ISSN 3080-6836 (Print)
ISSN 3080-6844 (Online)

Fundamental and Experimental Biology

2026

Volume 31, No. 3 (123)

Founded in 1996

Published 4 times a year

Karaganda
2026

Publisher: **NLC "Karaganda National Research University named after academician Ye.A. Buketov"**
Postal address: 28 University St., Karaganda 100024, Kazakhstan
E-mail: feb@buketov.edu.kz. Web-site: https://feb.buketov.edu.kz/

Fundamental and Experimental Biology. — 2026. — Vol. 31, Iss. 3(123). — 234 p. — ISSN 3080-6836 (Print) ISSN 3080-6844 (Online).

Proprietary: NLC "Karaganda National Research University named after academician Ye.A. Buketov".
Registered by the Ministry of Culture and Information of the Republic of Kazakhstan.

Rediscount certificate No. KZ45VPY00135989 dated 05.12.2025.

Signed in print 30.09.2026. Format 60×84 1/8. Photocopier paper. Volume 29,25 p.sh. Circulation 200 copies. Price upon request. Order № 126.

Printed in the Publishing house of NLC "Karaganda National Research University named after academician Ye.A. Buketov".
28 University St., Karaganda 100024, Kazakhstan. E-mail: printed@karnu-buketov.edu.kz.

CONTENTS

How to Cite: Bakytzhanova, M.S., Makhmudova, K.Kh., Aitymbetova, K.Sh., Murzatayeva, T.Sh., Yelubayeva, A.S. (2026). Seed morphology and seed coat micromorphology of *Linaria cretacea* Fisch. ex Spreng. from chalk outcrops of Western Kazakhstan. *Fundamental and Experimental Biology*, 31, 3 (123), 5-16. https://doi.org/10.31489/2026FEB3/5-16

Research article

https://doi.org/10.31489/2026FEB3/5-16

UDC 58.009 Received: 15.10.2025 | Accepted: 12.06.2026 | Published online: 30 September 2026

M.S. Bakytzhanova[1*], K.Kh. Makhmudova[2], K.Sh. Aitymbetova[3], T.Sh. Murzatayeva[4], A.S. Yelubayeva[5]

[1, 2]*Abai Kazakh National Pedagogical University, Faculty of Natural Sciences and Geography, Almaty, Kazakhstan;*
[2, 3, 4, 5]*Seed bank Laboratory, Institute of Botany and Phytointroduction, Almaty, Kazakhstan*
[*]*Corresponding author: maral.bakytzhanova@mail.ru*

Seed morphology and seed coat micromorphology of *Linaria cretacea* Fisch. ex Spreng. from chalk outcrops of Western Kazakhstan

The investigation of seed morphology and seed-coat micromorphology is important for taxonomy, ecology, and the conservation of rare endemic plants, particularly species restricted to specialized habitats such as chalk outcrops. In calciphilous plants with narrow distribution ranges, seed-coat micromorphology can serve as a useful diagnostic feature for species identification, clarification of taxonomic relationships, and the development of ex situ conservation measures. This study examined the morphological characteristics of the seeds and fruits of *Linaria cretacea* Fisch. ex Spreng., a rare calciphilous endemic species restricted to chalk outcrops in Western Kazakhstan, using scanning electron microscopy (SEM) and light microscopy. Macro- and microimages of the seeds were obtained, and their main morphometric parameters, including length, width, thickness, and shape index, were measured. Seed-coat sculpture was described at the primary, secondary, and tertiary levels following the classifications proposed by W. Barthlott and W. Stearn. The results showed that *L. cretacea* from the Aktobe Region is characterized by a cerebelliform primary sculpture with clearly defined anticlinal boundaries, a sharply tuberculate secondary sculpture with reticulate elements, and the absence of epicuticular wax. Comparison of the seed-coat traits identified in this study with published descriptions of the closely related species *L. vulgaris* and *L. genistifolia* revealed a set of diagnostically significant micromorphological differences. The possible adaptive role of seed-coat structure in chalk habitats with low water-retention capacity is also discussed. The findings are of both systematic and practical value, particularly for the identification of herbarium specimens and the development of protection and ex situ conservation protocols for this rare species.

Keywords: Linaria cretacea, Kazakhstan, calciphilous species, endemic species, seed morphology, scanning electron microscopy, light microscopy, features.

Introduction

The first information about the vegetation of chalk outcrops dates back to the works of I.A. Güldenstädt [1, 2]. In the 19th and early 20th centuries, the study of the flora of such habitats acquired a systematic character: significant contributions were made by Chernyaev [3], Litvinov [4, 5], Popov [6], Sagalaev [7], Sukachyov [8], Golitsyn [9], Klokov [10], Taliev [11–13], Kozo-Polyanskii [14–16], Kotov [17], Lavrenko [18] and others. The problem of the origin of chalk outcrops—natural or anthropogenic—was actively considered by classics of botany. Modern studies continue to clarify the composition of the flora and characteristics of chalk cliff communities, although a number of local and taxonomic issues remain insufficiently studied [19].

In carpological studies, seed macro- and micromorphology are considered key diagnostic characters in the taxonomy of angiosperms [20–22]. Of particular importance for taxonomic conclusions and evolutionary-functional interpretations are data on the ultrastructure of the seed coat obtained using SEM [23–26]. However, for a number of local, rare, and ecologically specialized taxa, data on seed microsculpture remain absent or are fragmentary.

Linaria cretacea Fisch. ex Spreng. is a perennial calciphyte with a taproot system that is strictly confined to chalk habitats within its Eastern European and Sub-Ural range. Its vegetative and reproductive traits (dwarfism, compact generative shoots, yellow corolla with a prominent spur) are consistent with life on steep chalk slopes and among rocky boulders.

Despite the recognized importance of seed traits in taxonomy and ecology, a comprehensive study of *L. cretacea's* seed micromorphology, combining modern SEM techniques, quantitative morphometrics, and comparison with related species, remains lacking. The seed morphology of representatives of the section *Linaria* has been described in the literature. However, specific information on primary and secondary sculpture, the degree of exotesta tortuosity, the presence/absence of epicuticular wax, and their functional interpretation are lacking for *L. cretacea* in the regional context of Cretaceous habitats in Kazakhstan.

This study examines the seed morphology and seed coat micromorphology of *L.cretacea* from the chalk outcrops of the Aktobe Region using scanning electron microscopy (SEM), light microscopy, and quantitative morphometric analysis. The research focuses on the description of the primary, secondary, and tertiary sculpture of the seed coat according to established classifications, comparison with closely related *Linaria species*, and evaluation of the taxonomic and adaptive significance of the identified traits in chalk habitats. Field material was collected from chalk massifs of the Aktobe Region during 2023–2025. Seeds were prepared for SEM following standard procedures, including fixation and gold sputtering, and the different levels of seed coat sculpture were described using accepted morphological terminology.

The identified seed-coat characters of *L.cretacea* were considered in comparison with published descriptions of selected representatives of the genus *Linaria*. This comparison was used to establish a general diagnostic framework and was not intended as a direct SEM-based species-to-species analysis of L. vulgaris and L. genistifolia. Because *L. cretacea* is a narrow chalk endemic, whereas related species of the genus occur in broader ecological settings, the literature data were employed only to indicate the possible taxonomic and ecological significance of the revealed seed traits.

The key result of the work is a deeper understanding of the micromorphology of a rare calciphilous species, the identification of diagnostic features for taxonomic purposes and herbarium identification, and the creation of a basis for subsequent studies of the ecology of germination and measures to conserve *L. cretacea* populations in chalk habitats.

Figure 1 presents images of *L.cretacea* growing on chalk slopes in the Aktobe Region, depicting the overall habit of the species and its typical habitat.

a) b)

Figure 1. *Linaria cretacea* in the Aktobe region: a) view of the plant; b) view of the seeds

Experimental

Material for carpological analysis was collected during June–July of 2023–2025 on the chalk massifs of the Aktobe Region (Tab. 1). For each sampling site, the coordinates, collection date, elevation above sea level, slope exposure, and general habitat characteristics were documented. For the morphometric and micro morphological study, 1,000 seeds (thousand-seed weight 0.20 g) collected from mature capsules of the two populations were analyzed.

Table 1

Characteristics of the studied sites of *Linaria cretacea*

Point number	Coordinates (latitude, longitude)	Elevation above sea level, m	Location	Slope aspect	Habitat characteristic
1	N49^{0}20′031′′ E 054°30′024′′	≈ 215 м	Akshatau Chalk	Southeast	A steep slope consisting of chalk marl and carbonate clays
2	N50^{0}32′069′′ E 054°54′341′′	≈ 235 м	Ishkargan Chalk	South	A gravel slope with exposed chalk bedrock

In the Aktobe Region of Western Kazakhstan, all major chalk outcrops were surveyed for *L. cretacea*, but the species was detected only at a few, markedly isolated locations. Intensive fieldwork in 2023–2025 showed that stable, self-maintaining populations are confined to the Akshatau and Ishkargan chalk massifs. On other chalk exposures, *L. cretacea* was either absent or represented by single, scattered plants, from which seed sampling is prohibited for conservation reasons. As a result, carpological material was collected only from these two populations, which constitute the main chalk massifs of the study area for this rare calciphilous endemic.

This study primarily sought to deliver a comprehensive qualitative and quantitative description of seed and seed-coat micromorphology at the species level. In this context, a rigorous statistical comparison between the two local populations was not pursued, as it lay outside the objectives of this initial investigation.

Seed and fruit morphology was investigated by light microscopy and scanning electron microscopy. The seed surface micromorphology of *L.cretacea* from the Aktobe Region was examined with JEOL JEM-1400 and JEOL JSM-6060LV scanning electron microscopes (JEOL Ltd., Tokyo, Japan). The analysis was performed on mature seeds. A total of 15 seeds were studied by SEM. To remove the cuticular layer, the seeds were kept in a chloroform–methanol mixture (1:1) for 48 h and then transferred through a graded ethanol series of 70 % and 90 %. After drying, the seeds were fixed directly onto specimen stubs with double-sided adhesive tape. Imaging at ×80 and ×100 magnification was used to record overall seed morphology, whereas ×500, ×800, and ×1500 magnifications were applied to examine the exo testa surface.

The resulting digital images were processed in Adobe Photoshop CS4. Seed surface descriptions were based on the shape of the principal cells, the structure of the anticlinal walls, including their thickness, sinuosity, and elevation above the surface, as well as the relief of the periclinal walls. Seed ultrastructure (primary, secondary and tertiary sculpture) was described using the terminology and morphotype categories proposed by Barthlott [23, 24], Stearn [25] and Segarra-Moragues & Mateu [26].

The terminology of W. Stearn and W. Barthlott [23, 25] was used to describe the ultrastructure of the seed coat. The classification provides for the distinction of three levels of sculpture—primary, secondary, and tertiary—with diagnostic features indicated (Tab. 2).

Table 2

Classification of seed ultrastructure according to W. Stearn and W. Barthlott with examples of morphotypes

Sculpture Level	Diagnostic Features	Examples of morphotypes	Characteristic features of *Linaria cretacea*
Primary	Exotesta cell shape, general pattern, type of anticlinal walls, border relief, curvature of outer periclinal walls	Comb-shaped, medulla-shaped, tuberculate, smooth	Cerebelliform; convolutions of slightly concave isodiametric cells; height 0.1–0.15 mm; margins recessed
Secondary	Relief of outer periclinal walls, location and shape of small elements	Reticulate, tuberculate, smooth, honeycomb	Low, closely spaced, acutely tuberculate cuticle deposits; tendency toward a reticulated pattern
Tertiary	Epicuticular secretions (wax: granules/flakes or absence)	Granules, scales, waxless	Epicuticular wax absent

The following parameters were assessed: seed shape; presence/absence of a wing; type of primary sculpture (comb-shaped, medulla-shaped, tuberculate, smooth); nature of cuticular deposits on the cell surface (reticular, papillary); tertiary sculpture (type of epicuticular wax or its absence).

Comparative information on other representatives of the genus *Linaria*, *including L. vulgaris* and *L. genistifolia*, was not obtained from original SEM observations in the present study and was used only as literature-based background for diagnostic interpretation.

For the morphometric analysis, measurements were obtained from the examined seed material in repeated observations. The quantitative data were summarized using descriptive statistical methods. For each measured trait, mean values, standard errors (Mean ± SE), and the minimum and maximum ranges were determined. Since the study was designed to provide an initial carpological and micromorphological characterization at the species level, no statistical comparison was carried out between the two sampled populations.

Results and Discussion

The fruits of *L.cretacea* are dry, multi-seeded capsules of oblong-round shape, approximately 3 mm in diameter. The locules are equal in size and dehisce through teeth at the apex (Fig. 2). The seeds gradually spill out through the resulting openings, driven by wind and stem vibrations.

The number of seeds in one capsule is 12–15, which is consistent with the data of Sutton and Viano [27]. The fruit weight is 3-4 mg, no more.

The passive seed dispersal range is determined by plant height and averages 12–35 cm—at the level of generative shoots. As a result, seeds are distributed within the parent patch of the coenopopulation, while their distant dispersal remains limited.

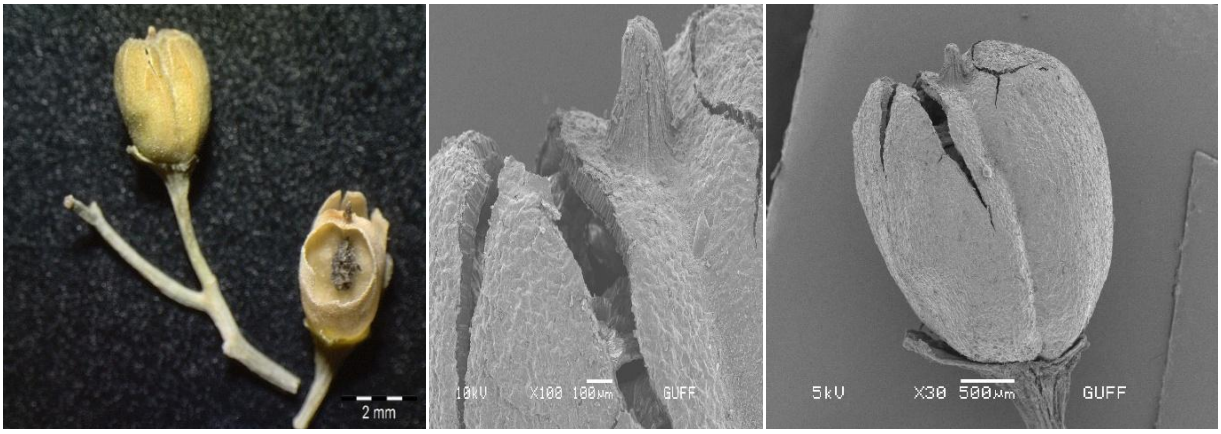

Figure 2. Macrophotography: general view of *Linaria cretacea* capsules

Morphometric characteristics of fruits are presented in Table 3.

Table 3

Morphometric parameters of *Linaria cretacea* fruits

Indicator	Mean ± SE	Minimum	Maximum
Capsule diameter, mm	3.02 ± 0.06	2.85	3.18
Number of seeds, pcs.	13.4 ± 1.1	12	15
Capsule length, mm	2.45 ± 0.08	2.30	2.60
Capsule width, mm	2.00 ± 0.07	1.80	2.20
Capsule weight, mg	3.5 ± 0.3	3.0	4.1
Shape	Oblong, rounded	–	–

The seeds of *L. cretacea* are small, elongate-reniform, and slightly curved; in cross section they are rounded with slight flattening on the dorsal side. Their mean dimensions are 1.20 ± 0.05 mm in length, 0.85 ± 0.04 mm in width, and 0.70 ± 0.03 mm in thickness (Tab. 4). The shape index (Length/Width) varies from 1.35 to 1.45, which indicates an elongated seed type (Fig. 3). The weight of 1000 seeds is 0.20 ± 0.01 g, confirming the very small size and low mass of the diaspores. Overall, the seeds are dark brown to black, slightly flattened, with a narrow marginal rim and a clearly expressed surface sculpture.

Table 4

Size and shape of *Linaria cretacea* seeds

Indicator	Mean ± SE	Minimum	Maximum
Length, mm	1.20 ± 0.05	1.00	1.85
Width, mm	0.85 ± 0.04	0.45	1.00
Thickness, mm	0.70 ± 0.03	0.25	0.55
Shape index (L/W)	1.41 ± 0.04	1.35	1.45
Form	Elongated, slightly reniform	–	–
Thousand-seed weight, g	0.20±0.01	0.18	0.22

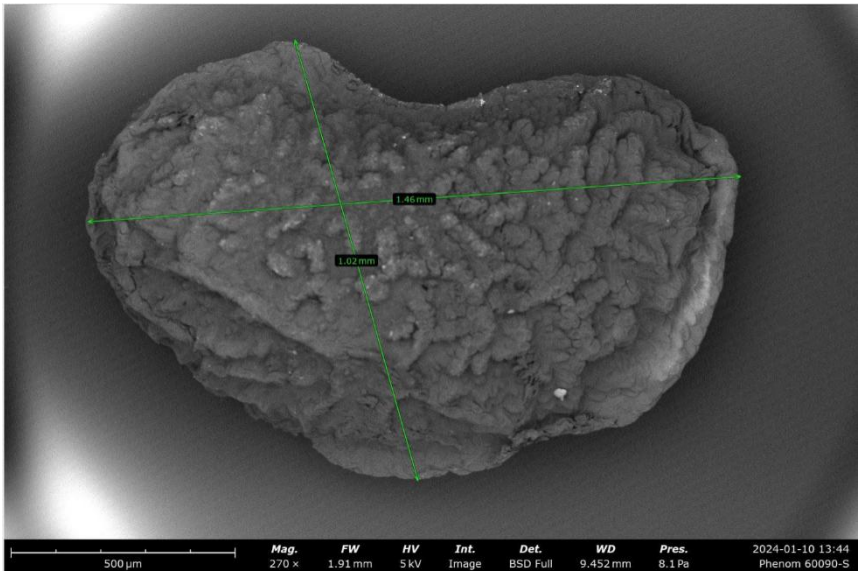

Figure 3. SEM image of *Linaria cretacea* seed, general view
(BSE mode, 5 kV, ×270; scale bar = 500 µm)

Observations under the light microscope showed that the seed surface is coarsely tuberculate and irregularly wrinkled, with a slight sheen. Examination by SEM provided a more detailed view of the seed coat ultrastructure and allowed the primary, secondary, and tertiary levels of sculpture to be distinguished.

In cross-section, the seed is characterized by a compact endosperm and a well-developed exotesta. The primary sculpture is cerebriform: the convolutions are formed by groups of slightly concave, isodiametric exotesta cells 0.10–0.15 mm high, often anastomosing. Cellular boundaries are deepened, with thin, discontinuous cuticular deposits.

The secondary sculpture is expressed by low, densely located, sharply tuberculate cuticular deposits, in places with a tendency to form a mesh pattern (Fig. 4).

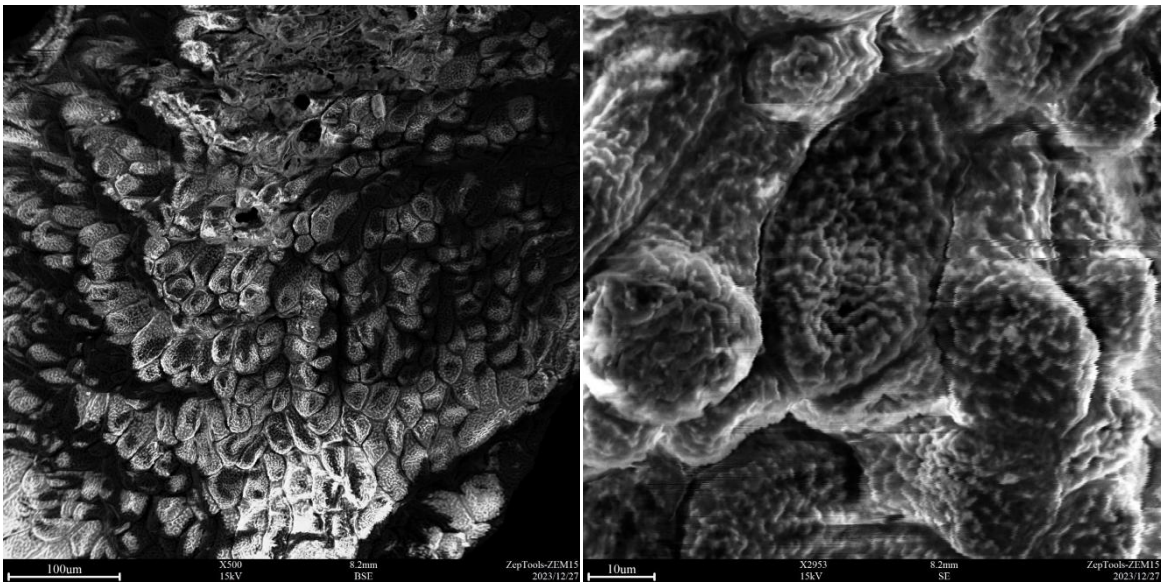

Figure 4. SEM images of the seed coat of *Linaria cretacea*, illustrating the cerebriform primary sculpture and the distinctly tuberculate secondary sculpture
(BSE mode, 15 kV, ×500, scale bar = 100 μm; SE mode, 15 kV, ×2953, scale bar = 10 μm)

SEM images (Fig. 4) demonstrate the ultrastructure of the *L. cretacea* seed coat with a characteristic cerebellar type of primary sculpture. The exotesta cells are isodiametric, slightly concave; the anticlinal boundaries are clearly deepened and form a sinuous folded pattern. The convolutions of varying width often anastomose, forming a branched network; their height is approximately 0.10–0.15 mm. Secondary sculpture is represented by dense, low, sharply tuberculate cuticular deposits, in places imparting a reticulate-like relief to the surface. Epicuticular wax is not observed: wax granules and scales are absent, which is consistent with previously described characteristics of the species. This microrelief likely increases the mechanical strength of the coat and promotes moisture retention, which is important for germination in chalky substrates with low water holding capacity.

No epicuticular wax was detected on the examined seeds, as neither wax granules nor wax scales were observed even at the highest magnification. The main characteristics of the primary, secondary, and tertiary levels of seed-coat sculpture in *L. cretacea* are summarized in Table 5.

Table 5

Characteristics of seed sculpture of *Linaria cretacea*

Sculpture Level	Diagnostic features	Morphotype	Characteristics of *L. cretacea*
Primary	Shape and relief of exotesta cells	Cerebelliform	Isodiametric cells are slightly concave; margins are indented.
Secondary	Microrelief of periclinal walls	Tubercular with reticular elements	Low, sharp tubercles; elements are often closely spaced.
Tertiary	Epicuticular secretions	Absent	Wax granules/scales are not detected.

Consequently, the morphological and anatomical features of the fruits and seeds *of L.cretacea* correspond to the conditions of chalk outcrops: they provide protection for diaspores, promote moisture retention, and limit long-distance transport, which supports the preservation of populations in highly specialized habitats.

The results obtained on the morphological and anatomical structure of the seeds of *Linaria cretacea* confirm several carpological characters previously reported for the genus and, at the same time, provide new diagnostic details for this rare chalk endemic [26, 27]. The cerebriform primary sculpture, with deeply marked anticlinal boundaries and no epicuticular wax, corresponds to the range of seed-coat characters described for *Linaria species* from arid and petrophytic habitats [23, 24, 26]. The secondary sculpture of *L. cretacea*, expressed as dense, sharply tuberculate cuticular deposits with a local tendency toward reticula-

tion, can be considered diagnostically informative; however, the present study is not intended as a direct SEM-based comparison with particular related species.

Only *L. cretacea* is illustrated in this paper, as the study is based on original morphological and micromorphological observations of this species, whereas comparisons with related taxa are derived from published descriptions. Based on a combination of traits—including seed shape, the types of primary and secondary sculpture, and the presence or absence of wax secretions—*L. cretacea* occupies a distinct position among closely related taxa. These characteristics are useful for clarifying the species' intrasectional taxonomic status and for reliably distinguishing the species from morphologically similar taxa, including in the analysis of herbarium specimens lacking flowering shoots.

To assess the diagnostic significance of the observed traits, the seed morphology of *L. cretacea* was compared with published descriptions of the closely related species *L. vulgaris* and *L. genistifolia*. The results of this comparison are presented in Table 6.

Table 6

Diagnostic comparison of seed characters in *Linaria cretacea* and related species based on published sources

Trait	*L. cretacea*	*L. vulgaris*	*L. genistifolia*
Seed shape	Elongated kidney-shaped	Discoid, reniform	Tetrahedral
Primary sculpture	Cerebelliform	Pectinate	Comb-shaped
Secondary sculpture	Acute tuberculate, partially reticulated	Papillary, partially reticular	Reticulate
Epicuticular wax	Absent	Granules	Granules
Seed size, mm	1.0–1.5 × 0.7–1.0	2.5–3.2 × 0.9–1.0	0.8–1.2 × 0.6–0.9
Note. Compiled from sources [26, 27]			

A comparison of the characters shows that *L. cretacea* differs from closely related species by a combination of an elongated kidney-shaped seed, a higher brain-shaped primary sculpture (0.10–0.15 mm), a sharply tuberculate secondary surface with elements of reticulation, and the absence of epicuticular wax, which makes this complex diagnostically significant for the identification of the species.

The unique structure of the *L. cretacea* seed coat can be interpreted as an adaptation to the conditions of chalk outcrops. The deep microrelief increases the mechanical strength of the coat and promotes the retention of a thin water film—an important factor for germination on low-water-holding substrates. These structural characteristics appear to influence not only protection, but also the course of germination. In *L. cretacea,* the pronounced cerebelliform primary relief, together with sharply tuberculate secondary elements and the absence of an epicuticular wax layer, affects both the rate and threshold of water uptake. Seeds are able to absorb moisture rapidly during short wetting episodes, while the water film retained in the surface sculpture slows drying and extends the time available for radicle emergence. In contrast, in related species with a smoother or wax-coated seed surface, comparable hydration may be reached only after longer or repeated moistening, which may partially account for interspecific differences in germination timing and success on chalk substrates. The absence of waxy secretions is likely due to the need for rapid moisture absorption during short-term precipitation. The sharp, tuberculate elements of the secondary sculpture likely enhance adhesion to microscopic irregularities, preventing seed washout and blowing away on steep slopes.

A morphoanatomical analysis of *L. cretacea* seeds revealed a complex of diagnostically significant traits: an elongated kidney-shaped form, a pronounced brain-shaped primary sculpture with deep anticlinal boundaries, a dense, acutely tuberculate secondary sculpture, and the absence of epicuticular wax. These features simultaneously distinguish the species from related taxa and possess obvious adaptive value for survival on chalk outcrops (increased seed coat strength, retention of a microfilm of moisture, and improved adhesion to the substrate). The results confirm the high informative value of seed coat micromorphology for the systematics of the section Linaria and enable the use of seed characters in taxonomic differentiation when working with herbarium material. The practical significance of the obtained data lies in the use in planning conservation measures for relict populations and in the design of experiments to assess seed viability (hydration, germination under conditions of limited moisture). To further clarify the evolutionary-ecological relationships, it is advisable to expand the sample by population, perform a comparable SEM analysis of closely related taxa, and conduct combined studies of the morphology and physiology of germination under different humidity and temperature conditions.

Conclusion

The fruits of *L. cretacea* are small, round-oblong capsules (≈3.2–3.4 mm in diameter), usually containing 12–15 seeds; the weight of one capsule is 3-4 mg or less. The seeds are small (length 1.0–1.5 mm; width 0.7–1.0 mm), elongated-reniform; the shape index L/W ≈ 1.35–1.45 indicates a pronounced elongation.

The primary sculpture is cerebellar: convolutions of slightly concave, isodiametric exotesta cells approximately 0.10–0.15 mm high with deeply anticlinal boundaries. Secondary sculpture consists of dense, sharply tuberculate cuticular deposits with a local tendency toward reticulation; tertiary sculpture (epicuticular wax) is absent in the specimens studied.

A combination of characters—the elongated kidney-shaped seed, the high brain-shaped primary sculpture, the nature of the secondary sculpture, and the absence of wax secretions—distinguishes *L. cretacea* from closely related taxa (e.g., *L. vulgaris*, *L. genistifolia*) and makes these micromorphological characters suitable for taxonomic differentiation, especially when analyzing herbarium material without flowers.

The structure of the seed coat—a pronounced microrelief and the absence of epicutinal wax granules—probably reflects adaptation to chalk habitats: deep relief increases the mechanical strength of the coat and retains a microfilm of moisture, while sharply tuberculate elements enhance adhesion to the microroughness of the substrate, reducing the risk of seeds being washed away or blown off slopes.

The short range of passive transfer (12–35 cm) combined with strict confinement to chalk substrates indicates limited potential dispersion and high local dependence of recruitment, which increases the vulnerability of populations to habitat disturbance.

The obtained micromorphological and morphometric information is suitable for monitoring and conservation of the species: it can be used for accurate identification of specimens, planning of seed collection and development of ex situ conservation protocols.

Further studies should cover a larger number of populations across the entire Eastern European-Subural part of the range in order to assess interpopulation variability of seed traits.

It is recommended to expand the sampling geography, conduct SEM studies of closely related taxa, conduct seed viability and germination tests, and develops protocols for seed collection and storage. The data obtained should be integrated into regional monitoring and management programs for chalk habitats to inform conservation and restoration measures.

The obtained data confirm the high informative value of seed coat micromorphological features for the taxonomy and ecology of calciphytes. Against the backdrop of declining suitable habitats, combining basic morphological research with practical conservation measures is key to the long-term conservation of *L. cretacea* and associated petrophyte communities.

Conflict of Interest

The authors declare no conflict of interest.

Author Contributions

The manuscript was written through the contributions of all authors. All authors have given approval to the final version of the manuscript. CRediT: **Bakytzhanova M.** — conceptualization, data curation, investigation, formal analysis, writing — original draft; **Makhmudova K.** — conceptualization, methodology, supervision, validation, writing — review and editing; **Aitymbetova K.** — investigation, methodology, data curation, formal analysis; **Murzatayeva T.** — supervision, project administration, resources, validation; **Yelubayeva A.** — investigation, visualization, data curation, technical assistance, editing.

References

1 Güldenstädt J.A. Reisen durch Rußland und im Caucasischen Gebürge / J.A. Güldenstädt. — St. Petersburg: Kaiserliche Akademie der Wissenschaften, 1787–1791. — Bd. I–II.

2 Гильденштедт И.А. Дневник путешествия в Россию в 1773–1774 гг. / И.А. Гильденштедт // Записки Одесского общества истории и древностей. — 1879. — Т. 11. — С. 180–229.

3 Черняев В.М. О произведениях растительного царства Курской губернии / В.М. Черняев // Журнал Министерства внутренних дел. — 1836. — Ч. 22, № 12. — С. 505–514.

4 Литвинов Д.И. О реликтовом характере флоры каменистых склонов в Европейской России / Д.И. Литвинов // Труды Ботанического музея Императорской Академии наук. — 1902. — Вып. 1. — С. 76–109.

5 Литвинов Д.И. О значении произрастания сосны и торфяной березки на меловых горах Центрально-Черноземного округа / Д.И. Литвинов // Бюллетень Общества естествоиспытателей при ВГУ. — 1927. — Т. 2, № 1. — С. 54–56.

6 Попов М.Г. Происхождение и эволюция покрытосеменных растений / М.Г. Попов // Филогения, флорогенетика, флорография, систематика: Избранные труды. — Киев: Наукова думка, 1983. — Ч. 2. — С. 281–290.

7 Сагалаев В.А. Флора степей и пустынь Юго-Востока европейской России, её генезис и современное состояние: автореф. дис. д-ра биол. наук / В.А. Сагалаев. — Москва, 2000. — 42 с.

8 Сукачёв В.Н. О болотной и меловой растительности Юго-Восточной части Курской губернии / В.Н. Сукачёв // Труды Общества испытателей природы при Императорском Харьковском университете. — 1902. — Т. 37. — С. 227–258.

9 Голицын С.В. «Сниженные альпы» и меловые иссопники Среднерусской возвышенности: автореф. дис. д-ра биол. наук / С.В. Голицын. — Воронеж, 1965. — 16 с.

10 Клоков М.В. Основные этапы развития равнинной флоры европейской части СССР / М.В. Клоков // Материалы по истории флоры и растительности СССР. — 1963. — Вып. 4. — С. 376–406.

11 Талиев В.И. Вегетация меловых обнажений Южной России / В.И. Талиев // Труды Общества испытателей природы при Императорском Харьковском университете. — 1904. — Т. 39, Вып. 1. — С. 81–254.

12 Талиев В.И. Дополнение к описанию меловой флоры / В.И. Талиев // Труды Общества испытателей природы при Императорском Харьковском университете. — 1905. — Т. 40, Вып. 1. — С. 1–282.

13 Талиев В.И. Дополнения к флоре меловых гор Южной России / В.И. Талиев // Труды Общества испытателей природы при Императорском Харьковском университете. — 1907. — Т. 40, Вып. 2. — С. 154–231.

14 Kozo-Poljanski B.M. Glaziale Pflanzenrelikte auf dem Orel-Kurskischen Plateau im Süden der Mittelrussischen Hochebene. Teil 1 / B.M. Kozo-Poljanski // Vegetationsbilder. — Jena: Fischer, 1928. — Reihe 19, H. 1/2. — Taf. 1–12.

15 Kozo-Poljanski B.M. Glaziale Pflanzenrelikte auf dem Orel-Kurskischen Plateau im Süden der Mittelrussischen Hochebene. Teil 2 / B.M. Kozo-Poljanski // Vegetationsbilder. — Jena: Fischer, 1929. — Reihe 19, H. 7/8. — Taf. 37–48.

16 Козо-Полянский Б.М. В стране живых ископаемых / Б.М. Козо-Полянский. — Москва, 1931. — 184 с.

17 Котов М.И. Ботанико-географический очерк растительности меловых обнажений на р. Оскол и её притоках / М.И. Котов // Журнал Русского ботанического общества. — 1927. — Т. 12, № 1-2. — С. 249–266.

18 Лавренко Е.М. Об эволюционных центрах флоры и возрасте украинского эндемизма / Е.М. Лавренко // Die Quartärperiode. — 1932. — Lieferung 4. — S. 27–43.

19 Golovanov Ya.M. Vegetation of chalk outcrops of Sub-Ural plateau and adjacent territories / Ya.M. Golovanov, S.M. Yamalov, M.V. Lebedeva, A.Yu. Korolyuk, L.M. Abramova, N.A. Dulepova // Vegetation of Russia. — 2021. — No. 40. — P. 3–42. https://doi.org/10.31111/vegrus/2021.40.3

20 Меликян А.П. Семейство Illiciaceae / А.П. Меликян; под ред. А.Л. Тахтаджяна // Сравнительная анатомия семян. — Ленинград: Наука, 1988. — Т. 2: Двудольные: Magnoliidae, Ranunculidae.

21 Меликян А.П. Семейство Winteraceae / А.П. Меликян, Е.Н. Немирович-Данченко; под ред. А.Л. Тахтаджяна // Сравнительная анатомия семян. — Ленинград: Наука, 1988. — Т. 2: Двудольные: Magnoliidae, Ranunculidae. — С. 44–47.

22 Данилова М.Ф. Сравнительная анатомия семян / М.Ф. Данилова; под ред. А.Л. Тахтаджяна. — СПб: Мир и Семья, 1996. — Т. 5: Двудольные: Rosidae I. — 240 с.

23 Barthlott W. Epidermal and seed surface characters of plants: Systematic applicability and some evolutionary aspects / W. Barthlott // Nordic Journal of Botany. — 1981. — Vol. 1, No. 3. — P. 345–355. https://doi.org/10.1111/j.1756-1051.1981.tb00704.x

24 Barthlott W. Microstructural features of seed surfaces / W. Barthlott; Eds. V.H. Heywood, D.M. Moore // Current Concepts in Plant Taxonomy. — London: Academic Press, 1984. — P. 95–105.

25 Stearn W.T. Botanical Latin: History, Grammar, Syntax, Terminology and Vocabulary / W.T. Stearn. — Portland: Timber Press, 1992. — 546 p.

26 Segarra-Moragues J.G. Seed morphology of Linaria species from eastern Spain: identification of species and taxonomic implications / J.G. Segarra-Moragues, I. Mateu // Botanical Journal of the Linnean Society. — 2001. — Vol. 137, No. 3. — P. 275–284. https://doi.org/10.1111/j.1095-8339.2001.tb01121.x

27 Sutton D.A. A Revision of the Tribe Antirrhineae / D.A. Sutton. — London: Oxford University Press for the British Museum (Natural History), 1988. — 322 p.

М.С. Бакытжанова, К.Х. Махмудова, К.Ш. Айтымбетова,
Т.Ш. Мурзатаева, А.С. Елубаева

Батыс Қазақстанның бор шөгінділерінен алынған *Linaria cretacea* Fisch. ex Spreng. тұқым қабығының морфологиясы және микроморфологиясы

Тұқым морфологиясы мен тұқым қабығының микроморфологиясын зерттеу сирек кездесетін эндемикалық өсімдіктердің, әсіресе кеуіп қалған жерлер сияқты мамандандырылған мекендеу орталарында мекендейтін түрлердің таксономиясы, экологиясы және сақталуы үшін өте маңызды. Таралу диапазоны тар кальцийлі өсімдіктерде тұқымның ультрақұрылымы түрлерін анықтау, таксономиялық байланыстарды нақтылау және *ex situ* сақтау шараларын әзірлеу үшін пайдалы

диагностикалық белгі ретінде қызмет ете алады. Зерттеуде Батыс Қазақстандағы кеуіп қалған жерлердегі сирек кездесетін кальцийлі эндемикалық түрі *Linaria cretacea* Fisch. ex Spreng. тұқымдары мен жемістерінің морфологиялық сипаттамалары сканерлеуші электронды микроскопия (SEM) және жарық микроскопиясы арқылы зерттелді. Тұқымдардың макро және микроскопиялық суреттері алынды, сондай-ақ олардың ұзындығы, ені, қалыңдығы және пішін индексі сияқты негізгі морфометриялық параметрлері өлшенді. Тұқым қабығының мүсіні В. Бартлотт пен В. Стерннің жіктемелеріне сәйкес бастапқы, екінші және үшінші деңгейлерде сипатталды. Нәтижелер Ақтөбе аймағынан алынған *L. cretacea* өсімдігінің антиклинальды шекаралары айқын анықталған мишық тәрізді бастапқы мүсінмен, торлы элементтері бар құрт туберкулезді екінші реттік мүсінмен және эпикутикулярлы балауыздың болмауымен сипатталатынын көрсетті. Анықталған тұқым қабығының ерекшеліктерін тығыз байланысты *L. vulgaris* және *L. genistifolia* түрлерінің жарияланған сипаттамаларымен салыстыру бірқатар диагностикалық маңызды микроморфологиялық айырмашылықтарды анықтады. Суды ұстау қабілеті төмен, кеуіп қалған жерлердегі тіршілік ету орталарындағы тұқым қабығы құрылымының бейімделу рөлі де талқыланды. Алынған деректердің жүйелік және практикалық маңызы бар, әсіресе гербарий үлгілерін анықтау және осы сирек кездесетін түрді қорғау және *ex situ* сақтау хаттамаларын әзірлеу үшін.

Кілт сөздер: Linaria cretacea, Қазақстан, кальцифилді түрлері, эндемикалық түрлері, тұқым морфологиясы, сканерлік электронды микроскопия, жарық микроскопиясы, ерекшеліктері.

М.С. Бакытжанова, К.Х. Махмудова, К.Ш. Айтымбетова,
Т.Ш. Мурзатаева, А.С. Елубаева

Морфология семян и микроморфология семенной оболочки *Linaria cretacea* Fisch. ex Spreng. из меловых отложений Западного Казахстана

Исследование морфологии семян и микроморфологии семенной оболочки имеет важное значение для таксономии, экологии и сохранения редких эндемичных растений, особенно видов, обитающих в специализированных местообитаниях, таких как меловые обнажения. У кальцифильных растений с узким ареалом распространения ультраструктура семян может служить полезным диагностическим признаком для идентификации видов, уточнения таксономических связей и разработки мер по сохранению ex situ. В данном исследовании с помощью сканирующей электронной микроскопии (СЭМ) и световой микроскопии были изучены морфологические характеристики семян и плодов *Linaria cretacea* Fisch. ex Spreng., редкого кальцифильного эндемичного вида меловых обнажений Западного Казахстана. Были получены макро- и микроизображения семян, а также измерены их основные морфометрические параметры, включая длину, ширину, толщину и индекс формы. Скульптура семенной оболочки была описана на первичном, вторичном и третичном уровнях в соответствии с классификациями В. Бартлотта и В. Штерна. Результаты показали, что *L. cretacea* из Актюбинской области характеризуется мозжечковидной первичной скульптурой с четко выраженными антиклинальными границами, резко бугорчатой вторичной скульптурой с сетчатыми элементами и отсутствием эпикутикулярного воска. Сравнение выявленных признаков семенной оболочки с опубликованными описаниями близкородственных видов *L. vulgaris и L. genistifolia* позволило выявить ряд диагностически значимых микроморфологических различий. Также рассматривается возможная адаптивная роль структуры семенной оболочки в меловых местообитаниях с низкой влагоудерживающей способностью. Полученные данные имеют как систематическое, так и практическое значение, особенно для идентификации гербарных образцов и для разработки протоколов защиты и сохранения ex situ этого редкого вида.

Ключевые слова: Linaria cretacea, Казахстан, кальцефильный вид, эндемичный вид, морфология семян, сканирующая электронная микроскопия, световая микроскопия, признаки.

References

1 Güldenstädt, J.A. (1787–1791). *Reisen durch Rußland und im Caucasischen Gebürge*. Saint Petersburg: Kaiserliche Akademie der Wissenschaften, Bd. I–II.

2 Güldenstädt, I.A. (1879). Dnevnik puteshestviia v Rossiiu v 1773–1774 gg. [Notes about journey to Russia in 1773–1774 years]. *Zapiski Odesskogo obshchestva istorii i drevnostei — Proceedings of the Odessa Society of History and Antiquities, 11,* 180–229 [in Russian].

3 Chernyaev, V.M. (1836). O proizvedeniiakh rastitelnogo tsarstva Kurskoi gubernii [About origin of plant kingdom in Kursk guberniya]. *Zhurnal Ministerstva vnutrennikh del — Journal of Ministry of Internal Affairs, 22*(12), 505–514 [in Russian].

4 Litvinov, D.I. (1902). O reliktovom kharaktere flory kamenistykh sklonov v Evropeiskoi Rossii [About relict character of flora of stony slopes in European Russia]. *Trudy Botanicheskogo muzeia Imperatorskoi Akademii nauk — Proceeding of Botanical Museum of Impair Society of Academy of Science, 1,* 76–109 [in Russian].

5 Litvinov, D.I. (1927). O znachenii proizrastaniia sosny i torfianoi berezki na melovykh gorakh Tsentralno-Chernozemnogo okruga [On the Significance of Pine and Peat Birch Growth on the Cretaceous Mountains of the Central Black Earth Region]. *Bulleten Obshchestva estestvoispytatelei pri Voronezhskom Gosudarstvennom Universitete — Bulletin of Society of Natural researchers of Voronezh State University, 2*(1), 54–56 [in Russian].

6 Popov, M.G. (1983). Proiskhozhdenie i evoliutsiia pokrytosemennykh rastenii [The Origin and Evolution of Angiosperms]. *Filogeniia, florogenetika, florografiia, sistematika: Izbrannye trudy — Phylogeny, Florogenetics, Florography, Systematics: Selected Works, 2*, 281–290. Kiev: Naukova dumka [in Russian].

7 Sagalaev, V.A. (2000). Flora stepei i pustyn Yugo-Vostoka evropeiskoi Rossii, ee genezis i sovremennoe sostoianie [Flora of the Steppes and Deserts of Southeastern European Russia: Its Genesis and Current State]. *Extended abstract of Doctor's thesis*. Moscow [in Russian].

8 Sukachyov, V.N. (1902). O bolotnoi i melovoi rastitelnosti Yugo-Vostochnoi chasti Kurskoi gubernii [On the Marsh and Chalk Vegetation of the Southeastern Part of the Kursk Governorate]. *Trudy Obshchestva ispytatelei prirody pri Imperatorskom Kharkovskom universitete — Proceedings of the Society of Naturalists at the Imperial Kharkiv University, 37*, 227–258 [in Russian].

9 Golitsyn, S.V. (1965). "Snizhennye alpy" i melovye issopniki Srednerusskoi vozvyshennosti [The "Lower Alps" and the Cretaceous Hyssop Grasslands of the Central Russian Uplands]. *Extended abstract of Doctor's thesis*. Voronezh [in Russian].

10 Klokov, M.V. (1963). Osnovnye etapy razvitiia ravninnoi flory evropeiskoi chasti SSSR [The Main Stages in the Development of the Lowland Flora of the European Part of the USSR]. *Materialy po istorii flory i rastitelnosti SSSR — Materials on history of flora and vegetation of USSR, 4*, 376–406 [in Russian].

11 Taliev, V.I. (1904). Vegetatsiia melovykh obnazhenii Yuzhnoi Rossii [Vegetation of Cretaceous Outcrops in Southern Russia]. *Trudy Obshchestva ispytatelei prirody pri Imperatorskom Kharkovskom universitete — Proceedings of the Society of Naturalists at the Imperial Kharkiv University, 39*(1), 81–254 [in Russian].

12 Taliev, V.I. (1905). Dopolnenie k opisaniiu melovoi flory [Supplement to the Description of the Cretaceous Flora]. *Trudy Obshchestva ispytatelei prirody pri Imperatorskom Kharkovskom universitete — Proceedings of the Society of Naturalists at the Imperial Kharkiv University, 40*(1), 1–282 [in Russian].

13 Taliev, V.I. (1907). Dopolneniia k flore melovykh gor Yuzhnoi Rossii [Additions to the Flora of the Cretaceous Mountains of Southern Russia]. *Trudy Obshchestva ispytatelei prirody pri Imperatorskom Kharkovskom universitete — Proceedings of the Society of Naturalists at the Imperial Kharkiv University*, *40*(2), 154–231 [in Russian].

14 Kozo-Poljanski, B.M. (1928). Glaziale Pflanzenrelikte auf dem Orel-Kurskischen Plateau im Süden der Mittelrussischen Hochebene. Teil 1. *Vegetationsbilder*. Jena: Fischer, 19(1/2); 1–12.

15 Kozo-Poljanski, B.M. (1929). Glaziale Pflanzenrelikte auf dem Orel-Kurskischen Plateau im Süden der Mittelrussischen Hochebene. Teil 2. *Vegetationsbilder*. Jena: Fischer, 19(7/8); 37–48.

16 Kozo-Polyanskii, B.M. (1931). *V strane zhivykh iskopaemykh* [In the Land of Living Fossils]. Moscow [in Russian].

17 Kotov, M.I. (1927). Botaniko-geograficheskii ocherk rastitelnosti melovykh obnazhenii na r. Oskol i ee pritokakh [A Botanical-Geographical Study of the Vegetation of Cretaceous Outcrops on the Oskol River and Its Tributaries]. *Zhurnal Russkogo botanicheskogo obshchestva — Journal of Russian Botanical Society, 12*(1-2), 249–266 [in Russian].

18 Lavrenko, E.M. (1932). Ob evoliutsionnykh tsentrakh flory i vozraste ukrainskogo endemizma [On the evolutionary centers of the flora and the age of Ukrainian endemism]. *Die Quartärperiode, Lieferung, 4*, 27–43 [in Russian].

19 Golovanov, Ya.M., Yamalov, S.M., Lebedeva, M.V., Korolyuk, A.Yu., Abramova, L.M., & Dulepova, N.A. (2021). Vegetation of chalk outcrops of Sub-Ural plateau and adjacent territories. *Vegetation of Russia*, 40, 3–42. https://doi.org/10.31111/vegrus/2021.40.3

20 Melikyan, A.P. (1988). Semeistvo Illiciaceae [Family Illiciaceae]. *Sravnitelnaia anatomiia semian. Vol. 2: Dvudolnye: Magnoliidae, Ranunculidae — Comparative Anatomy of Seeds. Vol. 2: Dicotyledons: Magnoliidae, Ranunculidae*. Leningrad: Nauka, 48–49 [in Russian].

21 Melikyan, A.P. & Nemirovich-Danchenko, E.N. (1988). Semeistvo Winteraceae [Family Winteraceae]. *Sravnitelnaia anatomiia semian. Vol. 2: Dvudolnye: Magnoliidae, Ranunculidae — Comparative Anatomy of Seeds. Vol. 2: Dicotyledons: Magnoliidae, Ranunculidae*. Leningrad: Nauka, 44-47 [in Russian].

22 Danilova, M.F. (1996). *Sravnitelnaia anatomiia semian. T. 5: Dvudolnye: Rosidae I* [Comparative seed anatomy. Vol. 5: Dicoteledons: Rosidae]. Saint Petersburg: Mir i Semia [in Russian].

23 Barthlott, W. (1981). Epidermal and seed surface characters of plants: Systematic applicability and some evolutionary aspects. *Nordic Journal of Botany, 1*(3), 345–355. https://doi.org/10.1111/j.1756-1051.1981.tb00704.x

24 Barthlott, W. (1984). Microstructural features of seed surfaces. In: Heywood V.H., Moore D.M. (Eds.), *Current Concepts in Plant Taxonomy*. London: Academic Press, 95–105.

25 Stearn, W.T. (1992). *Botanical Latin: History, Grammar, Syntax, Terminology and Vocabulary*. Portland: Timber Press.

26 Segarra-Moragues J.G., & Mateu I. (2001). Seed morphology of Linaria species from eastern Spain: identification of species and taxonomic implications. *Botanical Journal of the Linnean Society, 137*(3), 275–284. https://doi.org/10.1111/j.1095-8339.2001.tb01121.x.

27 Sutton, D.A. (1988). *A Revision of the Tribe Antirrhineae*. London: Oxford University Press for the British Museum (Natural History).

Information about the authors

Bakytzhanova Maral Sagyndykovna — PhD-student, Faculty of Natural Sciences and Geography, Abai Kazakh National Pedagogical University, Almaty, Kazakhstan; e-mail: maral.bakytzhanova@mail.ru, ORCID: http://orcid.org/0009-0006-1255-2971

Makhmudova Karina Khamidovna — Candidate of Biological Sciences, Senior Lecturer, Leading Researcher, Seed Bank Laboratory, Institute of Botany and Phytointroduction, Almaty, Kazakhstan; e-mail: carinamakhmudova2015@gmail.com, ORCID: https://orcid.org/0000-0003-0926-8196

Aitymbetova Klara Shardarbekovna — Candidate of Agricultural Sciences, Leading Researcher, Seed Bank Laboratory, Institute of Botany and Phytointroduction, Almaty, Kazakhstan; e-mail: aitklara@mail.ru, ORCID: https://orcid.org/0000-0003-3003-5223

Murzatayeva Tansara Shayakhmetovna — Candidate of Agricultural Sciences, Head of Seed Bank Laboratory, Institute of Botany and Phytointroduction, Almaty, Kazakhstan; e-mail: m.tansara@mail.ru, ORCID: https://orcid.org/0000-0002-3034-4205

Yelubayeva Aigerim Sauytovna — Junior Researcher, Seed Bank Laboratory, Institute of Botany and Phytointroduction, Almaty, Kazakhstan; e-mail: aigera_89_01@mail.ru, ORCID: https://orcid.org/0000-0003-4037-5707

How to Cite: Kumargazy, K.D., Satu, A.S., Khusanov, T., Temirkhanov, A.Zh., Nurbekova Zh.A. (2026). Organelle Dynamics during Salinity-Induced Programmed Cell Death in Plants. *Fundamental and Experimental Biology*, 31, 3 (123), 17-29. https://doi.org/10.31489/2026FEB3/17-29

Review Article

https://doi.org/10.31489/2026FEB3/17-29

UDC 581.19 Received: 12.12.2025 | Accepted: 18.02.2026 | Published online: 30.09.2026

K.D. Kumargazy[1], A.S. Satu[1], T. Khusanov[2], A.Zh. Temirkhanov[3], Zh.A. Nurbekova[1*]

[1]*Department of Biotechnology and Microbiology, L.N. Gumilyov Eurasian National University, Astana, Kazakhstan;*
[2]*The Institute of Microbiology of Academy of Sciences of Uzbekistan, Uzbekistan;*
[3]*Republican Collection of Microorganisms, Astana, Kazakhstan*
[*]*Corresponding author: zhadyrassyn.nurbekova@gmail.com*

Organelle Dynamics during Salinity-Induced Programmed Cell Death in Plants

Programmed cell death (PCD) is a complex mechanism induced by environmental stress (ePCD) or developmental processes (dPCD). ePCD can be triggered by various types of unfavorable abiotic conditions, including salinity stress. Exposure to high concentrations of salt not only alters plant morphological characteristics but also severely affects biochemical and molecular processes. Furthermore, plants activate numerous defense mechanisms that operate in different organelles within the plant cell. These mechanisms involve ionic, osmotic, and oxidative damage affecting the plasma membrane, mitochondria, chloroplasts, vacuoles, and nucleus. A major disturbance in the plasma membrane is characterized by impaired transport processes, ROS accumulation, and Ca^{2+} influx. Mitochondrial dysfunction is closely associated with excessive ROS accumulation, activation of protective pathways such as AOX, UCPs, and the GABA shunt, and cytochrome c release. Moreover, the photosynthetic rate is substantially reduced in association with a decline in chlorophyll content. Vacuoles integrate osmotic and ionic signals by sequestering Na^{+} through NHX antiporters and V-ATPase activity; however, when this system collapses, Ca^{2+} signals converge on the nucleus. Furthermore, the overproduction of ROS acts as a signaling molecule in the activation of EXECUTER proteins involved in chloroplast–nucleus communication. Salinization activates osmotic, ionic, and oxidative signaling pathways that ultimately result in chromatin degradation. Altogether, these interconnected processes contribute to the induction of PCD.

Keywords: Programmed cell death, salinity stress, reactive oxygen species, nitic oxide, phytohormones, enzyme.

Introduction

Programmed cell death (PCD) is a genetically regulated series of events resulting in cell death [1]. It eliminates unnecessarily damaged cells across all developmental stages, starting from germination to the plant's death [2]. PCD is classified into two distinct groups based on the mode of induction, triggered by environmental stress (ePCD) and triggered by developmental processes (dPCD) [3]. dPCD is involved in the latest stage of cell differentiation in various parts of the plant, controlling the formation of new cells; moreover, it may occur as a result of cell-to-cell signaling, and it is the final point of senescence in all plant tissues [1]. On the other hand, ePCD is induced by abiotic (drought, salinity, temperature, heavy metals, etc.) or biotic (pathogens, parasites, insects, etc.) stresses. In both types, PCD is a crucial step in plant growth and development, helping to control and respond to the internal or external stimuli in plants.

Among other defense mechanisms in a plant, PCD plays a key role during stress conditions, but it acts differently compared with other responses. In most cases, the defense systems have interplay with reactive oxygen species (ROS), which, in the case of PCD, is a main regulatory factor. However, during pPCD, damaged or highly affected cells by stress conditions are purposely killed in order not to affect the other living cells. So the plant can maintain a stable and acquired number of healthy living cells [4].

Review

Firstly, the term PCD was used by Lockshin and Williams (1964) and since then, many studies on the role in plant growth and development have been carried on. Several studies indicate that signaling pathways regulating PCD in both animals and plants are similar. PCD in plants is not only a developmental process, but also a significant response mechanism under salt stress. Salinity triggers ion imbalance, osmotic stress and oxidative damage, which can activate PCD pathways in plant cells [5]. Under salt stress,

overaccumulation of ROS becomes a "secondary stress" that impairs cellular function in organelles like chloroplasts, mitochondria, peroxisomes and the apoplast are principal sources of ROS under such conditions [6]. ROS accumulation under salinity not only damages molecular component, but also serves as a signaling cascade to initiate PCD. In salt-stressed cells, NADPH oxidases and mitochondrial respiration are activated, further enhancing ROS levels that lead to cell death [7]. NO acts as a redox-active signaling molecule, promoting survival at low concentrations but contributing to PCD at high levels, particularly when ROS are elevated. Crosstalk between NO and ROS regulates redox balance and forms peroxynitrite ($ONOO^-$), a potent oxidant that damages membranes, proteins, and nucleic acids, triggering PCD (a phenomenon called nitrosative burst) [8, 9]. Ionic imbalance, including high Na^+ influx and K^+ efflux, also contributes to PCD activation under salinity [7]. Calcium signaling is another critical regulator of salt-induced PCD, as elevated cytosolic Ca^{2+} activates downstream cascades, including ROS-producing enzymes like vacuolar processing enzymes (VPEs) and other cell death effectors [10]. Phytohormones coordinate stress responses and PCD: salicylic acid (SA) enhances antioxidant activity and reduces ROS-mediated cell death [11], while ethylene provides protection, as shown by higher salt-induced death in ethylene-insensitive Arabidopsis mutants (ein2-5, ein3-1) [12]. Jasmonic (JA) and gibberellins (GA) interact with SA pathways, redox balance and gene expression, influencing cell survival of PCD under salinity [13].

During PCD, various organelles play specific but interconnected roles. For example, the plasma membrane (PM) acts as the primary sensor of environmental stress, detecting ionic, osmotic and oxidative changes and initiating signaling cascades [21]. The mitochondria serve as one of the early stress sensors by releasing signaling factors, including the release of cytochrome c, which initiates further downstream cell death events [14]. Also, nuclear changes include chromatin condensation and nuclear degradation, triggered downstream of vacuole rupture during tracheary element differentiation and PCD in *Zinnia* plant [15]. Moreover, the vacuole undergoes tonoplast premeabilisation or rupture to release hydrolyses into cytoplasmic contents [16]. Finally, chloroplasts participate in ROS generation under stress and may experience thylakoid disorganization [17]. Altogether, these events are intertwined, forming cross-talk circuits that push the cell toward irreversible death.

Under salinity stress, PCD is a tightly regulated process in which stress signals like ROS, NO, Ca^{2+}, and phytohormones activate proteolytic enzymes and trigger organelle responses. Excessive salinity alters ions as well as redox balance, leading to structural and biochemical alterations in PM, mitochondria, chloroplasts, vacuoles and nuclei. These organelles communicate through ROS as well as calcium signaling, ensuring coordinated execution of cell death. Understanding their cross-talk during salinity stress gives valuable information about plant adaptations and the regulation of PCD during stress. In many studies, researchers described this mechanism mostly in animals; however, there are limited sources about plant PCD induced by salinity. Moreover, numerous amount of discoveries were made on the separate organelles, whereas few reviews summarise that knowledge about the relationship between plant organelles and PCD. Hence, in the following review, we will focus on detailed biochemical changes occurring in these organelles and their interconnections during salinity stress that lead to PCD.

1. Salinity stress

One of the most widespread stress factors affecting plants is salinization. It is estimated that by 2050, 50 % of cultivable land will be impacted by salinity stress [18]. It is described as a high concentration of sodium (Na^+), chloride (Cl^-), potassium (K^+), and sulfate (SO_4^{2-}) in a soil, which inhibits mineral uptake by roots. Further, these ions can subsequently be dissolved in water and transported to plant cells [18]. According to the type of salinity-inducing elements and pH, salinization is classified into two distinct groups: neutral and alkaline salinity. Neutral salinity is mainly induced by NaCl at pH = 6.998, and alkaline one is caused by sodium carbonate (Na2CO3) or potassium carbonate (K2CO3), where pH > 10.5 [19].

Salt stress conditions not only affect plant morphology but also exert profound effects on biochemical and molecular processes. Therefore, it affects many organelles within a plant cell, including the PM, mitochondria, vacuole, chloroplast and nucleus. Moreover, the homeostatic disturbance during high salinity exposure is classified into two stages known as primary (decline in plant growth and mineral absorption) and secondary (damage of biomolecules by ROS) [20].

2. Plasma Membrane (PM) dynamics under salinity stress

Plasma membrane (PM) serves as a vital interface between the plant cell and its environment, exhibiting high dynamism and changing structural and functional features in response to environmental stress-

es [21]. Under salinity, the PM becomes the primary sensor of ionic, osmotic and oxidative stresses, which act together and directly affect the behavior of PM channels [22]. The ionic aspect of salinity arises from toxic effects of specific ions, such as Na^+ and Cl^-, and from nutrient disruptions, while high salt concentrations lower water potential, causing water deficit or osmotic stress [23]. In addition, salt stress promoted the generation of ROS, including singlet oxygen, superoxide anion, hydrogen peroxide and hydroxyl radicals, causing oxidative stress in many plants [24].

Figure 1 indicates that PM-associated stress sensors, such as receptor-like kinases (RLKs) [25], glycosyl inositol phosphoryl ceramides (GIPCs) [26], and other membrane proteins, first detect high external salts. These sensors trigger downstream signaling pathways, notably the SOS (Salt Overly Sensitive) pathway, which attempts to regulate Na extrusion and maintain ionic homeostasis [25–28].

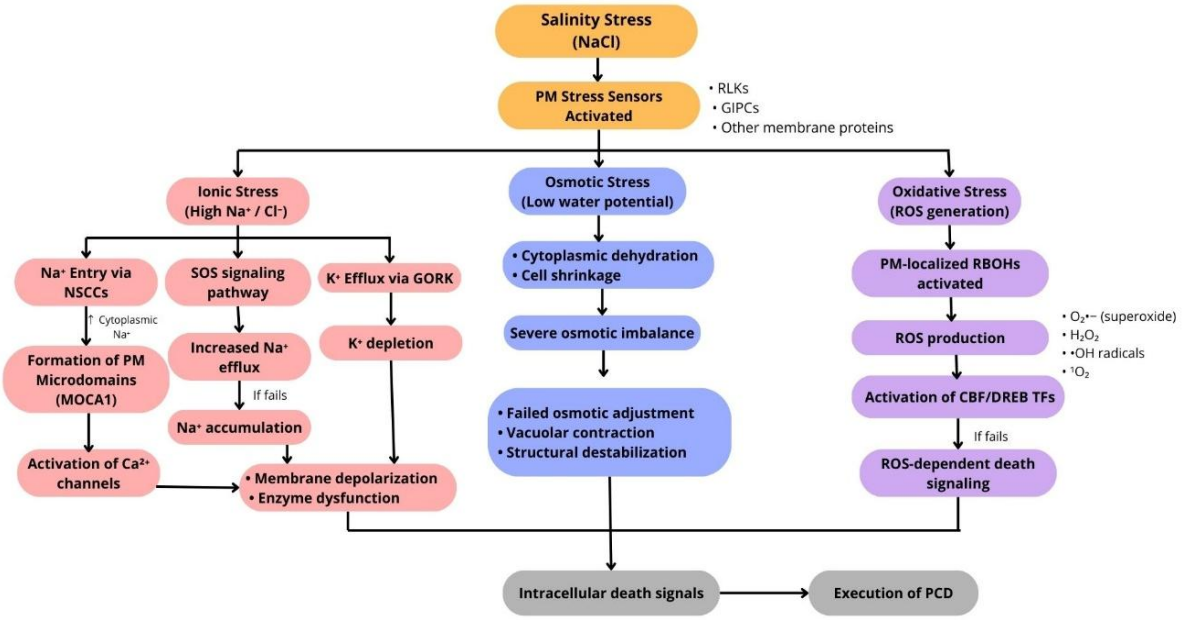

Figure 1. Plasma membrane function during salinity stress, which leads to PCD.
Created using Canva. Inspired by [43]

For ionic stress, Na^+ enters the cytoplasm through non-selective cation channels (NSCCs) like cyclic nucleotide-gated channels (CNGCs) [29] and glutamate-activated channels (GLRs) [30], while K^+ efflux occurs via outward-rectifying K^+ channels (GORK) [31]. High cytoplasmic Na^+ leads to the formation of PM microdomains (MOCA1), which in turn activate Ca^{2+} channels, resulting in a significant influx of Ca^{2+} into the cytoplasm. If the PM transporter, like SOS1, that plays a critical role in controlling the NHX antiporters in the vacuole, becomes overwhelmed [32], then cytoplasmic Na^+ accumulation and K+ depletion destabilize membrane potential and disrupt enzyme activity, generating strong intracellular death signals that contribute to PCD initiation [33].

Osmotic stress caused by high salt reduces water potential [34], leading to cytoplasmic dehydration and cell shrinkage. PM sensors, including RLKs and GIPCs, detect these changes, and the elevated Na^+ levels further trigger Ca^{2+} influx through PM channels [25, 26]. Under extreme stress, osmotic adjustment fails, resulting in vacuolar contraction and structural destabilization that amplify the intracellular death signal, further driving PCD [35].

Meanwhile, the PM acts as a major site for ROS production via NADPH oxidases (RBOH) [36]. ROS such as superoxide anion and hydrogen peroxide accumulate in the cytoplasm and apoplast, overwhelming detoxification mechanisms [37–39]. ROS production at the PM, combined with ionic and osmotic imbalances, acts as a death signal, activating downstream transcription factors (e.g. CBF/DREB) [40–42] and organelle-mediated PCD pathways, including mitochondrial dysfunction, vacuolar collapse and caspase-like protease activation [33].

Thus, under severe salinity stress, the PM integrates ionic, osmotic and oxidative stress signals, but rather than protecting the cell, its dysregulated responses converge to trigger PCD.

3. Mitochondrial Dynamics Under Salinity Stress

Mitochondria show a distinct and highly sensitive response to salinity stress because of their central roles in energy production, signaling and carbon metabolism [43]. Salt stress disturbs the normal balance of mitochondrial fission and fusion, leading to swelling, fragmentation and a decrease in membrane potential [44]. As ion homeostasis and osmotic balance shift under high salt, mitochondrial compartments sense cytosolic Na^+ accumulation and initiate early adaptive responses [45]. One of the earliest changes is a decline in the inner membrane potential (ΔΨm) due to the opening of permeability transition pores (PTPs) [46], as illustrated in Figure 2.

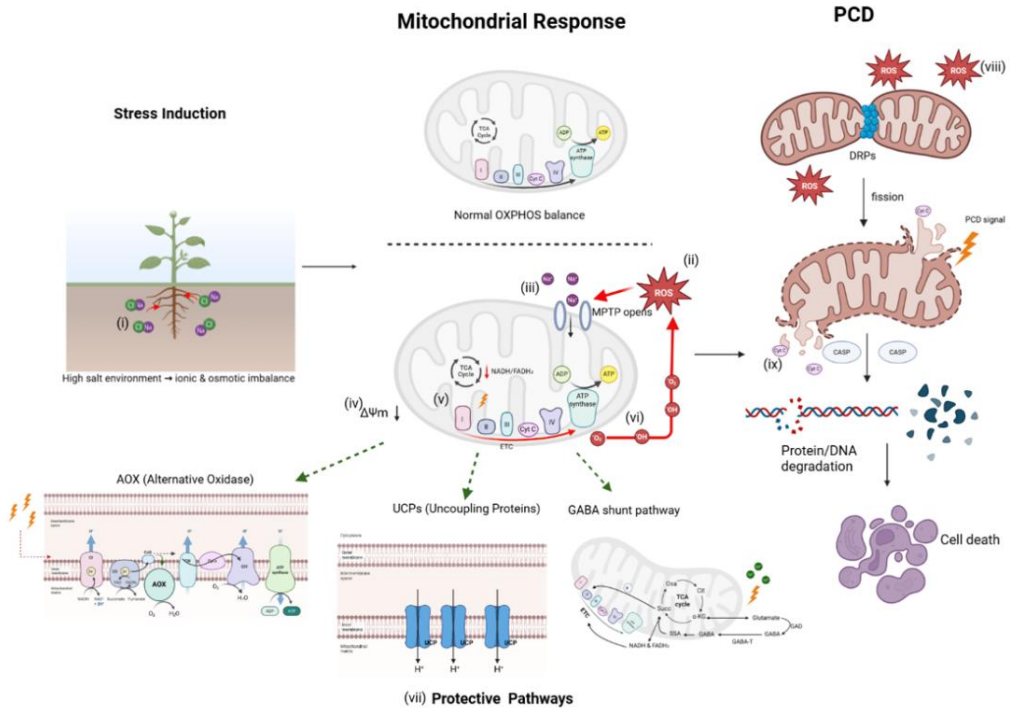

Figure 2. Mitochondrial response during salinity stress exposure.
Created using BioRender.com. Inspired by [43]

Mitochondrial oxidative phosphorylation (OXPHOS) depends on the electron transport chain (Complexes I-IV) and ATP synthase (Complex V) to generate ATP [47]. Complexes I, III and IV pump protons into the intermembrane space, creating an electrochemical gradient that drives ATP synthesis [48]. Under normal conditions, proton pumping and ATP production remain balanced, ensuring stable ΔΨm. However, salinity disrupts this balance, causing excess proton buildup, over-reduction of the ETC, and impaired ATP synthesis [49].

Salt stress affects the tricarboxylic acid (TCA) cycle, reducing the activity of key enzymes such as citrate synthase and isocitrate dehydrogenase [50]. This limits the supply of NADH and $FADH_2$ to the ETC, weakening OXPHOS and promoting electron leakage, which increases mitochondrial ROS production [6].

To restore homeostasis under salt stress, mitochondria activate Ca^{2+} transporters and bypass systems such as AOX and UCPs, which reduce redox pressure and help stabilize ΔΨm [49, 51]. AOX maintains NADH oxidation by bypassing Complexes III and IV, while UCPs mildly dissipate the proton gradient to limit ROS without fully stopping ATP production [52; 51]. Antioxidant defenses, including MnSOD and enzymes of the ascorbate-glutathione cycle, further detoxify ROS and support redox balance [51].

Salt stress also induced the GABA shunt, where glutamate is converted to GABA and then to succinate, supplying the TCA cycle and reducing ROS when photosynthesis and growth decline [53, 54].

Under severe salinity, excess ROS act as damage signals, activating DRP3A/DRP2B and promoting mitochondrial fragmentation [55, 56]. ROS also trigger mPTP opening, causing ΔΨm collapse and releasing cytochrome c, which activates caspase-like proteases and initiates irreversible PCD [57, 58]. When AOX, UCPs, antioxidant systems and the GABA shunt can no longer rebalance energy and redox status, ATP depletion worsens mitochondrial failure [43], driving the cell toward programmed death.

4. Chloroplast During Salinity Stress

Chloroplast is highly affected during exposure to high saline conditions. Many vital processes, which take place in chloroplasts, are declined, including photosynthesis. Those effects can be subdivided as osmotic and ionic stresses [59]. Osmotic stress is triggered by high salt concentration in soil, which disturbs the water absorption by roots, resulting in water deficit, and ionic stress is described as mechanical damage by an extreme amount of salt in transpiring leaf cells [60]. Munns proposed the idea of the biphasic model of plant response to salinity stress in 1993. Where he described the first phase as not salt-specific growth retardation due to water deficiency, while the second salt-specific phase is related to leaf death associated with rapid accumulation of salt in cytoplasm and cell walls [61]. Furthermore, it leads to stomatal closure, reduced chlorophyll content, decreased CO_2 concentration, and a decline in photosynthesis [62].

Exposure of plants to salinity stress leads to a decline in CO_2 assimilation, causing an over-reduction of photosystem II (PSII). This imbalance results in the formation of ROS, particularly singlet oxygen ($^1O_2$) [63]. In photosynthetically active leaves, chloroplasts serve as primary sites of ROS generation [64]. The major ROS species formed in chloroplasts include singlet oxygen ($^1O_2$), superoxide radicals (O_2^-), hydrogen peroxide (H_2O_2) and hydroxyl radicals (•OH) [65] (Tab. 1). Because radical forms of ROS are difficult to detect directly, most studies focus on measuring non-radical H_2O_2 accumulation as an indicator of oxidative stress under saline conditions [63].

Table 1

The effect of different concentrations of salinity on different plant species

	Plant species	Salt concentration (NaCl)	Chloroplast content	Photosynthetic efficiency	PCD marker	References
1.	A Korean wheat cultivar cv. Keumgang (*Triticum aestivum L.*)	150 mM for 1, 2, or 3 days	The levels of Chl a and b decreased to 79 % of the control at 1 day, 59 % at 2 days, and 53 % at 3 days	Photosynthetic rate decreased to 79 % at 1 day, 59 % at 2 days, and 53 % at 3 days	Proline contents rose to 102 % of the untreated control at 1 day, 104 % at 2 days, and 109 % at 3 days	[66]
2.	Barley (*Hordeum vulgare*)	100 and 200 mM	El Arich, Giza2000, Giza127 lose, respectively 33 %, 36 % and 43 % of their total chlorophyll content	A significant decrease only in Giza127 at 200mM NaCl	An increase in MDA content in almost all barley genotypes	[67]
3.	(*Vicia faba* L.)	60, 120, 240 mM	Chl a content decreased, reaching its lowest content, 0.270 and 0.426 mg/g fresh weight, at 240 mM	Due to the decline in photosynthetic pigments, decrease in photosynthetic rate as well	Decline in protein content	[68]
4.	Barley (*Hordeum vulgare* L.)	200 mM	Chl a content from 14 % to 41 %, chl b contents were reduced from 12 %, to 46.8 % and similarly, total chlorophyll contents were decreased from 10.3 % to 50.3 %	The efficiency of electron donation to PSI (Fv/Fo) and maximum quantum yield of PSII (Fv/Fm) was significantly reduced	Enhanced dissipation energy flux per reaction center (DIO/RC) in thylakoid membrane.	[69]
5.	Oat (*Avena sativa*)	48, 72, 96, 120, 144 $mmolL^{-1}$	At 96 $mmolL^{-1}$ NaCl, the content of chlorophyll a decreased to 0.86 times, while the content of chlorophyll b decreased to 0.7 times compared with the controls	Decline in photosynthetic rate due to the decrease in chloroplast content	The proline content in shoots was increased by 3.26 times under NaCl stress, and the proline content in roots by 3.41 times	[70]

5. Vacuole During Salinity Stress

Under saline conditions, plants rapidly experience osmotic, ionic and oxidative stress, while excess Na^+ and Cl^- disrupt cytosolic ion homeostasis, enzyme activation, biomolecule synthesis and hormonal imbalance [71]. Excess accumulation of these ions provokes the activation of vacuolar transport systems to sequester toxic ions into the vacuoles and maintain a favorable K^+/Na^+ ratio [72]. Vacuolar transport systems include Na^+/H^+ antiporters, V-ATPase, V-PPase, Ca^{2+}-ATPase, aquaporin, ABC transporters and etc. [73]. At the same time, some adjustments of the morphological and functional structure of the vacuole, such as vacuole enlargement (swelling), tonoplast remodeling, changes in cytosolic pH as a response to osmotic imbalance [74], and thereby protecting the cytoplasm from ion toxicity. These dynamic changes in vacuolar volume, tonoplast structure and internal environment, altogether contribute to the maintenance of turgor pressure [3] and support osmotic adjustment [67] during the early stages of salt stress, thus protecting the cytoplasm from rapid ionic stress damage.

However, failure to sequester excess Na into the vacuole causes severe cytosolic stress [75]. High salt levels induce ROS production, leading to oxidative damage of tonoplast lipids and proteins [76]. Under these conditions, cells shift to an energy-saving metabolic state, degrading stored reserves and nonessential components to supply metabolites for energy production and essential biosynthesis [77]. Elevated cytosolic Ca^{2+} further activated stress-signaling pathways that weaken vacuolar integrity. Early stress hormones such as salicylic acid (SA), gibberellin (GA) and ethylene trigger Ca^{2+} signaling and play critical roles in plant PCD [3; 10]. Disruption of the vacuolar Ca pumps ACA4 and ACA11 increases apoptosis-like cell death through an SA-dependent pathway [10], highlighting their role in linking vacuolar Ca^{2+} signaling to PCD onset [78]. Stress-induced autophagy often protects cells by restoring energy balance and suppressing PCD [79–81]. However, unknown signals can redirect autophagy into a pathway that promotes vacuole-dependent PCD [83, 82], characterized by tonoplast permeabilization and rupture, which releases hydrolases and drives cytoplasmic degradation [84, 77]. Vacuolar processing enzymes (VPEs) and other proteases can also initiate hypersensitive-response (HR) PCD under abiotic and biotic stress, and peroxisomal catalase removal via pexophagy may be required for HR activation [83, 86, 85]. Before tonoplast rupture, vacuoles show increased lytic activity as autophagy-derived cargo and stress-induced proteases accumulate [77]. Activation of VPE and related proteases triggers membrane collapse and release of acidic contents—a hallmark of vacuole-mediated PCD [85]. Disrupted coordination between autophagy and osmotic adjustment may contribute to tonoplast rupture [87]. Once the membrane collapses, hydrolases degrade the protoplast and later the cell wall. Notably, under severe energy deficiency, autophagy itself can act as a direct inducer of PCD [88].

6. Nucleus Under Salinity Stress

A number of processes are affected by salt exposure, including cell division. Cell division is a primary process determining the cell shape and its further development. High salinity conditions can alter symmetry and asymmetry ratio, meaning the distribution of cytoplasmic components between daughter cells during division [89]. Moreover, it severely disrupts the work of the cytoskeleton. Salt stress induced significant disturbances in the interactions among cytoskeletal components. It affects both ion transport regulation and the biosynthesis and regulation of various membrane and non-membrane proteins, including transporters and enzymes [90]. These can happen in individual cells. In some cases, cytoskeletal damage becomes irreversible, as components may form aberrant structures, including crystalline-like aggregates, which cannot be properly assembled and persist in daughter cells after division [91]. Additionally, earlier it was reported that the chloroplast proteins EXECUTER1 and EXECUTER2 transfer oxidative signals from the plastid to the nucleus [92]. Overaccumulation of ROS species in the nucleus resulted in cell death.

Another type of PCD regulation involved iron homeostasis. Iron is a crucial element that plays a key role in development, photosynthesis, chlorophyll biosynthesis and DNA synthesis through the formation of Fe-S clusters and heme groups [93]. Both ROS and NO can influence ion homeostasis in plant cells. Iron readily reacts with ROS to generate highly reactive and toxic species; for example, during the Fenton reaction, Fe^{2+} reacts with hydrogen peroxide (H_2O_2) to produce hydroxyl radicals (•OH), which can damage nucleic acids, proteins and lipids. NO is also a key element in maintaining iron balance; it helps sequester iron and reduce oxidative damage [94]. Furthermore, NO functions as a signaling molecule during ferritin synthesis, contributing to iron storage and cellular protection [93].

7. Interconnection of Cellular Organelles under Salinity Stress

Under salinity stress, plant organelles do not act independently; instead, they form an integrated signaling network in which ionic, osmotic and oxidative cues propagate rapidly between the plasma membrane (PM), mitochondria, chloroplasts, vacuole and nucleus. As shown in Figure 4, high Na^+ and Cl^- levels first disturb PM transport systems, driving Ca^{2+} influx and ROS accumulation that serve as early signals transmitted to internal organelles [22, 25, 36]. Mitochondria respond by altering $\Delta\Psi m$, increasing ROS production and activating protective pathways such as AOX, UCPs and the GABA shunt, but excessive stress leads to mPTP opening and cytochrome c release, linking mitochondrial dysfunction directly to PCD initiation [46, 51, 57]. Chloroplasts similarly generate large amounts of ROS due to PSII over-reduction, and these oxidative signals are relayed to the nucleus via chloroplast-nuclear communication pathways such as EXECUTER proteins, reinforcing stress-induced transcriptional reprogramming and DNA degradation [63, 92]. Vacuoles integrate osmotic and ionic signals by sequestering Na^+ through NHX antiporters and V-ATPase activity, but when this system collapses and Ca^{2+} converge on the nucleus, causing chromatin condensation and fragmentation, ultimately sealing the commitment to PCD [89]. Together, these interconnected organelles create a coordinated stress-response circuit in which membrane transport, ROS signaling, Ca^{2+} fluxes and protease activation collectively determine whether the cell adapts or undergoes PCD.

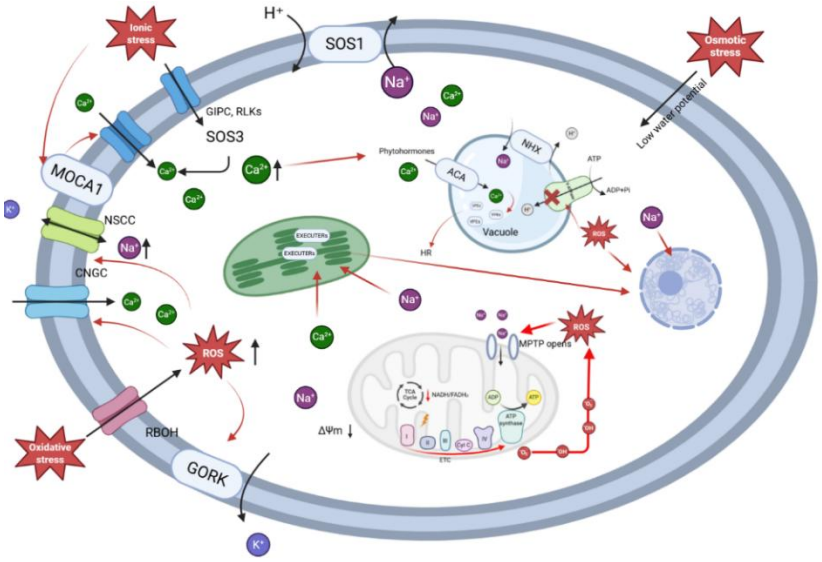

Figure 4. Interconnection of cellular organelles during salinity stress leading to PCD. Created using Biorender.com.

Future perspectives

Although significant progress has been made in understanding how individual organelles respond to salinity, their coordinated behavior during PCD remains insufficiently explored. Future research should focus on identifying the precise molecular signals, such as ROS, NO, Ca fluxes and phytohormone crosstalk that mediate communication between mitochondria, chloroplasts, vacuoles, the plasma membrane and nucleus under salt stress. Advancing imaging and omics technologies could help visualize real-time organelle interactions and uncover early biomarkers predicting the shift from stress tolerance to PCD. Moreover, engineering key regulators such as SOS transporters, vacuolar pumps, antioxidant systems, mitochondrial metabolic pathways (AOX, UCPs, GABA shunt), and chloroplast ROS-detoxifying components may provide new strategies for developing salt-tolerant crops. Integrating these findings will be essential for constructing comprehensive models of organelle-driven PCD and improving plant resilience in increasingly saline environments.

Conclusion

This review discussed the effect of high salinity exposure on the five main organelles in a plant cell, resulting in PCD. Over time, plants have developed a defensive system in order to protect themselves from high salinity. Indeed, although plants do not possess an equivalent to the animal adaptive immune system,

they deploy a number of defense mechanisms, and the severity of plant stress is tightly correlated with plant species, salt concentration and exposure longevity. The ratio between these two (plant defense system and severity of salinity) determines whether the plant will tolerate or activate PCD mechanisms. Hence, it is crucial to investigate the defensive mechanism and their interconnection in order to develop new strategies for producing plant species tolerant to salinity.

Funding

This research was funded by the Science Committee of the Ministry of Science and Higher Education of the Republic of Kazakhstan (Grant No. AP23483695).

Conflict of Interest

The authors declare no conflict of interest.

Author Contributions

The manuscript was written through contributions of all authors. All authors have given approval to the final version of the manuscript. CRediT: **Kumargazy K.D., Satu A.S.** — investigation, data curation, writing — original draft; **Temirkhanov A.Zh, Nurbekova Zh.A., Khusanov T.** — writing — review & editing; **Nurbekova Zh.A.** — supervision; **Temirkhanov A.Zh.** — project administration, funding acquisition.

References

1 Daneva, A., Gao, Z., Van Durme, M., & Nowack, M. K. (2016). Functions and Regulation of Programmed Cell Death in Plant Development. *Annual Review of Cell and Developmental Biology*, *32*(1), 441–468. https://doi.org/10.1146/annurev-cellbio-111315-124915

2 Fagundes, D., Bohn, B., Cabreira, C., Leipelt, F., Dias, N., Bodanese-Zanettini, M. H., & Cagliari, A. (2015). Caspases in plants: Metacaspase gene family in plant stress responses. *Functional & Integrative Genomics*, *15*(6), 639–649. https://doi.org/10.1007/s10142-015-0459-7

3 Jiang, C., Wang, J., Leng, H. -N., Wang, X., Liu, Y., Lu, H., Lu, M. -Z., & Zhang, J. (2021). Transcriptional Regulation and Signaling of Developmental Programmed Cell Death in Plants. *Frontiers in Plant Science*, *12*, 702928. https://doi.org/10.3389/fpls.2021.702928

4 Ye, C., Zheng, S., Jiang, D., Lu, J., Huang, Z., Liu, Z., Zhou, H., Zhuang, C., & Li, J. (2021). Initiation and Execution of Programmed Cell Death and Regulation of Reactive Oxygen Species in Plants. *International Journal of Molecular Sciences*, *22*(23), 12942. https://doi.org/10.3390/ijms222312942

5 Shabala, S. (2009). Salinity and programmed cell death: Unravelling mechanisms for ion specific signalling. *Journal of Experimental Botany*, *60*(3), 709–712. https://doi.org/10.1093/jxb/erp013

6 Liu, J., Fu, C., Li, G., Khan, M. N., & Wu, H. (2021). ROS Homeostasis and Plant Salt Tolerance: Plant Nanobiotechnology Updates. *Sustainability*, *13*(6), 3552. https://doi.org/10.3390/su13063552

7 Petrov, V., Hille, J., Mueller-Roeber, B., & Gechev, T. S. (2015). ROS-mediated abiotic stress-induced programmed cell death in plants. *Frontiers in Plant Science*, *6*. https://doi.org/10.3389/fpls.2015.00069

8 Zaninotto, F., Camera, S. L., Polverari, A., & Delledonne, M. (2006). Cross Talk between Reactive Nitrogen and Oxygen Species during the Hypersensitive Disease Resistance Response. *Plant Physiology*, *141*(2), 379–383. https://doi.org/10.1104/pp.106.078857

9 Wang, Y., Loake, G. J., & Chu, C. (2013). Cross-talk of nitric oxide and reactive oxygen species in plant programed cell death. *Frontiers in Plant Science*, *4*. https://doi.org/10.3389/fpls.2013.00314

10 Ren, H., Zhao, X., Li, W., Hussain, J., Qi, G., & Liu, S. (2021). Calcium Signaling in Plant Programmed Cell Death. *Cells*, *10*(5), 1089. https://doi.org/10.3390/cells10051089

11 Barwal, S. K., Shah, S. H., Pawar, A., Siddiqui, M. H., Agnihotri, R. K., Vimala, Y., & Wani, S. H. (2024). Mechanistic insights of salicylic acid-mediated salt stress tolerance in Zea mays L. seedlings. *Heliyon*, *10*(14), e34486. https://doi.org/10.1016/j.heliyon.2024.e34486

12 Pan, Y. -J., Liu, L., Lin, Y. -C., Zu, Y. -G., Li, L. -P., & Tang, Z. -H. (2016). Ethylene Antagonizes Salt-Induced Growth Retardation and Cell Death Process via Transcriptional Controlling of Ethylene-, BAG- and Senescence-Associated Genes in Arabidopsis. *Frontiers in Plant Science*, *7*. https://doi.org/10.3389/fpls.2016.00696

13 Zhu, Y., Wang, Q., Gao, Z., Wang, Y., Liu, Y., Ma, Z., Chen, Y., Zhang, Y., Yan, F., & Li, J. (2021). Analysis of Phytohormone Signal Transduction in Sophora alopecuroides under Salt Stress. *International Journal of Molecular Sciences*, *22*(14), 7313. https://doi.org/10.3390/ijms22147313

14 Schwarze, J., Carolan, J. C., Stewart, G. S., McCabe, P. F., & Kacprzyk, J. (2023). The boundary of life and death: Changes in mitochondrial and cytosolic proteomes associated with programmed cell death of Arabidopsis thaliana suspension culture cells. *Frontiers in Plant Science*, *14*, 1194866. https://doi.org/10.3389/fpls.2023.1194866

15 Obara, K., Kuriyama, H., & Fukuda, H. (2001). Direct Evidence of Active and Rapid Nuclear Degradation Triggered by Vacuole Rupture during Programmed Cell Death in Zinnia. *Plant Physiology*, *125*(2), 615–626. https://doi.org/10.1104/pp.125.2.615

16 Wertman, J., Lord, C. E., Dauphinee, A. N., & Gunawardena, A. H. (2012). The pathway of cell dismantling during programmed cell death in lace plant (Aponogeton madagascariensis) leaves. *BMC Plant Biology*, *12*(1), 115. https://doi.org/10.1186/1471-2229-12-115

17 Williams, B., & Dickman, M. (2008). Plant programmed cell death: Can't live with it; can't live without it. *Molecular Plant Pathology*, *9*(4), 531–544. https://doi.org/10.1111/j.1364-3703.2008.00473.x

18 Mustafa, G., Akhtar, M. S., & Abdullah, R. (2019). Global Concern for Salinity on Various Agro-Ecosystems. In M.S. Akhtar (Ed.), *Salt Stress, Microbes, and Plant Interactions: Causes and Solution* (pp. 1–19). Springer Singapore. https://doi.org/10.1007/978-981-13-8801-9_1

19 Stavi, I., Thevs, N., & Priori, S. (2021). Soil Salinity and Sodicity in Drylands: A Review of Causes, Effects, Monitoring, and Restoration Measures. *Frontiers in Environmental Science*, *9*, 712831. https://doi.org/10.3389/fenvs.2021.712831

20 Ondrasek, G., Rathod, S., Manohara, K. K., Gireesh, C., Anantha, M. S., Sakhare, A. S., Parmar, B., Yadav, B. K., Bandumula, N., Raihan, F., Zielińska-Chmielewska, A., Meriño-Gergichevich, C., Reyes-Díaz, M., Khan, A., Panfilova, O., Seguel Fuentealba, A., Romero, S. M., Nabil, B., Wan, C. (Craig), … Horvatinec, J. (2022). Salt Stress in Plants and Mitigation Approaches. *Plants*, *11*(6), 717. https://doi.org/10.3390/plants11060717

21 Conde, A., Chaves, M. M., & Geros, H. (2011). Membrane Transport, Sensing and Signaling in Plant Adaptation to Environmental Stress. *Plant and Cell Physiology*, *52*(9), 1583–1602. https://doi.org/10.1093/pcp/pcr107

22 Mansour, M. M. F. (2014). The plasma membrane transport systems and adaptation to salinity. *Journal of Plant Physiology*, *171*(18), 1787–1800. https://doi.org/10.1016/j.jplph.2014.08.016

23 Kingsbury, R. W., & Epstein, E. (1986). Salt Sensitivity in Wheat: A Case for Specific Ion Toxicity. *Plant Physiology*, *80*(3), 651–654. https://doi.org/10.1104/pp.80.3.651

24 Sharma, P., Jha, A. B., Dubey, R. S., & Pessarakli, M. (2012). Reactive Oxygen Species, Oxidative Damage, and Antioxidative Defense Mechanism in Plants under Stressful Conditions. *Journal of Botany*, *2012*, 1–26. https://doi.org/10.1155/2012/217037

25 Gandhi, A., & Oelmüller, R. (2023). Emerging Roles of Receptor-like Protein Kinases in Plant Response to Abiotic Stresses. *International Journal of Molecular Sciences*, *24*(19), 14762. https://doi.org/10.3390/ijms241914762

26 Jiang, Z., Zhou, X., Tao, M., Yuan, F., Liu, L., Wu, F., Wu, X., Xiang, Y., Niu, Y., Liu, F., Li, C., Ye, R., Byeon, B., Xue, Y., Zhao, H., Wang, H. -N., Crawford, B. M., Johnson, D. M., Hu, C., … Pei, Z. -M. (2019). Plant cell-surface GIPC sphingolipids sense salt to trigger Ca2+ influx. *Nature*, *572*(7769), 341–346. https://doi.org/10.1038/s41586-019-1449-z

27 Shi, H., Ishitani, M., Kim, C., & Zhu, J. -K. (2000). The *Arabidopsis thaliana* salt tolerance gene *SOS1* encodes a putative Na^+ /H^+ antiporter. *Proceedings of the National Academy of Sciences*, *97*(12), 6896–6901. https://doi.org/10.1073/pnas.120170197

28 Shi, H., Quintero, F. J., Pardo, J. M., & Zhu, J. -K. (2002). The Putative Plasma Membrane Na^+ /H^+ Antiporter SOS1 Controls Long-Distance Na^+ Transport in Plants. *The Plant Cell*, *14*(2), 465–477. https://doi.org/10.1105/tpc.010371

29 Phang, T., Shao, G., & Lam, H. (2008). Salt Tolerance in Soybean. *Journal of Integrative Plant Biology*, *50*(10), 1196–1212. https://doi.org/10.1111/j.1744-7909.2008.00760.x

30 Craig Plett, D., & Møller, I. S. (2010). Na^+ transport in glycophytic plants: What we know and would like to know. *Plant, Cell & Environment*, *33*(4), 612–626. https://doi.org/10.1111/j.1365-3040.2009.02086.x

31 Eisenach, C., Papanatsiou, M., Hillert, E., & Blatt, M. R. (2014). Clustering of the K^+ channel GORK of A rabidopsis parallels its gating by extracellular K^+. *The Plant Journal*, *78*(2), 203–214. https://doi.org/10.1111/tpj.12471

32 Qiu, Q. -S., Guo, Y., Quintero, F. J., Pardo, J. M., Schumaker, K. S., & Zhu, J. -K. (2004). Regulation of Vacuolar Na+/H+ Exchange in Arabidopsis thaliana by the Salt-Overly-Sensitive (SOS) Pathway. *Journal of Biological Chemistry*, *279*(1), 207–215. https://doi.org/10.1074/jbc.M307982200

33 Joseph, B., & Jini, D. (2010). Salinity Induced Programmed Cell Death in Plants: Challenges and Opportunities for Salt-tolerant Plants. *Journal of Plant Sciences*, *5*(4), 376–390. https://doi.org/10.3923/jps.2010.376.390

34 Mansour, M. M. F., Salama, K. H. A., & Allam, H. Y. H. (2015). Role of the Plasma Membrane in Saline Conditions: Lipids and Proteins. *The Botanical Review*, *81*(4), 416–451. https://doi.org/10.1007/s12229-015-9156-4

35 Hatsugai, N., Kuroyanagi, M., Yamada, K., Meshi, T., Tsuda, S., Kondo, M., Nishimura, M., & Hara-Nishimura, I. (2004). A Plant Vacuolar Protease, VPE, Mediates Virus-Induced Hypersensitive Cell Death. *Science*, *305*(5685), 855–858. https://doi.org/10.1126/science.1099859

36 Liu, M., Yu, H., Ouyang, B., Shi, C., Demidchik, V., Hao, Z., Yu, M., & Shabala, S. (2020). NADPH oxidases and the evolution of plant salinity tolerance. *Plant, Cell & Environment*, *43*(12), 2957–2968. https://doi.org/10.1111/pce.13907

37 Farvardin, A., González-Hernández, A. I., Llorens, E., García-Agustín, P., Scalschi, L., & Vicedo, B. (2020). The Apoplast: A Key Player in Plant Survival. *Antioxidants*, *9*(7), 604. https://doi.org/10.3390/antiox9070604

38 Hasanuzzaman, M., Raihan, Md. R. H., Masud, A. A. C., Rahman, K., Nowroz, F., Rahman, M., Nahar, K., & Fujita, M. (2021). Regulation of Reactive Oxygen Species and Antioxidant Defense in Plants under Salinity. *International Journal of Molecular Sciences*, *22*(17), 9326. https://doi.org/10.3390/ijms22179326

39 Pottosin, I., Velarde-Buendia, A. M., Bose, J., Zepeda-Jazo, I., Shabala, S., & Dobrovinskaya, O. (2014). Cross-talk between reactive oxygen species and polyamines in regulation of ion transport across the plasma membrane: Implications for plant adaptive responses. *Journal of Experimental Botany*, *65*(5), 1271–1283. https://doi.org/10.1093/jxb/ert423

40 Yan, J., Liu, Y., Yan, J., Liu, Z., Lou, H., & Wu, J. (2023). The salt-activated CBF1/CBF2/CBF3-GALS1 module fine-tunes galactan-induced salt hypersensitivity in *Arabidopsis*. *Journal of Integrative Plant Biology*, *65*(8), 1904–1917. https://doi.org/10.1111/jipb.13501

41 Liu, Q., Zhao, N., Yamaguch-Shinozaki, K., & Shinozaki, K. (2000). Regulatory role of DREB transcription factors in plant drought, salt and cold tolerance. *Chinese Science Bulletin*, *45*(11), 970–975. https://doi.org/10.1007/BF02884972

42 Zandkarimi, H., Ebadi, A., Salami, S. A., Alizade, H., & Baisakh, N. (2015). Analyzing the Expression Profile of AREB/ABF and DREB/CBF Genes under Drought and Salinity Stresses in Grape (Vitis vinifera L.). *PLOS ONE*, *10*(7), e0134288. https://doi.org/10.1371/journal.pone.0134288

43 Che-Othman, M. H., Millar, A. H., & Taylor, N. L. (2017). Connecting salt stress signalling pathways with salinity-induced changes in mitochondrial metabolic processes in C 3 plants. *Plant, Cell & Environment*, *40*(12), 2875–2905. https://doi.org/10.1111/pce.13034

44 Tang, H., & Zhu, H. (2022). Specific Changes in Morphology and Dynamics of Plant Mitochondria under Abiotic Stress. *Horticulturae*, *9*(1), 11. https://doi.org/10.3390/horticulturae9010011

45 Rozentsvet, O. A., Bogdanova, E. S., Nurminsky, V. N., Nesterov, V. N., & Chernyshov, M. Yu. (2023). Detergent-Resistant Membranes in Chloroplasts and Mitochondria of the Halophyte Salicornia perennans under Salt Stress. *Plants*, *12*(6), 1265. https://doi.org/10.3390/plants12061265

46 Vianello, A., Zancani, M., Peresson, C., Petrussa, E., Casolo, V., Krajňáková, J., Patui, S., Braidot, E., & Macrì, F. (2007). Plant mitochondrial pathway leading to programmed cell death. *Physiologia Plantarum*, *129*(1), 242–252. https://doi.org/10.1111/j.1399-3054.2006.00767.x

47 Eubel, H., Heinemeyer, J., Sunderhaus, S., & Braun, H. -P. (2004). Respiratory chain supercomplexes in plant mitochondria. *Plant Physiology and Biochemistry*, *42*(12), 937–942. https://doi.org/10.1016/j.plaphy.2004.09.010

48 Møller, I. M., Rasmusson, A. G., & Van Aken, O. (2021). Plant mitochondria — past, present and future. *The Plant Journal*, *108*(4), 912–959. https://doi.org/10.1111/tpj.15495

49 Schwarzländer, M., Logan, D. C., Johnston, I. G., Jones, N. S., Meyer, A. J., Fricker, M. D., & Sweetlove, L. J. (2012). Pulsing of Membrane Potential in Individual Mitochondria: A Stress-Induced Mechanism to Regulate Respiratory Bioenergetics in *Arabidopsis*. *The Plant Cell*, *24*(3), 1188–1201. https://doi.org/10.1105/tpc.112.096438

50 Barreto, P., Koltun, A., Nonato, J., Yassitepe, J., Maia, I. D. G., & Arruda, P. (2022). Metabolism and Signaling of Plant Mitochondria in Adaptation to Environmental Stresses. *International Journal of Molecular Sciences*, *23*(19), 11176. https://doi.org/10.3390/ijms231911176

51 Van Aken, O. (2021). Mitochondrial redox systems as central hubs in plant metabolism and signaling. *Plant Physiology*, *186*(1), 36–52. https://doi.org/10.1093/plphys/kiab101

52 Barreto, P., Okura, V., Pena, I. A., Maia, R., Maia, I. G., & Arruda, P. (2016). Overexpression of mitochondrial uncoupling protein 1 (UCP1) induces a hypoxic response in *Nicotiana tabacum* leaves. *Journal of Experimental Botany*, *67*(1), 301–313. https://doi.org/10.1093/jxb/erv460

53 Che-Othman, M. H., Jacoby, R. P., Millar, A. H., & Taylor, N. L. (2020). Wheat mitochondrial respiration shifts from the tricarboxylic acid cycle to the GABA shunt under salt stress. *New Phytologist*, *225*(3), 1166–1180. https://doi.org/10.1111/nph.15713

54 Ramos-Ruiz, R., Martinez, F., & Knauf-Beiter, G. (2019). The effects of GABA in plants. *Cogent Food & Agriculture*, *5*(1), 1670553. https://doi.org/10.1080/23311932.2019.1670553

55 Arimura, S. (2018). Fission and Fusion of Plant Mitochondria, and Genome Maintenance. *Plant Physiology*, *176*(1), 152–161. https://doi.org/10.1104/pp.17.01025

56 Ježek, J., Cooper, K. F., & Strich, R. (2021). The Impact of Mitochondrial Fission-Stimulated ROS Production on Pro-Apoptotic Chemotherapy. *Biology*, *10*(1), 33. https://doi.org/10.3390/biology10010033

57 Morciano, G., Naumova, N., Koprowski, P., Valente, S., Sardão, V. A., Potes, Y., Rimessi, A., Wieckowski, M. R., & Oliveira, P. J. (2021). The mitochondrial permeability transition pore: An evolving concept critical for cell life and death. *Biological Reviews*, *96*(6), 2489–2521. https://doi.org/10.1111/brv.12764

58 Vacca, R. A., Valenti, D., Bobba, A., Merafina, R. S., Passarella, S., & Marra, E. (2006). Cytochrome *c* is released in a Reactive Oxygen Species-Dependent Manner and Is Degraded via Caspase-Like Proteases in Tobacco Bright-Yellow 2 Cells en Route to Heat Shock-Induced Cell Death. *Plant Physiology*, *141*(1), 208–219. https://doi.org/10.1104/pp.106.078683

59 İbrahimova, U., Kumari, P., Yadav, S., Rastogi, A., Antala, M., Suleymanova, Z., Zivcak, M., Tahjib-Ul-Arif, Md., Hussain, S., Abdelhamid, M., Hajihashemi, S., Yang, X., & Brestic, M. (2021). Progress in understanding salt stress response in plants using biotechnological tools. *Journal of Biotechnology*, *329*, 180–191. https://doi.org/10.1016/j.jbiotec.2021.02.007

60 Parihar, P., Singh, S., Singh, R., Singh, V. P., & Prasad, S. M. (2015). Effect of salinity stress on plants and its tolerance strategies: A review. *Environmental Science and Pollution Research*, *22*(6), 4056–4075. https://doi.org/10.1007/s11356-014-3739-1

61 Munns, R. (1993). Physiological processes limiting plant growth in saline soils: Some dogmas and hypotheses. *Plant, Cell & Environment*, *16*(1), 15–24. https://doi.org/10.1111/j.1365-3040.1993.tb00840.x

62 Balasubramaniam, T., Shen, G., Esmaeili, N., & Zhang, H. (2023). Plants' Response Mechanisms to Salinity Stress. *Plants*, *12*(12), 2253. https://doi.org/10.3390/plants12122253

63 Gulzar, S., Hussain, T., Gul, B., & Hameed, A. (2020). Photosynthetic Adaptations and Oxidative Stress Tolerance in Halophytes from Warm Subtropical Region. In M. -N. Grigore (Ed.), *Handbook of Halophytes* (pp. 1–31). Springer International Publishing. https://doi.org/10.1007/978-3-030-17854-3_52-1

64 Wrzaczek, M., Brosché, M., & Kangasjärvi, J. (2013). ROS signaling loops—Production, perception, regulation. *Current Opinion in Plant Biology*, *16*(5), 575–582. https://doi.org/10.1016/j.pbi.2013.07.002

65 Wiciarz, M., Gubernator, B., Kruk, J., & Niewiadomska, E. (2015). Enhanced chloroplastic generation of H_2 O_2 in stress-resistant *Thellungiella salsuginea* in comparison to *Arabidopsis thaliana*. *Physiologia Plantarum*, *153*(3), 467–476. https://doi.org/10.1111/ppl.12248

66 Kamal, A. H. M., Cho, K., Kim, D. -E., Uozumi, N., Chung, K. -Y., Lee, S. Y., Choi, J. -S., Cho, S. -W., Shin, C. -S., & Woo, S. H. (2012). Changes in physiology and protein abundance in salt-stressed wheat chloroplasts. *Molecular Biology Reports*, *39*(9), 9059–9074. https://doi.org/10.1007/s11033-012-1777-7

67 Allel, D., Ben-Amar, A., & Abdelly, C. (2018). Leaf photosynthesis, chlorophyll fluorescence and ion content of barley (Hordeum vulgare) in response to salinity. *Journal of Plant Nutrition*, *41*(4), 497–508. https://doi.org/10.1080/01904167.2017.1385811

68 Abdul Qados, A. M. S. (2011). Effect of salt stress on plant growth and metabolism of bean plant Vicia faba (L.). *Journal of the Saudi Society of Agricultural Sciences*, *10*(1), 7–15. https://doi.org/10.1016/j.jssas.2010.06.002

69 Salim Akhter, M., Noreen, S., Mahmood, S., Athar, H. -R., Ashraf, M., Abdullah Alsahli, A., & Ahmad, P. (2021). Influence of salinity stress on PSII in barley (Hordeum vulgare L.) genotypes, probed by chlorophyll-a fluorescence. *Journal of King Saud University — Science*, *33*(1), 101239. https://doi.org/10.1016/j.jksus.2020.101239

70 Mu, Y., Lin, J., Mu, C., & Gao, Z. (2015). Effects of NaCl Stress on the Growth and Physiological Changes in Oat (*Avena sativa*) Seedlings. *Notulae Botanicae Horti Agrobotanici Cluj-Napoca*, *43*(2), 468–472. https://doi.org/10.15835/nbha4329972

71 Hao, S., Wang, Y., Yan, Y., Liu, Y., Wang, J., & Chen, S. (2021). A Review on Plant Responses to Salt Stress and Their Mechanisms of Salt Resistance. *Horticulturae*, *7*(6), 132. https://doi.org/10.3390/horticulturae7060132

72 Mansour, M. M. F. (2023). Role of Vacuolar Membrane Transport Systems in Plant Salinity Tolerance. *Journal of Plant Growth Regulation*, *42*(3), 1364–1401. https://doi.org/10.1007/s00344-022-10655-9

73 Martinoia, E., Maeshima, M., & Neuhaus, H. E. (2006). Vacuolar transporters and their essential role in plant metabolism. *Journal of Experimental Botany*, *58*(1), 83–102. https://doi.org/10.1093/jxb/erl183

74 Andrés, Z., Pérez-Hormaeche, J., Leidi, E. O., Schlücking, K., Steinhorst, L., McLachlan, D. H., Schumacher, K., Hetherington, A. M., Kudla, J., Cubero, B., & Pardo, J. M. (2014). Control of vacuolar dynamics and regulation of stomatal aperture by tonoplast potassium uptake. *Proceedings of the National Academy of Sciences*, *111*(17). https://doi.org/10.1073/pnas.1320421111

75 Shabala, S., & Cuin, T. A. (2008). Potassium transport and plant salt tolerance. *Physiologia Plantarum*, *133*(4), 651–669. https://doi.org/10.1111/j.1399-3054.2007.01008.x

76 Liu, C., Jiang, X., & Yuan, Z. (2024). Plant Responses and Adaptations to Salt Stress: A Review. *Horticulturae*, *10*(11), 1221. https://doi.org/10.3390/horticulturae10111221

77 Van Doorn, W. G., & Woltering, E. J. (2010). What about the role of autophagy in PCD? *Trends in Plant Science*, *15*(7), 361–362. https://doi.org/10.1016/j.tplants.2010.04.009

78 Kurusu, T., Yagala, T., Miyao, A., Hirochika, H., & Kuchitsu, K. (2005). Identification of a putative voltage-gated Ca^{2+} channel as a key regulator of elicitor-induced hypersensitive cell death and mitogen-activated protein kinase activation in rice. *The Plant Journal*, *42*(6), 798–809. https://doi.org/10.1111/j.1365-313X.2005.02415.x

79 Floyd, B. E., Pu, Y., Soto-Burgos, J., & Bassham, D. C. (2015). To Live or Die: Autophagy in Plants. In A.N. Gunawardena & P.F. McCabe (Eds), *Plant Programmed Cell Death* (pp. 269–300). Springer International Publishing. https://doi.org/10.1007/978-3-319-21033-9_11

80 Üstün, S., Hafrén, A., & Hofius, D. (2017). Autophagy as a mediator of life and death in plants. *Current Opinion in Plant Biology*, *40*, 122–130. https://doi.org/10.1016/j.pbi.2017.08.011

81 Zhou, L. -L., Gao, K. -Y., Cheng, L. -S., Wang, Y. -L., Cheng, Y. -K., Xu, Q. -T., Deng, X. -Y., Li, J. -W., Mei, F. -Z., & Zhou, Z. -Q. (2021). Short-term waterlogging-induced autophagy in root cells of wheat can inhibit programmed cell death. *Protoplasma*, *258*(4), 891–904. https://doi.org/10.1007/s00709-021-01610-8

82 Marshall, R. S., & Vierstra, R. D. (2018). Autophagy: The Master of Bulk and Selective Recycling. *Annual Review of Plant Biology*, *69*(1), 173–208. https://doi.org/10.1146/annurev-arplant-042817-040606

83 Hatsugai, N., Yamada, K., Goto-Yamada, S., & Hara-Nishimura, I. (2015). Vacuolar processing enzyme in plant programmed cell death. *Frontiers in Plant Science*, *6*. https://doi.org/10.3389/fpls.2015.00234

84 Hara-Nishimura, I., & Hatsugai, N. (2011). The role of vacuole in plant cell death. *Cell Death & Differentiation*, *18*(8), 1298–1304. https://doi.org/10.1038/cdd.2011.70

85 Lu, W., Deng, M., Guo, F., Wang, M., Zeng, Z., Han, N., Yang, Y., Zhu, M., & Bian, H. (2016). Suppression of OsVPE3 Enhances Salt Tolerance by Attenuating Vacuole Rupture during Programmed Cell Death and Affects Stomata Development in Rice. *Rice*, *9*(1), 65. https://doi.org/10.1186/s12284-016-0138-x

86 Jalili, S., Ehsanpour, A. A., & Javadirad, S. M. (2022). The role of melatonin on caspase-3-like activity and expression of the genes involved in programmed cell death (PCD) induced by in vitro salt stress in alfalfa (Medicago sativa L.) roots. *Botanical Studies*, *63*(1), 19. https://doi.org/10.1186/s40529-022-00348-7

87 Signorelli, S., Tarkowski, Ł. P., Van Den Ende, W., & Bassham, D. C. (2019). Linking Autophagy to Abiotic and Biotic Stress Responses. *Trends in Plant Science*, *24*(5), 413–430. https://doi.org/10.1016/j.tplants.2019.02.001

88 Teper-Bamnolker, P., Danieli, R., Peled-Zehavi, H., Belausov, E., Abu-Abied, M., Avin-Wittenberg, T., Sadot, E., & Eshel, D. (2021). Vacuolar processing enzyme translocates to the vacuole through the autophagy pathway to induce programmed cell death. *Autophagy*, *17*(10), 3109–3123. https://doi.org/10.1080/15548627.2020.1856492

89 Hu, Y., Fromm, J., & Schmidhalter, U. (2005). Effect of salinity on tissue architecture in expanding wheat leaves. *Planta*, *220*(6), 838–848. https://doi.org/10.1007/s00425-004-1401-8

90 Smith, L. G. (2003). Cytoskeletal control of plant cell shape: Getting the fine points. *Current Opinion in Plant Biology*, *6*(1), 63–73. https://doi.org/10.1016/S1369-5266(02)00012-2

91 Baranova, E. N., & Gulevich, A. A. (2021). Asymmetry of Plant Cell Divisions under Salt Stress. *Symmetry*, *13*(10), 1811. https://doi.org/10.3390/sym13101811

92 Lee, K. P., Kim, C., Landgraf, F., & Apel, K. (2007). EXECUTER1- and EXECUTER2-dependent transfer of stress-related signals from the plastid to the nucleus of *Arabidopsis thaliana*. *Proceedings of the National Academy of Sciences*, *104*(24), 10270–10275. https://doi.org/10.1073/pnas.0702061104

93 Hussain, A., Shah, F., Ali, F., & Yun, B. -W. (2022). Role of Nitric Oxide in Plant Senescence. *Frontiers in Plant Science*, *13*, 851631. https://doi.org/10.3389/fpls.2022.851631

94 Hsiao, H. -Y., Chung, C. -W., Santos, J. H., Villaflores, O. B., & Lu, T. -T. (2019). Fe in biosynthesis, translocation, and signal transduction of NO: Toward bioinorganic engineering of dinitrosyl iron complexes into NO-delivery scaffolds for tissue engineering. *Dalton Transactions*, *48*(26), 9431–9453. https://doi.org/10.1039/C9DT00777F

К.Д. Қумарғазы, А.С. Сату, Т. Хусанов, А.Ж. Темірханов, Ж.А. Нұрбекова

Өсімдіктердегі тұздылықтан туындаған бағдарламаланған жасуша өлімі кезіндегі органелла динамикасы

PCD (бағдарламаланған жасуша өлімі) — қоршаған орта стрестерінен (ePCD) немесе даму процестерінен (dPCD) туындаған күрделі механизм. ePCD әртүрлі қолайсыз абиотикалық жағдайлардан, соның ішінде тұздану стресінен туындауы мүмкін. Тұздың жоғары концентрациясының әсері өсімдіктердің морфологиялық ерекшеліктерін төмендетіп қана қоймай, сонымен қатар биохимиялық және молекулалық процестерге әсер етеді. Өсімдік әртүрлі органеллаларда болатын көптеген қорғаныс механизмдерін белсендіреді. Оған плазмалық мембранадағы, митохондриядағы, хлоропласттардағы, вакуольдегі және ядродағы иондық, осмостық және тотығу стрестері жатады. Плазмалық мембрананың негізгі бұзылуы тасымалдау жүйесінің төмендеуімен, ROS жинақталуымен және Ca2+ ағынымен сипатталады. Митохондриялық дисфункция ROS-тың жоғары жинақталуымен, AOX, UCP, GABA және цитохром с-ның бөлінуі сияқты қорғаныс жолдарының белсендірілуімен байланысты. Сонымен қатар фотосинтез жылдамдығы хлорофилл мөлшерінің төмендеуіне байланысты айтарлықтай төмендейді. Вакуольдер NHX антипортерлері және V-ATPase белсенділігі арқылы Na+ секвестрлейді және осмостық, иондық сигналдарды біріктіреді, бірақ бұл жүйе ыдырағанда Ca2+ ядрода жинақталады. ROS-тың артық мөлшерде генерациясы хлоропласт-ядролық байланыстағы EXECUTER ақуызы үшін сигналдық молекула ретінде әрекет етеді. Тұздану хроматиннің ыдырауына әкелетін осмостық, иондық және тотығу стресс сигналдарды белсендіреді. Қорытындылай келе, бұл өзара байланысты процестер PCD-ге әкеледі.

Кілт сөздер: бағдарламаланған жасуша өлімі, тұз стресі, реактивті оттегі түрлері, азот оксиді, фитогормондар, ферменттер.

К.Д. Кумаргазы, А.С. Сату, Т. Хусанов, А.Ж. Темирханов, Ж.А. Нурбекова

Динамика органелл при запрограммированной клеточной смерти растений, вызванной засолением

PCD (запрограммированная гибель клеток) — это сложный механизм, вызываемый экологическим стрессом (ePCD) или процессами развития (dPCD). ePCD может быть вызван различными типами неблагоприятных абиотических условий, включая солевой стресс. Воздействие высоких концентраций соли не только ухудшает морфологические особенности растений, но и серьезно влияет на биохимические и молекулярные процессы. Кроме того, растения активизируют многочисленные защитные механизмы, которые реализуются в различных органеллах растительной клетки. Они включают в себя ионное, осмотическое и окислительное повреждение плазматической мембраны, митохондрий, хлоропластов, вакуолей и ядер. Основные нарушения в плазматической мембране характеризуются снижением транспортной системы, накоплением АФК и притоком Ca2+. Митохондриальная дисфункция

связана с высоким накоплением АФК, активацией защитных путей, таких как AOX, UCP, GABA, и высвобождением цитохрома c. Вакуоли интегрируют осмотические и ионные сигналы, изолируя Na+ посредством антипортеров NHX и активности V-ATФазы, но когда эта система разрушается, Ca2+ концентрируется в ядре. Кроме того, скорость фотосинтеза значительно снижается из-за снижения содержания хлорофилла. Более того, избыточное производство АФК действует как сигнальная молекула для белков EXECUTER, обеспечивающих взаимодействие хлоропластов с ядрами. Засоление активирует осмотические, ионные и окислительные сигналы, которые приводят к деградации хроматина. В совокупности эти взаимосвязанные процессы приводят к образованию PCD.

Ключевые слова: запрограммированная гибель клеток, солевой стресс, активные формы кислорода, оксид азота, фитогормоны, ферменты.

Information about the authors

Kumargazy Karina Daurenkyzy — Fourth-Year Undergraduate Student, Department of Biotechnology and Microbiology, L.N. Gumilyov Eurasian National University, Astana, Kazakhstan; e-mail: karinakumargazy5@gmail.com; ORCID: https://orcid.org/0009-0002-0634-0316

Satu Albina Samatkyzy — Fourth-Year Undergraduate Student, Department of Biotechnology and Microbiology, L.N. Gumilyov Eurasian National University, Astana, Kazakhstan; e-mail: alekasatu@gmail.com; ORCID: https://orcid.org/0009-0003-6668-5380

Nurbekova Zhadyrassyn Akbergenkyzy — PhD, Associate Professor, Department of Biotechnology and Microbiology, L.N. Gumilyov Eurasian National University, Astana, Kazakhstan; e-mail: zhadyrassyn.nurbekova@gmail.com; ORCID: https://orcid.org/0009-0009-8766-4734

Khusanov Tokhir — PhD, Senior Researcher, The Institute of Microbiology of Academy of Sciences of Uzbekistan, Uzbekistan; e-mail: tohir_husanov@mail.ru; ORCID: https://orcid.org/0000-0002-2505-0026

Temirkhanov Aslan — Associate Professor, Candidate of Agricultural Sciences, Republican Collection of Microorganisms, Astana, Kazakhstan; e-mail: aszhte@gmail.com; ORCID: https://orcid.org/0000-0002-8716-1661

How to Cite: Alikul, A.B., Manapkyzy, D., Saparbaev, M.K., Taipakova, S.M. (2026). Evidence for asymmetric DNA strand inheritance in vertebrate mitochondria. *Fundamental and Experimental Biology*, 31, 3 (123), 30-42. https://doi.org/10.31489/2026FEB3/30-42

Review Article

https://doi.org/10.31489/2026FEB3/30-42

UDC 577.213:311.347 Received: 12.12.2025 | Accepted: 18.05.2026 | Published online: 30.09.2026

A.B. Alikul[1, 2*], D. Manapkyzy[2], M.K. Saparbaev[3], S.M. Taipakova[1, 2]

[1]*Department of Molecular Biology and Genetics, Faculty of Biology and Biotechnology, Al-Farabi Kazakh National University, Almaty, Kazakhstan;*
[2]*Scientific Research Institute of Biology and Biotechnology Problems, Al-Farabi Kazakh National University, Almaty, Kazakhstan;*
[3]*Group "Mechanisms of DNA Repair and Carcinogenesis", Université Paris-Saclay, Gustave Roussy Cancer Campus, Villejuif, Cedex, France*
[*]*Corresponding author: aliqul.ayzhan@gmail.com*

Evidence for asymmetric DNA strand inheritance in vertebrate mitochondria

A classical experiment performed by Meselson and Stahl in 1958 confirmed the semiconservative mechanism of DNA replication in cellular organisms. According to this mechanism, following DNA replication and cell division, each daughter cell inherits chromosomes consisting of one parental strand (W or C) and one newly synthesized complementary strand (C′ or W′). Since each DNA strand is replicated the same number of times during successive rounds of cell division, the W and C strands can be considered equivalent as a result of the coupling between cell division and semiconservative DNA replication. However, some non-cellular organisms, including single-stranded DNA and RNA viruses, do not conform to the concept of strand equivalence. A key feature of vertebrate mitochondrial genomes is a highly skewed nucleotide composition between the two complementary strands. This compositional asymmetry allows the strands to be separated by ultracentrifugation in an alkaline cesium chloride density gradient, yielding a heavy (H) strand enriched in guanine and thymine and a light (L) strand enriched in cytosine and adenine. Despite extensive research, the exact mechanism of human mitochondrial DNA replication and its relationship to nucleotide compositional bias remain unclear. In this review, we propose a conceptual model of asymmetric mitochondrial DNA strand inheritance to account for the strand-specific mutational asymmetry characteristic of vertebrate mtDNA.

Keywords: mitochondrial DNA, DNA strand equivalence, patterns of mutation, Chargaff's second parity rule, DNA replication.

Introduction

Mitochondrial DNA (mtDNA) in vertebrates consists of a compact circular molecule between 16–24 kb [1, 2]. In mammals, the mitochondrial genome is a circular DNA molecule of ~16.6 kb that carries 37 genes (13 protein-coding genes, 2 ribosomal RNAs and 22 transfer RNAs). The only major non-coding region, known as the control region or D-loop, contains key cis-acting elements essential for mtDNA transcription and replication, including the light-strand promoter (LSP) and heavy-strand promoter (HSP), which initiate transcription from the respective strands. Figure 1 presents a map of the human mitochondrial genome [3, 4].

The mitochondrial genome comprises two strands—the heavy (H) strand, enriched in guanine (G) and thymine (T), and the light (L) strand, enriched in cytosine (C) and adenine (A)—that exhibit marked differences in nucleotide composition. This compositional asymmetry contributes to distinct buoyant densities, enabling physical separation of the strands by alkaline CsCl density gradient centrifugation.

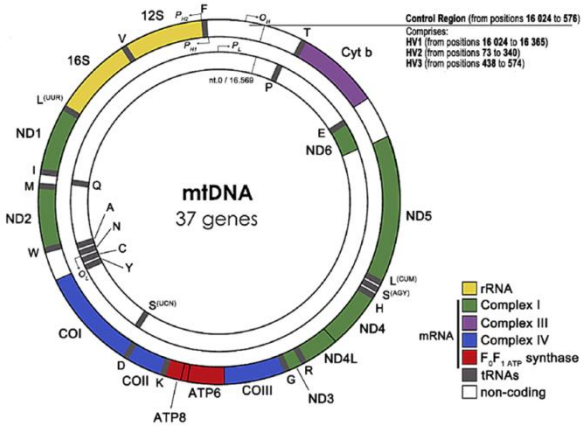

Figure 1. Structure of human mitochondrial DNA [5]

Table 1 quantifies these conserved patterns across vertebrates, illustrating how skew metrics (AT- and GC-skew) deviate from Chargaff's second parity rule and correlate with asymmetric replication dynamics. The pronounced H-strand skews—particularly negative AT- and GC-skews—facilitate strand displacement during replication and localize mutation hotspots near OriH [6, 7].

Table 1

Nucleotide composition and skews reveal conserved strand asymmetry in vertebrate mtDNA. H-strand G+T bias (vs. L-strand C+A enrichment) violates Chargaff's second parity rule across species. Skew metrics: AT-skew = (A–T)/(A+T); GC-skew = (G–C)/(G+C). Adapted from; own compilation

Species	Strand	A (%)	C (%)	G (%)	T (%)	AT-skew	GC-skew
Human	H	30.98	12.21	13.24	43.57	–0.168	–0.041
	L	29.65	28.21	12.21	30.98	+0.022	+0.398
Mouse	H	31.49	11.90	13.31	43.30	–0.156	–0.112
	L	30.12	27.31	11.90	30.67	+0.009	+0.393
Chicken	H	29.81	13.45	14.20	42.54	–0.177	–0.032
	L	28.92	27.45	13.45	30.18	+0.021	+0.328

The pronounced H-strand skews (Table 1)—particularly negative AT-skew and GC-skew—facilitate strand displacement during replication, underpin physical separation via alkaline CsCl density gradient centrifugation, and localize mutation hotspots near OriH.

MtDNA is inherited strictly maternally: paternal mtDNA is diluted in the zygote and actively degrades after fertilisation [8, 9]. Two main mechanisms are thought to underlie the absence of paternal mtDNA in the offspring. First, the small amount of mtDNA carried by sperm is negligible compared with the large number of maternal copies present in the oocyte and zygote, which leads to simple dilution [5, 10]. Second, an active degradation process selectively eliminates sperm-derived mitochondria after fertilisation [11–13]. Research revealed that a mammalian oocyte contains about 100,000 copies of mtDNA, which are distributed to daughter cells as the fertilized egg begins to divide [14]. However, mtDNA replication does not commence until after implantation. During development, only a small fraction of maternal mtDNA is designated for the germ line, eventually giving rise to primordial germ cells that will produce future oocytes. Despite the high mutation rate of mtDNA in somatic tissues, several protective mechanisms in the germline prevent the maternal transmission of deleterious mtDNA mutations [15]: (1) only a limited amount of the maternal mtDNA is passed on to the next generation [16]; (2) purifying selection within the maternal germline reduces mtDNA mutations that alter protein amino acids [17]; (3) embryos actively eliminate cells with high levels of mtDNA mutations affecting transfer RNA (tRNA) genes [18]; and (4) women with significant mtDNA mutations in their reproductive cells often face fertility problems [19].

Evidences suggest that mitochondrial DNA represent a vestigial genome of the alpha-proteobacterial endosymbiont captured ~1.5-2 billion years ago during eukaryogenesis, retaining ~5 % of progenitor genes while outsourcing bioenergetics to nuclear genome [20]. Remarkably conserved across Metazoa (human-chicken 93 % identity), mtDNA exhibits clade-specific rearrangements reflecting reductive evolution [21].

Strand asymmetry traces to ancestral displacement replication, paralleling T-odd/ssDNA bacteriophages and supporting alpha-proteobacterial phage-endosymbiont hypothesis [22]. Maternal uniparental inheritance precludes mtDNA recombination, yielding a low nonsynonymous/synonymous substitution ratio ($dN/dS \approx 0.2$) that indicates strong purifying selection. Tissue-specific mtDNA copy number variation and heteroplasmy thresholds then determine bioenergetic capacity [5, 23].

To understand the origin and maintenance of chain asymmetry, it is necessary to consider the mechanisms of mtDNA replication. Key proteins are polymerase γ (POLγ), TWINKLE helicase, and mitochondrial RNA polymerase (POLRMT), which synthesises primers [24, 25]. RNase H1 removes RNA primers [26].

Factors involved in mammalian mitochondrial DNA replication

Mammalian mitochondrial DNA (mtDNA) replication uses a specialised set of proteins that is distinct from the nuclear replication machinery [27]. DNA polymerase γ (POLγ) plays a central role as the only polymerase that synthesises both the H and L strands [28]. POLγ forms a heterotrimer: the catalytic subunit POLγA (~140 kDa, family A, related to T7 DNA polymerase) has 3′→5′ exonuclease activity (error <1 per 10^6 nt), while the two accessory subunits POLγB (~55 kDa, structurally similar to class IIa aminoacyl-tRNAsynthetases) increase processivity and stability of binding to the template [29, 30].

TWINKLE helicase (hexameric complex, ~420 kDa; 5′→3′ activity; homologous to T7 gp4) unwinds double-stranded DNA at the replication fork, while its limited priming capacity is supported by mitochondrial RNA polymerase (POLRMT), which synthesizes 25–75 nt RNA primers on single-stranded DNA templates. Mitochondrial single-stranded DNA-binding protein (mtSSB; tetrameric complex, ~60 kDa) prevents secondary structure formation, inhibits non-specific priming, and enhances the activities of both TWINKLE and POLγ [31–36]. Accessory polymerases (PrimPol, POLβ, POLθ, POLζ) focus on repair. TFAM (HMG box) packs mtDNA and initiates truncated transcripts for priming [27, 29, 36].

The D-loop in the control region is a docking station for nucleoids with an R-loop (7S DNA on the non-template strand), which ensures the organisation and separation of mtDNA [35, 37]. Depletion of MGME1 (ssDNA nuclease 5′→3′/3′→5′) leads to the accumulation of 7S DNA, confirming its role in D-loop turnover and prevention of linear fragments. MtSSB coordinates replication, increasing the efficiency of POLγ [34, 37].

mtDNA replication modes

Three primary models of mtDNA replication have been proposed for vertebrates: the classical strand-displacement model (SDM), the ribonucleotide incorporation throughout the lagging strand model (RITOLS), and the strand-coupled model (Fig. 2). These models have been confirmed by electron microscopy, two-dimensional agarose gel electrophoresis (2D-AGE), atomic force microscopy, analysis of DNA-RNA hybrids of replication intermediates, and ChIPmtSSB*in vivo* [38–43].

Figure 2 illustrates the topological differences: SDM features prolonged ssDNA displacement, RITOLS provides transient RNA protection, and SCM shows coupled forks. Each contributes to strand asymmetry maintenance.

Strand displacement model (SDM)

The classic SDM model was formulated in the early 1970s based on electron microscopic analysis of circular mitochondrial molecules containing extended single-stranded regions corresponding to the displaced parental strand. In these works, molecules were observed where one daughter strand was double-stranded and the other was partially or completely single-stranded, leading to the introduction of the term “strand displacement” to describe this mechanism [43, 45, 46]. Within the SDM, replication begins in the control region, near the origin of replication of the heavy chain (OriH), from where a new H chain is continuously synthesised on the L chain template [46]. As the replication fork progresses, the parental H-strand is displaced and remains in a single-stranded state, forming characteristic replication intermediates with an increasing length of the single-stranded segment [38]. The origin of L-strand replication (OriL) lies roughly two-thirds of the way around the circular mtDNA genome from OriH [40].

L-strand synthesis is initiated by mitochondrial RNA polymerase, which synthesises primers that are then extended by DNA polymerase γ (Pol γ), resulting in the formation of a functional analogue of the lagging strand, but without the classic Okazaki fragments [44, 48]. This asynchrony, as well as the prolonged existence of the single-stranded displaced H-strand, distinguishes SDM from nuclear DNA replication and served as the basis for the concept of "asynchronous chain synthesis" in mitochondria [47].

Later work using atomic force microscopy and 2D-AGE showed that SDM well explains the observed replication intermediates in mouse liver mitochondria and that there are additional L-strand initiation sites besides the classic OriL [45, 49].

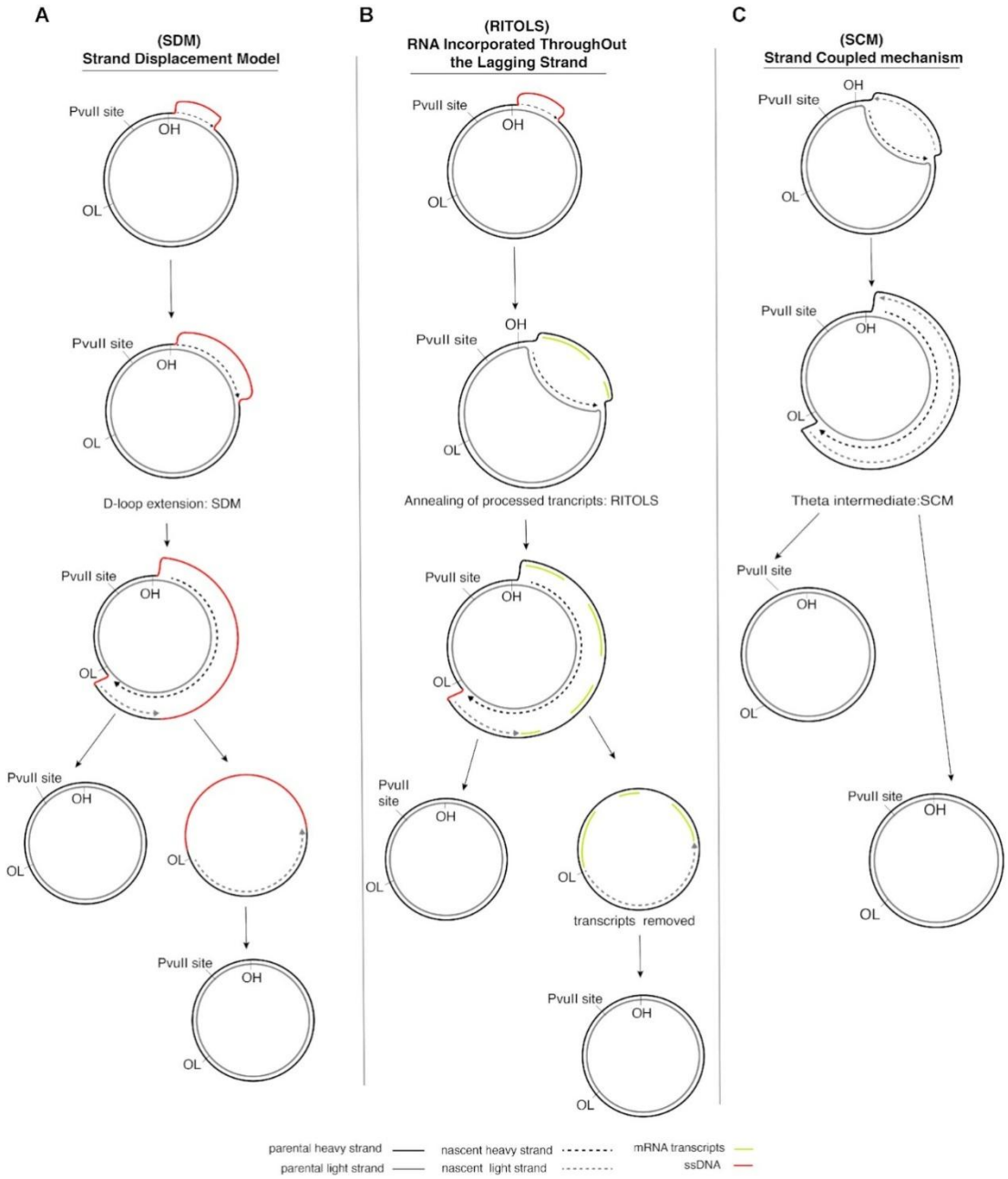

Figure 2. Schematics of the three main mtDNA replication models in vertebrates. (A) Strand-displacement model (SDM): leading-strand synthesis initiates at OriH, displacing the parental H strand (red) to form a D-loop until OriL activation and lagging-strand priming. (B) RITOLS model (RNA incorporation throughout the lagging strand): the displaced H strand is initially coated with RNA transcripts synthesized on the L strand ("bootlace" mechanism, yellow), later replaced by POLγ-synthesized DNA. (C) Strand-coupled model (SCM): bidirectional replication forks with coupled H/L-strand synthesis (Y-arc intermediates observed by 2D-AGE). Color code: black = parental strands; green = newly synthesized DNA; yellow = RNA [43, 44]

In summary, the defining features of SDM are: (1) strictly unidirectional, continuous H-strand synthesis initiating at OriH; (2) the displaced parental H-strand persisting as naked single-stranded DNA until OriL is reached approximately two-thirds around the genome; (3) L-strand synthesis commencing only after OriL is exposed, without Okazaki fragment formation; and (4) the prolonged single-stranded state of the parental H-strand as the principal source of its mutational vulnerability [38, 45, 46]. This model is best supported by electron microscopy and mtSSB occupancy data, and it provides the direct mechanistic basis for the replication-coupled mutational gradient that is the focus of the present work [39]. The key limitation of the pure SDM is its prediction of extended single-stranded intermediates that, in practice, appear partly RNA-coated in many experimental systems—a discrepancy addressed by the RITOLS model [40, 41].

The RITOLS model and the "bootlace" mechanism

With the development of methods that allow for the preservation of fragile replication intermediates and the analysis of DNA–RNA hybrids, it has been shown that many structures previously interpreted as extended single-stranded regions of the displaced H-strand actually contain long RNA tracts complementary to the L-strand [41, 46, 47]. These observations led to the formulation of the RNA Incorporated ThroughOut the Lagging Strand (RITOLS) model, according to which as the replication fork progresses, the displaced H-strand is temporarily covered by pre-synthesized transcripts that hybridize with the template and act as a temporary lagging strand [43, 47].

Metabolic labelling of isolated mitochondria with DNA and RNA precursors showed that RNA strands in these intermediates are not synthesised "on the fly" at the fork, but are preformed L-strand transcripts that are sequentially "threaded" (bootlaced) onto the displaced H-strand as the replication fork progresses [45, 47]. In the next stage, these RNA primers are gradually displaced and replaced by DNA synthesised by Pol γ, leading to the formation of a complete L-strand [41].

Thus, the RITOLS model largely retains the topology of SDM (initiation in the control region, the key role of OriH/OriL, and asynchronous strand synthesis), but radically reduces the lifetime of long single-stranded DNA segments by replacing them with stable DNA-RNA duplexes [43, 44, 50]. This is considered a potential adaptation necessary for maintaining mitochondrial genome integrity, given the relatively low replication rate of mtDNA compared to nuclear and bacterial DNA, and the high sensitivity of single-stranded DNA to breaks and deletions [44].

In summary, RITOLS shares with SDM its unidirectional initiation at OriH, its asynchronous activation of OriL, and its overall topology of leading-strand displacement. The critical distinction is mechanistic rather than topological: in RITOLS, the displaced parental H-strand is not naked ssDNA but is coated by preformed L-strand RNA transcripts via the "bootlace" threading mechanism, forming transient RNA–DNA duplexes that are subsequently matured into dsDNA by POLγ-mediated RNA replacement [41, 43]. This RNA coverage substantially shortens the window of H-strand single-stranded exposure compared to SDM, potentially reducing (but not eliminating) the mutational vulnerability of the H-strand [44]. Critically for the asymmetric inheritance model, both SDM and RITOLS produce the same net outcome: leading-strand (H-strand) synthesis is continuous and membrane-anchored, while lagging-strand (L-strand) synthesis is delayed and produces a diffusible daughter molecule [40, 43, 44]. The two models therefore differ in the degree, not the existence, of H-strand vulnerability, and both are fully compatible with the asymmetric strand inheritance model [50].

Synchronous (strand-coupled) replication

Along with SDM and RITOLS, analysis of replication intermediates using 2D-AGE revealed characteristic Y-shaped arcs (y-arcs) corresponding to double-stranded replication forks with synchronous synthesis of the leading and lagging strands [49]. Such structures are poorly consistent with the rigidly asymmetric model of pure chain displacement, as they suggest the existence of classical two-strand forks in significant portions of the mitochondrial genome [43].

However, mtSSBChIP-seq with a pronounced bias towards the displaced strand contradicts the uniform distribution of mtSSB expected in linked forks [51]. Y-loops likely reflect transient bidirectional progress or replication stress-induced structures rather than a dominant mechanism, as Kearns-type forms remain rare in vertebrates [64].

Refined models integrate elements of transient ligated replication before SDM dominance, reconciling 2D-AGE observations with single-stranded DNA persistence and asynchronous origin activation. Such a hybrid approach preserves the primacy of SDM while acknowledging the contribution of ligated forks in physiological variability [39].

In summary, the strand-coupled model (SCM) differs fundamentally from both SDM and RITOLS in its topology: it posits bidirectional replication forks in which H- and L-strand synthesis proceed simultaneously and in a coupled fashion, analogous to classical nuclear DNA replication [44]. The key evidence in its favour is the detection of Y-arc intermediates by 2D-AGE, consistent with double-stranded fork progression [49, 50].

However, SCM stands in direct conflict with several lines of evidence that support asynchronous displacement synthesis:

(1) mtSSBChIP-seq data show a strong bias of single-stranded DNA binding toward the displaced strand, incompatible with the uniform distribution expected at coupled forks [39, 51];

(2) the existence of a discrete OriL site and its delayed activation are mechanistically unnecessary under a fully coupled model [38, 40];

(3) the compositional asymmetry and mutation gradient from OriH to OriL are not readily explained by synchronous fork movement [50].

The current consensus therefore treats SCM not as an independent dominant mechanism but as a minor or context-specific mode—possibly reflecting replication stress, repair synthesis, or a transitional phase preceding SDM-type displacement [39]. Unlike SDM and RITOLS, SCM does not readily account for the persistent H-strand mutational bias that is the subject of the asymmetric inheritance model.

Consequences of replication asymmetry in mtDNA

The strand-specific mutational bias observed in vertebrate mtDNA arises from the interplay between replication dynamics, nucleotide compositional asymmetry, and limited DNA repair capacity. The heavy (H) strand, exhibiting G+T bias (~59 % G+T vs. 41 % in L-strand), remains predominantly single-stranded during leading-strand displacement synthesis from OriH (~6500 nucleotides before OriL activation), rendering it highly vulnerable to hydrolytic deamination of cytosine and adenine residues in DNA (C→U→T and A→Hx→G), polymerase slippage during POLγ processivity, and ROS-induced a basic sites/oxidized purine and pyrimidine bases [51].

L-strand priming at OriL initiates bidirectional lagging-strand synthesis, but the RITOLS "bootlace" mechanism provides only transient RNA coverage of nascent H-strand templates (~25-75 nt primers), leaving the displaced parental H-strand exposed [38]. Mitochondrial SSB (mtSSB) preferentially coats this ssDNA, yet protection proves incomplete compared to nuclear RPA dynamics (H-strand exposure: hours vs. nuclear replication ~minutes; replication cycle ~1 h [52]). Nucleoid architecture exacerbates asymmetry: TFAM compaction (~1 TFAM/10 bp) and selective membrane anchoring *via* H-strand-transcribed oxidative phosphorylation (OXPHOS) complexes (I, III, IV, V; ATP6/8) restrict H-strand-enriched nucleoids to high-replication niches near cristae, amplifying POLγ infidelity (error rate $1{:}10^{4}$ nt vs. nuclear $1{:}10^{8}$) and replication-associated mismatches [28].

Mitochondrial base excision repair (BER) operates at reduced efficiency (~10–50 % nuclear rates) for key lesions (8-oxoG glycosylase OGG1, AP-endonuclease APE1), with TFAM-dependent "transcription-coupled scanning" exhibiting strand bias toward transcriptionally hyperactive H-strand regions (14/15 transcripts) [53]. Replication forks frequently stall at D-loop damage hotspots, favoring mutagenic translesion synthesis (PrimPol/TLS polymerases) over faithful repair or double-strand break resolution (absent canonical HR/NHEJ) [54].

OXPHOS coupling imposes additional selection: H-strand anchoring facilitates rapid copy-number restoration post-damage but selects deletion mutants with replication advantage in aging tissues (e.g., "common delete" ΔmtDNA4977 amplifies in neurons). Maternal inheritance bottlenecks (~100–1000 germline mtDNA copies) impose purifying selection, yet somatic clonal expansion evades this filter [54–58].

Mutational bias in vertebrate mtDNA

Replication of mitochondrial DNA in vertebrates causes a strong asymmetry of mutations: in the heavy (H) strand A>G and C>T substitutions are dominant type of mutation (about 70 % of all mutations), whereas complementary L-strand exhibits T>C and G>A substitutions and very few A>G and C>T mutations [19, 57]. This strand-specific mutation pattern is maintained across all vertebrate species from fish to mammals, resulting in the observed nucleotide compositional bias between G+T-rich H-strand and C+A-rich L-strand.

The mutation frequency varies along the genome: the maximum is observed at the replication origin (OriH)—up to 10 times higher than at OriL [1]. This is directly related to the fact that the H-strand remains in a single-stranded state longer during replication according to the SDM and RITOLS models [42, 47, 59, 60–63].

The nucleotide compositional bias of vertebrate's mtDNA violates Chargaff's second parity rule: in the H-strand, adenine exceeds thymine by 20–40 %, and guanine exceeds cytosine by 30–50 %. Such a violation is typical for vertebrate'smtDNA and is absent in nuclear DNA [44].

In brain neurons, the asymmetry is even stronger: in the H-strand 85–90 % of somatic mutations consist of G>A substitutions which is 4-5 times more frequent than C>T [64]. This is characteristic of aging brain tissues—the putamen and the cortex. Main reasons: the H-strand remains longer in single-stranded form as compared to L-strand [65] and high levels of reactive oxygen species (ROS) in neurons cause guanine oxidation [66]; weak DNA repair in brain mitochondria [59]; neurons do not divide, as a result mutated mtDNA clonally expands [67].

In the brains of patients with Alzheimer's disease, mutations in the control region (D-loop) suppress mtDNA replication [68]. Point mutations and large deletions in mtDNA are associated with increased inci-

dence of age-related diseases across human and animal models. mtDNA accumulates mutations at rates ~10–100× higher than nuclear DNA, primarily due to elevated replication frequency (~500–10000 copies/cell/day), Polγ infidelity and proximity to ROS-generating ETC complexes. Somatic mutation burden in the human prefrontal cortex increases ~5-fold by age 80, dominated by transitions (purine↔pyrimidine) with oxidative transversions (G→T/C→A) as hallmarks of 8-oxoG lesions [69, 70]. Critically, H- and L-strands exhibit asymmetric accumulation: young brains show C→T bias on H-strand mirroring L-strand composition (31 %G vs. 13 %C), shifting to $T_L \rightarrow C_L$ dominance with age [64, 71].

The conceptual framework of asymmetric DNA strand inheritance in vertebrate mitochondria, originally proposed by Matkarimov and Saparbaev [72], provides a mechanistic explanation for the observed strand-biased mutation patterns in mtDNA. According to this model, the majority of mtDNA progeny after multiple replication rounds derives predominantly from the heavy (H) strand. This bias arises from asymmetric strand replication, which is anchored to the inner mitochondrial membrane via the D-loop structure [56, 72].

mtDNA replication initiates in the D-loop region where the parental H-strand serves as the template for leading-strand synthesis at OriH. This unidirectional replication displaces the parental H-strand, exposing OriL ~2/3 genome length away to trigger lagging L-strand synthesis. The H-strand remains anchored to the inner mitochondrial membrane *via* D-loop interactions and OXPHOS complexes, undergoing continuous replication cycles. In contrast, the L-strand replicates once to generate a diffusible daughter molecule containing the parental L-strand paired with newly synthesized H-strand (Fig. 3).

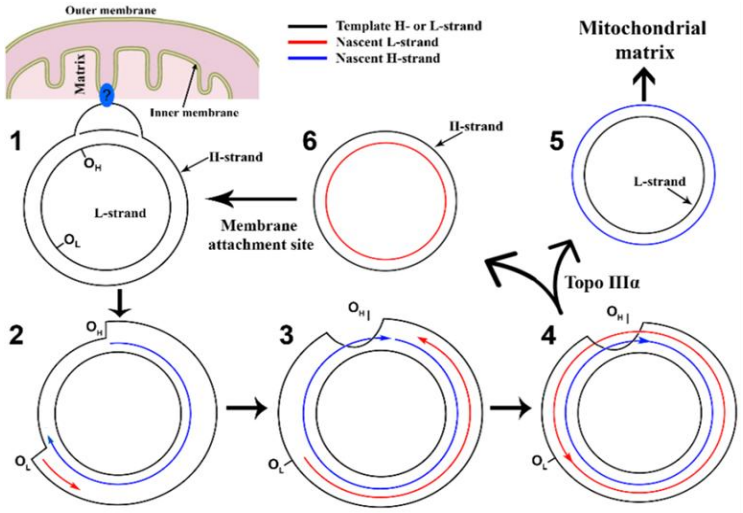

Figure 3. The model of asymmetrical mtDNA strand inheritance [71]

This asymmetric segregation occurs through SDM and RITOLS mechanisms [29, 73, 74] with certain features proposed by Matkarimov and Saparbaev [71]. Premature termination of leading H-strand synthesis creates a hemicatenane linking parental and daughter molecules [75] resolved by mitochondrial topoisomerase IIIα into two distinct mtDNA populations [76]. The resulting molecule containing the parental H-strand remains membrane-anchored for sustained replication, while the parental L-strand molecule diffuses freely through the matrix and is characterized by high transcriptional activity (L-strand is the transcribed strand for 12 out 13 mitochondrial protein-coding genes) [77].

This model elegantly explains the characteristic mutational bias or asymmetry: "transitions of T→C/G→A predominate on the L-strand template, while C→T/A→G occur on the H-strand", contradicting expected ROS-induced damage patterns but matching prolonged single-stranded H-strand exposure during asynchronous replication [72]. Preferential use of H-strand as a template for replication may explain long replication cycles (~2 hour/cycle), POLγ error rate ($1:10^4$ nt), and absence of 8-oxoG derived mutational signature in mtDNA from post-mitotic tissues.

This asymmetric replication strategy appears conserved across vertebrates, paralleling single-stranded bacteriophages (M13, φX174) [45, 78] and suggesting shared evolutionary origins. The model predicts testable mutation gradients peaking at OriH and requires validation through single-molecule long-read sequencing, nucleoid anchoring disruption experiments and quantitative replication dynamics modeling. Understand-

ing this fundamental replication asymmetry illuminates mitochondrial contributions to aging, neurodegeneration, and cancer evolution.

Alternative Hypotheses for Mutational Asymmetry

While the asymmetric strand inheritance model provides a compelling replication-centric framework, it is important to consider alternative and complementary hypotheses that have been proposed to explain strand-specific mutational bias in vertebrate mtDNA. A comprehensive evaluation of these alternatives provides a broader context for evaluating the asymmetric strand inheritance model and clarifies its scope and limitations [1].

An alternative explanation for H-strand mutational bias invokes transcriptional activity rather than replication dynamics. The L-strand serves as the template for the vast majority of mitochondrial transcripts (14 of 15 rRNA/mRNA genes in humans), making it the predominant transcribed strand, as a consequence during transcription H-strand remains in single-stranded form Transcription-coupled damage repair (TCR), well established in nuclear genomes [79] (may also operate in mitochondria and remove lesions from the template strand. Consequently, strand asymmetry in repair efficiency could amplify mutational bias even in the absence of replication-driven strand exposure [80], although the extent of this phenomenon and its mechanistic basis remain incompletely understood.

Additionally, the passage of mitochondrial RNA polymerase (POLRMT) through damaged or structurally unusual DNA regions may interfere with replication fork progression, giving rise to transcription–replication conflicts that can influence strand-specific mutational patterns. Distinguishing replication-driven from transcription-driven asymmetry requires strand-specific quantification of lesion loads and repair intermediates in cells with selectively inhibited [81] transcription or replication [82].

Reactive oxygen species (ROS) generated by the electron transport chain (ETC) represent a major source of mtDNA damage, primarily generating 8-oxodeoxyguanosine (8-oxoG) and oxidized cytosines [83]. Some authors have proposed that the spatial proximity of the H-strand, via its membrane-anchoring interactions with OXPHOS complexes, leads to its preferential exposure to superoxide and hydrogen peroxide generated in complexes I and III [84]. This model predicts an excess of G→T transversions (the hallmark of 8-oxoG mispairing) on the H-strand, a prediction that has partial support in aging somatic tissues [85]. However, ROS-based models alone cannot fully account for the predominance of hydrolytic deamination products (C→T and A→G transitions) in the observed mutation spectrum, suggesting that oxidative damage and replication exposure act synergistically rather than as exclusive mechanisms [7].

Structural features of mtDNA, including the D-loop and protein-binding sites, may also contribute to local variation in mutagenesis [86]. The D-loop region, described above as a specialized nucleoprotein structure, contains a persistently unpaired DNA segment that may increase its susceptibility to chemical damage and mutagenesis [86]. Because this region remains locally unpaired on at least one strand, it represents a site of elevated local mutagenicity independent of active replication [72]. TFAM binding throughout the mitochondrial nucleoid creates regions of constrained topology that may modulate polymerase slippage rates and base-excision repair access [87]. Mutational hotspots in the control region are observed across vertebrate species and correlate with D-loop boundaries, suggesting that structural rather than purely kinetic factors can concentrate damage [88]. Integrating structural mapping of protein occupancy (via ChIP-seq or CUT&RUN adapted for mitochondria) with mutation frequency data along the genome would help distinguish structural from replication-kinetic contributions to asymmetry [1].

Taken together, these alternative mechanisms are not mutually exclusive with the asymmetric strand inheritance model [72]. Rather, the asymmetric inheritance hypothesis provides the primary replication-based scaffold that explains the genome-wide gradient of mutation frequency from OriH to OriL, while transcription-coupled processes, ROS proximity, and structural features of the D-loop are also likely to contribute to the formation of local and context-dependent mutation rates [50, 85]. Future experimental designs should aim to decompose these contributions quantitatively, for example through strand-specific single-molecule sequencing in cells with disrupted nucleoid anchoring or selective POLRMT inhibition.

Conclusion

In conclusion, this review has examined the structural features of mtDNA, its replication mechanisms, and patterns of somatic mutation accumulation. The proposed theory of asymmetric strand inheritance offers a heuristic explanation for observed strand-specific mutational biases that challenge conventional replication models coupled to segregation via cell division. According to this theory, the leading chain (H-chain) undergoes continued DNA replication possibly via anchoring of OriH in the D-loop region to membrane, while the

lagging chain (L-chain) undergoes only one replication cycle and then detaches from the inner mitochondrial membrane and diffuses to matrix. The asymmetric nature of replication creates prerequisites for the accumulation of different types of mutations on Watson (top) and Crick (bottom) strands. Understanding this asymmetric strand inheritance model is crucial for elucidating mitochondrial aging, the pathogenesis of mitochondrial diseases, and tissue-specific mutation patterns. Consequently, further investigation into these mechanisms holds promise for developing novel diagnostic and therapeutic strategies for mitochondrial disorders.

Funding

This work was supported by grants from the Committee of Science of the Ministry of Science and Higher Education of the Republic of Kazakhstan grant AP19676334 to Taipakova S.M.; Manapkyzy D. and Alikul A.B. were supported by Abai-Verne Scholarship Program of the Ministry of Education and Science of the Republic of Kazakhstan and the Ministry of Europe and Foreign Affairs of the French Republic. The funders had no role in study design, data collection and analysis, decision to publish, or preparation of the manuscript.

Author Contributions

The manuscript was written through contributions of all authors. All authors have given approval to the final version of the manuscript. CRediT: **Alikul A.B.** — conceptualization, investigation, writing — original draft; **Manapkyzy D.** — data curation, formal analysis, visualization, writing — review & editing; **Saparbaev M.K.** — supervision, validation, writing — review & editing; **Taipakova S.M.** — supervision, writing — review & editing.

Conflict of Interest

The authors declare no conflict of interest.

References

1 Gomes-dos-Santos, A., Vilas-Arrondo, N., Machado, A. M., Román-Palacios, C., & Rocha, E. P. C. (2023). Mitochondrial replication's role in vertebrate mtDNA strand asymmetry. *Open Biology, 13*(12), 230181. https://doi.org/10.1098/rsob.230181

2 Boore, J. L. (1999). Animal mitochondrial genomes. *Nucleic Acids Research, 27*(8), 1767–1780.

3 Kolesnikov, A. A., & Gerasimov, E. S. (2012). Diversity of mitochondrial genome organization. *Biochemistry (Moscow), 77*(13), 1424–1435.

4 Lee, W. -J., Conroy, J., Howell, W. H., & Kocher, T. D. (1995). Structure and evolution of teleost mitochondrial control regions. *Journal of Molecular Evolution, 41*(1), 54–66.

5 Berk, A. J., & Clayton, D. A. (1974). Mechanism of mitochondrial DNA replication in mouse L-cells: asynchronous replication of strands, segregation of circular daughter molecules, aspects of topology and turnover of an initiation sequence. *Journal of Molecular Biology, 86*(4), 801–824.

6 Picard, M., Wallace, D. C., & Burelle, Y. (2016). The rise of mitochondria in medicine. *Mitochondrion, 30*, 105–116. https://doi.org/10.1016/j.mito.2016.07.003

7 Gibson, A., Gowri-Shankar, V, Higgs, P. G., & Rattray, M. (2005). A comprehensive analysis of mammalian mitochondrial genome base composition and improved phylogenetic methods. *Molecular Biology and Evolution, 22*(2), 251–264.

8 Noack, K., Zardoya, R., & Meyer, A. (1996). The complete mitochondrial DNA sequence of the bichir (Polypterusornatipinnis), a basal ray-finned fish: ancient establishment of the consensus vertebrate gene order. *Genetics, 144*(3), 1165–1180.

9 Clayton, D. A. (1982). Replication of animal mitochondrial DNA. *Cell, 28*(4), 693–705.

10 Gustafsson, C. M., Falkenberg, M., & Larsson, N. -G. (2016). Maintenance and expression of mammalian mitochondrial DNA. *Annual Review of Biochemistry, 85*, 133–160. https://doi.org/10.1146/annurev-biochem-060815-014402

11 Gyllensten, U., Wharton, D., Josefsson, A., & Wilson, A. C. (1991). Paternal inheritance of mitochondrial DNA in mice. *Nature, 352*, 255–257.

12 Wolff, J. N., & Gemmell, N. J. (2008). Lost in the zygote: the dilution of paternal mtDNA upon fertilization. *Heredity, 101*, 429–434.

13 Nishimura, Y., Yoshinari, T., Naruse, K., et al. (2006). Active digestion of sperm mitochondrial DNA in single living sperm revealed by optical tweezers. *Proceedings of the National Academy of Sciences of the USA, 103*, 1382–1387.

14 DeLuca, S. Z., & O'Farrell, P. H. (2012). Barriers to male transmission of mitochondrial DNA in sperm development. *Developmental Cell, 22*, 660–668.

15 Lee, W., et al. (2023). Molecular basis for maternal inheritance of human mitochondrial DNA. *Nature Genetics, 55*, 1632–1639.

16 Shoubridge, E. A., & Wai, T. (2007). Mitochondrial DNA and the mammalian oocyte. *Current Topics in Developmental Biology, 77*, 87–111. https://doi.org/10.1016/S0070-2153(06)77004-1

17 Larsson, N. G. (2010). Somatic mitochondrial DNA mutations in mammalian aging. *Annual Review of Biochemistry, 79*(1), 683–706.

18 Taylor, R. W., & Turnbull, D. M. (2005). Mitochondrial DNA mutations in human disease. *Nature Reviews Genetics, 6*(5), 389–402. https://doi.org/10.1038/nrg1606

19 Stewart, J. B., Freyer, C., Elson, J. L., & Larsson, N. G. (2008). Strong purifying selection in transmission of mammalian mitochondrial DNA. *PLoS Biology, 6*(1), e10. https://doi.org/10.1371/journal.pbio.0060010

20 Lima, A., et al. (2021). Cell competition acts as a purifying selection to eliminate cells with mitochondrial defects during early mouse development. *Nature Metabolism, 3*(8), 1091–1108.

21 Yang, L., et al. (2020). Mitochondrial DNA mutation exacerbates female reproductive aging via impairment of the NADH/NAD+ redox. *Aging Cell, 19*(9), e13206. https://doi.org/10.1111/acel.13206

22 Roger, A. J., Muñoz-Gómez, S. A., & Kamikawa, R. (2017). The origin and diversification of mitochondria. *Current Biology, 27*(21), R1177–R1192.

23 Ricchetti, M., Tekaia, F., & Dujon, B. (2004). Continued colonization of the human genome by mitochondrial DNA. *PLoS Biology, 2*(9), e273.

24 Park, C. B., & Larsson, N. G. (2011). Mitochondrial DNA mutations in disease and aging. *The Journal of Cell Biology, 193*(5), 809–818. https://doi.org/10.1083/jcb.201010024

25 Wallace, D. C., et al. (1988). Mitochondrial DNA mutation associated with Leber's hereditary optic neuropathy. *Science, 242*(4884), 1427–1430.

26 Xu, B., & Clayton, D. A. (1995). A persistent RNA–DNA hybrid is formed during transcription at a phylogenetically conserved mitochondrial DNA sequence. *Molecular and Cellular Biology, 15*, 580–589.

27 Fusté, J. M., et al. (2010). Mitochondrial RNA polymerase is needed for activation of the origin of light-strand DNA replication. *Molecular Cell, 37*, 67–78.

28 Cerritelli, S. M., et al. (2003). Failure to produce mitochondrial DNA results in embryonic lethality in Rnaseh1 null mice. *Molecular Cell, 11*, 807–815.

29 Falkenberg, M. (2018). Mitochondrial DNA replication in mammalian cells: overview of the pathway. *Essays in Biochemistry, 62*(3), 287–296. https://doi.org/10.1042/EBC20170100

30 Falkenberg, M., & Gustafsson, C. M. (2020). Mammalian mitochondrial DNA replication and mechanisms of deletion formation. *Critical Reviews in Biochemistry and Molecular Biology, 55*(6), 509–524. https://doi.org/10.1080/10409238.2020.1818684

31 Wanrooij, S., Fusté, J. M., & Farge, G., et al. (2008). Human mitochondrial RNA polymerase primes lagging-strand DNA synthesis in vitro. *Proceedings of the National Academy of Sciences of the USA, 105*(32), 11122–11127.

32 Park, J., Baruch-Torres, N., & Yin, Y. W. (2023). Structural and molecular basis for mitochondrial DNA replication and transcription in health and antiviral drug toxicity. *Molecules (Basel, Switzerland), 28*(4), 1796. https://doi.org/10.3390/molecules28041796

33 Oláhová, M., et al. (2021). POLRMT mutations impair mitochondrial transcription causing neurological disease. *Nature Communications, 12*(1), 1135.

34 Jiang, M., et al. (2021). The mitochondrial single-stranded DNA binding protein is essential for initiation of mtDNA replication. *Science Advances, 7*(27), eabf8631.

35 Shi, Y., Posse, V., & Zhu, X., et al. (2016). Mitochondrial transcription termination factor 1 directs polar replication fork pausing. *Nucleic Acids Research, 44*(12), 5732–5742.

36 Akbari, M., Nilsen, H. L., & Montaldo, N. P. (2022). Dynamic features of human mitochondrial DNA maintenance and transcription. *Frontiers in Cell and Developmental Biology, 10*, 984245.

37 Wanrooij, S., & Falkenberg, M. (2010). The human mitochondrial replication fork in health and disease. *Biochimica et Biophysica Acta (BBA) — Bioenergetics, 1797*(8), 1378–1388.

38 Nicholls, T. J., et al. (2014). Linear mtDNA fragments and unusual mtDNA rearrangements associated with pathological deficiency of MGME1 exonuclease. *Human Molecular Genetics, 23*(23), 6147–6162.

39 Matic, S., et al. (2018). Mice lacking the mitochondrial exonuclease MGME1 accumulate mtDNA deletions without developing progeria. *Nature Communications, 9*(1), 1202.

40 Yasukawa, T., & Kang, D. (2018). An overview of mammalian mitochondrial DNA replication mechanisms. *Journal of Biochemistry, 164*(3), 183–193. https://doi.org/10.1093/jb/mvy058

41 MirallesFusté, J., et al. (2014). In vivo occupancy of mitochondrial single-stranded DNA binding protein supports the strand displacement mode of DNA replication. *PLoS Genetics, 10*(12), e1004832.

42 Pohjoismäki, J. L., et al. (2010). Mammalian mitochondrial DNA replication intermediates are essentially duplex but contain extensive tracts of RNA/DNA hybrid. *Journal of Molecular Biology, 397*(5), 1144–1155.

43 Reyes, A., Kazak, L., Wood, S. R., et al. (2013). Mitochondrial DNA replication proceeds via a "bootlace" mechanism involving the incorporation of processed transcripts. *Nucleic Acids Research, 41*(11), 5837–5850. https://doi.org/10.1093/nar/gkt196

44 Yasukawa, T., et al. (2006). Replication of vertebrate mitochondrial DNA entails transient ribonucleotide incorporation throughout the lagging strand. *The EMBO Journal, 25*(22), 5358–5371. https://doi.org/10.1038/sj.emboj.7601392

45 Hsieh, C. L. (2019). Novel lines of evidence for the asymmetric strand displacement model of mitochondrial DNA replication. *Molecular and Cellular Biology, 39*(2), e00406-18. https://doi.org/10.1128/MCB.00406-18

46 Kosar, M., Piccini, D., Foiani, M., & Giannattasio, M. (2021). A rapid method to visualize human mitochondrial DNA replication through rotary shadowing and transmission electron microscopy. *Nucleic Acids Research, 49*(21), e121. https://doi.org/10.1093/nar/gkab770

47 Brown, T. A., et al. (2005). Replication of mitochondrial DNA occurs by strand displacement with alternative light-strand origins, not via a strand-coupled mechanism. *Genes & Development, 19*(20), 2466–2476.

48 McKinney, E. A., & Oliveira, M. T. (2013). Replicating animal mitochondrial DNA. *Genetics and Molecular Biology, 36*, 308–315.

49 Wanrooij, S., et al. (2008). Human mitochondrial RNA polymerase primes lagging-strand DNA synthesis in vitro. *Proceedings of the National Academy of Sciences of the USA, 105*(32), 11122–11127. https://doi.org/10.1073/pnas.0805399105

50 Holt, I. J., Lorimer, H. E., & Jacobs, H. T. (2000). Coupled leading- and lagging-strand synthesis of mammalian mitochondrial DNA. *Cell, 100*(5), 515–524.

51 Taanman, J. -W. (1999). The mitochondrial genome: structure, transcription, translation and replication. *Biochimica et Biophysica Acta (BBA) — Bioenergetics, 1410*(2), 103–123.

52 Xia, X. (2019). Is there a mutation gradient along vertebrate mitochondrial genome mediated by genome replication? *Mitochondrion, 46*, 30–40. https://doi.org/10.1016/j.mito.2018.06.004

53 Berk, A. J., & Clayton, D. A. (1974). Mechanism of mitochondrial DNA replication in mouse L-cells: asynchronous replication of strands, segregation of circular daughter molecules, aspects of topology and turnover of an initiation sequence. *Journal of Molecular Biology, 86*(4), 801–824.

54 Alexeyev, M., Shokolenko, I., Wilson, G., & LeDoux, S. (2013). The maintenance of mitochondrial DNA integrity — critical analysis and update. *Cold Spring Harbor Perspectives in Biology, 5*(5), a012641.

55 Sies, H., et al. (2022). Defining roles of specific reactive oxygen species (ROS) in cell biology and physiology. *Nature Reviews Molecular Cell Biology, 23*(7), 499–515. https://doi.org/10.1038/s41580-022-00456-z

56 Stewart, J. B., & Larsson, N. G. (2014). Keeping mtDNA in shape between generations. *PLoS Genetics, 10*(10), e1004670.

57 Ross, J. M., et al. (2013). Germline mitochondrial DNA mutations aggravate ageing and can impair brain development. *Nature, 501*(7467), 412–415.

58 Burger, G., Gray, M. W., & Lang, B. F. (2003). Mitochondrial genomes: anything goes. *Trends in Genetics, 19*, 709–716. https://doi.org/10.1016/j.tig.2003.10.012

59 Sanchez-Contreras, M., et al. (2023). The multi-tissue landscape of somatic mtDNA mutations indicates tissue-specific accumulation and removal in aging. *eLife, 12*, e83395. https://doi.org/10.7554/eLife.83395

60 Pohjoismäki, J. L., Forslund, J. M., Goffart, S., et al. (2018). Known unknowns of mammalian mitochondrial DNA maintenance. *BioEssays, 40*(9), 1800102.

61 Kirschner, R. H., Wolstenholme, D. R., & Gross, N. J. (1968). Replicating molecules of circular mitochondrial DNA. *Proceedings of the National Academy of Sciences of the USA, 60*(4), 1466–1472.

62 Ciesielski, L., Oliveira, M. T., & Kaguni, L. S. (2016). Animal mitochondrial DNA replication. *The Enzymes, 39*, 255–292.

63 Holt, I. J., & Jacobs, H. T. (2014). Unique features of DNA replication in mitochondria: a functional and evolutionary perspective. *BioEssays, 36*(11), 1024–1031.

64 Kennedy, S. R., Salk, J. J., Schmitt, M. W., & Loeb, L. A. (2013). Ultra-sensitive sequencing reveals an age-related increase in somatic mitochondrial mutations that are inconsistent with oxidative damage. *PLoS Genetics, 9*(9), e1003794. https://doi.org/10.1371/journal.pgen.1003794

65 Albrecht-Buehler, G. (2006). Asymptotically increasing compliance of genomes with Chargaff's second parity rules through inversions and inverted transpositions. *Proceedings of the National Academy of Sciences of the USA, 103*(47), 17828–17833. https://doi.org/10.1073/pnas.0605553103

66 MirallesFusté, J., et al. (2014). In vivo occupancy of mitochondrial single-stranded DNA binding protein supports the strand displacement mode of DNA replication. *PLoS Genetics, 10*(12), e1004832. https://doi.org/10.1371/journal.pgen.1004832

67 Williams, S. L., Mash, D. C., Züchner, S., & Moraes, C. T. (2013). Somatic mtDNA mutation spectra in the aging human putamen. *PLoS Genetics, 9*(12), e1003990. https://doi.org/10.1371/journal.pgen.1003990

68 Coskun, P. E., Beal, M. F., & Wallace, D. C. (2004). Alzheimer's brains harbor somatic mtDNA control-region mutations that suppress mitochondrial transcription and replication. *Proceedings of the National Academy of Sciences of the USA, 101*(29), 10726–10731. https://doi.org/10.1073/pnas.0403649101

69 Filograna, R., et al. (2021). Mitochondrial DNA copy number in human disease: the more the better? *FEBS Letters, 595*(8), 976–1002.

70 Ju, Y. S., et al. (2014). Origins and functional consequences of somatic mitochondrial DNA mutations in human cancer. *eLife, 3*, e02935.

71 Matkarimov, B. T., & Saparbaev, M. K. (2020). DNA repair and mutagenesis in vertebrate mitochondria: evidence for asymmetric DNA strand inheritance. In *Mechanisms of Genome Protection and Repair*, 77–10.

72 Fonseca, M. M., Harris, D. J., & Posada, D. (2014). The inversion of the control region in three mitogenomes provides further evidence for an asymmetric model of vertebrate mtDNA replication. *PLoS ONE, 9*(9), e106654. https://doi.org/10.1371/journal.pone.0106654

73 Holt, I. J., & Reyes, A. (2012). Human mitochondrial DNA replication. *Cold Spring Harbor Perspectives in Biology, 4*(12), a012971. https://doi.org/10.1101/cshperspect.a012971

74 Pohjoismäki, J. L. O., Forslund, J. M. E., Goffart, S., Torregrosa-Muñumer, R., & Wanrooij, S. (2018). Known unknowns of mammalian mitochondrial DNA maintenance. *BioEssays, 40*(9), 1800102. https://doi.org/10.1002/bies.201800102

75 Laurie, B., Katritch, V., Sogo, J., Koller, T., Dubochet, J., & Stasiak, A. (1998). Geometry and physics of catenanes applied to the study of DNA replication. *Biophysical Journal, 74*, 2815–2822. https://doi.org/10.1016/S0006-3495(98)77988-3

76 Nicholls, T. J., Nadalutti, C. A., Motori, E., Sommerville, E. W., Gorman, G. S., Basu, S., … Gustafsson, C. M. (2018). Topoisomerase 3α is required for decatenation and segregation of human mtDNA. *Molecular Cell, 69*(1), 9–23.e6. https://doi.org/10.1016/j.molcel.2017.11.033

77 Lynch, A. S., & Wang, J. C. (1993). Anchoring of DNA to the bacterial cytoplasmic membrane through cotranscriptional synthesis of polypeptides encoding membrane proteins or proteins for export: a mechanism of plasmid hypernegative supercoiling in mutants deficient in DNA topoisomerase I. *Journal of Bacteriology, 175*, 1645–1655.

78 Shutt, T. E., & Gray, M. W. (2006). Bacteriophage origins of mitochondrial replication and transcription proteins. *Trends in Genetics, 22*(2), 90–95. https://doi.org/10.1016/j.tig.2005.11.007

79 Hanawalt, P. C., & Spivak, G. (2008). Transcription-coupled DNA repair: two decades of progress and surprises. *Nature Reviews Molecular Cell Biology, 9*(12), 958–970. https://doi.org/10.1038/nrm2549

80 Touchon, M., Arneodo, A., d'Aubenton-Carafa, Y., & Thermes, C. (2004). Transcription-coupled and splicing-coupled strand asymmetries in eukaryotic genomes. *Nucleic Acids Research, 32*(17), 4969–4978. https://doi.org/10.1093/nar/gkh823

81 Shi, Y., Posse, V., Zhu, X., Hyvärinen, A. K., Jacobs, H. T., Falkenberg, M., & Gustafsson, C. M. (2016). Mitochondrial transcription termination factor 1 directs polar replication fork pausing. *Nucleic Acids Research, 44*(12), 5732–5742. https://doi.org/10.1093/nar/gkw302

82 Cluett, T. J., Akman, G., Reyes, A., Kazak, L., Mitchell, A., Wood, S. R., et al. (2018). Transcript availability dictates the balance between strand-asynchronous and strand-coupled mitochondrial DNA replication. *Nucleic Acids Research, 46*(20), 10771–10781. https://doi.org/10.1093/nar/gky852

83 Cadet, J., Douki, T., & Ravanat, J. L. (2010). Oxidatively generated base damage to cellular DNA. *Free Radical Biology and Medicine, 49*(1), 9–21. https://doi.org/10.1016/j.freeradbiomed.2010.03.025

84 Balaban, R. S., Nemoto, S., & Finkel, T. (2005). Mitochondria, oxidants, and aging. *Cell, 120(4)*, 483–495.

85 Degtyareva, N. P., Saini, N., Sterling, J. F., Placentra, V. C., Klimczak, L. J., Gordenin, D. A., & Doetsch, P. W. (2019). Mutational signatures of redox stress in yeast single-strand DNA and of aging in human mitochondrial DNA share a common feature. *PLoS Biology, 17*(5), e3000263. https://doi.org/10.1371/journal.pbio.3000263

86 Saccone, C., Attimonelli, M., & Sbisà, E. (1987). Structural elements highly preserved during the evolution of the D-loop-containing region in vertebrate mitochondrial DNA. *Journal of Molecular Biology, 192*(3), 503–511. https://doi.org/10.1016/0022-2836(86)90272-X

87 Brown, G. G., Gadaleta, G., Pepe, G., Saccone, C., & Sbisà, E. (1986). Structural conservation and variation in the D-loop-containing region of vertebrate mitochondrial DNA. *Journal of Molecular Biology, 192*(3), 503–511. https://doi.org/10.1016/0022-2836(86)90272-X

88 Ji, X., Guo, W., Gu, X., Guo, S., Zhou, K., & Su, L., et al. (2022). Mutational profiling of mtDNA control region reveals tumor-specific evolutionary selection involved in mitochondrial dysfunction. *eBioMedicine, 80*, 104058. https://doi.org/10.1016/j.ebiom.2022.104058

А.Б. Әліқұл, Д. Манапқызы, М.К. Сапарбаев, С.М. Тайпақова

Омыртқалылар митохондриясындағы ДНҚ тізбектерінің асимметриялық тұқым қуалауының дәлелдері

1958 жылы Мезельсон мен Сталь жүргізген классикалық эксперимент жасушалық организмдердегі ДНҚ репликациясының жартылай консервативті механизмін дәлелдеді. Бұл механизмге сәйкес, жасуша бөлінгеннен кейін әрбір еншілес жасуша бір ата-аналық тізбектен (W немесе C) және бір жаңадан синтезделген комплементарлы тізбектен (C' немесе W') тұратын хромосоманы иеленеді. Әрбір ДНҚ тізбегі жасуша әр бөлінген сайын бірдей үлгіде репликацияланатындықтан, W және C тізбектері жартылай консервативті репликация мен жасушалық бөліну нәтижесінде эквивалентті деп есептеледі. Алайда, кейбір жасушалық емес организмдер, мысалы, бір тізбекті ДНҚ немесе РНҚ вирустары, эквиваленттілік принципін сақтамайды. Сонымен қатар омыртқалылардың митохондриялық геномындағы екі тізбектің нуклеотидтік құрамының айқын теңсіздігі ерекше назар аударуға тұрарлық. Бұл теңсіздік сілтілі цезий хлориді градиентіндегі ультрацентрифугалау кезінде митохондриялық ДНҚ-ның екі тізбегінің — G+T-ге бай ауыр (H) және C+A-ға бай жеңіл (L)

тізбектерге бөлінуімен көрініс табады. Адам митохондрияларындағы ДНҚ репликациясы ұзақ жылдар бойы зерттеліп келе жатқанына қарамастан, репликация механизмі мен тізбектердің нуклеотидтік құрамындағы теңсіздіктің арасындағы ықтимал байланыс әлі де толық анықталмаған және ғылыми пікірталас тақырыбы болып отыр. Осыған байланысты бұл мақалада омыртқалылардың митохондриялық ДНҚ-сында байқалатын мутациялық паттерннің күшті ығысуын қарапайым эвристикалық жолмен түсіндіре алатын ДНҚ тізбектерінің асимметриялық тұқымқуалауы немесе олардың эквивалентті еместігі туралы ықтимал үлгісі ұсынылған.

Кілт сөздер: митохондриялық ДНҚ, ДНҚ тізбектерінің эквиваленттілігі, мутация заңдылықтары, Чаргаффтың екінші ережесі, репликация.

А.Б. Аликул, Д. Манапкызы, М.К. Сапарбаев, С.М. Тайпакова

Доказательства асимметричного наследования цепей ДНК в митохондриях позвоночных

Классический эксперимент, предложенный в 1958 году Мезельсоном и Сталем, подтвердил полуконсервативный механизм репликации ДНК в клеточных организмах, согласно которому после деления клеток каждая дочерняя клетка наследует хромосому, состоящую из одной родительской цепи (W или C) и одной новосинтезированной комплементарной цепи (C' или W'). Поскольку каждая цепь ДНК реплицируется одинаковое количество раз после каждого деления клетки, можно предположить, что цепи W и C эквивалентны как результат сочетания деления клетки и полуконсервативного механизма репликации ДНК. Однако некоторые неклеточные организмы, такие как оцДНК- и РНК-вирусы, игнорируют принцип эквивалентности цепей. Также стоит отметить интересную особенность митохондриального генома позвоночных с необычным дисбалансом нуклеотидного состава на двух нитях митохондриальной ДНК, что приводит к разделению на тяжелую (H) G+T-богатую и лёгкую (L) C+A-богатую нити ДНК при ультрацентрифугировании в щелочном градиенте хлористого цезия. Несмотря на многолетние исследования репликации ДНК в митохондриях человека, механизм этой репликации и возможная связь с дисбалансом нуклеотидного состава остаются предметом дискуссий. В связи с этим в данной статье мы предлагаем возможную модель асимметричного наследования нитей ДНК или неэквивалентности нитей ДНК, которая предоставляет простое эвристическое объяснение сильно смещенного паттерна мутаций в мтДНК позвоночных.

Ключевые слова: митохондриальная ДНК, эквивалентность цепей ДНК, закономерности мутаций, второе правило Чаргаффа, репликация.

Information about the authors

Alikul Ayzhan — PhD student, Department of Molecular Biology and Genetics, Faculty of Biology and Biotechnology, Al-Farabi Kazakh National University, Almaty, Kazakhstan; e-mail: aliqul.ayzhan@gmail.com; ORCID: https://orcid.org/0000-0002-4911-4936

Manapkyzy Diana — PhD, Scientific Research Institute of Biology and Biotechnology Problems, Al-Farabi Kazakh National University, Almaty, Kazakhstan; e-mail: manatkyzy.diana@gmail.com; ORCID: https://orcid.org/0000-0003-3371-4459

Saparbaev Murat — PhD, Professor, Group “Mechanisms of DNA Repair and Carcinogenesis”, CNRS UMR9019, Université Paris-Saclay, Gustave Roussy Cancer Campus, Villejuif, Cedex, France; e-mail: murat.saparbaev@gustaveroussy.fr; ORCID:https://orcid.org/0000-0002-4630-1074

Taipakova Sabira — PhD, Associated Professor, Department of Molecular Biology and Genetics, Faculty of Biology and Biotechnology, Al-Farabi Kazakh National University, Almaty, Kazakhstan; e-mail: sabira.taipakova@gmail.com; ORCID: https://orcid.org/0000-0001-9499-1682

How to Cite: Bayazitova, Z.E., Kurmanbayeva, A.S., Safronova, N.M., Zhaparova, S.B. (2026). Ecological and biological assessment of the state of soils and vegetation cover of the closed municipal solid waste landfill in Kokshetau. *Fundamental and Experimental Biology*, 31, 2 (122), 43-55. https://doi.org/10.31489/2026FEB3/43-55

Research Article
https://doi.org/10.31489/2026FEB3/43-55

UDC 504.054 Received: 16.02.2026 | Accepted: 8.06.2026 | Published online: 30.09.2026

Z.E. Bayazitova*, A.S. Kurmanbayeva, N.M. Safronova, S.B. Zhaparova

Kokshetau University named after Sh. Ualikhanov, Kokshetau, Kazakhstan
**Corresponding author: z_bayazitova@mail.ru*

Ecological and biological assessment of the state of soils and vegetation cover of the closed municipal solid waste landfill in Kokshetau

The ecological state of a closed municipal solid waste (MSW) landfill in Kokshetau, operated from 1960 to 2017 and lacking engineered protective systems, was assessed with a focus on heavy metal contamination and its effects on vegetation. Soil analysis revealed substantial exceedances of maximum permissible concentrations (MPCs) and background concentrations. Maximum concentrations reached 4230 mg/kg for Zn, 870 mg/kg for Cu, 299 mg/kg for Pb, 58 mg/kg for As, and 145 mg/kg for Ni, exceeding MPCs by 42.3, 15.8, 9.3, 29.0, and 3.6 times, respectively. Compared with background concentrations, these values were 48.1, 8.5, 19.9, 4.1, and 3.2 times higher, respectively. A pronounced radial contamination gradient was identified, with maximum concentrations in the central zone and a gradual decrease toward the periphery. However, even peripheral areas showed elevated concentrations relative to background levels, indicating persistent anthropogenic impact despite landfill closure. The geo-accumulation index (Igeo) classified the central soils as strongly to extremely contaminated, particularly with respect to Zn and Pb, while the phytotoxicity index (FTI) indicated a high level of phytotoxicity. Geobotanical analysis revealed substantial transformation of the vegetation, which was dominated by herbaceous and short-lived species, with annual species accounting for 49% of the recorded flora. The prevalence of *Asteraceae*, *Poaceae*, *Brassicaceae*, and *Chenopodiaceae* is consistent with adaptation to chemically stressed environments. The dominance of *Bassia scoparia* suggests its potential as a bioindicator of technogenically disturbed soils. Overall, the landfill represents a long-term anthropogenically transformed ecosystem requiring integrated environmental monitoring and reclamation measures.

Keywords: landfill of solid household waste, soil contamination, phytotoxicity, anthropogenic impact, heavy metals, ecosystem disturbance.

Introduction

Landfills of solid household waste (MSW), including closed and recultivated ones, remain long-term sources of soil pollution with heavy metals due to the accumulated “technogenic legacy”, lack/insufficiency of engineering protection (screens, filtrate collection) and the continued secondary intake of pollutants from surface runoff and dust transport [1]. International studies emphasize that soil pollution around landfills often persists for years and is accompanied by environmental risks to the soil and plant system, including the potential entry of metals into the biota [2].

For Kazakhstan, the problem is particularly significant against the background of an increase in the volume of accumulated waste and the need for environmentally sound management of landfill stock. Modern reviews and applied works on solid waste management in the Republic of Kazakhstan indicate the scale of waste accumulation and the importance of assessing the environmental effects of existing and closed facilities [3-4].

Kazakhstani studies demonstrate that landfills are capable of forming local anomalies in the content of Zn, Cu, Pb, As, Ni and other elements in soils, as well as influencing adjacent environmental components (including soils and groundwater) [5]. Thus, for the Karasai landfill (Almaty), soil pollution with heavy metals and its anthropogenic causes are shown. Similarly, earlier works on landfill sites emphasized the migration of heavy metals in the soil–water system, which makes an integrated approach to assessing the state of anthropogenic territories relevant [6]. In recent years, studies have been published on landfills in Kazakhstan (including in the Astana area), where excess of permissible levels of heavy metals and the need for environmental hazard assessment are noted, which confirms the current practical relevance of such work [7].

The study of closed landfills is of particular relevance, since the cessation of operation does not mean the cessation of exposure: pollutants can persist in soils and maintain a phytotoxic background, affecting the

restoration of vegetation and the structure of phytocenoses [8]. In this regard, it is important not only to record the concentrations of elements, but also to use integral indices (for example, Igeo) for a comparable assessment of the degree of anthropogenic accumulation and the allocation of functionally the most dangerous zones.

At the same time, an urgent task is not only to fix the level of pollution, but also to develop approaches to restoring disturbed ecosystems. It is necessary to study the prospects of biorecultivation of landfills using plant species resistant to stressful conditions, capable of functioning in conditions of increased heavy metal content and transformed water-salt regime [9]. This highlights the need for a comprehensive analysis combining chemical pollution indicators and a geobotanical assessment of the vegetation cover.

Geobotanical characteristics (the taxonomic structure of the flora, the proportion of short-lived life forms, and the dominance of ruderal/stress-tolerant species) can act as bioindicative signs of ecosystem transformation under the influence of metals, complementing the calculations of phytotoxicity (FTI) and making it possible to substantiate the ecological consequences for vegetation cover [10].

Thus, the relevance of this study is determined by: (1) the ecological significance of closed landfills as long-term sources of soil pollution with heavy metals [11]; (2) the lack of data on spatial heterogeneity of pollution within the body of the landfill; (3) the need to integrate chemical indicators (exceeding standards, Igeo, FTI) with the geobotanical assessment of vegetation cover transformation for scientifically based monitoring and selection of reclamation priorities in the conditions of Northern Kazakhstan.

Experimental

The study was performed at a closed solid waste landfill located in the eastern part of the city of Kokshetau (Akmola region, Northern Kazakhstan), on the border of the southwestern edge of the West Siberian Plain and the northern slopes of the Kokshetau upland (53.320833°N, 69.478333° E). The territory belongs to a moderately arid forest-steppe zone characterized by a sharply continental climate, a large annual temperature range, and insufficient precipitation.

The 36.5-hectare landfill was operated from 1960 to 2017. It is a multilayered waste body covered with soil, without waterproofing liners or leachate collection systems. The height of the garbage dumps reaches 5–7 m. Despite the official closure, unauthorized waste storage remains in some areas, which increases the anthropogenic burden on the ecosystem.

Soil sampling on the territory of a closed MSW landfill was carried out according to a radial gradient scheme in order to assess the spatial distribution of heavy metals depending on the distance from the center of the landfill. The zone of maximum capacity of a man-made body and the greatest accumulation of waste was considered as a conditional center. Figure 1 shows the sampling points from the closed MSW landfill in Kokshetau.

Ten sampling points were established within the landfill body and grouped into functional zones: the core (points 1–3, up to 50 m from the center), the middle zone (points 4–6, 50–150 m), and the marginal zone (points 7–10, 150–300 m). One control soil sample was collected outside the landfill's impact zone (5–10 km away) under comparable natural conditions and used as a background reference for pollution assessment (Tab. 1).

At each sampling point, one composite sample representing the site was collected. In total, 11 samples were analyzed (10 from the landfill and 1 background sample). The sampling design was aimed at assessing spatial variability; therefore, no replicates were taken, and each point was treated as an independent observation unit.

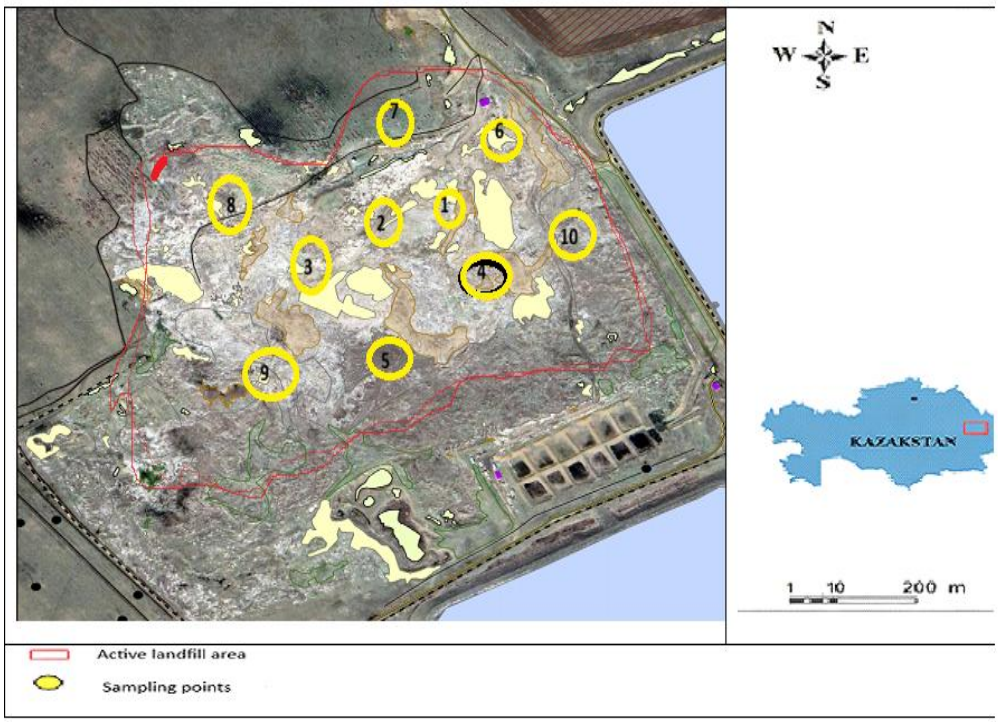

Figure 1. Map of the closed MSW landfill in Kokshetau (sampling points)

Table 1

The content of elements in soil samples of the closed MSW landfill in the city of Kokshetau

Samples	Zn	Cu	Mn	Sr	Pb	As	Ni
MPC	**100**	**55**	**1500**	**30**	**32.0**	**2.0**	**40**
Point 1	4230	760	1790	306	248	50	123
Point 2	2410	710	1830	389	299	45	145
Point 3	1620	870	1210	323	292	58	103
Point 4	1640	610	960	264	208	46	141
Point 5	1660	566	1140	225	151	42	124
Point 6	1100	440	1010	261	104	29	106
Point 7	249	237	930	211	128	29	76
Point 8	510	184	690	161	90	26	103
Point 9	235	144	660	126	71	24	62
Point 10	700	234	500	153	64	21	52
BACKGROUND	88	102	450	89	15	14	46

The sampling depth varied depending on the morphological position of the site. In the central part of the body of the landfill, samples were taken from a depth of 0–50 cm, which is due to the significant capacity of the anthropogenic horizon and the vertical migration of pollutants. In the middle and marginal parts of the body of the landfill, samples were taken from the upper soil layer (0–20 cm), which is most actively involved in the processes of interaction with vegetation.

This approach made it possible to identify the spatial gradient of soil pollution and assess the decrease in heavy metal concentrations as they moved away from the center of the landfill.

The total concentrations of heavy metals (Pb, Zn, Cu, Ni, As, Hg) in soil samples were determined using a portable X-ray fluorescence (XRF) analyzer, Olympus Vanta Pro series VCR, equipped with GeoChem software.

The analytical method is based on the X-ray fluorescence effect: when a sample is irradiated with primary X-rays, the atoms become excited and emit secondary (fluorescent) radiation. The energy spectrum of this radiation is characteristic of each chemical element, allowing both qualitative and quantitative determination.

The Olympus Vanta Pro analyzer is equipped with a 4 W X-ray tube with a rhodium (Rh) anode and a high-resolution large-area silicon drift detector (SDD, up to 50 mm²), ensuring high sensitivity and measurement accuracy for elements starting from magnesium (Mg) and above in the periodic table.

The instrument is also fitted with an integrated GPS module and a digital camera, enabling georeferencing of sampling locations and improving the accuracy of spatial analysis and contamination mapping.

The level of soil contamination was assessed by comparing the measured concentrations with the maximum permissible concentrations (MPCs) of heavy metals established by current sanitary and hygienic standards for soils. The background sample was used as a local geochemical reference for comparative assessment and for calculating integrated pollution indices [12].

Geobotanical studies were carried out on the territory of the closed MSW landfill in Kokshetau in August–October 2025. The vegetation survey was carried out by the route-site method with the laying of test areas (10 × 10 m) within the functional zones of the polygon body (core, middle and marginal parts) (Fig. 2), identified by the results of the analysis of the spatial distribution of heavy metals in soils.

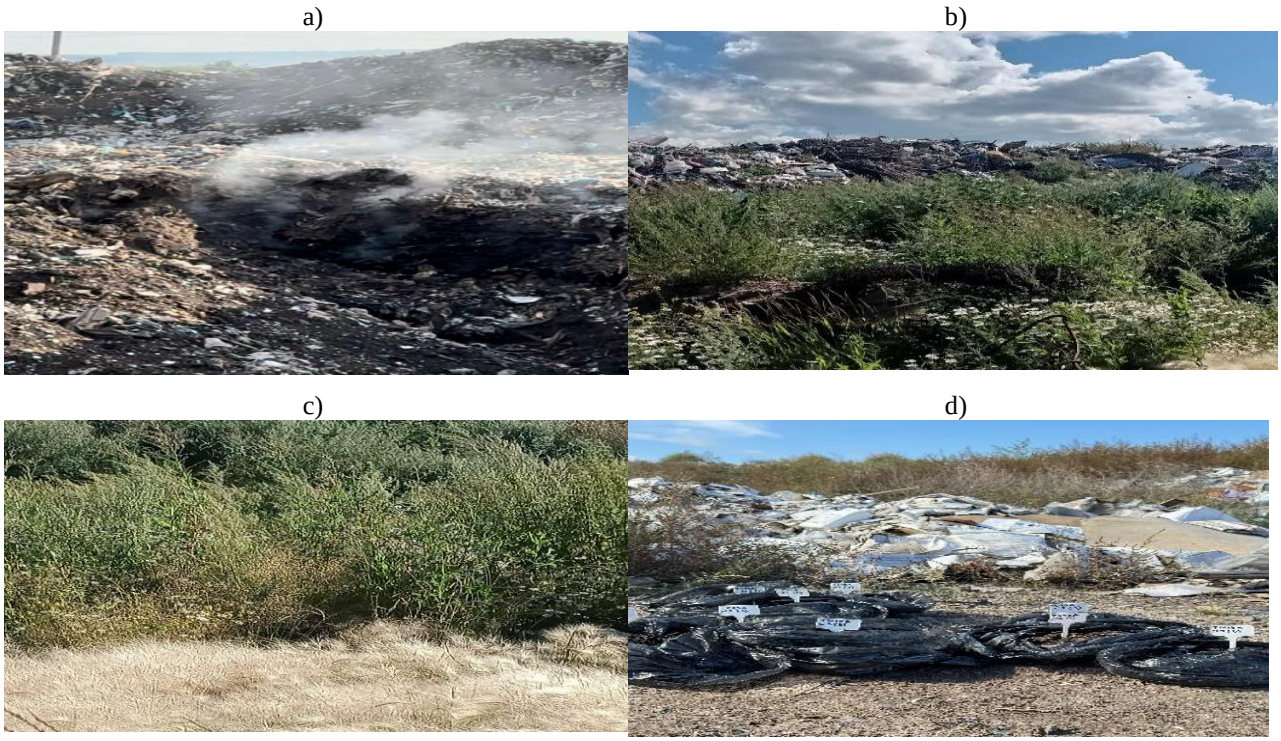

Figure 2. Closed municipal solid waste landfill in Kokshetau (53.320833° N; 69.478333° E):
(a) central part of the landfill body; (b) middle zone; (c) marginal zone;
(d) collected soil samples stored in polyethylene bags for subsequent laboratory analysis

A complete description of the vegetation cover was carried out at each site, with registration of all types of vascular plants. Taxonomic affiliation, life form, ecological group, and relative abundance were determined for each species; the projective coverage was assessed on the Brown–Blanke scale.

The interpretation of geobotanical data was carried out in comparison with concentrations of heavy metals and integrated pollution indicators (Igeo, phytotoxic index), which made it possible to assess the impact of anthropogenic soil pollution on the structure and composition of plant communities.

Statistical data processing included the calculation of descriptive indicators, analysis and geoaccumulation indices. The geoaccumulation index (Igeo) was calculated using a background control sample. The geoaccumulation index for each element was calculated using the formula:

$$I_{geo,i} = \log_2\left(\frac{C_i}{1.5 \cdot C_{i,fon}}\right) I_{geo,i} = \log_2\left(\frac{C_i}{1.5 \cdot C_{i,fon}}\right) \quad (1)$$

where *Ci* is the concentration of the element in the soil, mg/kg; *Ci,fon* is the background concentration in the control sample, mg/kg; the coefficient 1.5 takes into account the natural variability of background concentrations.

The phytotoxic index (FTI) was calculated as the average value of the multiplicities exceeding the maximum permissible concentration for Zn, Cu, Pb, As and Ni, after which the values obtained were averaged over the functional zones of the landfill to assess the spatial variability of soil phytotoxicity.

Results and Discussion

The results of the analysis of soil samples showed pronounced anthropogenic contamination of the territory of the closed landfill with heavy metals (Tab. 2). The maximum concentrations of zinc reached 4230 mg/kg, which exceeds the maximum permissible concentration by 42.3 times and the background values by 48.1 times. Significant exceedances were also recorded for arsenic (up to 29 MPC), copper (up to 15.8 MPC) and lead (up to 9.3 MPC). Nickel was characterized by more moderate but steady exceedances of standards (up to 3.6 MPC).

Table 2

Multiplicity of exceeding the maximum permissible concentration and background (maximum values)

Element	max C, mg/kg	C/MPC mg/kg	C/background mg/kg
Zn	4230	42,3	48,1
Cu	870	15,8	8,5
Pb	299	9,3	19,9
As	58	29,0	4,1
Ni	145	3,6	3,2

The data indicate the dominant role of Zn and As in forming the phytotoxic background of the landfill, due to their high biological activity and inhibitory effects on plant growth even at relatively low concentrations [13]. Elevated background exceedances of Pb and Cu reflect their long-term accumulation during landfill operation [14].

The observed contamination levels are consistent with those reported for MSW landfills worldwide, where elevated concentrations of Zn, Pb, Cu, and As and their accumulation in topsoil are commonly observed. Similar exceedance ranges and radial contamination gradients have been documented in Europe, China, and Central Asia [10, 11, 15], indicating the universal nature of heavy metal accumulation and migration in technogenically disturbed ecosystems.

Analysis of average metal concentrations across functional zones revealed a pronounced spatial gradient (Tab. 3). The highest levels were recorded in the landfill core (Zn — 2753, Cu — 780, Pb — 280 mg/kg), with decreasing concentrations toward the middle and marginal zones; however, even peripheral areas remained above background levels.

Table 3

Average concentrations by functional zones, mg/kg

The zone	Zn	Cu	Mn	Sr	Pb	As	Ni
Core (1-3)	2753	780	1610	339	280	51	124
Average (4-6)	1467	539	1037	250	154	39	124
Regional (7-10)	424	200	695	163	88	25	73

This pattern reflects the peculiarities of the landfill's functioning as a source of long-term anthropogenic impact: the central part is characterized by maximum accumulation of waste and filtrate, while partial dispersion of pollutants occurs as it moves away from it. Nevertheless, even the peripheral areas retain signs of sustained anthropogenic pollution, which underlines the long-term nature of the landfill's impact on the soil cover (Tab. 4) [14].

Table 4

Phytotoxic index (FTI) by zone

The zone	FTI	Evaluation
The core	15,81	Very high phytotoxicity
The middle part	10,38	High
The edge part	4,99	Moderate

The calculation of the geoaccumulation index made it possible to quantify the degree of soil contamination by individual elements (Tab. 5). For zinc, Igeo values in the central part of the landfill reached 5.0, which correspond to the class of extremely polluted soils. For lead, Igeo values at points 1–4 were in the range of 3.21–3.73, which also indicates severe and extreme contamination. Copper was characterized by Igeo values ranging from moderate to severe contamination, while arsenic corresponded to a moderate level of contamination at most points.

Table 5

Geoaccumulation Index (Igeo) for key elements

Point	Zn	Cu	Pb	As
1.0	5.0	2.31	3.46	1.25
2.0	4.19	2.21	3.73	1.1
3.0	3.62	2.51	3.7	1.47
4.0	3.64	2.0	3.21	1.13
5.0	3.65	1.89	2.75	1.0
6.0	3.06	1.52	2.21	0.47
7.0	0.92	0.63	2.51	0.47
8.0	1.95	0.27	2.0	0.31
9.0	0.83	-0.09	1.66	0.19
10.0	2.41	0.61	1.51	0.0

Igeo values decreased in the marginal zone of the polygon body, however, levels corresponding to moderate and severe pollution remained for a number of elements (Zn and Pb). This indicates that the anthropogenic impact of the landfill extends beyond its central part and forms a sustainably disturbed anthropogenic territory.

Such geoaccumulation index values are typical of areas with long-term waste accumulation and the absence of engineered barriers, which is confirmed by similar studies on closed landfills, where Igeo values for Zn and Pb often reach categories of strong to extreme contamination [11, 14].

An analysis of the spatial profile of the distribution of concentrations of heavy metals (Zn, Cu, Pb and As), shown in Figure 3, revealed a pronounced gradient of soil pollution from the central part of the closed landfill to its periphery. The maximum concentrations of all the studied elements were recorded in the central zone of the landfill body, reflecting the long-term accumulation of pollutants in the zone of maximum waste deposition [15].

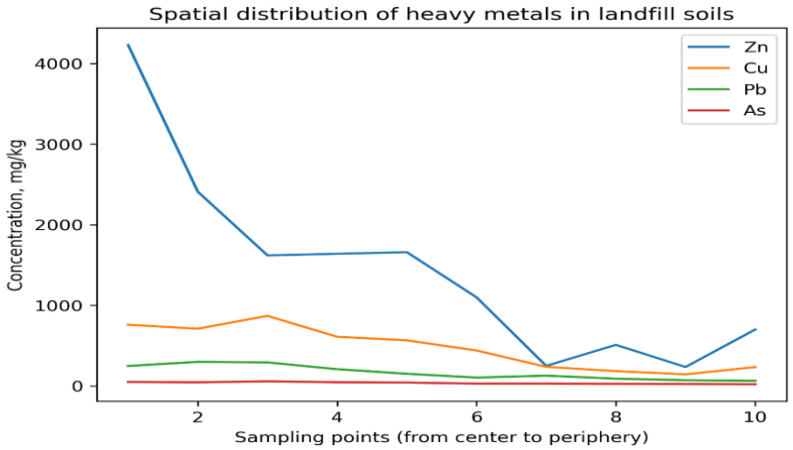

Figure 3. Spatial profile of the distribution of concentrations of heavy metals (Zn, Cu, Pb, As) from the center of the landfill to the periphery

The sharpest contrast is observed for zinc, whose concentrations in the central points exceed the values in the marginal zone by several times. A similar, though less pronounced, trend is observed for copper and lead, indicating similar mechanisms governing their input and migration within the landfill body. For arsenic,

concentrations also decrease with distance from the center, but its distribution profile is more smoothed, which may indicate increased mobility of this element and its redistribution with the filtrate [15].

The revealed pattern of distribution of heavy metals confirms that the central part of the landfill is the main zone of phytotoxic background formation. As they move away from the center, metal concentrations decrease, but even in the peripheral zone their levels remain above the background values, which indicates a stable anthropogenic impact and long-term persistence of pollution in the soil cover after the closure of the landfill [13].

The spatial distribution of heavy metals within the landfill is controlled by a combination of interrelated migration processes in a technogenically disturbed environment. A key mechanism is the infiltration of atmospheric precipitation through the landfill body: in the absence of impermeable liners and leachate collection systems, contaminated leachate is formed, promoting the vertical migration of dissolved and suspended metal forms, particularly in the central zone with maximum waste accumulation [16].

Surface runoff also plays a significant role by transporting fine contaminated material to lower relief areas and peripheral zones, explaining the persistence of elevated concentrations even at a distance from the landfill center [14]. Under conditions of sparse vegetation and a continental climate, aeolian transport further contributes to the dispersal of contaminated dust and secondary pollution of surrounding areas [15].

Microrelief additionally influences spatial differentiation: depressions act as accumulation zones for moisture, leachate, and fine particles, enhancing local metal concentrations and mobility, especially for arsenic [16].

Thus, the radial gradient of contamination results from the combined effects of infiltration, surface runoff, aeolian transport, and local accumulation, ensuring both vertical and horizontal migration of metals and their long-term persistence after landfill closure [10, 11].

The distribution of Zn, Cu, Pb, and As concentrations across the functional zones of the landfill body, shown in Figure 4, reflects significant differences in the environmental conditions of vegetation cover formation.

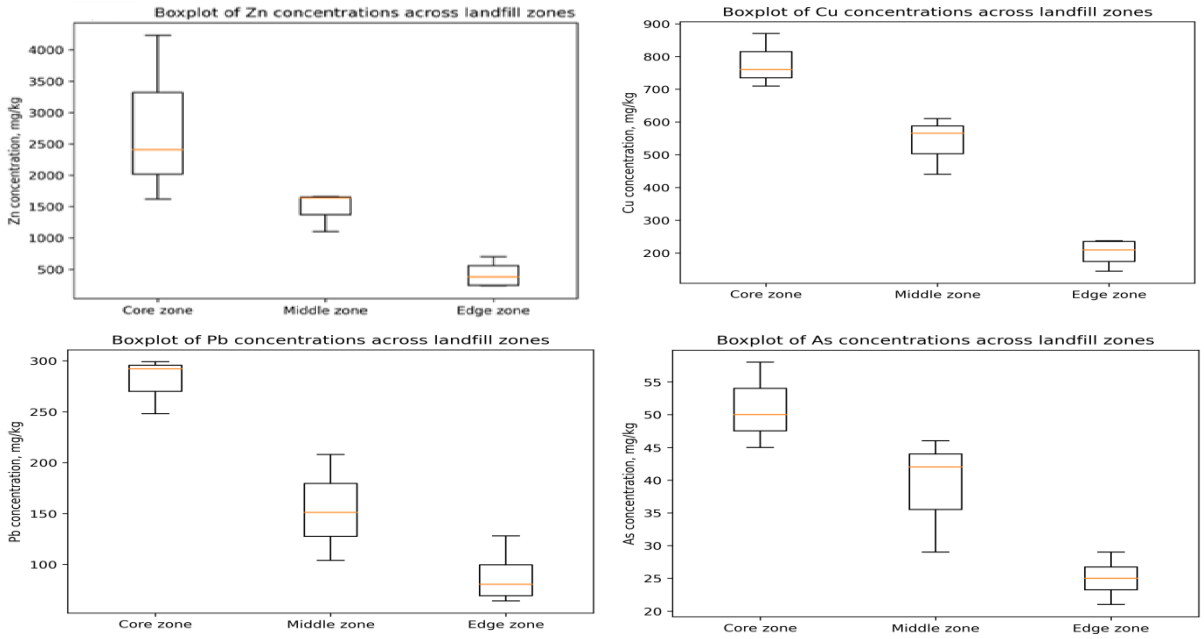

Figure 4. Boxplot of the distribution of Zn, Cu, Pb, and As concentrations by functional zones of the polygon body

The core of the landfill is characterized by the highest median values and significant variability in heavy metal concentrations, which indicates the formation of a pronounced phytotoxic background. Under these conditions, the development of zonal steppe phytocenoses is significantly limited, and the vegetation cover is mainly represented by ruderal and stress-tolerant species with a short life cycle [14].

In the middle part of the landfill, a decrease in pollution levels is accompanied by a partial increase in floral diversity, but persistent elevated concentrations of heavy metals continue to exert selective pressure on vegetation. In the marginal zone, where the median concentrations are minimal, there are signs of restoration

of zonal vegetation elements, but their sustainable development is hindered by residual soil pollution. Thus, the spatial differentiation of the heavy metal content is directly reflected in the structure and composition of the flora and determines the formation of specific anthropogenic phytocenoses on the territory of a closed landfill (Fig. 5).

The revealed high concentrations of heavy metals in the soils of a closed landfill have a decisive effect on the formation and spatial structure of vegetation cover. The recorded dominance of individual taxonomic groups and plant life forms reflects the adaptation of the flora to conditions of sustained anthropogenic and phytotoxic effects.

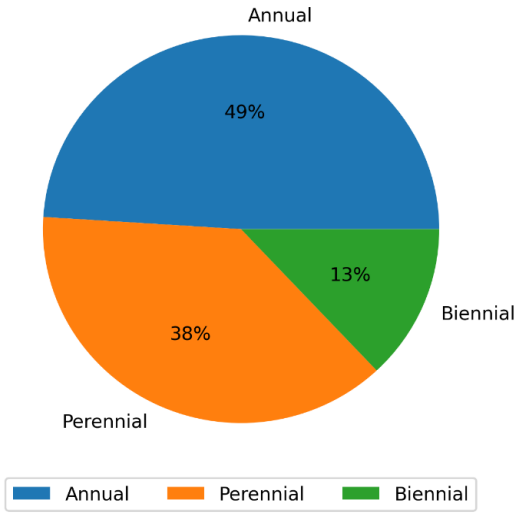

Figure 5. Distribution of plant life forms at the closed MSW landfill in Kokshetau

The found predominance of representatives of the *Asteraceae* (more than 25% of species), *Poaceae, Brassicaceae, and Chenopodiaceae* families is characteristic of anthropogenic disturbed ecosystems and is consistent with an increased content of Zn, Cu, Pb, and As in soils (Fig. 6). Many species of these families have high ecological plasticity, a short life cycle, and the ability to tolerate chemical stress, including heavy metal pollution. This is confirmed by the high participation of annual species (49%), while the share of perennials and biennials is 38% and 13%, respectively, which is typical for disturbed and technogenically transformed territories [12].

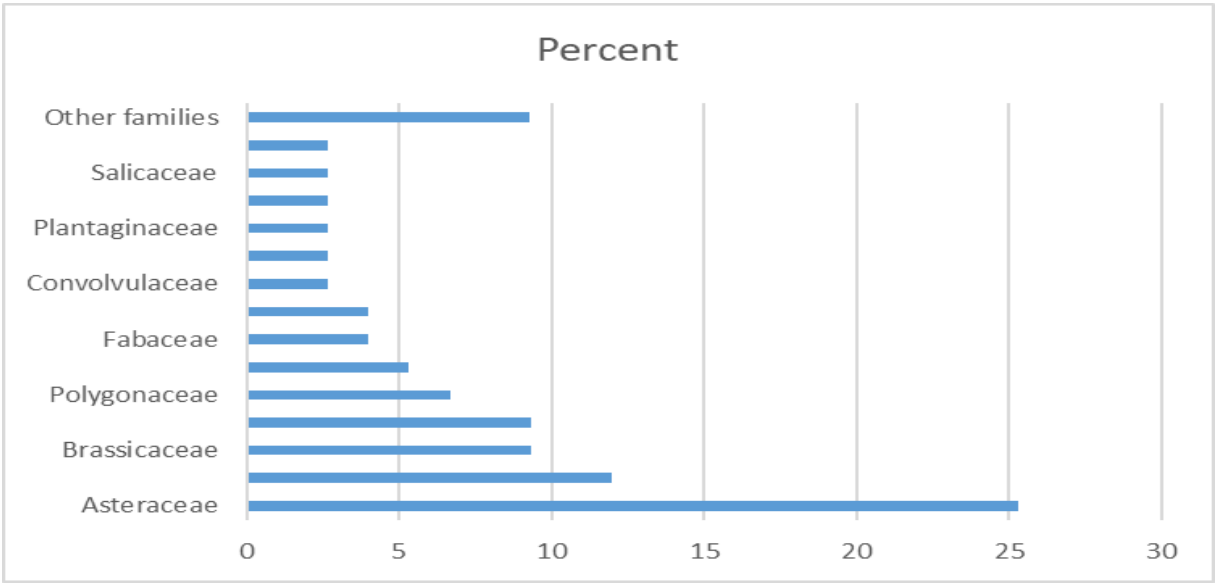

Figure 6. Floristic spectrum of plant species at the closed MSW landfill in Kokshetau (% of total species)

The low representation of woody plants and the predominance of herbaceous vegetation indicate unfavorable edaphic conditions for the formation of stable multi-tiered phytocenoses. Heavy metals, accumulating in the upper technogenically transformed horizon, limit the development of the deep root system and prevent the consolidation of tree species, which explains their sporadic presence in the form of single seedlings [13].

Geobotanical analysis showed that a substantial part of the flora is represented by meadow-steppe species typical of the regional vegetation. However, classical turf-grass steppes of the *Festuco-Brometea* class are largely degraded or only fragmentarily preserved. Their replacement by ruderal and stress-tolerant species indicates a profound transformation of natural phytocenoses under prolonged soil contamination.

The vegetation includes numerous ruderal and stress-tolerant species such as *Bassia scoparia*, *Atriplex patula*, *Chenopodium album*, *Artemisia* spp., and *Plantago major*, which are characteristic of technogenically disturbed environments. These species exhibit high tolerance to salinity, moisture deficit, and elevated heavy metal concentrations, forming the basis of secondary plant communities.

Particular importance is attached to wetland and halophytic species (*Phragmites australis*, *Suaeda prostrata*, *Atriplex patula*, *Persicaria hydropiper*) associated with moist areas and leachate accumulation zones. These habitats are characterized by altered hydrological conditions and increased metal mobility, enhancing selective pressure on vegetation and promoting the formation of specific local phytocenoses [16].

Several species can be considered ecological indicators. In particular, *Bassia scoparia*, *Atriplex patula*, and *Suaeda prostrata* indicate saline and technogenically disturbed soils, while *Phragmites australis* reflects zones of increased moisture and leachate accumulation. Their distribution highlights spatial heterogeneity and the degree of ecosystem transformation.

No widespread occurrence of aggressive invasive species was recorded; however, the presence of synanthropic plants indicates a high level of anthropogenic transformation of the vegetation cover.

The dominance of *Bassia scoparia* (average coverage 21.92%, frequency 50%) with high average projective coverage and frequency of occurrence is indicative from a geobotanical point of view. This species is known as a typical ruderal and halophytic element, resistant to salinity, moisture deficiency, and elevated concentrations of heavy metals. Its wide distribution and the formation of dense thickets in the most polluted areas of the landfill allow us to consider *Bassia scoparia* as a bioindicator of technogenically disturbed and phytotoxic substrates [17, 18].

Thus, the spatial structure of vegetation and its taxonomic composition in a closed landfill directly reflect the level and nature of soil contamination with heavy metals. The formed plant communities are stable anthropogenic phytocenoses dominated by species adapted to chemical stress and disturbed water-soil regime, which confirms the long-term and persistent impact of the landfill on the ecosystem.

Conclusion

The closed municipal solid waste landfill in Kokshetau is characterized by a high level of technogenic soil contamination with heavy metals, formed as a result of the long-term operation of the facility (1960–2017) and the lack of engineering protection systems. The maximum concentrations of zinc, copper, lead and arsenic are many times higher than the maximum permissible and background values, which indicates the persistent nature of soil contamination.

An analysis of the spatial distribution of pollutants revealed a pronounced radial-gradient nature of pollution: the highest levels of concentrations and multiplicity of excess standards were recorded in the central part of the landfill body, while as they move away to the periphery, their consistent decrease is noted. At the same time, concentrations of heavy metals exceeding the background values remain even in the marginal zone, which indicates a long-term preservation of anthropogenic impact after the closure of the landfill.

The calculation of the geoaccumulation index (Igeo) showed that the soils of the central part of the landfill belong to the categories of highly and extremely polluted, primarily by Zn and Pb. Igeo values decrease in the middle and marginal parts, however, levels corresponding to moderate and severe pollution remain for individual elements, which confirms the functional heterogeneity of the polygon body.

The values of the phytotoxic index (FTI) by functional zones indicate the formation of a pronounced phytotoxic background in the central and middle parts of the landfill. The decrease in FTI to the periphery reflects a decrease in chemical stress, but its levels remain sufficient to limit the development of zonal plant communities and maintain conditions of selective pressure on the flora.

Geobotanical studies have shown that soil pollution with heavy metals has a decisive effect on the structure and composition of vegetation cover. The flora of the landfill is mainly represented by herbaceous

and short-lived species, while the proportion of annual plants reaches 49%, which is typical for ecosystems with unstable and phytotoxic edaphic conditions.

The taxonomic structure of vegetation is characterized by the dominance of the *Asteraceae, Poaceae, Brassicaceae and Chenopodiaceae families*, typical of anthropogenic disturbed areas and resistant to chemical stress. The low representation of tree species indicates unfavorable soil conditions for the formation of stable multi-tiered phytocenoses.

The spatial distribution of plant communities is consistent with the soil pollution gradient: ruderal and stress-tolerant phytocenoses are formed in the central zones, while only partially preserved elements of zonal meadow-steppe vegetation are noted in the marginal part. The dominance of *Bassia scoparia* in the most polluted areas allows us to consider this species as a potential bioindicator of technogenically disturbed and phytotoxic substrates.

Considering the identified level of contamination and its spatial heterogeneity, a key priority for future work is the establishment of a systematic environmental monitoring program. Monitoring should include regular assessment of heavy metal concentrations in soils and vegetation, evaluation of phytotoxicity dynamics, and the use of geobotanical and bioindication methods to track ecosystem recovery processes.

A promising and environmentally sound approach to reclamation is phytoremediation, based on the use of pollution-tolerant plant species. Species selection should account for their ability to withstand high concentrations of heavy metals, accumulate them in biomass, stabilize the soil cover, and reduce contaminant mobility. The establishment of a stable vegetation cover will not only limit metal migration but also enhance the ecological resilience of the territory.

In general, a closed MSW landfill should be considered as a sustainably transformed anthropogenic ecosystem in which soil contamination with heavy metals continues to determine environmental conditions and biological processes even after the facility is discontinued. The results obtained emphasize the need to take into account accumulated anthropogenic pollution when assessing the ecological status and developing measures for the reclamation of such territories.

Funding

The research is funded by the Science Committee of the Ministry of Science and Higher Education of the Republic of Kazakhstan. It is supported through grant funding for scientific and/or scientific-technical projects for the years 2024–2026, with project duration of 36 months. Project title: Development of technology for reclamation of a closed solid waste landfill in the Akmola region by creating a model of artificial phytocenoses. Project IRN: AP23487981.

Author contribution

The manuscript was written through contributions of all authors. All authors have given approval to the final version of the manuscript. CRediT: **Bayazitova Z.E**. **—** attracting financing, research, writing a draft, editing, **Kurmanbayeva A.S. —** collecting samples, editing, conceptualization, data processing, methodology; **Safronova N.M**. **—** data processing, methodology, formal analysis, editing; **Japarova S.B**. **—** collecting samples, methodology, preparation of drawings.

Conflict of Interest

The authors declare no conflict of interest.

References

1 Štrbac S. Heavy metal concentrations in soil near illegal landfills: Ecological implications and ANN hazard prediction / S. Štrbac, L. Mandić, B. Škrbić, M. Marković // Journal of Soils and Sediments. — 2024. — Vol. 24(1). — P. 1–17. https://doi.org/10.1007/s11368-023-03637-1

2 Агаркова С.В. Проблемы утилизации твердых бытовых отходов / С.В. Агаркова // Вестник науки. — 2020. — Т. 2, № 3 (24). — С. 71–74.

3 Glazyrin S.A. Analysis of the efficiency and environmental impact of municipal solid waste incineration as a tool for sustainability development in Kazakhstan / S.A. Glazyrin, E.E. Kopishev, M.G. Zhumagulov, Z.A. Bimurzina, Y.K. Aibuldinov // Sustainability. — 2025. — Vol. 17(19). — Article ID 8696. https://doi.org/10.3390/su17198696

4 Kurmanbayeva A. Waste accumulation and geoecological assessment of the territories around the landfills in Kokshetau / A. Kurmanbayeva, Z. Bayazitova, A. Talal, A. Kakabayev, S. Zhaparova // International Journal of GEOMATE. — 2022. — Vol. 23, Iss. 96. — P. 179–185. https://doi.org/10.21660/2022.96. j2384

5 Inglezakis V.J. Municipal solid waste management in Kazakhstan: Astana and Almaty case studies / V.J. Inglezakis, K. Moustakas, G. Khamitovac, D. Tokmurzin, R. Rakhmatulina, B. Serik, Y. Abikak // Chemical Engineering Transactions. — 2017. — Vol. 56. — P. 565–570. https://doi.org/10.3303/CET1756095

6 Aibuldinov Y. K. Analysis of the composition and properties of municipal solid waste in various cities of Kazakhstan / Y.K. Aibuldinov, S.A. Glazyrin, E.E. Kopishev, M.G. Zhumagulov, Z.A. Bimurzina // Energies. — 2024. — Vol. 17(24). — Article ID 6426. https://doi.org/10.3390/en17246426

7 Kaliaskarova Z.K. Soil pollution with heavy metals on the land of the Karasai landfill of municipal solid waste in Almaty city / Z.K. Kaliaskarova, Zh.N. Aliyeva, A.S. Ikanova, E.S.M. Negim // News of the National Academy of Sciences of the Republic of Kazakhstan. Series of Geology and Technical Sciences. — 2019. — Vol. 6(438). — P. 256–267. https://doi.org/10.32014/2019.2518-170X.177.

8 Bayazitova Z.E. Assessment of ecological danger of seepage water solid waste landfill of Kokshetau / Z.E. Bayazitova, A.S. Kurmanbayeva, A.A. Kakabayev, S.B. Zhaparova, G.S. Baituk, A. Zandybay, G.E. Baikenova // Bulletin of Kazakh National Universitety. Ecological series. — 2022. — Vol. 70(1). — P. 46–55. https://doi.org/10.26577/EJE.2022.v70.i1.05

9 Курманбаева А.С. Биорекультивация полигонов твёрдых бытовых отходов / А.С. Курманбаева, З.Е. Баязитова, Н.М. Сафронова // Eurasian Journal of Applied Biotechnology. — 2024. — № 3S.

10 Akter S. Heavy metal contamination of surface soils: concentrations, sources, and ecological risks / S. Akter, A. Huq, M. Uddin // Environmental Geochemistry & Health. — 2025. — Vol. 198. — Article ID 165. https://doi.org/10.1080/03067319.2023.2280180

11 Qi J. Heavy metal contamination in soil and ecological risk assessment near waste disposal sites / J. Qi, Y. Zhang, X. Chen // PeerJ. — 2024. — Vol. 12. — e18510. https://doi.org/10.7717/peerj.18510

12 Гигиенические нормативы ПДК химических веществ в почве. — [Электронный ресурс]. — Режим доступа: https://adilet.zan.kz/rus/docs/V2100022595?utm_source=chatgpt.com

13 Broadley M. R. Zinc in plants / M. R. Broadley, P.J. White, J.P. Hammond, I. Zelko, A. Lux // New Phytologist. — 2007. — Vol. 173(4). — P. 677–702. https://doi.org/10.1111/j.1469-8137.2007.01996.x

14 Finnegan P. M. Arsenic toxicity: the effects on plant metabolism / P.M. Finnegan, W. Chen // Frontiers in Physiology. — 2012. — Vol. 3. — Article ID 182. https://doi.org/10.3389/fphys.2012.00182

15 Cai S. Assessment of metal pollution and effects of physicochemical factors on soil microbial communities around a landfill / S. Cai, S. Zhou, Q. Wang, J. Cheng, B. Zeng // Ecotoxicology and Environmental Safety. — 2024. — Vol. 271. — Article ID 115968. https://doi.org/10.1016/j.ecoenv.2024.115968

16 Khan S. Global soil pollution by toxic elements: Current status and future perspectives / S. Khan, M. Naushad, E.C. Lima, et al. // Science of the Total Environment. — 2021. — Vol. 778. — P. 146–171. https://doi.org/10.1016/j.scitotenv.2021.146171

17 Nagajyoti P. C. Heavy metals, occurrence and toxicity for plants / P.C. Nagajyoti, K.D. Lee, T.V.M. Sreekanth // Environmental Chemistry Letters. — 2010. — Vol. 8. — P. 199–216. https://doi.org/10.1007/s10311-010-0297-8

18 Prach K. Four opportunities for studies of ecological succession / K. Prach, L. R. Walker // Trends in Ecology & Evolution. — 2011. — No. 26. — P. 119–123. https://doi.org/10.1016/j.tree.2010.12.007

З.Е. Баязитова, А.С. Құрманбаева, Н.М. Сафронова, С.Б. Жапарова

Көкшетау қаласындағы қатты тұрмыстық қалдықтар жабық полигонының топырақ пен өсімдік жамылғысының жағдайын экологиялық және биологиялық бағалау

Көкшетау қаласындағы 1960–2017 жылдары пайдаланылған, инженерлік қорғаныс жүйелерімен жабдықталмаған жабық қатты тұрмыстық қалдықтар (ҚТҚ) полигонының экологиялық жағдайы ауыр металдармен ластану және оның өсімдік жамылғысына әсері тұрғысынан бағаланды. Топырақ талдауы Zn, Cu, Pb және As элементтері бойынша шекті рұқсат етілген және фондық концентрациялардың бірнеше есе артқанын көрсетті. Максималды концентрациялар келесідей болды: Zn — 4230 мг/кг, Cu — 870 мг/кг, Pb — 299 мг/кг, As — 58 мг/кг және Ni — 145 мг/кг, бұл шекті рұқсат етілген концентрациялардан тиісінше 42,3; 15,8; 9,3; 29,0 және 3,6 есе жоғары. Фондық мәндермен салыстырғанда элементтердің мөлшері Zn үшін 48,1 есе, Cu үшін 8,5 есе, Pb үшін 19,9 есе, As үшін 4,1 есе және Ni үшін 3,2 есе артқан. Ластанудың айқын радиалды-градиенттік сипаты анықталды: ең жоғары концентрациялар мен нормативтік көрсеткіштердің артуы полигон денесінің орталық бөлігінде тіркеліп, шеткі аймақтарға қарай біртіндеп төмендеген. Алайда шеткі учаскелердің өзінде фондық деңгейден жоғары концентрациялар сақталып, полигон жабылғаннан кейін де антропогендік әсердің тұрақты екенін көрсетті. Геоаккумуляция индексі (Igeo) бойынша орталық аймақ топырақтары, әсіресе Zn және Pb элементтері тұрғысынан, күшті және аса күшті ластанған санатқа жатқызылды. Фитоуыттылық индексі (FTI) орталық және ортаңғы аймақтарда айқын фитоуытты фонның қалыптасқанын растады. Геоботаникалық зерттеулер өсімдік қауымдастықтарының елеулі трансформацияға ұшырағанын көрсетті. Флора негізінен шөптесін және қысқа өмірлі түрлермен сипатталады, біржылдық өсімдіктердің үлесі 49 %-ды құрайды. Таксономиялық құрылымында

Asteraceae, Poaceae, Brassicaceae және Chenopodiaceae тұқымдастары басым, бұл антропогендік бұзылған және химиялық стресс жағдайларына тән. Жоғары деңгейде ластанған учаскелерде *Bassia scoparia* түрінің басымдығы оны техногендік бұзылған субстраттардың әлеуетті биоиндикаторы ретінде қарастыруға мүмкіндік береді. Жалпы алғанда, жабық ҚТҚ полигоны ауыр металдардың жинақталған ластануы экологиялық жағдай мен биологиялық үдерістерді айқындауды жалғастырып отырған тұрақты трансформацияланған антропогендік экожүйе. Бұл жағдай кешенді мониторинг пен рекультивация стратегияларын әзірлеудің қажеттілігін көрсетеді.

Кілт сөздер: қатты тұрмыстық қалдықтар полигоны, топырақтың ластануы, фитоуыттылық, антропогендік әсер, ауыр металдар, экожүйенің бұзылуы.

З.Е. Баязитова, А.С. Курманбаева, Н.М Сафронова, С.Б. Жапарова

Эколого - биологическая оценка состояния почв и растительного покрова закрытого полигона твёрдых бытовых отходов в г. Кокшетау

Проведена оценка экологического состояния закрытого полигона твёрдых бытовых отходов (ТБО) в г. Кокшетау, эксплуатировавшегося в 1960–2017 гг. и не оснащённого инженерными защитными системами, с акцентом на загрязнение тяжёлыми металлами и его влияние на растительный покров. Анализ почв выявил многократные превышения предельно допустимых и фоновых концентраций Zn, Cu, Pb и As. Максимальные концентрации составили: Zn — 4230 мг/кг, Cu — 870 мг/кг, Pb — 299 мг/кг, As — 58 мг/кг и Ni — 145 мг/кг, что превышает предельно допустимые концентрации соответственно в 42,3; 15,8; 9,3; 29,0 и 3,6 раза. По сравнению с фоновыми значениями содержание элементов увеличено в 48,1 раза для Zn, в 8,5 раза для Cu, в 19,9 раза для Pb, в 4,1 раза для As и в 3,2 раза для Ni. Установлен выраженный радиально-градиентный характер загрязнения: максимальные концентрации и кратность превышения нормативов зафиксированы в центральной части тела полигона с последующим постепенным снижением к периферии. Однако даже в краевых зонах отмечаются значения выше фоновых уровней, что свидетельствует о сохранении устойчивого антропогенного воздействия после закрытия объекта. Расчёт индекса геоаккумуляции (Igeo) показал, что почвы центральной части относятся к категории сильно и экстремально загрязнённых, прежде всего по Zn и Pb. Значения фитотоксического индекса (FTI) подтвердили формирование выраженного фитотоксического фона в центральной и средней зонах полигона. Геоботанические исследования выявили существенную трансформацию растительных сообществ. Флора представлена преимущественно травянистыми и короткоживущими видами; доля однолетних растений составляет 49 %. Таксономическая структура характеризуется доминированием семейств *Asteraceae, Poaceae, Brassicaceae* и *Chenopodiaceae*, типичных для нарушенных и химически стрессированных местообитаний. Преобладание *Bassia scoparia* в наиболее загрязнённых участках позволяет рассматривать данный вид как потенциальный биоиндикатор техногенно нарушенных субстратов. В целом закрытый полигон ТБО представляет собой устойчиво трансформированную антропогенную экосистему, в которой накопленное загрязнение тяжёлыми металлами продолжает определять экологические условия и биологические процессы, что подчёркивает необходимость комплексного мониторинга и разработки мер рекультивации.

Ключевые слова: полигон твёрдых бытовых отходов, загрязнение почв, фитотоксичность, антропогенное воздействие, тяжёлые металлы, нарушение экосистемы.

References

1 Štrbac, S., Mandić, L., Škrbić, B., & Marković, M. (2024). Heavy metal concentrations in soil near illegal landfills: Ecological implications and ANN hazard prediction. *Journal of Soils and Sediments, 24*(1), 1–17. https://doi.org/10.1007/s11368-023-03637-1

2 Agarkova, S. V. (2020). Problemy utilizatsii tverdykh bytovykh otkhodov [Problems of municipal solid waste disposal]. *Vestnik nauki — Science Bulletin, 2,* 3(24), 71–74 [in Russian].

3 Glazyrin, S. A., Kopishev, E. E., Zhumagulov, M. G., Bimurzina, Z. A., & Aibuldinov, Y. K. (2025). Analysis of the efficiency and environmental impact of municipal solid waste incineration as a tool for sustainability development in Kazakhstan. *Sustainability, 17*(19), 8696. https://doi.org/10.3390/su17198696

4 Kurmanbayeva, A., Bayazitova, Z., Talal, A., Kakabayev, A., & Zhaparova, S. (2022). Waste accumulation and geoecological assessment of the territories around the landfills in Kokshetau. *International Journal of GEOMATE, 23*(96), 179–185. https://doi.org/10.21660/2022.96. j2384

5 Inglezakis, V. J., Moustakas, K., Khamitovac, G., Tokmurzin, D., Rakhmatulina, R., Serik, B. & Abikak, Y. (2017). Municipal solid waste management in Kazakhstan: Astana and Almaty case studies. *Chemical Engineering Transactions, 56*, 565–570. https://doi.org/10.3303/CET1756095

6 Aibuldinov, Y. K., Glazyrin, S. A., Kopishev, E. E., Zhumagulov, M. G., & Bimurzina, Z. A. (2024). Analysis of the composition and properties of municipal solid waste in various cities of Kazakhstan. *Energies, 17*(24), 6426. https://doi.org/10.3390/en17246426

7 Kaliaskarova, Z. K., Aliyeva, Zh. N., Ikanova, A. S., & Negim, E. S. M. (2019). Soil pollution with heavy metals on the land of the Karasai landfill of municipal solid waste in Almaty city. *News of the National Academy of Sciences of the Republic of Kazakhstan. Series of Geology and Technical Sciences, 6*(438), 256–267. https://doi.org/10.32014/2019.2518-170X.177.

8 Bayazitova, Z. E., Kurmanbayeva, A. S., Kakabayev, A. A., Zhaparova, S. B., Baituk, G. S., Zandybay, A., & Baikenova, G. E. (2022). Assessment of ecological danger of seepage water solid waste landfill of Kokshetau. *Bulletin of Kazakh National Universiteti, Ecological series, 70*(1), 46–55. https://doi.org/10.26577/EJE.2022.v70.i1.05

9 Kurmanbayeva, A. S., Bayazitova, Z. E., & Safronova, N. M. (2024). Biorekultivatsiia poligonov tverdykh bytovykh otkhodov [Biorecultivation of municipal solid waste landfills]. *Eurasian Journal of Applied Biotechnology*, 3(Suppl.).

10 Akter, S., Huq, A., & Uddin, M. (2025). Heavy metal contamination of surface soils: concentrations, sources, and ecological risks. *Environmental Geochemistry & Health, 198*, 165. https://doi.org/10.1080/03067319.2023.2280180

11 Qi, J., Zhang, Y., & Chen, X. (2024). Heavy metal contamination in soil and ecological risk assessment near waste disposal sites. *PeerJ, 12*, e18510. https://doi.org/10.7717/peerj.18510

12 (2026). Gigienicheskie normativy PDK khimicheskikh veshchestv v pochve [Hygienic standards for maximum permissible concentrations (MPC) of chemical substances in soil]. *adilet.zan.kz*. Retrieved from https://adilet.zan.kz/rus/docs/V2100022595 [in Russian].

13 Broadley, M. R., White, P. J., Hammond, J. P., Zelko, I., & Lux, A. (2007). Zinc in plants. *New Phytologist, 173*(4), 677–702. https://doi.org/10.1111/j.1469-8137.2007.01996.x

14 Finnegan, P. M., & Chen, W. (2012). Arsenic toxicity: the effects on plant metabolism. *Frontiers in Physiology, 3*, 182. https://doi.org/10.3389/fphys.2012.00182

15 Cai, S., Zhou, S., Wang, Q., Cheng, J., & Zeng, B. (2024). Assessment of metal pollution and effects of physicochemical factors on soil microbial communities around a landfill. *Ecotoxicology and Environmental Safety, 271*, 115968. https://doi.org/10.1016/j.ecoenv.2024.115968

16 Khan, S., Naushad, M., Lima, E. C. et al. (2021). Global soil pollution by toxic elements: Current status and future perspectives. *Science of the Total Environment, 778*, 146–171. https://doi.org/10.1016/j.scitotenv.2021.146171

17 Nagajyoti, P. C., Lee, K. D., & Sreekanth, T. V. M. (2010). Heavy metals, occurrence and toxicity for plants. *Environmental Chemistry Letters, 8*, 199–216. https://doi.org/10.1007/s10311-010-0297-8

18 Prach, K., & Walker, L. R. (2011). Four opportunities for studies of ecological succession. *Trends in Ecology & Evolution*, 26, 119–123. https://doi.org/10.1016/j.tree.2010.12.007

Information about the authors

Bayazitova Zulfiya Erzatovna — Candidate of Biological Sciences, Professor, Department of Mining, Construction and Ecology, Sh. Ualikhanov Kokshetau University, Kokshetau, Kazakhstan; e-mail: z_bayazitova@mail.ru; ORCID: https://orcid.org/0000-0002-1106-0573

Kurmanbayeva Aigul Saparbekovna — Candidate of Biological Sciences, Professor, Department of Mining, Construction and Ecology, Sh. Ualikhanov Kokshetau University, Kokshetau, Kazakhstan; e-mail: akurmanbayeva@shokan.edu.kz; ORCID: https://orcid.org/0000-0002-6133-3226

Safronova Natalya Mikhailovna — Candidate of Biological Sciences, Professor, Department of Biology and Teaching Methods, Sh. Ualikhanov Kokshetau University, Kokshetau, Kazakhstan; e-mail: natalyasafronova@shokan.edu.kz; ORCID: https://orcid.org/0000-0001-5176-4404

Zhaparova Sayagul Beketovna — Candidate of Biological Sciences, Professor, Department of Mining, Construction and Ecology, Sh. Ualikhanov Kokshetau University, Kazakhstan; e-mail: zhaparova.saya77@gmail.com; ORCID: https://orcid.org/0000-0002-5346-5528

How to Cite: Vdovina, T.A., Anufrieva, O.A., Vinokurov, A.A., Danilova, A.N., Sumbembaev, A.A., Chernakova, A.A. (2026). Flora of anthropogenically disturbed territories of the Ridder Metallurgical Complex. *Fundamental and Experimental Biology*, 31, 3 (123), 56-65. https://doi.org/10.31489/2026FEB3/56-65

Research Article

https://doi.org/10.31489/2026FEB3/56-65

UDC 58.02 Received: 18.03.2026 | Accepted: 8.06.2026 | Published online: 30.09.2026

T.A. Vdovina, O.A. Anufrieva, A.A. Vinokurov, A.N. Danilova, A.A. Sumbembaev, A.A. Chernakova*

Altai Botanical Garden, Ridder, Kazakhstan
**Corresponding author: dolmatova-1986@bk.ru*

Flora of anthropogenically disturbed territories of the Ridder Metallurgical Complex

The aim of this study is to provide a comprehensive ecological assessment of the vegetation cover of technogenically disturbed territories of the Ridder Metallurgical Complex based on an analysis of floristic composition, life forms, and ecological plant groups, in order to determine succession pathways and substantiate biological reclamation measures. As part of the study, a comprehensive research program was implemented jointly with the IBBR "Institute of Plant Biology and Biotechnology" to investigate the phytocenoses of technogenic landscapes and the composition of their soils. The studied territory is characterized by a high degree of anthropogenic disturbance. The floristic composition was analyzed, comprising 126 species belonging to 38 families and 93 genera. The families Rosaceae (11 genera), Cyperaceae and Asteraceae (9 genera each), and Poaceae (7 genera) were the most prominent in the taxonomic spectrum. The spatial distribution, abundance, life forms, and condition of the plants were determined. A bioecological characterization of the species and their life forms (ecomorphs) was provided, and ecological groups of plants with respect to moisture requirements were identified. The results made it possible to assess the degree of disturbance of the territory and predict the direction of vegetation succession. The vegetation cover is predominantly composed of native, ecologically stable species, reflecting their adaptation to anthropogenic habitats. The findings contribute to the restoration of technogenically disturbed lands and their rehabilitation for integration into the biosphere.

Keywords: flora, species, technogenically disturbed territories, enterprises of the Ridder Metallurgical Complex, life form, plant condition, ecomorph, ecosystem.

Introduction

East Kazakhstan Region is one of the most anthropogenically transformed regions of Kazakhstan, where rich metal deposits, developed industry, mountainous relief, steppe and forest ecosystems are combined. This leads to a sharp contrast between natural and disturbed landscapes. The city of Ridder is located in the East Kazakhstan Region, within the Rudny Altai—a region rich in polymetallic ores (zinc, lead, copper, silver, gold). The presence of these deposits predetermined the industrial specialization of the territory, including ore mining, its beneficiation, and preparation of concentrates for metallurgical plants. The Ridder Metallurgical Complex (RMC) is one of the largest polymetallic enterprises in Kazakhstan, the intensive development of which has led to the accumulation of tailings storage facilities, soil and water pollution, and the formation of technogenic landscapes. With the growth of environmental problems, it became clear that without land restoration ecological balance is disrupted, fertile territories are lost, and the living conditions of the population deteriorate.

Land reclamation (industrial sites) of the Ridder Metallurgical Complex was actively carried out in the 1980s by employees of the Main Botanical Garden (Almaty) and the Altai Botanical Garden (Ridder). The work carried out was aimed at restoring the biological productivity and economic value of disturbed lands, as well as improving the conditions of the surrounding natural environment.

Studies on the flora of disturbed territories are presented in extensive literature [1–3]. One of the significant technogenic factors affecting the state of ecosystems and biodiversity is the high susceptibility of the soil and vegetation cover to the influence of heavy metals that accumulate in the soil. The results of studies conducted by domestic and foreign scientists show that these issues remain relevant to this day and acquire particular importance [4–8].

These studies directly contribute to the restoration of technogenically disturbed lands and their return to the biosphere fund. In order to restore disturbed areas and prevent their harmful impact on the natural environment, further reclamation is required, in the process of which the motivated formation of landscapes and the creation of a certain natural environment are always taken into account, as well as the study of mechanisms of natural restoration of ecosystems and the investigation of flora [9].

Plant communities (phytocenosis) are a set of plants growing together in the same territory, interconnected with each other and with the environment, performing ecosystem functions: soil-protective, water-regulating, environment-forming, and sanitary-hygienic. On anthropogenically disturbed lands, the structure of plant communities differs significantly from natural ones due to changes in soil, microclimate, and the level of anthropogenic impact.

Experimental

The names of accepted genera and species of vascular plants forming plant communities were verified with the online World Plants catalog of the website Plants of the World Online (POWO, 2025) [10]. The studies were carried out from May to October during the vegetation periods of 2023–2025, when active plant growth and vegetation occur. The Ridder Metallurgical Complex (RMC) belongs to the mountain-taiga zone. As a result of the research, 23 sample plots (loci) were established using random and regular methods in the zone of influence of harmful emissions (tailings of the Concentration Plant, the Zinc Plant, the Ridder and Sokolny mines). The size of the sampling plots ranged from 150 m² to 200 m² in the form of a square or rectangle. The coordinates of the plot locations were determined using a GPS navigator "Garmin". To assess the abundance–cover of species in phytocenoses of technogenic landscapes, the Braun-Blanquet method with the r–5 scale was used, which allows comparison of vegetation on experimental plots.

The vitality of species was determined using a 3-point scale: 3a—the species in a given phytocenosis completes the full development cycle and develops normally, including fruiting; 3b—the species passes through all stages of development but does not reach its usual size; 2—the species is vegetatively developed fairly well but does not bear fruit; 1—the species does not bear fruit and is strongly suppressed, with weak vegetation.

At each sample plot, the vital condition of all present trees, shrubs, and perennial herbs was assessed. The condition of woody plants was evaluated using a 5-point scale: 5—healthy trees without external signs of damage; 4—weakened trees with isolated damaged or drying leaves and branches; 3—strongly weakened trees with drying of branches up to 1/3; 2—drying trees with branch dieback up to 2/3; 1—with more than 2/3 of branches dried.

The distribution of plants according to the water regime was determined by plant moisture requirements: mesophytes, xeromesophytes, hygromesophytes, xerophytes, and hygrophytes. The biomorphological composition of the flora was determined according to the classical system of life-form classification (tree, shrub, semi-shrub, perennial herbaceous, biennial, annual—Raunkiær C. "The Life Forms of Plants and Statistical Plant Geography" (1907) [11].

Results and Discussion

The study of the flora of anthropogenically disturbed territories of the RMC was carried out on 23 plots, where the natural vegetation has been destroyed and significantly altered as a result of its activities (quarries, mines, dumps, tailings storage facilities) (Fig. 1).

Anthropogenic phytocenoses are plant communities that have formed or been significantly altered as a result of human activity. They differ from natural phytocenoses by their simplified structure, instability, and specific species composition, but they play an important role in landscape dynamics and the restoration of disturbed territories.

The formation of vegetation cover occurs in several stages (successions). Succession is a regular process of sequential replacement of plant communities in the same area over time. It occurs under the influence of changing environmental conditions, including those caused by human activity. For anthropogenically disturbed territories, succession is the main mechanism of natural ecosystem restoration [12–14].

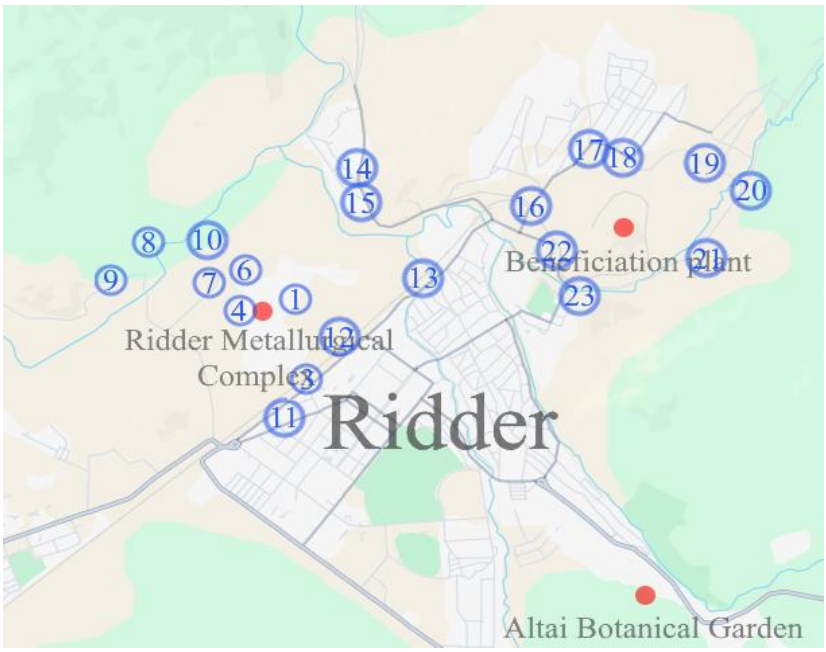

Figure 1. Location of the RMC experimental plots

The main stages of succession in anthropogenic territories include the herbaceous stage, an increase in species diversity, and the formation of a stable herbaceous cover composed of perennial herbaceous plants, mixed herbs, grasses, and legumes. This stage has ecological significance in active soil formation, accumulation of organic matter, and improvement of the microclimate. Soil is one of the most important components of the ecosystem and plays a crucial role in the formation and restoration of vegetation, especially on anthropogenically disturbed lands. The condition of the soil largely determines the possibility, speed, and direction of vegetation recovery.

The next shrub stage involves the appearance of woody-shrub forms, with increased competition for light and moisture. The tree stage forms a relatively stable plant community, with a structure approaching that of the natural vegetation of the zone. This is the final stage of succession under stable conditions.

When studying the spatial distribution of trees and shrubs on the plots, either even or grouped distribution patterns were observed.

During the study of the flora on the plots of the Ridder Metallurgical Complex, a species list was compiled. In the taxonomic list of 38 families, the leading families are Rosaceae — 11 genera, Cyperaceae and Asteraceae — 9 genera each, Poaceae — 7 genera, Fabaceae, Apiaceae, Plantaginaceae — 4 genera each, Brassicaceae, Caryophyllaceae, Malvaceae — 3 genera each. The remaining families include 1 to 2 genera (Tab. 1).

Table 1

Floristic composition of the plant cover of disturbed territories of the RMC

Family	Genus	Species
Sapindaceae	*Acer* L.	*Acer ginnala* Maxim., *Acer negundo* L., *Acer tataricum* L.
Salicaceae	*Populus* L.	*Populus laurifolia* Ledeb., *Populus tremula* L., *Populus nigra* L.
	Salix L.	*Salix acutifolia* Willd., *Salix alba* L., *Salix cinerea* L., *Salix integra* Thunb., *Salix rorida* Laksch., *Salix daphnoides* Vill., *Salix pentandra* L., *Salix viminalis* L.
Betulaceae	*Betula*L.	*Betula pendula* Roth, *Betula pubescens* Ehrh
Rosaceae	*Malus* Mill.	*Malus baccata* (L.) Borkh.
	Prunus L.	*Prunus padus* L.
	Sorbus L.	*Sorbus sibirica* Hedl
	Amelanchier Medik.	*Amelanchier alnifolia* (Nutt.) Nutt. ex M.Roem
	Spiraea L.	*Spiraea chamaedryfolia* L

Continuation of Table 1

Family	Genus	Species
Rosaceae	*Rosa* L.	*Rosa acicularis* Lindl
	Rubus L.	*Rubus saxatilis* L., *Rubus sachalinensis* Lévl
	Fragaria L.	*Fragaria viridis* (Duchesne) Weston
	Geum L.	*Geum urbanum* L.
	Agrimonia L.	*Agrimonia pilosa* Ledeb.
	Sorbaria(Ser.) A.Braun	*Sorbaria sorbifolia* (L.) A.Braun
Pinaceae	*Larix* Mill.	*Larix sibirica* Ledeb.
	Pinus L.	*Pinus sylvestris* L.
Oleaceae	*Fraxinus* L.	*Fraxinus pennsylvanica* Marshall
Adoxaceae	*Viburnum* L.	*Viburnum opulus* L.
Caprifoliaceae	*Lonicera* L.	*Lonicera tatarica* L.
Poaceae	*Calamagrostis* Adans.	*Calamagrostis epigeios* (L.) Roth, *Calamagrostis purpurea* (Trin.) Trin.
	Poa L.	*Poa pratensis* L., *Poa attenuata* Trin.
	Festuca L.	*Festuca pratensis* Huds., *Festuca rubra* L., *Festuca valesiaca* Schleich. ex Gaudin
	Phleum L.	*Phleum pratense* L., *Phleum phleoides* (L.) H.Karst.
	Phragmites Adans.	*Phragmites australis* (Cav.) Trin. ex Steud.
	Dactylis L.	*Dactylis glomerata* L.
	Bromopsis Fourr.	*Bromopsis inermis* (leyss.) Lindm.
	*Leymus*Hochst.	*Leymus angustus* (Trin.) Pilg
	Elymus L.	*Elymus repens* (L.) Gould, *Elymus* geniculatus (Trin.)
	Agrostis L.	*Agrostis stolonifera* L.
Cyperaceae	*Carex*L.	Carex *pediformis var. macroura* (Meinsh.) Kük
Asteraceae	*Artemisia* L.	*Artemisia absinthium* L.. *Artemisia vulgaris* L.
	Arctium L.	*Arctium tomentosum* Mill.
	Tanacetum L.	*Tanacetum vulgare* L.
	Achillea L.	*Achillea millefolium*L.
	Carduus L.	*Carduus crispus* L.. *Carduus nutans* L.
	Cirsium Mill.	*Cirsium vulgare* (Savi) Ten.
	Tussilago L.	*Tussilago farfara*L.
	Tripleurospermum Sch.Bip.	*Tripleurospermum perforatum* (Mérat) M.Lainz
	Galatella Cass.	*Galatella hauptii* (Ledeb.) Lindl., *Galatella punctata* (Waldst. & Kit.) Nees
	*Inula*L.	*Inula britannica* L..*Inula helenium* L.
	Echinops L.	*Echinops tricholepis* Trautv.
	Serratula L.	*Serratula coronata* L.
	Taraxacum F.H. Wigg.	*Taraxacum officinale* F.H. Wigg.
	Hieracium L.	*Hieracium umbellatum* L.
Fabaceae	*Vicia* L.	*Vicia sepium* L., *Vicia cracca* L., *Vicia silvatica* L.
	*Trifolium*L.	*Trifolium hybridum* L., *Trifolium lupinaster* L., *Trifolium repens* L., *Trifolium pratense* L.
	Medicago L.	*Medicago falcata* L.
	Melilotus Mill.	*Melilotus albus* Medik.
Brassicaceae	*Armoracia* Gaertn.	*Armoracia rusticana* P.Gaertn., B.Mey. & Scherb.
	*Bunias*L.	*Bunias orientalis* L.
	Berteroa DC.	*Berteroa incana* (L.) DC.
Apiaceae	*Angelica* L.	*Angelica decurrens* (Ledeb.) B. Fedtsch., *Angelica sylvestris* L.
	Heracleum L.	*Heracleum dissectum* Ledeb.
	Carum L.	*Carum carvi* L.
	Bupleurum L.	*Bupleurum longifolium* subsp. aureum (Fisch. ex Hoffm.) Soo
Lamiaceae	*Origanum* L.	*Origanum vulgare* L.
	Stachys L.	*Stachys silvatica* L.
Polygonaceae	*Aconogonon* Schrank**.**	*Aconogonon alpinum* (All.) Schur
Urticaceae	*Urtica* L.	*Urtica dioica* L.

Continuation of Table 1

Family	Genus	Species
Chenopodiaceae	*Chenopodium* L.	*Chenopodium album* L.
	Kochia Scop.	*Kochia prostrata* (L.) Schrad.
Typhaceae	*Typha* L.	*Typha angustifolia* L.
Valerianaceae	*Va*leriana L.	*Valeriana officinalis* L.
Caryophyllaceae	*Silene* L.	*Silene repens* Patrin ex Pers., *Silene vulgaris* (Moench) Garcke
	Gypsophila L.	*Gypsophila altissima* L.
	Dianthus L.	*Dianthus superbus* L.
Iridaceae	*Iris* L.	*Iris ruthenica* Ker Gawl.
Campanulaceae	*Campanula* L.	*Campanula* rapunculoides L.
Malvaceae	*Lavatera* L.	*Lavatera thuringiaca* L.
	Alcea Mill.	*Alcea nudiflora* (Lindl.) Boiss., *Alcea rosea* L.
	Malva L.	*Malva pusilla* Sm.
Boraginaceae	*Pulmonaria* L.	*Pulmonaria mollis* Wulfen ex Hornem.
Plantaginaceae	*Plantago* L.	*Plantago major* L.
	Linaria L.	*Linaria vulgaris* Mill.
	Veronica L.	*Veronica krylovii* Schichk.
	Dodartia L.	*Dodartia orientalis* L.
Euphorbiaceae	*Euphorbia* L.	*Euphorbia latifolia* C.A Mey.
Hypericaceae	*Hypericum* L.	*Hypericum perforatum* L.
Papaveraceae	*Chelidonium* L.	*Chelidonium majus* L.
Equisetaceae	*Equisetum* L.	*Equisetum sylvaticum* L., *Equisetum arvense* L., *Equisetum hyemale* L., *Equisetum palustre* L.
Asparagaceae	*Allium* L.	*Allium rubens* Schrad. ex Willd.
Geraniaceae	*Geranium* L.	*Geranium pratense* L.
Convolvulaceae	*Convolvulus* L.	*Convolvulus arvensis* L.
Grossulariaceae	*Ribes* L.	*Ribes aureum* Pursh
Scrophulariaceae	*Verbascum* L.	*Verbascum thapsus* L.
Rubiaceae	*Galium* L.	*Galium boreale* L. *Galium verum* L.
Crassulaceae	*Sedum* L.	*Sedum purpureum* (L.) Schult.
Onagraceae	*Epilobium* L.	*Epilobium angustifolium* L.

The most species-rich and dominant genera in the flora of the disturbed territories of the Ridder Metallurgical Complex are: *Trifolium* — 9 species (7.3 %), *Salix* — 8 species (6.5 %), *Equisetum* — 4 species (3.1 %), *Acer* and *Populus* — 3 species each (4.8 %). 11 genera have two species each, accounting for 11.4 %, while the remaining genera (66.9 %) have only 1 species.

The number of species per plot ranges from 14 to 23. Species abundance is as follows: 104 species (82.5 %) are represented on only some plots — from 1 to 7, and 12 species (9.6 %) are represented on 8 to 13 plots (Fig. 2).

They include: *Betula pendula*, *Betula pubescens*, *Malus baccata*, *Elymus repens*, *Phleum phleoides*, *Vicia sepium*, *Vicia cracca*, *Armoracia rusticana*, *Trifolium pratense*, *Trifolium hybridum*, *Tussilago farfara*, *Hypericum perforatum*

Species such as *Acer negundo*, *Populus laurifolia*, *Calamagrostis epigeios*, *Dactylis glomerata*, *Artemisia vulgaris*, *Arctium tomentosum*, *Cirsium vulgare*, *Echium vulgare*, *Convolvulus arvensis*, *Bunias orientalis*, and *Urtica dioica* are widely distributed on nearly all industrial plots, ranging from 14 to 22 sites, which corresponds to 7.9 % in percentage terms. Compared to 7 other industrial enterprises in the East Kazakhstan Region, the RMC exhibits the highest species diversity with 126 species — 157.5 %, which is associated with a richer natural flora. This accounts for almost half of the species (49.1 %) of the total number of species (255) across all surveyed industrial plots of the enterprises.

The ecological plasticity of plants plays a crucial role in the formation of vegetation cover on disturbed lands. This characteristic enables species to adapt to changing environmental conditions while maintaining viability, growth, and reproduction. For anthropogenically disturbed territories, ecological plasticity is one of the key factors for plant survival and successful colonization. On disturbed lands, the advantage is given to

plants that are resistant to soil compaction, tolerant to pollution, capable of rapid recovery after damage, and able to grow and disperse quickly. Typical plant groups include ruderal species, pioneer plants, weed herbs, and certain shrubs.

Species	Number of plots																						
	1	2	3	4	5	6	7	8	9	10	11	12	13	14	15	16	17	18	19	20	21	22	23
Acer negundo L.			+	+	+	+		+	+	+	+	+	+	+	+	+	+	+	+	+	+	+	
Acer tataricum L.			+								+						+						
Populus nigifolia Ledeb.	+		+	+			+																+
Populus tremula L.		+	+			+									+								
Populus balsamifera	+		+					+	+	+	+		+		+	+	+	+			+		
Betula pendula Roth		+	+	+			+	+	+		+		+	+		+						+	
Betula pubescens Ehrh.	+			+	+	+				+		+		+	+					+	+		
Malus baccata (L.) Borkh.	+				+							+	+		+		+						
Pinus sylvestris L.	+		+	+			+	+	+														
Viburnum opulus L.											+											+	
Padus avium Mill.										+	+	+						+					
Salix alba L.									+			+											
Salix cinerea L.			+	+		+					+	+									+		
Salix pentandra L.							+	+	+		+		+							+			
Salix daphnoides Vill.								+						+									
Salix viminalis L.		+					+				+							+	+				
Calamagrostis arundinacea (L.) Roth	+	+	+	+	+	+		+	+		+		+	+	+		+			+			
Elymus repens (L.) Nevski	+	+	+			+		+			+	+							+			+	+
Filipendula ulmaria																	+						
Dactylis glomerata L.	+	+			+	+	+	+	+	+	+	+	+		+		+	+	+	+	+	+	+
Phleum pratense L.		+						+	+						+				+				+
Phleum phleoides (L.) H. Karst.								+			+	+	+	+				+				+	
Artemisia vulgaris L.	+	+	+	+	+	+	+	+	+	+	+	+		+	+	+	+	+	+	+	+	+	+
Artemisia absinthium L.								+						+		+							
Artemisia commutata Mill.		+	+		+			+		+	+				+	+		+	+	+	+	+	+
Armerasia maritima Gaerta. Mey.			+							+	+		+					+	+				+
Vicia sepium L.	+		+		+					+			+					+	+				
Vicia cracca L.	+	+		+														+	+				+
Vicia sp.			+			+																+	
Coriaria myrtiseflora Bess.		+					+									+	+	+	+			+	+
Bunias orientalis L.	+	+			+				+	+					+	+		+				+	+
Achillea millefolium L.		+					+									+					+		
Rumex confertus Willd.	+									+					+						+		
Trifolium hybridum L.	+							+	+					+		+	+				+		
Trifolium pratense L.																							
Trifolium repens L.			+		+						+				+	+						+	
Cynanchum vulgare (Savi) Tetz.	+	+	+	+	+	+		+	+	+			+	+	+	+	+	+	+		+		+
Echium vulgare L.	+	+		+	+			+	+	+	+	+	+		+	+	+	+	+	+	+	+	
Convolvulus arvensis	+		+		+					+		+	+		+			+	+				+
Linaria vulgaris Mill		+			+	+			+			+	+	+	+	+		+					

Figure 2. Occurrence of certain species on the RMC experimental plots

The vitality of most species (52.0 %) growing on the plots was rated as 3a. These species complete the full development cycle and develop normally, including fruiting. They include: *Acer negundo*, *Malus baccata*, *Populus laurifolia*, *Elymus repens*, *Phleum phleoides*, *Trifolium pratense*, *Trifolium hybridum*, *Tussilago farfara*, *Hypericum perforatum*. About one-third of the species (30.0 %) received a 3b rating; they go through all developmental stages but do not reach their usual size. 16.6 % of species grow reasonably well but do not fruit, and 1.4 % of species are severely suppressed and do not fruit.

Under conditions of prolonged anthropogenic impact, it is important to provide an ecological-geographical analysis of the flora, reflecting their origin and connection with anthropogenic habitats. To assess the stability of plant communities and biodiversity on the RMC plots, biological groups of plants were identified: apophytes (native species), adventives, ruderal species, and synanthropic species. Considering that some species belong not only to one group but to two or three different groups—a phenomenon more common in species of the families Rosaceae, Asteraceae, Poaceae, Fabaceae, Plantaginaceae, Brassicaceae—the following distribution was observed. Native species occupy a special position, forming the basis (72.6 %) for

stabilizing the spatial structure; synanthropic species account for 10.0 %; ruderal plants of disturbed habitats make up 11.7 %; and adventive, invasive species make up 5.7 %, some of which exhibit aggressive behavior throughout the area, for example, *Acer negundo*.

The condition of woody plants is reflected in their morphological plasticity—the ability of a plant to change its external structure, in particular leaf size, plant height variation, development of a more robust root system, and modification of shoot form. Morphological plasticity helps plants adapt to deficits of moisture, light, and nutrients. Assessment of the vital condition of woody plants growing on the experimental plots showed that on the industrial sites near the Concentration Plant (tailings storage facilities), species such as *Betula pendula*, *Betula pubescens*, and *Populus laurifolia* exhibited a decrease in plant height by 15–18 %, reduction in growth by 14–16 %, and a 9 % reduction in leaf area compared to the control. Among the dominant grass species in the communities, *Dactylis glomerata* and *Phleum pratense*, most morphometric traits decreased, including plant height, stem thickness, and leaf blade area.

The life forms of the described species are classified according to the classical system of life-form classification (tree, shrub, semi-shrub, perennial herbaceous, biennial, annual). This classification is based on the method of overwintering and the position of generative buds relative to the soil surface. It is a simplified scheme often used in geobotany and vegetation ecology: 3 — woody plants over 5 m tall with a single stem; shrub—woody plants under 5 m, multi-stemmed; semi-shrub—semi-evergreen or low-growing subshrubs; perennial herbaceous—perennial herbs, including rhizomatous and tuberous forms; biennial–annual herbs—classified by lifespan. In these plants, aboveground parts die completely in winter but regenerate quickly.

According to this classification, on the disturbed territories of the RMC, perennial herbaceous plants dominate — 79 species (62.8 %), including rhizomatous species such as *Calamagrostis epigeios*, *Calamagrostis purpurea*, *Poa pratensis*, *Elymus repens*, *Agrostis stolonifera*, *Bromus inermis*, *Phragmites australis*, *Dactylis glomerata*, *Alopecurus pratensis*. These species have a high capacity to occupy open spaces, ensuring the stability of the vegetation cover and turf formation. Woody plants comprise 34 species, including 18 tree species (14.2 %) and 16 shrub species (13.4 %); semi-shrubs account for 7 species (5.5 %); annual herbs are represented by 5 species (3.9 %). Such biomorphological diversity demonstrates the resilience of plant communities on the RMC plots and their high capacity for self-restoration.

Grouping species by water regime shows that mesophytic species dominate the studied territory—38 species, accounting for 30.3 % of the total number of species. These are moderately moisture-loving plants, many of which have well-developed root systems. Xeromesophytes—34 species, make up 26.9 %. They are adapted to moisture deficiency through small or modified leaves, thick cuticles, and deep root systems, making them drought-resistant. Hygromesophytes include 24 species, accounting for 19.1 %. Xerophytes comprise 18 species (14.2 %), and 12 species are hydrophytes, representing only 9.5 % of the total species present. The identified groups reflect the morphological manifestation of colloidal-chemical issues in plants (Fig. 3).

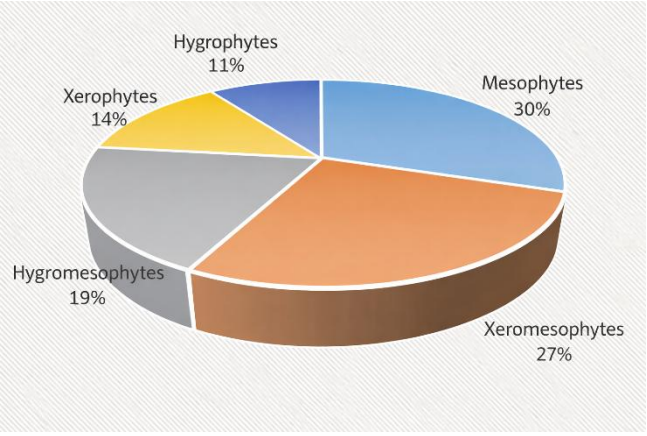

Figure 3. Distribution of species by water regime on RMC plots, methodology — (Raunkiær C., 1907)

Conclusion

The review of the flora includes ecological and geographical aspects. The conducted studies made it possible to assess the degree of disturbance of the territory and to predict the direction of succession. In the

vegetation cover, preference is given to local, ecologically stable species. The restoration of native vegetation can play a crucial role in forming resilient plant communities on the disturbed territories of the RMC.

The research concluded that a number of indicators (soil composition, ecological and biological characteristics of species) can be used to characterize vegetation condition as criteria for assessing environmental contamination with heavy metals. The biomorphological composition of the flora reflects the distribution of plants by life forms (biomorphs), which have evolved as adaptations to environmental conditions. Analysis of the biomorphological composition allowed for the assessment of the ecological state of the territory, the degree of anthropogenic disturbance, and the direction of succession. Ecological groups of plants were identified according to their moisture requirements.

The floristic composition studied includes 126 species from 38 families and 93 genera. The leading families are Rosaceae — 11 genera, Cyperaceae and Asteraceae — 9 genera each, Poaceae — 7 genera, Fabaceae, Apiaceae, Plantaginaceae — 4 genera each, Brassicaceae, Caryophyllaceae, Malvaceae — 3 genera each. The remaining families include 1 to 2 genera.

Within the phytocenoses, the spatial distribution, abundance, life form, and condition of the plants were determined. These studies contribute to the restoration of technogenically disturbed lands and their return to the biosphere fund. The study results allowed the identification of native and adventive species that predominate in plant communities.

Funding

The Committee of Science and Higher Education of the Republic of Kazakhstan, within the framework of project BR24992837 "Comprehensive Ecological Monitoring of the East Kazakhstan Region for Sustainable Development of the Agricultural Sector and Improvement of Environmental Quality", 2024–2026.

Conflict of Interest

The authors declare no conflict of interest.

Authors' contributions

The manuscript was prepared with the participation of all authors. All authors approved the final version of the manuscript. **T.A. Vdovina** — data analysis, manuscript writing; **O.A. Anufrieva** — floristic research; **A.A. Vinokurov** — floristic research; **A.N. Danilo**va — manuscript discussion and editing; **A.A. Sumbembaev** — floristic research, data analysis; **A.A. Chernakova** — data digitization and analysis.

References

1 Hajiyeva, G. N., & Ibrahimova, L. P. (2024). Ecological problems of technogenically disturbed lands on the Absheron Peninsula. *Journal of Geology, Geography and Geoecology, 33*(1), 70–76. https://doi.org/10.15421/112408

2 Stepanova, L. P., Pisareva, A. V., Bolmat, T. N., & Yelisarov, N. A. (2022). Ecological assessment of disturbances in the landscape structure of alluvial soils of floodplains under technogenesis influences. *IOP Conference Series: Earth and Environmental Science, 988*(4), Article 042024. https://doi.org/10.1088/1755-1315/988/4/042024

3 Kopach, P. I., Yakubenko, L. V., Mormul, T. M., Danko, T. T., Gorobets, N. V., & Halchenko, Z. S. (2022). Assessment of natural resource potential of territories disturbed by mining works in the context of effective use of post-technogenic landscape. *Geo-Technical Mechanics, 162*, 38–47. https://doi.org/10.15407/geotm2022.162.038

4 Osintseva, M. (2023). Assessment of soil properties in technogenically disturbed lands of Kemerovo Oblast — Kuzbass. *Qubahan Academic Journal, 3*(4), 77–92. https://doi.org/10.48161/qaj.v3n4a164

5 Ivakina, E. V. (2022). Habitat formation in technogenic landscapes. *IOP Conference Series: Earth and Environmental Science, 1045*(1), Article 012133. https://doi.org/10.1088/1755-1315/1045/1/012133

6 Shergina, O. V., Mironova, A. S., Mikhailova, T. A., & Badryanova, V. V. (2022). Assessment of effects of anthropogenic disturbance on plant communities and soils in urbanized territories. *IOP Conference Series: Earth and Environmental Science, 979*(1), Article 012162. https://doi.org/10.1088/1755-1315/979/1/012162

7 Ivanova, S., Vesnina, A., Fotina, N., & Prosekov, A. (2024). Technogenically disturbed lands of coal mines: Restoration methods**.** *Nature Environment and Pollution Technology, 23*(4), 2447–2452. https://doi.org/10.46488/NEPT.2024.v23i04.050

8 Dudnikova, T., Sushkova, S., Minkina, T., Barbashev, A., Ferreira, C. S. S., Antonenko, E., Shuvaev, E., & Bakoeva, G. (2023). Main factors in polycyclic aromatic hydrocarbons accumulations in the long-term technogenic contaminated soil. *Eurasian Journal of Soil Science, 12*(3), 282–289. https://doi.org/10.18393/ejss.1291033

9 Chaplygina, A. B., Filatova, O. V., Litvin, L. M., & Nykyforov, V. V. (2023). The main factors and prospects for the restoration of biodiversity in technogenic territories: On the example of the Poltava Mining and Processing Plant. *Biosystems Diversity*, *31*(1), 100–112. https://doi.org/10.15421/012311

10 (2024). Royal Botanic Gardens, Kew. *www.plantsoftheworldonline.org.* Retrieved from http://www.plantsoftheworldonline.org/

11 Raunkiaer, C. (1905). Types biologiques pour la géographie botanique. *Oversigt over Det Kongelige Danske Videnskabernes Selskabs Forhandlinger*, 347–437.

12 Litvinskaya, S. A. (2023). Transformation and features of plant successions of the Taman Peninsula in case of technogenic impact. *Russian Journal of Earth Sciences, 23*(5), 1–6. https://doi.org/10.2205/2023ES02SI18

13 Watkinson, A. D., Juckers, M., D'Andrea, L., Beckett, P., & Spiers, G. (2022). Ecosystem recovery of the Sudbury technogenic barrens 30 years post-restoration. *Eurasian Soil Science, 55*(5), 663–672. https://doi.org/10.1134/S106422932205012X

14 Faleyev, D., Ivanov, A., Petrov, S., & Smirnov, V. (2024). Changes in vegetation cover as a result of anthropogenic and technogenic impact on arid ecosystems of the Ashchykol depression (Betpak-Dala): Problems and prospects for the recultivation of uranium mines. *BIO Web of Conferences, 128*, Article 00006. https://doi.org/10.1051/bioconf/202412800006

Т.А. Вдовина, О.А. Ануфриева, А.А. Винокуров, А.Н. Данилова,
А.А. Сумбембаев, А.А. Чернакова

Риддер металлургиялық кешенінің антропогендік бұзылған аумақтарының флорасы

Жұмыстың мақсаты — Риддер металлургиялық кешені аумағындағы өнеркәсіптік бұзылған жерлерде қалыптасатын өсімдіктердің флоралық құрамын зерттеу арқылы оларды биологиялық рекультивациялау мәселесін шешу. Риддер металлургиялық кешенінің өнеркәсіптік бұзылған жерлеріндегі флораны зерттеу барысында Өсімдіктер биологиясы және биотехнологиясы институтымен бірлесіп техногендік ландшафттардың фитоценоздары мен топырақ құрамын зерттеуге бағытталған кешенді бағдарлама жүзеге асырылды. Бұл аумақ антропогендік әсердің жоғары деңгейімен сипатталады. Зерттеу нәтижесінде 38 тұқымдасқа, 93 туысқа жататын 126 түрден тұратын флоралық құрам анықталды. Таксономиялық тізімде жетекші орын алатын тұқымдастар: Rosaceae — 11 туыс, Cyperaceae және Asteraceae — 9 туыстан, Poaceae — 7 туыстан тұрады. Өсімдіктердің кеңістікте таралуы, саны, тіршілік формалары мен жағдайы айқындалды. Түрлердің биоэкологиялық сипаттамасы беріліп, тіршілік формалары (экоморфалары) анықталды, сондай-ақ өсімдіктердің ылғалға қатынасы бойынша экологиялық топтары ажыратылды. Жүргізілген зерттеулер аумақтың бұзылу дәрежесін бағалауға және сукцессия бағытын болжауға мүмкіндік берді. Өсімдік жамылғысының негізін антропогендік ортаға бейімделген жергілікті, экологиялық тұрғыдан тұрақты түрлер құрайды. Бұл зерттеулер техногендік бұзылған жерлерді қалпына келтіруге және оларды биосфералық қорға қайтаруға ықпал етеді.

Кілт сөздер: флора, түр, техногендік бұзылған аумақтар, Риддер металлургиялық кешенінің кәсіпорындары, тіршілік формасы, өсімдіктердің жағдайы, экоморфа, экожүйе.

Т.А. Вдовина, О.А. Ануфриева, А.А. Винокуров, А.Н. Данилова,
А.А. Сумбембаев, А.А. Чернакова

Флора антропогенно нарушенных территорий Риддерского металлургического комплекса

Цель работы — исследование флористического состава растений, формирующегося на нарушенных промышленностью землях в районе Риддерского металлургического комплекса для решения проблемы их биологической рекультивации. При проведении исследований на нарушенных промышленностью землях Риддерского металлургического комплекса совместно с ИББР «Институт биологии и биотехнологии растений» была реализована комплексная программа по изучению фитоценозов техногенных ландшафтов, почвенного состава. Данная территория характеризуется высокой степенью антропогенного воздействия. В результате исследований изучен флористический состав, насчитывающий 126 видов из 38 семейств, 93 родов. На лидирующих позициях в таксономическом списке такие семейства, как *Rosaceae* (одиннадцать родов), *Cyperaceae* и *Asteraceae*по (девять родов), *Poaceae* (семь родов). Определено их пространственное размещение, численность, жизненная форма, состояние растений. Приведена биоэкологическая характеристика видов, жизненная форма (экоморфа), выделены экологические группы растений по отношению к влаге. Проведенные исследования позволили оценить степень нарушенности территории, спрогнозировать направление сукцессии. В растительном

покрове основу составляют местные, экологически устойчивые виды, отражающие связь с антропогенным местообитанием. Данные исследования способствуют восстановлению техногенно нарушенных земель, возвращению их в биосферный фонд.

Ключевые слова: флора, вид, техногенно нарушенные территории, предприятия Риддерского металлургического комплекса, жизненная форма, состояние растений, экоморфа, экосистема.

Information about the authors

Vdovina Tatyana Afanasyevna — Candidate of Biological Sciences, Altai Botanical Garden, Ridder, Kazakhstan; e-mail: tvdovina2017@mail.ru; ORCID: https://orcid.org/0000-0002-1767-3047

Anufrieva Olga Alexandrovna — Senior Researcher, Altai Botanical Garden, Ridder, Kazakhstan; e-mail:anufrievaolgaalex59@yandex.kz; ORCID: https://orcid.org/0000-0001-9675-7654

Vinokurov Andrey Andreevich — Senior Researcher, Altai Botanical Garden, Ridder, Kazakhstan; e-mail:anvin64@mail.ru; ORCID: https://orcid.org/0000-0003-0154-8943

Danilova Alevtina Nikolaevna — Candidate of Biological Sciences, Altai Botanical Garden, Ridder, Kazakhstan; e-mail: a-n-danilova@yandex.ru; ORCID: https://orcid.org/0000-0002-1096-9339

Sumbembaev Aidar Aitkazyevich — PhD, General director, Altai Botanical Garden, Ridder, Kazakhstan; e-mail: aydars@list.ru; ORCID: https://orcid.org/0000-0003-0682-9162

Chernakova Anzhelika Alexandrovna — Junior Researcher, Altai Botanical Garden, Ridder, Kazakhstan; e-mail: dolmatova-1986@bk.ru; ORCID: https://orcid.org/0009-0007-6481-5611

How to Cite: Ibraimov, A.M., Yermagambetova, M.M., Makhmadzhanov, S.P., Ortaev, A.K. & Turuspekov, Y.K. (2026). Microsatellite-based genetic diversity evaluation of *Zea mays* L. accessions from different geographical origins. *Fundamental and Experimental Biology*, 31, 3 (123), 66-82. https://doi.org/10.31489/2026FEB3/66-82

Research article

https://doi.org/10.31489/2026FEB3/66-82

UDC 633.15Received: 3.04.2026 | Accepted: 16.04.2026 | Published online: 30.09.2026

A.M. Ibraimov[1], M.M. Yermagambetova[1], S.P. Makhmadzhanov[2], A.K. Ortaev[3], Y.K. Turuspekov[1*]

[1]*Institute of Plant Biology and Biotechnology, Almaty, Kazakhstan;*
[2]*Agricultural Experimental Station for Cotton and Melon Growing, Turkestan region, Kazakhstan;*
[3]*Krasnovodopad Agricultural Experimental Station, Turkestan region, Kazakhstan*
[*]*Corresponding author: yerlant@yahoo.com*

Microsatellite-based genetic diversity evaluation of *Zea mays* L. accessions from different geographical origins

The purpose of this study was to investigate the genetic diversity and population structure of 51 maize (*Zea mays* L.) accessions originating from Kazakhstan, China, and Europe using simple sequence repeat (SSR) markers. A total of 21 highly polymorphic SSR markers were used to genotype 255 individuals, enabling a comprehensive assessment of allelic variation and genetic relationships. The number of alleles per locus ranged from 1.0 to 2.7, with a mean of 1.517, while expected heterozygosity (*uHe*) averaged 0.192, indicating moderate genetic diversity among the accessions. Genetic diversity analysis by geographic origin revealed that European accessions exhibited the highest allelic richness (Na = 5.9) and genetic diversity, followed by Chinese and Kazakhstani accessions. Despite these differences, all groups exhibited 100% polymorphism, confirming the high informativeness of the selected SSR markers. Polymorphic information content (PIC) values ranged from 0.446 to 0.884, with an average of 0.712, indicating that markers such as *phi047*, *bnlg1520*, and *umc2189* were highly informative. Analysis of molecular variance (AMOVA) demonstrated that 70% of the total genetic variation was attributable to differences among accessions, indicating strong genetic differentiation (*Fst* = 0.702) and limited gene flow (*Nm* = 0.212). Cluster analysis, principal coordinate analysis, and STRUCTURE analysis consistently revealed clear genetic separation of the Chinese accessions, whereas European and Kazakhstani accessions showed closer genetic relationships and partial admixture. Overall, the findings highlight substantial genetic diversity and distinct population structure among the maize accessions, providing valuable insights for germplasm conservation and the selection of genetically diverse parental lines for breeding programs.

Keywords: Zea mays, Kazakhstan, molecular marker, SSR, genetic diversity, polymorphism, genetic structure, genotyping.

Introduction

Maize (*Zea mays* L.) is one of the most important cereal crops worldwide and ranks among the top three staple grains alongside wheat (*Triticum aestivum* L.) and rice (*Oryza sativa* L.) [1]. Owing to its high productivity, wide adaptability, and diverse end uses, maize plays a central role in global food security, livestock production, and industrial applications [2]. It is cultivated across a broad range of agroecological zones, from temperate to tropical regions, reflecting its remarkable genetic plasticity and capacity to adapt to diverse environmental conditions [3].

This extensive adaptability and phenotypic diversity are closely linked to the complex taxonomic structure of maize within the species *Zea mays*. Classification proposed by Hugh Iltis and John Doebley [4] provided a detailed subdivision of the *Zea mays* complex; however, it is now considered partly outdated due to advances in molecular systematic and revised taxonomic approaches. In contrast, modern authoritative databases such as Plants of the World Online (POWO) [5] adopt a simplified and currently accepted view, recognizing only three subspecies within *Zea mays*: *Zea mays* subsp. *mays*, *Zea mays* subsp. *parviglumis* Iltis & Doebley, and *Zea mays* subsp. *huehuetenangensis* (Iltis & Doebley) Doebley.

Within this group, subsp. *mays* is the domesticated form grown extensively across the globe, while subsp. *parviglumis* and subsp. *huehuetenangensis* are wild relatives, or teosintes. These wild subspecies are critical for tracing the evolutionary roots of maize and serve as vital resources for expanding its genetic diversity. Specifically, *Zea mays* subsp. *parviglumis* (Balsas teosinte) is identified as the immediate progenitor

of modern maize, with the distinct morphological variations between them arising from human-driven selection throughout the domestication process [6–8].

Within the cultivated subspecies *Zea mays* subsp. *mays*, an exceptionally high level of genetic and phenotypic diversity is observed, reflecting thousands of years of domestication, selection, and adaptation to diverse agroecological conditions. This diversity is expressed in numerous varieties (often referred to as kernel or endosperm types), which differ in grain structure, biochemical composition, and end-use applications [9].

Among the most widely recognized varieties, dent maize (*var. indentata*) is characterized by a combination of hard and soft endosperm, resulting in a depression at the crown of the kernel; it is predominantly used for animal feed and industrial processing, including starch and bioethanol production. Flint maize (*var. indurata*) possesses a hard outer endosperm layer, making it more resistant to mechanical damage and suitable for cultivation in cooler climates, as well as for food products such as grits and traditional dishes. Sweet maize (*var. saccharata*) is distinguished by mutations affecting sugar metabolism, resulting in high sugar content in immature kernels, and is widely consumed as a vegetable. Popcorn (*var. everta*) has a unique kernel structure with a hard pericarp and dense endosperm, allowing it to expand explosively when heated. Flour maize (*var. amylacea*) contains predominantly soft starch, facilitating milling into flour and its use in traditional foods, particularly in indigenous cultures. Waxy maize (*var. ceratina*) is rich in amylopectin and is valued in the food industry and for specialized starch applications [10–13].

This broad spectrum of forms within *Zea mays* subsp. *mays* highlights its remarkable genetic plasticity and adaptability. The diversity of kernel types is not only of economic importance but also reflects underlying allelic variation at key loci controlling starch composition, texture, and metabolic pathways. Such extensive intrasubspecific variation makes cultivated maize one of the most genetically diverse crop species and underscores its significance as a model organism for genetic, genomic, and breeding studies [14–16].

Given this high level of genetic diversity, reliable tools are required to accurately assess variation both within and among maize populations. Molecular markers have become essential in this context, providing a robust alternative to traditional agro-morphological evaluation. Among them, simple sequence repeat (SSR) markers are particularly widely used due to their high polymorphism, co-dominant inheritance, reproducibility, and genome-wide distribution [17, 18]. SSR markers enable precise detection of allelic variation, making them highly suitable for studies of genetic diversity, population structure, and relationships among plants [19].

Numerous studies have successfully applied SSR markers to characterize maize germplasm worldwide, revealing substantial levels of genetic variation and facilitating the development of core collections and breeding strategies [20–25]. These approaches have proven especially valuable for identifying unique alleles and underutilized genetic resources, which are critical for broadening the genetic base of modern breeding programs.

In maize, the use of SSR markers is particularly relevant due to the presence of numerous hybrid varieties, each with distinct parental contributions, as well as diverse local landraces. These hybrids, while improving yield and stress tolerance, can also reduce genetic diversity if a limited set of parental lines is repeatedly used. SSR-based analyses, therefore, provide an essential tool for evaluating and preserving genetic variation in both landraces and hybrids, supporting informed breeding and conservation efforts [26, 27].

Although SSR-based studies of maize have been widely conducted worldwide, research on maize genetic diversity using SSR markers in Kazakhstan remains scarce. Previous studies in the region have mostly focused on agro-morphological traits [28–31] or small panels of genotypes, such as the 21 accessions analyzed in our earlier work [32], which provided preliminary information but did not fully capture the genetic diversity of local germplasm.

This study extends prior research by examining 51 maize accessions, including local landraces from Kazakhstan and global hybrid varieties. This larger, more diverse panel enables a more comprehensive assessment of genetic diversity and population structure using SSR markers. Such analyses not only provide insights into the extent of variation within cultivated maize in Kazakhstan but also inform breeding programs by identifying genetically distinct lines and potential sources of beneficial alleles for future maize hybrid development.

Experimental

Plant material. The study included 51 accessions (hybrids) of common maize (*Zea mays* subsp. *mays* L.). By origin, accessions are divided into three groups: from Kazakhstan (17), China (10), and Europe (24). The European accessions were represented by Germany (9), Switzerland (7), Türkiye (3),

France (2), Russia (2), and Greece (1). The hybrids were developed using a population, single-, two- (F_1), and three-line hybrid systems. Seed material was provided by the Krasnovodopad Agricultural Experimental Station (AES) and the peasant farm (PF) "Sabyr" (Fig. 1; Tab. 1).

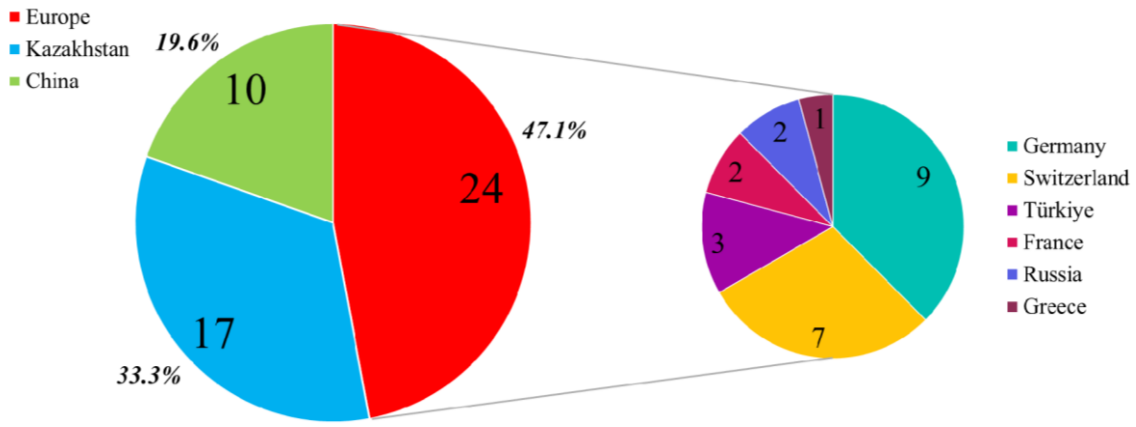

Figure 1. Distribution of maize accessions used in this study by country of origin

Table 1

Characteristics of maize accessions used for SSR genotyping

№	ID	Accessions	Country of origin	Developing system
1	ZM-001	Altai-319	Kazakhstan	Three-line hybrid
2	ZM-002	Gidro F2	Switzerland (Europe)	Two-line (F1) hybrid
3	ZM-003	Tulpar-539	Kazakhstan	Two-line (F1) hybrid
4	ZM-004	F2 S0069	Türkiye (Europe)	Two-line (F1) hybrid
5	ZM-005	ZPSK-704	Kazakhstan	Two-line (F1) hybrid
6	ZM-006	Altyn 739	Kazakhstan	Two-line (F1) hybrid
7	ZM-007	KazZP-777	Kazakhstan	Three-line hybrid
8	ZM-008	Mariam-419	Kazakhstan	Two-line (F1) hybrid
9	ZM-009	SV Bambus F2	Switzerland (Europe)	Two-line (F1) hybrid
10	ZM-010	Sunkar-779	Kazakhstan	Three-line hybrid
11	ZM-011	Fenikks Spartak	China	Two-line (F1) hybrid
12	ZM-012	Fenikks Atlant	China	Two-line (F1) hybrid
13	ZM-013	Fenikks Chelentano	China	Two-line (F1) hybrid
14	ZM-014	Fenikks Takelau	China	Two-line (F1) hybrid
15	ZM-015	Fenikks Bora-bora	China	Two-line (F1) hybrid
16	ZM-016	Fenikks Gobi	China	Two-line (F1) hybrid
17	ZM-017	LG31642	France (Europe)	Two-line (F1) hybrid
18	ZM-018	Fenikks Avrora	China	Two-line (F1) hybrid
19	ZM-019	LG31555	France (Europe)	Two-line (F1) hybrid
20	ZM-020	Fenikks Francheska	China	Two-line (F1) hybrid
21	ZM-021	Fenikks Bombei	China	Two-line (F1) hybrid
22	ZM-022	Symbat-1	Kazakhstan	Two-line (F1) hybrid
23	ZM-024	BG23-1637	Kazakhstan	Two-line (F1) hybrid
24	ZM-025	Briso	Germany (Europe)	Two-line (F1) hybrid
25	ZM-026	Skap 620	Russia (Europe)	Two-line (F1) hybrid
26	ZM-027	Hamilton	Greece (Europe)	Single-line (F1) hybrid
27	ZM-029	KVS Intelegenes	Germany (Europe)	Two-line (F1) hybrid
28	ZM-030	KVS Kaleido	Germany (Europe)	Two-line (F1) hybrid
29	ZM-038	Dala aru 446P	Kazakhstan	Population hybrid
30	ZM-039	KazLK444	Kazakhstan	Two-line (F1) hybrid
31	ZM-040	KazLK575	Kazakhstan	Two-line (F1) hybrid
32	ZM-041	KazLK780	Kazakhstan	Two-line (F1) hybrid
33	ZM-042	KazNIIZiR 90	Kazakhstan	Two-line (F1) hybrid

Continuation of Table 1

№	ID	Accessions	Country of origin	Developing system
34	ZM-044	KVS Alkanto	Germany (Europe)	Two-line (F1) hybrid
35	ZM-045	KVS Atako	Germany (Europe)	Three-line hybrid
36	ZM-048	KVS Elektro	Germany (Europe)	Two-line (F1) hybrid
37	ZM-049	Kerubino OK-69	Germany (Europe)	Two-line (F1) hybrid
38	ZM-050	Kefrankos	Germany (Europe)	Two-line (F1) hybrid
39	ZM-051	Kleopatras	Germany (Europe)	Two-line (F1) hybrid
40	ZM-056	M11G99	Türkiye (Europe)	Two-line (F1) hybrid
41	ZM-057	M-16C45	Türkiye (Europe)	Two-line (F1) hybrid
42	ZM-062	SI Bambus	Switzerland (Europe)	Two-line (F1) hybrid
43	ZM-063	SI Gladius	Switzerland (Europe)	Two-line (F1) hybrid
44	ZM-065	SI Kursor	Switzerland (Europe)	Two-line (F1) hybrid
45	ZM-066	SI Maileston	Switzerland (Europe)	Two-line (F1) hybrid
46	ZM-067	SI Fontero	Switzerland (Europe)	Two-line (F1) hybrid
47	ZM-069	Skap 301CB	Russia (Europe)	Two-line (F1) hybrid
48	ZM-070	Taulsizdik 20CB	Kazakhstan	Two-line (F1) hybrid
49	ZM-072	Tomiris	Kazakhstan	Three-line hybrid
50	ZM-073	Hyuaksi 948	China	Two-line (F1) hybrid
51	ZM-074	Turan480	Kazakhstan	Three-line hybrid

DNA extraction. Genomic DNA was extracted from 5-day-old maize seedlings (five replicates per accession) using a modified Dellaporta protocol [33]. The quality and quantity of the extracted DNA were assessed using a NanoDrop One spectrophotometer (Thermo Fisher Scientific Inc., USA) and 1 % agarose gel electrophoresis. For PCR analysis, genomic DNA was normalized to 100 ng/μl.

SSR genotyping. A set of 21 SSR markers (Tab. 2) was selected for genotyping 255 maize individuals based on their high levels of polymorphism, reproducibility, and informativeness, with five replicates per accession. These markers have been validated in previous studies, ensuring reliable and comparable results [20–25].

PCR parameters, including the annealing temperature (Ta), were individually optimized for each marker to achieve high amplification efficiency and specificity (Tab. 2). Each reaction was carried out in a total volume of 20 μL, comprising 100 ng of genomic DNA, 1 U of Taq DNA polymerase, 0.2 mM of each dNTP, 10 pM of each primer, 1.5 mM $MgCl_2$, and 1× Taq buffer. The thermal cycling program began with an initial denaturation at 94 °C for 3 minutes, followed by 35 cycles of denaturation at 94 °C for 30 seconds, annealing at the marker-specific Ta °C (Table 2) for 30 seconds, and extension at 72 °C for 1 minute, concluding with a final extension at 72 °C for 5 minutes.

PCR products were separated by capillary electrophoresis using the QIAxcel Connect System (QIAGEN, Germany) with the QIAxcel DNA High-Resolution Kit, QX Alignment Marker (15 bp/3 kb), and QX Size Marker (50 bp/1 kb). Sample analysis was performed using the standard OH500 protocol with a 20-second injection time. SSR alleles were identified by comparing fragment sizes to the reference DNA ladder.

Table 2

Characteristics of SSR markers used for analysis

№	Primer	Primer Sequence (5'-3')	Motif	Chr. No.	Ta (°C)	Associated genes and traits [34]
1	*bnlg1520*	F: TCCTCTTGCTCTCCATGTCC R: ACAGCTGCGTAGCTTCTTCC	(AG)22	2	58	-
2	*phi002*	F: CATGCAATCAATAACGATGGCGAGT R: TTAGCGTAACCCTTCTCCAGTCAGC	AACG	1	58	*agal2*, 100 kernel weight, leaf below flag leaf
3	*phi021*	F: TTCCATTCTCGTGTTCTTGGAGTGGTCCA R: CTTGATCACCTTTCCTGCTGTCGCCA	AG	4	58	*adh2*
4	*phi027*	F: GCGTACGTACGACGAAGACAC R: CACAGCACGTTGCGGATTTCTCT	(GCGCT)n	9	58	*wx1*, amino acids, leaf below flag leaf, metabolites

Continuation of Table 2

№	Primer	Primer Sequence (5'-3')	Motif	Chr. No.	Ta (℃)	Associated genes and traits [34]
5	*phi042*	F: ATGTGGCCATCATTCAATGCTGTAGAC R: ACACATGCAGGTGCAGCCAGA	CATA	9	60	*sus1*, photoperiod growing-degree days to silk, node number
6	*phi047*	F: GGAGATGCTCGCACTGTTCTC R: CTCCACCCTCTTTGACATGGTATG	ATC	3	62	*mybr17*
7	*phi058*	F: AGGTGCTGGACACAGACTTCAAC R: ACTGAGATCCAGGCTCCTCTTC	CCG	5	58	*col12*, tassel branch number, ear height, plant height
8	*phi061*	F: GACGTAAGCCTAGCTCTGCCAT R: AAACAAGAACGGCGGTGCTGATTC	TTCT-GTAT	9	58	*wx1*, amino acids, leaf below flag leaf, metabolites
9	*phi070*	F: GCTGAGCGATCAGTTCATCCAG R: CCATGGCAGGGTCTCTCAAG	AGCTG	6	58	*mlg3*
10	*phi076*	F: TTCTTCCGCGGCTTCAATTTGACC R: GCATCAGGACCCGCAGAGTC	AGCGGG	4	58	-
11	*phi079*	F: TGGTGCTCGTTGCCAAATCTACGA R: GCAGTGGTGGTTTCGAACAGACAA	AGATG	4	58	*gpc1*
12	*phi116*	F: TCCCTGCCGGGACTCCTG R: GCATACGGCCATGGATGGGA	ACTG/ACG	7	58	*phi116*
13	*phi127*	F: ATATGCATTGCCTGGAACTGGAAGGA R: AATTCAAACACGCCTCCCGAGTGT	AGAC	2	58	-
14	*umc1060*	F: ACAGGATTTGAGCTTCTGGACATT R: GGCCTCTCCTTCATCCTATTCAA	(CGG)5	5	58	*umc1060*
15	*umc1265*	F: GCCTAGTCGCCTACCCTACCAAT R: TGTGTTCTTGATTGGGTGAGACAT	(TCAC)4	2	58	*ereb197*, tassel spike length; leaf angle, tassel branch number
16	*umc1327*	F: AGGGTTTTGCTCTTGGAATCTCTC R: GAGGAAGGAGGAGGTCGTATCGT	(GCC)4	8	58	*umc1327*, anthesis date
17	*umc1403*	F: GTACAACGGAGGCATTCTCAAGTT R: TGTACATGGTGGTCTTGTTGAGGT	(GCA)4	1	58	*xyl5*, 100 kernel weight
18	*umc1446*	F: GCGCTGCTGCTTCTTAAATTATCT R: GATGAGACCACCTACAAGTTCGCT	(TAA)7	1	58	*kcs15*
19	*umc1545*	F: GAAAACTGCATCAACAACAAGCTG R: ATTGGTTGGTTCTTGCTTCCATTA	(AAGA)4	7	58	*hsp3*
20	*umc1941*	F: ACGACGAGACTCTGTTCTGGTTCT R: AGGAGGATTACGTCAATCTGTTCG	(CTG)10	5	58	*umc1941*, kernel row number
21	*umc2189*	F: CGTAAGTACAGTACACCAATGGGC R: ACACCGACTACAAGCCTCTCAACT	(CAG)4	1	58	*epf10*

Genetic diversity and Population structure analysis. Genetic diversity among the 51 maize accessions was evaluated using a set of diversity indices calculated with GenAlEx version 6.5 [35]. The parameters analyzed for SSR data included: the number of alleles per locus (*Na*), the effective number of alleles (*Ne*), Shannon's information index (*I*), Nei's genetic diversity index (*uh*), and the proportion of polymorphic loci (*%P*). In addition, levels of genetic differentiation among populations (*Fst*), expected Heterozygosity (*uHe*), and estimates of gene flow (*Nm)* were determined. Also, polymorphic information content (PIC) was calculated as described by Botstein et al. [36]. According to PIC values, SSR markers were categorized as PIC > 0.5 (highly informative), 0.25 < PIC ≤ 0.5 (moderately informative), and PIC ≤ 0.25 (slightly informative), following the classification proposed by Botstein et al. [36].

Analysis of Molecular Variance (AMOVA) was conducted to quantify the distribution of genetic variation within and among populations. Genetic structuring among individuals and populations was visualized using Principal Coordinate Analysis (PCoA). Initial PCoA by country of origin was performed in GenAlEx 6.5 [35] in a reduced-dimensional space. Additionally, a PCoA of 51 accessions was conducted in RStudio [37] to provide a clearer visualization of genetic relationships.

Patterns of genetic relationships among maize accessions were further examined using both distance-based and multivariate analytical methods. Genetic distance matrices were used to construct classical dendrograms to illustrate the relationships among accessions and their geographical origins. The analysis was performed using PAST software, version 3.19 [38], and the tvBOT online web application for visualizing the results [39].

The robustness of the clusters was assessed using bootstrap analysis with 1000 replicates. The population genetic structure was inferred using a Bayesian clustering approach implemented in STRUCTURE version 2.3.4 [40] under an admixture model with correlated allele frequencies. Runs were performed for K values ranging from 1 to 10, and the most probable number of genetic clusters was identified using the ΔK method of Evanno et al. [41], as implemented in the CLUMPAK platform [42]. STRUCTURE runs were performed using a burn-in period of 100,000 iterations followed by 100,000 MCMC repetitions. For each K value (K = 1-10), 10 independent runs were conducted to ensure consistency of clustering results. The STRUCTURE outputs were summarized and visualized using the CLUMPAK platform [42].

Results and Discussion

Genetic diversity across accessions. A total of 51 maize accessions, five replicates per accession, were genotyped using 21 simple sequence repeat (SSR) markers. Genetic diversity parameters varied markedly among the analyzed maize accessions (Tab. 3). The observed number of alleles (*Na*) ranged from 1.0 to 2.7, with a mean value of 1.517±0.023. The effective number of alleles (*Ne*) ranged from 1.0 to 2.3, with an average of 1.373±0.018 across all accessions.

Table 3

Genetic diversity by 51 maize accessions

№	Accession	*Na*	*Ne*	*I*	*uh*	*uHe*	*%P*
1	ZM-001	2.6	2.3	0.833	0.638	0.567	95.24 %
2	ZM-002	2.0	1.7	0.524	0.424	0.377	71.43 %
3	ZM-003	2.2	1.9	0.652	0.514	0.457	80.95 %
4	ZM-004	1.7	1.5	0.367	0.286	0.254	47.62 %
5	ZM-005	2.4	2.1	0.744	0.586	0.521	85.71 %
6	ZM-006	2.3	1.9	0.672	0.514	0.457	80.95 %
7	ZM-007	2.5	2.1	0.741	0.552	0.491	85.71 %
8	ZM-008	2.1	1.8	0.597	0.467	0.415	76.19 %
9	ZM-009	2.4	2.1	0.771	0.614	0.546	100.00 %
10	ZM-010	2.2	2.0	0.710	0.586	0.521	95.24 %
11	ZM-011	1.0	1.0	0.000	0.000	0.000	0.00 %
12	ZM-012	1.0	1.0	0.000	0.000	0.000	0.00 %
13	ZM-013	2.5	2.1	0.758	0.571	0.508	90.48 %
14	ZM-014	1.0	1.0	0.032	0.029	0.025	4.76 %
15	ZM-015	1.1	1.0	0.048	0.038	0.034	9.52 %
16	ZM-016	1.2	1.1	0.104	0.086	0.076	19.05 %
17	ZM-017	1.0	1.0	0.000	0.000	0.000	0.00 %
18	ZM-018	1.2	1.1	0.127	0.105	0.093	23.81 %
19	ZM-019	1.0	1.0	0.000	0.000	0.000	0.00 %
20	ZM-020	1.0	1.0	0.000	0.000	0.000	0.00 %
21	ZM-021	1.4	1.3	0.239	0.200	0.178	42.86 %
22	ZM-022	2.4	2.0	0.688	0.524	0.466	85.71 %
23	ZM-024	1.4	1.3	0.253	0.214	0.190	38.10 %
24	ZM-025	1.2	1.1	0.104	0.086	0.076	19.05 %
25	ZM-026	1.0	1.0	0.000	0.000	0.000	0.00 %
26	ZM-027	1.1	1.1	0.045	0.033	0.030	4.76 %
27	ZM-029	1.0	1.0	0.032	0.029	0.025	4.76 %
28	ZM-030	1.3	1.2	0.167	0.133	0.119	33.33 %
29	ZM-038	2.7	2.3	0.854	0.643	0.571	95.24 %
30	ZM-039	1.9	1.7	0.519	0.433	0.385	80.95 %
31	ZM-040	1.3	1.2	0.151	0.124	0.110	28.57 %
32	ZM-041	1.8	1.4	0.389	0.314	0.279	76.19 %

Continuation of Table 3

№	Accession	*Na*	*Ne*	*I*	*uh*	*uHe*	*%P*
33	ZM-042	2.3	1.9	0.693	0.543	0.483	90.48 %
34	ZM-044	1.0	1.0	0.000	0.000	0.000	0.00 %
35	ZM-045	1.0	1.0	0.000	0.000	0.000	0.00 %
36	ZM-048	1.0	1.0	0.000	0.000	0.000	0.00 %
37	ZM-049	1.0	1.0	0.000	0.000	0.000	0.00 %
38	ZM-050	1.1	1.1	0.077	0.062	0.055	9.52 %
39	ZM-051	1.0	1.0	0.024	0.019	0.017	4.76 %
40	ZM-056	1.1	1.0	0.048	0.038	0.034	9.52 %
41	ZM-057	1.6	1.4	0.353	0.295	0.262	57.14 %
42	ZM-062	1.1	1.0	0.048	0.038	0.034	9.52 %
43	ZM-063	1.1	1.1	0.071	0.057	0.051	14.29 %
44	ZM-065	1.0	1.0	0.000	0.000	0.000	0.00 %
45	ZM-066	1.1	1.1	0.056	0.048	0.042	9.52 %
46	ZM-067	1.1	1.0	0.048	0.038	0.034	9.52 %
47	ZM-069	1.9	1.7	0.481	0.390	0.347	61.90 %
48	ZM-070	2.0	1.8	0.528	0.414	0.368	66.67 %
49	ZM-072	1.5	1.4	0.290	0.248	0.220	42.86 %
50	ZM-073	1.0	1.0	0.000	0.000	0.000	0.00 %
51	ZM-074	1.1	1.1	0.080	0.067	0.059	14.29 %
Mean		1.517	1.373	0.273	0.216	0.192	36.79 %
SE		0.023	0.018	0.012	0.009	0.008	5.09 %

Note. *Na* — number of alleles per locus; *Ne* — effective number of alleles; *I* — Shannon's Information Index; *uh* — Nei's genetic diversity index; *uHe* — expected heterozygosity; *%P* — level of polymorphism; SE — standard error

Genetic diversity estimated using Shannon's information index (*I*) ranged from 0.000 to 0.854, with a mean value of 0.273. A similar pattern was observed for heterozygosity indices. The Nei's diversity index (*uh*) ranged from 0.000 to 0.643, while expected heterozygosity (*uHe*) varied from 0.000 to 0.571, with mean values of 0.216±0.009 and 0.192±0.008, respectively.

The highest levels of polymorphism (*%P*) were observed in ZM-009 (100.00 %) and in ZM-001, ZM-010, and ZM-038 (95.24 %). In contrast, several accessions, including ZM-011, ZM-012, ZM-017, ZM-019, ZM-020, ZM-026, ZM-044, ZM-045, ZM-048, ZM-049, ZM-065, and ZM-073, exhibited no polymorphism at all and showed minimal values for all diversity indices.

When comparing the present study with our previous work on 21 maize accessions cultivated in Kazakhstan [32], the mean values of *Na*, *Ne*, and PIC are lower in the expanded dataset of 51 accessions. The mean number of alleles per locus (*Na* = 1.52±0,023), effective alleles (*Ne* = 1.37±0.018), and PIC (0.712±0.01) were reduced compared to the earlier study (*Na* = 1.71±0.04; *Ne* = 1.52±0.03; PIC = 0.765±0.093), despite the inclusion of a larger number of accessions. This decrease can be attributed to the broader sampling, which incorporated genetically diverse and geographically distant accessions, introducing rare alleles that lower the average allele frequency. At the same time, the larger sample size improved the reliability of estimates, as reflected by smaller standard errors, providing a more robust and statistically representative picture of population-wide diversity. Genetic diversity parameters calculated by origin are presented in Table 4.

Table 4

Genetic diversity among the three groups of origin

№	Origin	*N*	*Na*	*Ne*	*I*	*uh*	*uHe*	*%P*
1	China	50	4.7	3.603	1.345	0.716	0.709	100.00 %
2	Europe	120	5.9	3.804	1.430	0.710	0.708	100.00 %
3	Kazakhstan	85	4.3	2.848	1.121	0.611	0.607	100.00 %
Mean		85.000	4.952	3.419	1.299	0.679	0.674	100.00 %
SE		3.629	0.200	0.152	0.043	0.016	0.016	0.00 %

Note. *N* — number of samples; *Na* — number of alleles per locus; *Ne* — effective number of alleles; *I* — Shannon's Information Index; *uh* — Nei's genetic diversity index; *uHe* — expected heterozygosity; *%P* — level of polymorphism; SE — standard error

The Chinese group, represented by 50 individuals, showed that the observed number of alleles (*Na*) was 4.7, while the effective number of alleles (*Ne*) reached 3.603. Shannon's information index (*I*) was 1.345. The Nei's diversity index (*uh*) and expected heterozygosity (*uHe*) were 0.716 and 0.709, respectively. The percentage of polymorphic loci (%P) was 100.00 %. The European group, comprising 120 individuals, had *Na* and *Ne* values of 5.9 and 3.804, respectively. Shannon's information index (*I*) reached 1.430. The values of *uh* and *uHe* were 0.710 and 0.708, respectively, with *%P* also equal to 100.00 %.

The Kazakhstani group included 85 individuals and showed an observed number of alleles (*Na*) of 4.3 and an effective number of alleles (*Ne*) of 2.848. Shannon's information index (*I*) was 1.121. The Nei's diversity index (*uh*) and expected heterozygosity (*uHe*) were 0.611 and 0.607, respectively. The percentage of polymorphic loci (*%P*) was 100.00 %. Mean values across all groups were 4.952±0.200 for *Na*, 3.419±0.152 for *Ne*, and 1.299±0.043 for Shannon's information index (*I*), while *uh* and *uHe* averaged 0.679±0.016 and 0.674±0.016, respectively.

These findings suggest that the European population harbors greater overall genetic variability, likely due to historical selection, extensive gene flow, and cultivation across diverse environments. The Shannon's information index (*I*), which reflects both allele richness and evenness, was also highest in European accessions (*I* = 1.430), followed by Chinese (*I* = 1.345) and Kazakhstani (*I* = 1.121) samples, further supporting the conclusion that European maize possesses the most diverse genetic structure.

The diversity observed in Chinese maize accessions reflects earlier findings that inbred lines in China are influenced by environmental conditions and human selection, resulting in high genetic variability [22, 43]. Waxy maize is reported to have originated in Southwestern China, where it displays substantial diversity in agronomic traits, highlighting the region as a center of diversity [44]. Consequently, while some diversity measures are slightly lower than in European accessions, Chinese maize still exhibits considerable allelic richness and heterozygosity, making it an important resource for breeding and conservation.

Kazakhstani populations exhibited intermediate genetic positions, reflecting their role as a transition zone between East Asian and European germplasm. The relatively lower polymorphism and reduced diversity indices observed in Kazakhstani accessions may be attributed to several factors. Local breeding and selection practices, often focused on adaptation to arid continental climates and specific agronomic requirements [30], may have led to the fixation of favorable alleles and the reduction of rare variants. Limited gene flow from distant European or Chinese germplasm compared to local populations could have constrained allelic richness, resulting in fewer effective alleles (*Ne*) and lower heterozygosity. Historical founder effects and population bottlenecks, common in geographically isolated or recently introduced germplasm, may also contribute to reduced genetic variability [45]. Together, these factors explain why Kazakhstani maize represents a genetically intermediate group: it shares allelic features with both European and East Asian populations but exhibits lower overall polymorphism due to local adaptation and limited gene exchange. A total of 51 maize accessions were evaluated using 21 SSR markers, all of which were polymorphic and included in analyses of genetic diversity and population structure (Tabl. 5).

Table 5

Genetic diversity by markers

№	Locus	*No*	*Na*	*Ne*	*I*	*uh*	*uHe*	*Fst*	*Nm*	*PIC*
1	*bnlg1520*	10	1.7	1.6	0.361	0.269	0.738	0.727	0.094	0.786
2	*phi002*	5	1.6	1.5	0.346	0.278	0.583	0.633	0.145	0.607
3	*phi021*	6	1.4	1.3	0.232	0.190	0.719	0.795	0.065	0.742
4	*phi027*	5	1.5	1.4	0.276	0.222	0.690	0.742	0.087	0.686
5	*phi042*	5	1.4	1.3	0.208	0.171	0.720	0.813	0.058	0.729
6	*phi047*	12	1.6	1.5	0.318	0.249	0.826	0.775	0.073	0.884
7	*phi058*	4	1.7	1.5	0.374	0.290	0.633	0.641	0.140	0.647
8	*phi061*	7	1.5	1.3	0.261	0.210	0.706	0.785	0.068	0.782
9	*phi070*	5	1.4	1.3	0.236	0.190	0.691	0.795	0.065	0.741
10	*phi076*	7	1.5	1.4	0.283	0.222	0.549	0.710	0.102	0.611
11	*phi079*	5	1.4	1.3	0.210	0.173	0.714	0.816	0.056	0.750
12	*phi116*	6	1.6	1.4	0.298	0.237	0.701	0.737	0.089	0.722
13	*phi127*	5	1.6	1.4	0.305	0.237	0.692	0.751	0.083	0.761
14	*umc1060*	6	1.6	1.5	0.330	0.253	0.759	0.747	0.085	0.800
15	*umc1265*	6	1.6	1.4	0.323	0.247	0.724	0.741	0.087	0.764

Continuation of Table 5

№	Locus	*No*	*Na*	*Ne*	*I*	*uh*	*uHe*	*Fst*	*Nm*	*PIC*
16	*umc1327*	4	1.3	1.2	0.145	0.116	0.455	0.792	0.066	0.446
17	*umc1403*	7	1.5	1.4	0.276	0.216	0.640	0.747	0.085	0.683
18	*umc1446*	4	1.4	1.3	0.208	0.161	0.635	0.814	0.057	0.692
19	*umc1545*	8	1.5	1.4	0.280	0.225	0.705	0.771	0.074	0.787
20	*umc1941*	7	1.3	1.2	0.188	0.157	0.516	0.766	0.076	0.536
21	*umc2189*	8	1.5	1.4	0.273	0.218	0.766	0.784	0.069	0.808
Mean		6.3	1.517	1.373	0.273	0.216	0.674	0.756	0.082	0.712
SE		2.0	0.023	0.018	0.012	0.009	0.016	0.011	0.005	0.100

Note. No — number of observed alleles; *Na* — number of alleles per locus; *Ne* — effective number of alleles; *I* — Shannon's Information Index; *uh*– Nei's genetic diversity index; *uHe* — expected heterozygosity; *Fst* — pairwise fixation index; *Nm* — gene flow value; PIC — polymorphic information content; SE — standard error

The number of observed alleles (*No*) varied noticeably across the SSR markers analyzed, ranging from 4 to 12, for a total of 132 alleles. The highest allelic richness was detected at locus *phi047* (*No* = 12), followed by *bnlg1520* (*No* = 10) and several loci, including *umc1545* and *umc2189* (*No* = 8). Intermediate values (*No* = 6–7) were observed for loci such as *phi021*, *umc1060*, *umc1265*, *umc1403*, and *umc1941*. In contrast, the lowest number of alleles (*No* = 4-5) was recorded for loci including *phi058*, *umc1327*, *umc1446*, *phi002*, *phi027*, and *phi079*. The loci also showed variation in allelic richness, with the number of alleles per locus (*Na*) ranging from 1.2 to 1.7. The highest values were observed for *bnlg1520* and *phi058* (1.7), while the lowest were recorded for *umc1327* and *umc1941* (1.2). Effective alleles (*Ne*) ranged from 1.2 to 1.6, with the greatest values at *bnlg1520*, *phi047*, *phi127*, *umc1060*, and *umc1265*.

Genetic diversity across loci also varied according to Shannon's Information Index (*I*), which spanned from 0.145 (*umc1327*) to 0.374 (*phi058*). Nei's diversity index (*uh*) ranged between 0.116 (*umc1327*) and 0.290 (*phi058*), whereas expected heterozygosity (*uHe*) extended from 0.455 (*umc1327*) to 0.826 (*phi047*). Population differentiation, measured by the fixation index (*Fst*), ranged from 0.056 (*phi079*) to 0.145 (*phi002*), while gene flow (*Nm*) varied from 0.446 (*umc1327*) to 0.884 (*phi047*). Polymorphic information content (PIC) values ranged from 0.446 (*umc1327*) to 0.884 (*phi047*), with a mean of 0.712±0.1. According to common criteria (PIC > 0.5 = highly informative markers), the most informative loci included *phi047* (0.884), *bnlg1520* (0.786), *phi021* (0.742), *phi058* (0.647), *phi127* (0.761), *umc1060* (0.800), and *umc2189* (0.808).

Despite these differences, the uniformly high level of polymorphism across all groups indicates that the SSR markers used in this study are highly informative and suitable for detecting genetic variation in maize. This is further supported by the high mean PIC value (0.712±0.1), confirming the strong discriminatory power of the selected loci. These findings are consistent with previous reports emphasizing the effectiveness of SSR markers in analyzing maize genetic structure [46]

Particular attention should be given to the most polymorphic markers identified in this study, such as *phi047*, *bnlg1520*, *umc1060*, and *umc2189*, which demonstrated the highest PIC values and allelic richness. These markers are not only effective for differentiating genotypes but are also associated with genes controlling important agronomic traits (Tab. 2). For example, markers such as *phi058* and *umc1265* are linked to traits including plant height, tassel architecture, and leaf angle, while *phi002* and *umc1403* are associated with kernel weight [47]. Similarly, markers such as *phi027* and *phi061* are connected to genes involved in starch biosynthesis (*wx1*) and carbohydrate metabolism, which directly influence grain quality [48]. In addition, the marker *phi047* has been reported to be associated with the *mybri17* gene, a transcription factor implicated in the regulation of photosynthetic processes and in enhancing photosynthetic efficiency in maize [49]. This highlights the potential of these SSR markers for marker-assisted selection, particularly to improve yield components, adaptation, and stress tolerance in maize breeding programs.

Analysis of Molecular Variance (AMOVA)

The distribution of genetic variation among and within maize accessions was assessed using analysis of molecular variance (AMOVA, Tab. 6). The results indicated that 70 % of the total genetic variation was attributable to differences among accessions, while the remaining 30 % was attributable to differences within accessions. The sum of squares (SS) for variation among accessions was 1445.608, with a mean square (MS) of 28.912 and an estimated variance of 5.329. In contrast, variation within accessions had an SS of 462.000, an MS of 2.265, and an estimated variance of 2.265. The total estimated variance across all accessions was 7.594. The fixation index (*Fst*) calculated from AMOVA was 0.702, reflecting the proportion of total genetic

variation attributable to differences among accessions. Correspondingly, the estimated number of migrants per generation (*Nm*) was 0.212, representing the relative level of gene flow among accessions.

According to population genetics theory, *Nm* values below 1 indicate that gene flow is insufficient to counteract genetic drift, leading to substantial differentiation among populations [50]. In our collection, the high among-accession variation can largely be explained by the fact that it includes maize varieties from multiple countries: Germany, Switzerland, France, Russia, Türkiye, Greece, China, and Kazakhstan. Because these accessions come from different breeding programs, climates, and agricultural traditions, they carry distinct allelic compositions, which lead to much greater genetic differences between accessions than within them.

Table 6

Results of Analysis of Molecular Variance

Source	*df*	*SS*	*MS*	*Est. Var.*	*%*	*Fst*	*Nm*
Among accessions	50	1445,608	28,912	5,329	70 %	0.702*	0.212*
Within accessions	204	462,000	2,265	2,265	30 %		
Total	254	1907,608		7,594	100 %		

Note. df — degrees of freedom; SS — sum of squares; MS — mean squared; Est.var. — estimates of variance; % — percentage of variation; *Fst* — pairwise fixation index; *Nm* — gene flow value; * $p < 0.001$

To assess the genetic relationships among countries of origin and 51 maize (*Zea mays*) accessions, a dendrogram was constructed using the classical method based on SSR marker data. The phylogenetic analysis by country of origin revealed a clear division into three distinct clusters. Accessions from China formed a highly discrete clade, a pattern robustly supported by a bootstrap value of 100. In contrast, samples from Europe and Kazakhstan clustered together within a common clade (bootstrap = 58), suggesting that these two groups share a closer genetic affinity with each other than with the Chinese lineage (Fig. 2A).

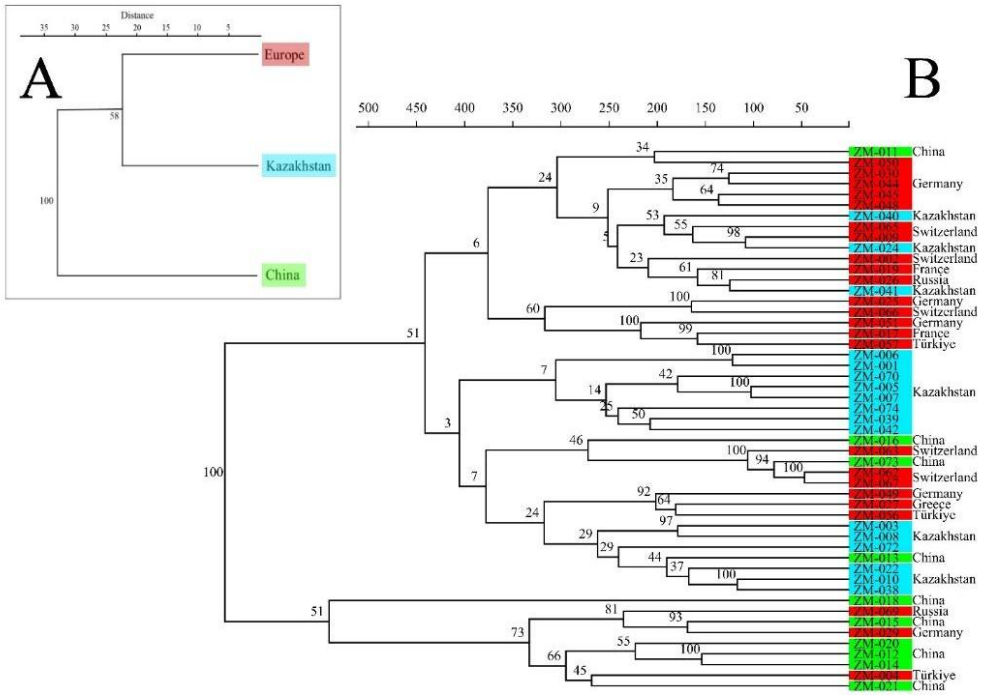

Figure 2. Dendrogram illustrating genetic relationships among *Zea mays* L.:
A — by origin, B — by each accession (color-coded according to the country of origin)

The phylogenetic analysis of the accessions reveals a similar pattern (Fig. 2B), dividing the studied accessions into three clusters based on genetic similarity coefficients and branching patterns, distinguishing European (Cluster I) and Kazakhstani (Cluster II) accessions from Chinese (Cluster III) accessions. Cluster I, located in the upper section of the dendrogram, consists primarily of European accessions and includes sam-

ples from Germany (ZM-050, ZM-030, ZM-044, ZM-045, ZM-048, ZM-025, ZM-051), Switzerland (ZM-065, ZM-009, ZM-002, ZM-066), France (ZM-019), Russia (ZM-026), and Türkiye (ZM-057). Also, this cluster consists of one Chinese (ZM-011) and a few Kazakhstani accessions (ZM-040, ZM-024, ZM-041). Cluster II represents a larger, more complex meta-cluster, subdivided into multiple subclades. The upper portion of Cluster II contains a stable Kazakhstani sub-group (ZM-001, ZM-005, ZM-006, ZM-007, ZM-039, ZM-042, ZM-070, ZM-074) supported by bootstrap values up to 100. Other mixed-origin subclades are present within Cluster II. One sub-clade (bootstrap 100) unites Swiss accessions (ZM-062, ZM-063, ZM-067) with a Chinese accession (ZM-073), while another highly supported sub-clade (bootstrap 97–100) groups Kazakhstani accessions (ZM-003, ZM-008, ZM-072, ZM-022, ZM-010, ZM-038) together with the Chinese accession ZM-013. Cluster III, located in the lower section of the dendrogram, is predominantly Chinese and includes accessions ZM-018, ZM-015, ZM-020, ZM-014, ZM-012, and ZM-021. In addition, individual accessions from Germany (ZM-029), Russia (ZM-069), and Türkiye (ZM-004) were also localized within this cluster.

The observed clustering pattern is consistent with the patterns detected in PCoA: the dendrogram revealed three main clusters that largely correspond to the geographic origin of the accessions. European accessions formed a distinct cluster, reflecting their relatively high genetic diversity and shared breeding history. Chinese accessions were grouped into a separate cluster, indicating moderate differentiation from both European and Kazakhstan accessions. The Kazakhstan accessions, while showing some internal substructuring, tended to cluster together, reflecting their closer genetic relatedness and narrower gene pool. Some accessions, however, exhibited intermediate positions between clusters, suggesting historical gene flow or shared ancestry. For example, certain European accessions (ZM-004, ZM-029, ZM-069) clustered near the Chinese group, suggesting shared alleles due to past germplasm exchange or common parental lines. Similarly, a few Kazakhstan accessions (ZM-024, ZM-040, and ZM-041) showed affinity with European accessions, suggesting limited introgression of exotic germplasm or residual heterogeneity within local populations.

Principal Coordinate Analysis (PCoA)

To further explore the genetic relationships among the three groups by origin and 51 maize (*Zea mays*) accessions, principal coordinate analysis was performed based on SSR marker data (Fig. 3).

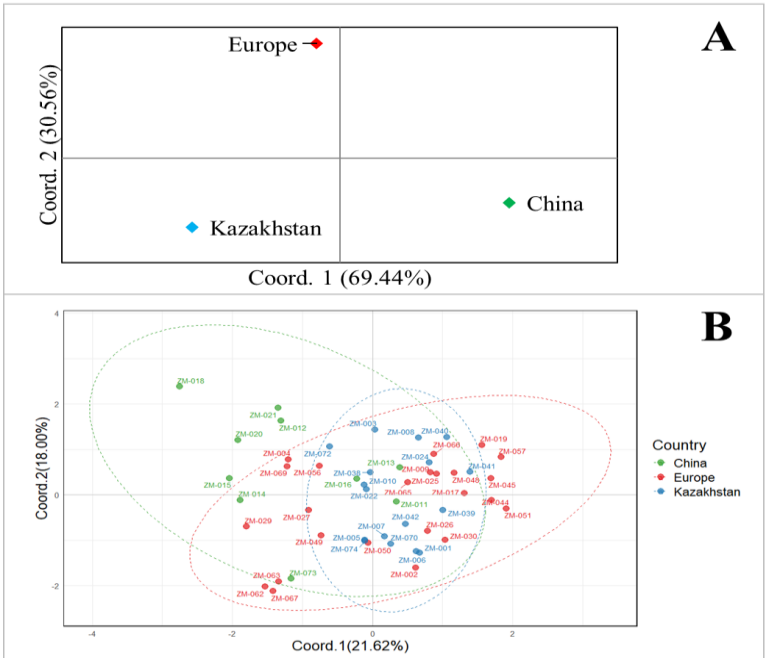

Figure 3. Principal Coordinate analysis plots based on SSR data:
A — by origin, B — by accession, each dot represents one accession, color-coded according to the country of origin

The Principal Coordinate Analysis (PCoA) revealed a distinct genetic separation by the samples' geographical origin. The first coordinate (Coord. 1), which accounted for 69.44 % of the total genetic variation, primarily differentiated the Chinese accessions from the Kazakhstani and European groups. The second co-

ordinate (Coord. 2), explaining an additional 30.56 % of the variance, provided further resolution by separating the European samples from those of Kazakhstani origin (Fig. 3A).

A similar analysis was performed among accessions. The first two principal coordinates accounted for 21.62 % and 18.00 % of the total genetic variation, respectively, together explaining 39.62 % of the observed variation (Fig. 3B). The PCoA plot revealed a relatively clear separation of the accessions into several groups, which is generally consistent with the clustering observed in the dendrogram (Fig. 2).

Accessions of Chinese origin (ZM-012, ZM-020, ZM-021, ZM-015, ZM-014) clustered together predominantly in the higher left quadrant. Notably, Chinese accessions ZM-018 and ZM-073 diverged from the core cluster, shifting toward the upper and lower regions of the plot, respectively. Also, accessions ZM-016, ZM-013, and ZM-011 settled in the central region of the plot, blending with samples from Kazakhstan and Europe. Kazakhstan accessions (ZM001, ZM-003, ZM-005, ZM006, ZM007, ZM010, ZM-074, ZM-070, ZM-024, and others) were mainly distributed in the middle of the plot, admixturing mainly with accessions of European origin. Accessions from European countries are split into two sides of the Coord. 1, and form two groups. The first group, to the left, consisted of Turkish (ZM-004, ZM-069), Russian (ZM-056), Greek (ZM-027), German (ZM-029, ZM-049, ZM-050), and Swiss (ZM-062, ZM-063, ZM-067) accessions. The second group, to the right, was composed of various accessions of European origin: Germany (ZM-025, ZM-030, ZM-044, ZM-045, ZM-048, ZM-051), Switzerland (ZM-002, ZM-009, ZM-065, ZM-066), Russia (ZM-026), Türkiye (ZM-057), and France (ZM-017, ZM-019).

Kazakhstani samples positioned between the European and Chinese clusters. This intermediate placement corroborates their role as a transition zone between East Asian and European germplasm, consistent with the reduced polymorphism observed in these populations. European accessions formed a relatively tight and distinct cluster, reflecting their high genetic diversity and structured allelic composition, while Chinese accessions showed greater spread within the cluster, indicating both high diversity and variability in allele distribution. Overall, the PCoA confirms the genetic distinctness of European, Chinese, and Kazakhstani maize populations, and visually supports the conclusions drawn from allele-based diversity indices.

These results are consistent with previous studies on crop and tree species, in which European accessions often exhibit higher genetic diversity than local or introduced populations. For example, analyses of walnut (*Juglans regia* L.) demonstrated that European genotypes had higher allelic richness and Shannon indices than Kazakhstani accessions, whereas Chinese populations often showed intermediate or variable values depending on the loci examined [51]. Similarly, population genetic studies in cultivated apples (*Malus* x *domestica* Borkh.) have reported that broader geographic distribution and historical gene flow in European populations contribute to higher *Na*, *Ne*, and heterozygosity values [52].

Population Structure Analysis

The population structure of the 51 maize accessions was analyzed using a model-based Bayesian clustering approach (STRUCTURE analysis) (Fig. 4). The highest ΔK value was observed at K = 2 (ΔK = 238.49111). The results indicated the presence of two distinct genetic clusters (K=2). The first cluster (represented in red) comprised predominantly accessions from Europe and Kazakhstan. The second cluster (green) was composed of Chinese, Kazakhstani, and a few European accessions.

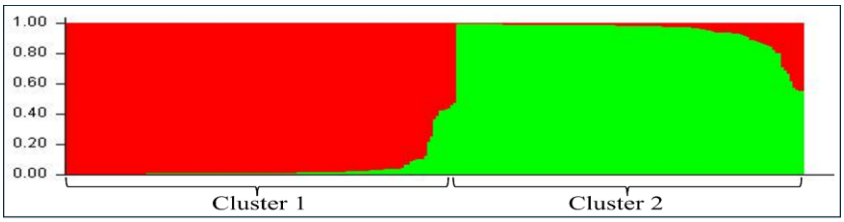

Figure 4. Population structure of 51 maize accessions. Distribution of maize accessions by clusters at K=2

This consolidation of European and Kazakhstani accessions into a single cluster suggests a high degree of shared ancestry or historical gene flow between these regions, which is consistent with known patterns of germplasm exchange and breeding practices. A similar pattern was observed in soybean (*Glycine max* L.), where Kazakhstani accessions clustered together with European genotypes, indicating close genetic relatedness and likely historical germplasm exchange between regions [53]. Examination of individual membership coefficients highlights both clear assignments and intermediate cases. For example, accessions such as ZM-024, ZM-029, ZM-065, and ZM-073 exhibited strong affiliation with the red cluster (>95 %), while

ZM-003, ZM-009, and ZM-014 were almost entirely assigned to the green cluster (>95 %), reflecting distinct lineage separation. Interestingly, some individuals displayed mixed ancestry, including ZM-002-1 (57 % red, 42 % green) and ZM-010-5 (44 % red, 56 % green), indicating historical admixture or residual heterogeneity within populations. Similarly, certain Kazakhstan samples, such as ZM-022-1 (63 % red, 37 % green) and ZM-022-3 (57.5 % red, 42.5 % green), showed partial assignment to both clusters, supporting the idea that local varieties have retained alleles from European germplasm.

Overall, this study confirms that SSR markers are highly effective for evaluating genetic diversity and population structure in *Zea mays* L. The most informative markers identified here offer valuable tools for characterizing additional maize accessions and can be directly applied in breeding programs, supporting both the conservation of genetic resources and the development of improved, locally adapted varieties.

Conclusion

The present study demonstrates substantial genetic diversity among 51 maize (*Zea mays* subsp. *mays*) accessions from Kazakhstan, China, and Europe, as revealed by analysis of 21 SSR markers. Significant genetic differentiation was observed among groups, largely corresponding to their geographic origin: European and Chinese accessions formed distinct clusters, while Kazakhstani landraces displayed unique genetic profiles. Accessions from geographically or breeding-similar backgrounds exhibited higher genetic similarity, whereas more distantly related lines showed greater differentiation, indicating that limited gene flow and breeding history contribute to the observed population structure. Several SSR markers exhibited high polymorphism and informativeness (*phi047*, *umc2189*, *bnlg1520*), confirming their suitability for evaluating genetic diversity and relationships among maize accessions. Importantly, many of the SSR markers used in this study are associated with key genes and agronomic traits, including kernel weight, starch composition, flowering time, and plant architecture, thereby enabling their potential use in marker-assisted selection and in identifying beneficial alleles for breeding programs. Thus, this study provides valuable insights into the genetic composition and structure of maize accessions in Kazakhstan and beyond. The findings provide a foundation for the preservation of local germplasm, the strategic selection of parental lines in hybrid development, and the broader use of genetic resources to enhance maize breeding, adaptability, and resilience across diverse agroecological conditions.

Funding

This research was funded by the Science Committee of the Ministry of Science and Higher Education (Program No.BR24992903).

Conflict of Interest

The authors declare no conflict of interest.

Author contribution

The manuscript was written through the contributions of all authors. All authors have given approval to the final version of the manuscript. CRediT: **Ibraimov A.M.** — formal analysis, investigation, writing — original draft, writing — review & editing; **Yermagambetova M.M.** — data curation, investigation, methodology, validation, writing — original draft, writing — review & editing; **Makhmadzhanov S.P.** — formal analysis, investigation, resources; **Ortaev A.K.** — formal analysis, investigation, resources; **Turuspekov Y.K.** — conceptualization, data curation, funding acquisition, methodology, project administration, supervision, validation, writing — original draft, writing — review & editing.

References

1 Fischer, R. A., & Edmeades, G. O. (2010). Breeding and cereal yield progress. *Crop science*, *50*, S-85. https://doi.org/10.2135/cropsci2009.10.0564.

2 Tanumihardjo, S. A., McCulley, L., Roh, R., Lopez-Ridaura, S., Palacios-Rojas, N., & Gunaratna, N. S. (2020). Maize agro-food systems to ensure food and nutrition security in reference to the Sustainable Development Goals. *Global Food Security*, *25*, 100327. https://doi.org/10.1016/j.gfs.2019.100327.

3 Leff, B., Ramankutty, N., & Foley, J. A. (2004). Geographic distribution of major crops across the world. *Global biogeochemical cycles*, *18*(1). https://doi.org/10.1029/2003GB002108.

4 Iltis, H. H., & Doebley, J. F. (1980). Taxonomy of Zea (Gramineae). II. Subspecific categories in the Zea mays complex and a generic synopsis. *American Journal of Botany*, *67*(6), 994–1004. https://doi.org/10.1002/j.1537-2197.1980.tb07731.x.

5 (2026). Plants of the World Online. Facilitated by the Royal Botanic Gardens, Kew. Published on the Internet. *powo.science.kew.org.* Retrieved from https://powo.science.kew.org/ Retrieved 27 March 2026.

6 Matsuoka, Y., Vigouroux, Y., Goodman, M. M., Sanchez G, J., Buckler, E., & Doebley, J. (2002). A single domestication for maize shown by multilocus microsatellite genotyping. *Proceedings of the National Academy of Sciences*, *99*(9), 6080–6084. https://doi.org/10.1073/pnas.052125199.

7 Adhikari, S., Joshi, A., Kumar, A., & Singh, N. K. (2021). Diversification of maize (Zea mays L.) through teosinte (Zea mays subsp. parviglumis Iltis & Doebley) allelic. *Genetic Resources and Crop Evolution*, *68*(7), 2983–2995. https://doi.org/10.1007/s10722-021-01170-z.

8 Wang, R. L., Stec, A., Hey, J., Lukens, L., & Doebley, J. (1999). The limits of selection during maize domestication. *Nature*, *398*(6724), 236–239. https://doi.org/10.1038/18435.

9 Kuleshov, N. N. (1933). World's diversity of phenotypes of maize. *Journal of the American Society of Agronomy*, *25*, 688–700.

10 Scott, P., Pratt, R. C., Hoffman, N., & Montgomery, R. (2019). Specialty corns. *Corn* (pp. 289–303). AACC International Press.

11 Santillán-Fernández, A., Salinas-Moreno, Y., Valdez-Lazalde, J. R., Bautista-Ortega, J., & Pereira-Lorenzo, S. (2021). Spatial delimitation of genetic diversity of native maize and its relationship with ethnic groups in Mexico. *Agronomy*, *11*(4), 672. https://doi.org/10.3390/agronomy11040672.

12 Wang, M., Wu, M., & Huo, H. (2007). Life-cycle energy and greenhouse gas emission impacts of different corn ethanol plant types. *Environmental Research Letters*, *2*(2), 024001. https://doi.org/10.1088/1748-9326/2/2/024001.

13 Klimek-Kopyra, A., Szmigiel, A., Zajac, T., & Kidacka, A. (2012). Some aspects of cultivation and utilization of waxy maize (Zea mays L. ssp. ceratina). *Acta Agrobotanica*, *65*(3). https://doi.org/10.5586/aa.2012.001.

14 Buckler, E. S., Gaut, B. S., & McMullen, M. D. (2006). Molecular and functional diversity of maize. *Current opinion in plant biology*, *9*(2), 172–176. https://doi.org/10.1016/j.pbi.2006.01.013.

15 Whitt, S. R., Wilson, L. M., Tenaillon, M. I., Gaut, B. S. & Buckler IV, E. S. (2002). Genetic diversity and selection in the maize starch pathway. *Proceedings of the National Academy of Sciences*, *99*(20), 12959–12962. https://doi.org/10.1073/pnas.202476999.

16 Chňapek, M., Balážová, Ž., Špaleková, A., Gálová, Z., Hromadová, Z., Číšecká, L., & Vivodík, M. (2024). Genetic diversity of maize resources revealed by different molecular markers. *Genetic Resources and Crop Evolution*, *71*(8), 4685–4703. https://doi.org/10.1007/s10722-024-01908-5.

17 Sagar, T., Kapoor, N., & Mahajan, R. (2023). Microsatellites as potential molecular markers for genetic diversity analysis in plants. *Molecular marker techniques: A potential approach of crop improvement* (pp. 81–101). Singapore: Springer Nature Singapore. https://doi.org/10.1007/978-981-99-1612-2_5.

18 Powell, W., Machray, G. C., & Provan, J. (1996). Polymorphism revealed by simple sequence repeats. *Trends in plant science*, *1*(7), 215–222. https://doi.org/10.1016/1360-1385(96)86898-1.

19 Kalia, R. K., Rai, M. K., Kalia, S., Singh, R. & Dhawan, A. K. (2011). Microsatellite markers: an overview of the recent progress in plants. *Euphytica*, *177*(3), 309–334. https://doi.org/10.1007/s10681-010-0286-9.

20 Shete, G. S., Nikam, S. D., Surbhaiyya, S. D., Jadhav, M. P., & Thakare, T. N. (2023). Analysis of genetic diversity in maize (Zea mays L.) variety using SSR markers. *International Journal of Plant & Soil Science*, *35*(15), 205–212. https://doi.org/10.9734/ijpss/2023/v35i153098.

21 Belalia, N., Lupini, A., Djemel, A., Morsli, A., Mauceri, A., Lotti, C., ... & Sunseri, F. (2019). Analysis of genetic diversity and population structure in Saharan maize (Zea mays L.) populations using phenotypic traits and SSR markers. *Genetic Resources and Crop Evolution*, *66*(1), 243–257. https://doi.org/10.1007/s10722-018-0709-3.

22 Vathana, Y., Sa, K. J., Lim, S. E., & Lee, J. K. (2019). Genetic diversity and association analyses of Chinese maize inbred lines using SSR markers. *Plant breeding and biotechnology*, *7*(3), 186–199. https://doi.org/10.9787/PBB.2019.7.3.186.

23 Aci, M. M., Revilla Temiño, P., Morsli, A., Djemel, A., Belalia, N., Kadri, Y., ... & Khelifi, L. (2013). *Genetic diversity in Algerian maize (Zea mays L) landraces using SSR markers.*

24 Suhasini, B., Ravikesavan, R., & Yuvaraja, A. (2023). Microsatellite marker based genetic diversity study in sweet corn in breds (Zea mays L. saccharata). *Plant Archives (09725210)*, *23*(2). DOI: 10.51470/PLANTARCHIVES.2023.v23.no2.058.

25 Patel, R., Memon, J., Kumar, S., Patel, D. A., Sakure, A. A., Patel, M. B., ... & Roychowdhury, R. (2024). Genetic diversity and population structure of maize (Zea mays L.) inbred lines in association with phenotypic and grain qualitative traits using SSR genotyping. *Plants*, *13*(6), 823. https://doi.org/10.3390/plants13060823.

26 Bocianowski, J., Nowosad, K., Wróbel, B., & Szulc, P. (2021). Identification of associations between SSR markers and quantitative traits of maize (Zea mays L.). *Agronomy*, *11*(1), 182. https://doi.org/10.3390/agronomy11010182.

27 Sherakhane, M., Lohithaswa, H. C., Sinchana Kashyap, G. S., Gowda, B., Siddaraju, R., & Keshavareddy, G. (2025). Genetic Purity Assessment of Maize Hybrid (Zea mays L.) and Its Parental Lines Employing SSR Markers. *Journal of Advances in Biology & Biotechnology*, *28*(2), 779–785. https://doi.org/10.9734/jabb/2025/v28i22038.

28 Sembayeva, A. S., Ospanbayev, Z., Zhapayev, R. K., Kenenbayev, S. B., Pejic, B., Kunypiyaeva, G. T., ... & Bekbauov, M. (2025). Corn hybrids assessment for grain yield under the soil tillage regimes and drip irrigation in Southeast Kazakhstan. *SABRAO Journal of Breeding and Genetics*, *57*(1). http://doi.org/10.54910/sabrao2025.57.1.5.

29 Tynykulov, M. (2022). Corn productivity in Northern Kazakhstan. *Izdenister Natigeler*, *3* (95), 54–62. https://doi.org/10.37884/3-2022/06.

30 Kudaibergenova, I., Kalashnikov, A., Balgabaev, N., Zharkov, V., & Angold, E. (2023). Effect of drip irrigation with foliar dressing of mineral fertilizer Kristalon and their impact on maize grain yield in Southern Kazakhstan. *SABRAO Journal of Breeding and Genetics*, *55*(5), 1855–1864. http://doi.org/10.54910/sabrao2023.55.5.36.

31 Malitskaya, N. V., Kusnetzova, M. A., Ashirbekov, M. Z., Ostretzova, I. B., Nurmukhametova, N. N., Zhumabayeva, S. E.,... & Shoykin, O. D. (2025). Evaluation of early maturing maize hybrids for yield-related traits in Akmola Region, Kazakhstan. *SABRAO Journal of Breeding & Genetics*, *57*(5). http://doi.org/10.54910/sabrao2025.57.5.20.

32 Yermagambetova, M. M., Ibraimov, A. M., Ortaev, A. K., Makhmadzhanov, S. P., & Turuspekov, Y. K. (2025). Genetic diversity analysis of *Zea mays* L. accessions based on microsatellite markers. *Eurasian Journal of Applied Biotechnology*, (3), 24–34. https://doi.org/10.11134/btp.3.2025.3.

33 Dellaporta, S. L., Wood, J., & Hicks, J. B. (1983). A plant DNA minipreparation: version II. *Plant molecular biology reporter*, *1*(4), 19–21. https://doi.org/10.1007/BF02712670.

34 Woodhouse, M. R., Cannon, E. K., Portwood, J. L., Gardiner, J. M., Hayford, R. K., Haley, O., & Andorf, C. M. (2025). Tools and resources at the maize genetics and genomics database (MaizeGDB). *Cold Spring Harbor Protocols*, *2025*(1), pdb-over108430. DOI: 10.1101/pdb.over108430.

35 Peakall, R. O. D., & Smouse, P. E. (2012). GenAlEx 6.5: genetic analysis in Excel. Population genetic software for teaching and research—an update. *Bioinformatics*, *28*(19), 2537–2539. https://doi.org/10.1093/bioinformatics/bts460.

36 Botstein, D., White, R. L., Skolnick, M., & Davis, R. W. (1980). Construction of a genetic linkage map in man using restriction fragment length polymorphisms. *American journal of human genetics*, *32*(3), 314. PMID: 6247908.

37 (2020). RStudio: Integrated Development for R. RStudio, PBC, Boston, MA. *www.rstudio.com.* Retrieved from http://www.rstudio.com/

38 Hammer, Ø., Harper, D. A., & Ryan, P. D. (2001). PAST: Paleontological statistics software package for education and data analysis. *Palaeontologia electronica*, *4*(1), 9.

39 Xie, J., Chen, Y., Cai, G., Cai, R., Hu, Z., & Wang, H. (2023). Tree Visualization By One Table (tvBOT): a web application for visualizing, modifying and annotating phylogenetic trees. *Nucleic acids research*, *51*(W1), W587–W592. https://doi.org/10.1093/nar/gkad359.

40 Pritchard, J. K., Stephens, M., & Donnelly, P. (2000). Inference of population structure using multilocus genotype data. *Genetics*, *155*(2), 945–959. https://doi.org/10.1093/genetics/155.2.945.

41 Evanno, G., Regnaut, S., & Goudet, J. (2005). Detecting the number of clusters of individuals using the software STRUCTURE: a simulation study. *Molecular ecology*, *14*(8), 2611–2620. https://doi.org/10.1111/ j.1365-294X.2005.02553.x.

42 Kopelman, N. M., Mayzel, J., Jakobsson, M., Rosenberg, N. A., & Mayrose, I. (2015). Clumpak: a program for identifying clustering modes and packaging population structure inferences across K. *Molecular ecology resources*, *15*(5), 1179–1191. https://doi.org/10.1111/1755 0998.12387.

43 Hao, D., Zhang, Z., Cheng, Y., Chen, G., Lu, H., Mao, Y., ... & Xue, L. (2015). Identification of genetic differentiation between waxy and common maize by SNP genotyping. *PLoS One*, *10*(11), e0142585. https://doi.org/10.1371/journal.pone.0142585.

44 Zheng, H., Wang, H., Yang, H., Wu, J., Shi, B., Cai, R., ... & Luo, L. (2013). Genetic diversity and molecular evolution of Chinese waxy maize germplasm. *Plos one*, *8*(6), e66606. https://doi.org/10.1371/journal.pone.0066606.

45 Wu, X., Li, Y., Li, X., Li, C., Shi, Y., Song, Y., ... & Wang, T. (2015). Analysis of genetic differentiation and genomic variation to reveal potential regions of importance during maize improvement. *BMC plant biology*, *15*(1), 256. https://doi.org/10.1186/s12870-015-0646-7

46 Nashath, M. N. F., Mubarak, A. N. M., & Kumara, A. D. N. T. (2023). *Exploring genetic diversity of maize* (*Zea mays* L.) *accessions in Sri Lanka by employing SSR markers on photosynthetic, canopy architectural and grain yield traits*.

47 Wallace, J. G., Bradbury, P. J., Zhang, N., Gibon, Y., Stitt, M., & Buckler, E. S. (2014). Association mapping across numerous traits reveals patterns of functional variation in maize. *PLoS genetics*, *10*(12), e1004845. https://doi.org/10.1371/journal.pgen.1004845.

48 Mishra, S. J., Gopinath, I., Muthusamy, V., Zunjare, R. U., Chand, G., Venkatesh, A. K., ... & Hossain, F. (2025). Unraveling the interactive effect of opaque2 and waxy1 genes on kernel nutritional qualities and physical properties in maize (*Zea mays* L.). *Scientific Reports*, *15*(1), 3425. https://doi.org/10.1038/s41598-025-87666-5.

49 Li, H., He, X., Lv, H., Zhang, H., Peng, F., Song, J., ... & Zhang, J. (2025). Epibrassinolide regulates Lhcb5 expression though the transcription factor of MYBR17 in maize. *Biomolecules*, *15*(1), 94. https://doi.org/10.3390/biom15010094.

50 Slatkin, M. (1985). Gene flow in natural populations. *Annual review of ecology and systematics*, 393–430.

51 Kairova, G., Taskuzhina, A., Yanin, K., Ismagulova, E., Oleichenko, S., Sarshayeva, M., ... & Gritsenko, D. (2025). First evaluation of genetic diversity and population structure of wild and cultivated Juglans regia in Kazakhstan. *Genetic Resources and Crop Evolution*, *72*(7), 8281–8292. https://doi.org/10.1007/s10722-025-02443-7.

52 Urrestarazu, J., Denancé, C., Ravon, E., Guyader, A., Guisnel, R., Feugey, L., ... & Durel, C. E. (2016). Analysis of the genetic diversity and structure across a wide range of germplasm reveals prominent gene flow in apple at the European level. *BMC plant biology*, *16*(1), 130. https://doi.org/10.1186/s12870-016-0818-0.

53 Zatybekov, A., Genievskaya, Y., Fang, C., Abugalieva, S., & Turuspekov, Y. (2025). Uncovering the genetic landscape of soybean accessions from Kazakhstan in comparison with global germplasm using whole genome resequencing. *BMC genomics*, *26*(1), 802. https://doi.org/10.1186/s12864-025-12024-8.

А.М. Ибраимов, М.М. Ермағамбетова, С.П. Махмаджанов,
А.К. Ортаев, Е.К. Туруспеков

Микросателлиттік маркерлерге негізделген әртүрлі географиялық аймақтардан алынған *Zea mays* L. үлгілерінің генетикалық алуантүрлілігін бағалау

Зерттеу жұмысының мақсаты — микросателлиттік (SSR) маркерлерді пайдалана отырып, Қазақстаннан, Қытайдан және Еуропадан алынған жүгерінің 51 сорттары мен гибридтерінің (*Zea mays* L.) генетикалық алуантүрлілігі мен құрылымын қарастыру. Барлығы 255 үлгіні генотиптеу үшін 21 жоғары полиморфты SSR маркері қолданылды, бұл аллельдік алуантүрлілік пен генетикалық қатынастарды кешенді бағалауға мүмкіндік берді. Локустағы аллельдердің саны 1,517 орташа мәнімен 1,0-ден 2,7-ге дейін өзгерді, ал күтілетін гетерозиготалық (*uHe*) орташа есеппен 0,192 құрады, бұл үлгілер арасындағы генетикалық алуантүрліліктің орташа деңгейін көрсетеді. Географиялық шығу тегі бойынша генетикалық алуантүрлілікті талдау еуропалық үлгілердің ең үлкен аллельдік байлығымен (*Na* = 5,9) және генетикалық алуантүрлілігімен, одан кейін қытайлық және қазақстандық топтармен сипатталатынын көрсетті. Осы айырмашылықтарға қарамастан, барлық топтар 100 % полиморфизмді көрсетті, бұл таңдалған SSR маркерлерінің жоғары ақпараттылығын растайды. Полиморфты ақпараттық мазмұнының (PIC) мәндері 0,446-дан 0,884-ке дейін, орташа мәні 0,712-ге дейін өзгерді, бұл *phi047*, *bnlg1520* және *umc2189* маркерлерінің жоғары ақпараттылығын көрсетті. Молекулалық дисперсияны (AMOVA) талдау жалпы генетикалық вариацияның 70 % үлгілер арасындағы айырмашылықтарға байланысты екенін көрсетті, бұл жоғары генетикалық дифференциацияны (*Fst* = 0,702) және шектеулі ген ағынын (*Nm* = 0,212) түсіндіреді. Кластерлік талдау, негізгі координаттарды талдау (PCoA) және STRUCTURE нәтижелері қытайлық үлгілердің нақты генетикалық бөлінуін дәйекті түрде анықтады, ал еуропалық және қазақстандық үлгілер жақынырақ генетикалық байланыстар мен ішінара араласуды көрсетті. Жалпы алғанда, нәтижелер жүгері үлгілері арасында айтарлықтай генетикалық алуантүрлілікті және айқын популяция құрылымын көрсетеді, бұл генетикалық ресурстарды сақтау және селекциялық бағдарламаларда генетикалық әртүрлі ата-аналық линияларды таңдау үшін құнды дерек көзі болады.

Кілт сөздер: *Zea mays*, Қазақстан, молекулалық маркерлер, SSR, генетикалық алуантүрлілік, полиморфизм, генетикалық құрылым, генотиптеу.

А.М. Ибраимов, М.М. Ермагамбетова, С.П. Махмаджанов,
А.К. Ортаев, Е.К. Туруспеков

Оценка генетического разнообразия образцов *Zea mays* L. из разных географических регионов на основе микросателлитных маркеров

Целью данного исследования было изучение генетического разнообразия и структуры 51 сорта и гибрида кукурузы (*Zea mays* L.), происходящих из Казахстана, Китая и Европы, с использованием маркеров простых повторяющихся последовательностей (SSR). Для генотипирования 255 образцов был применен 21 высокополиморфный SSR-маркер, что позволило провести всестороннюю оценку аллельной изменчивости и генетических взаимосвязей. Количество аллелей на локус варьировалось от 1,0 до 2,7, в среднем составляя 1,517, а ожидаемая гетерозиготность (*uHe*) в среднем составляла 0,192, что указывает на умеренное генетическое разнообразие среди образцов. Анализ генетического разнообразия по географическому происхождению показал, что европейские образцы демонстрируют наибольшее аллельное богатство (*Na* = 5,9) и генетическое разнообразие, за ними следуют китайские и казахстанские группы. Несмотря на эти различия, все группы показали 100 % полиморфизм, подтверждая высокую информативность выбранных SSR-маркеров. Значения PIC варьировались от 0,446 до 0,884 со средним значением 0,712, что указывает на высокую информативность таких маркеров, как *phi047*, *bnlg1520* и *umc2189*. Анализ AMOVA показал, что 70 % общей генетической изменчивости обусловлено различиями между образцами, что указывает на сильную генетическую дифференциацию (*Fst* = 0,702) и ограниченный генный поток (Nm = 0,212). Кластерный анализ, анализ PCoA

и результаты STRUCTURE выявили четкое разделение китайских образцов, в то время как европейские и казахстанские образцы показали более тесные генетические связи и частичное смешение. В целом, полученные результаты подчеркивают генетическое разнообразие и различную популяционную структуру среди образцов кукурузы, предоставляя ценную информацию для сохранения генофонда и отбора генетически разнообразных родительских линий в селекционных программах.

Ключевые слова: Zea mays, Казахстан, молекулярные маркеры, SSR, генетическое разнообразие, полиморфизм, генетическая структура, генотипирование.

Information about the authors

Ibraimov Alan Madiyarovich — Laboratory assistant of the Laboratory of Molecular Genetics, Institute of Plant Biology and Biotechnology, Almaty, Kazakhstan; e-mail: alan.ibraimov08@gmail.com; ORCID: https://orcid.org/0009-0007-1244-5209

Yermagambetova Moldir Makatkyzy — PhD, Senior Researcher of the Laboratory of Molecular Genetics, Institute of Plant Biology and Biotechnology, Almaty, Kazakhstan; e-mail: ermaganbetova.moldir@bk.ru; ORCID: https://orcid.org/0000-0002-4737-2384

Makhmadzhanov Sabir Partovich — Candidate of Agricultural Sciences, Head of laboratory at Agricultural Experimental Station for Cotton and Melon Growing, Atakent village, Kazakhstan; e-mail: max_s1969@mail.ru; ORCID: https://orcid.org/0009-0007-6664-5759

Ortaev Anarbai Kainarovich — Candidate of Agricultural Sciences, Director at Krasnovodopad Agricultural Experimental Station, Sarkyrama village, Kazakhstan; e-mail: anarbai_68@mail.ru; ORCID: https://orcid.org/0000-0001-5571-6055

Turuspekov Yerlan Kenesbekovich — Dr., Professor, Head of the Laboratory of Molecular Genetics, Institute of Plant Biology and Biotechnology, Almaty, Kazakhstan; e-mail: yerlant@yahoo.com; ORCID: https://orcid.org/0000-0001-8590-1745

How to Cite: Berliguzhin, M.T, Akhmedenov, K.M. & Yakupova, J.B.. (2026). Paleoecological reconstruction of the Late Pleistocene in the lower reaches of the Ural (Zhaiyk) River based on the materials of the Daryinsk Museum Collection. *Fundamental and Experimental Biology*, 31, 3 (123), 83-93. https://doi.org/10.31489/2026FEB3/83-93

Research Article

https://doi.org/10.31489/2026FEB3/83-93

UDC 903(574.1) Received: 9.02.2026 | Accepted: 8.06.2026 | Published online: 30.09.2026

M.T. Berliguzhin*, K.M. Akhmedenov, J.B. Yakupova

Makhambet Utemisov West Kazakhstan University, Uralsk, Kazakhstan
**Corresponding author: 88_max_88.88@inbox.ru*

Paleoecological reconstruction of the Late Pleistocene in the lower reaches of the Ural (Zhaiyk) River based on the materials of the Daryinsk Museum Collection

This article presents the results of a comprehensive study of a collection of Pleistocene mammal remains from the M.A. Sholokhov Memorial Museum (Daryinsk settlement, Baiterek District, West Kazakhstan Region). The material was collected from Late Pleistocene alluvial deposits in the lower reaches of the Ural (Zhaiyk) River and remained unidentified for a long time. Morphometric analyses allowed the collection to be documented and introduced into the scientific record for the first time, and enabled clarification of the taxonomic attribution of the large mammal remains. The collection includes skulls of *Bos primigenius* and *Bison priscus*, numerous postcranial elements and teeth of *Mammuthus primigenius*, a tooth of the transitional form *Mammuthus trogontherii chosaricus*, a femur of *Coelodonta antiquitatis* (Blumenbach, 1799), as well as antler beams of *Megaloceros giganteus* and *Cervus elaphus*. Comparative analyses following von den Driesch, Garutt, Dubrovo, and Foronova, together with comparisons with published series from the Ural–Volga–Caspian region, confirm the typical composition of the Pleistocene megafauna of Western Kazakhstan and indicate a broad spectrum of ecosystems, ranging from cold tundra–steppe environments to floodplain meadows. The results are significant for reconstructing Late Pleistocene palaeoecological conditions in the Ural–Caspian Lowland and for assessing environmental dynamics associated with climatic fluctuations.

Keywords: Late Pleistocene, Western Kazakhstan, Ural (Zhaiyk) River; megafauna, paleoecological reconstruction, museum collection, large mammals, Quaternary.

Introduction

The lower reaches of the Ural (Zhaiyk) River represent one of the key regions for the formation of Pleistocene paleofaunal complexes of the Ural–Caspian Lowland. Throughout the 20th century, numerous finds of large mammals from the glacial epochs were recorded in this area; however, a substantial part of the collected material remained outside scientific circulation. Among these collections, the Pleistocene megafaunal remains housed in the M.A. Sholokhov Memorial Museum in Daryinsk settlement (Baiterek District, West Kazakhstan Region) are of particular interest.

The collection consists of specimens gathered at different times from the lower reaches of the Ural (Zhaiyk) River, mainly from alluvial sand—gravel deposits attributed to the Late Pleistocene. A considerable portion of the material has not previously undergone systematic taxonomic identification, which has hindered the incorporation of these data into regional syntheses of Quaternary faunas.

The aim of this study is to conduct a detailed morphometric analysis and to establish the taxonomic composition of the large Pleistocene mammal fauna from this locality.

Experimental

The results of this study correspond to the UN Sustainable Development Goal 15 “Conservation of terrestrial ecosystems”. The studied collection comprises 37 catalogued osteological specimens representing several key taxa of Pleistocene megafauna.

Taxonomic composition of the material

1. Family Bovidae

Bos primigenius (Bojanus, 1825) — two skulls

Bison priscus (Bojanus, 1827) — two skulls

2. Order Proboscidea

Mammuthus primigenius — occipital parts of skulls, vertebrae, pelvic, humeral, tibial and ulnar elements, mandible, teeth, tusks, and a rib

Mammuthus trogontherii chosaricus (Dubrovo, 1966) — one molar tooth

3. Family Rhinocerotidae

Coelodonta antiquitatis (Blumenbach, 1799) — femur

4. Family Cervidae

Megaloceros giganteus — three horn rods

Cervus elaphus — horn rods (Fig. 1)

Figure 1. The museum's paleontological collection

Linear measurements were obtained using a digital caliper (Mitutoyo, Japan; accuracy ±0.01 mm) and an osteometric board for large skeletal element. The morphometric study of cranial and postcranial remains of mammals was carried out in accordance with the universal osteometric system of A. von den Driesch [1], which ensures the comparability of the results with international reference collections. Specialized methods were used for individual taxonomic groups, adapted to the anatomical and functional specifics of the respective taxa. The study of elephantine remains was based on the classical works of I.V. Dubrovo [2], the methodological schemes of V.E. Garutt and I.V. Foronova [3], and the refined measurement approaches proposed by A.V. Sher and V.E. Garutt [4]. Lamellar frequency was determined on the lateral surface of the crown; in the case of fragmented teeth, the count was made on a standard 5-centimeter section, with subsequent extrapolation to the full length of the crown. The thickness of the enamel was measured on the chewing surface by a series of 5–10 point measurements, averaged for the micron.

For representatives of the *Artiodactyla* order, specialized methodological complexes were used. When studying the *Bovidae* family, systems for measuring skulls and calculating diagnostic indices were used according to V.I. Gromova [5] and B.S. Rusanov [6]. The sex diagnosis of bison skulls was carried out in accordance with Rusanov's criteria, and the determination of Bison morphotypes was carried out using the method of A.A. Khromov [7], which takes into account the combination of braincase proportions and the morphology of horn rods. The measurement of skulls and antlers of the Cervidae family, as well as the calculation of indices, was carried out using the methodological developments of I.A. Vishlobokova [8] and G.G. Boeskorov [9], which allow for the correct assessment of intraspecific and interspecific variability.

The comprehensive use of these methods ensured the reliability of the taxonomic identification of the remains and allowed for a comparative morphological analysis with collections from Eastern Europe, Central Asia, and Siberia.

Geographical and geological setting

The paleontological locality is situated in the lower reaches of the Ural (Zhaiyk) River within the territory of the Baiterek District, West Kazakhstan Region. This area belongs to the southeastern part of the

Ural–Caspian Lowland, a vast accumulative plain characterized by thick successions of Quaternary deposits formed under conditions of prolonged fluvial and alluvial—deltaic sedimentation.

The landscape of the region is defined by a combination of floodplain, above-floodplain, and terrace levels, which developed successively under the influence of variations in the discharge of the Ural River, fluctuations of the Caspian Sea level, and climatic reorganizations during the Late Neopleistocene. The lower reaches of the Ural (Zhaiyk) River represent a wide alluvial valley with a well-developed system of oxbow lakes, pools, and channels, promoting the accumulation of organic material and the preservation of large mammal remains within sandy—loamy and gravel-sand deposits [10].

The paleontological materials housed in the M.A. Sholokhov Memorial Museum (Daryinsk settlement) were collected from similar Quaternary alluvial horizons. In the lower Ural region, the thickness of Pleistocene deposits reaches several tens of meters and is represented by interbedded sands, sandy loams, gravels, silts, and loams typical of channel, floodplain, and oxbow—lake facies. These sedimentary environments provided optimal conditions for the preservation of large osteological elements, including skulls, long bones, antlers, and tusks [11].

The sedimentary environment of the Late Pleistocene in the region was highly dynamic, involving cyclical changes in the hydrological regime that caused shifts in the Ural River channel, the formation of new terraces, and the accumulation of fresh fluvial deposits. These processes were directly linked to climatic fluctuations, marked by alternations of colder and warmer phases, which are reflected in the paleofaunal composition of the assemblages. The presence in the collection of remains of mammoth (*Mammuthus primigenius*), woolly rhinoceros (*Coelodonta antiquitatis*), steppe bison (*Bison priscus*), and aurochs (*Bos primigenius*) indicates the development of tundra–steppe and steppe landscapes typical of cold phases of the Late Pleistocene [12].

Thus, the geographical and geological position of the locality in the lower reaches of the Ural River determined the conditions of accumulation and preservation of the Pleistocene megafauna represented in the Daryinsk museum collection [13]. The combination of thick fluvial deposits, a dynamic river system, and climatically driven environmental changes provides a unique framework for reconstructing the paleoecological conditions of Western Kazakhstan during the Quaternary (Tab. 1).

Table 1

Stratigraphic correlation and faunal attribution of the Daryinsk section (Lower Ural River)

Layer	Depth (m)	Lithology	Age interpretation	Faunal content	Taphonomic interpretation
1	0-1	Modern floodplain grayish–brown loams with humus interlayers	Holocene	No Pleistocene fauna	Modern floodplain deposition
2	1–4	Light yellow–grey sandy loams with silty interbeds	Late Holocene — Early Neopleistocene	Aquatic microfauna (Planorbis, Lymnaea, Pisidium, Candona, Ilyocypris, Cyprideis)	Calm floodplain — oxbow deposition, minimal reworking
3	4–10	Medium–coarse channel sands with gravel–pebble lenses	Late Neopleistocene (MIS 3-2)	Sporadic reworked Pleistocene remains	High–energy channel transport
4	10–16	Cross–bedded sand — gravel deposits (main paleontological horizon)	Late Pleistocene (correlated with Khvalynian–Khazarian alluvial phases)	Concentration of megafauna (skulls, long bones, tusks, vertebrae)	Rapid burial in channel — nearshore facies; limited reworking of coarse material
5	16–22	Dense sandy loams and loams (oxbow — lacustrine facies)	Late Pleistocene (MIS 5-3 interstadials)	Mollusks and ostracods (Limnocythere postoncava, Candona, Cyprideis, Loxoconcha)	Alternation of freshwater and slightly brackish conditions
6	>22	Coarse, well–sorted ancient alluvial sands	Early–Middle Pleistocene	Reworked Mammuthus primigenius, Bos primigenius	Basal high–energy alluvial erosion

Layer 1. 0-1 m. Modern floodplain loams. The layer consists of greyish-brown loose loams with thin humus–rich interlayers. The sediment shows weak stratification and contains small inclusions of plant detritus. It was formed under modern floodplain conditions subjected to periodic seasonal flooding and deposition of fine–grained material in a low–energy environment. As the layer is of Holocene age, no remains of Pleistocene fauna were recorded.

Layer 2. 1–4 m. Floodplain sandy loams and silts. This layer is composed of light-yellow to light-grey fine-grained sandy loams with thin silty interbeds and rare lenses of plant detritus. The heterogeneous lenticular—laminated structure reflects alternating phases of quiet inundation and low—energy currents within an expanded floodplain. Lithological characteristics indicate formation during the Late Holocene—Early Neopleistocene. Large bone material is absent; however, aquatic microfauna occurs regularly. The microfaunal assemblage includes freshwater gastropods (Planorbis sp., Lymnaea sp.), small bivalves (Pisidium sp.), and ostracods of the genera Candona, Ilyocypris, and Cyprideis. The good preservation of valves, often found articulated, indicates calm depositional conditions and minimal reworking. The assemblage reflects shallow, weakly flowing floodplain—oxbow water bodies with fresh to slightly mineralized water.

Layer 3. 4–10 m. Channel sands with gravel–pebble lenses. The layer is represented by well–sorted medium — to coarse–grained sands with lenses of gravel and small pebbles [14]. Cross–bedding is common, and locally massive structures typical of high–energy channel flows are observed. Sedimentation occurred under conditions of a powerful and dynamically migrating Ural River channel, corresponding to cold stages of the Late Neopleistocene (MIS 3-2). Pleistocene faunal remains occur sporadically and in reworked condition, often showing traces of abrasion and transport.

Layer 4. 10–16 m. Sand–gravel deposits—main paleontological horizon. This unit includes coarse sands, gravels, and pebbles, partly cemented by iron compounds. Cross-bedded structures, channel infills, and evidence of repeated flood events are well expressed. This layer represents the main concentration horizon of Pleistocene megafauna, yielding skull fragments, long bones, tusks, and vertebrae. Their preservation is related to rapid burial within channel—nearshore facies and minimal reworking of coarse material. Lithological features are comparable with the Khvalynian and Khazarian alluvial horizons of the Caspian region. Microfauna is episodic and represented by reworked ostracods (Cyprideis, Candona) transported from adjacent oxbow and floodplain facies. Shells are frequently damaged, reflecting high–energy depositional conditions.

Layer 5. 16–22 m. Oxbow and floodplain—lacustrine sandy loams and loams. The deposits consist of dense brownish–yellow and grey sandy loams with silty and thin clay interlayers. The plastic, locally cloddy structure is typical of oxbow, floodplain—lacustrine, and shallow inundated environments [15]. The layer yields diverse mollusks and ostracods (Limnocythere postoncava, Candona sp., Cyprideis, Loxoconcha), typical of Late Pleistocene terraces of the Lower Volga and Caspian regions. The microfaunal assemblage reflects alternation of freshwater and slightly brackish conditions: euryhaline forms (Cyprideis, Loxoconcha) indicate minor influence of Caspian transgressions, whereas freshwater Candona and Ilyocypris indicate stable continental hydrology. The assemblage corresponds well to interstadial phases of MIS 5-3.

Layer 6. >22 m. Ancient alluvial sands of the Early–Middle Pleistocene. The sands are coarse-grained, well sorted, with gravel admixture and massive structure. These deposits formed under conditions of an ancient, more powerful river channel active during the Early–Middle Pleistocene. Reworked remains of ancient fauna (*Mammuthus primigenius, Bos primigenius*) occur, indicating erosion of older strata. Microfauna is extremely poor and represented by single reworked ostracods (Cyprideis, Denticulocythere) and mollusk fragments. The absence of autochthonous assemblages indicates high–energy flows, erosion, and intense reworking typical of basal alluvial deposits of an ancient channel system (Fig. 2).

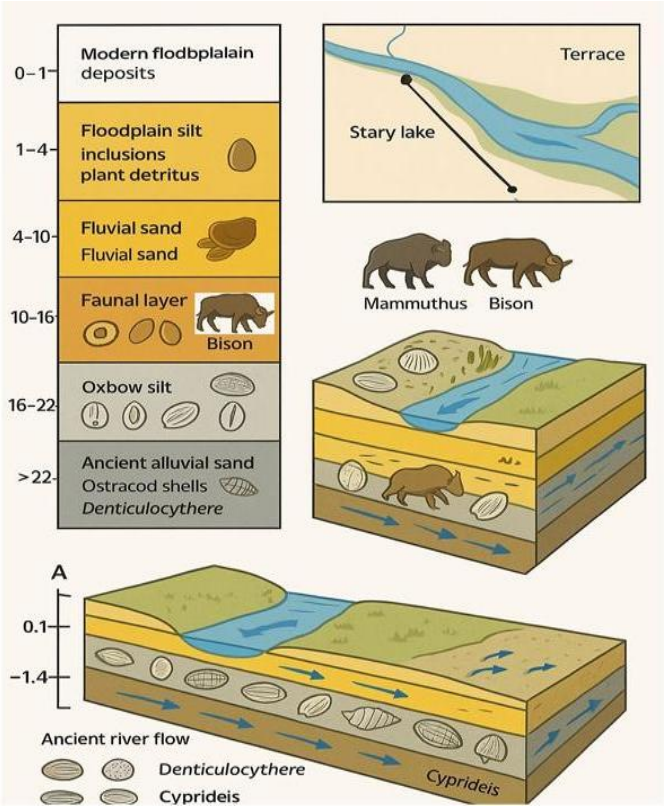

Figure 2. Lithological and stratigraphic scheme of the lower course of the Ural River with the location of layers, paleofauna, and microfauna (ostracods)

Description of osteological remains

The osteological material from the collection of the M.A. Sholokhov Memorial Museum is represented by diverse postcranial elements, teeth, and horn structures of large Late Pleistocene mammals [16; 230]. The preservation of most specimens is satisfactory, allowing detailed morphological analysis and reliable taxonomic identification. The assemblage characterizes a typical megafaunal complex of the alluvial deposits of the lower reaches of the Ural River.

The collection includes massive postcranial elements of the woolly mammoth *Mammuthus primigenius*. Tibiae are represented by large specimens reaching up to 1100 mm in length; the shaft is broad, with a minimum transverse diameter of about 140 mm and expansion in the midshaft up to 350 mm, corresponding to the hindlimb proportions of Late Pleistocene mammoths. Humeri are characterized by a well-developed deltoid tuberosity, a massive shaft (minimum diameters of 100–130 mm), and a moderately expanded distal epiphysis. The assemblage also includes cervical and thoracic vertebrae with wide articular surfaces and centrum heights of 160–180 mm; the dimensions of the articular processes and the morphology of the spinous processes correspond to a large representative of the genus Mammuthus. Fragments of hemipelves are also present, showing a well–developed acetabulum (140–160 mm in length), a high iliac shaft, and a wide obturator foramen, which is typical of adult individuals.

Among the mammoth dental remains, several molars of varying preservation are distinguished (Tab. 2). Large M3 reach up to 270 mm in length, include up to 20 lamellae, and are characterized by a high crown (up to 140 mm) and thin enamel (0.7-2 mm). Lamellar frequency ranges from 70 to 80 plates per 100 mm, which corresponds to the late form of No. 33, 36, 37 *Mammuthus primigenius*. Smaller teeth show 8–13 lamellae and moderate hypsodonty. The presence in the collection of a tooth with a crown height of 210 mm and lamella length up to 80 mm indicates the occurrence of the Khazarian form No. 34 *Mammuthus trogontherii chosaricus*, reflecting the probable stratigraphic heterogeneity of the reworked alluvial material (Fig. 3).

Table 2

Morphometric parameters of the third molar (M3) of Mammuthus from the Daryinsk section

Measurements	Crown length, mm	Maximum crown width, mm	Maximum crown height, mm	Total number of plates, pcs	Average length of one plate, mm	Frequency of plates per 10 cm, pcs	Enamel thickness, mm	Degree of erasure	Hypsodon index, (H/W), %	Crown Proportion Index (W/L), %
No.37	135	95	140	8	90	7	2	3	1,5 %	0,7 %
No. 34	140	90	210	8	80	7	0,8	1	2,3 %	0,60 %
No. 36	182	80	120	13	70	8	0,7	3	1,5 %	0,4 %
No. 33	270	80	140	20	10	8	2	2	1,75 %	0,3 %

The woolly rhinoceros Coelodonta antiquitatis is represented by a femur 530 mm in length with a massive shaft 160 mm in width. The distal end is expanded (200 mm), and the neck of the femoral head is constricted, fully corresponding to the proportions of the Late Pleistocene woolly rhinoceros. The development of the articular surfaces and the robustness of the shaft indicate an adult individual.

The collection includes substantial material of Bovidae, represented by the steppe bison *Bison priscus* and the aurochs *Bos primigenius*. Fragments of skulls and horn cores are preserved. Aurochs remains are characterized by narrow frontal regions of the skull, intercornual distances of 230 and 240 mm, and distances between horn tips along the curvature of 1300 and 1350 mm. Bison remains show a greater frontal width and massive horn cores with basal diameters of 120 and 140 mm and curvature lengths up to 395 mm, confirming attribution to the Late Pleistocene form Bison priscus.

Figure 3. Occlusal view of upper third molars (M3) of Mammuthus sp. from the Late Pleistocene deposits of the Lower Ural (Zhaiyk) River (Darinsk locality). (a; c; d) — *Mammuthus primigenius*, (b) — *Mammuthus trogontherii chosaricus)*

Several elements belong to *Megaloceros giganteus*, a large Late Pleistocene deer. The collection includes antler fragments with heights of 530 and 800 mm, corresponding to adult males of this species and indicating its presence in local faunal assemblages.

Mammoth tusks are also present, measuring 790 and 1120 mm in length. One specimen is characterized by a basal diameter of 230 mm, with diameters of 190 mm at one-third of the length and 160 mm at mid-length, indicating a large individual of *Mammuthus primigenius.* The tusks display typical curvature and moderate mediolateral flattening.

The mammoth mandible is represented by a fragment preserving the ramus and a tooth row 170 and 180 mm in length. The height of the ramus at the level of M3 reaches 150 mm, with a wall thickness of 110 mm; the diastema is long (109 mm), which is characteristic of adult woolly mammoths.

Overall, the osteological remains from the Daryinsk museum collection represent a typical Late Pleistocene faunal complex of the Ural–Caspian Lowland, including representatives of the mammoth fauna *(Mammuthus primigenius, Coelodonta antiquitatis, Bison priscus, Bos primigenius, Megaloceros giganteus).* The morphometric characteristics of the elements show good correspondence with published data and indicate the high scientific value and informative potential of this collection.

Results and Discussion

The taxonomic structure of the collection reflects a characteristic complex of Eurasian Pleistocene fauna formed under conditions of alternating cold and moderately cold climatic phases. The assembled material documents the wide distribution of different ecological groups of megafauna and allows reconstruction of a diverse paleoenvironment in the lower reaches of the Ural River during the Late Pleistocene.

A significant part of the collection belongs to the mammoth complex. Numerous postcranial elements and isolated teeth of *Mammuthus primigenius* confirm the existence of stable populations of the woolly mammoth in the region. The nature of fossilization and the degree of mechanical modification of the bones indicate their prolonged residence in channel and floodplain environments. Of particular interest is the presence of a tooth of *Mammuthus trogontherii chosaricus*, representing a transitional form between Middle and Late Pleistocene mammoths. This suggests that the collection includes materials of different ages and reflects a long-term occupation of the area by proboscideans [17, 18].

Steppe ungulates constitute another important component of the fauna. Skulls of *Bison priscus* and *Bos primigenius* confirm the wide development of open cold steppe landscapes in the lower Zhaiyk region, in agreement with reconstructions for the Volga–Ural interfluve. Alongside these taxa, more mesophilous forms are also present. The occurrence of antlers of *Megaloceros giganteus* indicates the existence of local habitats with increased humidity, such as floodplain meadows and areas with more productive herbaceous vegetation.

The presence of remains of the woolly rhinoceros *Coelodonta antiquitatis* further complements this picture. The recovered femur of this taxon is characteristic of cold-steppe, arid landscapes, confirming the alternation of cold and moderately cold phases in the region. Taken together, the taxonomic composition demonstrates a mosaic structure of paleolandscapes, in which tundra-steppe environments were combined with floodplain biotopes and more productive vegetation zones.

The state of preservation of the remains indicates that they were subjected to short-distance transport, deposited under channel and channel–floodplain flow conditions, partially reworked by the fluvial system, and did not undergo prolonged redeposition.

Most large bones (humeri, pelvic bones, tusks, massive skull fragments) are typical of sand–gravel facies of powerful alluvial streams. Horn rods of *Megaloceros giganteus* and fragments of rhinoceros bones may indicate more humid biotopes in close proximity to the main channel facies.

The combination of remains of mammoths (*Mammuthus primigenius*), steppe bison (*Bison priscus*), aurochs (*Bos primigenius*), woolly rhinoceros (*Coelodonta antiquitatis*), and *Megaloceros giganteus* allows reconstruction of: the existence of tundra—steppe landscapes; alternation of cold and moderate climatic phases; well–developed floodplain–meadow vegetation; and a complex system of Late Pleistocene climatic fluctuations [19].

This confirms the highly mosaic nature of Pleistocene landscapes and the strong dynamism of the natural environment. Analysis of morphometric parameters and faunal composition makes it possible to reconstruct episodes of climatic change, which is important for comparison with modern climate dynamics.

Conclusion

The study of the Pleistocene collection from the M.A. Sholokhov Memorial Museum allows us to introduce this significant material into scientific circulation for the first time and significantly expand our understanding of the megafauna of the lower reaches of the Ural River. The established taxonomic composition, which includes *Mammuthus primigenius, Mammuthus trogontherii chosaricus, Bison priscus, Bos primigenius, Coelodonta antiquitatis, Megaloceros giganteus,* and other forms, reflects the characteristic appearance of the Pleistocene communities in the region and demonstrates a wide range of ecological conditions, from cold tundra–steppe to floodplain–meadow biotopes. The combination of steppe, tundra–steppe, and forest–steppe elements highlights the complex mosaic of natural environments in the Late Pleistocene.

The collection has a high potential for subsequent comparative studies and reconstructions of paleoecological conditions, as it includes both massive elements of the postcranial skeleton and diagnostically valuable teeth and horns. The material demonstrates the dynamics of the natural environment and its response to climatic fluctuations, making it particularly important for analyzing long–term changes in the region's ecosystems. Thus, the collection from Daryinsk is a valuable source of information about the Quaternary fauna of Western Kazakhstan and opens up broad prospects for further paleontological and paleoecological research.

Funding

This research was funded by the Committee of Science of the Ministry of Science and Higher Education of the Republic of Kazakhstan (Grant No. BR 28712767 "Study of ecological, socio–demographic, economic–geographical, and paleobiogeographical aspects of the Urals and assessment of its natural resource potential").

Conflict of Interest

The authors declare no conflict of interest.

Author Contributions

The manuscript was written through contributions of all authors. All authors have given approval to the final version of the manuscript. CRediT: **Berliguzhin M.T. —** conceptualization, investigation, data curation, methodology, formal analysis, visualization, writing — original draft. **Akhmedenov K.M. —** supervision, methodology, validation, writing — review & editing, project administration. **Yakupova J.B. —** investigation, data curation, resources, visualization, writing — review & editing.

References

1 Driesch A. A guide to the measurement of animal bones from archaeological sites / A. Driesch // Peabody Museum Bulletin. — 1976. — № 1. — 136 p.

2 Дуброво И.А. Систематическое положение слона Хазарского фаунистического комплекса / И.А. Дубово // Бюллетень комиссии по изучению четвертичного периода. — 1966. — № 32. — С. 63–74

3 Гарутт В.Е. Исследования зубов вымерших слонов: методические рекомендации / В.Е. Гарутт, И.В. Форонова. — Новосибирск: Наука, 1976. — 35 с.

4 Шер А.В. О методике определения генерации коренных зубов вымерших слонов / А.В. Шер, В.Е. Гарутт // Труды Зоологического института АН СССР. — 1985. — Т. 131. — С. 93–103.

5 Громова В.И. Первобытный бык или тур (*Bos primigenius* Boj.) в СССР / В.И. Громова // Ежегодник Зоологического музея АН СССР. — 1931. — Т. 32. — С. 293–364.

6 Русанов Б.С. Ископаемые бизоны Якутии / Б.С. Рувсанов. — Якутск: Якутское книжное издательство, 1975. — 143 с.

7 Хромов А.А. Эволюция рода Bison и морфологические адаптации первобытных бизонов Bison priscus Bojanus из неоплейстоцена Поволжья / А.А. Хромов // Труды университета «Дубна». Экология и науки о Земле. — 2004. — Вып. 1. — С. 195–208

8 Вислобокова И.А. Ископаемые олени Евразии / И.А. Вислобокова // Труды ПИН АН СССР. — 1990. — Т. 240. — 208 с.

9 Боескоров Г.Г. К систематике и распространению баранов рода Ovis (Artiodactyla, Bovidae) в плейстоцене и голоцене Сибири и Дальнего Востока / Г.Г. Боескоров // Зоологический журнал. — 2001. — Т. 80, № 2. — С. 243–256.

10 Titov V. Data on elephants from Middle–Upper Pleistocene sediments of Astrakhan Volga area (Astrakhan Region, Russia) / V. Titov, M. Golovachev // VI International Conference on Mammoths and their Relatives. — Thessaloniki, 2014. — P. 200.

11 Larramendi A. Shoulder height, body mass and shape of proboscideans / A. Larramendi // Acta Palaeontologica Polonica. — 2016. — Vol. 61, No. 3. — P. 537–574.

12 Obada T. Mammuthus cf. chosaricus (Dubrovo, 1966) from Duruitoarea Veche, Republic of Moldova / T. Obada, A. David // Structura şi funcţionarea ecosistemelor în zona de interferenţă biogeografică. — Chişinău, 2008. — P. 209–211.

13 Яхимович В.Л. Плейстоцен нижнего течения р. Урал / В.Л. Яхимович и др. — Уфа, 1986. — 135 с.

14 Шкатова В.К. Значение нижнеуральского опорного разреза для стратиграфии и палеогеографии плейстоцена Западного Казахстана / В.К. Шкатович // Бюллетень комиссии по изучению четвертичного периода. — 1976. — № 45. — С. 73–82.

15 Якупова Д.Б. История изучения ископаемых позвоночных кайнозоя и мезозоя Западного Казахстана / Д.Б. Якупова, М.Т. Берлигужин, К.М. Ахмеденов // Материалы Международной научно-практической конференции «Биоразнообразие животного мира Казахстана». — Алматы, 2021. — С. 138.

16 Местонахождения ископаемых позвоночных фанерозоя Казахстана: справочник для палеонтологов, геологов и биологов / отв. ред. П.А. Тлеубердина. — Алматы, 2017. — 300 с.

17 Кожамкулова Б.С. Вымершие животные Казахстана (палеогеография позднего кайнозоя) / Б.С. Кожамкулова, Н.Н. Костенко. — Алма-Ата: Наука, 1984. — 104 с.

18 Labe B. Réhabilitation de Mammuthus intermedius (Jourdan, 1861), un mammouth (Mammalia, Elephantidae) du Pléistocène moyen récent d'Europe / B. Labe, C. Guérin // Comptes Rendus Palevol. — 2005. — Vol. 4. — P. 235–242.

19 Kahlke R.D. The origin of Eurasian Mammoth Faunas (Mammuthus-Coelodonta Faunal Complex) / R.D. Kahlke R.D. // Quaternary Science Reviews. — 2014. — Vol. 96. — P. 32–49.

М.Т. Берлигужин, К.М. Ахмеденов, Д.Б. Якупова

Дарьинск ауылы музей коллекциясының материалдары бойынша Орал (Жайық) өзенінің төменгі ағысы кеш плейстоценін палеоэкологиялық реконстукциялау

Мақалада М.А. Шолохов мемориалдық музейінің (Дарьинск ауылы, Бәйтерек ауданы, Батыс Қазақстан облысы) қорынан плейстоцендік сүтқоректілердің палеонтологиялық коллекциясын кешенді зерттеу нәтижелері ұсынылған. Материал кеш плейстоцен жасындағы аллювиалды шөгінділерден Жайық өзенінің төменгі ағысынан жиналған және ұзақ уақыт бойы анықталмаған. Жүргізілген морфометриялық зерттеулер коллекцияны алғаш рет ғылыми айналымға енгізуге және ірі сүтқоректілердің қалдықтарының таксономиялық байланысын нақтылауға мүмкіндік берді. Коллекцияға *Bos primigenius* және *Bison priscus* бас сүйектері, көптеген посткраниальды элементтер және *Mammuthus primigenius*, *Mammuthus trogontherii chosaricus* тістері, ортан жілік (*Coelodonta antiquitatis* (Blumenbach, 1799)) және мүйіз қалдықтары (*Megaloceros giganteus, Cervus elaphus*) кіреді. Салыстырмалы әдістерді қолдану (von den Driesch, Гарутт, Дуброво, Форонова) және Орал-Еділ-Каспий маңы аймақтарының жарияланған ғылыми мақалаларымен салыстыру Батыс Қазақстанның плейстоцендік мегафаунасының сипаттамалық келбетін растауға және суық далалық тундрадан жайылмалы-шалғынды биотоптарға дейінгі экожүйелердің кең спектрін анықтауға мүмкіндік берді. Алынған нәтижелер кеш плейстоцендегі Орал-Каспий ойпатының палеоэкологиялық жағдайларын қайта құру және климаттық ауытқуларға байланысты табиғи жағдайлардың динамикасын бағалау үшін маңызды. Материал плейстоцен кешенінің типтік құрылымын және дала, ылғалды орманды дала элементтерінің болуын көрсетеді. Бұл жинақты ғылыми айналымға енгізу аймақтың төрттік фаунасы туралы мәліметтер базасын кеңейтеді және одан әрі салыстырмалы, палеобиогеографиялық және палеоэкологиялық зерттеулерге, сондай-ақ қазіргі экожүйелердің ықтимал өзгеру тенденцияларын модельдеуге негіз жасайды.

Кілт сөздер: кеш плейстоцен, Батыс Қазақстан, Орал (Жайық) өзені, мегафауна, палеоэкологиялық реконструкциялау, музей коллекциясы, ірі сүтқоректілер, төрттік кезең.

М.Т. Берлигужин, К.М. Ахмеденов, Д.Б. Якупова

Палеоэкологическая реконструкция позднего плейстоцена нижнего течения реки Урал (Жайык) по материалам музейной коллекции п. Дарьинск

В работе представлены результаты комплексного изучения палеонтологической коллекции плейстоценовых млекопитающих из фондов Мемориального музея М.А. Шолохова (п. Дарьинск, район Байтерек, Западно-Казахстанская область). Материал был собран в нижнем течении реки Урал (Жайык) из аллювиальных отложений позднеплейстоценового возраста и на протяжении длительного времени оставался неопределённым. Проведённые нами морфометрические исследования позволили впервые ввести коллекцию в научный оборот и уточнить таксономическую принадлежность остатков крупных млекопитающих. Коллекция включает черепа *Bos primigenius* и *Bison priscus*, многочисленные посткраниальные элементы и зубы *Mammuthus primigenius*, зуб переходной формы *Mammuthus trogontherii chosaricus*, бедренную кость (*Coelodonta antiquitatis* (Blumenbach, 1799)), а также рога *Megaloceros giganteus* и *Cervus elaphus*. Использование сравнительных методик (von den Driesch, Гарутт, Дуброво, Форонова) и сопоставление с опубликованными сериями из регионов Урал — Волга — Прикаспий позволили подтвердить характерный облик плейстоценовой мегафауны Западного Казах-

стана и выявить широкий спектр экосистем — от холодных тундростепей до пойменно-луговых биотопов. Полученные результаты важны для реконструкции палеоэкологических условий Урало-Каспийской низменности в позднем плейстоцене и для оценки динамики окружающей среды, связанной с климатическими колебаниями.

Ключевые слова. Поздний плейстоцен, Западный Казахстан, река Урал (Жайык), мегафауна, палеоэкологическая реконструкция, музейная коллекция, крупные млекопитающие, четвертичный период.

References

1 Driesch, A. (1976). A guide to the measurement of animal bones from archaeological sites. *Peabody Museum Bulletin,* 1, 136.

2 Dubrovo, I. A. (1966). Sistematicheskoe polozhenie slona Khazarskogo faunisticheskogo kompleksa [Systematic position of the elephant of the Khazar faunal complex]. *Biulleten Komissii po izucheniiu chetvertichnogo perioda — Bulletin of the Commission on Quaternary Studies,* 32, 63–74 [in Russian].

3 Garutt, V. E., & Foronova, I. V. (1976). *Issledovaniia zubov vymershikh slonov: metodicheskie rekomendatsii* [Studies of teeth of extinct elephants: methodological recommendations]. Novosibirsk: Nauka [in Russian].

4 Sher, A. V., & Garutt, V. E. (1985). O metodike opredeleniia generatsii korennykh zubov vymershikh slonov [Methodology for determining molar generations in extinct elephants]. *Trudy Zoologicheskogo instituta Akademii Nauk SSSR — Proceedings of the Zoological Institute of the USSR Academy of Sciences, 131*, 93–103 [in Russian].

5 Gromova, V. I. (1931). Pervobytnyi byk ili tur (*Bos primigenius* Boj.) v SSSR [The aurochs (*Bos primigenius* Boj.) in the USSR]. *Ezhegodnik Zoologicheskogo muzeia Akademii Nauk SSSR — Yearbook of Zoological Museum of the Academy of Sciences of the USSR, 32*, 293–364 [in Russian].

6 Rusanov, B. S. (1975). *Iskopaemye bizony Yakutii* [Fossil bisons of Yakutia]. Yakutsk: Yakutskoe knizhnoe izdatelstvo [in Russian].

7 Khromov, A. A. (2004). Evoliutsiia roda Bison i morfologicheskie adaptatsii pervobytnykh bizonov Bison priscus Bojanus iz neopleistotsena Povolzhia [Evolution of the genus Bison and morphological adaptations of primitive bison]. *Trudy universiteta «Dubna». Ekologiia i nauki o Zemle — Proceedings of Dubna University, series Ecology and Earth Science, 1*, 195–208 [in Russian].

8 Vislobokova, I. A. (1990). Iskopaemye oleni Evrazii [Fossil deer of Eurasia]. *Trudy Paleontologicheskogo instituta Akademii Nauk SSSR — Proceedings of the Paleontological Institute of the USSR Academy of Sciences, 240*, 208 [in Russian].

9 Boeskorov, G. G. (2001). K sistematike i rasprostraneniiu baranov roda *Ovis* (Artiodactyla, Bovidae) v pleistotsene i golotsene Sibiri i Dalnego Vostoka [To systematics and distribution of sheep of the genus *Ovis* (Artiodactyla, Bovidae) in the Pleistocene and Holocene of Siberia and the Far East]. *Zoologicheskii Zhurnal — Zoological Journal, 80*(2), 243–256 [in Russian].

10 Titov, V., & Golovachev, M. (2014). Data on elephants from Middle–Upper Pleistocene sediments of Astrakhan Volga area (Astrakhan Region, Russia). *VI International Conference on Mammoths and their Relatives*, 200. Thessaloniki.

11 Larramendi, A. (2016). Shoulder height, body mass and shape of proboscideans. *Acta Palaeontologica Polonica, 61*(3), 537–574.

12 Obada, T., & David, A. (2008). Mammuthus cf. chosaricus (Dubrovo, 1966) from Duruitoarea Veche, Republic of Moldova. *Structura şi funcţionarea ecosistemelor în zona de interferenţă biogeografică*, 209–211. Chisinau: Stiinta.

13 Yakhimovich, V. L. et al. (1986). *Pleistotsen nizhnego techeniia reki Ural* [Pleistocene of the Lower Ural River]. Ufa [in Russian].

14 Shkatova, V. K. (1976). Znachenie nizhneuralskogo opornogo razreza dlia stratigrafii i paleogeografii pleistotsena Zapadnogo Kazakhstana [Significance of the Lower Ural reference section for stratigraphy and paleogeography of the Pleistocene of Western Kazakhstan]. *Biulleten komissii po izucheniiu chetvertichnogo perioda — Quaternary Commission Bulletin*, 45, 73–82 [in Russian].

15 Yakupova, D. B., Berliguzhin, M. T., & Akhmedenov, K. M. (2021). *Istoriia izucheniia iskopaemykh pozvonochnykh kainozoia i mezozoia Zapadnogo Kazakhstana* [History of study of fossil vertebrates of Western Kazakhstan]. Almaty [in Russian].

16 Tleuberdina, P. A. (Ed.). (2017). *Mestonakhozhdeniia iskopaemykh pozvonochnykh fanerozoia Kazakhstana: spravochnik dlia paleontologov, geologov i biologov* [Locations of fossil vertebrates of the Phanerozoic of Kazakhstan]. Almaty [in Russian].

17 Kozhamkulova, B. S., & Kostenko, N. N. (1984). *Vymershie zhivotnye Kazakhstana (paleogeografiia pozdnego kainozoia)* [Extinct animals of Kazakhstan (Paleogeography of the Late Cenozoic)]. Alma-Ata: Nauka [in Russian].

18 Labe, B., & Guérin, C. (2005). Réhabilitation de Mammuthus intermedius (Jourdan, 1861), un mammouth (Mammalia, Elephantidae) du Pléistocène moyen récent d'Europe. *Comptes Rendus Palevol, 4*, 235–242.

19 Kahlke, R. D. (2014). The origin of Eurasian mammoth faunas (Mammuthus-Coelodonta Faunal Complex). *Quaternary Science Reviews, 96*, 32–49.

Information about the authors

Berliguzhin Maxot Tynyshtykovich — Master of Natural Sciences, Senior Lecturer in Biology, Chemical Sciences and the Environment, Makhambet Utemisov West Kazakhstan University; Uralsk, Kazakhstan; e-mail: 88_max_88.88@inbox.ru; ORCID: https://orcid.org/0000-0001-7926-2991

Akhmedenov Kazhmurat Maksutovich — Candidate of Geographical Sciences, Professor, Deputy Chairman of the Board, Vice-Rector for Research and International Relations, Makhambet Utemisov West Kazakhstan University; Uralsk, Kazakhstan; e-mail: kazhmurat78@mail.ru; ORCID: http://orcid.org/0000-0001-7294-0913

Yakupova Jamilya Bolatovna — Master in Chemical Ecology, Senior Lecturer in Educational programs for training biology, chemistry, and geography lecturer, Makhambet Utemisov West Kazakhstan University; Uralsk, Kazakhstan; e-mail: yakupova_j@mail.ru; ORCID: https://orcid.org/0000-0003-3875-1224

How to Cite: Matai, Zh.M., Jantassov, S.K. & Ibragimova, G.M. (2026). Bacterial and Fungal Contamination during Garlic (*Allium sativum* L.) Initiation in In Vitro Culture. *Fundamental and Experimental Biology*, 31, 3 (123), 94-102. https://doi.org/10.31489/2026FEB3/94-102

Research Article

https://doi.org/10.31489/2026FEB3/94-102

UDC 581.143:633.88 Received: 3.04.2026 | Accepted: 12.06.2026 | Published online: 30 September 2026

Zh.M. Matai[1, 2*], S.K. Jantassov[2], G.M. Ibragimova[3]

[1]*Almaty Technological University, JSC, Almaty, Kazakhstan;*
[2]*Kazakh Research Institute of Fruit and Vegetable Growing, LLP, Almaty, Kazakhstan*
[*]*Corresponding author: sayajan_91@mail.ru*

Bacterial and Fungal Contamination during Garlic (*Allium sativum* L.) Initiation in In Vitro Culture

The present study investigated bacterial and fungal contamination occurring during the establishment of garlic (*Allium sativum* L.) in vitro cultures. The aim of the study was to assess the level of contamination in explants and evaluate the effectiveness of standard surface sterilization protocols. The scientific novelty of the study lies in the first comprehensive assessment in Kazakhstan of bacterial and fungal contamination occurring during the establishment of garlic in vitro cultures. The experiments demonstrated that conventional sterilization methods, including ethanol and disinfectant treatments, did not ensure complete decontamination of the plant material. Consequently, microbial contamination was observed at the early stages of cultivation, resulting in partial or complete necrosis of explants and reduced efficiency of micropropagation. The degree of contamination varied among garlic cultivars, suggesting an influence of genotype and the physiological condition of the donor plants. Microscopic analysis indicated the predominance of fungal morphotypes consistent with genera such as *Fusarium*, *Penicillium*, and *Aspergillus*, as well as the presence of diverse bacterial microflora. However, accurate taxonomic identification of the contaminants requires further molecular genetic analysis. The results demonstrate that microbial contamination remains a critical limiting factor for the successful establishment of garlic in vitro cultures. Therefore, improved pre-treatment of plant material, optimization of sterilization protocols, and refinement of culture conditions are required. The practical significance of the study lies in the development of more effective approaches to reducing contamination, thereby increasing the success rate of micropropagation and facilitating the establishment of healthy in vitro collections.

Keywords: garlic, *Allium sativum* L., in vitro, microbial contamination, explants, Fusarium, Penicillium.

Introduction

Garlic (*Allium sativum* L.) is a vegetatively propagated crop, which facilitates the accumulation and persistence of infectious agents in planting material. A significant proportion of phytopathogens may remain latent during the growing season; however, they become activated during storage, leading to substantial post-harvest losses [1].

According to numerous studies, the most common pathogens affecting garlic include fungi of the genera *Fusarium*, *Penicillium*, *Botrytis*, and *Sclerotium*, as well as bacteria belonging to the genera *Pectobacterium*, *Pantoea*, and *Pseudomonas* [2, 3]. The species composition of pathogens and the degree of infection vary depending on the soil and climatic conditions of the cultivation region.

A particular concern is the presence of latent internal infections that persist within bulb tissues. Even when standard surface sterilization protocols are applied during the introduction of plants into in vitro culture, microorganisms localized in internal tissues may become activated and cause contamination of explants. This results in necrosis, tissue decay, and reduced efficiency of micropropagation [4, 5].

Fungal diseases, including fusariosis, penicilliosis, neck rot, and white rot, are among the main factors reducing the quality of planting material during storage. The mycelium of pathogens can spread through the vascular system of plants, block conductive tissues, and produce toxic metabolites, thereby intensifying degenerative processes. Bacterial infections, in turn, are primarily manifested as soft rot affecting cloves and the basal plate of bulbs [6].

Preventive measures, including quarantine, removal of infected plants, and control of natural vectors, remain the primary strategies for limiting pathogen spread. Unlike other agricultural crops, where modern

approaches to developing genetic resistance—such as transformation, genome editing, or cross-protection—are applied, their use in garlic is restricted due to the lack of efficient regeneration systems.

Therefore, maintaining the phytosanitary purity of planting material relies primarily on pathogen elimination and the cultivation of healthy plants under controlled conditions. Since garlic is vegetatively propagated and does not produce viable seeds, obtaining pathogen-free material is achievable through in vitro methods, such as meristem culture, thermotherapy, chemotherapy, and cryotherapy [7, 8].

Bacterial contamination is typically manifested by turbid growth of the medium, unpleasant odors, and meristem necrosis [9]. Fungal contamination appears as mycelial growth on the surface of the substrate or plant tissues, which also leads to the death of explants. The primary sources of contamination are endophytic microorganisms residing within garlic cloves, as well as spores of microorganisms present on the surface [10–12].

Several approaches are employed to minimize the risk of contamination, including meticulous sterilization of the starting material, the use of antimicrobial agents, careful control of culture conditions, and the selection of cultivars with high resistance to infections. Despite these measures, contamination remains a significant challenge, affecting the efficiency of garlic micropropagation and the quality of the resulting in vitro collection. Therefore, addressing bacterial and fungal contamination is a key aspect of successful garlic introduction into in vitro culture and requires an integrated approach using modern sterilization techniques and microorganism control methods [13, 14].

Effective contamination management is essential for establishing a healthy in vitro garlic collection, particularly when working with infection-sensitive cultivars, and for the subsequent application of micropropagation in breeding and biotechnological programs [15, 16]. Consequently, a comprehensive investigation of bacterial and fungal contamination in garlic planting material following low-temperature storage, prior to its introduction into in vitro culture, is highly relevant.

Experimental

The study was conducted in the biotechnology laboratory of the "Potato Breeding, Seed Production, and Biotechnology" Department at the Kazakh Research Institute of Horticulture, Branch "Kainar", during 2024-2025.

Three garlic (*Allium sativum* L.) cultivars "Arman", "Zailiyskiy", and "Dunganskiy" were used as research objects. Visually healthy cloves were selected for in vitro culture, and the basal plate portion was used as explants.

The plant material was stored in a dry environment at approximately 10 °C for 7-8 months prior to the experiment. Culture initiation was carried out under aseptic conditions in a laminar flow cabinet.

All manipulations were performed under aseptic conditions using a laminar airflow cabinet (ESCO, Singapore). Sterilization was carried out using an autoclave (Tuttnauer, Germany) at a temperature of 121 °C, a pressure of 1.1 atm, and an exposure time of 20 min to ensure complete sterility of culture media and instruments. Microscopic analysis was conducted using a light microscope (Olympus, Japan).

Sterilization of the plant material was performed in two stages. The first stage involved the removal of external contaminants: washing the plant material in running water for 30–60 min, soaking the cloves in a 10 % solution of household soap for 40–60 min, followed by rinsing in running water and immersion in a 0.1 % potassium permanganate solution for 15–20 min.

The second stage was performed under laminar flow conditions and included surface sterilization of explants with 70 % ethanol for 30 s, followed by immersion in 1 % sodium hypochlorite solution for 20 min, and subsequent rinsing three times with sterile distilled water. This sterilization protocol was applied to reduce external microbial contamination and ensure aseptic conditions for in vitro culture initiation [17, 18].

The experiment was conducted in three biological replicates, each comprising 13–15 explants. Explants were cultured on Murashige and Skoog (MS) medium supplemented with 3 % sucrose and 0.7 % agar, adjusted to pH 5.8. Cultures were maintained at 24 ± 2 °C under a 16/8 h photoperiod with a light intensity of 40–50 μmol m^{-2} s^{-1}.

Contamination levels were assessed on days 3, 7, and 14 of cultivation. Statistical analysis was performed using Microsoft Excel. Data are presented as mean values calculated from replicates. Microorganism identification was carried out based on morphological characteristics using diagnostic keys; however, the results are considered preliminary and require confirmation by molecular genetics methods.

Microorganism identification was additionally performed using light microscopy and requires further validation by molecular techniques, including PCR analysis using 16S rRNA markers for bacteria and ITS regions for fungi.

The percentage of contamination was calculated as the ratio of contaminated explants to the total number of cultured explants. Results are presented as mean ± standard deviation. Differences among cultivars were analyzed using analysis of variance (ANOVA), followed by Tukey's post hoc test to determine statistically significant differences ($p < 0.05$). Each experiment was conducted in three biological replicates.

Results and Discussion

The introduction of cloves from the "Arman", "Zailiyskiy", and "Dunganskiy" garlic cultivars into in vitro culture revealed that explants contamination by various phytopathogens was observed within the first week. Bacterial growth was detected by day 3, while fungal pathogen development became evident after 6-7 days (Fig. 1).

Table 1

Contamination Levels of Explants of Different Garlic Cultivars

№	Garlic Cultivar	Total Number of Explants	Number of Infected Explants	*Fusarium*, %	*Penicillium*, %	*Aspergillus*, %	*Pseudomonas*, %	Total Infected, %
1	Arman	45	35	64.5	14.2	9.1	12.1	77.8
2	Zailiyskiy	44	29	25.4	28.7	13.0	31.0	65.9
3	Dunganskiy	41	28	26.3	32.1	9.2	33.2	68.5

The results presented in the table characterize the structure of microbial contamination of garlic explants by cultivar and allow for the assessment of the contribution of individual pathogen groups to the overall level of infection. The analysis included fungi of the genera *Fusarium*, *Penicillium*, and *Aspergillus*, as well as bacteria of the genus *Pseudomonas*. The indicators reflect the relative prevalence of the identified microorganisms and their share in the total infection of the studied samples.

The highest proportion of infected explants was observed in the "Arman" cultivar, which is associated with the particular internal tissue structure and the accumulation of pathogens during storage. Overall, differences in cultivar sensitivity to fungal and bacterial infections were noted.

Fungi of the genera *Fusarium*, *Penicillium*, and *Aspergillus*, as well as bacteria of the genus *Pseudomonas*, were detected in the garlic explants. In the "Arman" cultivar, *Fusarium* (64.5 %) and *Pseudomonas* (12.1 %) predominated. In the "Zailiyskiy" cultivar, *Penicillium* (28.7 %) and *Fusarium* (25.4 %) were the main fungal pathogens, while *Pseudomonas* bacteria accounted for 31.0 % of contamination. In the "Dunganskiy" cultivar, the most frequently observed microorganisms were *Penicillium* (32.1 %), *Fusarium* (26.3 %), and *Pseudomonas* (33.2 %).

The observed differences in pathogenic microflora composition are associated with the biological traits of the cultivars. Cultivars with less developed aerial bulbs and weak scape formation tend to accumulate higher levels of fungal and bacterial infections in their internal tissues (Fig. 2). Despite rigorous surface sterilization, internal infections persisted and became apparent in the explants during in vitro culture.

Table 2

Average Percentage of Bacterial and Fungal Contamination of Garlic Explants

№	Garlic Cultivar	Bacterial Contamination (*Pseudomonas*), % ± SD	Fungal Contamination (*Fusarium* + *Penicillium* + *Aspergillus*), % ± SD
1	Arman	12.1 ± 1.0	87.8 ± 2.5
2	Zailiyskiy	31.0 ± 2.0*	65.9 ± 2.0*
3	Dunganskiy	33.2 ± 1.8*	68.5 ± 2.1*

*Differences were considered statistically significant at $p < 0.05$.

The obtained results indicate the persistence of latent microbial infections in garlic planting material, which become evident at the early stages of in vitro culture (Fig. 1). Contamination levels varied among cultivars, which should be taken into account when organizing micropropagation and the sanitation of planting material.

Figure 1. In vitro culture of garlic showing *Penicillium* contamination. Scale bar = 0.1 cm.

In Figure 2A, colonies of *Penicillium* can be observed developing in the lower part of the plant material, indicating partial contamination. This highlights the necessity of thorough sterilization and strict control of explant cleanliness during in vitro culture.

In Figure 2B, branched conidia and the characteristic mycelium of *Penicillium* are visible, confirming contamination at the cellular level. This image emphasizes the need for strict control of medium sterility and careful material sterilization prior to culture initiation.

In Figure 3, sickle-shaped multicellular macroconidia of *Fusarium* isolated from infected garlic (*Allium sativum* L.) tissues are shown. The conidia exhibit an elongated, curved shape with 3–5 transverse septa, tapered ends, and a hyaline structure. The observed morphological characteristics are typical of *Fusarium* species and confirm the fungal nature of the infection.

Figure 2. Microscopic image of *Penicillium* colonies on a garlic (*Allium sativum* L.) explant in in vitro culture. (A) Fungal structures observed on explant surface. (B) Abundant fungal hyphae and spores indicating contamination. Magnification ×600. Scale bar = 10 µm.

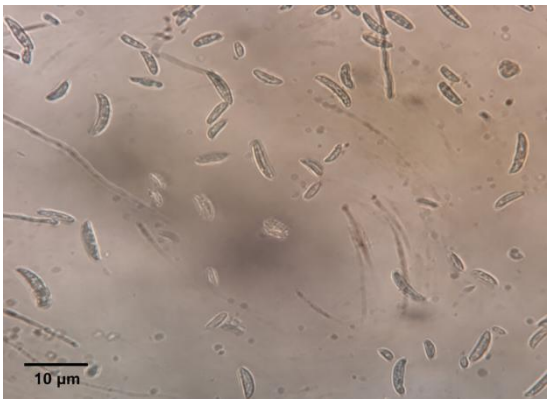

Figure 3. Macroconidia of *Fusarium* isolated from infected garlic (*Allium sativum* L.) tissues. Magnification ×600. Scale bar = 10 µm

These results are consistent with previous studies indicating the widespread occurrence of latent infections in garlic planting material. The higher contamination levels observed in certain cultivars may be associated with anatomical features of the tissues, as well as prolonged low-temperature storage, which promotes the development of hidden microflora. At the same time, the incomplete decontamination following surface sterilization suggests possible localization of microorganisms within internal tissues; however, additional studies, including isolation of pure cultures, are required to confirm the endophytic nature of the infection.

The results obtained indicate that contamination of garlic explants becomes apparent at the early stages of in vitro culture, which is consistent with previous studies reporting the widespread occurrence of latent infections in vegetatively propagated crops. The early onset of bacterial contamination (by day 3) followed by the subsequent development of fungal microflora reflects the different growth dynamics of microorganisms under in vitro conditions.

The observed predominance of fungi of the genera *Fusarium*, *Penicillium*, and *Aspergillus*, as well as bacteria of the genus *Pseudomonas*, aligns with literature data on the most common garlic phytopathogens associated with storage and subsequent cultivation. This confirms that even visually healthy planting material may harbor latent infections.

Differences in contamination levels and structure among cultivars suggest a possible influence of plant genotypic characteristics, including tissue anatomy, density of protective layers, and their permeability to microorganisms. Additionally, prolonged storage at low temperatures may have contributed to the persistence and partial activation of latent microflora.

It was established that the application of the standard surface sterilization protocol does not ensure complete decontamination of explants. This suggests a likely localization of microorganisms within internal tissues (endophytic infection), which are inaccessible to sterilizing agents. Similar conclusions have been reported in studies on the cultivation of garlic and other vegetatively propagated crops.

It should be noted that microorganism identification in this study was based on morphological characteristics, which limits the accuracy of taxonomic assignment, particularly for bacterial microflora. Therefore, further research should focus on molecular-genetic identification using PCR and sequencing methods.

A limitation of the present study is the relatively small sample size and the descriptive nature of the statistical analysis, which does not allow a full assessment of the significance of differences between cultivars. Nevertheless, the obtained data provide a general overview of contamination structure and can serve as a basis for further investigations.

The practical significance of this work lies in the necessity of considering the identified contamination features when developing protocols for introducing garlic into in vitro culture. Promising directions include optimization of sterilization schemes, including the use of combined methods (thermotherapy, antibiotics, fungicides), as well as the preliminary selection of planting material with a low level of infection.

Thus, the results of this study confirm the complex and multifactorial nature of contamination during in vitro garlic cultivation and highlight the need for a comprehensive approach to address this issue.

Conclusion

The conducted study demonstrated that garlic planting material of the "Arman", "Zailiyskiy", and "Dunganskiy" cultivars harbors latent microbial infections, which persist in bulb tissues after prolonged storage and become apparent upon introduction into in vitro culture.

It was established that the use of a standard surface sterilization protocol does not ensure complete decontamination of explants, as evidenced by the high levels of contamination observed at early stages of cultivation. The microbial community was dominated by fungi of the genera *Fusarium*, *Penicillium*, and *Aspergillus*, as well as bacteria of the genus *Pseudomonas*, indicating the complex nature of the infection.

The study showed that the level and composition of contamination vary depending on the cultivar, which should be considered when developing protocols for micropropagation and sanitation of garlic planting material.

The obtained results have practical significance for plant biotechnology and highlight the need to improve the preparation of planting material, including optimization of sterilization procedures and implementation of additional decontamination strategies.

Future work should focus on molecular-genetic identification of microorganisms and expansion of the sample size to increase the reliability of the results.

Funding

This study was conducted within the framework of the scientific and technical program BR22885335, "Sustainable Development of Breeding, Seed Production, Biotechnology, and Innovative Agrotechnologies for Potato, Vegetable, and Melon Crops in Kazakhstan" for 2024–2026, funded by the Ministry of Agriculture of the Republic of Kazakhstan under the program-targeted financing scheme.

Conflict of Interest

The authors declare no conflict of interest.

Author Contributions

The manuscript was written through contributions of all authors. All authors have given approval to the final version of the manuscript. CRediT: **Jantassov S.K. —** conceptualization, methodology, supervision, formal analysis; **Matai Zh.M. —** investigation, data curation, formal analysis, writing — original draft, conducted in vitro experiments, performed data analysis, and draft writing; **Ibragimova G.M.** — validation, writing — review & editing, visualization.

References

1 Середин Т.М. Распространение и вредоносность микозов на культуре чеснока озимого в условиях Московской области / Т.М. Середин, Л.И. Герасимова, Е.Г. Козарь, И.А. Енгалычева, Е.В. Баранова // Овощи России. — 2018. — № 6. — С. 84–90. DOI: 10.18619/2072-9146-2018-6-84-90.

2 Шестакова К.С. Селекционно-иммунологическая характеристика устойчивости чеснока озимого (*Allium sativum* L.) к фузариозным гнилям: автореф. дис. канд. с. -х. наук / К.С. Шестокова. — М., 2009. — 23 с.

3 Cremer J. Detection and distribution of viruses infecting garlic crops in Australia / J. Cremer, P. Campbell, V. Steele, D. Persley, J. Thomas, S. Harper, C. Gambley // Plants. — 2021. — Vol. 10(5). — P. 1013. doi:10.3390/plants10051013

4 Moharam M.H.A. Pathogenic fungi in garlic cloves and first report of clove rot of stored bulbs caused by Fusarium proliferatum in Upper Egypt / M.H.A. Moharam, E.S. Farrag, M.D.A. Mohamed // Journal of Plant Pathology. — 2013. — Vol. 95. — P. 2096–2103. doi:10.1080/03235408.2013.785122.

5 Степанова М.Ю. Указатель возбудителей болезней сельскохозяйственных растений / М.Ю. Степанова. — Л., 1978. — 500 с.

6 Тимина Л.Т. Комплекс патогенов на овощных культурах в условиях центрального региона РФ / Л.Т. Тимина, И.А. Енгалычева // Овощи России. — 2015. — № 3-4. — С. 123–129. DOI: 10.18619/2072-9146-2015-3-4-123-129.

7 Хмельницкая И.И. Распространение грибов *Aspergillus* в почвах различных регионов России / И.И. Хмельницкая // 1 съезд микологов. Современная микология в России. — М., 2002. — С. 53-54.

8 Саттон Д. Определитель патогенных и условно-патогенных грибов / Д. Саттон, А. Фоторгилл, М. Ринальди. — М.: Мир, 2001. — 464 с.

9 Поляков А.В. Регенерация растений чеснока озимого (*Allium sativum* L.) in vitro из воздушных луковичек / А.В. Поляков, М.А. Азопкова, Н.Н. Лебедева, И.В. Муравьёва // Овощи России. — 2018. — № 4. — С. 20–25. DOI: 10.18619/2072-9146-2018-4-20-25.

10 Поляков А.В. *In vitro* регенерация растений чеснока озимого (*Allium sativum* L.) из воздушных луковичек / А.В. Поляков, М.А. Азопкова, Н.Н. Лебедева, И.В. Муравьёва // Вестник МГОУ. Естественные науки. — 2018. — № 4. — С. 115–124. DOI: 10.18384/2310-7189-2018-4-115-124.

11 Shim S.T. Natural microflora of pre-processed garlic and their resistance to garlic antimicrobial activity / S.T. Shim, K.H. Kyung // Food Microbiology. — 1999. — Vol. 16(2). — P. 165–172.

12 Ounis S. Co-Occurrence of *Stromatinia cepivora* and *Fusarium proliferatum* Fungi on Garlic: In Vitro Investigation of Pathogen–Pathogen Interactions and In Planta Screening for Resistance of Garlic Cultivars / S. Ounis, G. Turóczi, J. Kiss // Plants. — 2025. — Vol. 14(3). — Article ID 440. DOI: 10.3390/plants14030440

13 Abachi H. Garlic Bulb Decay and Soft Rot Caused by the Cross-Kingdom Pathogen *Burkholderia gladioli* / H. Abachi, M. Moallem, S.M. Taghavi // Plant Disease. — 2024. — Vol. 108(3). — P. 684–693. DOI: 10.1094/PDIS-08-23-1603-RE

14 Anum H. Different Preharvest Diseases in Garlic and Their Eco-Friendly Management / H. Anum et al. // Plants. — 2024. — Vol. 13(2). — Article ID 267. DOI:10.3390/plants13020267

15 Mohy S. Biological control of garlic white and basal rot pathogens in vitro and under field conditions / S. Mohy, T.M. Elameen, R. Khalaphallah, N.M.S. Hassan // SVU-International Journal of Agricultural Sciences. — 2024. — Vol. 6(4). — P. 12–23. DOI: 10.21608/svuijas.2024.319563.1393

16 Gasser K. Fusarium dry rot in garlic: hidden infection of planting material leading to high infestation rates during storage of the resulting harvest / K. Gasser, S. Steinkellner, K. Hage-Ahmed // Journal of Crop Health. — 2025. — Vol. 77. — Article ID 132. DOI: 10.1007/s10343-025-01202-z

17 Dedecan O. First report of *Stemphylium eturmiunum* from garlic (*Allium sativum* L.) growing areas of Türkiye / O. Dedecan, N. Güneş et al. // Crop Protection. — 2025. — Vol. 25(1). DOI: 10.1016/j.cropro.2025.107253

18 Sharma S. In vitro and field efficacy of fungicide treatments against Fusarium bulb rot of garlic / S. Sharma, S. Mandal, C.S. Cramer // Horticulturae. — 2024. — Vol. 148(2). — P. 321–328. DOI: 10.3390/horticulturae10050527

Ж.М. Матай, С.К. Джантасов, Г.М. Ибрагимова

Сарымсақты (*Allium sativum* L.) *in vitro* дақылына енгізу кезіндегі бактериялық және саңырауқұлақтық контаминация

Зерттеу жұмысында сарымсақты (*Allium sativum* L.) *in vitro* дақылына енгізу барысында туындайтын бактериялық және саңырауқұлақтық контаминация зерттелді. Зерттеудің мақсаты — эксплантардағы контаминация деңгейін бағалау және стандартты беткі стерилизациялау протоколдарының тиімділігін анықтау. Зерттеудің ғылыми жаңалығы — Қазақстанда алғаш рет сарымсақты *in vitro* дақылына енгізу кезінде кездесетін бактериялық және саңырауқұлақтық контаминацияға кешенді бағалау жүргізілді. Тәжірибелер нәтижесінде этанолмен және дезинфекциялаушы ерітінділермен өңдеуді қамтитын дәстүрлі стерилизация әдістері өсімдік материалын толық залалсыздандыруды қамтамасыз етпейтіні анықталды. Соның салдарынан өсірудің бастапқы кезеңдерінде микробтық инфекция дамып, эксплантардың жартылай немесе толық некрозына және микроклональды көбейту тиімділігінің төмендеуіне әкелді. Контаминация деңгейінің сарымсақ сорттарына байланысты өзгеретіні анықталды, бұл донор өсімдіктердің генотипі мен физиологиялық күйінің әсерін көрсетеді. Микроскопиялық талдау нәтижесінде *Fusarium*, *Penicillium*, *Aspergillus* туыстарына жататын саңырауқұлақтардың басым екені, сондай-ақ әртүрлі бактериялық микрофлораның бар екені анықталды. Дегенмен контаминанттарды нақты анықтау үшін қосымша молекулалық-генетикалық зерттеулер жүргізу қажет. Алынған нәтижелер контаминацияның сарымсақты *in vitro* дақылына сәтті енгізудегі негізгі шектеуші факторлардың бірі болып қала беретінін көрсетті. Осыған байланысты өсімдік материалын алдын ала өңдеу әдістерін жетілдіру, сондай-ақ стерилизациялау протоколдары мен өсіру жағдайларын оңтайландыру қажет. Зерттеудің практикалық маңыздылығы — контаминацияны азайтудың тиімді тәсілдерін әзірлеу арқылы микроклональды көбейту тиімділігін арттыру және сау *in vitro* коллекциялар құру мүмкіндігімен сипатталады.

Кілт сөздер: сарымсақ, *Allium sativum* L., *in vitro*, микробтық контаминация, эксплланттар, *Fusarium*, *Penicillium.*

Ж.М. Матай, С.К. Джантасов, Г.М. Ибрагимова

Бактериальная и грибковая контаминация при введении чеснока (*Allium sativum* L.) в культуру in vitro

В настоящем исследовании изучалась бактериальная и грибная контаминация, возникающая при введении чеснока (*Allium sativum L.*) в культуру in vitro. Целью работы являлась оценка уровня контаминации эксплантов, а также определение эффективности стандартных протоколов поверхностной стерилизации. Научная новизна исследования заключается в том, что впервые в Казахстане проведена

комплексная оценка бактериальной и грибной контаминации при введении чеснока в культуру in vitro. В ходе экспериментов установлено, что традиционные методы стерилизации, включая обработку этанолом и дезинфицирующими растворами, не обеспечивают полной деконтаминации растительного материала. В результате на ранних этапах культивирования наблюдалось развитие микробной инфекции, приводящее к частичному или полному некрозу эксплантов и снижению эффективности микроклонального размножения. Установлено, что степень контаминации варьирует в зависимости от сорта чеснока, что свидетельствует о влиянии генотипа и физиологического состояния донорных растений. Микроскопический анализ выявил преобладание грибов родов *Fusarium*, *Penicillium* и *Aspergillus*, а также наличие разнообразной бактериальной микрофлоры. Однако точная идентификация контаминантов требует проведения дополнительных молекулярно-генетических исследований. Полученные результаты показывают, что контаминация остаётся одним из основных ограничивающих факторов успешного введения чеснока в культуру in vitro. В связи с этим необходима оптимизация предпосевной обработки растительного материала, а также совершенствование протоколов стерилизации и условий культивирования. Практическая значимость исследования заключается в разработке более эффективных подходов к снижению контаминации, что позволит повысить эффективность микроклонального размножения и создать здоровые in vitro коллекции.

Ключевые слова: чеснок, *Allium sativum* L., *in vitro*, микробная контаминация, экспланты, *Fusarium*, *Penicillium*.

References

1 Seredin, T.M., Gerasimova, L.I., Kozar, E.G., Engalycheva, I.A., & Baranova, E.V. (2018). Rasprostranenie i vredonosnost mikozov na kulture chesnoka ozimogo v usloviiakh Moskovskoi oblasti [Prevalence and Harmfulness of Fungal Diseases in Winter Garlic Cultivars in the Moscow Region]. *Ovoshchi Rossii — Vegetables of Russia*, 6, 84–90. DOI: 10.18619/2072-9146-2018-6-84-90 [in Russian].

2 Shestakova, K.S. (2009). Selektsionno-immunologicheskaia kharakteristika ustoichivosti chesnoka ozimogo (*Allium sativum* L.) k fuzarioznym gniliam [Breeding and immunological characteristics of winter garlic (*Allium sativum* L.) resistance to Fusarium rots]. *Extended abstract of candidate's thesis.* Moscow [in Russian].

3 Cremer, J., Campbell, P., Steele, V., Persley, D., Thomas, J., Harper, S., & Gambley, C. (2021). Detection and distribution of viruses infecting garlic crops in Australia. *Plants*, *10*(5), 1013. DOI: 10.3390/plants10051013

4 Moharam, M.H.A., Farrag, E.S., & Mohamed, M.D.A. (2013). Pathogenic fungi in garlic cloves and first report of clove rot of stored bulbs caused by Fusarium proliferatum in Upper Egypt. *Journal of Plant Pathology*, *95*, 2096–2103. DOI: 10.1080/03235408.2013.785122

5 Stepanova, M.Yu. et al. (1978). *Ukazatel vozbuditelei boleznei selskokhoziaistvennykh rastenii* [Index of Pathogens of Agricultural Plants]. Leningrad [in Russian].

6 Timina, L.T., & Engalycheva, I.A. (2015). Kompleks patogenov na ovoshchnykh kulturakh v usloviiakh tsentralnogo regiona [Pathogen Complex on Vegetable Crops in the Central Region of the Russian Federation]. *Ovoshchi Rossii — Vegetables of Russia*, 3-4, 123–129. DOI: 10.18619/2072-9146-2015-3-4-123-129 [in Russian].

7 Khmelnickaya, I.I. (2002). Rasprostranenie gribov *Aspergillus* v pochvakh razlichnykh regionov Rossii [Distribution of *Aspergillus* fungi in soils of various regions of Russia]. *1 sezd mikologov. Sovremennaia mikologiia v Rossii — 1st Congress of Mycologists. Modern Mycology in Russia*, 53-54. Moscow [in Russian].

8 Satton, D., Fotergill, A., & Rinaldi, M. (2001). *Opredelitel patogennykh i uslovno-patogennykh gribov* [A Field Guide to Pathogenic and Opportunistic Fungi]. Moscow: Mir [in Russian].

9 Polyakov, A.V., Azopkova, M.A., Lebedeva, N.N., & Muravyova, I.V. (2018). Regeneratsiia rastenii chesnoka ozimogo (*Allium sativum* L.) in vitro iz vozdushnykh lukovichek [In vitro regeneration of winter garlic (*Allium sativum* L.) from aerial bulbs]. *Ovoshchi Rossii — Vegetablexs of Russia*, 4, 20–25. DOI: 10.18619/2072-9146-2018-4-20-25 [in Russian].

10 Polyakov, A.V., Azopkova, M.A., Lebedeva, N.N., & Muravyova, I.V. (2018). In vitro regeneratsiia rastenii chesnoka ozimogo (*Allium sativum* L.) iz vozdushnykh lukovichek [In vitro regeneration of winter garlic (*Allium sativum* L.) plants from aerial bulbs]. *Vestnik Moskovskogo gosudarstvennogo oblastnogo universiteta. Seriia: Estestvennye nauki — Bulletin of the Moscow State Regional University, Series: Natural Sciences*, 4, 115–124. DOI: 10.18384/2310-7189-2018-4-115-124 [in Russian].

11 Shim, S.T., & Kyung, K.H. (1999). Natural microflora of pre-processed garlic and their resistance to garlic antimicrobial activity. *Food Microbiology*, *16(2)*, 165–172.

12 Ounis, S., Turóczi, G., & Kiss, J. (2025). Co-occurrence of *Stromatinia cepivora* and *Fusarium proliferatum* on garlic: in vitro investigation of pathogen–pathogen interactions and in planta screening for resistance of garlic cultivars. *Plants*, *14*(3), 440. DOI: 10.3390/plants14030440

13 Abachi, H., Moallem, M., & Taghavi, S.M. (2024). Garlic bulb decay and soft rot caused by the cross-kingdom pathogen *Burkholderia gladioli*. *Plant Disease*, *108*(3), 684–693. DOI: 10.1094/PDIS-08-23-1603-RE

14 Anum, H. et al. (2024). Different preharvest diseases in garlic and their eco-friendly management. *Plants*, *13*(2), 267. DOI: 10.3390/plants13020267

15 Mohy, S., Elameen, T.M., Khalaphallah, R., & Hassan, N.M.S. (2024). Biological control of garlic white and basal rot pathogens in vitro and under field conditions. *SVU International Journal of Agricultural Sciences*, *6*(4), 12–23. DOI: 10.21608/svuijas.2024.319563.1393

16 Gasser, K., Steinkellner, S., & Hage Ahmed, K. (2025). Fusarium dry rot in garlic: hidden infection of planting material leading to high infestation rates during storage of the resulting harvest. *Journal of Crop Health*, *77*, 132. DOI: 10.1007/s10343-025-01202-z

17 Dedecan, O., Güneş, N. & et al. (2025). First report of *Stemphylium eturmiunum* from garlic (*Allium sativum* L.) growing areas of Türkiye. *Crop Protection, 25*(1). DOI: 10.1016/j.cropro.2025.107253

18 Sharma, S., Mandal, S., & Cramer, C.S. (2024). In vitro and field efficacy of fungicide treatments against Fusarium bulb rot of garlic. *Horticulturae, 148*(2), 321–328. DOI: 10.3390/horticulturae10050527

Information about the authors

Matai Zhansaya — PhD-student of the Department of Biotechnology, Almaty Technological University; Researcher of the Agrochemistry Laboratory, LLP "Kazakh Research Institute of Fruit and Vegetable Growing", Almaty, Kazakhstan; e-mail: zhansaya.matay.91@mail.ru; ORCID: https://orcid.org/0009-0001-8819-0296

Jantassov Serik — Head of the Department of Vegetable and Melon Crop Breeding and Seed Production, LLP "Kazakh Research Institute of Fruit and Vegetable Growing", Almaty, Kazakhstan; e-mail: s_jantassov@mail.ru; ORCID: https://orcid.org/0000-0001-5407-9605

Ibragimova Gulnara — Leading researcher of the Department of Vegetable and Melon Crop Breeding and Seed Production, LLP "Kazakh Research Institute of Fruit and Vegetable Growing", Almaty, Kazakhstan; e-mail: gulnara.0868@mail.ru; ORCID: https://orcid.org/0009-0005-5662-4175

How to Cite: Sarsenbayeva, U., Almasbekova, A., Sharipov, K. Taipakova, S. & Saparbayev, M. (2026). The role of mutations in the MUTYH gene in the development of colorectal cancer. *Fundamental and Experimental Biology*, 31, 3 (123), 103-111. https://doi.org/10.31489/2026FEB3/103-111

Review Article

https://doi.org/10.31489/2026FEB3/103-111

UDC 575.113:616.351‑006.6 Received: 14.12.2025 | Accepted: 8.06.2026 | Published online: 30 September 2026

U. Sarsenbayeva[1, 2, 3*], A. Almasbekova[1, 2, 3], K. Sharipov[2, 3], S. Taipakova[1], M. Saparbayev[4]

[1]*Al-Farabi Kazakh National University, Almaty, Kazakhstan;*
[2]*M. Aitkozhin Institute of Molecular Biology and Biochemistry, Almaty, Kazakhstan;*
[3]*S. Asfendiyarov Kazakh National Medical University, Almaty, Kazakhstan;*
[4]*University Paris-Saclay, Gustave Roussy Cancer Campus, Villejuif, France*
[*]*Corresponding author: ulansarsenbayeva@gmail.com*

The role of mutations in the MUTYH gene in the development of colorectal cancer

Mutations in the MUTYH gene, which encodes a DNA glycosylase, are associated with an increased risk of colorectal cancer (CRC), particularly in individuals with hereditary MUTYH-associated polyposis (MAP). MUTYH is an essential component of the base excision repair (BER) pathway, where it removes adenine residues that are mispaired with 8-oxoguanine (8-oxoG), a major product of oxidative DNA damage. Loss of MUTYH function caused by pathogenic variants promotes the accumulation of oxidative DNA damage-associated mutations, including G:C→T:A transversions, thereby contributing to genomic instability and colorectal tumorigenesis. This review examines the pathogenic mechanisms underlying MAP and its characteristic phenotypic features. Structural and functional studies indicate that many pathogenic MUTYH variants result in reduced adenine DNA glycosylase activity, leading to impaired base excision repair. Potential therapeutic strategies aimed at restoring or compensating for defective MUTYH function are being investigated, including approaches based on synthetic lethality. Increasing attention is also being paid to molecular genetic testing for biallelic pathogenic variants in the MUTYH gene, particularly in individuals with clinical or family histories suggestive of hereditary colorectal cancer or polyposis. Identification of such variants may enable more precise risk assessment and facilitate personalized surveillance and preventive management. Overall, advances in understanding the role of MUTYH in genome maintenance have provided important insights into the pathogenesis of MAP and created opportunities for improving the diagnosis, risk stratification, and management of colorectal cancer.

Keywords: base excision repair, adenine DNA glycosylase, DNA repair, MUTYH, colorectal cancer.

Introduction

Colorectal cancer (CRC) is one of the most common types of cancer worldwide. It is the third most common cause of illness and the second most common cause of cancer-related death. Its development reflects a multifactorial process driven by the interplay of genetic predisposition, epigenetic alterations, and environmental influences. Although most CRC cases are sporadic, approximately 5–10 % are associated with inherited genetic defects. Among the best-characterized hereditary CRC syndromes are Lynch syndrome, caused by deficiencies in the DNA mismatch repair (MMR) system, and familial adenomatous polyposis (FAP), which arises from pathogenic mutations in the APC gene [1, 2].

Nevertheless, a subset of patients presenting with multiple colorectal polyps or early-onset CRC lacks detectable mutations in either APC or MMR genes. The identification of biallelic mutations in MUTYH led to the recognition of a distinct hereditary condition known as MUTYH-associated polyposis (MAP) [3, 4]. The MUTYH gene encodes a DNA glycosylase that functions within the base excision repair (BER) pathway, which is essential for protecting the genome from oxidative DNA damage, particularly lesions involving 8-oxoguanine (8-oxoG) [5, 6].

A unique feature of MUTYH is its role in preventing G: C→T: A transversion mutations by excising adenines mispaired with 8-oxoG during DNA replication. When MUTYH activity is compromised, these mutagenic lesions persist, leading to the accumulation of somatic mutations in critical cancer-related genes, most notably APC, a hallmark molecular feature of MAP-associated tumors [4, 7].

This review summarizes current knowledge on the biological function of MUTYH in DNA repair, the molecular basis and clinical characteristics of MAP, and the consequences of MUTYH dysfunction for ge-

nome stability. In addition, it discusses the diagnostic relevance of MUTYH mutations and emerging perspectives for targeted and preventive therapeutic strategies.

Base Excision Repair and the Role of MUTYH

Base excision repair (BER) represents the principal DNA repair pathway responsible for the removal of non-bulky base lesions arising from oxidation, deamination, and alkylation. This pathway is initiated by DNA glycosylases, which recognize damaged bases and cleave the N-glycosidic bond between the base and the deoxyribose, generating an apurinic/apyrimidinic (AP) site. Some glycosylases additionally possess β-lyase activity, allowing cleavage of the DNA backbone at the 3′ side of the AP site and thereby influencing the subsequent steps of repair [8, 9].

Among BER glycosylases, MUTYH occupies a unique position. Unlike most glycosylases, which directly excise damaged bases, MUTYH removes undamaged adenines mispaired with oxidized guanine (8-oxo-7,8-dihydroguanine, 8-oxoG) during DNA replication. This activity prevents the fixation of G: C→T: A transversion mutations, one of the most frequent mutational outcomes of oxidative stress. Loss of MUTYH function leads to the accumulation of somatic mutations in cancer-related genes, including APC, and underlies the development of MUTYH-associated polyposis (MAP). MUTYH operates in concert with other repair enzymes: OGG1 excises 8-oxoG opposite cytosine, whereas MTH1 sanitizes the nucleotide pool by hydrolyzing oxidized dNTPs. Together, these enzymes form a coordinated, multi-layered defense against 8-oxoG-induced mutagenesis [10, 11].

BER proceeds through two main subpathways: single-nucleotide BER (SN-BER) and long-patch BER (LP-BER). In SN-BER, only the damaged nucleotide is replaced, whereas LP-BER involves the removal and resynthesis of a short DNA segment comprising 2–10 nucleotides. When the initiating glycosylase possesses AP-lyase activity, the repair process proceeds through strand incision followed by gap filling by DNA polymerase β and ligation mediated by XRCC1 and DNA ligase III. In contrast, glycosylases lacking lyase activity rely on APE1-mediated incision, followed by strand displacement synthesis involving PCNA, DNA polymerases δ/ε, FEN1, and DNA ligase I. The selection of either pathway depends on the nature of the lesion and the biochemical properties of the initiating enzyme, ensuring flexibility and accuracy of repair under conditions of oxidative stress or during replication [8, 12, 13] (Fig. 1).

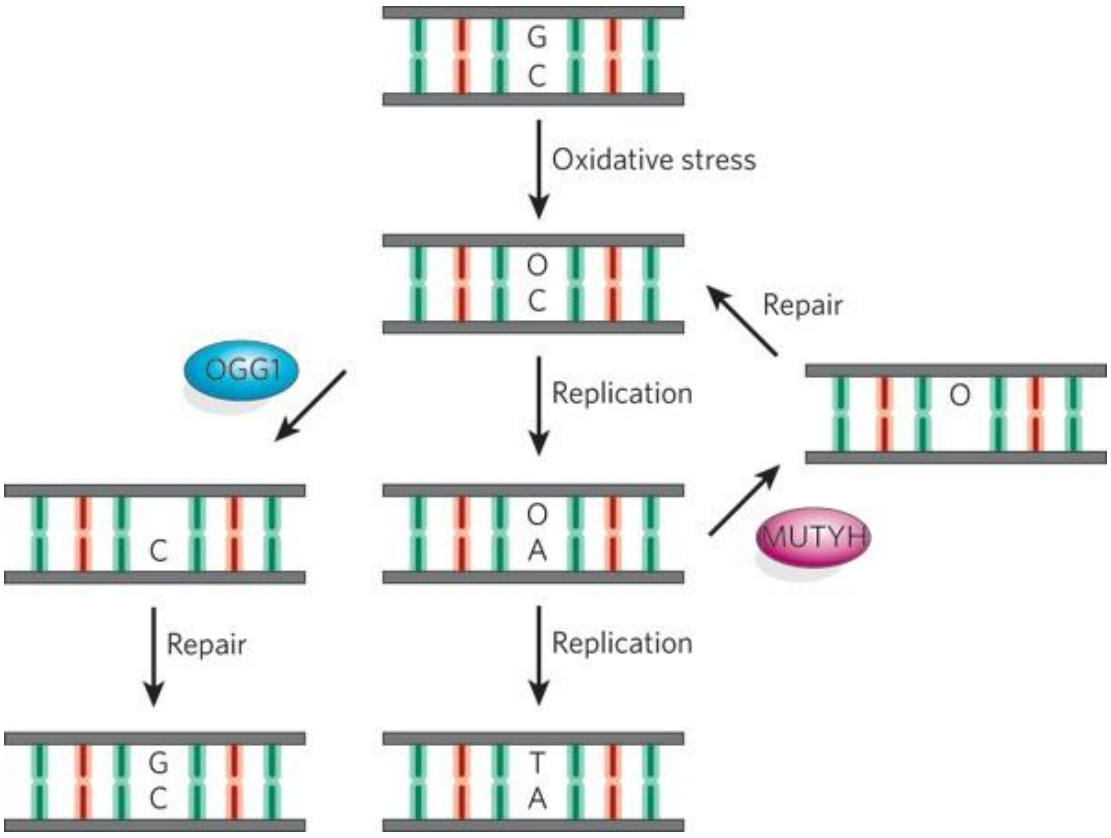

Figure 1. Short-patch base excision repair (BER) pathway for 8-oxoG lesions [8]

Oxidative damage to guanine resulting in 8-oxoG formation is particularly mutagenic. If unrepaired, 8-oxoG can mispair with adenine during DNA synthesis, leading to G: C→T: A transversions. Such mutations are frequently detected in early stages of colorectal carcinogenesis [9]. Consistent with this observation, MUTYH deficiency is associated with a characteristic mutational signature dominated by G: C→T: A substitutions, which represents a molecular hallmark of MAP [11, 14].

Human MUTYH consists of an N-terminal catalytic domain responsible for adenine excision and a C-terminal domain involved in recognition of 8-oxoG. These structural features are conserved in the bacterial homolog MutY, highlighting the evolutionary preservation of MUTYH function [11]. A defining structural element of MUTYH is a highly conserved [4Fe–4S] cluster located within the C-terminal domain. This metallocluster, characteristic of the helix–hairpin–helix (HhH) DNA glycosylase superfamily, plays a critical role in maintaining protein stability and facilitating substrate recognition [15].

Biochemical and structural studies indicate that the [4Fe–4S] cluster does not participate directly in redox catalysis but instead contributes to DNA binding and lesion detection. By stabilizing the HhH-GPD motif, the cluster enables proper alignment of MUTYH with the DNA duplex and supports the base-flipping mechanism required for identifying adenines mispaired with 8-oxoG. Disruption of the Fe–S cluster, whether through mutagenesis or impaired metal coordination, markedly reduces DNA binding affinity and glycosylase activity [16, 17]. Crystallographic analyses further demonstrate that the cluster is positioned at the protein–DNA interface, suggesting a role in recognizing the distinctive structural and electronic properties of 8-oxoG [15].

The human MUTYH gene is located on chromosome 1p34.1, spans about 11.2 kb, and contains 16 exons. It partially overlaps with the TOE1 gene, suggesting a complex regulatory framework at this locus. Multiple alternative promoters produce different transcription variants that encode isoforms with distinct subcellular localizations. Nuclear isoforms mainly repair genomic DNA, while the mitochondrial isoform protects mitochondrial DNA from oxidative damage. This targeting helps MUTYH maintain genomic integrity in different cellular compartments (Fig. 2) [18].

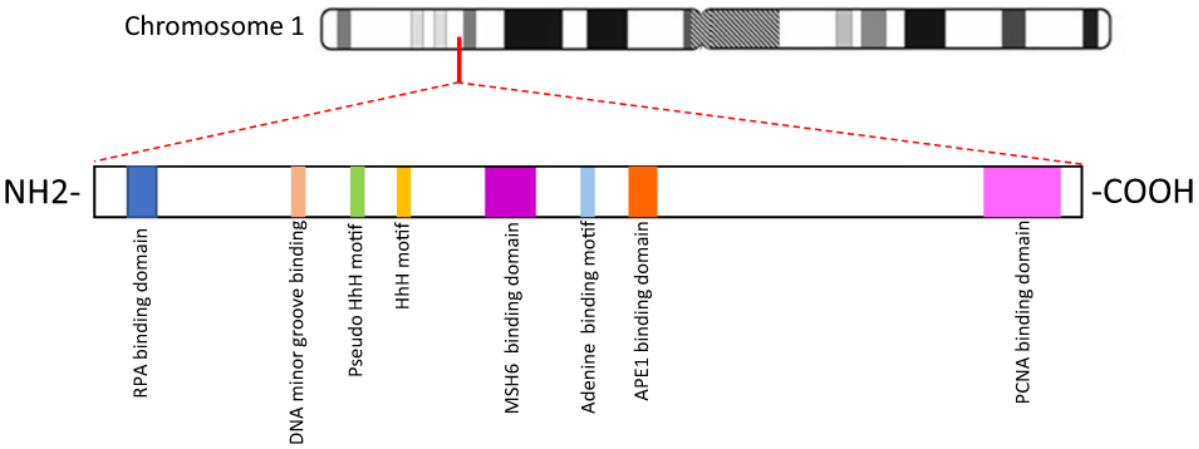

Figure 2: The chromosomal localization and functional domains of MUTYH [18]

Recent studies have improved the understanding of MUTYH's functions by showing its interaction with mismatch repair proteins, especially MSH6, which helps detect DNA damage and form the repair complex. Post-translational modifications, such as phosphorylation and ubiquitination, play a crucial role in controlling the stability, subcellular localization, and catalytic activity of MUTYH. These regulatory mechanisms provide fine control over BER and help prevent excessive or aberrant base excision [8, 18, 19].

Importantly, MUTYH acts as a mismatch-specific rather than a damage-specific glycosylase. By excising adenine from 8-oxoG: A mismatches, MUTYH creates a substrate for correct cytosine incorporation, thereby allowing OGG1 a second opportunity to remove the oxidized guanine. The efficiency of this repair process depends on DNA structure, chromatin context, and replication status, underscoring the adaptive role of MUTYH in proliferating cells (Tab. 1) [20–24].

Table 1

Functional roles of MUTYH in genome maintenance and disease prevention

Role of MUTYH	Molecular mechanism	Biological significance	Clinical implications	Key references
Removal of mispaired adenine opposite 8-oxoG	Hydrolysis of N-glycosidic bond; recognition of A:8-oxoG via HhH-GPD domain	Prevents G: C→T: A transversions; maintains replication fidelity	Loss of function → MAP phenotype; accumulation of APC mutations	[8, 10]
Cooperation with OGG1 and MTH1 (8-oxoG defense axis)	Acts downstream of OGG1 and in coordination with MTH1 to counteract oxidative lesions during and after replication	Provides multi-layered protection against oxidative mutagenesis	Disruption of this axis increases oxidative mutational burden; the strongest clinical evidence for CRC is associated with biallelic MUTYH deficiency	[8, 9]
Crosstalk with mismatch repair (MSH6)	Physical and functional interaction with MSH6 enhances mismatch recognition and repair complex assembly	Improves post-replicative repair efficiency	May contribute to Lynch-like molecular features in a subset of MUTYH-deficient tumors	[23, 24]
Coordination with the DNA replication machinery	Interaction with PCNA localizes MUTYH to replication forks	Enables rapid correction of mismatches arising during DNA synthesis	Impaired interaction increases mutational load and cancer susceptibility	[15, 19]
Function of the [4Fe-4S] cluster	Stabilizes DNA-binding conformation and supports allosteric control	Ensures accurate lesion recognition and structural integrity of the enzyme	Variants destabilizing the Fe-S cluster are associated with severe loss-of-function phenotypes	[15]
Regulation by post-translational modifications	Phosphorylation and ubiquitination modulate stability, localization, and activity	Fine-tunes BER according to cell cycle and stress conditions	Dysregulation may contribute to cancer susceptibility	[23]
Tumor suppression beyond the colon	Prevention of oxidative mutagenesis in multiple tissues	Extends protective role beyond colorectal epithelium	Supports the concept of a broader “MUTYH-associated tumor spectrum”	[4]

Discovering and expanding the role of MUTYH in cancer susceptibility

The discovery of MUTYH-associated polyposis (MAP) was a watershed moment in our understanding of hereditary colorectal cancer syndromes (CRC). Before this, the majority of hereditary CRC cases were linked to dominant mutations in the APC gene (familial adenomatous polyposis) or the mismatch repair (MMR) genes (Lynch syndrome). However, in certain cases, mutations in these canonical genes were not related with numerous adenomas or early development of prostate cancer.

In 2002, a British family was identified as having multiple occurrences of colon cancer and a high frequency of G: C to T: A transversions in the APC gene, indicating a failure to repair oxidative DNA damage. Sequencing showed harmful mutations in the MUTYH (Y179C and G396D) gene implicated in basic excision repair (BER), resulting in the discovery of a novel condition, MAP (MUTYH-associated polyposis) [25].

A comprehensive case-control research found that carriers with biallelic MUTYH mutations had an 18-fold increased risk of cancer, confirming the significance of this finding [23]. Interestingly, heterozygous carriers had a minor but statistically significant increase in cancer risk (risk factor = 1.5), implying MUTYH plays a broader role in cancer propensity [24].

MUTYH was initially linked to colorectal tumor growth, but new research suggests that it plays a larger biological role in preserving genomic stability in many tissues. Its primary role is to remove adenines that are incorrectly linked to 8-oxoguanine, so protecting the genome from oxidative stress-induced mutations. Studies on MUTYH-deficient mice have revealed an increased frequency of spontaneous mutations as well as an increase in the number of tumors not only in the gastrointestinal tract but also in the lungs, liver, and lym-

phatic system. When subjected to oxidative stressors like potassium bromate or ionizing radiation, these mice develop more varied and severe tumors than wild-type controls.

At the molecular level, MUTYH is involved in transcriptional repair and interacts with mismatch repair proteins such as MSH6, implying a function in coordinating numerous genome maintenance mechanisms [22]. Furthermore, posttranslational changes including phosphorylation, ubiquitination, and interaction with replication-related proteins like PCNA, influence MUTYH function and cellular location [21].

Furthermore, discoveries have highlighted the epigenetic control of MUTYH. For example, Alfeghaly et al. (2019) discovered that the long non-coding RNA ANRIL controls the expression of DNA repair genes, including MUTYH, implying that tissue-specific expression and cancer risk may be generated by RNA regulation [23].

Clinically, MUTYH allelic mutations have been observed in tumors other than the colon, including ovarian, endometrial, and probably kidney cancers; the degree and causation of these connections are currently being investigated. As genome-wide association studies (GWAS) and genetic screening panels for many malignancies become increasingly popular, the whole spectrum of MUTYH tumor suppressor activity is expected to broaden.

As Curia, Catalano, and Acetoet al. point out, MUTYH is increasingly recognized as a multifunctional genome caregiver rather than a CRC-specific tumor suppressor. Its involvement in oxidative DNA repair, interaction with essential repair proteins, stress signaling, and vulnerability to epigenetic modification highlight its importance in cellular homeostasis and cancer prevention [26].

The clinical implications of MUTYH mutations in colorectal cancer

The discovery of MUTYH-associated polyposis (MAP) had far-reaching clinical implications, especially in the field of genetic counseling, diagnosis, and treatment of colorectal cancer (CRC). As an autosomal recessive disease, MAP is a problem distinct from dominantly inherited syndromes such as familial adenomatous polyposis (FAP) and Lynch syndrome. For the disease to develop, individuals must inherit two harmful mutations, one from each parent, while heterozygous (monoallelic) carriers are usually asymptomatic. This complicates the risk assessment based solely on family history and highlights the need for molecular diagnostics [26, 27].

Genetic testing for MUTYH mutations is currently standard practice in individuals with multiple colorectal adenomas (usually 10–100), especially when no pathogenic variants have been identified in the APC gene [29]. In European populations, the most common mutational variants are Y165C and G382D, which are usually included in targeted testing programs. Next-generation sequencing (NGS) has expanded the possibilities of detecting rare and population-specific mutations [30].

After the diagnosis of MAP, clinical guidance is based on enhanced surveillance. Colonoscopy should begin in the third decade of life with a follow-up interval of 1-2 years, depending on the prevalence of the adenoma and histological examination. Preventive colectomy may be recommended for patients with a high prevalence of adenoma or dysplasia, similar to treatment for advanced FAP [31]. Screening of the upper gastrointestinal tract, such as esophagogastroduodenoscopy, is also recommended due to the increased risk of developing duodenal and gastric polyps [32].

Comprehensive testing of family members is required. Relatives of those affected should undergo genetic counseling and, if necessary, mutation testing. Early detection of carriers of biallelic genes allows timely implementation of surveillance strategies, potentially preventing CRC [33]. Although MAP does not develop in monoallelic carriers, some studies suggest a slightly increased risk of CRC, especially in the presence of environmental or genetic cofactors.

MUTYH is increasingly being included in multigenic panels to determine cancer predisposition, which is beneficial for patients with atypical phenotypes or lack of family history. However, broader testing increases the likelihood of identifying variants with uncertain significance (VUS), which complicates clinical interpretation, especially in individuals without overt polyposis [34].

Emerging data on the epigenetic regulation of MUTYH may suggest new diagnostic and prognostic approaches. Long non-coding RNAs (lncRNAs) such as ANRIL have been shown to modulate the expression of DNA repair genes, including MUTYH, suggesting that transcriptomic profiling can improve risk stratification [20].

Thus, the identification of MUTYH as the main gene in hereditary CRC has had a profound impact on clinical practice, providing more accurate risk assessment, personalized follow-up, and integration of

MUTYH testing into complex cancer genetics. Recent advances in genomics and transcriptomics are expected to further improve clinical care for MAP and related conditions [28].

Major studies conducted over the past decade confirm the multifaceted role of MUTYH in maintaining genomic integrity and preventing hereditary cancers, particularly colorectal cancer. Biallelic mutations lead to MUTYH dysfunction, resulting in the formation of MAP, characterized by numerous adenomatous polyps and a significantly increased risk of CRC. Epidemiological data indicate an 18-fold higher risk in biallelic carriers, while heterozygous carriers show a moderately increased risk.

MUTYH is necessary for the basic excision repair (BER) pathway, removing adenines improperly incorporated into 8-oxoG, and supplementing the activity of OGG1 and MTH1 to protect against mutagenesis caused by reactive oxygen species. Recent studies have highlighted its interaction with other repair pathways, including mismatch repair (MMR), and the effect of posttranslational modifications on MUTYH activity and localization [35].

Conclusion

In conclusion, identifying MUTYH-associated polyposis (MAP) has improved our understanding of hereditary colorectal cancer. It emphasizes the key role of base excision repair in preventing tumor formation. The MUTYH protein ensures the maintenance of genomic stability by removing adenine mistakenly paired with oxidized guanine, thereby preventing the accumulation of mutations. This mechanism is an important component of the dynamic balance between DNA damage and repair. The functions of MUTYH are not limited to colorectal tissue but also include participation in the cellular response to oxidative stress and epigenetic regulatory processes, indicating its broader systemic significance. It has been shown that molecular genetic testing for MUTYH mutations improves the accuracy of individual risk assessment and clinical management in hereditary colorectal cancer. However, challenges persist in the interpretation of variants and the assessment of cancer risk in cases not limited to the colon. It is suggested that future research into the regulatory mechanisms of MUTYH may result in the identification of novel biomarkers and targeted therapeutic strategies. Overall, MUTYH demonstrates the capacity for molecular insights to be translated into enhanced clinical practice for hereditary cancer syndromes.

Funding

This work was prepared within the framework of U.B. Sarsenbayeva's dissertation project "Development of a method for detecting the activity of mismatch-specific adenine-DNA glycosylases for the study of aberrant repair in cancer cells" and was supported by Abai-Verne Scholarship Program of the Ministry of Science and Higher Education of the Republic of Kazakhstan, and the Ministry of Europe and Foreign Affairs of the French Republic supported U. Sarsenbayeva and A. Almasbekova. The funding agencies did not influence the content of this review.

Conflict of Interest

The authors declare no conflict of interest.

Author Contributions

The manuscript is a review article prepared through the joint contribution of all authors. All authors have read and approved the final version of the manuscript. CRediT: **Sarsenbayeva U.** — conceptualization, literature collection and analysis, writing — original draft. **Almasbekova A**. — literature collection and analysis. **Sharipov K.** — critical analysis, writing — review & editing. **Taipakova S.** — data curation, writing — review & editing, critical analysis, final text preparation. **Saparbayev M.** — data curation, writing — review & editing, critical analysis, final text preparation.

References

1 Siegel, R. L., Miller, K. D., Fuchs, H. E., & Jemal, A. (2022). Cancer statistics, 2022. *CA: A Cancer Journal for Clinicians, 72*(1), 7–33. https://doi.org/10.3322/caac.21708

2 Kantor, M., Sobrado, J., Patel, S., Eiseler, S., & Ochner, C. (2017). Hereditary colorectal tumors: A literature review on MUTYH-associated polyposis. *Gastroenterology Research and Practice, 2017*, Article ID 8693182. https://doi.org/10.1155/2017/8693182

3 Venesio, T., Balsamo, A., D'Agostino, V. G., & Ranzani, G. N. (2012). MUTYH-associated polyposis (MAP), the syndrome implicating base excision repair in inherited predisposition to colorectal tumors. *Frontiers in Oncology, 2*, Article ID 83. https://doi.org/10.3389/fonc.2012.00083

4 Curia, M. C., Catalano, T., & Aceto, G. M. (2020). MUTYH: Not just polyposis. *World Journal of Clinical Oncology, 11*(7), 428–449. https://doi.org/10.5306/wjco.v11.i7.428

5 Nakamura, T., Okabe, K., Hirayama, S., Chirifu, M., Ikemizu, S., Morioka, H., Nakabeppu, Y., & Yamagata, Y. (2021). Structure of the mammalian adenine DNA glycosylase MUTYH: Insights into the base excision repair pathway and cancer. *Nucleic Acids Research, 49*(12), 7154–7163. https://doi.org/10.1093/nar/gkab492

6 Kairupan, C., & Scott, R. J. (2007). Base excision repair and the role of MUTYH. *Hereditary Cancer in Clinical Practice, 5*, Article ID 199.https://doi.org/10.1186/1897-4287-5-4-199

7 Guarinos, C., Juárez, M., Egoavil, C., Castillejo, A., Barberá, V. M., Pérez-Cabornero, L., Sánchez-Heras, A. B., Castellví-Bel, S., Llor, X., & Castells, A. (2014). Prevalence and characteristics of MUTYH-associated polyposis in patients with multiple adenomatous and serrated polyps. *Clinical Cancer Research, 20*(5), 1158–1168. https://doi.org/10.1158/1078-0432.CCR-13-1490

8 David, S. S., O'Shea, V. L., & Kundu, S. (2007). Base-excision repair of oxidative DNA damage. *Nature, 447*, 941–950. https://doi.org/10.1038/nature05978

9 Dizdaroglu, M., Coskun, E., & Jaruga, P. (2017). Repair of oxidatively induced DNA damage by DNA glycosylases: Mechanisms of action, substrate specificities and excision kinetics. *Mutation Research/Reviews in Mutation Research, 763*, 212–245. https://doi.org/10.1016/j.mrrev.2017.02.001

10 Al-Tassan, N., Chmiel, N., Maynard, J., Fleming, N., Livingston, A. L., Williams, G. T., Hodges, A. K., Davies, D. R., David, S. S., Sampson, J. R., & Cheadle, J. P. (2002). Inherited variants of MYH associated with somatic G: C→T: A mutations in colorectal tumors. *Nature Genetics, 30*, 227–232. https://doi.org/10.1038/ng828

11 Buisine, M. P., Bonadona, V., Baert-Desurmont, S., Frebourg, T., Olschwang, S., Parc, Y., Taieb, J., Saurin, J. C., & Laurent-Puig, P. (2020). MUTYH-associated polyposis: Review and update of the French recommendations. *Bulletin du Cancer, 107*(5), 586–600. https://doi.org/10.1016/j.bulcan.2020.02.004

12 Wallace, S. S. (2014). Base excision repair: A critical player in many games. *DNA Repair, 19*, 14–26. https://doi.org/10.1016/j.dnarep.2014.02.011

13 Majumdar, C., Demir, M., Merrill, S. R., Pande, P., & David, S. S. (2024). FSHing for DNA damage: Key features of MutY detection of 8-oxoguanine: adenine mismatches. *Accounts of Chemical Research, 57*(7), 1019–1031. https://doi.org/10.1021/acs.accounts.3c00759

14 Talhaoui, I., Matkarimov, B. T., Tchenio, T., Zharkov, D. O., & Saparbaev, M. K. (2017). Aberrant base excision repair pathway of oxidatively damaged DNA. *Free Radical Biology and Medicine, 107*, 266–277. https://doi.org/10.1016/j.freeradbiomed.2016.11.040

15 Trasviña-Arenas, C. H., Dissanayake, U. C., Tamayo, N., Merrill, S. R., Demir, M., Majumdar, C., & David, S. S. (2025). Structure of human MUTYH and functional profiling of cancer-associated variants. *Nature Communications, 16*, Article ID 1234. https://doi.org/10.1038/s41467-025-58361-w

16 Nuñez, N., Majumdar, C., Lay, K. T., & David, S. S. (2018). Fe–S clusters and MutY base excision repair glycosylases. *Methods in Enzymology, 599*, 21–68. https://doi.org/10.1016/bs.mie.2017.11.035

17 McDonnell, K. J., Chemler, J. A., Bartels, P. L., Sloggett, S., Viner, R., Chatterjee, N., Barton, J. K., & David, S. S. (2018). A human MUTYH variant linking colonic polyposis to redox degradation of the $[4Fe–4S]^{2+}$ cluster. *Nature Chemistry, 10*, 752–759. https://doi.org/10.1038/s41557-018-0068-x

18 Magrin, L., Fanale, D., Brando, C., Corsini, L. R., Calò, V., Bazan, V., & Russo, A. (2022). MUTYH-associated tumor syndrome: The other face of MAP. *Oncogene, 41*, 2531–2539. https://doi.org/10.1038/s41388-022-02304-y

19 Banda, D. M., Nuñez, N. N., Burnside, M. A., Bradshaw, E. M., & David, S. S. (2017). Repair of 8-oxoG: A mismatches by the MUTYH glycosylase. *Free Radical Biology and Medicine, 107*, 202–215. https://doi.org/10.1016/j.freeradbiomed.2017.01.008

20 Grasso, F., Di Meo, S., De Luca, G., & Venditti, P. (2015). The MUTYH base excision repair gene protects against inflammation-associated colorectal carcinogenesis. *Oncotarget, 6*(27), 19671–19684. https://doi.org/10.18632/oncotarget.4284

21 Trasviña-Arenas, C. H., Demir, M., Lin, W. -J., & David, S. S. (2021). Structure, function and evolution of the helix–hairpin–helix DNA glycosylase superfamily. *DNA Repair, 108*, Article ID 103231. https://doi.org/10.1016/j.dnarep.2021.103231

22 Manlove, A. H., McKibbin, P. L., Doyle, E. L., Majumdar, C., Hamm, M. L., & David, S. S. (2017). Structure–activity relationships reveal key features of 8-oxoguanine: adenine mismatch detection by the MutY glycosylase. *ACS Chemical Biology, 12*(9), 2335–2344. https://doi.org/10.1021/acschembio.7b00389

23 Limpose, K. L., Corbett, A. H., & Doetsch, P. W. (2017). BERing the burden of damage: Pathway crosstalk and post-translational modification of base excision repair proteins regulate DNA damage management. *DNA Repair, 56*, 51–64. https://doi.org/10.1016/j.dnarep.2017.06.007

24 Markkanen, E., Dorn, J., & Hübscher, U. (2015). Mutagenic processing of 8-oxoguanine- and 8-oxoadenine-containing DNA by human DNA polymerases η and κ. *DNA Repair, 21*, 58–67. https://doi.org/10.1016/j.dnarep.2014.06.007

25 Sanchez-Mete, L., Mosciatti, L., Casadio, M., Vittori, L., Martayan, A., & Stigliano, V. (2023). MUTYH-associated polyposis: Is it time to change upper gastrointestinal surveillance? *World Journal of Gastrointestinal Oncology, 15*(11), 1891–1899. https://doi.org/10.4251/wjgo.v15.i11.1891

26 Curia, G., Catalano, F., & Aceto, S. (2023). The multifaceted role of MUTYH in cancer and beyond: From molecular mechanisms to therapeutic opportunities. *Biomedicines, 11*(10), Article ID 2700. https://doi.org/10.3390/biomedicines11102700

27 Morcillo, M., Yagüe, M. L., Pérez-Cabornero, M., Infante, E., Lastra, E., & Urioste, M. (2020). Molecular pathogenesis of MUTYH-associated polyposis and implications for clinical management. *Cancers, 12*(9), Article ID 2680. https://doi.org/10.3390/cancers12092680

28 Weren, R. D. A., Ligtenberg, M. J. L., Kets, C. M., de Voer, R. M., Verwiel, E. T. P., Spruijt, L., van Zelst-Stams, W. A. G., Jongmans, M. C. J., & Hoogerbrugge, N. (2021). Cancer risks associated with monoallelic MUTYH pathogenic variants: A retrospective cohort study. *Genetics in Medicine, 23*(7), 1340–1346. https://doi.org/10.1038/s41436-021-01234-9

29 Nielsen, M., Joerink-van de Beld, M. C., Jones, N., Vogt, S., Tops, C. M., Vasen, H. F. A., Sampson, J. R., Aretz, S., & Hes, F. J. (2009). Analysis of MUTYH Genotypes and Colorectal Phenotypes in Patients With MUTYH-Associated Polyposis. *Gastroenterology, 136*(2), 471–476. https://doi.org/10.1053/j.gastro.2008.10.056

30 Vogt, S., Jones, N., Christian, D., Engel, C., Nielsen, M., Kaufmann, A., Steinke, V., Vasen, H. F. A., & Hes, F. J. (2009). Expanded extracolonic tumor spectrum in MUTYH-associated polyposis. *Gastroenterology, 137*(6), 1976–1985. e1–10. https://doi.org/10.1053/j.gastro.2009.08.052

31 Win, A. K., Young, J. P., Lindor, N. M., Tucker, K. M., Ahnen, D. J., & Young, G. P. (2012). Colorectal and other cancer risks for carriers and noncarriers from families with a DNA mismatch repair gene mutation: a prospective cohort study. *Journal of Clinical Oncology, 30*(9), 958–964. https://doi.org/10.1200/JCO.2011.39.5590

32 Nieuwenhuis, M. H., and Vasen, H. F. A. (2007). Correlations between genotype and phenotype of familial adenomatous polyposis. *Critical Reviews in Oncology/Hematology, 61*, 153–161. https://doi.org/10.1016/j.critrevonc.2006.07.004

33 Lubbe, S. J., Di Bernardo, M. C., Chandler, I. P., & Houlston, R. S. (2009). Clinical Implications of the Colorectal Cancer Risk Associated With MUTYH Mutation. *Journal of Clinical Oncology, 27*(24), 3975–3980. https://doi.org/10.1200/JCO.2008.21.6853

34 Lucci-Cordisco, E., Amenta, S., Panfili, A., Del Valle, J., Capellá, G., & Pineda, M. (2022). Variants of uncertain significance (VUS) in cancer predisposing genes: What are we learning from multigene panels? *European Journal of Medical Genetics, 65*(1), 104400. https://doi.org/10.1016/j.ejmg.2021.104400

35 Nielsen, M., Morreau, H., Vasen, H. F. A., & Hes, F. J. (2011). MUTYH-associated polyposis (MAP). *Critical Reviews in Oncology/Hematology, 79*(1), 1–16. https://doi.org/10.1016/j.critrevonc.2010.05.011

У. Сарсенбаева, А. Алмасбекова, К. Шарипов,
С. Тайпакова, М. Сапарбаев

MUTYH геніндегі мутацияның колоректальды қатерлі ісіктің дамуындағы рөлі

MUTYH геніндегі мутациялар ДНҚ-гликозилазаны кодтай отырып, колоректальды қатерлі ісіктің (КРҚІ) дамуында, әсіресе MUTYH-пен байланысты полипоз (MAP) жағдайларында маңызды рөл атқарады. Бұл фермент ДНҚ-ның негіздерін эксцизиялық репарациялау (BER) үдерісінің негізгі компоненті және ДНҚ-ның тотығу зақымдануының өнімі болып саналатын 8-оксогуанинмен (8-охоG) қате жұптасқан адениндерді жоюға жауап береді. MUTYH функциясының патогенді мутациялар салдарынан бұзылуы G: C→T: A типті трансверсиялардың жинақталуына әкеліп, геномдық тұрақсыздықтың күшеюіне және тоқ ішек эпителий жасушаларының қатерлі трансформациясына себеп болады. Бұл шолуда MUTYH дисфункциясының колоректальды қатерлі ісіктің дамуымен байланысын дәлелдейтін молекулалық, функционалдық және клиникаға дейінгі деректер жинақталған. MAP синдромының патогенетикалық механизмдері мен фенотиптік ерекшеліктері талқыланып, MUTYH-тың әртүрлі нұсқаларында ферментативтік белсенділіктің төмендейтінін көрсететін құрылымдық талдаулардың нәтижелері ұсынылады. Қазіргі уақытта MUTYH функциясын қалпына келтіруге бағытталған терапиялық стратегиялар, соның ішінде гендік терапия, фармакологиялық модуляция және синтетикалық өлім қағидаттарына негізделген тәсілдер зерттелуде. Отбасылық анамнезінде колоректальды қатерлі ісігі бар адамдарда MUTYH генінің биаллельді мутацияларын ерте молекулалық скринингтен өткізуге ерекше назар аударылады, өйткені бұл деректер алдын алу мен емдеудің дербестендірілген тәсілдерін қалыптастыру үшін маңызды негіз бола алады. MUTYH-тың геном тұтастығын сақтаудағы рөлін терең түсіну колоректальды қатерлі ісікті диагностикалау, қауіп-қатерді бағалау және таргеттік терапияны дамыту үшін жаңа мүмкіндіктер ашады.

Кілт сөздер: негіздерді эксцизиялық репарациялау, аденин-ДНҚ-гликозилаза, ДНҚ репарациясы, MUTYH, колоректальды қатерлі ісік.

У. Сарсенбаева, А. Алмасбекова, К. Шарипов,
С. Тайпакова, М. Сапарбаев

Роль мутации в гене MUTYHв развития колоректального рака

Мутации в гене MUTYH, который кодирует ДНК-гликозилазу, играют ключевую роль в развитии колоректального рака (КРР), особенно в случаях наследственного полипоза, ассоциированного с MUTYH (MAP). Этот фермент является важной частью процесса репарации оснований (BER), ответственного за удаление аденинов, неправильно связанных с 8-оксогуанином (8-oxoG), побочным продуктом окислительного повреждения ДНК. Потеря функции MUTYH из-за вредных мутаций приводит к накоплению трансверсий G:C→T:A, что приводит к нестабильности генома и злокачественной трансформации эпителиальных клеток толстой кишки. В этом обзоре обобщены молекулярные, функциональные и доклинические данные, подтверждающие связь дисфункции MUTYH с развитием КРР. В нем обсуждаются патогенетические механизмы и фенотипические особенности MAP, представлены результаты структурного анализа, показывающие снижение ферментативной активности в различных вариантах MUTYH. В настоящее время изучаются терапевтические стратегии, направленные на восстановление функции MUTYH, включая генную терапию, фармакологическую модуляцию и использование синтетической летальности. Особое внимание уделяется раннему молекулярному скринингу на наличие биаллельных мутаций MUTYH у лиц с семейным анамнезом КРР, поскольку он может служить основой для персонализированных подходов к профилактике и лечению. Понимание роли MUTYH в поддержании целостности генома открывает новые возможности для диагностики, оценки риска и таргетной терапии колоректального рака.

Ключевые слова: удаление основания, аденин-ДНК гликозилаза, репарация ДНК, MUTYH, колоректальный рак.

Information about the authors

Sarsenbayeva Ulan — PhD-student, Department of Biotechnology, al-Farabi Kazakh National University, Senior lecturer of the Department of Biochemistry, S. Asfendiyarov Kazakh National Medical University, Almaty, Kazakhstan; e-mail: ulansarsenbayeva@gmail.com; ORCID: https://orcid.org/0009-0003-9292-0153

Almasbekova Adina — PhD-student, Department of Biomedicine, al-Farabi Kazakh National University, Senior lecturer of the Department of Biochemistry, S. Asfendiyarov Kazakh National Medical University, Almaty, Kazakhstan; e-mail: almasbekovaadina94@gmail.com; ORCID: https://orcid.org/0009-0005-9957-1747

Sharipov Kamalidin — Doctor of Biological Sciences, Professor, General Director of the M.A. Aitkhozhin Institute of Molecular Biology and Biochemistry, Head of the Department of Biochemistry, S. Asfendiyarov Kazakh National Medical University, Almaty, Kazakhstan; e-mail: sharipov.k@kaznmu.kz; ORCID: https://orcid.org/0000-0001-5946-5521

Taipakova Sabira — PhD, Associate Professor of the Department of Molecular Biology and Genetics, Al-Farabi Kazakh National University, Almaty, Kazakhstan; e-mail: sabira.taipakova@gmail.com; ORCID: https://orcid.org/0000-0001-9499-1682

Saparbayev Murat — Candidate of Biological Sciences, Head of the Laboratory “Mechanisms of DNA Repair and Carcinogenesis”, Gustave Roussy Cancer Center, Villejuif, France; e-mail: murat.saparbaev@gustaveroussy.fr; ORCID: https://orcid.org/0000-0002-4630-1074

How to Cite: Smayelova, K.A., Abdukadirova, Zh.A., Anarbekova, G.D., Kozhamzharova, A.S., Izbastina, K.S. & Aitzhanova, M.O. (2026). Floristic diversity, geobotanical structure and ecological significance of plant communities of *Tanacetum vulgare* L. in the foothill ecosystems of Southeast Kazakhstan. *Fundamental and Experimental Biology*, 31, 3 (123), 112-126. https://doi.org/10.31489/2026FEB3/112-126

Research Article

https://doi.org/10.31489/2026FEB3/112-126

UDC 581.412+581.5+582.5/.9 Received: 5.01.2026 | Accepted: 8.06.2026 | Published online: 30.09.2026

K.A. Smayelova[1*], Zh.A. Abdukadirova[1], G.D. Anarbekova[2], A.S. Kozhamzharova[3], K.S. Izbastina[4, 5], M.O. Aitzhanova[2]

[1]*Al-Farabi Kazakh National University, Almaty, Kazakhstan;*
[2]*Kazakh National Women's Teacher training University, Almaty, Kazakhstan;*
[3]*S.D. Asfendiyarov Kazakh National Medical University, Almaty, Kazakhstan;*
[4]*Astana Botanical Garden, Astana, Kazakhstan;*
[5]*S. Seifullin Kazakh AgroTechnical Research University, Astana, Kazakhstan*
**Corresponding author: karlyga505@gmail.com*

Floristic diversity, geobotanical structure and ecological significance of plant communities of *Tanacetum vulgare* L. in the foothill ecosystems of Southeast Kazakhstan

The article presents the results of a comprehensive study of the floristic diversity, geobotanical structure, and ecological significance of plant communities of *Tanacetum vulgare* L. growing in the foothill ecosystems of southeastern Kazakhstan. The relevance of the study is determined by the multifunctional significance of common tansy, a multipurpose plant used for food, fodder, technical, and ornamental purposes, as well as in traditional and conventional medicine. In the context of increasing anthropogenic pressure and the transformation of natural ecosystems, studying the ecological and coenotic role of this species is of particular scientific and practical importance. It was established that *Tanacetum vulgare* L. plant communities are characterized by high floristic diversity and a predominance of mesophytic and mesoxerophytic species. The studied species occurs as a constant or subdominant component of the herbaceous layer, demonstrating high ecological plasticity and resistance to changing environmental conditions. The obtained results expand our understanding of the structure and functioning of foothill phytocenoses and may be used for biodiversity monitoring, ecosystem status assessment, and the rational and sustainable use of plant resources in southeastern Kazakhstan.

Keywords: *Tanacetum vulgare* L., floristic diversity, geobotanical structure, phytocenosis, ecological significance, foothill ecosystems, Southeast Kazakhstan.

Introduction

Accelerated landscape modification driven by expanding land use and increasing climatic variability has intensified the need to investigate vegetation processes in ecotonal territories [1]. Foothill ecosystems represent transitional zones that connect steppe plains with mountain systems and function as dynamic interfaces where species exchange, environmental gradients, and structural heterogeneity converge. Owing to their complex topography and microclimatic variability, these landscapes are particularly sensitive to both natural fluctuations and anthropogenic disturbances [2–5].

The functional integrity of plant communities is closely linked to their taxonomic diversity and spatial organization. Ecosystems with high species richness typically demonstrate greater resistance to environmental stress through niche differentiation and functional complementarity. In contrast, reduced floristic complexity often results in diminished soil stabilization capacity, altered hydrological regulation, and lower primary productivity. In foothill belts, where environmental gradients overlap with human activity, evaluating vegetation structure and species composition is essential for forecasting successional shifts and ecosystem transformation [6–8].Within this ecological framework, plant communities incorporating *Tanacetum vulgare* L. offer a valuable model for integrated geobotanical analysis. The species exhibits wide ecological amplitude and occurs across meadow, meadow-steppe, forest-steppe, and riparian habitats from lowland areas to middle mountain elevations. Its morphological and physiological adaptations—including a well-developed perennial root system, high regenerative ability, prolonged vegetative phase, and tolerance to moderate grazing and trampling—enable long-term persistence under semi-natural and moderately disturbed

conditions. Depending on habitat characteristics, *T. vulgare* may function as a constant community component or achieve subdominant status, influencing interspecific competition and vegetation structure [9].

Beyond its ecological adaptability, *T.vulgare* possesses considerable medicinal and biochemical significance. The aerial parts of the plant contain 0.1-0.3 % essential oil, rich in monoterpenes and oxygenated compounds. The principal constituents of the essential oil include β-thujone (up to 60–70 % of the oil fraction depending on population), camphor (10–20 %), borneol (5–10 %), and pinene derivatives [10, 11]. In addition to volatile compounds, the plant accumulates sesquiterpene lactones (including tanacetin), flavonoids such as luteolin and quercetin (total flavonoid content typically exceeding 2-2.5 % in dry matter), hydroxycinnamic acids, alkaloids (~0.04 %), and tannins. These secondary metabolites are responsible for documented anti-inflammatory, antimicrobial, antiparasitic, choleretic, and antioxidant properties, which explain the long-standing application of the species in traditional medicine and its current use in phytopharmaceutical and cosmetic industries. Extracts of *T. vulgare* are also utilized in the production of botanical insecticides and repellents due to their bioactive terpene composition. However, the relatively high concentration of thujone-a neurotoxic monoterpene ketone—necessitates controlled dosage and scientifically grounded application standards [12].

Therefore, understanding the ecological distribution and population structure of this species is important not only for vegetation science but also for sustainable management of medicinal plant resources. At the same time, increased anthropogenic disturbance may alter community equilibrium by enhancing the competitive advantage of *T. vulgare*, potentially leading to reduced floristic evenness. Such structural shifts may influence overall ecosystem functioning, particularly in transitional foothill landscapes where species interactions are strongly modulated by environmental gradients [13, 14]. Despite its wide Eurasian distribution and recognized pharmacological relevance, the structural role and coenotic contribution of *T. vulgare* in the foothill ecosystems of Southeast Kazakhstan remain insufficiently characterized. The scarcity of comprehensive regional geobotanical assessments limits objective evaluation of vegetation dynamics, species interactions, and successional development under changing environmental conditions [15].

Accordingly, the present study aims to analyze the floristic diversity, spatial structure, and ecological significance of plant communities containing *T. vulgare* L. in the foothill zone of Southeast Kazakhstan, and to identify the environmental drivers that determine its distribution patterns and functional role within phytocenoses.

Experimental

Field investigations were carried out in the foothill ecosystems of the Kapchagay (Konayev) region, Southeast Kazakhstan, within the northern slope of the Ile Alatau mountain system. The study area is located within the geographic range of 43.70°–43.95° N and 76.90°–77.30° E (WGS84, EPSG:4326). Vegetation cover is represented by meadow, meadow-steppe, and typical foothill plant communities. The spatial distribution of the sampling sites is shown in Figure 1. The absolute elevation of the surveyed sites ranged from 600 to 1,200 m above sea level (a.s.l.), corresponding to the lower and middle foothill belt. Elevation values were recorded using a handheld GPS device and subsequently verified using the SRTM-based Digital Elevation Model (DEM) available in Google Earth Pro (Fig. 1).

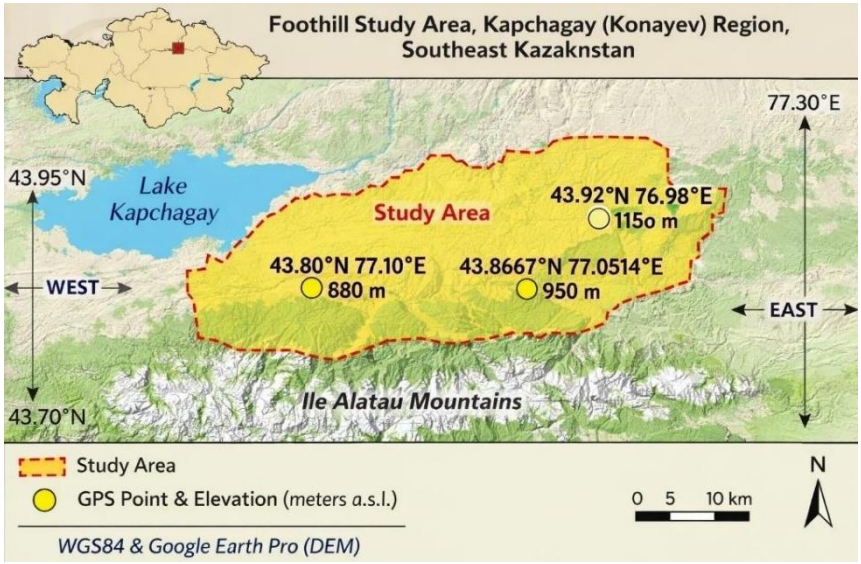

Figure 1. Geographic location and spatial arrangement of the studied cenopopulations of *Tanacetum vulgare* in the foothill coastal zone of South-East Kazakhstan (Kapchagay area)

The soil cover of the foothill coastal zone of the Kapchagay region is predominantly composed of chestnut-type gray-brown soils and soddy-meadow soils formed under a temperate continental climate with pronounced seasonal variability in precipitation and temperature. Gray-brown soils are mainly distributed on well-drained northern and northeastern slopes. They are characterized by light to medium loamy texture, moderate humus content in the upper horizons, carbonate accumulation in subsurface layers, and a neutral to slightly alkaline soil reaction (pH 7.0-8.2). Their relatively low water-holding capacity is typical of semi-arid steppe environments and supports meadow-steppe phytocenoses domiwenated by xeromesophytic species [16].

Soddy-meadow soils occur within the coastal belt of the Kapchagay Reservoir and in moisture-accumulating depressions. These soils exhibit higher organic matter content in surface horizons, improved structural aggregation, and increased moisture availability, creating favorable edaphic conditions for mesophytic perennial grasses. The soil moisture regime varies along the topographic gradient, remaining moderate on elevated slopes and increasing in areas adjacent to the reservoir due to capillary water rise and local microclimatic effects. Anthropogenic pressure is assessed as low to moderate and is associated with seasonal recreational use, localized livestock grazing, and partial agricultural transformation. These factors contribute to localized soil compaction and enhanced spatial heterogeneity of vegetation cover [16]. The existing soil conditions represent a transitional edaphic environment between meadow and meadow-steppe ecosystems, providing favorable ecological conditions for the stable persistence of *T. vulgare* populations. Climatically, the region belongs to a temperate continental semi-arid zone, characterized by warm summers and relatively mild winters.

Fieldwork was conducted during the active growing season, specifically in May and June 2025, corresponding to the flowering and seed formation stages of most plant species. This period ensured accurate taxonomic identification based on morphological characteristics. The research program included route surveys, establishment of transects and sampling plots, and detailed geobotanical descriptions of plant communities. Route surveys were conducted to identify vegetation diversity, locate areas where *T. vulgare* occurs, and preliminarily assess its growth conditions in different ecotypes [17].

The study focused on one population of *T.vulgare*, within which three cenopopulations were distinguished according to habitat conditions. Within each cenopopulation, three transects were established. Each transect corresponded to a permanent 10 × 10 m (100 m²) sampling plot. The total number of transects was nine (3 cenopopulations × 3 transects). Transects were located within three vegetation types: meadow communities, meadow-steppe communities, and typical foothill communities [18]. Sampling plots were selected within homogeneous vegetation patches to minimize edge effects. In the geobotanical and floristic survey, a complete inventory of higher vascular plants was conducted within each 100 m² plot [19]. For each species, the following parameters were recorded: presence, abundance, projective cover (%), and spatial distribution pattern within the community. Species identification was performed during flowering and fruiting stages

based on morphological characteristics of vegetative and generative organs using regional floras and identification manuals [20]. Plant specimens collected in the study area were identified using Flora of Kazakhstan (Volumes I–IX) and the Illustrated Guide to Plants of Kazakhstan [20, 21]. Species abundance was assessed using the Braun–Blanquet cover-abundance scale and the Hult–Drude scale, allowing comparability with classical geobotanical studies. Projective cover (%) was visually estimated within each 100 m² plot. Spatial distribution patterns were classified as uniform, grouped (clustered), or patchy [22]. The vertical and horizontal structure of phytocenoses was analyzed, including stratification, density of the herb layer, and the position of dominant and subdominant species.

For *T. vulgare* additional parameters were evaluated, including frequency of occurrence, cenotic position within the community (dominant, subdominant, or accompanying species), and its contribution to total projective cover. In biodiversity assessment and statistical analysis, species richness (S) was calculated as the total number of higher vascular plant species per 100 m² plot. Floristic diversity was evaluated using the Shannon–Weaver index (H′) [23] and Simpson index (D) [24].

Results and Discussion

During the study, the population of *T. vulgare* was investigated in the foothill zone of the Kapchagay (Konaev) region on the northern slope of the Ile Alatau mountain system, within the coordinate range of 43.70°–43.95° N and 76.90°–77.30° E (WGS84, EPSG:4326). Phytocoenotic Structure and Ecological Characteristics of Cenopopulation I (430-500 m above sea level, near the reservoir belt). Cenopopulation I, examined within the foothill ecosystems of Southeastern Kazakhstan, occupies humid meadow-forest sites situated at elevations of 430–500 m above sea level in close proximity to the reservoir. Due to the specific features of microrelief, this territory is relatively well moistened; its soils belong to the soddy-meadow type and it is characterized by favorable light conditions associated with open habitats. Such environmental conditions allow the formation of a plant community distinguished by high density and stable structural organization. The floristic composition of the community developed in a mesophytic direction. Perennial grasses occupy a leading position in the species structure. The principal dominants and subdominants include *Poa pratensis*, *Festuca pratensis*, *Dactylis glomerata*, and *Phleum pratense*. These species are characterized by high frequency values and considerable projective cover. Their well-developed root systems stabilize soil structure and contribute to moisture retention.

Among Fabaceae, *Trifolium pratense*, *Medicago falcata*, and *Melilotus officinalis* are widely distributed. Through nitrogen fixation processes, they enhance soil fertility and participate in maintaining the trophic balance of the community. Among Asteraceae, *Achillea millefolium*, *Taraxacum officinale*, and *T.vulgare* perform an important phytocoenotic role. In Cenopopulation I, *T/ vulgare* was recorded at the subdominant level. Its projective cover averaged 8–12 %, reaching up to 15 % in certain microsites. The sufficient number of generative shoots indicates a stable population state. Within the community, *Tanacetum vulgare* is relatively evenly distributed and, together with the dominant grasses, contributes to maintaining the structural integrity of the phytocoenosis. The overall vegetation cover density reached 95–100 %. Such a high projective cover confirms the high productivity of the phytocoenosis and sufficient moisture availability. The soil surface is almost entirely covered by herbaceous vegetation, and bare patches are practically absent. The community is characterized by a distinct four-layered structure.

The uppermost layer (1.5-3.0 m) consists of sparsely distributed woody and shrub species, including *Salix alba*, *Salix triandra*, *Rosa iliensis*, and *Elaeagnus oxycarpa*. This layer regulates the light regime, reduces wind speed, and creates specific microclimatic conditions. The second layer (60–110 cm) is composed of tall perennial herbaceous species. In this layer, *D. glomerata*, *T. vulgare*, and *A. millefolium* predominate. This layer forms the main vertical profile of the phytocoenosis.

Cenopopulation I, studied within the foothill ecosystems of Southeastern Kazakhstan, occupies humid meadow-forest sites situated at elevations between 430 and 500 m above sea level in close proximity to the reservoir. Owing to specific microrelief features, this area is relatively well moistened; its soils belong to the soddy-meadow type and are characterized by favorable light conditions associated with open habitats. Such environmental settings enable the formation of a plant community distinguished by high density and stable structural organization. The floristic composition of the community has developed predominantly in a mesophytic direction. Perennial grasses occupy a leading position in the species structure. The principal dominants and subdominants include *P. pratensis*, *F. pratensis*, *D. glomerata*, and *P. pratense*. These species are characterized by high frequency values and considerable projective cover. Their well-developed root systems stabilize soil structure and contribute to moisture retention.

Among the Fabaceae, *T. pratense*, *M. falcata*, and *M. officinalis* are widely distributed. Through nitrogen fixation processes, they enhance soil fertility and participate in maintaining the trophic balance of the community. Among the Asteraceae, *A. millefolium*, *T.officinale*, and *Tanacetum vulgare* perform an important phytocoenotic role.

Tanacetum vulgare in Cenopopulation I was recorded at the subdominant level. Its projective cover averaged 8–12 %, reaching up to 15 % in certain microsites. The sufficient number of generative shoots indicates a stable population condition. Within the community, *T. vulgare* is distributed relatively evenly and, together with the dominant grasses, contributes to maintaining the structural integrity of the phytocoenosis.

The overall vegetation cover density reached 95–100 %. Such a high projective cover confirms the high productivity of the phytocoenosis and sufficient moisture availability. The soil surface is almost entirely covered with herbaceous vegetation, and bare patches are practically absent. The community is characterized by a distinct four-layered structure. The uppermost layer (1.5-3.0 m) consists of sparsely distributed woody and shrub species, including *Salix alba*, *Salix triandra*, *Rosa iliensis*, and *Elaeagnus oxycarpa*. This layer regulates the light regime, reduces wind speed, and creates specific microclimatic conditions. The second layer (60–110 cm) is composed of tall perennial herbaceous species. In this layer, *D. glomerata*, *T. vulgare*, and *A. millefolium* predominate. This layer forms the main vertical profile of the phytocoenosis.

The third layer (30–60 cm) was composed of dominant grasses and formed the main bulk of community biomass. Within this layer, *P. pratensis*, *F. pratensis*, *D. glomerata*, and in some sites *Bromus inermis* predominated. These species were distinguished by high projective cover and well-developed vegetative reproduction capacity. Their dense turf-forming root systems stabilize soil structure and contribute to maintaining its aggregate composition. This particular layer ensures the overall density of vegetation cover, shades the soil surface, and reduces the intensity of moisture evaporation. In addition, it moderates seasonal temperature fluctuations and creates favorable microclimatic conditions for plants of the lower layers. The stable development of the third layer serves as a key indicator of phytocoenosis productivity and ecological stability.

The fourth layer (5–30 cm) consisted of low-growing mesophytic and eurytopic species. This layer included *Plantago major*, *V. chamaedrys*, *Potentilla anserina*, *T. officinale*, and other low herbaceous plants. These species form a dense ground cover that prevents erosion processes. The lower-layer plants participate in the accumulation of organic residues and humus formation, thereby playing an important role in increasing soil fertility. Furthermore, this layer facilitates regeneration processes and ensures rapid recovery of vacant microsites. The ecological plasticity of species within the lower layer enhances the adaptive capacity of the community to changing environmental conditions.

Thus, the third and fourth layers maintain the structural integrity of the phytocoenosis and ensure its functional stability. While the third layer forms the primary biomass component, the fourth layer performs soil-protective and regenerative functions. The interaction between these layers allows the community to maintain ecological balance.

Structurally, Cenopopulation I represents a stable, uniform, and ecologically balanced system. According to both Hult–Drude and Braun–Blanquet scales, the high proportion of dominant categories indicates strong biomass concentration and dense vegetation cover. The relatively low proportion of rare species reflects a high level of structural stability.

From an ecological perspective, this cenopopulation develops in a hydromesophytic direction and is dependent on the moisture regime. The combination of elevation and microclimatic conditions supports high phytocoenosis productivity and stable vertical organization. Under these conditions, *T. vulgare* maintains a stable subdominant position and functions as an integral structural component of the community. Cenopopulation I belongs to the humid meadow-forest type and represents a structurally well-developed and ecologically stable phytocoenosis. Its high vegetation cover density, clearly expressed stratification, and predominance of mesophytic species indicate that this system is developing under relatively favorable ecological conditions.

As a result of the study, 50 species of higher vascular plants were recorded within the territory of Cenopopulation I. Due to its proximity to the reservoir, the community was characterized as hydromesophytic. According to the Frequency (%) structure, species were grouped as follows: — High frequency (≥60 %) — 8 species (16 %) *(P. pratensis*, *F. pratensis*, *D. glomerata*, *Artemisia vulgaris*, etc.); Medium frequency (30–59 %) — 22 species (44 %);– Low frequency (<30 %) — 20 species (40 %).

According to the Hult–Drude cover-abundance scale, the distribution of species within Cenopopulation I was as follows: Cop3-Cop2 (dominants and subdominants) — 14 species (28 %); Cop1 (moderate abundance) — 18 species (36 %); Sp (rare) — 12 species (24 %); Sol (solitary individuals) — 6 species (12 %). The proportion of 14 species belonging to the Cop2 — Cop3 categories indicates the for-

mation of an ecologically significant structural core within the community. This group primarily includes perennial grasses and stable mesophytic elements that determine the vertical structure of the phytocoenosis, vegetation density, and the main portion of biomass accumulation. The relatively high proportion of the Cop1 category (36 %) enhances the structural diversity of the community and provides additional ecological stability to the dominant core. Species within this group form secondary structural components of the phytocoenosis and contribute to spatial mosaicity. The combined proportion of Sp and Sol categories (36 %) demonstrates the considerable presence of species occurring as rare or solitary individuals. Such species are often adapted to specific ecological niches or may represent temporary succession elements. The relatively high share of Cop2–Cop3 categories (28 %), together with the predominance of Cop1 species, confirms that the phytocoenosis is dense, well-developed, and structurally stable. This pattern is directly associated with the hydromesophytic character of Cenopopulation I and the favorable moisture regime. Overall, the data obtained according to the Hult–Drude scale indicate that Cenopopulation I represents an ecologically balanced meadow community with a clearly expressed dominant structure and relative resistance to anthropogenic impact.

To assess species abundance and vegetation cover levels in Cenopopulation I, both the Hult–Drude and Braun–Blanquet scales were applied. The results of the two scales were mutually consistent and confirmed the structural stability of the community. According to the Hult–Drude scale: Cop3–Cop2(dominant/subdominant) — 28 % of species; Cop1 — 36 %; Sp + Sol — 36 %. These indicators demonstrate the presence of a clearly formed dominant core within the phytocoenosis, while secondary and rare elements ensure structural diversity.

According to the Braun–Blanquet scale: Classes III-IV (moderate to high cover) — 36 %; Class II — 40 %; Class I + — 24 %.Thus, the predominance of classes III-II confirms the high overall vegetation density (80–90 %). Cop2-Cop3 categories largely correspond to Braun–Blanquet classes III-IV, indicating that dominant and subdominant species are widely distributed and possess high projective cover. Cop1 species mainly correspond to Braun–Blanquet class II, meaning these species are stable structural components but not absolutely dominant. Sp and Sol categories correspond to Braun–Blanquet classes I and +, reflecting species that occur rarely or at the periphery of the community. In the ecological interpretation of the community structure, dominant species were mainly represented by perennial grasses. Subdominants consisted of mesophytic and mesoxerophytic perennials, whereas rare species were primarily ruderal or successional elements. Such a structural organization ensures high biomass production, well-developed stratification, stable microclimate formation, and relative resilience to anthropogenic disturbance (Tab. 1).

Table 1

Floristic diversity and ecological structure of Cenopopulation I (430–500 m a.s.l.) of *Tanacetum vulgare* in the Kapchagay foothills (South-East Kazakhstan)

No	Species	Frequency, %	Hult–Drude	Braun–Blanquet	Ecological group
1	*Equisetum arvense*	25	2	II	Mesophyte
2	*Phragmites australis*	30	3	III	Hygrophyte
3	*Typha angustifolia*	15	2	II	Hygrophyte
4	*Poa pratensis*	40	3	III	Mesophyte
5	*Festuca pratensis*	35	3	III	Mesophyte
6	*Dactylis glomerata*	45	3	III	Mesophyte
7	*Bromopsis inermis*	45	3	III	Xeromesophyte
8	*Agrostis stolonifera*	30	3	III	Hygromesophyte
9	*Phleum pratense*	30	3	III	Mesophyte
10	*Stipa capillata*	40	3	III	Xerophyte
11	*Allium decipiens*	15	2	II	Xerophyte
12	*Carex colchica*	25	2	II	Hygromesophyte
13	*Juncus compressus*	20	2	II	Hygrophyte
14	*Trifolium pratense*	35	3	III	Mesophyte
15	*Trifolium repens*	30	3	III	Mesophyte
16	*Medicago falcata*	40	3	III	Mesophyte
17	*Melilotus officinalis*	30	3	III	Xeromesophyte
18	*Vicia cracca*	25	2	II	Mesophyte
19	*Achillea millefolium*	45	3	III	Mesophyte

Continuation of Table 1

No	Species	Frequency, %	Hult–Drude	Braun–Blanquet	Ecological group
20	*Taraxacum officinale*	30	3	III	Mesophyte
21	*Tanacetum vulgare*	25	2	II	Xeromesophyte
22	*Artemisia austriaca*	20	2	II	Xerophyte
23	*Artemisia vulgaris*	50	4	IV	Xeromesophyte
24	*Xanthium spinosum*	20	2	II	Mesophyte
25	*Onopordon acanthium*	15	2	II	Xerophyte
26	*Conyza canadensis*	20	2	II	Mesophyte
27	*Dodartia orientalis*	20	2	II	Xerophyte
28	*Verbascum songoricum*	15	2	II	Xeromesophyte
29	*Galium verum*	25	2	II	Xeromesophyte
30	*Plantago major*	25	2	II	Mesophyte
31	*Plantago lanceolata*	30	3	III	Xeromesophyte
32	*Convolvulus arvensis*	20	2	II	Mesophyte
33	*Thlaspi arvense*	20	2	II	Mesophyte
34	*Descurainia sophia*	20	2	II	Mesophyte
35	*Berteroa incana*	15	2	II	Xeromesophyte
36	*Rosa iliensis*	10	1	I	Xeromesophyte
37	*Polygonum aviculare*	30	3	III	Mesophyte
38	*Salix alba*	20	2	II	Hygromesophyte
39	*Salvia stepposa*	35	3	III	Xeromesophyte
40	*Papaver rhoeas*	40	3	III	Xeromesophyte
41	*Urtica dioica*	20	2	II	Hygrophyte
42	*Euphorbia palustris*	35	3	III	Hygrophyte
43	*Elymus repens*	40	3	III	Mesophyte
44	*Capsella bursa-pastoris*	20	2	II	Mesophyte
45	*Rumex acetosa*	25	2	II	Mesophyte
46	*Rumex crispus*	20	2	II	Mesophyte
47	*Chenopodium album*	15	2	II	Xeromesophyte
48	*Atriplex patula*	15	2	II	Xeromesophyte
49	*Thymus marschallianus*	20	2	II	Xerophyte
50	*Campanula patula*	15	2	II	Mesophyte
51	*Stellaria graminea*	20	2	II	Mesophyte

Cenopopulation II (500–570 m above sea level). Cenopopulation II is located in the upper part of the altitudinal gradient and represents a transitional meadow-steppe type. As a result of the study, 45 species of higher vascular plants were identified within this cenopopulation. The taxonomic structure was classified into two divisions, three classes, and 17 families. The majority of the flora is represented by angiosperms (Magnoliophyta), whereas the division Equisetophyta is represented by only a single species. Among the classes, dicotyledons (Magnoliopsida) occupy the leading position, indicating an increasing contribution of steppe elements within the community. At the same time, the monocotyledonous class (Liliopsida) also plays a significant role in the taxonomic structure of the community. A total of 14 species belonging to the class Liliopsida were identified, the majority of which are representatives of the family Poaceae. Grasses form the dominant and subdominant structure of the community and constitute the main component of phytocoenotic biomass. Species such as *P. pratensis*, *F. pratensis*, *Stipa capillata*, *Aegilops cylindrica*, and *Bromopsis inermis* were distinguished by high frequency and cover values. These species form the principal part of the second vertical layer (II layer) within the phytocoenosis and ensure the overall density of vegetation cover.

The predominance of Poaceae reflects the ecological specificity of this transitional ecosystem. With increasing elevation and a relatively reduced moisture regime, the proportion of xerophytic and xeromesophytic grasses increases. According to literature data, these species are characterized by drought tolerance and well-developed root systems, contributing to soil stabilization and the reduction of erosion processes. In addition, monocotyledonous species contribute to maintaining the microclimatic stability of the community. Dense grass cover shades the soil surface, reduces moisture evaporation, and moderates seasonal temperature fluctuations. Such conditions create favorable circumstances for the stable persistence of other mesophytic and xeromesophytic species.

Within the family structure, Poaceae and Asteraceae occupy leading positions, which is characteristic of meadow-steppe phytocenoses. Families such as Fabaceae, Brassicaceae, and Lamiaceae also contribute significantly to the overall floristic composition. Hygrophytic elements decrease in abundance, while the proportion of xerophytic and xeromesophytic species increases.

From an ecological perspective, Cenopopulation II is characterized by the predominance of xeromesophytic and xerophytic species alongside mesophytes. This pattern is directly associated with changes in altitude and the moisture regime. As the distance from the reservoir increases, the direct influence of surface and capillary moisture decreases, leading to a higher proportion of drought-tolerant species. In terms of floristic composition and taxonomic structure, Cenopopulation II corresponds to a transitional meadow-steppe type. Compared to Cenopopulation I, its structure displays a more pronounced xeromesophytic character and a spatially mosaic organization. These features indicate the ecological flexibility of *Tanacetum vulgare* and its capacity to tolerate varying moisture conditions.

Analysis of frequency values among the 45 recorded species revealed three principal groups. Species with high frequency (≥60 %) comprised 9 taxa (20 %), including P. pratensis, F. pratensis, A. vulgaris, Stipa capillata, and Aegilops cylindrica. Species with moderate frequency (40–59 %) accounted for 18 taxa (40 %), while low-frequency species (<40 %) also represented 18 taxa (40 %).

Most of the high-frequency species belong to xerophytic and xeromesophytic ecological groups. Grasses and wormwood species within this category form the dominant structural framework of the community. Their elevated frequency reflects drought tolerance, well-developed root systems, and effective vegetative reproduction. These adaptive traits confirm that Cenopopulation II has developed under relatively drier environmental conditions associated with increasing elevation.

The group of moderately frequent species (40 %) contributes substantially to the ecological diversity of the phytocenosis. This group is largely composed of mesophytic and mesoxerophytic taxa that, together with the dominants, maintain structural integrity and prevent complete xerophytization of the community. Such a configuration is typical of transitional ecosystems, where both meadow and steppe elements coexist.

Low-frequency species (40 %) occur sporadically or are confined to localized microhabitats. A considerable portion of these taxa are ruderal or occupy peripheral ecological niches. Their relatively high proportion reflects the mosaic spatial organization and ecological heterogeneity of Cenopopulation II. Structural analysis of frequency data demonstrates a clear predominance of xerophytic and xeromesophytic steppe elements. The dominance of steppe grasses and *A.* species among high-frequency taxa indicates a directional ecological shift toward drier environmental conditions. Simultaneously, the increased share of moderate- and low-frequency species suggests enhanced spatial heterogeneity and structural complexity of the phytocenosis. These transformations are associated with altitudinal gradients and moisture variability, reflecting ecological reorganization of the community. The obtained data further emphasize the high ecological plasticity of *Tanacetum vulgare* and its ability to adapt to diverse moisture and edaphic conditions.

According to the Hult–Drude cover–abundance scale, species distribution within Cenopopulation II was structured as follows: Cop2 (dominants) — 8 species (18 %), Cop1 (subdominants) — 17 species (38 %), Sp (sparse) — 14 species (31 %), and Sol (solitary individuals) — 6 species (13 %). These proportions indicate a relatively weaker dominant core and a more spatially heterogeneous organization of the community. The reduced proportion of Cop2 species suggests uneven biomass concentration, while the elevated representation of the Sp category reflects increased ecological niche differentiation and community heterogeneity.

In comparison with Cenopopulation I, the number of dominant species decreased, whereas the proportion of rare taxa increased. This shift confirms structural transformation associated with changes in altitude and moisture availability. Although the dominant layer remains present in Cenopopulation II, it exhibits a distinctly mosaic distribution pattern rather than forming a uniform phytocoenotic core.

According to the Braun–Blanquet cover-abundance assessment, species were distributed as follows: IV class — 5 species, III class — 15 species, II class — 17 species, and I plus (+) — 8 species. The predominance of III–II categories indicates that the phytocenosis has not undergone structural degradation and retains overall stability. However, the reduced number of species in the IV category demonstrates a decline in vegetation density compared to Cenopopulation I, with total projective cover estimated at approximately 75–85 %.

The obtained results for Cenopopulation II reflect a noticeable reorganization of community structure. A decrease in cover uniformity suggests that vegetation is no longer spatially continuous but instead exhibits a mosaic pattern. The relative weakening of the dominant layer also affects the vertical organization of the phytocenosis. In contrast to Cenopopulation I, biomass in this case is not evenly concentrated but distributed

heterogeneously across different microsites. This pattern is associated with a reduced proportional cover of dominant species and a simultaneous increase in the spatial contribution of subdominant and sparse taxa. As a result, the structural framework of the community becomes less compact, and the phytocenosis acquires a more dynamic character.

The relative thinning of the lower layer is likewise linked to changes in environmental conditions. With increasing elevation and a less stable moisture regime, the proportion of mesophytic and hygrophytic elements declines. This shift affects both the density and species richness of the lower stratum and may potentially slow regeneration processes. In addition, uneven distribution of light and soil moisture restricts the full development of the ground layer. The observed reduction in cover density and the attenuation of the dominant structure in Cenopopulation II indicate that the community is undergoing ecological adjustment. The phytocenosis appears to be transitioning gradually from a meadow type toward a steppe type. Such structural transformation confirms the ability of *Tanacetum vulgare* populations to persist under varying altitudinal and moisture conditions, demonstrating a high degree of ecological plasticity (Tab. 2).

Table 2

Floristic diversity and ecological structure of Cenopopulation II (500–570 m a.s.l.) of *Tanacetum vulgare* in the Kapchagay foothills (South-East Kazakhstan)

No	Species	Frequency, %	Hult–Drude	Braun–Blanquet	Ecological group
1	*Poa pratensis*	75	Cop2	III	Mesophyte
2	*Festuca pratensis*	70	Cop2	III	Mesophyte
3	*Dactylis glomerata*	65	Cop2	III	Mesophyte
4	*Stipa capillata*	60	Cop2	IV	Xerophyte
5	*Bromopsis inermis*	55	Cop1	III	Xeromesophyte
6	*Elymus repens*	50	Cop1	II–III	Mesophyte
7	*Anisantha tectorum*	50	Cop1	III	Xerophyte
8	*Aegilops cylindrica*	65	Cop2	IV	Xerophyte
9	*Eremopyrum orientale*	30	Cop1	II	Xerophyte
10	*Taeniatherum crinitum*	25	Cop1	II	Xerophyte
11	*Artemisia austriaca*	60	Cop2	IV	Xerophyte
12	*Artemisia frigida*	55	Cop1	III	Xerophyte
13	*Artemisia vulgaris*	70	Cop2	IV	Xeromesophyte
14	*Tanacetum vulgare*	55	Cop1	II–III	Xeromesophyte
15	*Achillea millefolium*	60	Cop2	III	Mesophyte
16	*Taraxacum officinale*	40	Cop1	II	Mesophyte
17	*Salvia stepposa*	50	Cop1	III	Xeromesophyte
18	*Thymus marschallianus*	45	Cop1	II	Xerophyte
19	*Convolvulus arvensis*	40	Cop1	II	Mesoxerophyte
20	*Plantago lanceolata*	45	Cop1	II	Mesoxerophyte
21	*Plantago major*	30	Sp	I	Mesophyte
22	*Galium verum*	50	Cop1	III	Xeromesophyte
23	*Medicago falcata*	55	Cop1	III	Mesoxerophyte
24	*Melilotus officinalis*	45	Cop1	II	Xeromesophyte
25	*Trifolium pratense*	50	Cop1	III	Mesophyte
26	*Trifolium repens*	35	Sp	II	Mesophyte
27	*Vicia cracca*	30	Sp	II	Mesophyte
28	*Thlaspi arvense*	25	Sp	II	Mesophyte
29	*Descurainia sophia*	25	Sp	II	Mesophyte
30	*Berteroa incana*	30	Sp	II	Xeromesophyte
31	*Polygonum aviculare*	35	Sp	II	Mesophyte
32	*Papaver rhoeas*	45	Cop1	III	Xeromesophyte
33	*Rosa iliensis*	20	Sol	I	Xeromesophyte
34	*Elaeagnus oxycarpa*	15	Sol	I	Xeromesophyte
35	*Salix alba*	15	Sol	I	Hygromesophyte
36	*Tamarix ramosissima*	20	Sol	I	Haloxerophyte
37	*Dodartia orientalis*	30	Sp	II	Xerophyte
38	*Verbascum songoricum*	25	Sp	II	Xeromesophyte

Continuation of Table 2

No	Species	Frequency, %	Hult–Drude	Braun–Blanquet	Ecological group
39	*Onopordon acanthium*	20	Sol	I	Xerophyte
40	*Xanthium spinosum*	30	Sp	II	Mesophyte
41	*Chenopodium album*	25	Sp	II	Xeromesophyte
42	*Atriplex patula*	25	Sp	II	Xeromesophyte
43	*Rumex acetosa*	30	Sp	II	Mesophyte
44	*Rumex crispus*	25	Sp	II	Mesophyte
45	*Urtica dioica*	20	Sol	I	Hygrophyte

The conducted research demonstrated that plant communities involving *T. vulgare*, although belonging to a single population, exhibit clear structural and ecological differentiation along the altitudinal gradient. Within the elevation range of 430–570 m above sea level, the two cenopopulations differ significantly in floristic composition, dominant structure, vegetation density, and ecological orientation.

Cenopopulation I (430–500 m) is located closer to the reservoir in a relatively well-moistened zone. A total of 50 species of higher vascular plants were recorded here, and the community developed under hydromesophytic conditions. Vegetation cover is dense (80–90 %, reaching up to 95 % in some sites), and the dominant layer is well expressed. According to the Hult–Drude scale, the proportion of Cop2–Cop3 categories reached 28 %, indicating the presence of a stable dominant core within the phytocenosis. The Braun–Blanquet assessment confirmed this pattern: the predominance of species belonging to cover classes III–IV reflects sufficient biomass concentration and uniform vegetation cover. In this community, mesophytic grasses form the structural framework, while *T. vulgare* acts as a stable subdominant species with a relatively even spatial distribution.

Cenopopulation II (500–570 m) is situated at a higher altitudinal level and is characterized by relatively drier ecological conditions. A total of 45 species were identified, indicating a slight decrease in species richness. The floristic composition shows an increased proportion of xeromesophytic and xerophytic elements, corresponding to a transitional meadow-steppe type. According to the Hult–Drude scale, the proportion of Cop2 species decreased to 18 %, while the share of sparse (Sp) species increased to 31 %. This pattern indicates a weakening of the dominant structure and the development of a more mosaic spatial organization. Within the Braun–Blanquet system, the number of species assigned to class IV decreased, whereas classes II–I increased in proportion. Total vegetation cover declined to 75–85 %. These changes suggest reduced uniformity of biomass distribution and a relative weakening of the dominant layer.

The results obtained from both scales are consistent: the reduction of Cop2 species corresponds to a decrease in the number of class IV species. This confirms structural reorganization of the community and reflects its transition to a more dynamic ecological state. While Cenopopulation I possesses a clearly expressed and stable dominant core, Cenopopulation II demonstrates an increased proportion of subdominant and sparse species, resulting in a comparatively loosened structural configuration.

Altitude and moisture regime exert a direct influence on phytocenotic organization. In the lower belt near the reservoir, mesophytic elements predominate and vegetation cover remains dense and uniform. In contrast, in the higher belt, drought-tolerant species increase in abundance, and the ecological orientation shifts toward steppe conditions. However, this change represents a transitional stage rather than complete transformation.

T. vulgare remains present under both ecological conditions, demonstrating high ecological plasticity. In Cenopopulation I, it occurs as a stable subdominant with relatively even distribution, whereas in Cenopopulation II its cover slightly decreases and distribution becomes less uniform. Nevertheless, the species maintains viability across different moisture and altitudinal regimes. Thus, comparative analysis shows that although both cenopopulations belong to a single population, the altitudinal gradient significantly influences their structural organization, floristic composition, and dominant patterns. Cenopopulation I corresponds to a stable meadow-type community, whereas Cenopopulation II exhibits features of a transitional meadow-steppe system. These findings scientifically substantiate the altitude-dependent structural differentiation of plant communities involving *T. vulgare*.

The high uniformity is primarily due to the developed three-tiered structure of the phytocenoses and the significant proportion of mesophytic rhizomatous grasses (*Poa pratensis, F. pratensis, D. glomerata*), which form a stable background for the grass stand and prevent the monopolization of space by individual species. Despite the persistent presence of *T.vulgare* as a subdominant, this species does not disrupt the uniform dis-

tribution of floristic elements or suppress associated mesophytic species. The uniform distribution of species within the population contributes to the maintenance of high functional stability of the phytocenoses, including effective microclimate regulation, soil stabilization, and the preservation of an optimal water regime. Thus, the population can be considered a standard (reference) meadow community of the foothill ecosystems of southeastern Kazakhstan, characterized by a highly uniform species distribution, sustainability, and ecological stability.

Application of the Braun-Blanquet scale allowed us to identify a pronounced hierarchical structure of the phytocenoses of population 1 and quantitatively characterize the contribution of individual species to the formation of the herbaceous layer. Category 3 (26–50 %) included the dominant grass species *P. pratensis* L. and *F. pratensis* Huds, which form the main background of the herbage and ensure high community density. Category 2 (6–25 %) included subdominant species: *T. vulgare* L., *D. glomerata* L., *T. pratense* L., *M. falcata* L., *Galium verum* L., and *A. millefolium*L. It was in this group that *T.vulgare* exhibited the greatest cenotic stability. Category 1 (1–5 %) was represented by assectator species: *P. major* L., *V.chamaedrys* L., *Potentilla anserina* L., *T. officinale* F.H. Wigg., *Ranunculus acris* L., *Rumex acetosa* L., which form the regenerative and stabilizing ground layer. Categories r and + (<1 %) included single and rare species*: Capsellabursa-pastoris* L., *Stellaria media* L., *Chenopodiumalbum* L., indicating local anthropogenic influence and micromosaic nature of phytocenoses. The altitudinal gradient in the study area revealed a distinct differentiation in the floristic composition and geobotanical structure of plant communities, accompanied by a consistent change in species frequency. Vertical zonation is due to the complex influence of climatic, edaphic, and orographic factors, primarily changes in air temperature, moisture regime, and slope exposure. The lower part of the altitudinal belt (430–500 m a.s.l.) is characterized by the development of xerophytic-xeromesophytic wormwood-grass communities with the participation of ruderal and halophytic elements. The greatest floristic diversity and maximum occurrence rates are noted here. The dominant species are *Aegilops cylindrica* (90 %, score V), *A. vulgaris (85 %,* scores IV–V), *Stipa capillata, Anisantha tectorum, Leymus angustus,* and *A. frigida*. These species form a dense turf cover and determine the overall physiognomic appearance of the phytocoenosis. The high frequency of ruderal species (*Polygonum aviculare, Tanacetum vulgare, Xanthium strumarium, Descurainia sophia)* indicates significant anthropogenic impact and soil compaction. In the mid-altitude zone, a gradual transition from xerophytic to xeromesophytic-mesophytic meadow-steppe communities is observed. The proportion of mesophytic grasses and legumes increases: *P. pratensis, F. pratensis, D. glomerata, T. pratense*, and *M. officinalis*, accompanied by an increase in the projective cover of the grass stand.

The frequency of xerophytes (*Artemisia frigida, Aegilops cylindrica*, and *Taeniatherum crinitum*) decreases slightly, while mesophytic species tend to increase in frequency, which is associated with a more favorable moisture regime and lower thermal stress. In the upper altitude zone, mesophytic meadow-forest communities with tree and shrub forms develop. The frequency of occurrence of mesophytic and hygromesophytic species increases: *Picea schrenkiana, Pinus sylvestris, Carex colchica, Rosa iliensis, Schoenoplectus lacustris*. The proportion of ruderal and xerophytic elements significantly decreases, reflecting reduced anthropogenic load and a more stable hydrothermal regime. Thus, a clear zonal change in phytocenoses is observed along the altitudinal gradient: from xerophytic-wormwood-grass communities of the lower belt through xeromesophytic-meadow-steppe communities of the middle belt to mesophytic meadow-forest communities of the upper belt. Changes in species frequency along the altitudinal profile reflect the adaptation of the flora to changing conditions of moisture, temperature, and the degree of anthropogenic impact.

Conclusion

The comprehensive study conducted in the foothill ecosystems of Southeastern Kazakhstan revealed clear structural and floristic differentiation of plant communities involving *Tanacetum vulgare* L. along the altitudinal gradient within 430–570 m above sea level. The identified differences correspond to measurable changes in vegetation cover, dominance structure, and species composition.

Two phytocoenotic variants were distinguished within a single population of *Tanacetum vulgare* L. In the lower altitudinal belt (430–500 m a.s.l.), located closer to the reservoir, meadow-type communities were recorded. This cenopopulation included 50 vascular plant species and was characterized by high projective cover (95–100 %) and a well-developed dominant structure. According to the Hult–Drude scale, Cop2–Cop3 categories accounted for 28 %, Cop1 for 36 %, and Sp + Sol for 36 %. The Braun–Blanquet assessment indicated the predominance of classes III–IV, and total vegetation cover ranged between 80–90 %, reaching up

to 95 % in certain plots. These parameters reflect a relatively concentrated biomass distribution and a clearly expressed dominant core.

In contrast, in the upper altitudinal belt (500–570 m a.s.l.), the community exhibited features of a transitional meadow-steppe type. This cenopopulation contained 45 vascular plant species, and total vegetation cover decreased to 75–85 %. According to the Hult–Drude scale, the proportion of Cop2 species declined to 18 %, while sparse species (Sp) increased to 31 %. The Braun–Blanquet scale showed a reduction in class IV species to five, with classes II–III predominating. These changes indicate a decrease in dominance concentration and a more heterogeneous spatial distribution of vegetation.

Comparative analysis demonstrated that increasing elevation is associated with a reduction in total vegetation cover, a decline in dominance intensity, and an increased proportion of xerophytic and xeromesophytic elements. The concordance between the Hult–Drude and Braun–Blanquet assessments confirms that the decrease in Cop2 abundance corresponds to a reduction in high cover classes, providing consistent quantitative evidence of structural transformation along the altitudinal gradient.

Floristic analysis showed that Poaceae and Asteraceae were the leading families in both cenopopulations, which is typical for foothill meadow and transitional meadow-steppe phytocoenoses. Species richness remained relatively high (50 species in Cenopopulation I and 45 species in Cenopopulation II), reflecting the floristic variability of the study area.

T.vulgare maintained a subdominant position in both ecological conditions. In Cenopopulation I, its projective cover ranged between 8–12 % and its distribution was relatively uniform, whereas in Cenopopulation II, its cover decreased to 5–10 % and spatial distribution became less uniform. Despite these changes, the species remained a consistent structural component of both communities.

Overall, the study provides quantitative evidence of altitude-related structural differentiation of *T. vulgare* communities in the foothill ecosystems of Southeastern Kazakhstan. Cenopopulation I corresponds to a meadow-type phytocoenosis with higher vegetation density and more concentrated dominance, whereas Cenopopulation II represents a transitional meadow-steppe community characterized by reduced cover and increased representation of xeromesophytic species.

Conflict of Interest

The authors declare no conflict of interest.

Author contribution

The manuscript was written through contributions of all authors. All authors have given approval to the final version of the manuscript. CRediT: **Smayelova K.A**. — conceptualization, data curation, investigation, visualization, writing — original draft; **Abdukadirova Zh.A.** — project administration, resources, supervision; **Anarbekova G.D., Kozhamzharova A.S.** — writing — review & editing; **Izbastina K.S., Aitzhanova M.O.** — methodology, formal analysis.

References

1 Sene A.M. Perte et lutte pour la biodiversité: Perceptions et débats contradictoires / A.M. Sene // Vertigo — La Revue électronique en sciences de l'environnement. — 2010. — No. 10. — P. 1–9.

2 Mace G.M. Biodiversity and ecosystem services: A multilayered relationship / G.M. Mace, K. Norris, A.H. Fitter // Trends in Ecology & Evolution. — 2012. — Vol. 27. — P. 19–26.

3 Bureau D. Biodiversité en danger: Quelle réponse économique / D. Bureau, J.C. Bureau, K. Schubert // *Notes du* Conseil d'Analyse Économique. — 2024. — No. 59. — P. 1–12.

4 Menioui M. Biological diversity in Morocco / M. Menioui // Global Biodiversity. — Apple Academic Press, 2018. — P. 133–171.

5 Anisa Q. Phytosociological method for the evaluation of biodiversity and medicinal plants / Q. Anisa, P. Arsen // Albanian Journal of Agricultural Sciences. — 2018. — Vol. 17. — P. 45–55.

6 Magurran A.E. Biological Diversity: Frontiers in Measurement and Assessment / A.E. Magurran, B.J. McGill (Eds.). — Oxford: Oxford University Press, 2011. — 345 p.

7 Jost L. Entropy and diversity / L. Jost // Oikos. — 2010. — Vol. 113, No. 2. — P. 363–375.

8 Chao A. Unifying species diversity, phylogenetic diversity, functional diversity / A. Chao, C. -H. Chiu, L. Jost // Annual Review of Ecology, Evolution, and Systematics. — 2014. — Vol. 45. — P. 297–324.

9 Wolf V.C. Genetic and chemical variation of *Tanacetum vulgare* in plants of native and invasive origin / V.C. Wolf, A. Gassmann, B.M. Clasen, A.G. Smith, C. Müller // Biological Control. — 2012. — Vol. 61, No. 3. — P. 240–245.

10 Ojeda-Prieto L., et al. Intraspecific chemical variation of *Tanacetum vulgare* affects plant growth and reproductive traits in field plant communities / L. Ojeda-Prieto, et al. // Plant Biology. — 2025. — Vol. 27, No. 5. — P. 785–801.

11 Stutz S. *Tanacetum vulgare* L. (Asteraceae) / S. Stutz, A.S. McClay, R.A. De Clerck-Floate // Biological Control Programmes in Canada, 2013–2023 // CAB International. — 2024. — P. 569–574.

12 Koblanova S. Diversity of Birch and Alder Forests in the Kostanay Region of Kazakhstan / S. Koblanova, S. Mukhtubayeva, A. Kakimzhanova, A. Orazov, D. Dyussembekova, G. Abileva // Forests. — 2024. — Vol. 15, No. 10. — Article 1680.

13 Zeng G. The relationships between plant community stability and diversity across different grassland types and their association with environmental factors in the Habahe Forest Area, Xinjiang / G. Zeng, M. Ye, M. Li, W. Chen, Q. He, X. Pan, X. Zhang, J. Che, J. Qian, Y. Lv // Diversity. — 2024. — 16(8). — Article 499.

14 Sparrow B.D. A vegetation and soil survey method for ecosystem surveillance monitoring / B.D. Sparrow,W. Edwards, S.E.M. Munroe, et al. // Frontiers in Ecology and Evolution. — 2020. — Vol. 8. — Article 157.

15 Biurrun I. Vegetation classification and survey: Five years and looking ahead / I. Biurrun, J. Dengler, W. Willner // Vegetation Classification and Survey. — 2025. — Vol. 6. — P. 1–11.

16 Yapiyev V. Top soil physical and chemical properties in Kazakhstan across a north-south gradient / V. Yapiyev, C.P. Gilman, T. Kabdullayeva, A. Suleimenova, A. Shagadatova, A. Duisembay, S. Naizabekov, S. Mussurova, K. Sydykova, I. Raimkulov, L. Kabimoldayev, A. Abdrakhmanova, S. Omarkulova, D. Nurmukhambetov, A. Kudarova, D. Malgazhdar, C. Schönbach, V. Inglezakis V. // Scientific Data. — 2018. — Vol. 5. — Article 180242.

17 Moldakhanova N., et al. Analysis of changes in the ecological space of the Ili River after the construction of the Kapchagay Reservoir / N. Moldakhanova, et al. // Evergreen. — 2023. — P. 29–35.

18 Заугольнова Л.Б. Структура и динамика ценопопуляций растений / Л.Б. Заугольнова. — Москва: Наука, 1994. — 364 с.

19 Greig-Smith P. Quantitative Plant Ecology / P. Greig-Smith. — 2nded. — London: Butterworths, 1964. — 256 p.

20 Иллюстрированный определитель растений Казахстана [в 2-х т.] / сост. М.С. Байтенов, А.П. Гамаюнова и др. — Алма-Ата: Наука КазССР, 1972. — Т. 1. — 571 с.

21 Флора Казахстана. — Алма-Ата, 1965. — Т. 8: Паслёновые–Сложноцветные. — 447 с.

22 Braun-Blanquet J. *Plant Sociology:* The Study of Plant Communities / J. Braun-Blanquet. — Moscow: Mir Publishers, 1964. —439 p.

23 Shannon C.E. The Mathematical Theory of Communication / C.E. Shannon, W. Weaver // Urbana: University of Illinois Press, 1949. — 144 p.

24 Simpson E.H. Measurement of diversity / E.H. Simpson // Nature. — 1949. — Vol. 163. — P. 688.

Қ.А. Смаелова, Ж.А. Абдукадирова, Г.Д. Анарбекова, А.С. Қожамжарова,
К.С. Избастина, М.О. Айтжанова

Оңтүстік-Шығыс Қазақстанның тау етегіндегі экожүйелеріндегі *Tanacetum vulgare* L. өсімдіктер қауымдастығының флористикалық әртүрлілігі, геоботаникалық құрылымы және экологиялық маңызы

Мақалада Оңтүстік-Шығыс Қазақстанның тау бөктері экожүйелерінде өсетін *Tanacetum vulgare L.* өсімдіктер бірлестіктерінің флоралық әртүрлілігі, геоботаникалық құрылымы және экологиялық маңызына жүргізілген кешенді зерттеу нәтижелері ұсынылған. Зерттеудің өзектілігі кәдімгі пижманың көпфункционалды маңыздылығымен айқындалады, себебі ол адамзат тарапынан тағамдық, мал азықтық, техникалық және сәндік мақсаттарда, сондай-ақ халықтық және ғылыми медицинада кеңінен қолданылатын әмбебап өсімдік. Антропогендік жүктеменің күшеюі және табиғи экожүйелердің трансформациялануы жағдайында аталған түрдің экологиялық және ценотикалық рөлін зерттеу ерекше ғылыми әрі практикалық мәнге ие. Зерттеу нәтижесінде *Tanacetum vulgare L.* қатысатын өсімдік қауымдастықтары жоғары флоралық әртүрлілікпен және мезофитті әрі мезоксерофитті түрлердің басым болуымен сипатталатыны анықталды. Зерттелген түр шөптесін саты-сы тұрақты немесе субдоминант компоненті ретінде көрініс беріп, өзгермелі орта жағдайларына жоғары экологиялық икемділік пен төзімділік танытады. Алынған нәтижелер тау бөктері фитоценоздарының құрылымы мен қызмет ету ерекшеліктері туралы түсінікті кеңейтіп, биоалуантүрлілікті мониторингілеуде, экожүйелердің жай-күйін бағалауда және Оңтүстік-Шығыс Қазақстандағы өсімдік ресурстарын ұтымды пайдалануда қолданылуы мүмкін.

Кілт сөздер: Tanacetum vulgare L., флоралық әртүрлілік, геоботаникалық құрылым, фитоценоз, экологиялық маңызы, тау бөктері экожүйелері, фитопрепарат, Оңтүстік-Шығыс Қазақстан.

К.А. Смаелова, Ж.А. Абдукадирова, Г.Д. Анарбекова, А.С. Қожамжарова,
К.С. Избастина, М.О. Айтжанова

Флористическое разнообразие, геоботаническая структура и экологическое значение растительных сообществ *Tanacetum vulgare* L. в предгорных экосистемах Юго-Восточного Казахстана

В статье представлены результаты комплексного исследования флористического разнообразия, геоботанической структуры и экологической значимости растительных сообществ с участием *Tanacetum vulgare* L., произрастающих в предгорных экосистемах Юго-Восточного Казахстана. Актуальность исследования определяется многофункциональной значимостью пижмы обыкновенной, являющейся универсальным растением, используемым человеком в пищевых, кормовых, технических и декоративных целях, а также в народной и научной медицине. В условиях усиления антропогенной нагрузки и трансформации природных экосистем изучение экологической и ценотической роли данного вида приобретает особую научную и практическую значимость. Установлено, что растительные сообщества с участием *Tanacetum vulgare* L. характеризуются высоким флористическим разнообразием и преобладанием мезофитных и мезоксерофитных видов. Исследуемый вид выступает постоянным или субдоминантным компонентом травяного яруса, демонстрируя высокую экологическую пластичность и устойчивость к изменяющимся условиям среды. Полученные результаты расширяют представления о структуре и функционировании предгорных фитоценозов и могут быть использованы при мониторинге биоразнообразия, оценке состояния экосистем и рациональном использовании растительных ресурсов Юго-Восточного Казахстана.

Ключевые слова: Tanacetum vulgare L., флористическое разнообразие, геоботаническая структура, фитоценоз, экологическая значимость, предгорные экосистемы, фитопрепарат, Юго-Восточный Казахстан.

References

1 Sene, A.M. (2010). Perte et lutte pour la biodiversité: Perceptions et débats contradictoires. *VertigO — La revue électronique en sciences de l'environnement*, (10), 1–9.

2 Mace, G. M., Norris, K., & Fitter, A. H. (2012). Biodiversity and ecosystem services: A multilayered relationship. *Trends in Ecology & Evolution, 27*, 19–26. https://doi.org/10.1016/j.tree.2011.08.006.

3 Bureau, D., Bureau, J. C., & Schubert, K. (2024). Biodiversité en danger: Quelle réponse économique. *Notes du Conseil d'Analyse Économique*, (59), 1–12.

4 Menioui, M. (2018). Biological diversity in Morocco. *Global biodiversity* (pp. 133–171). Apple Academic Press.

5 Anisa, Q., & Arsen, P. (2018). Phytosociological method for the evaluation of biodiversity and medicinal plants. *Albanian Journal of Agricultural Sciences, 17*, 45–55.

6 Magurran, A. E., & McGill, B. J. (Eds.). (2011). *Biological diversity: Frontiers in measurement and assessment*. Oxford University Press.

7 Jost, L. (2010). Entropy and diversity. *Oikos, 113*(2), 363–375. https://doi.org/10.1111/j.1600-0706.2009.01847.x.

8 Chao, A., Chiu, C. -H., & Jost, L. (2014). Unifying species diversity, phylogenetic diversity, and functional diversity. *Annual Review of Ecology, Evolution, and Systematics, 45*, 297–324. https://doi.org/10.1146/annurev-ecolsys-120213-091540.

9 Wolf, V. C., Gassmann, A., Clasen, B. M., Smith, A. G., & Müller, C. (2012). Genetic and chemical variation of *Tanacetum vulgare* in plants of native and invasive origin. *Biological Control, 61*(3), 240–245. https://doi.org/10.1016/j.biocontrol.2012.03.010

10 Ojeda-Prieto, L., et al. (2025). Intraspecific chemical variation of *Tanacetum vulgare* affects plant growth and reproductive traits in field plant communities. *Plant Biology, 27*(5), 785–801.

11 Stutz, S., McClay, A. S., & De Clerck-Floate, R. A. (2024). *Tanacetum vulgare* L. (Asteraceae). *Biological Control Programmes in Canada,* 2013–2023 (pp. 569–574). CAB International.

12 Koblanova, S., Mukhtubayeva, S., Kakimzhanova, A., Orazov, A., Dyussembekova, D., & Abileva, G. (2024). Diversity of birch and alder forests in the Kostanay region of Kazakhstan. *Forests, 15*(10), Article 1680. https://doi.org/10.3390/f15101680.

13 Zeng, G., Ye, M., Li, M., Chen, W., He, Q., Pan, X., Zhang, X., Che, J., Qian, J., & Lv, Y. (2024). The relationships between plant community stability and diversity across different grassland types and their association with environmental factors in the Habahe Forest Area, Xinjiang. *Diversity, 16*(8), Article 499. https://doi.org/10.3390/d16080499.

14 Sparrow, B. D., Edwards, W., Munroe, S. E. M., et al. (2020). A vegetation and soil survey method for ecosystem surveillance monitoring. *Frontiers in Ecology and Evolution, 8,* Article 157. https://doi.org/10.3389/fevo.2020.00157.

15 Biurrun, I., Dengler, J., & Willner, W. (2025). Vegetation classification and survey: Five years and looking ahead. *Vegetation Classification and Survey, 6,* 1–11. https://doi.org/10.3897/VCS.148065.

16 Yapiyev, V., Gilman, C. P., Kabdullayeva, T., Suleimenova, A., Shagadatova, A., Duisembay, A., Naizabekov, S., Mussurova, S., Sydykova, K., Raimkulov, I., Kabimoldayev, I., Abdrakhmanova, A., Omarkulova, S., Nurmukhambetov, D., Kudarova, A., Malgazhdar, D., Schönbach, C., & Inglezakis, V. (2018). Top soil physical and chemical properties in Kazakhstan across a north–south gradient. *Scientific Data, 5,* Article 180242. https://doi.org/10.1038/sdata.2018.242.

17 Moldakhanova, N., et al. (2023). Analysis of changes in the ecological space of the Ili River after the construction of the Kapchagay Reservoir. *Evergreen,* 29–35.

18 Zaugolnova, L.B. (1994). *Struktura i dinamika tsenopopuliatsii rastenii* [Structure and dynamics of plant coenopopulations]. Moscow: Nauka [in Russian].

19 Greig-Smith, P. (1964). *Quantitative plant ecology* (2nd ed.). Butterworths. 256 p.

20 Baitenov, M.S., Gamaiunova, A.P., et al. (Comp.). (1972). *Illiustrirovannyi opredelitel rastenii Kazakhstana* [Illustrated guide to the plants of Kazakhstan]. (Vols. 1-2, Vol. 2). Alma-Ata: Nauka KazSSR [in Russian].

21 (1965). *Flora Kazakhstana* [Flora of Kazakhstan]. Vol. 8: Solanaceae–Asteraceae. Alma-Ata [in Russian].

22 Braun-Blanquet, J. (1964). *Plant sociology: The study of plant communities.* Moscow: Mir Publishers.

23 Shannon, C.E., & Weaver, W. (1949). The mathematical theory of communication. *Urbana, IL: University of Illinois Press,* 144.

24 Simpson, E.H. (1949). Measurement of diversity. *Nature, 163*, 688. https://doi.org/10.1038/163688a0.

Information about the authors

Smayelova Karlyga Azhikulovna — PhD, Al-Farabi Kazakh National University, Almaty, Kazakhstan; e-mail: karlyga505@gmail.com; ORCID: https://orcid.org/0009-0005-2099-3147

Abdukadirova Zhansaya Abdymuratovna — PhD, Al-Farabi Kazakh National University, Almaty, Kazakhstan; e-mail: zhansina88@mail.ru; ORCID: https://orcid.org/0000-0003-3905-7349

Anarbekova Gulshat Dzhumabaevna — Candidate of Biological Sciences, Associate Professor, Kazakh National Women's Teacher training University, Almaty, Kazakhstan; e-mail: g7348749@gmail.com; ORCID: https://orcid.org/0000-0001-9424-2913

Kozhamzharova Assel Seidakhmetkyzy — Candidate of Chemical Sciences, Associate Professor of the Department of Pharmaceutical and Toxicological Chemistry, Kazakh National Medical University named after S.D. Asfendiyarov, Almaty, Kazakhstan; e-mail: assel_kozhamzharova@mail.ru; ORCID: https://orcid.org/0000-0002-6688-6209

Izbastina Klara Serzhanovna — PhD, Associate Professor Astana Botanical Garden, Committee of Forestry and Animal World of the Ministry of Ecology and Nature Conservation, S. Seifullin Kazakh AgroTechnical Research University, Astana, Kazakhstan; e-mail: izbastina.k@gmail.com; ORCID: https://orcid.org/0000-0002-6418-1950

Aitzhanova Mira Onlanbekovna — Candidate of Biological Sciences (Senior Lecturer), Department of Biology, Kazakh National Women's Teacher training University, Almaty, Kazakhstan; e-mail: aytzhanova.m@qyzpu.edu.kz; ORCID: https://orcid.org/0000-0002-7067-9296

How to Cite: Amangeldina, A.A., Zhumina, A.G., Zeinidenov, A.K., Aimukhanov, A.K., Shakeyev, K.T., Sagyngali, U.K., Shestakov, D.V. (2026). Cell Cultures as a Platform for Optical Diagnostics and Toxicological Analysis: Cancer Predictors and Cytotoxicity of Organic Compounds. *Fundamental and Experimental Biology*, 31, 3 (123), 127-136. https://doi.org/10.31489/2026FEB3/127-136

Review Article

https://doi.org/10.31489/2026FEB3/127-136

UDC 616-006:543.429.2 Received: 16.02.2026 | Accepted: 12.06.2026 | Published online: 30 September 2026

A.A. Amangeldina[1], A.G. Zhumina[1*], A.K. Zeinidenov[1], A.K. Aimukhanov[1], K.T. Shakeyev[2, 3], U.K. Sagyngali[2], D.V. Shestakov[2]

[1]*Buketov Karaganda National Research University, University str., 28, 100028 Karaganda, Kazakhstan;*
[2]*Department of Surgical Diseases, Karaganda Medical University, Karaganda 100012, Republic of Kazakhstan;*
[3]*Department of Surgical Diseases, Karaganda Medical University. Concurrently Head of Surgical Service, "Multidisciplinary Hospital No. 3, Karaganda" (Oncology Dispensary)*
[*]*Corresponding author: bioassel@gmail.com*

Cell Cultures as a Platform for Optical Diagnostics and Toxicological Analysis: Cancer Predictors and Cytotoxicity of Organic Compounds

This review examines the use of cell cultures as an experimental platform for optical diagnostics and the assessment of the cytotoxic effects of organic compounds. *In vitro* models, including primary cell cultures, immortalized cell lines, and tumor cell lines, are used to investigate biochemical changes associated with malignant transformation and cytotoxic effects. Particular emphasis is placed on Raman and infrared spectroscopy as label-free methods for detecting molecular alterations and evaluating dose-dependent cellular responses to organic compounds. The review covers studies using human cell lines, including MCF-7, HeLa, A549, HepG2, HL-60, and U-937, with particular attention to documented changes in lipid and protein composition, structural abnormalities, and metabolic adaptations. The integration of cellular models with optical methods enables the acquisition of reproducible and quantitatively measurable indicators of biochemical changes, thereby supporting the development of novel diagnostic approaches and the assessment of compound toxicity. The findings highlight the scientific value of cell cultures as a versatile platform for both fundamental and applied research in oncology and toxicology.

Keywords: cell cultures, cytotoxicity, organic compounds, Raman spectroscopy, infrared spectroscopy, optical diagnostics, *in vitro*.

Introduction

Cell cultures are widely employed as experimental tools in applied, fundamental, and biological research, representing one of the principal *in vitro* models [1]. They are valued for being convenient and readily controllable systems [2], enabling the study of cellular structural, functional, and metabolic features under both normal and pathological conditions [3]. Additionally, *in vitro* cultures allow the assessment of various chemical and physical factors within precisely defined experimental settings [4].

Due to their ease of cultivation and high reproducibility, cell cultures are widely used in oncology, toxicology, and pharmacology [5]. They offer a convenient experimental platform for controlled *in vitro* studies. Cell cultures are frequently used to investigate cellular mechanisms, assess the toxicity of substances, and prescreen potentially effective compounds [6, 7].

In recent years, the application of cell cultures in combination with optical research methods has gained particular relevance. Optical microscopy, along with fluorescent and spectroscopic techniques, enables the monitoring of changes in cell morphology, structure, and biochemical state without disrupting the sample [8, 9]. These capabilities make such methods promising for the early detection of malignant cell transformation, as well as for evaluating the cytotoxic effects of various organic compounds at the cellular level [10].

Scientific literature reports various findings on the use of cell cultures in oncological research and toxicological analysis. These studies demonstrate optical methods are applied to both tumor and non-tumor cell lines to study cellular changes and assess the various chemical compounds toxicity [11–13]. At the same time, various publications consider these aspects separately, focusing either on the cell cultures biological characteristics or on individual optical methods without a comprehensive examination [14, 15]. This indicates the relevance of using cell culture analysis as a unified experimental platform for optical diagnostics and toxicological assessment.

A key issue in this field is the lack of a comprehensive understanding of the capabilities and limitations of using cell cultures to identify optical predictors of malignant transformation and to assess the cytotoxic effects of organic compounds. The criteria for interpreting optical data obtained from cell models, as well as their relevance to preclinical research, remain insufficiently defined [16].

The object of this study is cell cultures employed in biomedical research, while the subject is their application in optical diagnostics of malignant transformations and the toxicological assessment of organic compounds. The aim of this review article is to analyze and systematize the scientific literature on the use of cell cultures as a platform for optical diagnostics and toxicological evaluation. To achieve this goal, the article addresses the following objectives: to review the main types of cell cultures and their applications; to analyze the advantages and limitations of cell cultures as *in vitro* models; to describe the optical methods employed to study cell cultures in oncology.

Experimental

A systematic approach was employed to analyze the scientific literature for this review. The primary sources of information included the international databases PubMed, Web of Science, and Scopus, as well as open-access scientific journals publishing research in the fields of cell biology, oncology, toxicology, and spectroscopy. Inclusion criteria encompassed studies focused on the use of cell cultures (primary, immortalized, and tumor cell lines) as models for investigating biochemical changes associated with malignant transformation and the cytotoxicity of organic compounds, as well as studies employing spectroscopic methods for the quantitative and qualitative analysis of cellular components. Studies lacking experimental data or without a detailed description of spectroscopic methods were excluded. Data were systematically organized to analyze cell line types, studied compounds, applied spectroscopic approaches (Raman and FTIR), and identified biochemical changes. The collected materials were used to summarize current trends, compare results across studies, and highlight prospects for the development of optical diagnostics and *in vitro* toxicological analysis.

Main types of cell cultures and their applications

Cell cultures are experimental systems consisting of populations of cells maintained outside the organism under controlled *in vitro* conditions. Such conditions ensure cell viability, support proliferation, and preserve essential biological functions. Consequently, cell cultures are widely used as model systems for the investigation of cellular processes, the study of pathological alterations, including malignant transformation, and the assessment of the cytotoxic effects of chemical compounds [17, 18].

Cell cultures are classified into three main types based on their source and biological characteristics: primary cultures, immortalized cell lines, and tumor cell lines [19, 20].

Primary cell cultures are obtained directly from body tissues and maintained *in vitro* without prolonged adaptation or targeted genetic modification. As a result, they largely preserve the morphological, functional, and metabolic characteristics of the original tissue, including specific cellular phenotypes and regulatory mechanisms [21]. For example, primary human mammary epithelial cells (HMECs) have been isolated and cultured from mammary tissue to study fundamental aspects of breast biology and diseases, including early stages of breast cancer development [22]. Primary human hepatocytes isolated from resected liver tissue are frequently used as physiologically relevant models to study drug metabolism, cytochrome P450 regulation and response to xenobiotics *in vitro* [23]. Similarly, primary adult cardiomyocytes isolated from human myocardium were cultured to evaluate electrophysiological properties and cardiotoxic responses to therapeutic compounds, demonstrating their utility in cardiovascular research and drug safety assessment [24]. Their close resemblance to native tissue underlies their high biological relevance, making primary cultures an important tool in fundamental research [25]. They are widely employed to investigate cellular mechanisms underlying tumor development, to study disruptions in cellular regulation [26], and to experimentally assess the effects of various chemical compounds at the cellular level [27].

Immortalized cell lines are characterized by their ability to undergo an unlimited number of cell divisions, making them a convenient and stable platform for long-term, reproducible experiments. This enables the standardization of experimental conditions and the comparability of results across different studies. For example, the Jurkat T-lymphoblastic cell line, derived from human T-lymphoblastic leukemia, is routinely used in an *in vitro* model to study signaling pathways during T-cell activation and their functional roles, in-

cluding studies of T-cell receptor (TCR) signaling pathways and cytokine production in response to stimulation protocols [28]. Similarly, the HEK293 cell line, an immortalized human kidney cell line, is commonly used as a host system for transient expression studies, recombinant protein production, and viral vector production due to its high transfection and robust growth properties [29]. Immortalized hepatoma cell lines, such as Huh7 cells play a key role in virological research as they enable efficient replication of hepatitis C virus (HCV) RNA in culture and allow the screening of antiviral compounds that would otherwise be difficult to evaluate in primary hepatocyte systems [30]. Their role as model systems for studying the molecular mechanisms of cell activity, analyzing signaling pathways, and performing pharmacological and toxicological screening of various compounds confirms their importance for basic and applied research. Immortal cell lines also play a key role in the development and validation of cell-model-based diagnostic methods, such as reporter assays generated on transformed cell lines to detect biomarker-mediated responses [31].

Tumor cell lines are derived from malignant neoplasms of various origins. Their distinguishing feature is the disruption of growth, proliferation, and cell cycle regulation, which makes them a valuable tool for studying tumor cell biology [32]. For example, human breast adenocarcinoma MCF-7 and hepatocellular carcinoma HepG2 cell lines are frequently used in cancer research to study metabolic changes and stress responses in tumor cells; studies have shown how metabolic inhibition and hypoxic conditions affect viability and apoptotic markers in these tumor cell lines, providing insight into regulatory pathways associated with carcinogenesis [33]. In another study, a range of human ovarian tumor cell lines, including IGROV1, OVCAR-3, OVCAR-4, OVCAR-5, OVCAR-8, and SK-OV-3, were used to characterize the antitumor activity of the chemotherapeutic agent irofulven. Significant antiproliferative effects were demonstrated in vitro, and the suitability of these cell lines for the preclinical evaluation of cytotoxic compounds was confirmed [34]. The human cervical cancer cell line HeLa is derived from a malignant epithelial tumor. Fourier-transform infrared spectroscopy (FTIR) and Raman spectroscopy were used to investigate changes in the protein and lipid composition of HeLa cells following cytotoxic and pharmacological stimulation. For example, FTIR and Raman imaging of HeLa cells treated with the adaptogen withaferin A revealed dose-dependent biochemical changes in lipid-related spectral regions and protein secondary structures. This suggests alterations in cellular metabolism and response to chemical substances [35]. Further studies demonstrated that cell cycle-dependent changes in the FTIR spectra of HeLa cells correlate with changes in amide I and II bands, which are associated with protein conformation and cell state [36]. Raman spectroscopy combined with atomic force microscopy was also used to detect changes in the DNA, lipid, and protein composition of HeLa cells after exposure to external substances such as nanoparticles. This confirmed that the vibrational signatures reflect molecular adaptation to the treatment [37]. These studies demonstrate the suitability of HeLa cells for assessing cytotoxic effects and for investigating biochemical reactions in solid tumor models using optical methods.

In contrast, the human leukemia cell lines HL-60 and U-937 are derived from hematological malignancies and grow in suspension, making them suitable models for toxicological and spectroscopic investigations. Leukemia cell cultures have been extensively studied using Raman spectroscopy and Fourier-transform infrared spectroscopy (FTIR) to identify alterations in protein, lipid, and nucleic acid composition associated with cytotoxic effects and apoptosis [38, 39]. The combined use of solid tumor and leukemia cell lines allows for a comparative evaluation of cytotoxic effects and molecular reactions in different cancers using optical spectroscopic methods.

Tumor cell lines of various origins are frequently used to model solid and hematological malignancies *in vitro*. These lines are employed to investigate the mechanisms of carcinogenesis, analyze the phenotypic and molecular characteristics of malignant cells, and identify potential cellular markers of tumor transformation. In applied research, such cultures are used to assess antitumor activity and the cytotoxic effects of organic compounds using various analytical techniques, including optical methods, which provide information on structural, functional, and biochemical changes in cells [40].

Cell cultures as an experimental model in vitro: advantages and limitations

Cell cultures are regarded as a common *in vitro* model in biomedical research, owing to the ability to maintain strict control over experimental conditions and achieve highly reproducible results when studying cellular processes. The use of cell cultures enables the analysis of the effects of various factors on cells under standardized conditions, which is particularly important for oncology and toxicology studies [41].

The main advantages of cell cultures are the strict control of experimental conditions, including the composition of the culture medium, the concentration of the compounds being studied, the temperature, and the exposure time. These conditions ensure reproducible results and enable quantitative analysis of cellular responses. Moreover, cell cultures offer high experimental flexibility, enabling the variation of study parameters and the modeling of diverse biological conditions.

A significant benefit of cell models is the ability to investigate cellular mechanisms at the molecular and subcellular levels [42]. The use of cell cultures facilitates the analysis of proliferation, apoptosis, metabolic changes, and the structural organization of cells. This makes them indispensable for studies of carcinogenesis as well as for assessing the cytotoxic effects of chemical compounds [43].

Despite their advantages, cell cultures as *in vitro* models have several limitations. One limitation is the simplified nature of the system compared to *in vivo* conditions, as cell cultures do not fully reflect complex intercellular and tissue interactions, nor the influence of systemic factors present in the organism. This restricts the direct extrapolation of results to whole-organism contexts [44]. Another limitation is the variability of cellular characteristics during long-term culture, particularly for immortalized and tumor cell lines. Such changes can affect morphology, metabolism, and gene expression, which must be considered when interpreting results. Additionally, study outcomes may depend on the specific cell line used and the culture conditions applied [45].

Cell cultures represent an effective and informative *in vitro* model with several significant advantages, but careful interpretation of data and consideration of their limitations are essential.

Optical methods for the identification of cancer-related predictors in cell cultures

Optical spectroscopic techniques are widely applied to examine molecular changes associated with tumor phenotypes and are recognized as effective tools for identifying cancer-related predictors *in vitro*. By analyzing the spectral properties of cell cultures, researchers can detect variations in biochemical composition corresponding to different levels of malignancy and tumor aggressiveness. Among these methods, Raman and infrared (IR) spectroscopy stand out in oncology research due to their label-free operation and high molecular specificity. For example, investigations of urothelial carcinoma cell lines, including T24a, T24p, RT4, HT‑1376, and J82, using both Raman and FTIR imaging, have revealed that the spectral signatures reflect critical molecular differences between malignant and non-malignant cells, correlating with malignancy grade and invasive potential. These findings support the use of such spectroscopic profiles as reproducible indicators of cancer-related molecular changes *in vitro* [46]. The use of well-characterized tumor cell lines provides a controlled experimental platform for correlating spectral signatures with specific malignant phenotypes, facilitating the identification of reproducible molecular predictors of cancer development [47].

Raman spectroscopy is widely applied to characterize the biochemical profiles of tumor cell lines and to distinguish them from less aggressive cellular models. Studies involving breast cancer cell lines such as MDA-MB-231, MDA-MB-468, HCC-1143, and MCF-7 have demonstrated that both Raman and infrared spectral analyses can reveal molecular features characteristic of distinct tumor subtypes. In these models, Raman spectra have been shown to reflect differences in cellular lipid organization, protein secondary structure, and nucleic acid content, which are associated with variations in tumor aggressiveness. Such spectral distinctions enable the differentiation of highly invasive cell lines from less aggressive ones, supporting the use of Raman-based molecular fingerprints as potential predictors of tumor behavior [48].

Several studies have shown that Raman spectroscopy is sensitive to biochemical adaptations and metabolic features of tumor cells [49]. For instance, comparative analyses of the MDA-MB-231 and MCF-7 cell lines indicate that the intensity of spectral bands associated with lipid and protein components correlates with cellular aggressiveness and metastatic potential. In these investigations, elevated lipid-associated Raman signals were linked to increased membrane remodeling and altered energy metabolism in more aggressive cells. The application of multivariate statistical methods, including principal component analysis (PCA), allows the identification of informative spectral features and facilitates reliable discrimination between tumor cell lines [50]. As a result, cell line-specific spectral profiles can be generated and further explored as quantitative predictors of malignant phenotype and progression.

Infrared spectroscopy, particularly Fourier-transform infrared (FTIR) spectroscopy, complements Raman analysis by detecting the absorption of infrared radiation by specific molecular functional groups [51]. Studies of tumor cell lines have shown that alterations in amide I and amide II bands, as well as lipid-

associated spectral regions, reflect biochemical shifts characteristic of malignant transformation. Using breast cancer cell lines such as MCF-7 and more aggressive counterparts, FTIR spectroscopy has been shown to detect differences in protein-to-lipid ratios and conformational changes in cellular macromolecules. These FTIR-derived spectral features provide reproducible indicators of tumor-associated biochemical remodeling and can be employed to distinguish cell populations with different malignant potentials [52].

Overall, the application of Raman and infrared spectroscopic techniques to cell cultures enables the detection of stable molecular changes associated with tumor development. The resulting spectral profiles reflect key biochemical characteristics of malignant cells, including alterations in lipid metabolism, protein structure, and nucleic acid content, and may be considered potential predictors of cancer. Consequently, cell cultures serve as an effective and informative experimental platform for the development and validation of optical diagnostic approaches aimed at identifying cancer-related predictors in oncology research [53].

Cell cultures as a model for the assessment of cytotoxicity of organic compounds using optical methods

Cell cultures are widely used in toxicological studies to assess the cytotoxic effects of organic compounds, as they allow for the direct analysis of chemical impacts on cells derived from various tissues under controlled conditions [54]. In such studies, Raman and infrared spectroscopy are applied as optical techniques for detecting biochemical alterations in cells induced by toxic agents without the use of labels or destructive sample preparation [55].

Liver cell lines, particularly HepG2, are among the most commonly used models for evaluating the cytotoxicity of organic compounds with potential hepatotoxic effects. Several studies employing this model have investigated the impact of organic solvents, such as dimethylformamide and ethanol, as well as aromatic hydrocarbons and pharmacologically active compounds [56, 57]. Exposure to these substances induces alterations in lipid and protein components of HepG2 cells, which can be detected in both Raman and FTIR spectra. Spectral features associated with membrane integrity disruption and metabolic dysfunction have been shown to correlate with reduced cell viability, allowing these changes to be considered indicators of cytotoxic effects [58].

The HeLa and A549 cell lines are widely used in studies aimed at assessing the cytotoxicity of organic compounds in epithelial cells. In HeLa cells, Fourier-transform infrared (FTIR) spectroscopic analysis has been applied to detect biochemical changes in protein and lipid regions following exposure to pharmacologically active and toxic agents [59]. FTIR spectra of HeLa cells reveal alterations in amide I/II bands and lipid-related regions corresponding to cellular responses, including cell cycle arrest and phenotypic changes induced by external compounds [60]. Raman spectroscopy has also been successfully applied to live HeLa cells, demonstrating that vibrational signatures can provide detailed molecular information (including lipids and proteins) when HeLa cells are examined under different experimental conditions [61]. In A549 models, FTIR spectroscopy has been used to monitor apoptosis and cytotoxicity induced by toxic agents, including predominantly organic compounds as well as inorganic toxicants such as arsenic trioxide, demonstrating shifts in spectral regions associated with proteins, lipids, nucleic acids, and carbohydrates [62]. The combined application of Raman and infrared spectroscopy enables a more comprehensive characterization of cellular responses to toxic exposure, revealing complementary biochemical insights into membrane integrity, protein conformation, and metabolic disfunction.

The MCF-7 breast cancer cell line is frequently employed to evaluate the cytotoxicity of organic antitumor compounds, natural bioactive substances, and synthetic organic molecules considered as potential therapeutic agents. In such studies, Raman and FTIR spectroscopy have been used to detect changes in the protein and lipid composition of cells, reflecting structural damage and disturbances in cellular energy metabolism [63]. The resulting spectral data have been applied for the comparative assessment of toxic effects and for the analysis of dose-dependent cellular responses [64].

In a number of studies, cell cultures have been used to construct dose-dependent models of cytotoxicity for organic compounds of various chemical classes, including aromatic compounds, alcohols, ketones, and pharmacologically active molecules. The use of a single cell line in combination with Raman and infrared spectroscopy allows the generation of reproducible spectral profiles that reflect the extent of cellular damage at different toxicant concentrations [65, 66]. These spectral profiles complement conventional cell viability assays and can be employed for the quantitative evaluation of cytotoxic effects *in vitro*.

The main cell lines, studied compounds, and applied spectroscopic methods are summarized in Table 1.

Table 1

Application of cell lines and optical methods in cytotoxicity studies

Cell line	Type of organic compounds	Method	Main detected changes	References
HepG2	Organic solvents, aromatic compounds	Raman, FTIR	Changes in lipid and protein components	[67]
HeLa	Pharmacologically active compounds	Raman, FTIR	Shifts in amide bands and lipid regions	[68]
A549	Toxic organic compounds	FTIR	Apoptosis-associated spectral changes	[62]
MCF-7	Organic antitumor compounds	Raman, FTIR	Protein-lipid balance disorders	[69]

Thus, the integration of cell culture models with Raman and infrared spectroscopy represents an effective platform for assessing the cytotoxicity of organic compounds [66]. This approach enables the identification of molecular and biochemical changes induced by toxic exposure and supports the use of spectral characteristics for the comparative analysis and evaluation of the potential toxicity of organic substances [69].

Conclusions

The review demonstrates cell cultures serve as a versatile platform for research in optical diagnostics and toxicological analysis. The use of primary, immortalized, and tumor cell lines allows for the reproducible assessment of biochemical and structural changes resulting from both malignant transformation and exposure to organic compounds. Application of Raman and infrared spectroscopy facilitates the identification of molecular cancer markers, structural alterations in proteins and lipids, and cellular metabolic adaptations. The compiled data confirm the effectiveness of cell models for both quantitative and qualitative analysis of biochemical processes, as well as their potential in the development of new diagnostic approaches and the *in vitro* assessment of compound toxicity. Future research should focus on standardizing spectroscopic analysis methods and expanding the use of cell models for the predictive evaluation of biochemical and pharmacological effects of substances.

Acknowledgments

This research is funded by the Science Committee of the Ministry of Science and Higher Education of the Republic of Kazakhstan (Grant No. AP26102549).

Author Contributions

The manuscript was written through contributions of all authors. All authors have given approval to the final version of the manuscript. CRediT: **Amangeldina A.A**. — conceptualization, data curation, investigation, writing draft; **Zhumina A.G**. — supervision, conceptualization, data curation, formal analysis, writing — review and editing; **Zeinidenov A.K**. — supervision, conceptualization, formal analysis; **Aimukhanov A.K.** — formal analysis, writing — review and editing; **Shakeyev K.T**. — investigation, data curation, editing; **Sagyngali U.K**. — investigation, data curation, editing; **Shestakov D.V.** — investigation, data curation, editing.

References

1 Segeritz, C. P., &Vallier, L. (2017). Cell culture: Growing cells as model systems in vitro. *Basic science methods for clinical researchers* (pp. 151–172). https://doi.org/10.1016/B978-0-12-803077-6.00009-6

2 Jubelin, C., Muñoz-Garcia, J., Griscom, L., et al. (2022). Three-dimensional in vitro culture models in oncology research. *Cell Bioscience, 12,* 155. https://doi.org/10.1186/s13578-022-00887-3

3 Thomson, A. B. R., & Wild, G. (1995). Cell culture systems in the elucidation of cellular and molecular mechanisms associated with intestinal adaptation. *Biochimica et Biophysica Acta (BBA) — Molecular Basis of Disease, 1258*(1), 1–12. https://doi.org/10.1016/0955-2863(95)00035-X

4 Poteser, M. (2017). Cell-based in vitro models in environmental toxicology: A review. *Biomonitoring, 4*(1). https://doi.org/10.1515/bimo-2017-0002

5 Riss, T. L., Moravec, R. A., Duellman, S. J., & Niles, A. L. (2021). Treating cells as reagents to design reproducible assays. *SLAS Discovery, 26*(10), *1256–1267*. https://doi.org/10.1177/24725552211039754

6 Kitaeva, K. V., Rutland, C. S., Rizvanov, A. A., & Solovyeva, V. V. (2020). Cell culture based in vitro test systems for anticancer drug screening. *Frontiers in Bioengineering and Biotechnology, 8*, 322. https://doi.org/10.3389/fbioe.2020.00322

7 Allen, D. D., Caviedes, R., Cárdenas, A. M., Shimahara, T., Segura-Aguilar, J., & Caviedes, P. A. (2005). Cell lines as in vitro models for drug screening and toxicity studies. *Drug Development and Industrial Pharmacy, 31*(8), 757–768. https://doi.org/10.1080/03639040500216246

8 Hickey, S. M., Ung, B., Bader, C., Brooks, R., Lazniewska, J., Johnson, I. R. D., et al. (2021). Fluorescence microscopy—An outline of hardware, biological handling, and fluorophore considerations. *Cells, 11*(1), 35. https://doi.org/10.3390/cells11010035

9 Voros, C., Bauer, D., Migh, E., Grexa, I., Végh, A. G., Szalontai, B., et al. (2023). Correlative fluorescence and Raman microscopy to define mitotic stages at the single-cell level: Opportunities and limitations in the AI era. *Biosensors, 13*(2), 187. https://doi.org/10.3390/bios13020187

10 Tolstik, E., Gongalsky, M. B., Dierks, J., Brand, T., Pernecker, M., Pervushin, N. V., et al. (2022). Raman and fluorescence micro-spectroscopy applied for the monitoring of sunitinib-loaded porous silicon nanocontainers in cardiac cells. *Frontiers in Pharmacology, 13*, 962763. https://doi.org/10.3389/fphar.2022.962763

11 Evers, D. J., Hendriks, B., Lucassen, G., &Ruers, T. (2012). Optical spectroscopy: Current advances and future applications in cancer diagnostics and therapy. *Future Oncology, 8*(3), 307–320. https://doi.org/10.2217/fon.12.15

12 Ziemba, B. (2025). Advances in cytotoxicity testing: From in vitro assays to in silico models. *International Journal of Molecular Sciences, 26*(22), 11202. https://doi.org/10.3390/ijms262211202

13 Khalef, L., Lydia, R., Filicia, K., & Moussa, B. (2024). Cell viability and cytotoxicity assays: Biochemical elements and cellular compartments. *Cell Biochemistry and Function, 42*(3), e4007. https://doi.org/10.1002/cbf.4007

14 Ávila, F. J. (2024). A review of non-linear optical imaging techniques for cancer detection. *Optics, 5*(4), 416–433. https://doi.org/10.3390/opt5040031

15 Li, Y., Li, Z., Li, Y., & Gao, X. (2024). Optical molecular imaging in cancer research: Current impact and future prospect. *Oncology and Translational Medicine, 10*(5), 212–222. https://doi.org/10.1097/ot9.0000000000000056

16 Schneckenburger, H., & Richter, V. (2021). Challenges in 3D live cell imaging. *Photonics, 8*(7), 275. https://doi.org/10.3390/photonics8070275

17 Zhao, C. (2023). Cell culture: In vitro model system and a promising path to in vivo applications. *Journal of Histotechnology, 46*(1), 1–4. https://doi.org/10.1080/01478885.2023.2170772

18 Zink, D., Chuah, J. K. C., & Ying, J. Y. (2020). Assessing toxicity with human cell‐based in vitro methods. *Trends in Molecular Medicine, 26*(6), 570–582. https://doi.org/10.1016/j.molmed.2020.01.008

19 Weiskirchen, S., Schröder, S. K., Buhl, E. M., & Weiskirchen, R. (2023). A beginner's guide to cell culture: Practical advice for preventing needless problems. *Cells, 12*(5), 682. https://doi.org/10.3390/cells12050682

20 Pipiya, V. V., Gilazieva, Z. E., Issa, S. S., Rizvanov, A. A., & Solovyeva, V. V. (2024). Comparison of primary and passaged tumor cell cultures and their application in personalized medicine. *Exploratory Targeted Antitumor Therapy, 5*(3), 581–599. https://doi.org/10.37349/etat.2024.00237

21 Piwocka, O., Musielak, M., Ampuła, K., et al. (2024). Navigating challenges: Optimising methods for primary cell culture isolation. *Cancer Cell International, 24*, 28. https://doi.org/10.1186/s12935-023-03190-4

22 Qian, L., Yan, J., Chen, S., Abbas Karekad, M. M., Wu, Y., Wu, X., Xu, X., & Zhang, X. (2024). Isolation and culture of primary human mammary epithelial cells. *Journal of Visualized Experiments*, (207). https://doi.org/10.3791/66638

23 Gómez-Lechón, M. J., Donato, M. T., Castell, J. V., & Jover, R. (2004). Human hepatocytes in primary culture: The choice to investigate drug metabolism in man. *Current Drug Metabolism, 5*(5), 443–462. https://doi.org/10.2174/1389200043335414

24 Zhou, B., Shi, X., Tang, X., et al. (2022). Functional isolation, culture and cryopreservation of adult human primary cardiomyocytes. *Signal Transduction and Targeted Therapy, 7*, 254. https://doi.org/10.1038/s41392-022-01044-5

25 Harper, J. M. (2024). Primary cell culture as a model system for evolutionary molecular physiology. *International Journal of Molecular Sciences, 25*(14), 7905. https://doi.org/10.3390/ijms25147905

26 Miserocchi, G., Mercatali, L., Liverani, C., et al. (2017). Management and potentialities of primary cancer cultures in preclinical and translational studies. *Journal of Translational Medicine, 15*, 229. https://doi.org/10.1186/s12967-017-1328-z

27 Esparza-López, J., Martínez-Aguilar, J. F., & Ibarra-Sánchez, M. J. (2019). Deriving primary cancer cell cultures for personalized therapy. *Revista de Investigación Clínica, 71*(6), 369–380. https://doi.org/10.24875/RIC.19002832

28 Carrasco-Padilla, C., Aguilar-Sopeña, O., Gómez-Morón, A., et al. (2023). T cell activation and effector function in the human Jurkat T cell model. *Methods in Cell Biology, 178*, 25–41. https://doi.org/10.1016/bs.mcb.2022.09.012

29 Tan, E., Chin, C. S. H., Lim, Z. F. S., & Ng, S. K. (2021). HEK293 cell line as a platform to produce recombinant proteins and viral vectors. *Frontiers in Bioengineering and Biotechnology, 9*, 796991. https://doi.org/10.3389/fbioe.2021.796991

30 Sainz, B. Jr., Barretto, N., Yu, X., Corcoran, P., & Uprichard, S. L. (2012). Permissiveness of human hepatoma cell lines for HCV infection. *Virology Journal, 9*, 30. https://doi.org/10.1186/1743-422X-9-30

31 Chalak, M., Hesaraki, M., Mirbahari, S. N., Yeganeh, M., Abdi, S., Rajabi, S., & Hemmatzadeh, F. (2024). Cell immortality: In vitro effective techniques to achieve and investigate its applications and challenges. *Life, 14*(3), 417. https://doi.org/10.3390/life14030417

32 Mirabelli, P., Coppola, L., & Salvatore, M. (2019). Cancer cell lines are useful model systems for medical research. *Cancers (Basel), 11*(8), 1098. https://doi.org/10.3390/cancers11081098

33 Doczi, J., Karnok, N., Bui, D., et al. (2023). Viability of HepG2 and MCF-7 cells is not correlated with mitochondrial bioenergetics. *Scientific Reports, 13*, 10822. https://doi.org/10.1038/s41598-023-37677-x

34 Van Laar, E. S., Izbicka, E., Weitman, S., Medina-Gundrum, L., Macdonald, J. R., & Waters, S. J. (2004). Antitumor activity of irofulven against human ovarian cancer cell lines, human tumor colony-forming units, and xenografts. *International Journal of Gynecological Cancer, 14*(5), 824–831. https://doi.org/10.1111/j.1048-891X.2004.014515.x

35 Pięta, E., Chrabąszcz, K., Pogoda, K., Suchy, K., Paluszkiewicz, C., & Kwiatek, W. M. (2023). Adaptogenic activity of withaferin A on human cervical carcinoma cells using high-definition vibrational spectroscopic imaging. *Biochimica et Biophysica Acta (BBA) — Molecular Basis of Disease, 1869*(2), 166615. https://doi.org/10.1016/j.bbadis.2022.166615

36 Boydston-White, S., Romeo, M., Chernenko, T., Regina, A., Miljković, M., & Diem, M. (2006). Cell-cycle-dependent variations in FTIR micro-spectra of single proliferating HeLa cells: Principal component and artificial neural network analysis. *Biochimica et Biophysica Acta, 1758*(7), 908–914. https://doi.org/10.1016/j.bbamem.2006.04.018

37 Miletić, M., Aškrabić, S., Rüger, J., Vasić, B., Korićanac, L., Mondol, A. S., Dellith, J., Popp, J., Schiebe, I. W., & Dohčević-Mitrović, Z. (2020). Combined Raman and AFM detection of changes in HeLa cervical cancer cells induced by CeO_2 nanoparticles — Molecular and morphological perspectives. *Analytical Methods, 12*, 483–494. https://doi.org/10.1039/C9AN02518A

38 Fazio, E., Trusso, S., Franco, D., Nicolò, M. S., Allegra, A., Neri, F., Musolino, C., & Guglielmino, S. P. (2016). A micro-Raman spectroscopic investigation of leukemic U-937 cells in aged cultures. *Spectrochimica Acta Part A: Molecular and Biomolecular Spectroscopy, 159*, 21–29. https://doi.org/10.1016/j.saa.2016.01.032

39 Gasparri, F., & Muzio, M. (2003). Monitoring of apoptosis of HL60 cells by Fourier-transform infrared spectroscopy. *Biochemical Journal, 369*(Pt 2), 239–248. https://doi.org/10.1042/BJ20021021

40 Wang, J., Lin, K., Hu, H., Qie, X., Huang, W. E., Cui, Z., Gong, Y., & Song, Y. (2021). In vitro anticancer drug sensitivity sensing through single-cell Raman spectroscopy. *Biosensors, 11*(8), 286. https://doi.org/10.3390/bios11080286

41 Hirsch, C., & Schildknecht, S. (2019). In vitro research reproducibility: Keeping up high standards. *Frontiers in Pharmacology, 10*, 1484. https://doi.org/10.3389/fphar.2019.01484

42 Fontana, F., Marzagalli, M., Sommariva, M., Gagliano, N., & Limonta, P. (2021). In vitro 3D cultures to model the tumor microenvironment. *Cancers, 13(12)*, 2970. https://doi.org/10.3390/cancers13122970

43 Xu, R., Karrow, N. A., Shandilya, U. K., Sun, L. -h., & Kitazawa, H. (2020). In-vitro cell culture for efficient assessment of mycotoxin exposure, toxicity and risk mitigation. *Toxins, 12*(3), 146. https://doi.org/10.3390/toxins12030146

44 Urzì, O., Gasparro, R., Costanzo, E., De Luca, A., Giavaresi, G., Fontana, S., & Alessandro, R. (2023). Three-dimensional cell cultures: The bridge between in vitro and in vivo models. *International Journal of Molecular Sciences, 24(*15), 12046. https://doi.org/10.3390/ijms241512046

45 Polikov, V., Block, M., Zhang, C., Reichert, W. M., & Hong, J. S. (2008). *In vitro models for neuroelectrodes: A paradigm for studying tissue–materials interactions in the brain.* In W.M. Reichert (Ed.), Indwelling neural implants: Strategies for contending with the in vivo environment (Chapter 4). CRC Press/Taylor & Francis.

46 Kujdowicz, M., Placha, W., Mech, B., Chrabaszcz, K., Okoń, K., & Malek, K. (2021). In vitro spectroscopy-based profiling of urothelial carcinoma: A Fourier transform infrared and Raman imaging study. *Cancers, 13*(1), 123. https://doi.org/10.3390/cancers13010123

47 Nieva, C., Marro, M., Santana-Codina, N., Rao, S., Petrov, D., & Sierra, A. (2012). The lipid phenotype of breast cancer cells characterized by Raman microspectroscopy: Towards a stratification of malignancy. *PLoS ONE, 7*(10), e46456. https://doi.org/10.1371/journal.pone.0046456

48 Santos, I. P., Martins, C. B., Batista de Carvalho, L. A. E., Marques, M. P. M., & Batista de Carvalho, A. L. M. (2022). Who's who? Discrimination of human breast cancer cell lines by Raman and FTIR microspectroscopy. *Cancers, 14*(2), 452. https://doi.org/10.3390/cancers14020452

49 Elumalai, S., Managó, S., & De Luca, A. C. (2020). Raman microscopy: Progress in research on cancer cell sensing. *Sensors (Basel), 20*(19), 5525. https://doi.org/10.3390/s20195525

50 Chaturvedi, D., Balaji, S. A., Bn, V. K., Ariese, F., Umapathy, S., & Rangarajan, A. (2016). Different phases of breast cancer cells: Raman study of immortalized, transformed, and invasive cells. *Biosensors (Basel), 6*(4), 57. https://doi.org/10.3390/bios6040057

51 Su, K. -Y., & Lee, W. -L. (2020). Fourier transform infrared spectroscopy as a cancer screening and diagnostic tool: A review and prospects. *Cancers, 12*(1), 115. https://doi.org/10.3390/cancers12010115

52 Lasalvia, M., Capozzi, V., & Perna, G. (2021). Comparison of FTIR spectra of different breast cell lines to detect spectral biomarkers of pathology. *Infrared Physics & Technology, 115*, 103976. https://doi.org/10.1016/j.infrared.2021.103976

53 Short, K. W., Carpenter, S., Freyer, J. P., & Mourant, J. R. (2005). Raman spectroscopy detects biochemical changes due to proliferation in mammalian cell cultures. *Biophysical Journal, 88*(6), 4274–4288. https://doi.org/10.1529/biophysj.103.038604

54 Owen, C. A., Selvakumaran, J., Notingher, I., Jell, G., Hench, L. L., & Stevens, M. M. (2006). In vitro toxicology evaluation of pharmaceuticals using Raman micro-spectroscopy. *Journal of Cellular Biochemistry, 99*(1), 178–186. https://doi.org/10.1002/jcb.20884

55 Baker, M. J., Trevisan, J., Bassan, P., Bhargava, R., Butler, H. J., Dorling, K. M., Fielden, P. R., Fogarty, S. W., Fullwood, N.J., Heys, K. A., Hughes, C., Lasch, P., Martin-Hirsch, P. L., Obinaju, B., Sockalingum, G. D., Sulé-Suso, J., Strong, R. J., Walsh,

M. J., Wood, B.R., … Martin, F. L. (2014). Using Fourier transform IR spectroscopy to analyze biological materials. *Nature Protocols, 9*(8), 1771–1791. https://doi.org/10.1038/nprot.2014.110

56 Schoonen, W. G., de Roos, J. A., & Westerink, W. M. (2005). Cytotoxic effects of 110 reference compounds on HepG2 cells and for 60 compounds on HeLa, ECC-1 and CHO cells. II. Mechanistic assays on NAD(P)H, ATP and DNA contents. *Toxicology In Vitro, 19*(4), 491–503. https://doi.org/10.1016/j.tiv.2005.01.002

57 Kim, S., Kang, K., Kim, H., & Seo, M. (2024). In vitro toxicity screening of fifty complex mixtures in HepG2 cells. *Toxics, 12*(2), 126. https://doi.org/10.3390/toxics12020126

58 Xing, Y., Li, J., Yang, J., Li, J., Pang, W., Martin, F. L., & Xu, L. (2023). Application of spectrochemical analysis with chemometrics to profile biochemical alterations in nanoplastic-exposed HepG2 cells. *Environmental Pollution, 336,* 122309. https://doi.org/10.1016/j.envpol.2023.122309

59 Nešić, M. D., Dučić, T., Liang, X., Algarra, M., Mi, L., Korićanac, L., Žakula, J., Kop, T. J., Bjelaković, M. S., Mitrović, A., & Gojgić Cvijović, G. D. (2020). SR-FTIR spectro-microscopic interaction study of biochemical changes in HeLa cells induced by Levan-C60, Pullulan-C60, and their cholesterol-derivatives. *International Journal of Biological Macromolecules, 165(Pt B),* 2541–2549. https://doi.org/10.1016/j.ijbiomac.2020.10.141

60 Zhang, F. Q., Qi, J., & Yang, Z. G. (2011). Cell-cycle-dependent variations in the FTIR spectroscopy of HeLa cells treated with trichostatin A. *Guang Pu Xue Yu Guang Pu Fen Xi, 31*(8), 2076–2080.

61 Gargotti, M., Efeoglu, E., Byrne, H. J., & Casey, A. (2018). Raman spectroscopy detects biochemical changes due to different cell culture environments in live cells in vitro. *Analytical and Bioanalytical Chemistry, 410*(28), 7537–7550. https://doi.org/10.1007/s00216-018-1371-5

62 Liu, H., Su, Q., Wu, Q., Fang, W., Yang, D., Zheng, W., & Wang, X. (2018). FTIR spectroscopic study on apoptosis of lung cancer cell line A549 induced by arsenic trioxide. *Infrared Physics & Technology, 95,* 102–108. https://doi.org/10.1016/j.infrared.2018.08.017

63 Mignolet, A., Wood, B. R., & Goormaghtigh, E. (2018). Intracellular investigation on the differential effects of four polyphenols on MCF‑7 breast cancer cells by Raman imaging. *Analyst, 143*(1), 258–269. https://doi.org/10.1039/C7AN01460K

64 Wu, B. B., Gong, Y. P., Wu, X. H., Chen, Y. Y., Chen, F. F., Jin, L. T., Cheng, B. R., Hu, F., & Xiong, B. (2015). Fourier transform infrared spectroscopy for the distinction of MCF-7 cells treated with different concentrations of 5-fluorouracil. *Journal of Translational Medicine, 13,* 108. https://doi.org/10.1186/s12967-015-0468-2

65 Efeoglu, E., Casey, A., & Byrne, H. J. (2016). In vitro monitoring of time and dose dependent cytotoxicity of aminated nanoparticles using Raman spectroscopy. *Analyst, 141*(18), 5417–5431. https://doi.org/10.1039/c6an01199c

66 Byrne, H. J., Bonnier, F., Efeoglu, E., Moore, C., & McIntyre, J. (2020). In vitro label free Raman microspectroscopic analysis to monitor the uptake, fate and impacts of nanoparticle based materials. *Frontiers in Bioengineering and Biotechnology, 8,* 544311. https://doi.org/10.3389/fbioe.2020.544311

67 Junhom, C., Weerapreeyakul, N., Tanthanuch, W., & Thumanu, K. (2016). FTIR microspectroscopy defines early drug resistant human hepatocellular carcinoma (HepG2) cells. *Experimental Cell Research, 340*(1), 74–82. https://doi.org/10.1016/j.yexcr.2015.12.007

68 Kamat, S., Kumari, M., & Jayabaskaran, C. (2022). Infrared spectroscopy and flow cytometry studies on the apoptotic effect of nano-chrysin in HeLa cells. *Spectrochimica Acta Part A: Molecular and Biomolecular Spectroscopy, 282,* 121666. https://doi.org/10.1016/j.saa.2022.121666

69 Ahmad, M. S., Mirza, B., Hussain, M., Hanif, M., Ali, S., Walsh, M. J., & Martin, F. L. (2008). ATR-FTIR spectroscopy detects alterations induced by organotin(IV) carboxylates in MCF-7 cells at sub-cytotoxic/-genotoxic concentrations. *PMC Biophysics, 1*(1), 3. https://doi.org/10.1186/1757-5036-1-3

А.А. Амангельдина, А.Г. Жумина, А.К. Зейниденов, А.К. Аймуханов,
К.Т. Шакеев, Ұ.К. Сағынғали, Д.В. Шестаков

Жасуша өсіндісі оптикалық диагностика және токсикологиялық талдау платформасы ретінде: қатерлі ісік предикторлары және органикалық қосылыстардың цитотоксикалық әсері

Шолу мақалада жасуша өсіндісін оптикалық диагностика және органикалық қосылыстардың цитотоксикалық әсерін бағалау үшін эксперименттік платформа ретінде пайдалану қарастырылған. Қатерлі трансформациямен және уытты әсерлермен байланысты биохимиялық өзгерістерді зерттеу үшін бастапқы өсіндісі, сондай-ақ өлмейтін және ісік жасуша желілерін қоса алғанда, *in vitro* модельдері қолданылды. Молекулалық өзгерістерді анықтау және органикалық қосылыстарға дозаға тәуелді жасушалық реакцияларды бағалау үшін таңбасыз әдістер ретінде Раман және инфрақызыл спектроскопияға ерекше назар аударылды. Қарастырылған зерттеулер липидтер мен ақуыз құрамының құжатталған өзгерістеріне, құрылымдық ауытқуларға және метаболикалық бейімделулерге назар аудара отырып, MCF-7, HeLa, A549, HepG2, HL-60 және U-937 сияқты адам

жасуша желілерін қамтиды. Жасуша модельдерін оптикалық әдістермен біріктіру биохимиялық өзгерістердің қайталанатын және сандық тұрғыдан маңызды көрсеткіштерін алуға мүмкіндік жасайды, бұл жаңа диагностикалық тәсілдерді әзірлеу және қосылыстың уыттылығын бағалау үшін мүмкіндіктер береді. Қорытындыда жасуша өсіндісінің онкология мен токсикологиядағы іргелі және қолданбалы зерттеулер үшін жан-жақты платформа ретіндегі ғылыми құндылығы атап өтілген.

Кілт сөздер: жасуша өсіндісі, цитотоксикалық әсер, органикалық қосылыстар, Раман спектроскопиясы, инфрақызыл спектроскопия, оптикалық диагностика, *in vitro.*

А.А. Амангельдина, А.Г. Жумина, А.К. Зейниденов, А.К. Аймуханов, К.Т. Шакеев, Ұ.К. Сағынғали, Д.В. Шестаков

Культуры клеток как платформа для оптической диагностики и токсикологического анализа: предикторы рака и цитотоксичность органических соединений

В данной обзорной статье мы рассматриваем использование клеточных культур в качестве экспериментальной платформы для оптической диагностики и оценки цитотоксического действия органических соединений. Для исследования биохимических изменений, связанных со злокачественной трансформацией и токсическим действием, используются модели in vitro, включая первичные культуры, а также иммортализованные и опухолевые клеточные линии. Особое внимание уделяется рамановской и инфракрасной спектроскопии как безметочным методам обнаружения молекулярных изменений и оценки дозозависимых клеточных ответов на органические соединения. Рассмотренные исследования включают клеточные линии человека, такие как MCF-7, HeLa, A549, HepG2, HL-60 и U-937, с акцентом на документированные изменения в липидном и белковом составе, структурные аномалии и метаболические адаптации. Интеграция клеточных моделей с оптическими методами позволяет получать воспроизводимые и количественно значимые показатели биохимических изменений, предоставляя возможности для разработки новых диагностических подходов и оценки токсичности соединений. В выводах подчеркивается научная ценность клеточных культур как универсальной платформы для фундаментальных и прикладных исследований в онкологии и токсикологии.

Ключевые слова: клеточные культуры, цитотоксичность, органические соединения, рамановская спектроскопия, инфракрасная спектроскопия, оптическая диагностика, *invitro.*

Information about the authors

Amangeldina Aruzhan Ayankyzy — PhD Student, Buketov Karaganda National Research University, Karaganda, Kazakhstan; email: apysi@mail.ru; ORCID: 0009-0001-0439-8402

Zhumina Assel Galymovna — PhD, Associate Professor, Buketov Karaganda National Research University, Karaganda, Kazakhstan; e-mail: bioassel@gmail.com; ORCID: 0000-0002-0904-4726

Zeinidenov Assylbek Kalkenovich — PhD, Associate Professor, Buketov Karaganda National Research University, Karaganda, Kazakhstan; e-mail: a.k.zeinidenov@gmail.com; ORCID: 0000-0001-9780-5072

Aimukhanov Aitbek Kaliyevich — Candidate of Physics and Mathematics Sciences, Professor, Buketov Karaganda National Research University, Karaganda, Kazakhstan; e-mail: aitbekaimukhan@gmail.com; ORCID:0000-0002-4384-5164

Shakeyev Kairat Tanabayevich — Doctor of Medical Sciences, Professor, Department of Surgical Diseases, Karaganda Medical University, Concurrently Head of Surgical Service, Multidisciplinary Hospital No. 3, Karaganda, Kazakhstan; e-mail: kayrat.shakeev@bk.ru; ORCID:0000-0002-7802-1464

Sagyngali Uldana Kamidollakyzy — PhD Student, Department of Surgical Diseases, Karaganda Medical University, Karaganda, Kazakhstan; e-mail: uldanka.2012@mail.ru; ORCID:0009-0004-8951-2703

Shestakov Dmitriy Vladimirovich — PhD student, Department of Surgical Diseases, Karaganda Medical University, Karaganda, Kazakhstan; e-mail: dshestakov008@gmail.com; ORCID: 0000-0001-7251-093X

How to Cite: Ualiyeva, R.M., Kaverina, M.M., Osipova, A.V., Koppaev, A.E., Chaizabekova, M.A. & Zhangazin, S.B. (2026). Species identification of crops and weeds in wheat fields using hyperspectral data and machine learning algorithms. *Fundamental and Experimental Biology*, 31, 3 (123), 137-151. https://doi.org/10.31489/2026FEB3/137-151

Research article

https://doi.org/10.31489/2026FEB3/137-151

UDC 57.08:581:004.8 Received: 12.12.2025 | Accepted: 18.02.2026 | Published online: 30.09.2026

R.M. Ualiyeva[1], M.M. Kaverina[2*], A.V. Osipova[3], A.E. Koppaev[4], M.A. Chaizabekova[5], S.B. Zhangazin[6]

[1, 2, 3, 4, 5]*Toraighyrov University, Pavlodar, Kazakhstan;*
[6]*L.N. Gumilyov Eurasian National University, Astana, Kazakhstan*
[*]*Corresponding author: k.ma96@mail.ru*

Species identification of crops and weeds in wheat fields using hyperspectral data and machine learning algorithms

Based on the relationship established between the morphological and anatomical properties of plant tissues and the recognition performance of a machine learning algorithm, a comprehensive assessment of the limitations of ML algorithms, using Random Forest as an example, was conducted for the first time for the multiclass identification of crops and weeds in the agroecosystems of northeastern Kazakhstan. The study identifies the principal biological factors underlying the optical overlap of classes in the hyperspectral feature space. Data were collected using a hyperspectral sensor operating in the VIS–NIR range. Spectral profiles were analyzed by assessing variance distribution using principal component analysis and constructing reflectance curves. Classification of the extracted data was performed using the Random Forest algorithm. Spring wheat (*Triticum aestivum*) at different phenological stages and five dominant weed species (*Euphorbia virgata, Descurainia sophia, Vicia hirsuta, Fallopia convolvulus*, and *Echinochloa crus-galli*) were selected as the study objects. The algorithm demonstrated an overall classification accuracy of 72.94% on the test data for crop-weed discrimination. High identification accuracy was achieved for wheat (MCC = 0.994), attributable to its spectral stability and pronounced red-edge features (680–730 nm). Lower accuracy in the intra-class separation of weed species was associated with species-specific anatomical characteristics: the thick cuticle of *Euphorbia virgata* increased reflectance, the complex structure of *Vicia hirsuta* contributed to spectral dispersion, and similarities in mesophyll structure between *Echinochloa crus-galli* and other grasses resulted in optical overlap with crop features. Thus, the model enables reliable crop–weed discrimination, which is important for precision agriculture and targeted agrochemical application.

Keywords: hyperspectral sensing, spring wheat, weeds, machine learning, species identification, species differentiation, spectral signatures, precision agriculture.

Introduction

Wheat is an important crop that ensures food security [1], accounting for approximately one-fifth of the total current global food demand [2]. However, despite the global prevalence of its cultivation areas, these regions are characterised by a number of problems that impede the implementation of initiatives in this direction [1]. One of the key destructive factors affecting cultivation and leading to substantial economic losses is the infestation of crop stands with weeds [3], which is caused by the delay and slowdown of crop growth, leading to reduced productivity and harvest quality [4] due to competition with weeds for sunlight, essential nutrients, territory, and water resources [5, 6]. According to FAO data, the share of annual crop losses due to weeds amounts to approximately 10 % [7, 8]. Traditional control methods, based on the blanket application of herbicides to field areas infested with weed vegetation, are associated with high labour intensity, increased financial costs, soil degradation, and negative environmental impacts [4, 9].

In the context of precision agriculture, the SSWM (Site-Specific Weed Management) strategy is gaining relevance [3, 10, 11], involving the targeted application of protective agents only in locations where specific species of undesirable plants (weeds) are detected [12], which allows for a manifold reduction of the pesticide load on ecosystems [13]. The basis of this strategy is the automated and accurate identification of weeds against the background of crop vegetation [14], which remains a challenging task to this day due to the morphological similarity of plants, especially at early developmental stages.

Standard digital RGB cameras have significant limitations when classifying species with similar visual characteristics. A promising alternative to them is hyperspectral systems, which, unlike traditional RGB and

multispectral imaging [14], record the reflectance of objects in hundreds of narrow spectral bands, thereby enabling the acquisition of detailed, unique spectral signatures of plants that reflect not only external morphological characteristics but also structural features of tissues, as well as internal chemical composition (chlorophyll, anthocyanin, carotenoid content, etc.) [15]. This makes it possible to distinguish species of crops and weeds based on species identification models, detect stress conditions, and conduct phytosanitary monitoring of crops at various stages of plant development [16].

One of the key research directions is the identification of weed vegetation in wheat crops [17]. However, despite the capabilities of hyperspectral sensors, the spectral information extracted in the form of hypercubes is characterised by high redundancy and dimensionality, which requires the application of comprehensive raw data processing methods. Machine learning and deep learning methods have become the primary tools for analysing such data arrays. The application of hyperspectral images in conjunction with machine learning algorithms enables the effective differentiation of several weed species using PLS-DA, SVM, and multilayer neural networks (MLP), with the MLP model demonstrating the best results with classification accuracy reaching nearly 100 % [18]. The combination of UAV imaging and convolutional neural networks allows for the accurate localisation of infestation hotspots and the assessment of the impact of weeds on wheat yield and biomass [4]. This is based on the difference in spectral signatures of leaves of crop and weed plants [19]. Traditional classifiers such as SVM, RF, and LDA [3, 20] demonstrate high performance in classification tasks when appropriate preprocessing parameters and feature sets are selected [21]. The combination of UAV-based hyperspectral imaging and deep neural networks enables the prediction of wheat yield and plant phenotyping with high accuracy, while the application of CNNs [3, 14, 21], Transformer models, and other artificial intelligence algorithms significantly enhances the efficiency of hyperspectral cube processing and the automation of crop analysis [22].

Despite significant advances in this field, there is still insufficient data on the application of hyperspectral imaging for the identification of weed vegetation and its differentiation from cereal crops, with this issue being particularly relevant for the regions of Central Asia specialising in grain cultivation. In this regard, the aim of this study is to investigate the application of hyperspectral imaging technology, as well as the possibilities of integrating hyperspectral sensing and machine learning for the species-level identification of crop and weed vegetation. The results of this study may help reduce the environmental burden and increase the efficiency of agroecosystem monitoring through more precise application of plant protection products, aligning with SDG 2 “Zero Hunger”, particularly the tasks of implementing innovative agricultural technologies and ensuring sustainable agriculture.

Experimental

The objects of the study were samples of crop and weed vegetation. The study crop was spring wheat (*Triticum aestivum* L., 1753). The weed vegetation was represented by the following five dominant species: *Euphorbia virgata* Waldst. & Kit., 1803; *Descurainia sophia* (L.) Webb ex Prantl, 1887 (syn. *Sisymbrium sophia* L., 1753); *Vicia hirsuta* (L.) Gray, 1821 (syn. *Ervum hirsutum* L., 1753); *Fallopia convolvulus* (L.) Á. Löve, 1970 (syn. *Polygonum convolvulus* L., 1753); *Echinochloa crus-galli* (L.) P. Beauv., 1812 (syn. *Panicum crus-galli* L., 1753). Sampling of both crop and weed vegetation was conducted in the northeast of Pavlodar Region, Republic of Kazakhstan, during the main developmental stages of spring wheat according to the BBCH scale: 10–20, 25–35, 39–59, and 61–75. The weather and climatic conditions of the study areas were characterised by a sharply continental climate with an average daily temperature during the growing season of +17.5 °C, average precipitation levels ranging from 40 to 48 mm, NE and SW winds with a speed of about 4 m/s, dark chestnut and chestnut medium-loamy soils with a calcareous composition and alkaline reaction (average pH 7.5).

For the analysis and subsequent imaging, 120 plant samples were selected: *Triticum aestivum* — 20, *Euphorbia virgata* — 20, *Descurainia sophia* — 20, *Vicia hirsuta* — 20, *Fallopia convolvulus* — 20, *Echinochloa crus-galli* — 20. The collected samples were transported from the fields to the Laboratory of Biological Research at Toraighyrov University (Pavlodar, Kazakhstan) for spectral studies. The acquisition, preprocessing, and processing of raw spectral data were performed using a FigSpec FS-13 hyperspectral camera (CHNSpec Technology, Hangzhou, China) with a CMOS detector and Breeze software (Umeå, Sweden). Hyperspectral imaging was conducted in the visible and NIR range with a spatial step of 2.5 nm at 1.92 thousand pixels, each with a size of 5.86 μm. The raw three-dimensional hypercubes, for the extraction of informative data, were preliminarily subjected to reference calibration (Spectralon, 99 %; Labsphere, Inc., North Sutton, NH, USA), noise elimination, smoothing, normalisation, and centering. Multidimensional lay-

er-by-layer visualisation and spatial dimensionality reduction were performed based on a PCA model with the extraction of principal components using Variance Scatter and the spectral representation of pixels from key informative regions via Raw Spectrum. PC1 and PC2 were used for the analysis of feature variability (t[1] reflects the main spectral differences between features, while t[2] determines additional variable characteristics). The formation of labeling in the dataset for further training and the selection of working pixels were carried out manually, followed by the segmentation of plant samples into distinct regions. The extracted sample regions, totaling 538, were used to develop a working model based on the Random Forest machine learning algorithm, and were divided into two main sets: the training set included 358 sample regions—66.5 % of the entire dataset; the test set comprised 180 sample regions—33.5 % of the dataset. The training of the RF-based model was performed using cross-validation. The workflow of the algorithm, from the import of raw data to training, is presented in Figure 1.

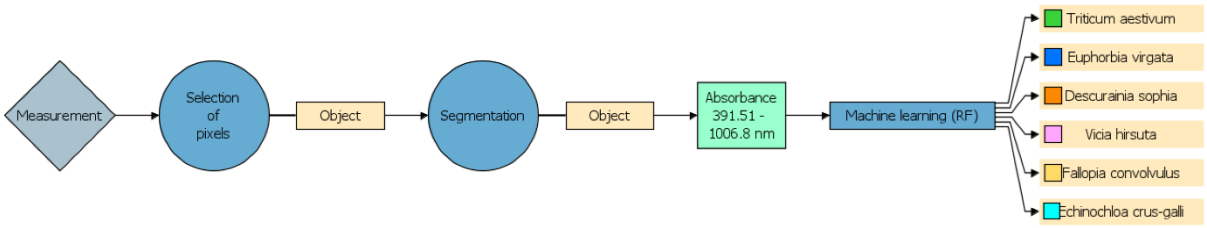

Figure 1. Algorithm workflow from raw data import to the application of machine learning

The extracted spectral reflectance data were processed using descriptive statistics and analysis of variance (ANOVA), with statistical significance set at $p<0.05$. The obtained indicators for species identification and differentiation of weed and crop vegetation are presented in the format of a Confusion Matrix. The assessment of classification quality was conducted using metrics such as Precision, Recall, and F1-score, while Accuracy and MCC were calculated to evaluate the performance of the model and the obtained results, allowing for the determination of the machine learning model's operability and its applicability to individual species of the studied weed and crop vegetation.

Results and Discussion

Spectral analysis

The figures present hyperspectral images of wheat and weed vegetation of agroecosystems, Raw Spectrum plots with curves reflecting the spectral characteristics of plant regions, and Variance Scatter diagrams. The hyperspectral image is rendered in pseudo-colours that correspond to the level of light reflectance intensity. Warm colours (red, yellow) denote areas with high reflectance, while cool colours (cyan, blue) represent zones of low reflectance. The Raw Spectrum plot contains curves reflecting the spectral characteristics of a specific part of the hyperspectral image. The plot represents a basic presentation of spectral data, showing the dependence of the object's reflectance coefficient on wavelength (400–1000 nm), where this indicator is a key source of information about the physiological state of plant tissues. The Variance Scatter diagrams reflect the distribution of objects in the principal component space.

Figure 2 presents hyperspectral images, Raw Spectrum plots, and a Variance Scatter diagram of a young wheat plant (Sample 1) and a plant at the heading stage (Sample 2). The spectral curves of the Raw Spectrum plot for Sample 1 are in the range of 500–780 nm. It was established that the most intense curves (purple and cyan), corresponding to the brightest areas of the hyperspectral image (coleoptile and spike), reach a reflectance coefficient of about 50–53 % in the wavelength region of 620–650 nm. The minimum values are characteristic of the red curve, whose reflectance coefficient does not exceed 10–12 %. For the green and red curves, a pronounced red edge region and a sharp increase in reflectance between 680 and 730 nm are recorded after 680 nm, driven by the transition from strong chlorophyll absorption to high reflectance in the near-infrared region. Along with this, it was revealed that after 730–780 nm, the reflectance coefficient gradually decreases. For the wheat spike (Sample 2), the spectral curves have a similar shape but are distinguished by lower reflectance amplitude. The maximum reflectance coefficient values of the most intense areas reach 37.5 % in the 600–650 nm range. The red curve, corresponding to regions with minimum reflectance, is characterised by a coefficient of about 7.5 % at the first peak and 20 % at the second peak. At the same time, the red edge in the 680–730 nm interval is observed for all curves of the plot; however, the

curves of the spikelet glumes have lower reflectance within the second peak. The Variance Scatter diagrams reflect the distribution of spectral variability of the data in the principal component space. Accordingly, it was revealed that for the young wheat plant, the first component t[1] explains 64.5 % of the total variance, and the second component t[2] explains 14.6 %, which may indicate high spectral heterogeneity of tissues among the leaf, coleoptile, and root. For the wheat spike, the first principal component already explains 82.2 % of the total variance, and the second component only 5.21 %. The more compact distribution of points and the dominance of the first component indicate a more homogeneous spectral structure of the spike compared to the young plant.

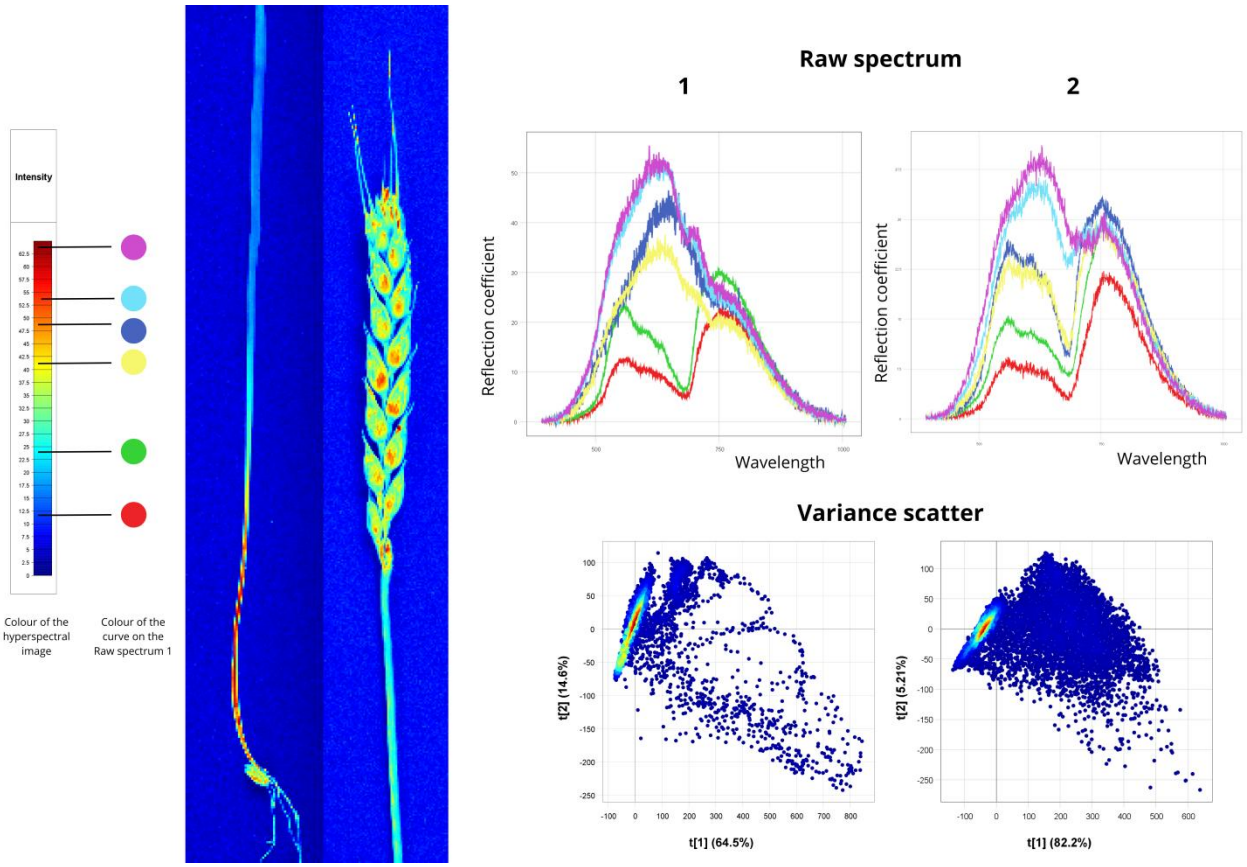

Figure 2. Wheat spectral profile

Figure 3 presents the weed vegetation and Variance Scatter diagrams, and Figure 4 presents the Raw Spectrum plots.

The Raw Spectrum plots reflect the spectral characteristics of different parts of the weed plants presented in the hyperspectral images. The spectral curves of Sample 1 demonstrate the highest reflectance values among all plants. The maximum reflectance coefficient of the purple curve reaches 75–77 % in the 610–650 nm range, which corresponds to areas of the root zone. The cyan and blue spectra have reflectance coefficients corresponding to 60–67 %. The yellow curve has its first peak recorded in the wavelength region of 500–730 nm, with a reflectance coefficient of 45 %, and its second peak noted in the region of 730–750 nm with a reflectance coefficient within 30–35 %, also belonging to the root part. The green curve reflects the leaf veins and stem of the weed and has a reflectance coefficient of 28 %. The red spectrum displays the spectral characteristics of the leaves with a reflectance coefficient not exceeding 14-15 %. For Sample 2, the maximum reflectance of the purple curve reaches 25–35 %, and the reflectance peak is noted in the wavelength region of about 620–650 nm, which corresponds to the root zone of the weed. The cyan, blue, and yellow curves are distinguished by a reflectance coefficient in the range of 20–27 % and belong to the stem and leaves. The red curve has a reflectance coefficient of 7 % and corresponds to individual shaded areas of the weed leaves. In the green spectral region, reflectance reaches up to 10 %, followed by a sharp increase to 25 % after 700 nm. The presence of the red edge in the region of 700 nm was also revealed for all spectral curves except the purple one.

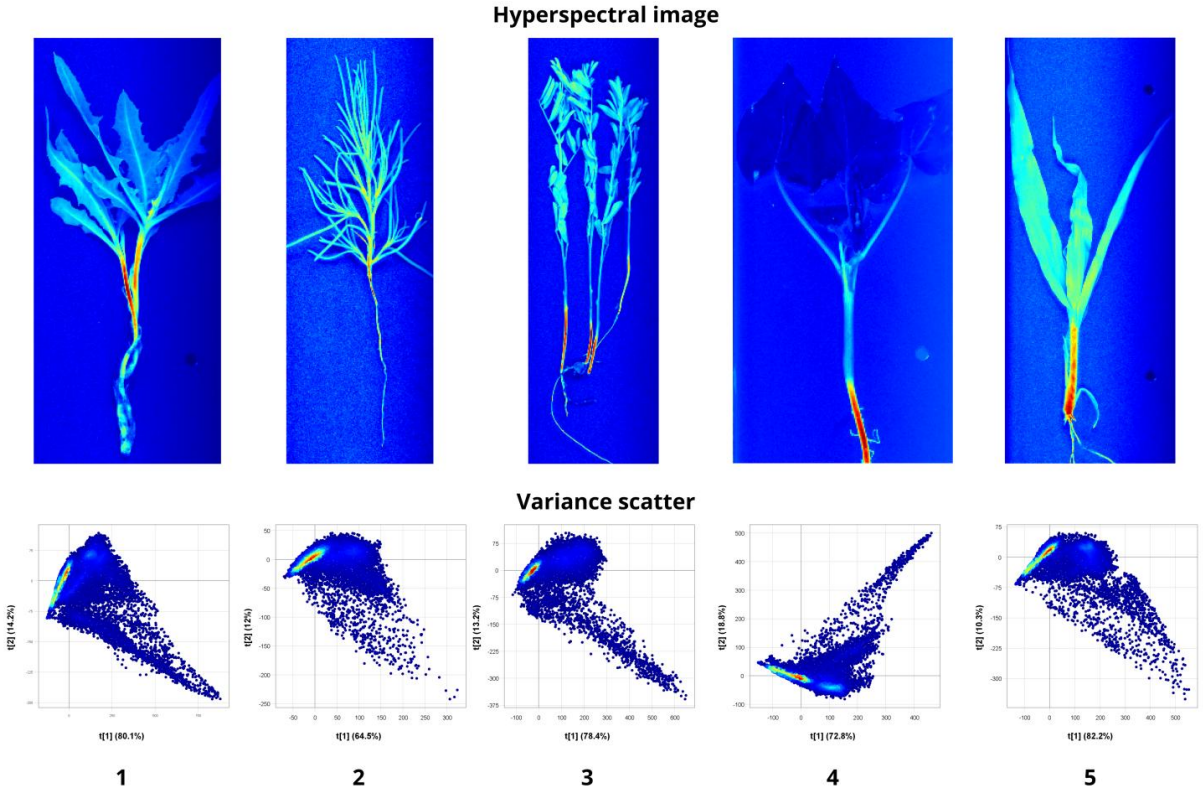

Figure 3. Hyperspectral images and Variance Scatter of weeds
(1 — *Euphorbia virgata*, 2 — *Descurainia sophia*, 3 — *Vicia hirsuta*,
4 — *Fallopia convolvulus*, 5 — *Echinochloa crus-galli*)

For Sample 3, the maximum value of the purple spectrum reaches 60 % in the region of 620–650 nm. The cyan, blue, and yellow curves have reflectance coefficients of 40–53 %, corresponding to root areas. The red and green spectra display the leaves and stems, having reflectance coefficients of 10–15 % at the first peak and 20–30 % at the second peak, and a clearly pronounced red edge is observed in the 680–730 nm interval.

For Sample 4, the maximum reflectance coefficient of the purple curve is 60 %, the cyan is 50 %, the blue corresponds to 30–35 %, and the yellow to 20–30 %, which relate to the root and near-root parts. The green spectrum has a reflectance coefficient of 5 %, and the red curve is characterised by a minimum value of 5 % in the visible range. In the 670–700 nm region, a deep reflectance minimum is observed, followed by a sharp red edge in the 700–740 nm range, with the reflectance coefficient reaching 25 % for the green and 15 % for the red curve, where the former spectrum belongs to stem areas and the latter to leaves.

All curves of Sample 5 have two peaks due to the formation of the red edge in the 700–740 nm range, after which reflectance gradually decreases in the near-infrared range beyond 780 nm. The first peak is in the 500–730 nm wavelength range, and the second peak is in the 730–780 nm region. The reflectance coefficient of the purple curve reaches 51 % at the first peak and 40 % at the second, the cyan 37.5 % and 35 %, the blue 30 % and 35 %, the yellow 27 % and 30 %, the green 15 % and 25 %, and the red 10 % and 15 %, respectively. The purple, cyan, and blue curves display the near-root part, the yellow and green curves display the leaves, and the red curve corresponds to individual shaded areas of the leaves.

The formation of a dense cluster of points in the region of low values of the second component and an elongated spectral tail, reflecting the heterogeneity of plant tissues and differences between leaves, stems, and root zones, is characteristic of all samples. The highest value of the second component is observed in *Vicia hirsuta* (18.8 %), indicating the heterogeneity of the plant's spectral characteristics. At the same time, in *Descurainia sophia*, the first component explains the lowest percentage of variance among all samples (64.5 %), and its variance diagram shows a wide distribution of points and a less pronounced cluster compactness. The fifth sample (*Echinochloa crus-galli*) exhibited the lowest value of the second component and the greatest dominance of the first (82.2 %), indicating the relative homogeneity of the spectral data of this weed species.

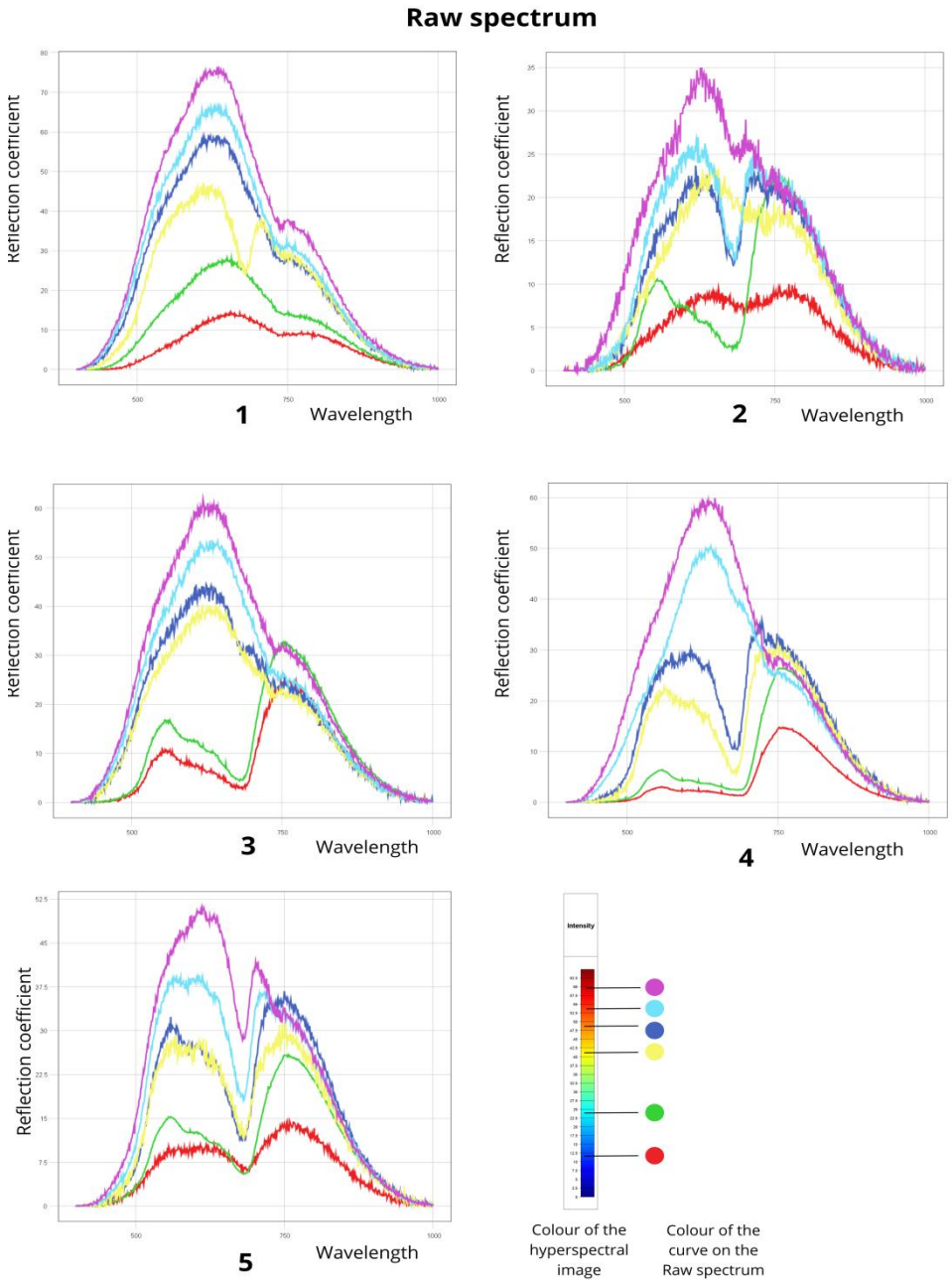

Figure 4. Raw spectra of weeds
(1 — Euphorbia virgata, 2 — Descurainia sophia, 3 — Vicia hirsuta,
4 — Fallopia convolvulus, 5 — Echinochloa crus-galli)

The obtained spectral differences between wheat and weed vegetation are driven by a combination of biophysical properties of plant tissues, including chlorophyll content, mesophyll anatomy, cuticle thickness, cell wall structure, the number of intercellular spaces, and the level of tissue water retention. The most significant differences were observed in the red-edge and NIR ranges, associated with the physiological state of plants and the structural features of leaf tissue. The spectral curves of the green parts of the studied objects demonstrate the reflectance pattern of photosynthetic vegetation, with low reflectance in the blue and red regions of the spectrum due to chlorophyll absorption, an increase in reflectance in the green region, and the formation of the red edge in the 680–730 nm range. The red edge is formed due to the combination of strong light absorption by chlorophyll in the red region of the spectrum and intense multiple scattering in the near-infrared range. The spectral curves of the root and near-root zones, due to the absence of photosynthetic activity and the presence of other pigments, do not exhibit a red-edge feature and reflect light throughout the wavelength range from 500 to 780 nm.

The higher reflectance values of the young wheat plant compared to the spike are explained by the anatomical features of the vegetative organs. The leaves and coleoptile of the young plant contain developed spongy parenchyma and a large amount of intercellular space, which enhances internal light scattering and leads to increased reflectance in the NIR region. In addition, young tissues are characterised by high chlorophyll content and an active photosynthetic apparatus, which contributes to the formation of a more pronounced red edge. In contrast, the tissues of the spike have a denser structure, a smaller proportion of intercellular spaces, and a higher content of mechanical tissues, which reduces the intensity of internal scattering and lowers the reflectance coefficient. Similar patterns have been described in studies of the spectral structure of cereal crops, where it has been shown that the transition from vegetative to generative organs is accompanied by a decrease in red edge amplitude and a reduction in reflectance in the near-infrared range due to changes in tissue structure and decreased chlorophyll content [23, 24]. The pronounced red edge in young wheat leaves and individual weed plants indicates a high content of photosynthetically active pigments and a developed internal cellular structure. According to research data, the position and steepness of the red edge are closely related to chlorophyll concentration, biomass, and plant water status. An increase in chlorophyll content causes a shift of the red edge toward longer wavelengths (red shift), whereas a decrease in physiological activity and water stress leads to a reduction in amplitude and a smoothing of the red edge [25–28].

The differences among weed species are also associated with their morphological and anatomical characteristics. *Euphorbia virgata* was characterised by the highest reflectance values, especially in the near-root zone. This may be explained by the presence of thick, succulent tissues, a developed system of vascular elements, and the presence of amyloplasts. Spurges contain a significant amount of milky sap and possess a comparatively thick cuticle, which enhances internal light scattering and increases the reflectance properties of the tissues. The broad leaves of *Euphorbia virgata* form a more uniform reflectance surface compared to narrow-leaved species. *Descurainia sophia* exhibited the lowest values of the first principal component and high spectral heterogeneity. This species has highly dissected, filiform leaves, resulting in pronounced variability in reflection angles and shadow zones. The thin, linear leaves reduce the volume of multiple internal scattering, and the heterogeneous leaf orientation leads to a broadening of the point cloud on the Variance Scatter diagram. *Vicia hirsuta* is characterised by the highest value of the second component, indicating pronounced intra-tissue heterogeneity of spectral characteristics. This species has a complex, branching shoot structure and combines thin leaves and stems with varying degrees of lignification and moisture content. This leads to differences in reflectance between individual plant organs and the formation of a wide spectral dispersion. In *Fallopia convolvulus*, the deep minimum in the 670–700 nm region and the subsequent sharp increase in reflectance are associated with intense chlorophyll absorption and a strong contrast between the leaf blade and the vascular tissues of the stem. The presence of a pronounced red edge indicates the preservation of an active photosynthetic apparatus. *Echinochloa crus-galli* demonstrated the most homogeneous spectral structure. Its broad leaves and relatively uniform tissue anatomy provide similar light reflectance conditions over most of the plant surface.

The main difference between weed vegetation and wheat is the higher spectral variability and a wider range of reflectance. The young wheat plant was characterised by a relatively smooth and stable spectral curve shape with a maximum reflectance coefficient of about 50–53 %, whereas in some weed species, especially *Euphorbia virgata* and *Vicia hirsuta*, reflectance reached 60–77 %.

Analysis of statistical indicators

In the course of the study, the reflectance characteristics of spring wheat and five weed species at different stages of ontogenesis were analysed, as well as the spectral contrast characteristics within the VNIR range. The reflectance indicators clearly demonstrate variability among the studied plant species, as well as within a species depending on the phenological phase. Wheat exhibited a pronounced decrease in reflectance during the transition from the young plant stage to the heading stage with mean and maximum reflectance coefficient (RC) values within 31.50 % and 53 % for the first variant and 22.50 % and 37.50 % for the second, respectively. Among the studied weeds, the maximum reflectance values were found in *Euphorbia virgata*, which applies both to the mean reflectance (45.50 %) of the plant tissues of this species and to the maximum (77 %). These characteristics, along with a delta reflectance of 63 %, represented the highest values among all weed species and across all studied wheat growth stages. However, alongside this, certain groups of weeds were identified whose spectral characteristics are approximately similar in their manifestation to the crop vegetation during certain phenophases. The closest indicators in terms of value are the reflectance-absorption characteristics of *Echinochloa crus-galli*, with a mean RC value within 30.50 %, which clearly demonstrates the similarity of the spectral characteristics of this weed species to the young wheat

plant (mean RC=31.50 %). A similarity was also established for such spectral reflectance characteristics as rate of change and CV: for the young spring wheat plant—27.56 % and 5.46 %, and for the weed—26.28 % and 5.21 %, respectively. *Vicia hirsuta* (mean RC=35 %) has values that differ somewhat more but are not greatly distant from those of young wheat. On the other hand, the reflectance patterns of *Descurainia sophia* (21 %) and *Fallopia convolvulus* (26.50 %) are highly similar to those of heading wheat (22.50 %). At the same time, the highest coefficient of variation was recorded for the latter weed and was equal to 22.52 %, which is an indicator of high intraspecific heterogeneity of reflectance properties in this species (Tab. 1).

Table 1

Reflectance characteristics of wheat and weeds

№	Sample		Reflectance (%)		Mean	Standard deviation	CV	Rate of change	ΔReflectance
			min	max					
1	*Triticum aestivum*	Young plant	10	53	31.50	5.46	17.34	27.56	43,00
		Ear-bearing wheat plant	7.5	37.5	22.50	3.81	16.93	19.23	30,00
2	*Euphorbia virgata*		14	77	45.50	8.00	17.58	40.38	63.00
3	*Descurainia sophia*		7	35	21.00	3.56	16.93	17.95	28.00
4	*Vicia hirsuta*		10	60	35.00	6.35	18.14	32.05	50.00
5	*Fallopia convolvulus*		3	50	26.50	5.97	22.52	30.13	47.00
6	*Echinochloa crus-galli*		10	51	30.50	5.21	17.07	26.28	41.00

The assessment of the spectral characteristics of the wavelength range within VIS-NIR demonstrated the identity of macroparameters for the two groups of studied vegetation (“Wheat” and “Weeds”), corresponding to the wavelength interval of 500–780 nm. It was also observed that both groups demonstrated a spectral bandwidth of 280 nm, a contrast ratio of 1.56, a relative bandwidth of 0.22, and a normalised contrast of 0.36 (Tab. 2).

Table 2

Spectral contrast features across the visible-to-near-infrared spectral region

№	Samples	Wavelength (nm)		Spectral bandwidth	Contrast ratio	Relative bandwidth	Normalised contrast
		λ_{min}	λ_{max}				
1	*Wheat*	500	780	280	1.56	0.22	0.36
2	*Weeds*	500	780	280	1.56	0.22	0.36

The main key task in precision smart farming is the reliable and accurate differentiation of crop and weed vegetation for the subsequent targeted application of herbicides. The obtained data on the statistical indicators of the spectra made it possible to identify a number of features and limitations associated with the automated identification and differentiation of plant species. First and foremost, an obvious phenological dependence of differentiation was revealed. In accordance with the reflectance characteristic indicators, it was established that using only reflectance amplitude to create a single static “crop/weed” segregation model is not feasible. Due to the fact that the reflectance indicators within the species (wheat) drop by nearly a third (from 31.50 % to 22.50 %) by the time of heading, this indicates that the model’s efficiency for differentiation depends specifically on the phenological phase of monitoring. It was established that at the early stages of vegetation, young wheat can be easily distinguished, for example, from *Descurainia sophia* (mean difference of about 10 %), but in relation to *Echinochloa crus-galli*, a “spectral mimicry” effect may arise (mean RC difference = 1 %), which may be related to this plant’s belonging to the category of grass weeds. However, by the heading stage, wheat, according to its spectral profile (22.50 %), begins to overlap with *Descurainia sophia* (21 %) and may have similar spectral features to *Fallopia convolvulus* (26.50 %), while *Vicia hirsuta* (35 %) and *Echinochloa crus-galli* (30.50 %) contrast quite clearly with the crop. On the other hand, our data indicates that *Euphorbia virgata* can be consistently identified across all wheat development stages, owing to its anomalously high reflectance (45.50 %).

It was established that for interspecific identification, the use of standard broadband vegetation indices or multispectral cameras with wide spectral bands is ineffective due to the identical nature of their fundamental spectral contrast features. This is related to the similarity of the cellular structure of the leaves and the

chlorophyll content in the tissues of the studied plant samples, which influences the shape of the spectral curve.

Machine learning

The identified differences in hyperspectral characteristics between wheat and weed vegetation, as well as among individual weed species, formed the basis for constructing the classification model. The confusion matrix of the classification model demonstrates varying efficiency in recognising wheat and individual weed species based on hyperspectral features. The training model showed 84.9 % correctly classified samples. The model performed best with wheat—96.9 % correctly classified samples. The worst results were obtained for *Echinochloa crus-galli*, whose classification accuracy amounted to 68.4 % (Fig. 5, 6).

A

Actual classes	Total	Triticum aestivum	Euphorbia virgata	Descurainia sophia	Vicia hirsuta	Fallopia convolvulus	Echinochloa crus-...	No class
Triticum aestivum	87 (48.3%)	86 (98.9%)						1 (1.15%)
Euphorbia virgata	18 (10%)		4 (22.2%)		1 (5.56%)		2 (11.1%)	11 (61.1%)
Descurainia sophia	26 (14.4%)			22 (84.6%)			2 (7.69%)	2 (7.69%)
Vicia hirsuta	15 (8.33%)				8 (53.3%)		2 (13.3%)	5 (33.3%)
Fallopia convolvulus	16 (8.89%)		2 (12.5%)	4 (25%)		0		10 (62.5%)
Echinochloa crus-galli	18 (10%)		1 (5.56%)	1 (5.56%)	4 (22.2%)		3 (16.7%)	9 (50%)
# Predicted	180 (100%)	86 (47.8%)	7 (3.89%)	27 (15%)	13 (7.22%)	0	9 (5%)	38 (21.1%)
Correctly	123 (68.3%)							
Incorrectly	57 (31.7%)							
Precision		100%	57.1%	81.5%	61.5%	0%	33.3%	
Recall		98.9%	22.2%	84.6%	53.3%	0%	16.7%	
F-score		99.4%	32%	83%	57.1%	0%	22.2%	

B

Actual classes	Total	Triticum aestivum	Euphorbia virgata	Descurainia sophia	Vicia hirsuta	Fallopia convolvulus	Echinochloa crus-...	No class
Triticum aestivum	65 (18.2%)	63 (96.9%)						2 (3.08%)
Euphorbia virgata	48 (13.4%)		36 (75%)		2 (4.17%)			10 (20.8%)
Descurainia sophia	100 (27.9%)		1 (1%)	95 (95%)				4 (4%)
Vicia hirsuta	72 (20.1%)			1 (1.39%)	60 (83.3%)		1 (1.39%)	10 (13.9%)
Fallopia convolvulus	35 (9.78%)			2 (5.71%)		24 (68.6%)		9 (25.7%)
Echinochloa crus-galli	38 (10.6%)		2 (5.26%)	1 (2.63%)			26 (68.4%)	9 (23.7%)
# Predicted	358 (100%)	63 (17.6%)	39 (10.9%)	99 (27.7%)	62 (17.3%)	24 (6.7%)	27 (7.54%)	44 (12.3%)
Correctly	304 (84.9%)							
Incorrectly	54 (15.1%)							
Precision		100%	92.3%	96%	96.8%	100%	96.3%	
Recall		96.9%	75%	95%	83.3%	68.6%	68.4%	
F-score		98.4%	82.8%	95.5%	89.6%	81.4%	80%	

Figure 5. Confusion Matrix (A — Test, B — Train)

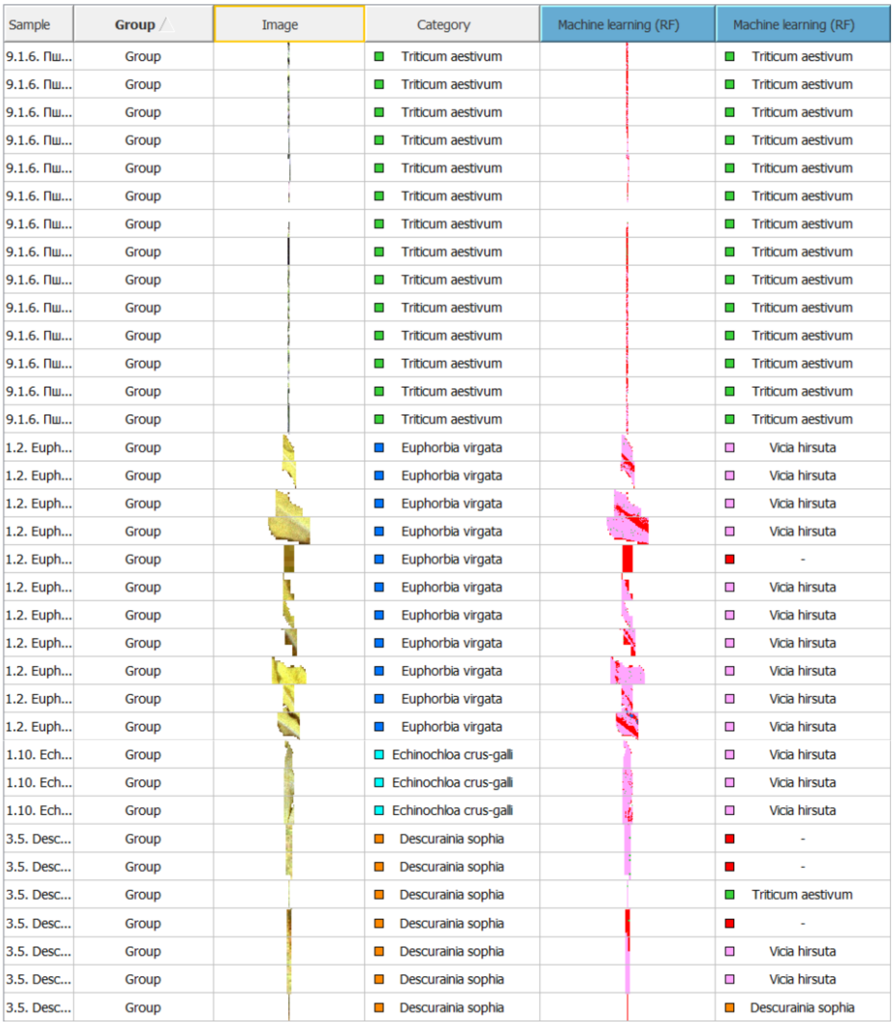

Sample	Group	Image	Category	Machine learning (RF)	Machine learning (RF)
9.1.6. Пш...	Group		Triticum aestivum		Triticum aestivum
9.1.6. Пш...	Group		Triticum aestivum		Triticum aestivum
9.1.6. Пш...	Group		Triticum aestivum		Triticum aestivum
9.1.6. Пш...	Group		Triticum aestivum		Triticum aestivum
9.1.6. Пш...	Group		Triticum aestivum		Triticum aestivum
9.1.6. Пш...	Group		Triticum aestivum		Triticum aestivum
9.1.6. Пш...	Group		Triticum aestivum		Triticum aestivum
9.1.6. Пш...	Group		Triticum aestivum		Triticum aestivum
9.1.6. Пш...	Group		Triticum aestivum		Triticum aestivum
9.1.6. Пш...	Group		Triticum aestivum		Triticum aestivum
9.1.6. Пш...	Group		Triticum aestivum		Triticum aestivum
9.1.6. Пш...	Group		Triticum aestivum		Triticum aestivum
9.1.6. Пш...	Group		Triticum aestivum		Triticum aestivum
9.1.6. Пш...	Group		Triticum aestivum		Triticum aestivum
1.2. Euph...	Group		Euphorbia virgata		Vicia hirsuta
1.2. Euph...	Group		Euphorbia virgata		Vicia hirsuta
1.2. Euph...	Group		Euphorbia virgata		Vicia hirsuta
1.2. Euph...	Group		Euphorbia virgata		Vicia hirsuta
1.2. Euph...	Group		Euphorbia virgata		-
1.2. Euph...	Group		Euphorbia virgata		Vicia hirsuta
1.2. Euph...	Group		Euphorbia virgata		Vicia hirsuta
1.2. Euph...	Group		Euphorbia virgata		Vicia hirsuta
1.2. Euph...	Group		Euphorbia virgata		Vicia hirsuta
1.2. Euph...	Group		Euphorbia virgata		Vicia hirsuta
1.2. Euph...	Group		Euphorbia virgata		Vicia hirsuta
1.10. Ech...	Group		Echinochloa crus-galli		Vicia hirsuta
1.10. Ech...	Group		Echinochloa crus-galli		Vicia hirsuta
1.10. Ech...	Group		Echinochloa crus-galli		Vicia hirsuta
3.5. Desc...	Group		Descurainia sophia		-
3.5. Desc...	Group		Descurainia sophia		-
3.5. Desc...	Group		Descurainia sophia		Triticum aestivum
3.5. Desc...	Group		Descurainia sophia		-
3.5. Desc...	Group		Descurainia sophia		Vicia hirsuta
3.5. Desc...	Group		Descurainia sophia		Vicia hirsuta
3.5. Desc...	Group		Descurainia sophia		Descurainia sophia

Figure 6. Classification results

The overall classification result of the test model was 68.3 % (123 correctly classified samples out of 180), while 31.7 % of samples were assigned by the model to incorrect classes. The highest classification accuracy was achieved for wheat, where 86 out of 87 samples were correctly identified, corresponding to a recall of 98.9 %. The virtually complete absence of false-positive results indicates the high spectral uniqueness of wheat compared to weed vegetation. This is likely associated with the relatively homogeneous anatomical structure of the leaves and coleoptile, the characteristic red edge shape, and the stable reflectance distribution in the near-infrared range. The best results among the weed plants were obtained for *Descurainia sophia*. The model correctly classified 22 out of 26 samples of this species, corresponding to a recall of 84.6 % and a precision of 81.5 %. The high classification accuracy may be due to the plant's specific morphology, with thin, filiform leaves and relatively low reflectance coefficients compared to other weeds. For *Vicia hirsuta*, the classification quality in the test set proved to be moderate: recall was 53.3 %, and precision — 61.5 %. The majority of samples were erroneously assigned to the "No class" category (33.3 %) and partially confused with *Echinochloa crus-galli*. *Vicia hirsuta* is characterised by a branching shoot structure and the presence of leaves with varying orientations, which leads to wide spectral dispersion. Low classification quality was observed for *Euphorbia virgata* and *Echinochloa crus-galli*. For *Euphorbia virgata*, recall reached only 22.2 %, despite relatively high reflectance coefficients. Most samples were erroneously classified as "No class" (61.1 %) or confused with *Echinochloa crus-galli*. A likely reason is the high variability of reflectance among the near-root zone, leaves, and stem of the plant. *Euphorbia virgata* has thick, succulent tissues, a developed system of vascular elements, and a heterogeneous distribution of moisture, which causes a significant change in spectral characteristics within a single plant. Because of a limited number of training examples, the model was unable to extract stable spectral features of this species. *Echinochloa crus-*

galli was also characterised by low recall (16.7 %) and precision (33.3 %). Some samples were erroneously assigned to *Vicia hirsuta* and the "No class" category. The reason may be the similarity of the spectral characteristics of *Echinochloa crus-galli* to wheat and other grass plants. As a representative of the *Poaceae* family, this species possesses linear leaves, similar mesophyll anatomy, and a close red edge position, which complicates class separation in multidimensional spectral space. For *Fallopia convolvulus*, the model failed to correctly classify any samples in the training data. Recall and precision were 0 %. The majority of objects were erroneously classified as "No class" or confused with *Descurainia sophia*. Such a result may be associated with the high spectral dissimilarity among different parts of the weed, the low reflectance intensity of the leaves, and an insufficient amount of training data. The high proportion of objects in the "No class" category (21.1 % of all predictions) indicates insufficient separability of certain spectral features and the presence of overlap between classes (Fig. 5).

According to the generalised statistical indicators of the algorithm (Tab. 3), the model demonstrates high potential in solving the basic task of classification and differentiation of crop and weed vegetation, which is confirmed by the Macro Accuracy value of 0.82214. In contrast, the decrease in this indicator on the test dataset (Macro Accuracy Test = 0.63123), the Log Loss metric (0.66778), and the cross-validation accuracy (CV Macro Accuracy = 0.72645) clearly reflect the natural complexity of working with the optical characteristics of biological objects. Such a change in the metric indicates spectral overlap between certain plant species within the "Weeds" categorical group, which, in turn, may be resolved in the future by expanding the database of spectral signatures and data for analysis, enabling more confident feature generalisation.

Table 3

Algorithm statistics

Algorithm name	Macro Accuracy	Log Loss	Log Loss Reduction	Micro Accuracy	Macro Accuracy Test	CV Macro Accuracy
Random Forest	0.82214	0.66778	0.61251	0.83544	0.63123	0.72645

Table 4 presents the accuracy and correlation metrics (MCC) for the algorithm used, confirming that the algorithm effectively copes with separating the crop plant from the weed background, with an average accuracy of 72.94 % in the test set.

Table 4

Quality assessment metrics for machine learning sample sets

Metrics	*Triticum aestivum*	*Euphorbia virgata*	*Descurainia sophia*	*Vicia hirsuta*	*Fallopia convolvulus*	*Echinochloa crus-galli*
Random Forest (Train)						
Binary Accuracy	96.92	75.00	95.00	83.33	68.57	68.42
Balanced Accuracy	98.45	87.47	97.46	91.63	84.30	84.19
MCC	0.984	0.831	0.954	0.897	0.827	0.811
Random Forest (Test)						
Binary Accuracy	98.85	22.22	84.62	53.33	0.00	16.67
Balanced Accuracy	99.45	61.07	92.25	76.60	50.00	58.29
MCC	0.994	0.355	0.829	0.572	-	0.234

Wheat demonstrated exceptional recognition stability, where binary accuracy rose from 96.92 % at the training stage to 98.85 % on the test set, and Balanced Accuracy from 98.45 % to 99.45 %. At the same time, the MCC value in the test set was determined to be 0.994, which confirms the uniqueness of the spectral characteristics of the crop, as well as the reliability of the model's performance in its identification. Regarding the recognition of specific weeds, it was also established that the model effectively distinguishes species with uniquely characteristic morphology. In particular, *Descurainia sophia* deserves special attention, maintaining high classification performance on the test data (Binary Accuracy=84.62, MCC=0.829), which demonstrates the algorithm's ability to capture and identify stable patterns of optical characteristics, particularly for fine-leaved plants. For the intra-class differentiation of a number of weed plants (*Euphorbia virgata*,

Vicia hirsuta, *Fallopia convolvulus*, *Echinochloa crus-galli*), classification proved to be a more challenging task, which was demonstrated by a decline in the metric indicators on the test set. However, this is substantiated by biological features. In particular, the signs of anatomical affinity of grass weeds (*Echinochloa crus-galli*) with the studied crop obviously create difficulties for separating these classes in the basic spectral space. Alongside this, a reason may be the high internal heterogeneity, forming a wide dispersion of spectral values (multidirectional leaf orientation in *Vicia hirsuta*, uneven moisture distribution in the dense tissues of *Euphorbia virgata*). It was found that these variability features were actually insufficient to form a single universal set of rules for recognising these species within the group (Tab. 4).

Thus, the results show that hyperspectral analysis possesses high efficiency for recognising wheat and certain weed species; however, classification accuracy depends on the spectral homogeneity of the plant and the degree of overlap of its spectral characteristics with those of other species. Species with unique morphology and a stable spectral profile are classified most successfully, whereas plants with complex shoot morphology or similar tissue anatomy exhibit a higher level of classification errors.

Conclusion

The conducted analysis of spectral characteristics and machine learning results allowed for drawing principal conclusions regarding the prospects for automated species-level identification of crop and weed vegetation. It was established that hyperspectral sensing, in combination with the Random Forest ML algorithm, proved the high validity and success of crop vegetation segregation from the weed background, which addresses the main task of precision agriculture. The spectral stability of spring wheat enables the model to identify it with high accuracy (MCC=0.994). A dependence of recognition on the anatomical specificity of the plant and the phenological phase was also revealed; in particular, the morphological features of *Descurainia sophia* form stable patterns, allowing the algorithm to perform accurate identification. However, the spectral proximity of green biomass across the broad VIS-NIR range (500–780 nm) requires the expansion of the spectral database for the application of standard metrics. The attempt to separate complex weed species from one another, such as grass weeds or species with high tissue heterogeneity, manifests in a decrease in the predictive ability of the model, which is an obvious consequence of their intraspecific variability and, as a result, spectral overlaps. Moreover, the application of the RF algorithm, with an overall accuracy of 72.94 % on the test set, formed a reliable basis for performing basic “crop-weed” classification. To transition toward high-precision multiclass identification and intra-group weed differentiation, it is essential to extract narrow-band spectral markers, balance complex training datasets, and integrate textural features, thereby compensating for optical overlaps. In conclusion, the developed classification model demonstrates potential for integration into site-specific herbicide application systems by solving the task of reliable crop preservation, thereby providing a foundation for further optimisation of machine learning algorithms in intra-class weed differentiation.

Funding

This research is funded by the Science Committee of the Ministry of Science and Higher Education of the Republic of Kazakhstan (Grant No. AP26197815 “Development of an intelligent monitoring system for wheat agrocenosis through the synergistic integration of hyperspectral imaging and LiDAR using computer vision technologies”.

Conflict of Interest

Authors declare no conflict of interest.

Author contribution

The manuscript was written through contributions of all authors. All authors have given approval to the final version of the manuscript: **Ualiyeva R.M.** — conceptualization, formal analysis, supervision, editing; **Kaverina M.M.** — methodology, investigation, analysis, writing draft; **Osipova A.V.** — methodology, investigation, analysis, writing draft; **Koppaev A.E.** — research, data collection; **Chaizabekova M.A.** — research, data collection; **Zhangazin S.B.** — data curation, analysis.

References

1 Kettlewell, P., Byrne, R., & Jeffery, S. (2023). Wheat area expansion into northern higher latitudes and global food security. *Agriculture, Ecosystems & Environment, 351*, 108499. https://doi.org/10.1016/j.agee.2023.108499

2 Gooding, M.J. (2023). Wheat. *ICC Handbook of 21st Century Cereal Science and Technology*, 121–130. Academic Press https://doi.org/10.1016/B978-0-323-95295-8.00027-7

3 Mensah, B., Rai, N., Betitame, K., & Sun, X. (2024). Advances in weed identification using hyperspectral imaging: A comprehensive review of platform sensors and deep learning techniques. *Journal of Agriculture and Food Research, 18*, 101388. https://doi.org/10.1016/j.jafr.2024.101388

4 Liu, T., Zhao, Y., Wang, H., Wu, W., Yang, T., Zhang, W., Zhu, S., Sun, C., & Yao, Z. (2024). Harnessing UAVs and deep learning for accurate grass weed detection in wheat fields: a study on biomass and yield implications. *Plant Methods, 20*. https://doi.org/10.1186/s13007-024-01272-6

5 Zhang, Y., Wang, M., Zhao, D., Liu, C., & Liu, Z. (2023). Early weed identification based on deep learning: A review. *Smart Agricultural Technology, 3*,100123. https://doi.org/10.1016/j.atech.2022.100123

6 Che'Ya, N.N., Dunwoody, E., & Gupta, M. (2021). Assessment of Weed Classification Using Hyperspectral Reflectance and Optimal Multispectral UAV Imagery. *Agronomy, 11*(7), 1435. https://doi.org/10.3390/agronomy11071435

7 FAO (Food and Agriculture Organization of the United Nations). *www.fao.org.* Retrieved from https://www.fao.org/home/en/

8 Danilov, R., Kremneva, O., & Pachkin, A. (2023). Identification of the Spectral Patterns of Cultivated Plants and Weeds: Hyperspectral Vegetation Indices. *Agronomy, 13*(3), 859. https://doi.org/10.3390/agronomy13030859

9 Pantazi, X. -E., Moshou, D., & Bravo, C. (2016). Active learning system for weed species recognition based on hyperspectral sensing. *Biosystems Engineering, 146*, 193–202. https://doi.org/10.1016/j.biosystemseng.2016.01.014

10 Rai, N., Zhang, Y., Ram, B.G., Schumacher, L., Yellavajjala, R.K., Bajwa, S., & Sun, X. (2023). Applications of deep learning in precision weed management: A review. *Computers and Electronics in Agriculture, 206*, 107698. https://doi.org/10.1016/j.compag.2023.107698

11 Ronay, I., Lati, R.N., & Kizel, F. (2024). Weed Species Identification: Acquisition, Feature Analysis, and Evaluation of a Hyperspectral and RGB Dataset with Labeled Data. *Remote Sensing, 16*(15), 2808. https://doi.org/10.3390/rs16152808

12 Luo, T., Zhao, J., Gu, Y., Zhang, S., Qiao, X., Tian, W., & Han, Y. (2023). Classification of weed seeds based on visual images and deep learning. *Information Processing in Agriculture, 10*(1), 40–51. https://doi.org/10.1016/j.inpa.2021.10.002

13 Vasileiou, M., Kyrgiakos, L.S., Kleisiari, C., Kleftodimos, G., Vlontzos, G., Belhouchette, H., & Pardalos, P.M. (2024). Transforming weed management in sustainable agriculture with artificial intelligence: A systematic literature review towards weed identification and deep learning. *Crop Protection, 176*, 106522. https://doi.org/10.1016/j.cropro.2023.106522

14 Ram, B.G., Oduor, P., Igathinathane, C., Howatt, K., & Sun, X. (2024). A systematic review of hyperspectral imaging in precision agriculture: Analysis of its current state and future prospects. *Computers and Electronics in Agriculture, 222*, 109037. https://doi.org/10.1016/j.compag.2024.109037

15 Mishra, P., Lohumi, S., Khan, H.A., & Nordon, A. (2020). Close-range hyperspectral imaging of whole plants for digital phenotyping: Recent applications and illumination correction approaches. *Computers and Electronics in Agriculture, 178*, 105780. https://doi.org/10.1016/j.compag.2020.105780

16 Kiani, S., & Jafari, A. (2012). Crop Detection and Positioning in the Field Using Discriminant Analysis and Neural Networks Based on Shape Features. *Journal of Agricultural Science and Technology, 14*, 755–765. https://dor.isc.ac/dor/20.1001.1.16807073.2012.14.4.10.6

17 Gutjahr, C., & Gerhards, R. (2010). Decision rules for site-specific weed management. *Precision Crop Protection — the Challenge and Use of Heterogeneity*, 223–239. Dordrecht: Springer Netherlands. https://doi.org/10.1007/978-90-481-9277-9_14

18 Li, Y., Al-Sarayreh, M., Irie, K., Hackell, D., Bourdot, G., Reis, M.M., & Ghamkhar, K. (2021). Identification of Weeds Based on Hyperspectral Imaging and Machine Learning. *Frontiers in Plant Science, 11*, 611622. https://doi.org/10.3389/fpls.2020.611622

19 Smith, A.M., & Blackshaw, R.E. (2003). Weed-Crop Discrimination Using Remote Sensing: A Detached Leaf Experiment. *Weed Technology, 17*(4), 811–820. https://doi.org/10.1614/WT02-179

20 Liu, B., Li, R., Li, H., You, G., Yan, S., & Tong, Q. (2019). Crop/Weed Discrimination Using a Field Imaging Spectrometer System. *Sensors, 19*(23), 5154. https://doi.org/10.3390/s19235154

21 Wieme, J., Mollazade, K., Malounas, I., Zude-Sasse, M., Zhao, M., Gowen, A., Argyropoulos, D., Fountas, S., & Van Beek, J. (2022). Application of hyperspectral imaging systems and artificial intelligence for quality assessment of fruit, vegetables and mushrooms: A review. *J Wieme, Biosystems Engineering, 222*, 156–176. https://doi.org/10.1016/j.biosystemseng.2022.07.013

22 Moghimi, A., Yang, C., & Anderson, J.A. (2020). Aerial hyperspectral imagery and deep neural networks for high-throughput yield phenotyping in wheat. *Computers and Electronics in Agriculture, 172*, 105299. https://doi.org/10.1016/j.compag.2020.105299

23 Cheng, Y., He, W., Zheng, F., Zhang, F., Bai, B., Sun, N., Wang, W., & Geng, H. (2025). Genome-wide association study of wheat chlorophyll dynamics under drought and irrigation using multispectral UAV phenotyping. *Frontiers in Plant Science, 16*, 1607862. https://doi.org/10.3389/fpls.2025.1607862

24 Railyan, V.Ya., & Korobov, R.M. (1993). Red edge structure of canopy reflectance spectra of triticale. *Remote Sensing of Environment, 46*(2), 173–182. https://doi.org/10.1016/0034-4257(93)90093-D

25 Filella, I., & Penuelas, J. (1994). The red edge position and shape as indicators of plant chlorophyll content, biomass and hydric status. *International Journal of Remote Sensing, 15*(7), 1459–1470. https://doi.org/10.1080/01431169408954177

26 Horler, D.N.H., Dockray, M., Barber, J., & Barringer, A.R. (1983). Red edge measurements for remotely sensing plant chlorophyll content. *Advances in Space Research, 3*(2), 273–277. https://doi.org/10.1016/0273-1177(83)90130-8

27 Mutanga, O., & Skidmore, A.K. (2007). Red edge shift and biochemical content in grass canopies. *ISPRS Journal of Photogrammetry and Remote Sensing, 62*(1), 34–42. https://doi.org/10.1016/j.isprsjprs.2007.02.001

28 Clevers, J.G., & Gitelson, A. (2013). Remote estimation of crop and grass chlorophyll and nitrogen content using red-edge bands on Sentinel-2 and -3. *International Journal of Applied Earth Observation and Geoinformation, 23*, 344–351. https://doi.org/10.1016/j.jag.2012.10.008

Р.М. Уалиева, М.М. Каверина, А.В. Осипова, А.Е. Коппаев,
М.А. Чайзабекова, С.Б. Жангазин

Машиналық оқыту алгоритмдерін пайдалану арқылы гиперспектралды деректер негізінде бидай егістіктеріндегі дақыл және арамшөп өсімдіктерін түрлік анықтау

Алғаш рет Қазақстанның солтүстік-шығысындағы агроценоздар жағдайында дақыл өсімдіктер мен арамшөптерді көпкласты жіктеу кезінде машиналық оқыту алгоритмдерінің (Random Forest мысалында) шектеулеріне өсімдік тіндерінің морфологиялық-анатомиялық қасиеттері мен тану тиімділігі арасындағы өзара байланысты негізге ала отырып кешенді бағалау жүргізілді. Жұмыста гиперспектралды белгілер кеңістігінде кластардың оптикалық қабаттасуына әкелетін биологиялық табиғаттағы негізгі факторлар негізделді. Деректер VIS-NIR диапазонында гиперспектралды сенсор көмегімен жиналды. Спектрлік профильдерді талдау бас компоненттер әдісі арқылы дисперсия құрылымын бағалау және шағылысу спектрлерін құру негізінде жүзеге асырылды. Алынған деректерді жіктеу Random Forest алгоритмі арқылы орындалды. Зерттеу нысандары ретінде әртүрлі фенофазалардағы жаздық бидай (*Triticum aestivum*) егістіктері және арамшөптердің бес басым түрі (*Euphorbia virgata, Descurainia sophia, Vicia hirsuta, Fallopia convolvulus, Echinochloa crus-galli*) таңдалды. Алгоритм «дақыл-арамшөп» деңгейінде объектілерді тиімді ажыратып, тест деректерінде 72,94 % жалпы жіктеу дәлдігін көрсетті. Бидайды анықтау дәлдігі жоғары деңгейде (MCC=0.994) болып, бұл оның спектрлік тұрақтылығы мен red edge (680-730 нм) аймағындағы айқын белгілермен түсіндіріледі. Арамшөптерді түрлік деңгейде ажырату дәлдігінің төмендеуі олардың анатомиялық ерекшеліктерімен байланысты екені анықталды: *Euphorbia virgata*-ның қалың кутикулярлық қабаттары жоғары шағылысу мәндерін тудырады; *Vicia hirsuta*-ның күрделі морфологиялық құрылымы спектрлік ауытқуды күшейтеді; ал *Echinochloa crus-galli* мезофилінің дәнді дақылдарға ұқсас құрылымы кейбір спектрлік белгілердің оптикалық қабаттасуына әкеледі. Осылайша, әзірленген модель мәдени өсімдіктер мен арамшөптерді сенімді ажыратып, дәлме-дәл егіншілік технологиялары мен агрохимикаттарды мақсатты қолдану жүйелерін енгізуге негіз қалайды.

Кілт сөздер: гиперспектралды зондтау, жаздық бидай, арамшөптер, машиналық оқыту, түрлік анықтау, түрлерді ажырату, спектрлік қолтаңбалар, дәлме-дәл егіншілік.

Р.М. Уалиева, М.М. Каверина, А.В. Осипова, А.Е. Коппаев,
М.А. Чайзабекова, С.Б. Жангазин

Видовая идентификация культурной и сорной растительности в посевах пшеницы по гиперспектральным данным с использованием алгоритмов машинного обучения

Впервые проведена комплексная оценка ограничений ML-алгоритмов (на примере Random Forest) при мультиклассовой идентификации культурных растений и сорняков в агроценозах северо-востока Казахстана на основе установления взаимосвязи между морфолого-анатомическими свойствами растительных тканей и эффективностью распознавания алгоритмом машинного обучения. В работе обоснованы основные причины биологической природы, проявляющиеся в оптическом перекрытии классов в пространстве гиперспектральных признаков. Сбор данных проведен гиперспектральным сенсором в диапазоне VIS-NIR. Анализ спектральных профилей проведен на основе оценки распределения дисперсии методом главных компонент и построения кривых отражения. Классификация извлеченных данных выполнена на основе алгоритма Random Forest. В качестве объектов исследования выбраны

посевы яровой пшеницы (*Triticum aestivum*) на разных фенофазах и пять доминирующих видов сорной растительности (*Euphorbia virgata, Descurainia sophia, Vicia hirsuta, Fallopia convolvulus, Echinochloa crus-galli*). Алгоритм показал эффективность сегрегации по типу «культура-сорняк» с общей точностью классификации на тестовых данных 72,94 %. Выявлена высокая точность идентификации пшеницы (MCC=0,994) за счет спектральной стабильности и выраженных признаков red edge (680–730 нм). Установлено, что снижение точности при попытке внутриклассового разделения сорняков связано с анатомическими особенностями отдельных представителей (плотные кутикулярные слои *Euphorbia virgata* приводят к проявлению высоких показателей отражения по сравнению с остальными видами; сложная архитектура *Vicia hirsuta* вызывает критический спектральный разброс; сходство строения мезофилла *Echinochloa crus-galli* с культурой, учитывая его принадлежность к злаковым, приводит к частичному оптическому слиянию с некоторыми признаками). Таким образом, разработанная модель позволяет решить главную задачу — обеспечение надежной дифференциации культурной растительности от сорного фона, что является важным условием для формирования технологического базиса точного земледелия и внедрения систем таргетного применения агрохимикатов.

Ключевые слова: гиперспектральное зондирование, яровая пшеница, сорная растительность, машинное обучение, видовая идентификация, видовая дифференциация, спектральные сигнатуры, точное земледелие.

Information about the authors

Ualiyeva Rimma Meyramovna — PhD, Professor, Department of Biology and Ecology, Toraighyrov University, Pavlodar, Kazakhstan; e-mail: ualiyeva.r@gmail.com; ORCID: https://orcid.org/0000-0003-3551-5007

Kaverina Mariya Mikhailovna — Corresponding author, Junior Researcher, Department of Biology and Ecology, Toraighyrov University, Pavlodar, Kazakhstan; e-mail: k.ma96@mail.ru; ORCID: https://orcid.org/0000-0002-3838-7656

Osipova Anastasiya Vyacheslavovna — Master's student, Department of Biology and Ecology, Toraighyrov University, Pavlodar, Kazakhstan; e-mail: aanastasiyaaa@internet.ruж ORCID: https://orcid.org/0000-0002-3947-5252

Koppaev Altynbek Erkebulanovich — Master's student, Department of Biology and Ecology, Toraighyrov University, Pavlodar, Kazakhstan; e-mail: altynbek_koppaev@mail.ru; ORCID: https://orcid.org/0009-0004-0476-9017

Chaizabekova Meruyert Askarovna — Master of Natural Sciences, Department of Biology and Ecology, Toraighyrov University, Pavlodar, Kazakhstan; e-mail: meruyert130797@gmail.com; ORCID: https://orcid.org/0009-0004-0468-956X

Zhangazin Sayan Berikovich — PhD, Associate Professor, Acting Deputy Director for Research at the Institute of Natural Sciences, Eurasian National University named after L.N. Gumilyov, Astana, Kazakhstan; e-mail: sayanzhangazin@gmail.com; ORCID: https://orcid.org/0000-0002-5813-8331

How to Cite: Yertayeva, T.G., Belgibay, S.D., Artykbayeva, D.E., Baikarayev, Z.M. & Iksat, N.N. (2026). Antioxidant defense in plants during RNA virus infection: the role of key enzymes. *Fundamental and Experimental Biology*, 31, 3 (123), 152-169. https://doi.org/10.31489/2026FEB3/152-169

Review Article

https://doi.org/10.31489/2026FEB3/152-169

UDC 57.577 Received: 12.12.2025 | Accepted: 18.02.2026 | Published online: 30.09.2026

T.G. Yertayeva, S.D. Belgibay, D.E. Artykbayeva, Z.M. Baikarayev, N.N. Iksat*

Rustem Omarov Plant Biotechnology Laboratory, L.N. Gumilyov Eurasian National University, Astana, Kazakhstan
**Corresponding author: nurguliksat@gmail.com*

Antioxidant defense in plants during RNA virus infection: the role of key enzymes

In recent decades, the issue of crop resistance to biotic stressors has gained particular relevance in the context of global food security. Among biotic factors, viral infections occupy a special position, causing significant yield losses and disrupting physiological processes in plants. RNA viruses are characterized by high adaptability and the ability to effectively reprogram host cellular metabolism, a process accompanied by disruption of redox homeostasis. The generation of reactive oxygen species (ROS) constitutes one of the key events in this process and is characterized by functional duality: ROS act as signaling molecules that initiate defense responses, whereas their excessive accumulation leads to damage to cellular components. Alterations in redox homeostasis are accompanied by activation of the plant antioxidant system, which encompasses both enzymatic and non-enzymatic defense mechanisms. Despite considerable advances in the study of redox processes in plants, the interplay between redox regulation mechanisms and antioxidant system functioning under viral infection remains insufficiently characterized and requires further investigation. In this regard, the aim of the present review is to systematize and analyze current knowledge of the roles of reactive oxygen species and key antioxidant enzymes in the regulation of immune responses in plants infected with RNA viruses.

Keywords: oxidative stress, plant antioxidant system, viral infection, plant immunity.

Introduction

In recent decades, the issue of crop resistance to biotic stressors has become particularly relevant in the context of ensuring global food security. Among biotic factors, viral infections occupy a special place, causing significant yield losses and disrupting plant physiological processes. RNA viruses are characterised by high adaptability and the ability to effectively modify the host's cellular metabolism, which is accompanied by a disruption of redox homeostasis. The generation of reactive oxygen species (ROS) represents one of the key stages of this process, characterised by functional duality: on the one hand, ROS act as signalling molecules that initiate defence responses; on the other, their excessive accumulation leads to damage to cellular components. Changes in redox homeostasis are accompanied by the activation of the plant antioxidant system, which includes both enzymatic and non-enzymatic defence mechanisms. Despite significant progress in the study of redox processes in plants, the integration of redox regulation mechanisms and the functioning of the antioxidant system under conditions of viral infection remains insufficiently described to date and requires further analysis. In this regard, the aim of this review is to systematise and analyse current understanding of the role of ROS and key enzymes of the antioxidant system in the regulation of the plant immune response during RNA virus infection.

1. Generation of Reactive Oxygen Species during RNA Virus Infection.

Reactive oxygen species (ROS) are highly reactive oxygen-containing molecules, including free radicals such as the superoxide anion ($O_2^{-}\cdot$), the hydroxyl radical ($\cdot OH$), and hydrogen peroxide (H_2O_2). The compounds listed above are natural products of cellular metabolism and are formed predominantly in the mitochondria during the functioning of the electron transport chain [1]. Under physiological conditions, ROS act as signalling molecules performing regulatory functions in the control of cell proliferation and differentiation, as well as in the activation of the immune response via redox-dependent signalling pathways [2].

However, excessive accumulation of ROS within the cell leads to the development of oxidative stress, accompanied by a disruption of redox homeostasis. Under these conditions, ROS actively interact with major

cellular macromolecules—lipids, proteins and nucleic acids—causing lipid peroxidation, oxidative modification of proteins and damage to genetic material, ultimately leading to the destabilisation of cell membranes, disruption of organelle functions and cell death [3].

Oxidative stress can be induced both by abiotic factors, including extreme temperatures, ultraviolet radiation and exposure to toxic compounds, and by biotic factors, such as bacterial, fungal or viral infections [4, 5]. In viral infections, changes in redox homeostasis are caused not only by the damaging effect but also by the functional reorganisation of cellular processes aimed at ensuring viral replication. In particular, RNA viruses actively interact with the cell's membrane structures, forming replication complexes on the surface of mitochondria, the endoplasmic reticulum and other organelles, which is accompanied by an increase in ROS production. These replication complexes are virus-induced membrane structures formed by the recruitment of intracellular organelles and serving as a platform for viral RNA synthesis [6, 7]. In plant RNA viruses, their organisation has specific features: in *Tobacco mosaic virus* (TMV), replication is associated with the membranes of the endoplasmic reticulum, in *Tomato bushy stunt virus* (TBSV)—with the membranes of peroxisomes and mitochondria, where invaginations form, creating isolated microcompartments, whereas *in Cucumber mosaic virus* (CMV) intracellular membrane structures and chloroplasts are involved in the process. Such a spatial organisation of replication is inevitably accompanied by disruption of the function of the relevant organelles and alterations in electron transport, leading to oxidative stress [8, 9].

An additional contribution to the excessive accumulation of ROS is made by the activation of NADPH oxidases and changes in the functioning of mitochondria and chloroplasts, which enhance the formation of O_2^-. In this context, ROS act not only as a by-product but also as a regulatory factor involved in the activation of signalling pathways that contribute to the maintenance of viral replication. RNA viruses are characterised by their ability to maintain ROS levels within a functionally significant range, as a moderate increase in their concentration facilitates the viral life cycle, whereas excessive accumulation is accompanied by the development of oxidative damage to the cell and a limitation of the infectious process.

The balance between ROS formation and neutralisation under conditions of viral infection is determined by the functional state of the cell's antioxidant system—an evolutionarily conserved defence mechanism capable of counteracting oxidative stress [6, 10].

2. Plant antioxidant defense system.

Under stress conditions such as viral infection, the maintenance of redox homeostasis in plants is ensured by the coordinated functioning of the antioxidant defence system (Fig. 1). Antioxidants are molecules capable of inhibiting free radical reactions, thereby preventing the development of cellular damage [11].

This system consists of enzymatic and non-enzymatic components (Fig. 2), which are localised in various cellular structures and regulated in response to the physiological state of the cell. In this context, antioxidant defence is formed as an integrated system that functions in a coordinated manner and mutually enhances the effectiveness of ROS detoxification during viral infections.

The enzymatic components of the plant antioxidant system (including superoxide dismutase, catalases, ascorbate peroxidase and glutathione reductase) are regarded as the main component of primary antioxidant defence, ensuring rapid enzymatic detoxification of ROS induced by viral infection.

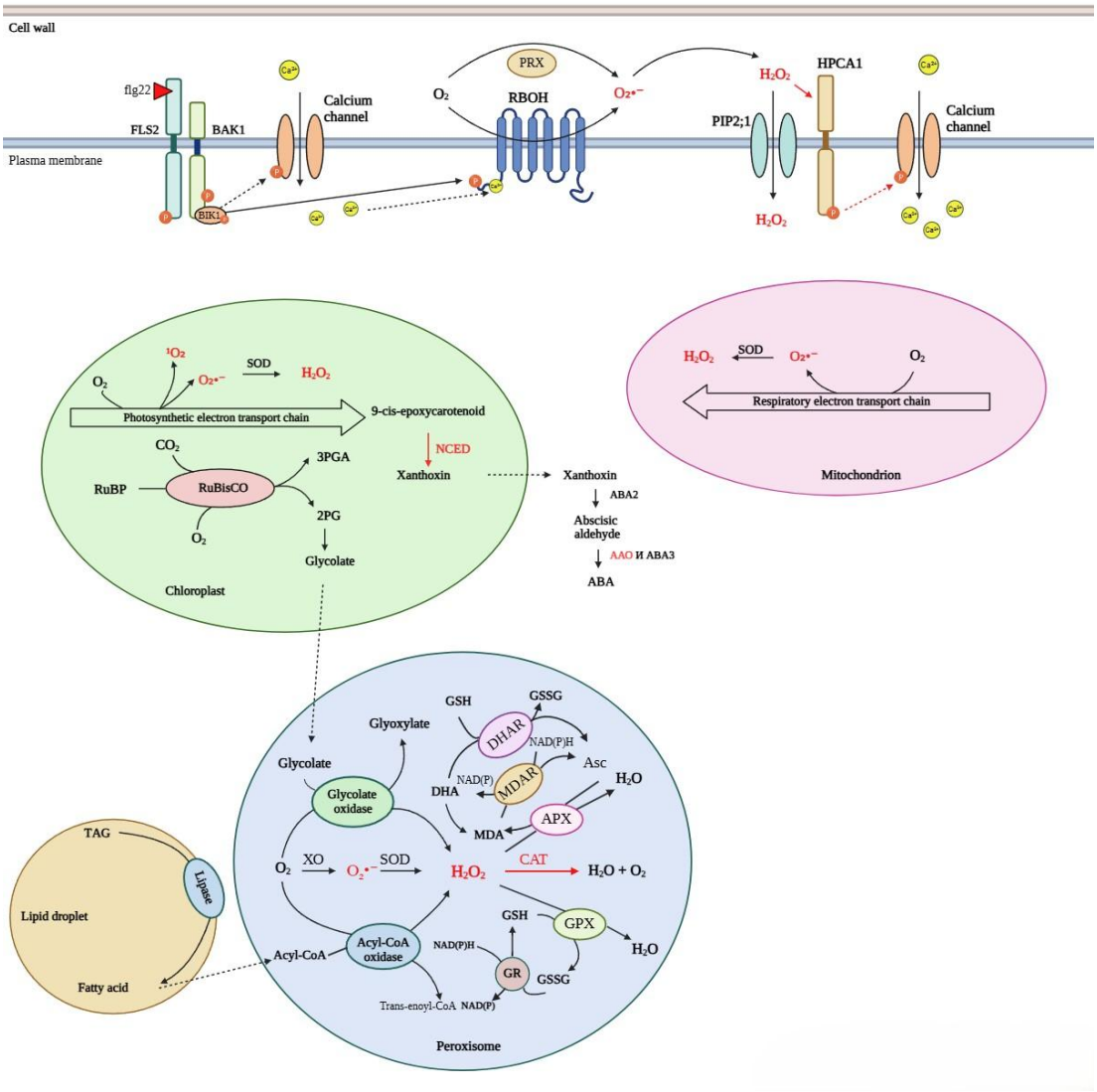

Figure 1. Plant antioxidant system.

Note. Compiled by the authors.

Non-enzymatic antioxidants (ascorbate, glutathione, tocopherols, carotenoids and phenolic compounds) constitute a pool of low-molecular-weight redox-active compounds that primarily perform buffering, reducing and stabilising functions in maintaining cellular redox [12–14].

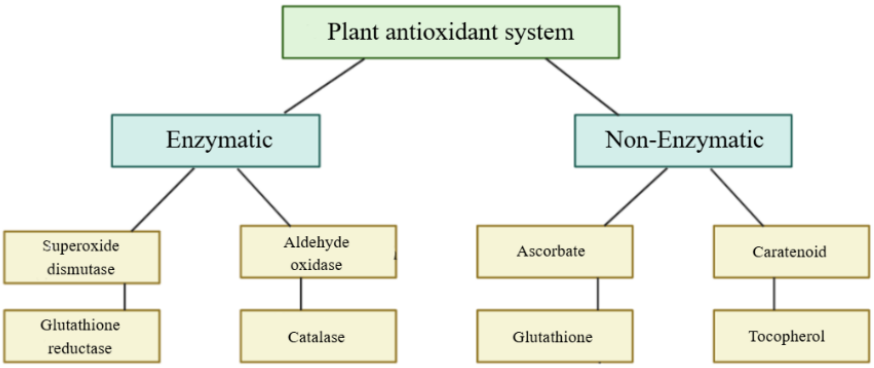

Figure 2. Enzymatic and non-enzymatic components of the antioxidant system

2.1 Non-enzymatic Antioxidants

Non-enzymatic antioxidants are low-molecular-weight compounds that play an important role in neutralising free radicals by donating electrons or hydrogen atoms. These compounds are divided into two categories: hydrophilic antioxidants, such as glutathione, ascorbate and phenolic compounds, and lipophilic membrane antioxidants, which include carotenoids. Among hydrophilic antioxidants, ascorbate (AsA) occupies a special place—one of the key water-soluble antioxidants in plants, playing an important role in maintaining the redox balance during viral infection. The redox state of ascorbate, regulated by the activity of ascorbate oxidase (AO), determines the apoplast's ability to participate in signal transduction associated with the activation of the plant's defence responses during a viral attack. In this context, AsA is involved not only in the neutralisation of ROS but also in the signalling regulation of the immune response. The biosynthesis of ascorbate is predominantly carried out via the Smirnov–Wheeler pathway, where the final step is the oxidation of L- galactono-1,4-lactone in the mitochondria. Due to its structure, AsA is capable of directly neutralising ROS, including $O_2^{-}\cdot$ and $\cdot OH$, and also acts as an electron donor for ascorbate peroxidase (APX) during the reduction of H_2O_2 [15, 16]. AsA functions as a redox buffer, coordinating antioxidant defence and immune signalling in infected cells [17]. Alongside ascorbate, glutathione (GSH)—a low-molecular-weight tripeptide—is one of the main antioxidants in plant cells during viral infection. Upon viral entry, there is enhanced ROS generation, accompanied by the accumulation of GSH in the cytosol, chloroplasts and mitochondria [18]. It is important to note that GSH participates in the ascorbate–glutathione cycle, ensuring the reduction of dehydroascorbate to ascorbate via the enzyme dehydroascorbate reductase (DHAR) [19, 20]. In this context, the GSH/GSSG ratio serves as an indicator of the cell's redox status and regulates the activation of defence response genes. Consequently, glutathione plays a dual role—as an antioxidant and a signalling molecule—ensuring thiol redox homeostasis during viral [21–23]. Regarding lipid lipophilic antioxidants, carotenoids belong to the group of isoprenoid compounds, characterized by significant structural diversity [24]. They consist of eight isoprene units, with most carotenoids deriving from the linear tetraterpene phytoene. These low-molecular-weight metabolites protect the photosynthetic apparatus by preventing the formation of reactive oxygen species through the quenching of excited chlorophyll and triplet sensitizers, whilst simultaneously reducing the level of lipid peroxidation [25].

Non-enzymatic antioxidants include functionally diverse redox-active compounds involved in maintaining cellular homeostasis. Individual representatives differ in their localisation, mechanisms of action and degree of involvement in redox regulation. A comparative characterisation of the main components of the plant antioxidant system and their roles in viral infection is presented in Table 1.

Table 1

The importance of non-enzymatic antioxidants in antiviral response

Antioxidant	Localization	Role in Antiviral Response (RNA Viruses)	Sources
Ascorbate (Vitamin C)	Cytosol, chloroplasts, mitochondria; apoplast	Maintains redox homeostasis, participates in ROS detoxification, and enhances resistance to Turnip mosaic virus (TuMV) and Cucumber mosaic virus (CMV).	[26]
Glutathione (GSH)	Cytosol, nucleus, mitochondria, chloroplasts; apoplast/cell wall	Supports the ascorbate-glutathione cycle and influences HR and resistance to Potato virus Y (PVY) and TuMV.	[27]
Carotenoids	Chloroplast thylakoid membranes; plastoglobules	During virus-induced chloroplast dysfunction and chlorosis, carotenoids are expected to play a crucial role in controlling $^1O_2$.	[28]

2.2 Enzymatic antioxidants

SOD acts as a key enzyme in the first line of antioxidant defence; however, its reaction product, H_2O_2, is itself a toxic compound capable of converting into highly reactive OH in the presence of Fe^{2+} via the Fenton reaction. The detoxification of H_2O_2 is the next essential stage in cellular antioxidant defence. This func-

tion is performed by two other first-line defence enzymes, CAT and GR, which, together with SOD, form a coordinated enzymatic system for the neutralisation of ROS [29].

2.2.1 Superoxide dismutase

Superoxide dismutase (SOD) is a metal-containing enzyme and one of the most effective components of the antioxidant defence system of plant cells against ROS. SOD catalyses the dismutation of $O_2^{-}\cdot$ to form H_2O_2 and O_2 (Fig. 1) [30].

Depending on the metal cofactor, SOD exists in several isoforms: Cu/Zn-SOD, Mn-SOD and Fe-SOD. The Cu/Zn-SOD isoform is localised in the cytoplasm, peroxisomes, chloroplasts and apoplast, whilst Fe-SOD is found in plant chloroplasts, and Mn-SOD is localised in the mitochondrial matrix and in peroxisomes [31].

Sequence alignment, as well as structural and evolutionary studies, have revealed homology between Mn-SOD and Fe-SOD, whereas Cu/Zn-SOD has been found to be distinctly related to either Mn- or Fe-SOD [32]. Cu/Zn-SOD is activated either via a CCS-dependent pathway, which requires the covalent binding of a Cu chaperone to the Cu^{2+} ion, or via a CCS- independent mechanism [33]. The presence of two activation pathways is of significant physiological importance, as it ensures the preservation of the enzyme's catalytic activity even if one of the mechanisms is disrupted, thereby maintaining the functionality of the antioxidant system and the cell's resistance to oxidative stress.

The regulation of SOD under conditions of viral infection is characterised by multi-level modification, affecting both post-translational processes and the subcellular localisation of the enzyme. It has been established that infection with the bamboo mosaic virus (BaMV) in *Brachypodium distachyon* and *Nicotiana benthamiana* is accompanied by the accumulation of the full-length Cu/Zn-SOD precursor protein (PrNbCSD2) in the cytoplasm. This effect is attributed to the virus disrupting the processing of the PrNbCSD2 transit peptide, which impedes its normal function. The consequence is an excessive accumulation of H_2O_2 in infected cells, associated with the development of chlorotic mosaic symptoms [34].

However, the neutralisation of ROS is not limited to the action of a single enzyme: the product of the reaction catalysed by SOD, hydrogen peroxide, is itself a toxic compound and requires further decomposition. This function is performed by catalase, which catalyses the dismutation of H_2O_2 into water and molecular oxygen, thereby ensuring the cell's antioxidant response [35].

2.2.2 Catalase

Catalase (CAT) catalyses a two-step reaction for the decomposition of hydrogen peroxide and is localised in peroxisomes. In the first step, H_2O_2 oxidises the iron (Fe^{2+}) ion in the active site of CAT to form iron peroxide. It is known that at low concentrations of H_2O_2, the enzyme can remain in this intermediate state (compound I). However, at higher concentrations of H_2O_2, it acts as a reducing agent for compound I, thereby regenerating the enzyme and releasing water and oxygen [36].

$$\text{CAT-Fe-OH} + H_2O_2 \rightarrow \text{CAT-Fe-OOH} + H_2O \text{ (Stage 1)} \quad (1)$$

$$\text{CAT-Fe-OOH} + H_2O_2 \rightarrow \text{CAT-Fe-OH} + H_2O + O_2 \text{ (Stage 2)} \quad (2)$$

The sources of H_2O_2 in plant cells are chloroplasts, mitochondria and peroxisomes. In all these compartments, H_2O_2 is synthesised following the dismutation of $O_2^{-}\cdot$ by SOD. Furthermore, H_2O_2 is generated by glycolate oxidase in peroxisomes [37] (Fig. 1).

Three distinct classes I, II and III have been identified based on *Nicotiana tabacum* genes. Class I CATs play a role in photosynthetic tissues and are involved in neutralising H_2O_2, which is produced during photosynthesis. Class II predominates in vascular tissues and lignification in response to ABA and during ageing, whereas class III is expressed in seeds and reproductive tissues, and its activity is high during fatty acid catabolism in the glyoxylate cycle in glyoxysomes. Three CAT isoforms (CAT1, CAT2, CAT3) have been identified in *Zea mays*. These isoforms are identical in their coding region and differ only in variable intron segments. Furthermore, the promoter sequence also differs in these different isoforms. The *Arabidopsis* genome also contains three CAT genes [38]. Recently, seven CAT genes were identified in *Gossypium* using genome-wide association studies (GWAS) [39]. The number of CAT genes varies among different plants; for example, there are three in *O. sativa*, *C. pepo* and *Cucumis sativus*, two in *Hordeum spp*. and one in *Ipomoea batatas*, *Ricinus communis* and *S. lycopersicum* [40].

Viral infections have mixed effects on catalase activity; however, in most cases, a functional suppression is observed. For example, in *Arabidopsis thaliana*, upon infection, the 2b protein interacts with the

CAT3 isoenzyme, inhibiting its activity and causing the development of necrosis [41]. A similar effect is observed during infection with maize chlorotic mottle virus (MCMV) in *Zea mays*, where the P31 protein binds to ZmCAT1, suppressing its activity, which is accompanied by the accumulation of H_2O_2, suppression of PR genes (ZmPR3, ZmPR4, ZmPR5) and enhanced viral replication; additional suppression of catalase isoform expression further enhances this effect [42]. Furthermore, the involvement of the PVX viral protein HC-Pro triggers a more intensive generation of H_2O_2 compared to mutant forms. This suggests that viral factors play a direct role in regulating the cellular oxidative status.

CAT ensures the effective decomposition of H_2O_2 predominantly in peroxisomes however, in mitochondria, where CAT is virtually absent, the detoxification of H_2O_2 and lipid hydroperoxides is carried out by other enzymes. Maintaining redox homeostasis in these compartments requires the involvement of glutathione-dependent enzymes, the key one being GR.

2.2.3 Glutathione Reductase

Glutathione reductase (GR) is one of the main enzymes of the plant antioxidant system, involved in maintaining the balance between reduced (GSH) and oxidised (GSSG) glutathione. Maintaining this ratio is a critical condition for the effective neutralisation of ROS accumulating during viral infections. GR functions in close cooperation with other enzymes, in particular glutathione-S-transferases (GST), glutathione peroxidases (GPX) and γ-glutamyltransferases (GGT), providing comprehensive protection of cells against oxidative stress [43].

A review of the literature indicates that viral infections have a varied effect on GR activity depending on the host plant's resistance: *Turnip mosaic virus* (TuMV) and *Arabidopsis thaliana*: in resistant mutants (rbohF and rbohD/F), an increase in GR activity was observed, whereas in susceptible plants (Col-0 and rbohD), GR activity decreased 7 days post-infection [44]. *Cucumber mosaic virus* (CMV) and *Cucumis sativus*: treatment of plants with glycine betaine and chitosan led to a significant increase in GR activity, accompanied by a reduction in disease severity and viral accumulation [45]. Alongside changes in enzymatic activity, viral infections modulate the expression of glutathione system genes: TuMV and *A. thaliana*: resistant mutants demonstrated increased expression of the GSTU13 and GSTU19 genes, which correlated with a restriction of viral spread. In susceptible plants, the expression of these genes decreased 7 days post-infection [46].

These patterns are consistent with data obtained in other model systems and reflect the context-dependent nature of glutathione system regulation during viral infection. Thus, in *Solanum lycopersicum* infected with ToLCNDV, the SlGR3 isoform is significantly induced at the transcript and protein levels, whereas its suppression via virus-induced gene silencing (VIGS) leads to increased viral DNA accumulation and loss of resistance [47]. At the same time, during TuMV infection in *Arabidopsis thaliana*, the activity of the glutathione peroxidase-like enzyme (GPXL) decreases in susceptible genotypes and increases in resistant ones, accompanied by a change in the GSH/GSSG ratio, which reflects the redox state of the cell and determines the outcome of the infection [48].

GR plays a central role in ensuring the regeneration of reduced glutathione and thereby maintaining the functionality of the entire glutathione-dependent antioxidant system. However, under conditions of viral stress, not only ROS but also highly reactive aldehydes accumulate in the cell—by-products of the oxidative degradation of lipids and carbohydrates, which are themselves capable of damaging proteins, nucleic acids and membranes. The neutralisation of these compounds requires the involvement of specialised enzymes, one of which is AO.

2.2.4 Aldehyde oxidase

Aldehyde oxidase (AO) is a common molybdenum-iron-flavoprotein that oxidises various aldehydes to carboxylic acids [49]. The mechanism of action of AO is characteristic of molybdeno-flavoproteins: in the active site, molybdenum binds the aldehyde and transfers the oxygen group, reducing it, after which electrons are sequentially transported through two iron-sulphur clusters and FAD to an O_2 molecule. In the process, superoxide and, predominantly, hydrogen peroxide are formed [50]. Collectively, AO performs key regulatory functions in plant metabolism, catalysing the final stages of phytohormone biosynthesis by oxidising their aldehyde precursors. Four AO genes (AAO1–AAO4) have been identified in the *Arabidopsis thaliana* genome, exhibiting different substrate affinities and tissue localisation (Tab. 2) [51].

Table 2

Major isoforms of AO and their biochemical properties

Isoform	Structure	Localization	Biochemical function	Source
AAO1	Homodimer (denoted as AOα)	Seeds, roots, seedlings	IAAld → IAA. Participates in the alternative auxin biosynthesis pathway and oxidizes benzaldehyde	[52]
AAO2	Forms homo- and heterodimers, often in combination with AAO1 (AOβ)	Seedlings, roots, and senescing leaves	Participates in the alternative auxin biosynthesis pathway and oxidizes benzaldehyde	
AAO3	Homodimer	Leaves (vascular tissues), seeds, roots	ABAld → ABA. Key enzyme of the final stage of abscisic acid biosynthesis	
AAO4	Homodimer	Developing fruits (siliques), pollen	Benzaldehyde → Benzoic acid. Participates in the metabolism of secondary compounds in seeds	

The data obtained reflect the functional specialisation of isoforms: AAO1–AAO2 are involved in growth and development processes (biogenesis of secondary metabolites, oxidation of aldehydes), AAO3—in the synthesis of ABA under stress conditions, AAO4—in the detoxification of aldehydes and the utilisation of O_2 metabolites in fruits [52].

Since the effectiveness of antioxidant defence is determined by the preservation of functionally significant molecular mechanisms, it seemed appropriate to assess the degree of evolutionary conservation of the enzymes under investigation. Analysis of amino acid sequences and the construction of phylogenetic trees allow us to identify the level of conservation of functionally important domains, as well as to establish phylogenetic relationships between the proteins under investigation in different plant species. A high degree of conservatism in antioxidant enzymes may indirectly indicate the fundamental role of these proteins in maintaining redox homeostasis and plant adaptation to stressors, including viral infection. In this regard, key enzymes of the antioxidant system were examined and a comparative phylogenetic analysis was conducted.

Phylogenetic analysis

A search for the amino acid sequences of enzymes in the antioxidant system—SOD, CAT, GR and AO—was conducted in the NCBI Protein database. For the analysis, representatives of dicotyledonous plants (Eudicots) belonging to various families were selected: Solanaceae (*Solanum tuberosum*, *Solanum lycopersicum*, *Nicotiana tabacum*), Fabaceae (*Glycine max*, *Cicer arietinum*), Cucurbitaceae (*Cucumis sativus*), Rosaceae (*Malus domestica*) and Brassicaceae (*Arabidopsis thaliana*). Comparing representatives of phylogenetically distant families within a single class enabled the identification of both conserved and variable regions of protein sequences and also allowed the evaluation of the evolutionary relationships of the enzymes under investigation at the level of eudicots as a whole.

The criteria for sequence selection were the presence of full-length, experimentally validated records without fragmentary regions, a high degree of genomic annotation for each of the included species, and comparability of the species composition of the sample for all four enzymes, which ensured the validity of the comparative analysis. The exception was the analysis of AO, which included seven species instead of eight due to the absence of a full-length validated sequence for *Cucumis sativus* in the NCBI database.

Multiple alignment of amino acid sequences was performed using the MUSCLE method in MEGA 11.

To assess the evolutionary conservatism of the enzymes under study, phylogenetic trees were constructed based on the alignment of SOD, CAT, GR and AO amino acid sequences from selected dicotyledonous plant species (Figs. 3–6).

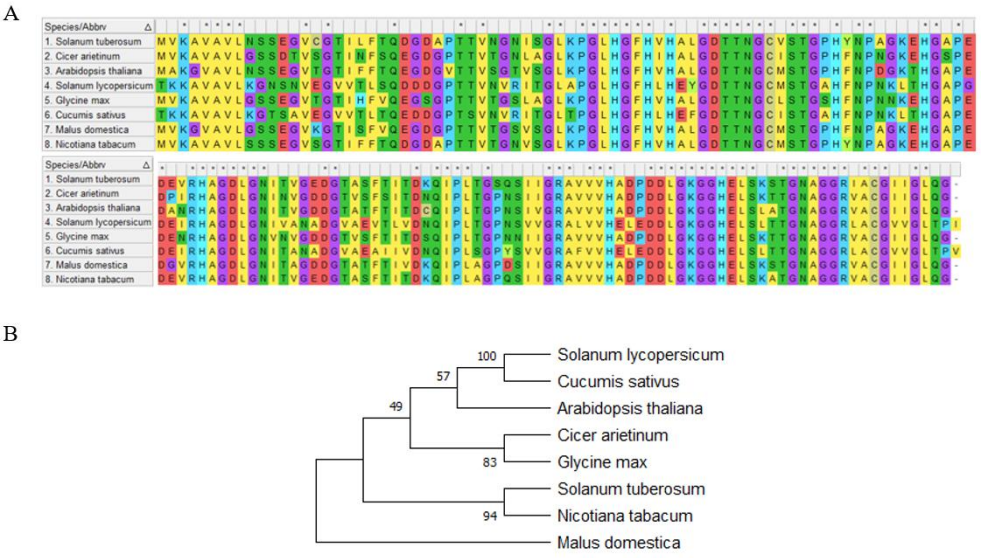

Figure 3. SOD phylogenetic tree and alignment of amino acid residues from different plant species:
A — MUSCLE alignment (MEGA 11); colors reflect the physicochemical properties of amino acids.
Conservatism: "*" — identity, ":"/ "." — similarity, B — The Maximum Likelihood tree (500 bootstrap replications).
The length of the branches is proportional to the number of amino acid substitutions per site

The SOD phylogenetic tree is characterised by clear clustering, reflecting the systematic position of the species. The genus *Solanum* is grouped with high support (94 %), the family Solanaceae forms a single, connected cluster, whilst *Glycine max* and *Cicer arietinum* are grouped separately in accordance with their membership of the Fabaceae. *Malus domestica* occupies an independent position on the tree. Sequence alignment shows 90 % identity within *Solanum* and 70–80 % between families, indicating the conservation of functionally significant domains of the catalytic centre. At the level of deep branches, bootstrap support drops to 40–50 %, reflecting the limited resolution of a single gene for reconstructing ancient phylogenetic relationships.

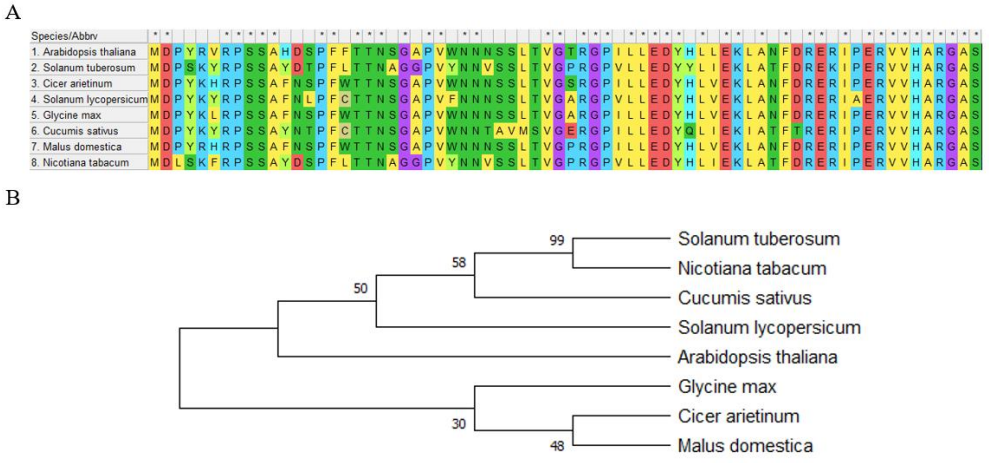

Figure 4. Comparative analysis of the amino acid sequences of catalase (CAT) in eight plant species:
A — MUSCLE alignment (MEGA 11); colors reflect the physicochemical properties of amino acids.
Conservatism: "*" — identity, ":"/ "." — similarity, B — The Maximum Likelihood tree (500 bootstrap replications).
The length of the branches is proportional to the number of amino acid substitutions per site

The topology of the CAT tree generally agrees with that of SOD, but differs in having higher bootstrap support values within key clusters. The *Solanum tuberosum–Nicotiana tabacum* pair is grouped with maximum support of 99 %, indicating exceptional conservatism of CAT within the Solanaceae family. Fabaceae are grouped with 80–85 % support, whilst *Arabidopsis thaliana* and *Malus domestica* again occupy isolated

positions. The consistency of the SOD and CAT tree topologies may indicate their co-evolution, driven by functional interdependence: SOD generates H_2O_2, the immediate detoxification of which is provided by CAT.

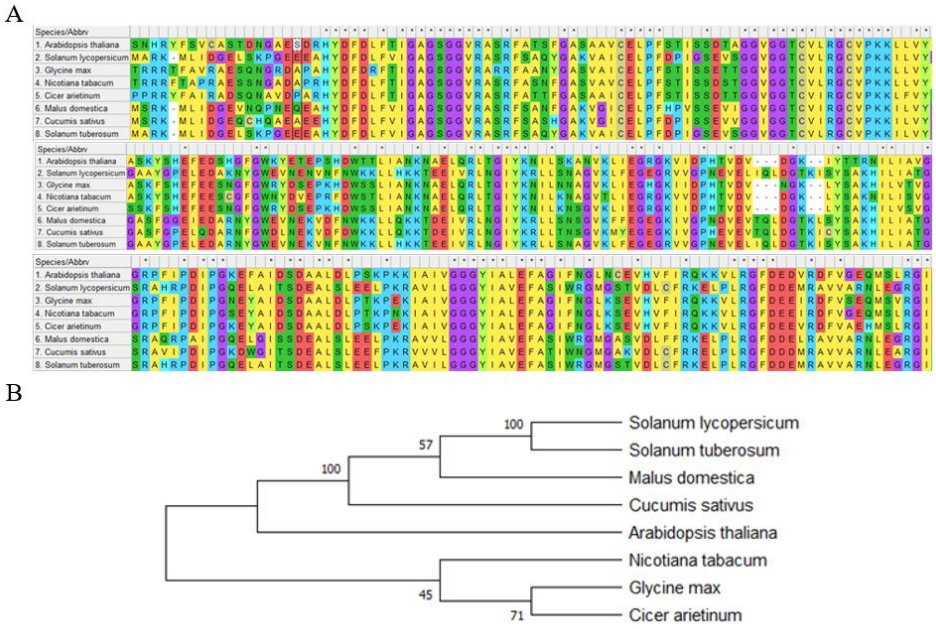

Figure 5. Comparative analysis of amino acid sequences of glutathione reductase (GR) in eight plant species: A — MUSCLE alignment (MEGA 11); colors reflect the physicochemical properties of amino acids.

Conservatism: "*" — identity, ":"/ "." — similarity, B — The Maximum Likelihood tree (500 bootstrap replications). The length of the branches is proportional to the number of amino acid substitutions per site

Phylogenetic analysis of GR revealed a number of topological features that distinguish this enzyme from SOD and CAT. *Solanum lycopersicum* and *Solanum tuberosum* are grouped together with maximum bootstrap support, confirming the high conservation of GR within the genus. Notably, *Malus domestica*, which occupied an isolated position on the SOD and CAT trees, is grouped together with representatives of the genus *Solanum* in this analysis with 100 % support. *Glycine max* and *Cicer arietinum* are grouped together with 71 % support. The partial divergence of the GR tree topology from the SOD and CAT trees may reflect differences in the intensity of evolutionary pressure on this enzyme in dicotyledonous plants, which is associated with its broader functional role in maintaining cellular redox balance.

Among all the enzymes considered, AO exhibits the most structured phylogenetic topology with two distinct monophyletic groups: Solanaceae (100 % support) and Fabaceae (100 % support), whilst *Malus domestica* occupies a sister position (75 %), and *Arabidopsis thaliana* occupies a basal position. High support values for deep nodes (75–85 %) and identity of functionally important domains exceeding 92 % within dicots indicate a slower evolutionary rate of the AO gene and pronounced purifying selection aimed at preserving the enzyme's catalytic structure.

Phylogenetic analysis of the amino acid sequences of SOD, CAT, GR and AO in dicotyledonous plants revealed a high degree of conservatism of the enzymes under study within closely related taxa. The highest bootstrap support values were recorded within the genus Solanum and amounted to 94 %, 99 %, 100 % and 100 % for SOD, CAT, GR and AO, respectively. Representatives of the Fabaceae family were consistently grouped together in all four analyses, reflecting the conservation of the amino acid sequences of these enzymes within the family. The topologies of the resulting trees are generally consistent with the systematic position of the taxa under study, confirming the validity of the analysis. The results obtained indicate the evolutionary conservatism of the enzymes of the antioxidant system in dicotyledonous plants and their functional significance in the mechanisms of cellular defence against oxidative stress during viral infection.

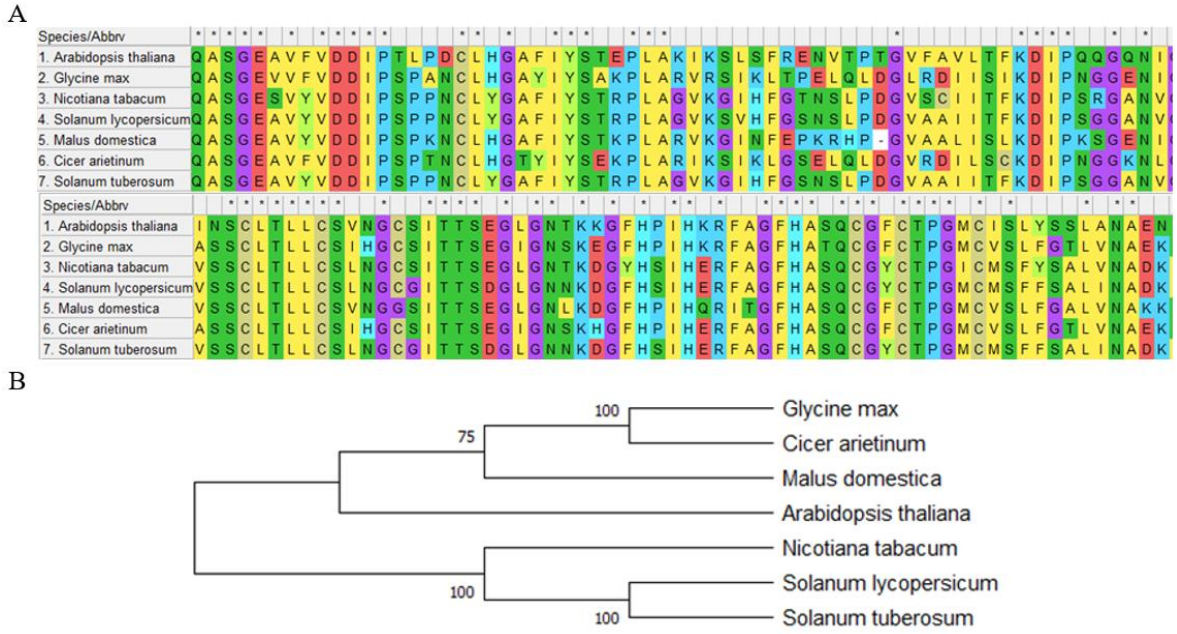

Figure 6. Comparative analysis of amino acid sequences of aldehyde oxidase (AO) in seven plant species: A — MUSCLE alignment (MEGA 11); colors reflect the physicochemical properties of amino acids

Conservatism: "*" — identity, ":"/ "." — similarity, B — The Maximum Likelihood tree (500 bootstrap replications). The length of the branches is proportional to the number of amino acid substitutions per site

The data obtained suggest that the evolutionary conservation of the enzymes under investigation is due to their key functional role in the mechanisms by which cells defend themselves against oxidative stress. At the same time, phylogenetic analysis characterises each enzyme in isolation, whereas their protective function is realised within a single, coordinated system. To assess the nature of molecular interactions between the components of this system, a network analysis of protein-protein interactions among the enzymes under investigation was conducted.

4. Network Analysis of Antioxidant Enzyme Interactions

While phylogenetic analysis characterized the evolutionary conservation of each enzyme individually, the efficiency of antioxidant protection during RNA virus infection is determined not by the properties of isolated proteins, but by the degree of their coordination within an integrated redox-regulatory network. Viral infection triggers simultaneous ROS generation across multiple cellular compartments, including chloroplasts, mitochondria, peroxisomes, and the apoplast, causing antioxidant enzymes to function as interconnected elements of a multicomponent system. To assess the structural organization and functional integration of these components, protein–protein interaction (PPI) analysis was performed using the STRING database (v12.0, https://string-db.org) with a confidence threshold of ≥ 0.800. The resulting interactomes revealed pronounced network organization characterized by dense intracluster connectivity and functional modularity. Within the *Arabidopsis thaliana* interactome, CAT1-2 occupies a central hub position (Fig. 7), coordinating key ROS-associated pathways.

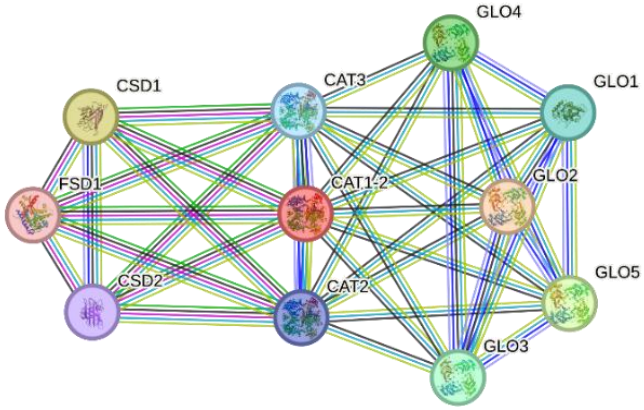

Figure 7. Functional interaction network of catalase (CAT1-2)
The network was constructed in STRING for *A. thaliana*. Colored nodes represent primary interaction partners.

Edge types: teal lines—curated database evidence, pink lines—experimental data, black lines—co-expression.

Results

The analysis identified ten high-confidence interaction partners of CAT1-2 (Tab. 3), predominantly represented by glycolate oxidases (GLO1–GLO5), superoxide dismutases (CSD1, CSD2, FSD1), as well as catalase isoforms CAT2 and CAT3.

Table 3

Functional interaction partners of CAT1-2 identified via STRING database analysis

Protein	Description	Score
GLO2	(S)-2-hydroxy-acid oxidase GLO2	0.950
CSD1	Superoxide dismutase [Cu-Zn] 1	0.942
GLO5	Peroxisomal oxidase GLO5	0.932
GLO4	Peroxisomal oxidase GLO4	0.931
GLO3	Peroxisomal oxidase GLO3	0.930
GLO1	(S)-2-hydroxy-acid oxidase GLO1	0.930
CAT3	Catalase-3	0.906
CAT2	Catalase-2	0.902
CSD2	Superoxide dismutase [Cu-Zn] 2, chloroplastic	0.878
FSD1	Superoxide dismutase [Fe] 1, chloroplastic	0.823

The most robust interactions were detected between CAT1-2 and glycolate oxidase family proteins, including GLO2 (0.950), GLO5 (0.932), GLO4 (0.931), and GLO1/GLO3 (0.930), indicating tight functional integration between catalase-dependent peroxide detoxification and photorespiratory metabolism and confirming the existence of a well-coordinated peroxisomal redox regulation module.

Strong associations with cytosolic CSD1 (0.942), chloroplastic CSD2 (0.878), and iron-containing FSD1 (0.823) demonstrate that antioxidant regulation during viral infection operates through coordinated multi-compartmental ROS buffering rather than isolated enzymatic reactions, linking chloroplasts, cytosol, and peroxisomes into a unified system. This organization is particularly critical under viral infection, where oxidative stress develops simultaneously across multiple intracellular compartments, necessitating rapid redistribution of redox-buffering capacity throughout the cell (Fig. 8).

A further characteristic feature of the CAT1-2 interactome is strong connectivity among catalase isoforms CAT2 (0.902) and CAT3 (0.906), suggesting functional redundancy and the presence of compensatory mechanisms that maintain network stability under pathogen-induced oxidative damage and reduce the likelihood of complete disruption of hydrogen peroxide detoxification pathways.

Analysis of the CSD1 interaction network revealed a similarly high level of structural integration across multiple cellular compartments (Fig. 8).

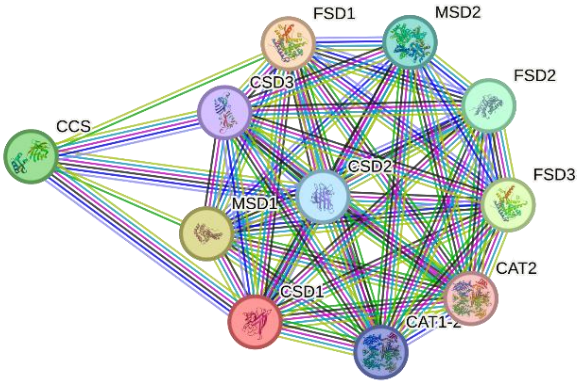

Figure 8. Network analysis of superoxide dismutase CSD1 interactions
Visualization was performed using the STRING database (A. thaliana). Nodes represent different SOD types (CSD, FSD, MSD), the chaperone CCS, and catalases (CAT). The combined confidence score for primary interaction partners exceeds 0.900.

Edge types: teal lines—curated database evidence, pink lines—experimental data, black lines—co-expression.

The reconstructed interactome comprised a broad set of functional partners identified via STRING analysis (Tab. 4), including Cu/Zn-containing superoxide dismutases, chloroplastic Fe-SOD isoforms (FSD1–FSD3), mitochondrial Mn-SOD proteins (MSD1–MSD2), catalases CAT1-2 (score = 0.942) and CAT2 (score = 0.893), as well as the copper chaperone CCS (score = 0.991). Thus, the interaction profile of CSD1 reflects the formation of a highly interconnected cross-compartmental antioxidant network that integrates ROS regulatory systems across chloroplasts, mitochondria, cytosol, and peroxisomes.

Table 4

Functional interaction partners of CSD1 identified via STRING database analysis (*A. thaliana*)

Protein	Description	Localization
FSD1	Superoxide dismutase [Fe] 1	Chloroplast
MSD1	Superoxide dismutase [Mn] 1	Mitochondria
FSD3	Superoxide dismutase [Fe] 3	Chloroplast
CCS	Copper chaperone for SOD	Chloroplast/cytosol
FSD2	Superoxide dismutase [Fe] 2	Chloroplast
MSD2	Superoxide dismutase [Mn] 2	Mitochondria
CSD2	Superoxide dismutase [Cu-Zn] 2	Chloroplast
CAT1-2	Catalase-1	Peroxisome
CSD3	Superoxide dismutase [Cu-Zn] 3	-
CAT2	Catalase-2	Peroxisome

Partners are ranked by combined confidence score in descending order. The network encompasses all major SOD isoforms across chloroplastic (FSD1–3, CSD2), mitochondrial (MSD1-2), and cytosolic compartments, the copper chaperone CCS, and peroxisomal catalases (CAT1-2, CAT2), reflecting the broad integration of CSD1 into the plant antioxidant defense network.

Particularly strong interactions were observed between CSD1 and chloroplast-localized FSD isoforms, supporting the existence of coordinated ROS regulation between the cytosolic and chloroplastic compartments during oxidative stress. At the same time, the inclusion of mitochondrial MSD proteins within the same interaction cluster suggests that mitochondrial ROS-associated pathways are also structurally integrated into the global antioxidant network. This multi-compartmental organization implies that oxidative stress induced by viral infection is regulated at the level of the entire cell through synchronized interactions among multiple organelle-associated antioxidant defense systems (Fig. 9).

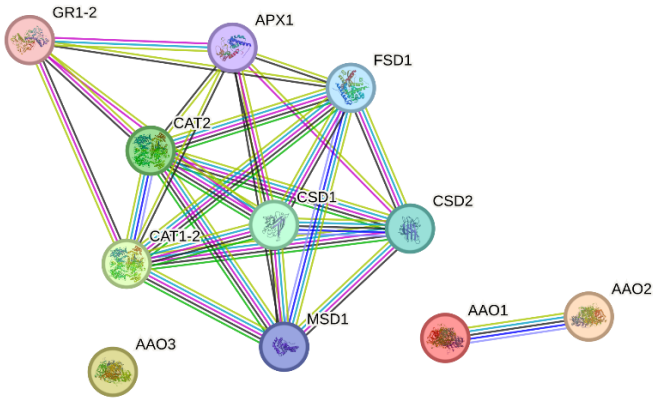

Figure 9. Comprehensive protein-protein interaction network of antioxidant defense and aldehyde metabolism systems. Analysis was performed in STRING (*A. thaliana*). Network nodes correspond to proteins (SOD, CAT, APX, GR, and AAO isoforms). Pronounced clustering is observed: the core direct ROS detoxification system (SOD–CAT–APX–GR) operates distinctly from the aldehyde oxidase module (AAO1–3).

Edge types: teal lines—curated database evidence, pink lines—experimental data, black lines—co-expression

The interaction between CSD1 and the copper chaperone CCS (score = 0.991) highlights the importance of post-translational regulation in antioxidant defense architecture, indicating that adaptation during infection depends not only on transcriptional responses but also on mechanisms controlling enzyme assembly and cofactor delivery.

Reconstruction of the combined antioxidant interactome revealed two major functional modules (Fig. 9). The first comprised core ROS detoxification enzymes, including SOD isoforms, catalases, ascorbate peroxidase, and glutathione reductase, forming a densely connected central redox-buffering scaffold. GLO-like peroxisomal glycolate oxidases (GLO1–GLO5; scores 0.930–0.950) constituted a tightly integrated peroxisomal submodule directly linked to CAT1-2 as the primary H_2O_2-scavenging component. In contrast, aldehyde oxidase proteins AAO1–AAO3 formed a relatively segregated cluster with limited direct connectivity to the core network, indicating that aldehyde oxidase-associated metabolic routes operate as a coordinated but structurally distinct regulatory system.

Conclusion on PPI Analysis of the Arabidopsis thaliana Antioxidant System

PPI network reconstruction of key antioxidant enzymes in *Arabidopsis thaliana* using STRING revealed a modular topology reflecting the functional architecture of the redox regulatory system under pathogen-induced stress. The analyzed network, comprising 11 protein nodes represented by SOD isoforms (CSD1, CSD2, FSD1, MSD1), catalases (CAT1-2, CAT2), ascorbate peroxidase (APX1), glutathione reductase (GR1-2), and aldehyde oxidases (AAO1-AAO3), demonstrated high-confidence associations (combined score ≥ 0.823) verified by experimental data, curated databases, and co-expression analysis.

The network separates into two functionally distinct modules. The core antioxidant module (SOD–CAT–APX–GR) is characterized by high inter-node connectivity spanning cytosolic, chloroplastic, mitochondrial, and peroxisomal compartments, implementing sequential ROS detoxification: dismutation of superoxide ($O_2^{-}\cdot$ to H_2O_2 by SOD isoforms), followed by H_2O_2 degradation via catalases and APX1, and regeneration of reduced ascorbate through the ascorbate-glutathione cycle involving GR1-2, thereby forming a closed metabolic circuit maintaining redox homeostasis during oxidative burst. The aldehyde oxidase cluster (AAO1-AAO3) functions as a relatively autonomous unit mediating auxin and abscisic acid biosynthesis. The absence of direct protein contacts between AAO proteins and the SOD-CAT core indicates that crosstalk between hormonal signaling and antioxidant defense operates predominantly at the transcriptional level rather than through physical protein complex formation.

Discussion

The obtained data indicate that reactive oxygen species during RNA viral infection perform a dual function determined by their concentration, subcellular localization, and temporal characteristics of generation. A moderate increase in H_2O_2 and superoxide anion levels is necessary to trigger the host plant's defensive signaling cascades, whereas their excessive accumulation activates cell death mechanisms that limit the spread

of infection [53]. The localization specificity of viral replication complexes is also of considerable importance: in TMV they are associated with endoplasmic reticulum membranes, in TBSV with peroxisomes and mitochondria, and in CMV with elements of the endomembrane system. This indicates that viruses specifically form organelle-specific redox microenvironments and exploit ROS as a tool for regulating their own life cycle, rather than merely as a byproduct of cellular stress [54, 55].

Viral proteins can interfere with the plant antioxidant system through various mechanisms. The CMV 2b protein interacts with catalase CAT3 of *Arabidopsis* and suppresses its activity, leading to H_2O_2 accumulation and the development of necrotic processes. The MCMV P31 protein inhibits ZmCAT1 in maize, simultaneously reducing PR gene expression and enhancing viral replication. A different mechanism is observed in Bamboo mosaic virus, where processing of the transit peptide of Cu/Zn-SOD PrNbCSD2 is disrupted, preventing the enzyme from being transported to the chloroplast and causing loss of functional activity without direct suppression of synthesis. Tomato chlorosis virus (ToCV) acts even more indirectly: its p22 protein disrupts α-tocopherol biosynthesis through interaction with the FBN1.1-VTE1 complex, creating heightened vulnerability in the cellular compartment where singlet oxygen production is most intense. Despite the mechanistic differences, the common thread among all these strategies is not the complete suppression of the antioxidant system, but rather its targeted modulation in specific cellular structures [56, 57].

Reconstruction of the PPI network of key antioxidant enzymes of *Arabidopsis thaliana* using the STRING platform revealed pronounced modular organization playing an important role in the systemic redox response. The core direct ROS detoxification system—comprising SOD, CAT, APX, and GR—is characterized by high inter-protein interaction density and multi-compartmental organization. The isoforms CSD1, CSD2, FSD1, FSD2, FSD3, MSD1, and MSD2 function in concert, providing compartment-specific neutralization of superoxide anion with subsequent degradation of H_2O_2 by catalases and ascorbate peroxidase. The particularly high combined scores for the CSD1-FSD1 and CSD1-MSD1 pairs reflect evolutionarily established functional redundancy of the system. The aldehyde oxidase cluster—AAO1, AAO2, and AAO3—operates relatively autonomously and does not form direct protein contacts with the SOD-CAT core, indicating that the link between the antioxidant response and hormonal reprogramming during infection is predominantly regulatory in nature.

The glutathione system demonstrates a pronounced context-dependence of response. Increased GR activity and changes in the GSH/GSSG ratio correlate with resistance in *rbohF Arabidopsis* mutants during TuMV infection, whereas in susceptible genotypes enzyme activity decreases. Identification of tomato SlGR3 as a causative resistance component against Tomato leaf curl New Delhi virus (ToLCNDV) via VIGS verification demonstrates that cellular redox status can serve as a kind of epigenetic switch determining the outcome of viral infection. Nevertheless, certain limitations of this study must be acknowledged. All PPI analyses were conducted using *Arabidopsis thaliana* as a model, so extrapolation to crop plants with different multigene family compositions requires caution. Furthermore, the static nature of network analysis does not reflect the dynamic post-translational modifications occurring during infection. Data on non-enzymatic antioxidants, including carotenoids and tocopherols, also remain predominantly indirect. Despite this, the findings provide an important conceptual framework for developing biotechnological approaches to enhance plant resistance. Promising directions include marker-assisted selection based on ascorbate and glutathione loci, as well as the application of exogenous biostimulants capable of enhancing GR-mediated protection during viral infection.

Conclusions

The present review systematically analyzes the role of reactive oxygen species and the antioxidant defense system in plant-RNA virus interactions. The data collectively demonstrate that ROS occupy a central position in this relationship, functioning simultaneously as triggers of host immune responses and as regulatory factors exploited by viruses to facilitate their own replication cycle. The dual nature of ROS signaling—protective at moderate concentrations and cytotoxic upon excessive accumulation—determines the outcome of infection and reflects the evolutionary arms race between plant hosts and RNA viruses.

The enzymatic components of the antioxidant system—superoxide dismutase, catalase, glutathione reductase, and aldehyde oxidase—do not function as isolated units but form a highly integrated, multi-compartmental network. Protein-protein interaction analysis of key *Arabidopsis thaliana* antioxidant enzymes via the STRING platform confirmed this architecture, revealing two functionally distinct modules: a densely interconnected core ROS detoxification system (SOD-CAT-APX-GR) spanning cytosolic, chloroplastic, mitochondrial, and peroxisomal compartments, and a relatively autonomous aldehyde oxidase

cluster (AAO1-AAO3) linked to phytohormone biosynthesis. The absence of direct protein contacts between these modules suggests that crosstalk between antioxidant defense and hormonal signaling operates predominantly at the transcriptional level.

Phylogenetic analysis of SOD, CAT, AO, and GR across eight dicotyledonous species confirmed the high evolutionary conservation of these enzymes, particularly within closely related taxa, underscoring their fundamental and indispensable role in cellular redox homeostasis. The functional redundancy observed within multigene families—multiple SOD isoforms across compartments, multiple CAT isoenzymes—provides a buffering capacity that prevents complete antioxidant collapse even when individual components are suppressed by viral effector proteins.

The reviewed literature demonstrates that RNA viruses have evolved diverse and precise strategies to manipulate the host antioxidant system: direct inhibition of catalase activity by CMV 2b and MCMV P31, disruption of SOD transit peptide processing by Bamboo mosaic virus, and impairment of tocopherol biosynthesis by ToCV p22. Crucially, these mechanisms share a common logic—not wholesale destruction of antioxidant capacity, but fine-tuned modulation that maintains ROS within a range permissive for viral replication while avoiding irreversible cellular damage.

Taken together, these findings establish redox regulation as a central battlefield in plant-virus interactions and provide a conceptual basis for the development of novel resistance strategies. Biotechnological approaches targeting the enhancement of GR-mediated glutathione regeneration, marker-assisted selection at ascorbate and glutathione biosynthesis loci, and the application of exogenous antioxidant biostimulants represent promising directions for improving crop resistance to RNA viral pathogens.

Funding

This research was funded by the Science Committee of the Ministry of Science and Higher Education of the Republic of Kazakhstan, grant number AP27508003.

Conflict of Interest

The authors declare no conflicts of interest.

Author contribution

The manuscript was written through contributions of all authors. All authors have given approval to the final version of the manuscript. CRediT: **Iksat N.N.** — conceptualization, supervision, writing original draft preparation, writing review and editing; **Yertayeva T.G**. — writing original draft preparation, writing review and editing; **Belgibay S.D**. — writing original draft preparation, writing review and editing; **Artykbayeva D.E**. — writing original draft preparation, writing review and editing; **Baikarayev Z.M**. — writing original draft preparation, writing review and editing.

References

1 Panda, S. K. et al. (2024). Functionality of reactive oxygen species (ROS) in plants: toxicity and control in poaceae crops exposed to abiotic stress. *Plants*, *13*(15), 2071. https://doi.org/10.3390/plants13152071

2 Mittler, R. et al. (2022). Reactive oxygen species signalling in plant stress responses. *Nature Reviews Molecular Cell Biology*, *23*(10), 663–679. https://doi.org/10.1038/s41580-022-00499-2

3 Chandimali, N. et al. (2025). Free radicals and their impact on health and antioxidant defenses: a review. *Cell Death Discovery*, *11*(19). https://doi.org/10.1038/s41420-024-02278-8

4 Hasanuzzaman, M. et al. (2020). Reactive oxygen species and antioxidant defense in plants under abiotic stress: revisiting the crucial role of a universal defense regulator. *Antioxidants*, *9*(8), 681. https://doi.org/10.3390/antiox9080681

5 Sahu, P. K. et al. (2022). ROS generated from biotic stress: Effects on plants and alleviation by endophytic microbes. *Front. Plant Sci*., *13*, 1042936. https://doi.org/10.3389/fpls.2022.1042936

6 Xu, Y. et al. (2024). The role of reactive oxygen species in plant-virus interactions. *Plant Cell Rep*, *43*(8), 197. https://doi.org/10.1007/s00299-024-03280-1

7 Zhang, Q. et al. (2025). Replication organelles of plant positive-strand RNA viruses: a boost in knowledge following new imaging approaches. *Annual Review of Phytopathology*, *63*, 451–476. https://doi.org/10.1146/annurev-phyto-121823-032017

8 Nguyen-Dinh, V., & Herker, E. (2021). Ultrastructural features of membranous replication organelles induced by positive-stranded RNA viruses. *Cells*, *10*(9), 2407. https://doi.org/10.3390/cells10092407

9 Garcia-Ruiz, H. (2018). Susceptibility genes to plant viruses. *Viruses*, *10*(9), 484. https://doi.org/10.3390/v10090484

10 Wang, L. et al. (2019). NADPH oxidases, essential players of hormone signalings in plant development and response to stresses. *Plant Signaling & Behavior*, *14*(10), 1657343. https://doi.org/10.1080/15592324.2019.1657343

11 Dumont, S., & Rivoal, J. (2019). Consequences of oxidative stress on plant glycolytic and respiratory metabolism. *Front. Plant Sci.*, *10*, 853. https://doi.org/10.3389/fpls.2019.00166

12 Zhou, Y. et al. (2017). Genome-wide identification and transcriptional expression analysis of cucumber superoxide dismutase (SOD) family in response to various abiotic stresses. *International Journal of Genomics*, *2017*, 7243973. https://doi.org/10.1155/2017/7243973

13 Rajput, V. D. et al. (2015). Effects of high salinity on physiological and anatomical indices in the early stages of *Populus euphratica* growth. *Russ J Plant Physiol*, *62*(2), 229–236. https://doi.org/10.1134/S1021443715020168

14 Zhou, Y. et al. (2018). Genome-wide identification of glutathione peroxidase (GPX) gene family and their response to abiotic stress in cucumber. *3 Biotech*, *8*(3), 159. https://doi.org/10.1007/s13205-018-1185-3

15 Jaleel, C. A. et al. (2009). Antioxidant defense responses: physiological plasticity in higher plants under abiotic constraints. *Acta Physiol Plant*, 31(3), 427–436. https://doi.org/10.1007/s11738-009-0275-6

16 Das, K., & Roychoudhury, A. (2014). Reactive oxygen species (ROS) and response of antioxidants as ROS-scavengers during environmental stress in plants. *Front. Environ. Sci.*, *2*, 53. https://doi.org/10.3389/fenvs.2014.00053

17 Barata-Soares, A. D. et al. (2004). Ascorbic acid biosynthesis: a precursor study on plants. *Braz. J. Plant Physiol.*, *16*, 147–154. https://doi.org/10.1590/S1677-04202004000300004

18 Sharma, P. & et al. (2012). Reactive oxygen species, oxidative damage, and antioxidative defense mechanism in plants under stressful conditions. *Journal of Botany*, *2012*, 217037. https://doi.org/10.1155/2012/217037

19 Tausz, M. et al. (2004). The glutathione system as a stress marker in plant ecophysiology: is a stress-response concept valid? *J Exp Bot*, *55*(404), 1955–1962. https://doi.org/10.1093/jxb/erh194

20 Hasanuzzaman, M. et al. (2019). Regulation of ascorbate-glutathione pathway in mitigating oxidative damage in plants under abiotic stress. *Antioxidants*, *8*(9), 384. https://doi.org/10.3390/antiox8090384

21 Mandal, M. et al. (2022). Reactive oxygen species (ROS) and reactive nitrogen species (RNS) in plants– maintenance of structural individuality and functional blend. *Advances in Redox Research*, *5*, 100039. https://doi.org/10.1016/j.arres.2022.100039

22 Rodrigues de Queiroz, A. et al. (2023). The effects of exogenously applied antioxidants on plant growth and resilience. *Phytochem Rev*, *22*(2), 407–447. https://doi.org/10.1007/s11101-023-09862-3

23 Chai, Y. -C., & Mieyal, J. J. (2023). Glutathione and glutaredoxin–key players in cellular redox homeostasis and signaling. *Antioxidants*, *12*(8), 1553. https://doi.org/10.3390/antiox12081553

24 Havaux, M. (2014). Carotenoid oxidation products as stress signals in plants. *The Plant Journal*, *79*(4), 597–606. https://doi.org/10.1111/tpj.12386

25 Castro, J. L. S. et al. (2018). Ascorbic acid toxicity is related to oxidative stress and enhanced by high light and knockdown of chloroplast ascorbate peroxidases in rice plants. *Theor. Exp. Plant Physiol.*, *30*(1), 41–55. https://doi.org/10.1007/s40626-018-0100-y

26 Fujiwara, A. et al. (2016). Ascorbic acid accumulates as a defense response to Turnip mosaic virus in resistant *Brassica rapa* cultivars. *J Exp Bot*, *67*(14), 4391–4402. https://doi.org/10.1093/jxb/erw223

27 Otulak-Kozieł, K. et al. (2022). Glutathione modulation in PVYNTN susceptible and resistant potato plant interactions. *International Journal of Molecular Sciences*, *23*(7), 3567. https://doi.org/10.3390/ijms23073797

28 Shukla, K. et al. (2025). Phytohormones and emerging plant growth regulators in tailoring plant immunity against viral infections. *Physiologia Plantarum*, *177*(2), e70171. https://doi.org/10.1111/ppl.70171

29 Ighodaro, O. M., & Akinloye, O. A. (2018). First line defence antioxidants-superoxide dismutase (SOD), catalase (CAT) and glutathione peroxidase (GPX): Their fundamental role in the entire antioxidant defence grid. *Alexandria Journal of Medicine*, *54*(4), 287–293. https://doi.org/10.1016/j.ajme.2017.09.001

30 Saxena, P. et al. (2022). Superoxide dismutase as multipotent therapeutic antioxidant enzyme: role in human diseases. *Biotechnol Lett*, *44*(1), 1–22. https://doi.org/10.1007/s10529-021-03200-3

31 Fink, R. C., & Scandalios, J. G. (2002). Molecular evolution and structure–function relationships of the superoxide dismutase gene families in angiosperms. *Archives of Biochemistry and Biophysics*, *399*(1), 19–36. https://doi.org/10.1006/abbi.2001.2739

32 Stephenie, S. et al. (2020). An insight on superoxide dismutase (SOD) from plants for mammalian health enhancement. *Journal of Functional Foods*, *68*, 103917. https://doi.org/10.1016/j.jff.2020.103917

33 Dehury, B. et al. (2013). *In silico* analyses of superoxide dismutases (SODs) of rice (*Oryza sativa* L.). *J. Plant Biochem. Biotechnol.*, *22*(1), 150–156. https://doi.org/10.1007/s13562-012-0121-6

34 Leitch, J. M. et al. (2012). Post-translational modification of Cu/Zn superoxide dismutase under anaerobic conditions. *Biochemistry*, *51*(2), 677–685. https://doi.org/10.1021/bi201353y

35 Lin, K. -Y. et al. (2022). MiR398-regulated antioxidants contribute to Bamboo mosaic virus accumulation and symptom manifestation. *Plant Physiology*, *188*(1), 593–607. https://doi.org/10.1093/plphys/kiab451

36 Bowler, C. et al. (1992). Superoxide dismutase and stress tolerance. *Annual Review of Plant Biology*, *43*, 83–116. https://doi.org/10.1146/annurev.pp.43.060192.000503

37 Wang, P. et al. (2024). Reactive oxygen species: Multidimensional regulators of plant adaptation to abiotic stress and development. *Journal of Integrative Plant Biology*, *66*(3), 330–367. https://doi.org/10.1111/jipb.13601

38 Mishra, N. et al. (2023). Achieving abiotic stress tolerance in plants through antioxidative defense mechanisms. *Frontiers in Plant Science*, *14*, 1110622. https://doi.org/10.3389/fpls.2023.1110622

39 Wang, W. et al. (2019). The catalase gene family in cotton: genome-wide characterization and bioinformatics analysis. *Cells*, *8*(2), 86. https://doi.org/10.3390/cells8020086

40 Zandi, P., et Schnug, E. (2022). Reactive oxygen species, antioxidant responses and implications from a microbial modulation perspective. *Biology*, *11*(2), 155. https://doi.org/10.3390/biology11020155

41 Inaba, J. et al. (2011). Virus-induced necrosis is a consequence of direct protein-protein interaction between a viral RNA-silencing suppressor and a host catalase. *Plant Physiol.*, *156*(4), 2026–2036. https://doi.org/10.1104/pp.111.180042

42 Jiao, Z. et al. (2022). Advances in research on maize lethal necrosis, a devastating viral disease. *Phytopathol Res*, *4*(1), 14. https://doi.org/10.1186/s42483-022-00117-1

43 Kozieł, E. et al. (2024). Glutathione-the "master" antioxidant in the regulation of resistant and susceptible host-plant virus-interaction. *Front. Plant Sci*., *15*, 1373801. https://doi.org/10.3389/fpls.2024.137380

44 Otulak-Kozieł, K. et al. (2023). Glutathione contribution in interactions between Turnip mosaic virus and *Arabidopsis thaliana* mutants lacking respiratory burst oxidase homologs D and F. *International Journal of Molecular Sciences*, *24*(8), 7128. https://doi.org/10.3390/ijms24087128

45 Sofy, A. R. et al. (2020). Improving regulation of enzymatic and non-enzymatic antioxidants and stress-related gene stimulation in Cucumber mosaic cucumovirus-infected cucumber plants treated with glycine betaine, chitosan and combination. *Molecules*, *25*(10), 2341. https://doi.org/10.3390/molecules25102341

46 Otulak-Kozieł, K. et al. (2022). AtGSTU19 and AtGSTU24 as moderators of the response of *Arabidopsis thaliana* to Turnip mosaic virus. *International Journal of Molecular Sciences*, *23*(19), 11531. https://doi.org/10.3390/ijms231911531

47 Sharma, N. et al. (2021). Genomic dissection of ROS detoxifying enzyme encoding genes for their role in antioxidative defense mechanism against Tomato leaf curl New Delhi virus. *Genomics*, *113*(3), 889–899. https://doi.org/10.1016/j.ygeno.2021.01.022

48 Seo, M. et al. (1998). Higher activity of an aldehyde oxidase in the auxin-overproducing superroot1 mutant of *Arabidopsis thaliana*. *Plant Physiol*., *116*(2), 687–693. https://doi.org/10.1104/pp.116.2.687

49 Koshiba, T. et al. (1996). Purification and properties of flavin- and molybdenum-containing aldehyde oxidase from coleoptiles of maize. *Plant Physiol*., *110*(3), 781–789. https://doi.org/10.1104/pp.110.3.781

50 Jiao, Z. et al. (2022). Advances in research on maize lethal necrosis, a devastating viral disease. *Phytopathol Res*, *4*(1), 14. https://doi.org/10.1186/s42483-022-00117-1

51 Ori, N. et al. (1997). TAO1, a representative of the molybdenum cofactor containing hydroxylases from tomato. *Journal of Biological Chemistry*, *272*(2), 1019–1025. https://doi.org/10.1016/S0021-9258(19)77568-1

52 Srivastava, S. et al. (2017). Aldehyde oxidase 4 plays a critical role in delaying silique senescence by catalyzing aldehyde detoxification. *Plant Physiology*, *173*(4), 1977–1997. https://doi.org/10.1104/pp.16.01939

53 Apel, K., & Hirt, H. (2004). Reactive oxygen species: metabolism, oxidative stress, and signal transduction. *Annual Review of Plant Biology*, *55*, 373–399. https://doi.org/10.1146/annurev.arplant.55.031903.141701

54 Verchot, J. (2011). Wrapping membranes around plant virus infection. *Current Opinion in Virology*, *1*(5), 388–395. https://doi.org/10.1016/j.coviro.2011.09.009

55 Schoelz, J. E. et al. (2011). Intracellular Transport of Plant Viruses: Finding the Door out of the Cell. *Molecular Plant*, *4*(5), 813–831. https://doi.org/10.1093/mp/ssr070

56 Keurentjes, J. J. B. et al. (2011). Redefining plant systems biology: from cell to ecosystem. *Trends in Plant Science*, *16*(4), 183–190. https://doi.org/10.1016/j.tplants.2010.12.002

57 Gill, S. S., & Tuteja, N. (2010). Reactive oxygen species and antioxidant machinery in abiotic stress tolerance in crop plants. *Plant Physiology and Biochemistry*, *48*(12), 909–930. https://doi.org/10.1016/j.plaphy.2010.08.016

Т.Ғ. Ертаева, С.Д. Белгібай, Д.Е. Артыкбаева, Ж.М. Байқараев, Н.Н. Иқсат

Өсімдіктердің РНҚ вирустарымен инфекциялануы кезіндегі антиоксиданттық қорғанысы: негізгі ферменттердің рөлі

Соңғы онжылдықтарда ауылшаруашылық дақылдарының биотикалық стрессорларға төзімділігі мәселесі жаһандық азық-түлік қауіпсіздігін қамтамасыз ету тұрғысынан ерекше өзектілікке ие болды. Биотикалық факторлардың ішінде өнімділіктің айтарлықтай төмендеуіне және өсімдіктердің физиологиялық процестерінің бұзылуына әкелетін вирустық инфекциялар ерекше орын алады. РНҚ вирустары жоғары бейімделгіштікпен және иесінің жасушалық метаболизмін тиімді түрде өзгерту қабілетімен сипатталады, бұл процесс редокс-гомеостаздың бұзылуымен қатар жүреді. Белсенді оттегі түрлерінің (БОТ) түзілуі бұл процестің негізгі кезеңдерінің бірі және функционалдық екіұдайлықпен сипатталады: БОТ қорғаныс реакцияларын қоздыратын сигналдық молекулалар ретінде әрекет етеді,

ал олардың шамадан тыс жиналуы жасушалық компоненттердің зақымдалуына әкеледі. Редокс-гомеостаздағы өзгерістер ферментативті және ферментативті емес қорғаныс механизмдерін қамтитын өсімдіктердің антиоксиданттық жүйесінің белсендірілуімен жалғасады. Редокс-процестерді зерттеудегі айтарлықтай жетістіктерге қарамастан, вирустық инфекция жағдайында редокс-реттелу механизмдерінің интеграциясы және антиоксиданттық жүйенің жұмыс істеуі бүгінгі күнге дейін жеткілікті түрде сипатталмаған және әрі қарай талдауды қажет етеді. Осыған байланысты, бұл шолудың мақсаты — РНК вирустарымен инфекцияланған өсімдіктердегі иммундық жауапты реттеудегі белсенді оттегі түрлері мен антиоксиданттық жүйенің негізгі ферменттерінің рөлі туралы қазіргі түсініктерді жүйелеу және талдау.

Кілт сөздер: оксидативтік стресс, өсімдіктің антиоксиданттық құрылымы, вирустық инфекция, өсімдік иммунитеті.

Т.Г. Ертаева, С.Д. Белгибай, Д.Е. Артыкбаева, Ж.М. Байкараев, Н.Н. Иксат

Антиоксидантная защита растений при инфицировании РНК-вирусами: роль ключевых ферментов

В последние десятилетия проблема устойчивости сельскохозяйственных культур к биотическим стрессорам приобрела особую актуальность в контексте обеспечения глобальной продовольственной безопасности. Среди биотических факторов особое место занимают вирусные инфекции, вызывающие значительные потери урожая и нарушающие физиологические процессы растений. РНК-вирусы характеризуются высокой адаптивностью и способностью эффективно модифицировать клеточный метаболизм хозяина, что сопровождается нарушением редокс-гомеостаза. Генерация активных форм кислорода (АФК) является одним из ключевых этапов этого процесса и характеризуется функциональной двойственностью: АФК выступают в роли сигнальных молекул, инициирующих защитные реакции, в то время как их избыточное накопление приводит к повреждению клеточных компонентов. Изменения редокс-гомеостаза сопровождаются активацией антиоксидантной системы растений, включающей как ферментативные, так и неферментативные механизмы защиты. Несмотря на значительные успехи в изучении редокс-процессов, интеграция механизмов редокс-регуляции и функционирование антиоксидантной системы в условиях вирусной инфекции к настоящему времени остаются недостаточно описанными и требуют дальнейшего анализа. В связи с этим целью настоящего обзора является систематизация и анализ современных представлений о роли активных форм кислорода и ключевых ферментов антиоксидантной системы в регуляции иммунного ответа у растений, инфицированных РНК-вирусами.

Ключевые слова: окислительный стресс, антиоксидантная система растений, вирусная инфекция, иммунитет растений.

Information about the authors

Yertayeva Tomiris Galymzhankyzy — Bachelor of Natural Sciences, Junior Researcher of Rustem Omarov Plant Biotechnology Laboratory, Department of Biotechnology and Microbiology, L.N. Gumilyov Eurasian National University, Astana, Kazakhstan; e-mail: tomirisertaeva@gmail.com; ORCID 0009-0000-7273-0385

Belgibay Sauat Didaruly — Bachelor of Natural Sciences, Junior Researcher of Rustem Omarov Plant Biotechnology Laboratory, Department of Biotechnology and Microbiology, L.N. Gumilyov Eurasian National University, Astana, Kazakhstan; e-mail: sbelgibaj@gmail.com; ORCID: 0009-0005-9988-0144

Artykbayeva Dana Erbolatovna — Master of Natural Sciences, Junior Researcher of Rustem Omarov Plant Biotechnology Laboratory, Department of Biotechnology and Microbiology, L.N. Gumilyov Eurasian National University, Astana, Kazakhstan; e-mail: artykbayeva_dye_1@enu.kz; ORCID: 0009-0008-0588-6660

Baikarayev Zhaksat Matatuly — Bachelor of Natural Sciences, Junior Researcher of Rustem Omarov Plant Biotechnology Laboratory, Department of Biotechnology and Microbiology, L.N. Gumilyov Eurasian National University, Astana, Kazakhstan; e-mail: baikarayev_zhm@enu.kz, ORCID: 0009-0008-4415-0103

Iksat Nurgul Nurkanatkyzy — PhD, Acting Associate Professor of the Department of Biotechnology and Microbiology, L.N. Gumilyov Eurasian National University, Astana, Kazakhstan; e-mail: nurguliksat@gmail.com, ORCID: 0000-0003-1278-5207

How to Cite: Turarova, Ye.M., Osmonali, B.B., & Mamurova, A.T. (2026). Ecological and geographical characteristics of the subgenus *Cercidotrix* Bunge in Betpak-Dala. *Fundamental and Experimental Biology*, 31, 3 (123), 170-182. https://doi.org/10.31489/2026FEB3/170-182

Data Paper

https://doi.org/10.31489/2026FEB3/170-182

UDC 581.526.325:581.9 (574.54) Received: 20.12.2025 | Accepted: 15.05.2026 | Published online: 30.09.2026

Ye.M. Turarova[1, 2], B.B. Osmonali[2], A.T. Mamurova[1]

[1]*Kazakh National University named after Al-Farabi, Almaty, Kazakhstan;*
[2]*Institute of Botany and Phytointroduction, Almaty, Kazakhstan*
[*]*Corresponding author: turarova-erkejan@mail.ru*

Ecological and geographical characteristics of the subgenus *Cercidotrix* Bunge in Betpak-Dala

In the present study, data on the species composition and geographic distribution of representatives of the subgenus *Cercidotrix* Bunge in the Betpak-Dala region have been systematized and clarified for the first time based on an analysis of herbarium collections (AA, MW, LE, TASH) and recent field observations. The scientific novelty of the study lies in the integration of literature sources and herbarium data to refine the ecological and geographic characteristics of *Cercidotrix* Bunge representatives in the desert ecosystem of Betpak-Dala, thereby enabling a more comprehensive assessment of their biodiversity and ecological traits. The analysis of ecological and geographic data for the genus *Astragalus* L. demonstrates that the collection and systematization of this information have been carried out for the first time both in Betpak-Dala and in Kazakhstan as a whole.

Keywords: Astragalus, Cercidotrix, Betpak-Dala, ecology, geography, herbarium, life form, ecological group.

Introduction

The Fabaceae family consists of valuable forage plants. It includes such major genera as *Astragalus*, *Lathyrus*, *Medicago* (alfalfa), *Melilotus* (sweet clover), *Oxytropis*, *Trifolium* (clover), *Vicia* (vetch), and others. After grasses, legumes are the most important group of flowering plants for humans in terms of practical significance. In legume seeds, the main storage substances are protein, as well as starch and fatty oil, which determine their high nutritional and fodder value. The legume family includes about 550 genera and 13,000 species distributed throughout the world, making it one of the largest families in the global flora. In Kazakhstan, 42 genera and about 650 species are found [1]. *Astragalus* L., is one of the largest genuses of flowering plants in the Leguminosae family [2].

The genus *Astragalus* L. is a very large Holarctic genus, comprising more than 2,000 species, of which about 900 occur in the former USSR and 308 in Kazakhstan. Most species of Astragalus remain poorly studied in terms of their chemical composition, forage value, and other properties. Some of them serve as good forage plants, while others contain alkaloids, glycosides, or saponins and are poisonous [3, 4]. Active ingredients from Astragalus sp. They are used in nutrition, and their use in the treatment of neurological diseases is attracting increasing attention [3]. Many Astragalus species have extremely limited ranges and are endemic to Kazakhstan; there are 75 such endemic species, which is more than 25 % of the total [5, 6].

Species of the genus *Astragalus* L. are annual or perennial herbaceous plants, subshrubs, and less commonly shrubs, with well-developed or strongly shortened stems. They are usually covered with simple or bifurcate hairs, and more rarely glabrous (hairless) [6].

Betpak-Dala is one of the largest clay deserts in the world. This vast natural region stretches 170 kilometers from north to south and about 500 kilometers from west to east, covering an area of 75,000 square kilometers on the Kazakh plains—two and a half times the size of modern-day Belgium. Almost entirely uninhabited, Betpak-Dala captivates with its diverse landscape. Its proximity to the Kazakh Uplands is reflected in the region's rocky areas, low hills, and small depressions.

Among the CIS countries, about 900 species of the genus *Astragalus* L. are recorded. At present, a new representative of the genus *Astragalus* L., namely *Astragalus mollis*, has been identified in Azerbaijan [7]. In Kazakhstan, 309 species occur, 11 of which are listed in the Red Book. In the Betpak-Dala Desert, 17 species

are found, belonging to 11 sections of the subgenus *Cercidotrix* Bunge *(Astragalus* L.). According to the Flora of Kazakhstan, two species—*Astragalus sumneviczii* and *Astragalus karatjubeki*—are endemic [8, 9].

The objective of the present study is to investigate the ecological and geographical characteristics of the subgenus *Cercidotrix* Bunge (*Astragalus* L.) in the desert ecosystem of Betpak-Dala, including the determination of species composition, geographic distribution (Fig. 1), predominant life forms, ecological niches, and patterns of distribution across different habitat types.

Scientific novelty:

1. For the first time, data on the species composition and geographic distribution of representatives of the subgenus *Cercidotrix* Bunge in the Betpak-Dala region have been systematized and clarified.

2. An integrated analysis of herbarium material and literature sources has been conducted, allowing a more precise determination of the ecological and geographical characteristics of the subgenus in the desert ecosystem.

3. Based on the analysis of ecological and geographical features of the genus *Astragalus* L., it is important to note that this study and data collection have been carried out for the first time both for the genus *Astragalus* L. in Betpak-Dala and for the territory of Kazakhstan as a whole.

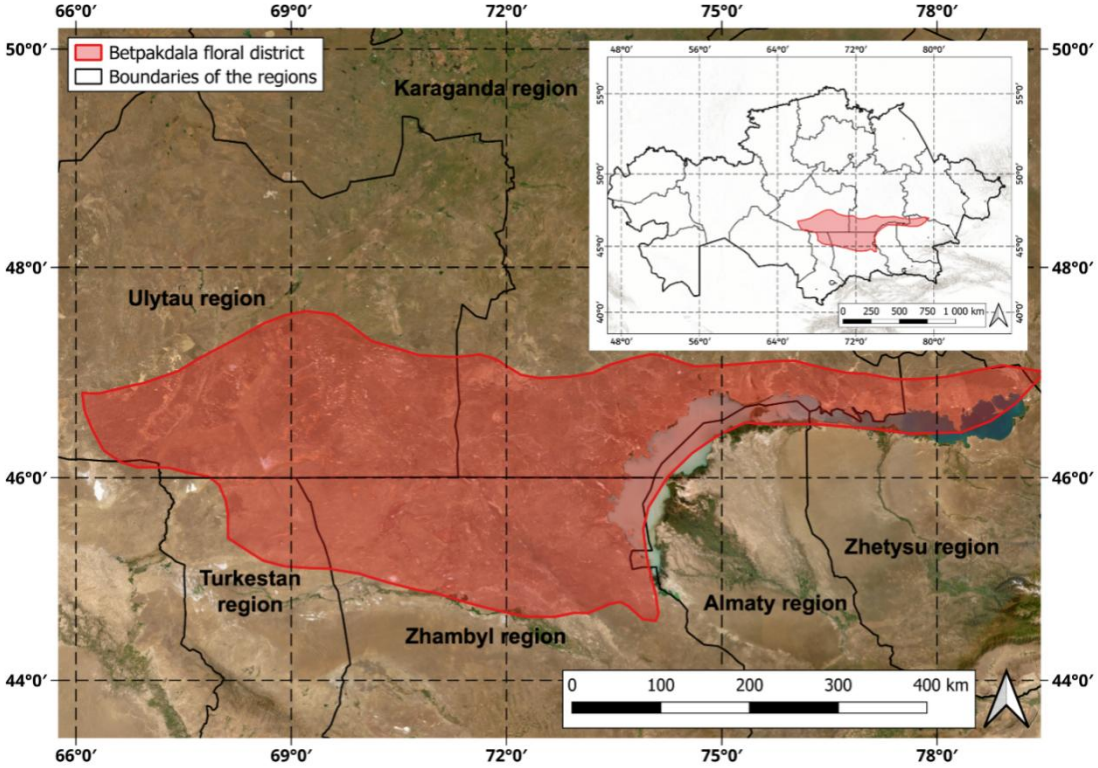

Figure 1. Map of the location of the Betpak-Dala floristic region within the territory of Kazakhstan

Experimental

The research work used classical botanical (ecologo-systematic; ecologo-geographical) methods. In the course of the work, herbarium materials collected on the territory of Betpak-Dala were studied through the internet resources of the collection fund of the Institute of Botany and phytointroduction (AA), herbarium of Moscow University (MW), herbarium of St. Petersburg State University (LE), the Central herbarium fund of Uzbekistan (TASH) and iNaturalist and GBIF (Global Biodiversity Information Facility). Herbarium collection is carried out according to the method of Skvortsov A. K. (1977) [7; 10–25]. To identify the collected materials, fundamental reports were used: "Flora of Kazakhstan" (1961) [5], "Illustrated determinant of Kazakhstan" (1969), "Determinant of Middle Asia and Kazakhstan" (1972) and "Flora of the USSR". The ecological conditions of the species were studied based on the works of Raunkiaer C. (1934), Serebryakov I.G. (1964), Shennikov (1950), and Poplavskaya (1950) [26–30]. To assess the statistical significance of differences in species distribution across ecological groups, the basic formula for calculating percentages in statis-

tics was used. A total of 17 species were distributed among three groups: 7 species (41.2 %) as hemicryptophytes, 7 species (41.2 %) as phanerophytes, and 3 species (17.6 %) as chamaephytes.

Results and Discussion

The CIS of Astragalus includes about 900 species among countries [10]. *Astragalus* L. there are 309 species of the genus, of which 11 species are listed in the Red Book [9]. Representatives of the genus *Astragalus* L. in the genus *Cercidotrix* Bunge found in the territory of Betpak-Dala are classified into 11 sections [10, 31]. Studies of the species of the subgenus *Cercidotrix* Bunge (*Astragalus* L.) occurring in Betpak-Dala, along with the examination of herbarium material, showed that the studied subgenus has a wide ecological amplitude and is fairly well distributed in this area. The total number of species in the studied territory is 17, which can be seen in Table 1:

Table 1

Taxonomic composition of species of genus *Astragalus* L.
(compiled from Flora of Kazakhstan)

№	Section	Subsection	Species
1	Xiphidium Bge.	Xiphidium	*Astragalus arbuscula*
			A. polyceras
			A. scleroxylon
			A. virgatus
		Macrotropida R. Kam	*A. compressus*
2	Ammodendron		*A. brachypus*
			A. karatjubeki
3	Corethrum Bge		*A. Kronenburgii*
4	Ammodytes (Stev.) Bge		*A. ammodytes*
5	Erioceras Bge.		*A. arcuatus*
6	Tamias Bge		*A. Turczaninovii*
7	Paracystium Gontsch.		*A. Sumneviczii*
			A. lasiophyllus
8	Scabriseta R. Kam.		*A. scabrisetus*
9	Pseudohelmia R. Kam.		*A. Krascheninikovii*
10	Bucharica B. Fedtsh.		*A. macropetalus*
11	Bulimioides Bge.		*A. unijugus*

Abstract

Astragalus kronenburgii B. Fedtsch. ex Kneuck.

Perennial herbaceous plant. It grows on gravelly, woody, and rocky slopes in the foothills and low mountains.

It blooms in May and bears fruit until June and July.

It occurs in the floristic regions of Betpak-Dala, Dzungarian Alatau, Zailiysky Kungey Alatau, Chu-Ili Mountains, Karatau, and Western Tien Shan.

General distribution worldwide: Kyrgyzstan, Uzbekistan [8, 9].

A. ammodytes Pall.

Perennial herbaceous plant. Grows on sandy soils.

Flowering occurs from May to June; fruiting from May to July.

It is found in the floristic regions of Irtysh, Semipalatinsk, Aktobe, Western and Eastern Low Hills, Zaysan, Aral Sea region, Kyzylorda, Betpak-Dala, and Turkestan.

General distribution worldwide: Altai, China, Mongolia, Tuva, Uzbekistan, and Xinjiang [8, 9].

A. arcuatus Kar. et Kir.

Perennial herbaceous plant. Grows on rocky slopes of hills.

Flowering occurs from June to July.

It is found in the floristic regions of Irtysh, Kokshetau, Aktobe, Mugodzhar, Emba, Turgay, Western and Eastern Low Hills, Ulytau, Karkaraly, Zaysan, Betpak-Dala, Altai, Dzungarian Alatau, and Karatau.

General distribution worldwide: Eastern European part of Russia, Mongolia [8, 9].

A. Turczaninowii Kar. et Kir.

Perennial herbaceous plant. Grows in desert zones on stabilized hummocky sands, in river valleys, saxaul thickets, and on sandy loams along mountain foothills.

Flowering occurs from April to June; fruiting from May to June.

It is found in the floristic regions of Aktobe, Turgay, Western Low Hills, Aral Sea region, Kyzylorda, Betpak-Dala, Muyunkum, Balkhash-Alakol, Kyzylkum, Turkestan, Tarbagatai, Dzungarian Alatau, Chu-Ili Mountains, and Karatau.

General distribution worldwide: Afghanistan, Turkmenistan, Uzbekistan [8, 9].

A. Sumneviczii Pavlov.

Perennial herbaceous plant. Grows on compacted sands and sandy-clay hills.

Flowering occurs from May to June; fruiting from June to July.

It is found in the floristic region of Betpak-Dala.

General distribution worldwide: Endemic [8, 9].

A. lasiophyllus Ledeb.

Perennial herbaceous plant. Grows in sagebrush and saltwort-sagebrush deserts, on outcrops of chalk and tertiary clays.

Flowering occurs in (April) May; fruiting from May to June.

It is found in the floristic regions of Aktobe, Emba, Western Low Hills, Northern Ust-Urt, Buzachi, Mangyshlak, Aral Sea region, Betpak-Dala, Balkhash-Alakol, Dzungarian Alatau, Zailiysky Kungey Alatau, Chu-Ili Mountains, and Karatau.

General distribution worldwide: Eastern European part of Russia, Mongolia, Northern European part of Russia, Uzbekistan, and Xinjiang [8, 9].

A. scabrisetus Bonge.

Perennial herbaceous plant. Grows on sands, sandy-stony slopes, and clayey areas.

Flowering occurs from April to May; fruiting in June.

It is found in the floristic regions of Aktobe, Turgay, Western and Eastern Low Hills, Karkaraly, Zaysan, Northern Ust-Urt, Mangyshlak, Aral Sea region, Betpak-Dala, Balkhash-Alakol, Kyzylkum, Dzungarian Alatau, Zailiysky Alatau, Chu-Ili Mountains, and Karatau.

General distribution worldwide: Mongolia, Uzbekistan, Xinjiang [8, 9].

A. arbuscula Pall.

Bushy shrub. Grows in steppes and sagebrush deserts, occasionally on sands, more often on rocky and pebble soils, in forested foothills and dry slopes of low mountains.

Flowers in May; fruits in June.

It is found in the floristic regions of Irtysh, Turgay, Western and Eastern Low Hills, Karkaraly, Zaysan, Betpak-Dala, Balkhash-Alakol, Altai, Tarbagatai, Dzungarian Alatau, Zailiysky Alatau, and Chu-Ili Mountains.

General distribution worldwide: Altai, Mongolia, Xinjiang [8, 9].

A. polyceras Kar. et Kir.

Bush. Grows on gravelly and clayey solonchak soils, at the edges of sands, and in desert steppes among sagebrush.

Flowering occurs from April to May; fruiting in May.

It is found in the floristic regions of the Caspian Lowland, Western Low Hills, Betpak-Dala, Balkhash-Alakol, and Dzungarian Alatau.

General distribution worldwide: Xinjiang [8, 9].

A. scleroxylon Bunge

Subshrub. Grows on solonetzic red clays, gravelly soils of buttes and dry stream beds, less commonly on sandy soils of desert low mountains.

Flowering occurs from May to June.

It is found in the floristic regions of Betpak-Dala, Muyunkum, Kyzylkum, Turkestan, and Karatau.

General distribution worldwide: Uzbekistan [8, 9].

A. compressus Ledeb.

Subshrub. Grows on gravelly and sandy steppe areas in intermontane depressions and valleys.

Flowers in May; fruits in July.

General distribution worldwide: Altai, North-Central China, Mongolia, Xinjiang [8, 9].

A. virgatus Pall.

Perennial herbaceous plant. Grows in sandy and desert steppes, feather grass and feather grass-fescue steppes, in meadow depressions among sandy ridges, on clayey cliffs, and fallow lands.

Flowering occurs from May to June; fruiting from June to August.

It is found in the floristic regions of the Spur of the General Syrt, Tobol-Ishim, Irtysh, Caspian Lowland, Aktobe, Mugodzhar, Emba, and Betpak-Dala.

General distribution worldwide: Bulgaria, Central European part of Russia, Eastern European part of Russia, Hungary, Crimea, North Caucasus, Romania, Southern European part of Russia, Ukraine, and Western Siberia [8, 9].

A. kraschenninnikovii Kamelin

Bush. Grows along the edges of dry spring streams in clayey deserts.

Flowering occurs from May to June.

It is found in the floristic region of Betpak-Dala.

General distribution worldwide: Endemic [8, 9].

A. macropetalus Schrenk

Perennial herbaceous plant. Grows on gravelly mountain foothills and slopes, in clayey ephemeral deserts and dry steppes.

Flowering occurs from April to July; fruiting from May to June.

It is found in the floristic regions of Kyzyl-Orda, Betpak-Dala, Balkhash-Alakol, Chu-Ili Mountains, Karatau, and Western Tien Shan.

General distribution worldwide: Uzbekistan [8, 9].

A. brachypus Schrenk ex Fisch. & C.A. Mey.

Perennial herbaceous plant. Grows on sands, weathered sandstones, sandy solonetzic soils, and in desert shrub thickets.

Flowering occurs from April to June; fruiting from June to July.

It is found in the floristic regions of the Caspian Lowland, Western Low Hills, Aral Sea region, Kyzyl-Orda, Betpak-Dala, Muyunkum, Balkhash-Alakol, and Zailiysky Alatau.

General distribution worldwide: Kyrgyzstan, Xinjiang [8, 9].

A. karatjubeki Golosk.

Subshrub. Grows on coastal sands.

Flowering occurs from May to June; fruiting from June to July.

It is found in the floristic regions of Betpak-Dala and Balkhash-Alakol.

General distribution worldwide: Endemic [8, 9].

A. unijugus Bunge.

A small shrub. Grows in clayey and sandy deserts on takyrs, edges of solonchaks, calcareous loams, and sandy loams. Flowering occurs from May to June; fruiting in June. It is found in the floristic regions of Western Low Hills, Kyzyl-Orda, Betpak-Dala, and Balkhash-Alakol. General distribution worldwide: Xinjiang [8, 9].

Cercidotrix Bunge (*Astragalus* L.) description of herbarium specimens of representatives of the genus can be seen in Table 2.

Table 2

Comparative data on the presence of species of the genus *Cercidotrix* Bunge in herbarium collections (AA, MW, LE, TASH, GBIF and iNaturalist)

№	Name of the species by FK	AA	MW, GBIF, iNaturalist	LE
1	*Astragalus arbuscula* Pall.	3	4	3
2	*A. polyceras* Kar. & Kir.	4	2	-
3	*A. scleroxylon* Bunge	1	1	3
4	*A. virgatus* Pall.	-	-	-
5	*A. compressus* Ledeb.	-	-	-
6	*A. brachypus* Schrenk ex Fisch. & C.A. Mey.	-	-	-
7	*A. karatjubeki* Golosk.	1	-	-
8	*A. Kronenburgii* B.Fedtsch. ex Kneuck.	2	-	-
9	*A. ammodytes* Pall.	4	-	-
10	*A. arcuatus* Kar. & Kir.	5	-	-
11	*A. Turczaninovii* Kar. et Kir.	6	-	5
12	*A. Sumneviczii* Pavlov	-	2	1
13	*A. lasiophyllus* Ledeb.	8	-	1
14	*A. scabrisetus* Bong.	2	1	2
15	*Astragalus kokaschikii* Gamajun	1	-	-
16	*A. macropetalus* Schrenk	3	1	18
17	*A. unijugus* Bunge	10	3	2
	Species in total	50	14	35

Note. FK —Flora of Kazakhstan; AA — on the Herbarium of the Institute of Botany and Phytointroduction; MW — on the Herbarium of Moscow University; III — on the Herbarium of Saint Petersburg State University

In the herbarium of the Institute of Botany and Phytointroduction (AA), a total of 50 specimens related to this subgenus were collected. The most frequently encountered and mostly collected between 1934–1941 were *Astragalus unijugus* (20.8 %) and *Astragalus lasiophyllus* (14.6 %). In the digital herbarium "Noevkovcheg" at Moscow State University (MW), 14 specimens were collected. Most of these were gathered in 1951, with the most common species being *Astragalus arbuscula* (33.3 %), *A. polyceras* (16.7 %), and *A. unijugus* (16.7 %). In the herbarium of Saint Petersburg State University (LE), the majority of the specimens were collected between 1958–1960. The predominant species were *Astragalus macropetalus* (48.5 %) and *A. turczaninovii* (18.2 %). In the National Herbarium of Uzbekistan (TASH), 6 specimens were recorded, including 4 specimens of *Astragalus arbuscula* (66.7 %) and 2 specimens of *A. ammodytes* (33.3 %). Figure 2 shows several species of herbarium specimens of the subgenus *Cercidotrix* Bunge collected from the Betpak-Dala Desert. Analysis of herbarium collections showed that *A. unijugus Bunge*, *A. lasiophyllus*, and *A. turczaninovii* are widespread and exhibit a high degree of distribution.

Based on herbarium specimens, a distribution map of species of the subgenus Cercidotrix Bunge within the floristic regions of Kazakhstan was compiled (Fig. 3). According to the obtained data, the species *A. kokaschikii* Gamajun and *Astragalus sumneviczii* Pavl. are recorded only from a single locality, which confirms their status as rare and narrowly endemic species.

In this study, among the species belonging to the subgenus *Cercidotrix* Bunge (Astragalus L.), two species are included in the Red Book. Considering these species individually:

Astragalus kokaschikii Gamajun is a rare local endemic species with a limited distribution range. It flowers in June. The species is known from only one locality—the clay desert of Betpak-Dala, where it grows along the banks of the dried-up Kokashyk riverbeds. Its extremely low abundance is a consequence of economic and anthropogenic activities. As a conservation measure, the establishment of the Betpak-Dala Nature Reserve has been proposed. It is necessary to determine the current state of the populations and develop appropriate conservation measures [9].

Astragalus sumneviczii Pavl. is a rare local endemic species. It is a perennial plant 4–15 cm in height. The species flowers from May to July and bears fruit from June to July. It grows on compacted sandy soils of the Betpak-Dala region (Fig. 4). Due to anthropogenic activities, the probability of extinction of the species is high. As a preventive conservation measure, the organization of the Betpak-Dala Nature Reserve is recommended. It is necessary to assess the current condition of the species in nature and establish protection measures [9].

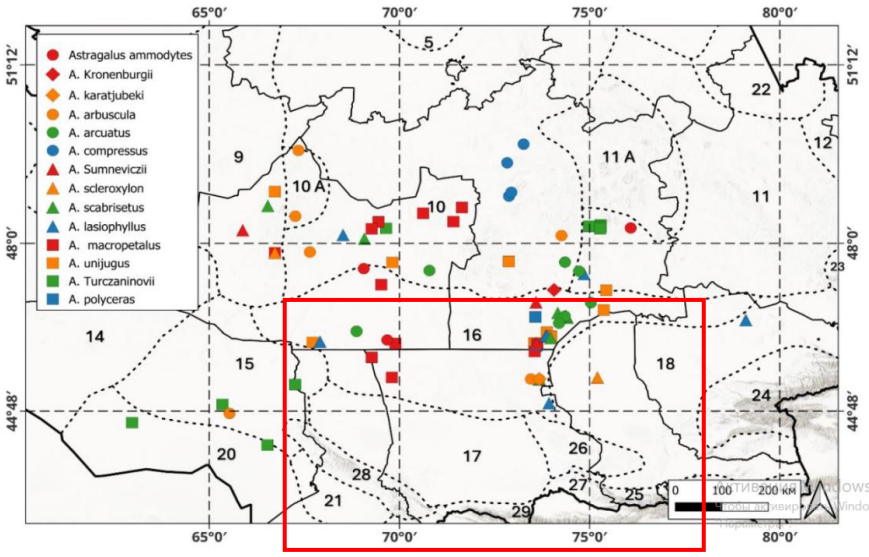

Figure 3. Map of the distribution of species of the subgenus *Cercidotrix* Bunge in the floristic regions of Kazakhstan

Astragalus virgatus
Pall Herbarium MW

Astragalus compressus Ledeb.
Herbarium MW

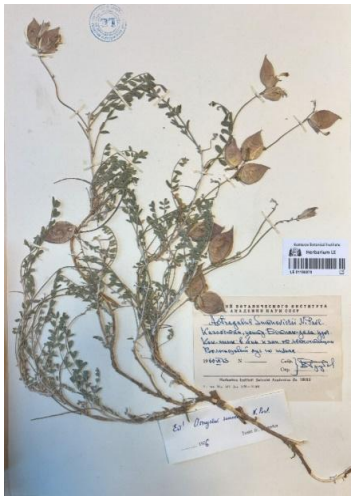

Astragalus Sumneviczii Pavlov.
Herbarium LE

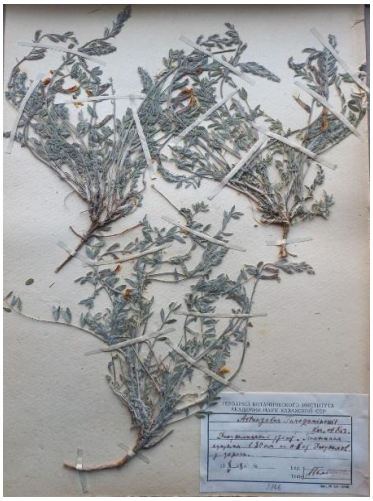

Astragalus Turczaninowii Kar.&Kir
Herbarium AA

Astragalus ammodytes Pall
Herbarium LE

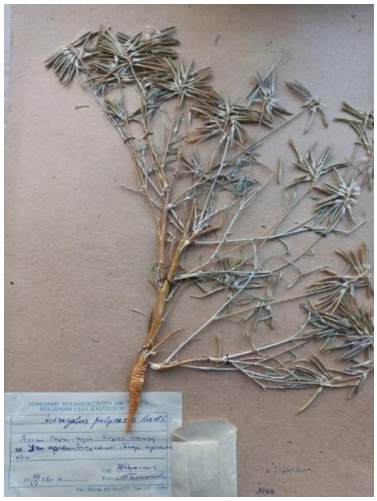

Astragalus polyceras Kar. et Kir.
Herbarium AA

Figure 4. Herbarium specimens of species of the subgenus *Cercidotrix* Bunge. in the Betpak-Dala

Species of the subgenus *Cercidotrix* Bunge, found in the territory of Betpak-Dala, grow in various ecological groups due to the adaptation of representatives of a related branch to the soil. In our research work, we can identify 3 different groups. These are: sandy, rocky-gravel, clay-salt marshes. The species adapted to these groups can be divided as shown in Figure 5. Regarding soil conditions, these plants are frequently found on sandy soils; therefore, they are classified as psammophytes. Psammophytes are plants that grow on sandy soils. They possess a xeromorphic structure and a well-developed root system. In psammophytes, adventitious buds are formed on the roots depending on the accumulation of sand, while adventitious roots develop on the stems when they become covered with sand [3].

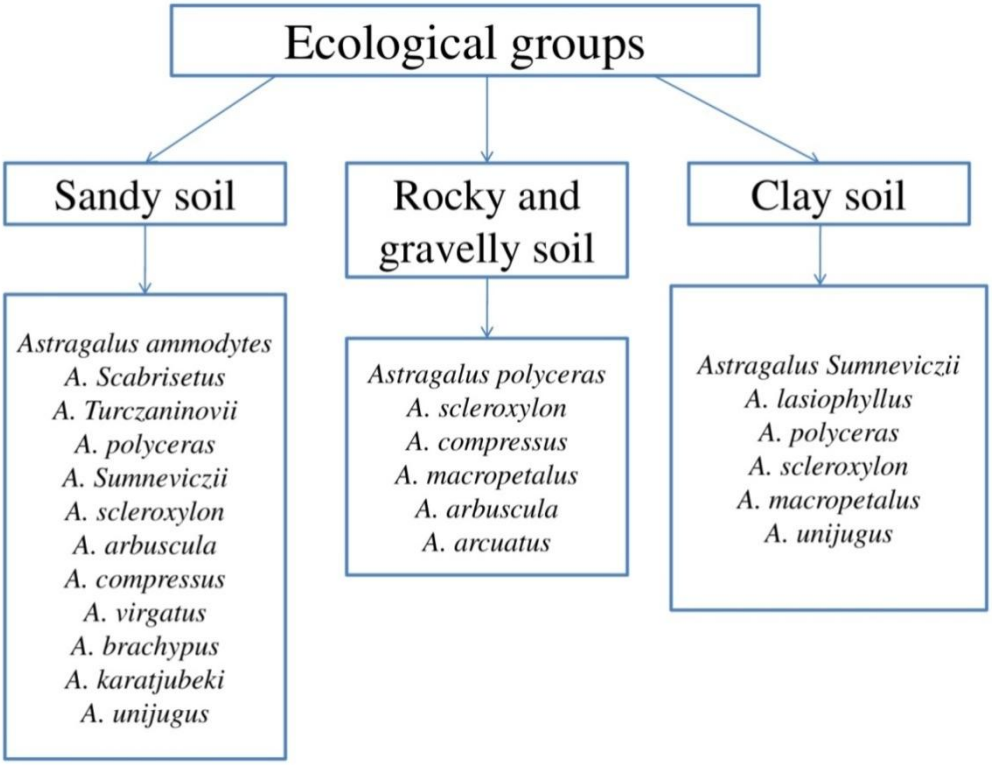

Figure 5. Ecological groups of species of the subgenus *Cercidotrix* Bunge (*Astragalus* L.)

Astragalus is a polymorphic genus that includes a variety of life forms: annual ephemeral herbs, as well as perennial herbaceous, shrubby, subshrub, and branched forms. Currently, there are 2,455 species of these plants worldwide [26, 27].

Analysis of life forms according to I.G. Serebryakov showed that the identified species belong only to certain groups. The predominant life forms are perennial plants (9 species), shrubs (2 species), subshrubs (2 species), sub-shrubs (3 species), and dwarf semi-shrubs (1 species) which can be seen in Table 3.

Ecological analysis of the subgenus indicates a wide distribution of xerophytes and mesophytes in desert and gravelly habitats [26, 27].

Table 3

Life forms according to I.G. Serebryakov

№	Species	Types life form
1	*Astragalus ammodytes*	Perennial grasses
2	*Astragalus arbuscula*	Bush
3	*Astragalus arcuatus*	Perennial grasses
4	*Astragalus brachypus*	Subshrub
5	*Astragalus compressus*	Subshrub
6	*Astragalus karatjubeki*	Subshrub
7	*Astragalus kokaschikii*	Bush
8	*Astragalus Kronenburgii*	Perennial grasses
9	*Astragalus lasiophyllus*	Perennial grasses

Continuation of Table 3

№	Species	Types life form
10	*Astragalus macropetalus*	Perennial grasses
11	*Astragalus polyceras*	Subshrub
12	*Astragalus scabrisetus*	Perennial grasses
13	*Astragalus scleroxylon*	Subshrub
14	*Astragalus Sumneviczii*	Perennial grasses
15	*Astragalus Turczaninovii*	Perennial grasses
16	*Astragalus unijugus*	Shrub
17	*Astragalus virgatus*	Perennial grasses

In the course of a study by C. Raunkier, the life forms *of Cercidotrix* Bunge species were identified. Of these, 41.2 % are hemicryptophytes (7 species), phanerophytes — 41.2 % (7 species) and hametophytes — 17.6 % (3 species) in Figure 2 [30].

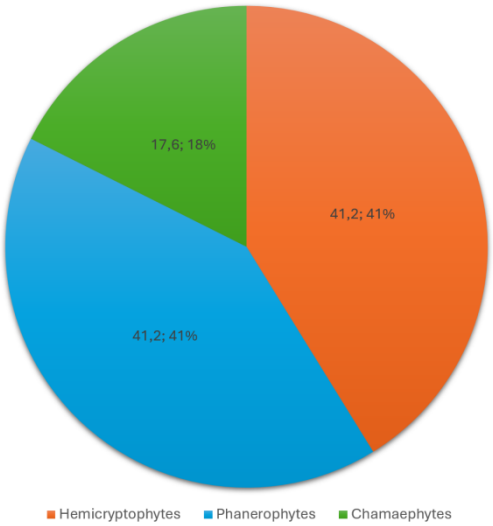

Figure 5. Life forms of representatives of the related branch of *Cercidotrix* Bunge according to C. Raunkier

Conclusion

Thus, on the basis of field studies, collection of information on scientific publications and analysis of the herbarium fund, it was found that 17 species of representatives of the genus *Astragalus* L grow on the territory of Betpak-Dala. Ranking by ecological groups and life forms was carried out. Depending on moistening conditions xerophyte species prevail, perennial herbaceous, bushes plants dominate by life form. Species with fodder value were identified.

Funding

This research was funded by the Ministry of Ecology and Natural Resources of the Republic of Kazakhstan: BR23591088 “Creating the Ulytau Plant Cadastre as Kazakhstan Law tasks” implementation “On Plant World” for sustainable use of region botanical resources” (2024–2026).

Conflict of interest

The authors declare no conflict of interest.

Author contribution

The manuscript was written through contributions of all authors. All authors have given approval to the final version of the manuscript. CRediT: **Turarova Ye.M.** — conceptualization, project administration; investigation, writing, review and editing; **Osmonali B.B.** — methodology, validation, data curation; **Mamurova A.T. —** project administration, supervision.

References

1 Яковлев Г.П. Бобовые земного шара / Г.П. Яковлев. — Л.: Наука, 1991. — 144 с.

2 Ганбаров Д.Ш. Новое местонахождение вида Astragalus mollis M. Bieb. (Fabaceae) во флоре Нахичевани (Азербайджан) / Д.Ш. Ганбаров, Е.А. Асланова, Н.К. Аббасов // Бюллетень науки и практики. — 2023. — Т. 9, № 11. — С. 75–79.

3 Heba-Tallah, Abd Elrahim Abd Elkader. *Astragalus* species: Phytochemistry, biological actions and molecular mechanisms underlying their potential neuroprotective effects on neurological diseases / Heba-Tallah Abd Elrahim Abd Elkader, Amina Essawy, Ahmed S.Al-Shami // Phytochemistry. — October 2022. — Vol. 202. — 113293 https://doi.org/10.1016/j.phytochem.2022.113293

4 Li X. A review of recent research progress on the astragalus genus / X. Li, L. Qu, Y. Dong, L. Han, E. Liu, S. Fang, Y. Zhang, T. Wang // Molecules. — 2014. — 19(11). — 18850–18880. doi: 10.3390/molecules191118850. PMID: 25407722; PMCID: PMC6270929.

5 Павлов Н.В. Флора Казахстана: [в 9-и т.] / Н.В. Павлов. — Алма-Ата: Изд-во АН КазССР, 1961. — Т. 5. — 515 с.

6 Сергалиева М.У. Растения рода Астрагал: перспективы применения в фармации / М.У. Сергалиева, М.В. Мажитова М.А. Самотруева // Астраханский медицинский журнал. — 2015. — Т. 10, № 2. — С. 17–31.

7 Серегин А. Гербарий Московского университета (MW) / А. Серегин. — 2026. — Версия 1.416. Московский государственный университет им. Ломоносова. Набор данных о встречаемости https://doi.org/10.15468/cpnhcc, доступ получен через GBIF.org 13.01.2026. https://www.gbif.org/occurrence/1799016501

8 Голоскоков В.П. Иллюстрированный определитель растений Казахстана [в 2-х т.]. / В.П. Голоскоков — Алма-Ата: Изд-во «Наука» Казахской ССР, 1972. — Т. 2 — 572 с.

9 Байтенов М.С. Қазақстанның Қызыл кітабы / М.С. Байтенов, Р.О. Закирова, Е.М. Абенов. — 2-бас., өңд. және толықт. — Астана, ЖШС «АртPrintXXI», 2014. — 2-ші том: Өсімдіктер. — Б. 169.

10 Plants of the World Online. — POWO, 2024. — [Electronic resource]. — Access mode: https://powo.science.kew.org

11 GBIF | Global Biodiversity Information Facility, 2025. — [Electronic resource]. — Access mode: https://www.gbif.org/

12 iNaturalist. — [Electronic resource]. — Access mode: https://www.inaturalist.org/

13 Цифровой гербарий МГУ. — [Электронный ресурс]. — Режим доступа: https://plant.depo.msu.ru/

14 Серегин А. Гербарий Московского университета (MW) [Электронный ресурс] / А. Серегин. — 2026. — Версия 1.416. Московский государственный университет им. Ломоносова. Набор данных о встречаемости. https://doi.org/10.15468/cpnhcc, доступ получен через GBIF.org 13.01.2026. — Режим доступа: https://www.gbif.org/occurrence/1799016467

15 Серегин А. Гербарий Московского университета (MW) / А.Серегин. — 2026. — Версия 1.416. Московский государственный университет им. Ломоносова. Набор данных о встречаемости https://doi.org/10.15468/cpnhcc, доступ получен через GBIF.org 13.01.2026. https://www.gbif.org/occurrence/1799016536

22 Серегин А. Гербарий Московского университета (MW) / А.Серегин. — 2026. — Версия 1.416. Московский государственный университет им. Ломоносова. Набор данных о встречаемости https://doi.org/10.15468/cpnhcc, доступ получен через GBIF.org 13.01.2026. https://www.gbif.org/occurrence/1799016518

17 Серегин А. Гербарий Московского университета (MW) / А.Серегин. — 2026. — Версия 1.416. Московский государственный университет им. Ломоносова. Набор данных о встречаемости https://doi.org/10.15468/cpnhcc, доступ получен через GBIF.org 13.01.2026. https://www.gbif.org/occurrence/1799018480

18 Серегин А. Гербарий Московского университета (MW) / А. Серегин. — 2026. — Версия 1.416. Московский государственный университет им. Ломоносова. Набор данных о встречаемости https://doi.org/10.15468/cpnhcc, доступ получен через GBIF.org 13.01.2026. https://www.gbif.org/occurrence/1799018507

19 Серегин А. Гербарий Московского университета (MW) / А. Серегин. — 2026. — Версия 1.416. Московский государственный университет им. Ломоносова. Набор данных о встречаемости https://doi.org/10.15468/cpnhcc, доступ получен через GBIF.org 13.01.2026. https://www.gbif.org/occurrence/1799067546

20 Серегин А. Гербарий Московского университета (MW) / А. Серегин. — 2026. — Версия 1.416. Московский государственный университет им. Ломоносова. Набор данных о встречаемости https://doi.org/10.15468/cpnhcc, доступ получен через GBIF.org 13.01.2026. https://www.gbif.org/occurrence/1697719225

21 Серегин А. Гербарий Московского университета (MW) / А. Серегин. — 2026. — Версия 1.416. Московский государственный университет им. Ломоносова. Набор данных о встречаемости https://doi.org/10.15468/cpnhcc, доступ получен через GBIF.org 13.01.2026. https://www.gbif.org/occurrence/1799019092

22 Серегин А. Гербарий Московского университета (MW) / А. Серегин. — 2026. — Версия 1.416. Московский государственный университет им. Ломоносова. Набор данных о встречаемости https://doi.org/10.15468/cpnhcc, доступ получен через GBIF.org 13.01.2026. https://www.gbif.org/occurrence/1799017904

23 Серегин А. Гербарий Московского университета (MW) / А. Серегин. — 2026. — Версия 1.416. Московский государственный университет им. Ломоносова. Набор данных о встречаемости https://doi.org/10.15468/cpnhcc, доступ получен через GBIF.org 13.01.2026. https://www.gbif.org/occurrence/1799019387

24 Серегин А. Гербарий Московского университета (MW) / А. Серегин. — 2026. — Версия 1.416. Московский государственный университет им. Ломоносова. Набор данных о встречаемости https://doi.org/10.15468/cpnhcc, доступ получен через GBIF.org 13.01.2026. https://www.gbif.org/occurrence/1799019418

25 Серегин А. Гербарий Московского университета (MW) / А. Серегин. — 2026. — Версия 1.416. Московский государственный университет им. Ломоносова. Набор данных о встречаемости https://doi.org/10.15468/cpnhcc, доступ получен через GBIF.org 13.01.2026. https://www.gbif.org/occurrence/1799019422

26 Серебряков И.Г. Экологические группы и жизненные формы растений / И.Г. Серебряков // Ботаника (Анатомия и морфология растений). — М., 1978. — С. 431–461.

27 Серебряков И.Г. Жизненные формы высших растений и их изучение / И.Г. Серебряков // Полевая ботаника. — М. — Л.: Наука, 1964. — Т. III. — С. 146–205.

28 Поплавская Г.И. Экология растений / Г.И. Поплавская. — М.: Советская наука, 1948. — 296 с.

29 Raunkiaer C. The Life forms of plants and statistical plant geography / C. Raunkiaer. — Oxford: Clarendon press, 1934. — 632 p.

30 Павленко А.В. Род Astragalus L. во флоре юго-западного Копетдага (Туркменистан) / А.В. Павленко // Проблемы ботаники Южной Сибири и Монголии. «Камелинские чтения». Специальный выпуск. — 2024. — Т. 23, №1. — С. 211–217.

31 Селевин В.А. Введение в естественно-историческое изучение Бетпак-дала / В.А. Селевин // Труды САГУ. XII-а. — 1935 г. — География. Вып.12.

Е.М. Турарова, Б.Б. Осмонали, А.Т. Мамурова

Бетпақдала аумағындағы *Cercidotrix* Bunge туыстармағы өкілдерінің экологиялық-географиялық ерекшеліктері

Мақалада алғаш рет Бетпақдала аумағындағы *Cercidotrix* Bunge тармағының түр құрамы мен географиялық таралуы туралы деректер жүйелендіріліп, нақтыланды. Бұл зерттеу гербарий коллекция қорларының (AA, MW, LE, TASH) талдауы мен қазіргі өрістік бақылауларға негізделген. Зерттеудің ғылыми жаңалығы әдеби деректер мен гербарий материалдарын интеграциялау арқылы Бетпақдала шөл экожүйесіндегі *Cercidotrix* Bunge өкілдерінің экологиялық-географиялық ерекшеліктерін нақтылау, бұл олардың биоалуантүрлілігін және экологиялық сипаттарын тереңірек бағалауға мүмкіндік береді. Жүргізілген экологиялық-географиялық талдау көрсеткендей, *Astragalus* L. туысына қатысты деректерді жинау және жүйелеу алғаш рет Бетпақдалада және жалпы Қазақстан аумағында жүзеге асырылды.

Кілт сөздер: *Astragalus, Cercidotrix*, Бетпақдала, экология, география, гербарий, тіршілік формасы, экологиялық топ.

Е.М. Турарова, Б.Б. Осмонали, А.Т. Мамурова

Эколого-географические особенности представителей рода *Cercidotrix* Bunge, встречающихся на территории Бетпакдалы

В настоящей работе впервые систематизированы и уточнены данные о видовом составе и географическом распространении представителей подрода *Cercidotrix* Bunge на территории Бетпакдалы на основе анализа гербарных коллекций (AA, MW, LE, TASH) и современных полевых наблюдений. Научная новизна исследования заключается в интеграции литературных источников и гербарных данных для уточнения эколого-географических характеристик представителей *Cercidotrix* Bunge в пустынной экосистеме Бетпакдалы, что позволяет глубже оценить их биоразнообразие и экологические особенности. Проведенный анализ эколого-географических данных рода *Astragalus* L. показывает, что сбор и систематизация информации выполнены впервые как для Бетпакдалы, так и для территории Казахстана в целом.

Ключевые слова: Astragalus, Cercidotrix, Бетпакдала, экология, география, гербарий, жизненная форма, экологическая группа.

References

1 Yakovlev, G.P. (1991). *Bobovye zemnogo shara* [Legumes of the World]. Leningrad: Nauka [in Russian].

2 Ganbarov, D.Sh., Aslanova, E.A., & Abbasova, N.K. (2023). Novoe mestonahozhdenie vida *Astragalus mollis* M. Bieb. (Fabaceae) vo flore Nahichevani (Azerbaidzhan). *Biulleten nauki i praktiki — Bulletin of Science and Practice, 9*(11), 75–79 [in Russian].

3 Heba-Tallah, Abd Elrahim Abd Elkader, Amina Essawy, Ahmed S. Al-Shami. (2022). *Astragalus* species: Phytochemistry, biological actions and molecular mechanisms underlying their potential neuroprotective effects on neurological diseases. *Phytochemistry, 202*, 113293. https://doi.org/10.1016/j.phytochem.2022.113293

4 Li, X., Qu, L., Dong, Y., Han, L., Liu, E., Fang, S., Zhang, Y., & Wang, T. (2014). A review of recent research progress on the astragalus genus. *Molecules, 19*(11), 18850–18880. doi: 10.3390/molecules191118850.

5 Pavlov, N.V. (1956–1966). *Flora Kazakhstana* [Flora of Kazakhstan]. Vols. 1–9. Vol. 5. Alma-Ata: Nauka Izdatelstvo Akademii Nauk Kazakhskoi SSR [in Russian].

6 Sergalieva, M.U., Mazhitova, M.V., & Samotrueva, M.A. (2015). Rasteniia roda Astragal: perspektivy primeneniia v farmatsii [Astragalus Species: Potential Applications in Pharmacy]. *Astrakhanskii meditsinskii zhurnal — Astrakhan Medical Journal, 10*(2), 17–31 [in Russian].

7 Seregin, A. (2026). Gerbarii Moskovskogo universiteta (MV) [Moscow University Herbarium (MW)]. Version 1.422. Lomonosov Moscow State University. Occurrence dataset https://doi.org/10.15468/cpnhcc accessed via GBIF.org on 2026-02-24. https://www.gbif.org/occurrence/1799016501

8 Goloskokov, V.P. (1972). *Illiustrirovannii opredelitel rastenii Kazakhstana* [Illustrated Guide to the Plants of Kazakhstan]. Alma-Ata: Nauka [in Russian].

9 Baitenov, M.S., Zakirova, R.O. & Abenov, E.M. (2014). *Kazakhstannyn Qyzyl kitaby* [Red Book of Kazakhstan]. Astana: «ArtPrintXXI» [in Kazakh].

10 (2024). Plants of the World Online (POWO). *powo.science.kew.org*. Retrieved from https://powo.science.kew.org

11 (2025). GBIF | Global Biodiversity Information Facility. *www.gbif.org.* Retrieved from https://www.gbif.org/

12 iNaturalist. *www.inaturalist.org.* Retrieved from https://www.inaturalist.org/

13 Tsifrovoi gerbarii Moskovskogo gosudarstvennogo universiteta [Digital Herbarium of Moscow State University]. *plant.depo.msu.ru.* Retrieved from https://plant.depo.msu.ru/

14 Seregin, A. (2026). Gerbarii Moskovskogo universiteta (MV) [Moscow University Herbarium (MW)]. Version 1.422. — Lomonosov Moscow State University. Occurrence dataset https://doi.org/10.15468/cpnhcc accessed via GBIF.org on 2026-02-24. https://www.gbif.org/occurrence/1799016467

15 Seregin, A. (2026). Gerbarii Moskovskogo universiteta (MV) [Moscow University Herbarium (MW)]. Version 1.422. Lomonosov Moscow State University. Occurrence dataset https://doi.org/10.15468/cpnhcc accessed via GBIF.org on 2026-02-24. https://www.gbif.org/occurrence/1799016536

16 Seregin, A. (2026). Gerbarii Moskovskogo universiteta (MV) [Moscow University Herbarium (MW)]. Version 1.422. Lomonosov Moscow State University. Occurrence dataset https://doi.org/10.15468/cpnhcc accessed via GBIF.org on 2026-02-24. https://www.gbif.org/occurrence/1799016518

17 Seregin, A. (2026). Gerbarii Moskovskogo universiteta (MV) [Moscow University Herbarium (MW)]. Version 1.422. Lomonosov Moscow State University. Occurrence dataset https://doi.org/10.15468/cpnhcc accessed via GBIF.org on 2026-02-24. https://www.gbif.org/occurrence/1799018480

18 Seregin A (2026). Gerbarii Moskovskogo universiteta (MV) [Moscow University Herbarium (MW)]. Version 1.422. Lomonosov Moscow State University. Occurrence dataset https://doi.org/10.15468/cpnhcc accessed via GBIF.org on 2026-02-24. https://www.gbif.org/occurrence/1799018507

19 Seregin, A. (2026). Gerbarii Moskovskogo universiteta (MV) [Moscow University Herbarium (MW)]. Version 1.422. Lomonosov Moscow State University. Occurrence dataset https://doi.org/10.15468/cpnhcc accessed via GBIF.org on 2026-02-24. https://www.gbif.org/occurrence/1799067546

20 Seregin, A. (2026). Gerbarii Moskovskogo universiteta (MV) [Moscow University Herbarium (MW)]. Version 1.422. Lomonosov Moscow State University. Occurrence dataset https://doi.org/10.15468/cpnhcc accessed via GBIF.org on 2026-02-24. https://www.gbif.org/occurrence/1697719225

21 Seregin A. (2026). Gerbarii Moskovskogo universiteta (MV) [Moscow University Herbarium (MW)]. Version 1.422. Lomonosov Moscow State University. Occurrence dataset https://doi.org/10.15468/cpnhcc accessed via GBIF.org on 2026-02-24. https://www.gbif.org/occurrence/1799019092

22 Seregin, A. (2026). Gerbarii Moskovskogo universiteta (MV) [Moscow University Herbarium (MW)]. Version 1.422. Lomonosov Moscow State University. Occurrence dataset https://doi.org/10.15468/cpnhcc accessed via GBIF.org on 2026-02-24. https://www.gbif.org/occurrence/1799017904

23 Seregin, A. (2026). Gerbarii Moskovskogo universiteta (MV) [Moscow University Herbarium (MW)]. Version 1.422. Lomonosov Moscow State University. Occurrence dataset https://doi.org/10.15468/cpnhcc accessed via GBIF.org on 2026-02-24. https://www.gbif.org/occurrence/1799019387

24 Seregin, A. (2026). Gerbarii Moskovskogo universiteta (MV) [Moscow University Herbarium (MW)]. Version 1.422. Lomonosov Moscow State University. Occurrence dataset https://doi.org/10.15468/cpnhcc accessed via GBIF.org on 2026-02-24. https://www.gbif.org/occurrence/1799019418

25 Seregin, A. (2026). Gerbarii Moskovskogo universiteta (MV) [Moscow University Herbarium (MW)]. Version 1.422. Lomonosov Moscow State University. Occurrence dataset https://doi.org/10.15468/cpnhcc accessed via GBIF.org on 2026-02-24. https://www.gbif.org/occurrence/1799019422

26 Serebryakov, I.G. (1978). Ekologicheskie gruppy i zhiznennye formy rastenii [Plant Ecological Groups and Life Forms]. *Botanika (Anatomiia i morfologiia rastenii) — Botany (Plant anatomy and morphology).* Moscow [in Russian].

27 Serebryakov, I.G. (1964). Zhiznennye formy vysshikh rastenii i ikh izuchenie [Life Forms of Vascular Plants and Their Investigation]. *Polevaia botanika — Field botany.* Vol. III. Moscow-Leningrad: Nauka [in Russian].

28 Poplavskaya, G.I. (1948). *Ekologiia rastenii* [Ecology of Plants]. Moscow: Sovetskaia nauka [in Russian].

29 Raunkiaer, C. (1934). *The Life Forms of Plants and Statistical Plant Geography*. Oxford: Clarendon Press.

30 Pavlenko, A.V. (2023). Rod Astragalus L. vo flore yugo-zapadnogo Kopetdaga (Turkmenistan) [The Genus Astragalus L. in the Flora of the Southwestern Kopetdag (Turkmenistan)]. *Problemy botaniki Yuzhnoi Sibiri i Mongolii. «Kamelinskie chteniia». Spetsialnyi vypusk — Problems of botany in Southern Siberia and Mongolia. "Kamelin readings". Special issue, 23*(1), 211–217 [in Russian].

31 Selevin, V.A. (1935). *Vvedenie v estestvenno-istoricheskoe izuchenie Betpak-dala* [Introduction to the Natural-Historical Study of Betpak-Dala]. Tashkent: Trudy SAGU [in Russian].

Information about the authors

Turarova Yerkezhan Murzabekkyzy — Master of Science, Department of Zoology, Histology, and Cytology, Kazakh National University named after Al-Farabi, Senior Laboratory Assistant of Plant World Cadastre Laboratory "Institute of Botany and Phytointroduction", Almaty, Kazakhstan; e-mail: turarova-erkejan@mail.ru; ORCID: 0009-0005-8295-7926

Osmonali Bektemir Birimkululy — PhD, Head of the Plant World Cadastre Laboratory "Institute of Botany and Phytointroduction", Almaty, Kazakhstan; e-mail: be96ka_kz@mail.ru; ORCID: 0000-0003-3060-8597

Mamurova Asem Tleuzhanovna — Candidate of Biological Sciences, Acting professor, Faculty of Biology and Biotechnology, Kazakh National University named after Al-Farabi, Almaty, Kazakhstan; e-mail: amamurova81@mail.ru; ORCID: 0000-0002-4676-9443

How to Cite: Yessimseitova, A.K., Maller, A.V., Dyussembekova, D.A., Islamova, S., Nurtaza, A.S. & Kakimzhanova, A.A. (2026). The influence of explant type and plant growth regulators on callus induction of *Malus niedzwetzkyana*. *Fundamental and Experimental Biology*, 31, 3 (123), 183-191. https://doi.org/10.31489/2026FEB3/183-191

Research Article

https://doi.org/10.31489/2026FEB3/183-191

UDC 57.085.23 Received: 15.12.2026 | Accepted: 06.06.2026 | Published online: 30.09.2026

A.K. Yessimseitova[1, 3], A.V. Maller[2], D.A. Dyussembekova[1, 3], S. Islamova[1], A.S. Nurtaza[1, 3], A.A. Kakimzhanova[1, 3*]

[1]National Center for Biotechnology, Astana, Kazakhstan;
[2]L.N. Gumilyov Eurasian National University, Astana, Kazakhstan;
[3]LLP "Greenlab", Astana, Kazakhstan
**Corresponding author: kakimzhanova@biocenter.kz*

The influence of explant type and plant growth regulators on callus induction of *Malus niedzwetzkyana*

Malus niedzwetzkyana is a rare and valuable wild apple species characterised by a high anthocyanin content. This species is of considerable interest as a promising source of bioactive compounds. In this study, we investigated the effect of explant type on callus induction and its morphological characteristics. Stems and leaves from 40-day-old in vitro-grown plants maintained on Murashige-Skoog (MS) medium were used as explants. The results showed that stem explants had a higher callus induction rate than leaf explants, at 100% and 86.7%, respectively. MS medium supplemented with different concentrations of 2,4-dichlorophenoxyacetic acid (2,4-D) (2.5, 3.0, and 3.5 mg/L) and 6-benzylaminopurine (BAP) (0.5 and 1.0 mg/L) significantly affected callus diameter, fresh and dry weight, and dry matter content ($p < 0.001$). The combination of 3.5 mg/L 2,4-D and 0.5 mg/L BAP in MS medium was optimal, resulting in the formation of a uniform, loose callus with a pinkish-burgundy colour. Thus, our results provide a basis for the establishment of suspension cultures and the biotechnological production of biologically active compounds from *Malus niedzwetzkyana*.

Keywords: callus, *Malus niedzwetzkyana*, plant growth regulators, Murashige-Skoog medium, *in vitro*, auxin, cytokinin.

Introduction

Against the backdrop of the rapid disappearance of natural ecosystems, *in vitro* biotechnological methods are becoming an important tool for the conservation of rare and endangered plant species [1].

One such rare and valuable wild species is *Malus niedzwetzkyana* Dieck, which grows in Central Asia, including Kazakhstan (Karatau and Zailiyskiy Alatau), Kyrgyzstan (Jalal-Abad region) and western China (Xinjiang Uyghur Autonomous Region). This species is of particular interest due to its unique chemical composition and ornamental qualities [2].

A distinctive feature of the *Malus niedzwetzkyana* is the intense red colouration not only of the fruit but also of other parts of the plant—the flowers, leaves, and even the wood. This colouration is due to the high content of anthocyanins—natural pigments from the flavonoid group. These compounds not only impart a bright red colour but also possess powerful antioxidant, anti-inflammatory and anti-cancer properties [3].

These characteristics make the *Malus niedzwetzkyana* of great interest not only as an ornamental and genetic resource of Central Asian flora, but also as a promising source of bioactive compounds for use in the pharmaceutical, food and biotechnology industries. In Kazakhstan, this species is listed in the Red Book, which restricts its widespread use and the collection of wild material [2].

In this context, the development of sustainable biotechnological methods for the cultivation and utilisation of the *Malus niedzwetzkyana* has become particularly important. Such approaches will help to preserve the genetic diversity and natural populations of the species, whilst enabling the production of valuable bioactive compounds without harming ecosystems [4].

One of the modern and promising methods for obtaining valuable compounds from rare or endangered plant species is the use of cell technologies, in particular, the production of callus cultures [5]. In plant tissue culture, the term "callus" refers to a dense mass of undifferentiated cells that form when plant tissue is cultured on a growth medium under controlled conditions *in vitro* [6].

Virtually any part of a plant can be used to produce callus cultures. Explant samples taken from plant tissues grow slowly *in vitro*, forming a cell mass whose colour varies from amorphous and colourless to pale brown [1]. Various callus-inducing factors may be employed to achieve optimal callus formation. Changes in external factors, such as culture medium types, plant growth regulators (PGRs), sucrose concentrations, culture medium pH and incubation temperature, are among the factors that can influence the induction potential and morphology of the induced callus [7].

Despite extensive research into the tissue culture of various species of the genus *Malus*, data on the optimisation of callus formation conditions in *Malus niedzwetzkyana* remain limited. This lack of understanding necessitates the experimental selection of explant type, culture media and PGRs to induce and establish a stable, actively growing callus culture.

This study aimed to investigate the effect of explant type and PGRs concentration (2,4-D and BAP) on the induction and morphological characteristics of *Malus niedzwetzkyana* callus tissue for the subsequent production of suspension cultures and bioactive compounds.

Experimental

Study materials

The research was conducted at the Laboratory of Biotechnology and Plant Breeding at the National Centre for Biotechnology (Astana). *Malus niedzwetzkyana* plants *in vitro* culture, previously obtained by microclonal propagation according to the protocol [8], were used as explants. The *in vitro* shoots were maintained in culture by transferring them to fresh medium of the same composition every 40 days.

Effect of explant type on callus induction

To induce callus, leaves and stems of *Malus niedzwetzkyana in vitro* culture were used as explants to select the most suitable type of explant. Stem and leaf segments measuring 0.3-0.5 cm, taken from plants grown in vitro, were inoculated onto Murashige-Skoog (MS) basal medium [9] containing 30 g/l sucrose and 7 g/l agar, with 2,4-dichlorophenoxyacetic acid (2,4-D) (2.5 mg/L) and 6-benzylaminopurine (BAP) (0.5 mg/L). All chemicals used for analysis were supplied by Sigma-Aldrich (St. Louis, MO). Explantlets grown on MS medium without PGRs were used as a control. Before adding agar, the pH of the medium was adjusted to 5.8, and it was autoclaved at 121 °C for 15 minutes. Cultivation was carried out in a controlled-environment room at a temperature of 25±2 °C with a 12-hour photoperiod and relative humidity of 60–65 %. After 30 days of cultivation, morphological observation was carried out to select a suitable type of explant.

The effect of PGRs concentration on callus formation

To optimise the hormonal composition of the culture medium, the effect of various concentrations of PGRs 2,4-D (2.5; 3.0; 3.5 mg/L) and BAP (0.5; 1.0 mg/L) on the induction of callus formation in stem explants of *Malus niedzwetzkyana* was investigated. The stems were cut into segments measuring 0.3-0.5 cm and inoculated onto MS medium containing 30 g/l sucrose and 7 g/l agar. A total of six treatment were studied: Ⅰ — (2,4-D 2.5 mg/L + BAP 0.5 mg/L); Ⅱ — (2,4-D 3.0 mg/L + BAP 0.5 mg/L); Ⅲ — (2,4-D 3.5 mg/L + BAP 0.5 mg/L); Ⅳ — (2,4-D 2.5 mg/L + BAP 1.0 mg/L); Ⅴ — (2,4-D 3.0 mg/L + BAP 1.0 mg/L); Ⅵ — (2,4-D 3.5 mg/L + BAP 1.0 mg/L). All treatments were cultured in a climate-controlled chamber at a temperature of 25±2 °C with a 12-hour photoperiod and relative humidity of 60–65 %. After 40 days of culture, callus growth parameters were measured.

Measurement of callus growth parameters and statistical analysis

To assess the morphogenetic potential, the colour and texture of the callus were determined visually. The growth parameters of the induced callus were assessed by fresh weight (FW), dry weight (DW) and dry matter (DM). To determine dry weight, the fresh callus was dried in an oven at 45 °C until a constant weight was achieved (Binder ED115, Tuttlingen, Germany). The dry matter of callus was calculated using the formula:

$$DM\ (\%) = (DW/FW) \times 100$$

Statistical analysis was performed using Python. The data obtained were analysed using one-way analysis of variance (ANOVA). Tukey's HSD test was used for pairwise comparison of mean values. Results are presented as mean ± standard deviation. Differences between treatments were considered statistically significant at $p < 0.05$.

Results and Discussion

Effect of explant type on callus induction

The first signs of cell dedifferentiation and callus formation were observed 10–15 days after inoculation, manifesting as cell swelling and proliferation at the cut surfaces of the explants. No callus formation was observed on the control MS medium without the addition of PGRs. On the MS medium (2,4-D — 2.5 mg/L and BAP — 0.5 mg/L), the extent of callus formation varied depending on the type of explant. On leaf explants, callus formed in several zones: along the edges of the leaf blade and in its central part (Fig. 1). On stem explants, callus tissue began to develop from the transverse cuts on both sides. A comparative analysis showed that callus formation was significantly more pronounced on stem explants: the callus induction rate was 100 % for stems and 86.7 % for leaves. Consequently, stem explants were used for further studies.

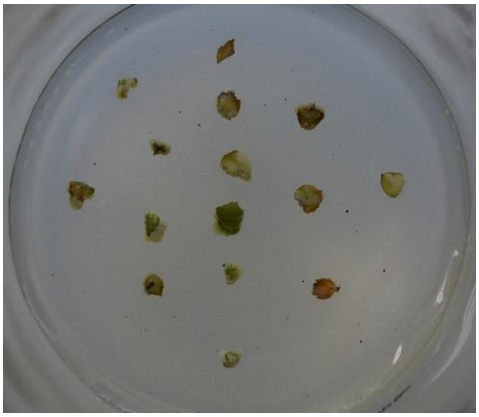

a — callus from a leaf explant

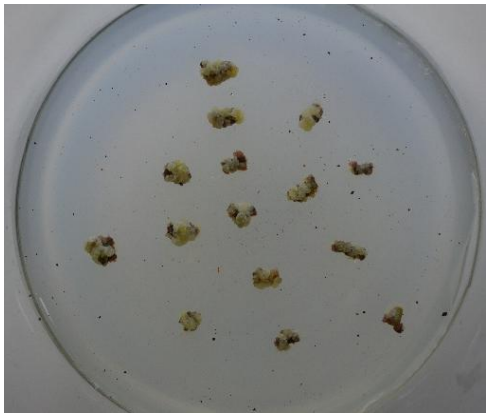

b — callus from a stem explant

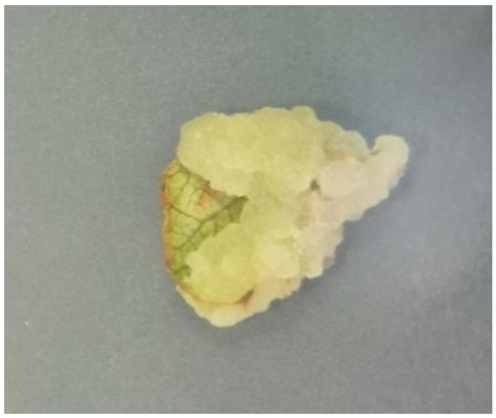

c — leaf explant under a microscope (×15)

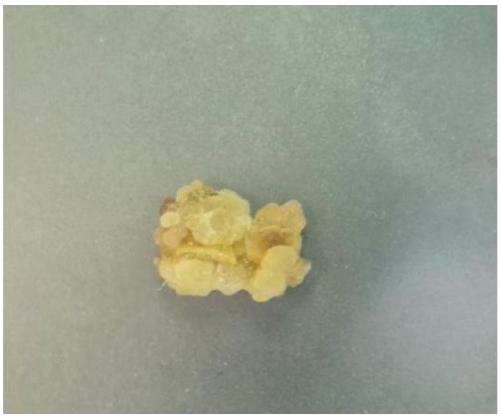

d — stem explant under a microscope (×15)

Figure 1. Callus induction from leaf and stem explants of *Malus niedzwetzkyana*

The effect of PGRs on the growth and development of callus cultures

Various combinations of the PGRs 2,4-D (2.5, 3.0 and 3.5 mg/L) and BAP (0.5 and 1.0 mg/L) had a marked effect on the morphological and growth characteristics of callus tissue. All PGR combinations tested resulted in 100 % callus induction from stem explants of *Malus niedzwetzkyana.*

As shown in Table 1, all PGR combinations significantly affected callus diameter, fresh weight (FW), dry weight (DW) and dry matter (DM) ($p < 0.001$). The largest callus diameter (13.20 ± 3.76 mm) and the highest dry weight (0.045 ± 0.019 g) were observed in treatment I (2,4-D 2.5 mg/L + BAP 0.5 mg/L). The highest fresh weight was recorded in treatment II (2,4-D 3.0 mg/L + BAP 0.5 mg/L) and amounted to 0.342 ± 0.204 g. With an increase in PGR concentration, a gradual decrease in all growth parameters was observed: the minimum values for diameter (5.93±2.55 mm), fresh weight (0.048±0.033 g) and dry weight (0.014±0.007 g) were recorded in treatment VI (2,4-D 3.5 mg/L + BAP 1.0 mg/L).

The dry matter content showed the opposite trend: in treatments I-III, the dry matter was at its lowest (12.09–16.03 %), indicating a high water content and a loose callus structure. In treatments IV-VI, a significant increase in dry matter (31.97–34.75 %) was observed, indicating the formation of a denser and more compact callus. Thus, increasing the BAP concentration from 0.5 to 1.0 mg/L had a more pronounced inhibitory effect on callus growth parameters and promoted the formation of denser, more compact tissue compared with an increase in 2,4-D concentration.

Table 1

Effect of various combinations of plant growth regulators (2,4-D and BAP) on the fresh weight, dry weight and dry matter of callus

Treatment	2,4-D (mg/L)	BAP (mg/L)	Callus diameter (mm)	Fresh callus weight (g)	Dry callus weight (g)	Dry matter (%)	Callus colour and texture
I	2,5	0,5	13,20±3,76	0,301±0,133	0,045±0,019	16,03±5,92	Yellowish with white flecks, heterogeneous
II	3,0	0,5	12,80±3,57	0,342±0,204	0,039±0,017	12,56±2,83	Creamy yellow with pink and burgundy flecks, heterogeneous
III	3,5	0,5	10,80±4,11	0,194±0,109	0,023±0,015	12,09±4,05	Creamy yellow with pink and burgundy flecks, crumbly
IV	2,5	1,0	6,93±1,87	0,070±0,039	0,022±0,008	33,10±6,44	White and yellow with brown patches, mottled
V	3,0	1,0	6,07±0,96	0,061±0,059	0,017±0,016	34,75±18,10	Greenish-yellow with purple flecks, dense
VI	3,5	1,0	5,93±2,55	0,048±0,033	0,014±0,007	31,97±5,37	Green and greenish-white, compact
Significance			***	***	***	***	

****: p<0.001, **: p<0.01, *: p<0.05.* The data are presented as the mean ± standard deviation, n = 15.

Visual inspection revealed that the calluses in all treatments were predominantly yellowish or greenish yellow in colour (Fig. 1a, c). With an increase in the concentration of 2,4-D to 3.0 mg/L in combination with both 0.5 mg/L BAP (treatment II) and 1.0 mg/L BAP (treatment V), the appearance of a pronounced reddish-purple hue was observed. With a further increase in the concentration of 2,4-D to 3.5 mg/L (treatments III and VI), the intensity of pigmentation decreased; however, in treatments with 1.0 mg/L BAP (VI), an intensification of the greenish colour and the appearance of dense nodular structures were noted, indicating the onset of differentiation processes. The best texture loose, uniform, creamy-yellow with pinkish-burgundy flecks was demonstrated by treatment III (2,4-D 3.5 mg/L + BAP 0.5 mg/L), making it the most suitable for further cultivation.

In terms of structure, the callus tissues of treatments I-III (BAP 0.5 mg/L) had a heterogeneous and loose structure, with treatment III easily breaking down into individual cells and cell aggregates. Increasing the BAP concentration to 1.0 mg/L (treatments IV-VI) led to the formation of a dense callus structure; furthermore, organogenesis of the callus tissue was observed.

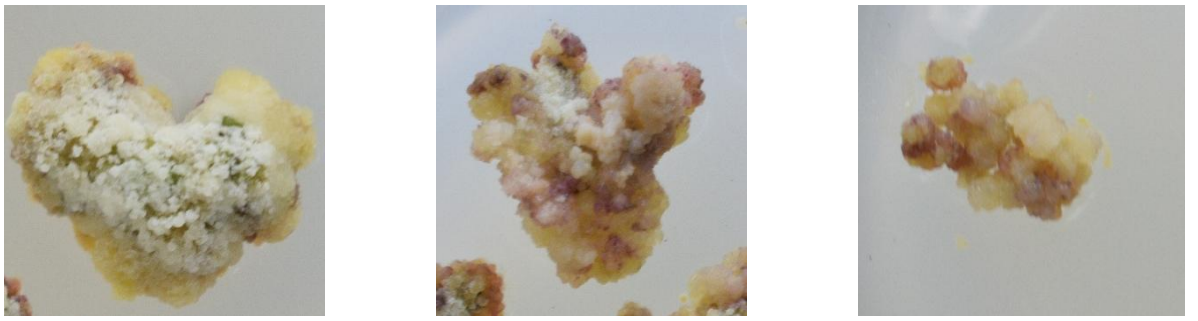

a — 2.5 mg/L 2,4-D + 0.5 mg/L BAP

b — 3.0 mg/L 2,4-D + 0.5 mg/L BAP

c — 3.5 mg/L 2,4-D + 0.5 mg/L BAP

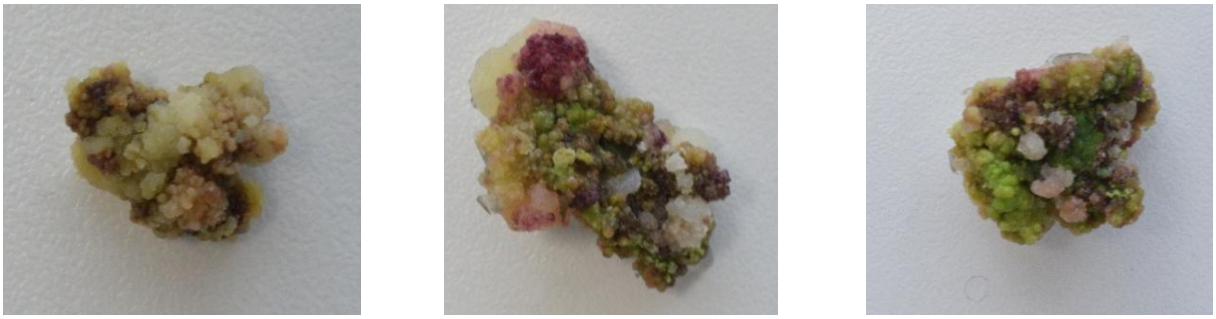

d — 2.5 mg/L 2,4-D + 1.0 mg/L BAP

e — 3.0 mg/L 2,4-D + 1.0 mg/L BAP

f — 3.5 mg/L of 2,4-D + 1.0 mg/L of BAP

Figure 2. Callus formation on MS medium supplemented with different combinations of 2,4-D and BAP

A detailed morphological examination of the calli revealed differences in texture and colouration between the treatments. The calli of treatment III (2,4-D 3.5 mg/L + 6-BAP 0.5 mg/L) had a uniform, loose, granular texture that easily disintegrated into individual cell aggregates, and were cream-yellow in colour with pinkish-burgundy inclusions (Fig. 1c). In contrast, the calli of treatment II (2,4-D 3.0 mg/L + 6-BAP 0.5 mg/L) had a denser, heterogeneous texture in the form of large aggregates with pink-burgundy inclusions (Fig. 1b). It should be noted that the pink-burgundy colour of the calli in both treatments is due to the presence of anthocyanins, which accumulate in *Malus niedzwetzkyana*. Although treatment II demonstrated the highest fresh weight (0.342±0.204 g), treatment III was preferable for suspension culture.

The calli from the treatments with a higher concentration of BAP (1.0 mg/L) differed significantly in morphology. Treatment Ⅳ (2,4-D 2.5 mg/L + BAP 1.0 mg/L) was characterised by a denser, heterogeneous texture with brownish areas, which may indicate oxidative processes in the callus tissue (Fig. 1d). Treatment Ⅴ (2,4-D 3.0 mg/L + BAP 1.0 mg/L) was distinguished by the most pronounced anthocyanin pigmentation with intense purple spots, as well as the presence of green nodular structures, indicating the onset of organogenesis processes. In treatment Ⅵ (2,4-D 3.5 mg/L + BAP 1.0 mg/L), a greenish colouration predominated with a dense, compact callus structure, indicating enhanced cell differentiation at high concentrations of both growth regulators. Thus, increasing the BAP concentration to 1.0 mg/L generally contributed to the compaction of callus tissue and the intensification of differentiation processes, making these treatments less suitable for obtaining suspension cultures compared to treatment III

The choice of explant type is one of the key factors influencing the efficiency of callus induction [10]. In this study, stem explants of *Malus niedzwetzkyana* demonstrated a higher morphogenetic capacity compared to leaf explants. Callus induction was 100 % for stem explants and 86.7 % for leaf explants. This is consistent with the study by Zhang et al. (2020), which showed that callus induction from stem explants of the wild apple (*Malus sieversii*) occurred more rapidly and with higher efficiency compared to leaf explants, whereas leaf explants were highly sensitive to medium composition and died in the absence of auxin [11]. The greater ability of stem explants to form callus can be explained by the large number of meristem-like cells in the vascular tissues of the stem, which are known to possess a greater capacity for dedifferentiation [12].

Plant growth regulators play a key role at all stages of plant development, influencing cell growth, differentiation, physiological responses and the production of secondary metabolites. Under *in vitro* conditions,

they are one of the key factors controlling callus formation and cell proliferation, and their optimal type and concentration must be determined experimentally for each species, genotype and explant [13]. Auxins and cytokinins are essential for cell division and morphogenesis. Auxins are considered the primary inducers of callus formation, promoting cell wall softening through acidification and activating the expression of genes associated with growth and development. Cytokinins complement this effect by directly regulating the cell cycle, thereby maintaining sustained cell division and morphogenetic activity [14].

According to the results of our study, a low concentration of BAP (0.5 mg/L) is more effective than a high concentration (1.0 mg/L). The 2,4-D and BAP had a marked and statistically significant effect on all the callus formation parameters studied ($p < 0.001$). The auxin 2,4-D, in combination with a low concentration of cytokinin (BAP 0.5 mg/L), stimulated active cell proliferation and the formation of loose, well-growing callus tissue. Increasing the BAP concentration to 1.0 mg/L had a marked inhibitory effect on growth parameters, which is consistent with the general pattern that in cultures containing low concentrations of cytokinin and high concentrations of auxin, callus cultures grow excessively, and the callus structure becomes soft and loose, but as the concentration of cytokinin increases, the callus tissue becomes stiffer [15].

Studies conducted on *Abies koreana* showed that a combination of the NAA, 2,4-D and BAP had a positive effect on callus formation. The callus proliferation coefficient at a high concentration of 2,4-D (3.0 mg/L) was high, amounting to 1147.6 % compared to the initial mass of fresh callus [16]. A comparison with data on closely related species of the *Rosaceae* family shows that optimal concentrations and PGR types vary significantly depending on the genotype. Thus, in studies by Menbari et al. (2021), it was found that the maximum callus induction rate (100 %) was achieved on MS medium containing 2.0 mg/L 2,4-D and 1.0 mg/L BAP. The same combination of PGRs also resulted in the highest fresh and dry callus biomass (2.754 g and 0.37 g, respectively). Furthermore, callus formation occurred more rapidly compared with other combinations. The authors also noted that this combination yielded the best callus quality, characterised by a loose texture and a yellowish-white colour [17].

The results obtained are consistent with the literature on the key role of the auxin-to-cytokinin ratio in the regulation of callus formation. The best indicators of fresh callus mass and texture were achieved using 2,4-D at a concentration of 2.5-3.5 mg/L in combination with BAP at 0.5 mg/L, which is slightly higher than the concentrations described for other species of the genus *Malus*. This appears to reflect the genetic characteristics of *Malus niedzwetzkyana*.

Treatment III (2,4-D 3.5 mg/L + BAP 0.5 mg/L) was identified as optimal not only in terms of the morphological characteristics of the callus loose texture and low dry matter content, but also in terms of its suitability for the subsequent establishment of suspension cultures. Thus, treatment III ensures the production of callus most suitable for establishing suspension cultures and studying the bioactive compounds of this species.

Conclusion

This study investigated callus formation in leaf and stem explants of *Malus niedzwetzkyana*. It was found that stem explants possess higher morphogenetic activity compared to leaf explants and demonstrate 100 % callus induction. The optimal PGR composition of the medium for callus formation was determined. Among the PGR combinations tested, the MS medium supplemented with 2,4-D at a concentration of 3.5 mg/L and BAP at a concentration of 0.5 mg/L proved to be the most promising for the cultivation of uniform, loose callus tissue. The pinkish-burgundy colour of the calli formed, due to the accumulation of anthocyanins, demonstrates the high biosynthetic potential of this species and opens up prospects for the use of *Malus niedzwetzkyana* callus and suspension cultures for the biotechnological production of biologically active substances.

Funding

This work was supported by the Ministry of Science and Higher Education of the Republic of Kazakhstan under programme BR28713087, “Fundamental and applied aspects of obtaining and targeted synthesis of biologically active substances from medicinal plants *in vitro* culture”, for the period 2025–2027.

Conflict of interest

The authors declare no conflict of interest.

Author Contributions

The manuscript was written through contributions of all authors. All authors have given approval to the final version of the manuscript. CRediT: **Kakimzhanova A.A**. — conceptualization, investigation, writing draft; **Yessimseitova A.K., Dyussembekova D.A., Islamova S.S., Nurtaza A.S.** — data curation, analysis, methodology, data collection; **Maller A.V.** — investigation, data analysis.

References

1 Efferth T. Biotechnology applications of plant callus cultures / T. Efferth // Engineering. — 2019. — Vol. 5, No. 1. — P. 50–59. https://doi.org/10.1016/j.eng.2018.11.006

2 Kolchenko M. Wild *Malus niedzwetzkyana* Dieck ex Koehne as a genetic resource for fire blight resistance / M. Kolchenko, A. Nurtaza, A. Pozharskiy, D. Dyussembekova, A. Kapytina, G. Nizamdinova, M. Khusnitdinova, A. Taskuzhina, A. Kakimzhanova, D. Gritsenko // Horticulturae. — 2023. — Vol. 9, No. 10. — P. 1066. https://doi.org/10.3390/horticulturae9101066

3 Khoo H.E. Anthocyanidins and anthocyanins: Colored pigments as food, pharmaceutical ingredients, and the potential health benefits / H.E. Khoo, A. Azlan, S.T. Tang, S.M. Lim // Food & Nutrition research. — 2017. — Vol. 61, No. 1. — P. 1361779. https://doi.org/10.1080/16546628.2017.1361779

4 Мамонов Л.К. Степень изученности видов, родов и семейств флоры Казахстана и перспективы дальнейших исследований / Л.К. Мамонов, Р.А. Музычкина, Н.Г. Гемеджиева, Ю.И. Васильев, Г.Т. Ситпаева, Н.А. Рябушкина, Г.С. Муканова // Введение в фитохимические исследования и выявление биологической активности веществ растений. — Алматы, 2008. — С. 24.

5 Babich O. Evaluation of the conditions for the cultivation of callus cultures of *Hyssopus officinalis* regarding the yield of polyphenolic compounds / O. Babich, S. Sukhikh, A. Pungin, L. Astahova, E. Chupakhin, D. Belova, A. Prosekov, S. Ivanova // Plants. — 2021. — Vol. 10, No. 5. — P. 915. https://doi.org/10.3390/plants10050915

6 Sidik N.J. A Mini review of plant tissue culture: the role of media optimization, growth regulators in modern agriculture, callus induction and the applications / N.J. Sidik, H.M. Agha, A.A. Alkamil, M. M.S. Alsayadi, A.A. Mohammed // AUIQ Complementary Biological System. — 2024. — Vol. 1, No. 2. — P. 96–109. https://doi.org/10.70176/3007-973X.1019

7 Osman N.I. Effects of variations in culture media and hormonal treatments upon callus induction potential in endosperm explant of *Barringtonia racemosa* L. / N.I. Osman, N.J. Sidik, A. Awal // Asian Pacific Journal of Tropical Biomedicine. — 2016. — Vol. 6, No. 2. — P. 143–147. https://doi.org/10.1016/j.apjtb.2015.10.007

8 Nurtaza A. Micropropagation of the endangered species *Malus niedzwetzkyana* for conservation biodiversity in Kazakhstan / A. Nurtaza, G. Magzumova, A. Yessimseitova, V. Karimova, A. Shevtsov, D. Silayev, V. Lutsay, Y. Ramankulov, A. Kakimzhanova // In Vitro Cellular & Developmental Biology. — 2021. — Vol. 57, No. 6. — P. 965–976. https://doi.org/10.1007/s11627-021-10174-4

9 Murashige T. (1962). A revised medium for rapid growth and bio assays with tobacco tissue cultures / T. Murashige, F. Skoog // Physiologia plantarum. — 1962. — Vol. 15, No. 3. https://doi.org/10.1111/j.1399-3054.1962.tb08052.x

10 Rahayu S. The effect of types and concentrations of auxins on callus induction of *Centella asiatica* / S. Rahayu, I. Roostika, N. Bermawie // Nusantara Bioscience. — 2016. — Vol. 8, No. 2. — P. 283-7. https://doi.org/10.13057/nusbiosci/n080224

11 Zhang Y. An efficient in vitro regeneration system from different wild apple (*Malus sieversii*) explants / Y. Zhang, T.A. Bozorov, D.X. Li, P. Zhou, X.J. Wen, Y. Ding, D.Y. Zhang // Plant Methods. — 2020. — Vol. 16, No. 1. — P. 56. https://doi.org/10.1186/s13007-020-00599-0

12 Kaňuková Š. Establishment of stem cell-like cells of *Sida hermaphrodita* (L.) rusby from explants containing cambial meristems / Š. Kaňuková, M. Gubišová, L. Klčová, D. Mihálik, J. Kraic // International Journal of Molecular Sciences. — 2022. — Vol. 23, No. 14. — P. 7644. https://doi.org/10.3390/ijms23147644

13 Song W. Improvement of culture conditions and plant growth regulators for *in vitro* callus induction and plant regeneration in *Paeonia lactiflora* Pall / W. Song, Y. Song, X. Liu, X. Zhang, R. Xin, S. Duan, S. Guan, X. Sun // Plants. — 2023. — Vol. 12, No. 23. — P. 3968. https://doi.org/10.3390/plants12233968

14 Hazrati R. Factors affecting the growth, antioxidant potential, and secondary metabolites production in hazel callus cultures / R. Hazrati, N. Zare, R. Asghari-Zakaria, P. Sheikhzadeh, M. Johari-Ahar // AMB Express. — 2022. — Vol. 12, No. 1. — P. 109. https://doi.org/10.1186/s13568-022-01449-z

15 Rahmati Z. et al. Optimization of culture medium for *in vitro* callogenesis in *Taxus baccata* L. and *T. berevifolia* Nutt / Z. Rahmati, V. Payam Nour, K. Ghasemi Bezdi, P. Ebrahimi // Forest and Wood Products. — 2017. — Vol. 70, No. 3. — P. 381–391.

16 Guo G. Explant, medium, and plant growth regulator (PGR) affect induction and proliferation of callus in *Abies koreana* / G. Guo, B.R Jeong // Forests. — 2021. — Vol. 12, No. 10. — P. 1388. https://doi.org/10.3390/f12101388

17 Menbari A. Establishment of callus and cell suspension cultures of Granny Smith apple fruit and antityrosinase activity of their extracts / A. Menbari, B. Bahramnejad, M. Abuzaripoor, E. Shahmansouri, M. A. Zarei // Scientia Horticulturae. — 2021. — Vol. 286. — P. 110222. https://doi.org/10.1016/j.scienta.2021.110222

А.К. Есимсеитова, А.В. Маллер, Д.А. Дюсембекова, С.С. Исламова,
А.С. Нұртаза, А.А. Какимжанова

Malus niedzwetzkyana каллус индукциясына эксплант түрі және өсімдік гормондарының әсері

Недзвецкий алмасы (*Malus niedzwetzkyana*) — антоцианиннің жоғары мөлшерімен сипатталатын сирек кездесетін және бағалы жабайы түр. Бұл түр биоактивті қосылыстардың перспективалы көзі ретінде елеулі қызығушылық тудырады. Осы зерттеуде эксплант түрінің каллус индукциясына және оның морфологиялық сипаттамаларына әсері зерттелген. 40 күн *in vitro* жағдайында Мурасиге-Скуг (МС) қоректік ортасында өсірілген өсімдіктердің сабағы мен жапырақтары эксплант ретінде алынды. Нәтижелер көрсеткендей, сабақ эксплантгары жапырақ эксплантгарына қарағанда каллус түзу қабілетін жоғарырақ көрсетті, тиісінше 100 % және 86,7 %. 2,4-дихлорофеноксиацетикалық қышқылдың (2,4-D) әртүрлі концентрациялары бар МС ортасы (2,5; 3,0; 3,5 мг/л) және 6-бензиламинопурин (БАП) (0,5; 1,0 мг/л) концентрациялары диаметрге, жаңа және құрғақ салмаққа, сондай-ақ құрғақ зат мөлшеріне ($p < 0,001$) елеулі әсер етті. МС ортасы мен 3,5 мг/л концентрациядағы 2,4-D және 0,5 мг/л БАП үйлесімі оңтайлы, бұл қызғылт-қою қызыл түсті біртекті әрі борпылдақ каллустың түзілуін қамтамасыз етті. Осылайша, алынған нәтижелер Недзвецкий алмасының суспензиялық өсірінділерін алу және биологиялық белсенді заттарды биотехнологиялық жолмен өндіру үшін негіз бола алады.

Кілт сөздер: каллус, *Malus niedzwetzkyana*, өсу реттегіштері, Мурасиге-Скуг ортасы, *in vitro*, ауксин, цитокинин.

А.К. Есимсеитова, А.В. Маллер, Д.А. Дюсембекова, С.С. Исламова,
А.С. Нұртаза, А.А. Какимжанова

Влияние типа экспланта и гормонов растений на индукцию каллуса яблони Недзвецкого (*Malus niedzwetzkyana*)

Яблоня Недзвецкого (*Malus niedzwetzkyana*) — редкий и ценный дикорастущий вид, который характеризуется высоким содержанием антоцианов. Этот вид представляет значительный интерес как перспективный источник биологически активных веществ. В настоящем исследовании мы изучали влияние типа экспланта на индукцию каллуса и его морфологические характеристики. В качестве эксплантов использовали стебли и листья 40-дневных растений, выращенных в условиях *in vitro*, которые культивировали на среде Мурасиге-Скуга (МС). Результаты показали, что экспланты стебля демонстрировали более высокую способность к образованию каллуса по сравнению с эксплантами листьев — 100 % и 86,7 % соответственно. Среда МС с различными концентрациями 2,4-дихлорфеноксиуксусной кислоты (2,4-D) (2,5; 3,0; 3,5 мг/л) и 6-бензиламинопурина (БАП) (0,5; 1,0 мг/л) оказала значительное влияние на диаметр, свежую и сухую массу, а также содержание сухого вещества ($p < 0,001$). Сочетание среды МС с 2,4-D в концентрации 3,5 мг/л и БАП 0,5 мг/л являлось оптимальным, что обеспечивало образование однородного и рыхлого каллуса розово-бордового цвета. Таким образом, полученные нами результаты служат основой для получения суспензионных культур и биотехнологического получения биологически активных веществ яблони Недзвецкого.

Ключевые слова: каллус, *Malus niedzwetzkyana*, регуляторы роста, среда Мурасиге-Скуга, *in vitro*, ауксин, цитокинин.

References

1 Efferth, T. (2019). Biotechnology applications of plant callus cultures. *Engineering*, *5*(1), 50–59. https://doi.org/10.1016/j.eng.2018.11.006

2 Kolchenko, M., Nurtaza, A., Pozharskiy, A., Dyussembekova, D., Kapytina, A., Nizamdinova, G., ... & Gritsenko, D. (2023). Wild *Malus niedzwetzkyana* Dieck ex Koehne as a genetic resource for fire blight resistance. *Horticulturae*, *9*(10), 1066. https://doi.org/10.3390/horticulturae9101066

3 Khoo, H.E., Azlan, A., Tang, S.T., & Lim, S.M. (2017). Anthocyanidins and anthocyanins: Colored pigments as food, pharmaceutical ingredients, and the potential health benefits. *Food & Nutrition research*, *61*(1), 1361779. https://doi.org/10.1080/16546628.2017.1361779

4 Mamonov, L.K., Muzychkina, R.A., Gemedzhieva, N.G., Vasiliev, Yu.I., Sitpaeva, G.T., Ryabushkina, N.A., & Mukanova, G.S. (2008). Stepen izuchennosti vidov, rodov i semeistv flory Kazakhstana i perspektivy dalneishikh issledovanii [The degree of study of species, genera and families of the flora of Kazakhstan and prospects for further research]. *Vvedenie v*

fitokhimicheskie issledovaniia i vyiavlenie biologicheskoi aktivnosti veshchestv rastenii — Introduction to phytochemical research and identification of biological activity of plant substances, 24. Almaty [in Russian].

5 Babich, O., Sukhikh, S., Pungin, A., Astahova, L., Chupakhin, E., Belova, D., ... & Ivanova, S. (2021). Evaluation of the conditions for the cultivation of callus cultures of *Hyssopus officinalis* regarding the yield of polyphenolic compounds. *Plants*, *10*(5), 915. https://doi.org/10.3390/plants10050915

6 Sidik, N.J., Agha, H.M., Alkamil, A.A., Alsayadi, M.M. S., & Mohammed, A.A. (2024). A Mini review of plant tissue culture: the role of media optimization, growth regulators in modern agriculture, callus induction and the applications. *AUIQ Complementary Biological System*, *1*(2), 96–109. https://doi.org/10.70176/3007-973X.1019

7 Osman, N.I., Sidik, N.J., & Awal, A. (2016). Effects of variations in culture media and hormonal treatments upon callus induction potential in endosperm explant of *Barringtonia racemosa* L. *Asian Pacific Journal of Tropical Biomedicine*, *6*(2), 143–147. https://doi.org/10.1016/j.apjtb.2015.10.007

8 Nurtaza, A., Magzumova, G., Yessimseitova, A., Karimova, V., Shevtsov, A., Silayev, D., ... & Kakimzhanova, A. (2021). Micropropagation of the endangered species *Malus niedzwetzkyana* for conservation biodiversity in Kazakhstan. *In Vitro Cellular & Developmental Biology*, *57*(6), 965–976. https://doi.org/10.1007/s11627-021-10174-4

9 Murashige, T., & Skoog, F. (1962). A revised medium for rapid growth and bio assays with tobacco tissue cultures. *Physiologia plantarum*, *15*(3). https://doi.org/10.1111/j.1399-3054.1962.tb08052.x

10 Rahayu, S., Roostika, I., & Bermawie, N. (2016). The effect of types and concentrations of auxins on callus induction of *Centella asiatica*. *Nusantara Bioscience*, *8*(2), 283-7. https://doi.org/10.13057/nusbiosci/n080224

11 Zhang, Y., Bozorov, T. A., Li, D. X., Zhou, P., Wen, X. J., Ding, Y., & Zhang, D. Y. (2020). An efficient in vitro regeneration system from different wild apple (*Malus sieversii*) explants. *Plant Methods*, *16*(1), 56. https://doi.org/10.1186/s13007-020-00599-0

12 Kaňuková, Š., Gubišová, M., Klčová, L., Mihálik, D., & Kraic, J. (2022). Establishment of Stem Cell-like Cells of *Sida hermaphrodita* (L.) Rusby from Explants Containing Cambial Meristems. *International Journal of Molecular Sciences*, *23*(14), 7644. https://doi.org/10.3390/ijms23147644

13 Song, W., Song, Y., Liu, X., Zhang, X., Xin, R., Duan, S., ... & Sun, X. (2023). Improvement of Culture Conditions and Plant Growth Regulators for In Vitro Callus Induction and Plant Regeneration in *Paeonia lactiflora* Pall. *Plants*, *12*(23), 3968. https://doi.org/10.3390/plants12233968

14 Hazrati, R., Zare, N., Asghari-Zakaria, R., Sheikhzadeh, P., & Johari-Ahar, M. (2022). Factors affecting the growth, antioxidant potential, and secondary metabolites production in hazel callus cultures. *AMB Express*, *12*(1), 109. https://doi.org/10.1186/s13568-022-01449-z

15 Rahmati, Z., Payam Nour, V., Ghasemi Bezdi, K., & Ebrahimi, P. (2017). Optimization of culture medium for *in vitro* callogenesis in *Taxus baccata* L. and *T. berevifolia* Nutt. *Forest and Wood Products*, *70*(3), 381–391.

16 Guo, G., & Jeong, B.R. (2021). Explant, medium, and plant growth regulator (PGR) affect induction and proliferation of callus in *Abies koreana. Forests*, *12*(10), 1388. https://doi.org/10.3390/f12101388

17 Menbari, A., Bahramnejad, B., Abuzaripoor, M., Shahmansouri, E., & Zarei, M. A. (2021). Establishment of callus and cell suspension cultures of Granny Smith apple fruit and antityrosinase activity of their extracts. *Scientia Horticulturae*, *286*, 110222. https://doi.org/10.1016/j.scienta.2021.110222

Information about the authors

Yessimseitova Assel Kairatovna — PhD student, Senior researcher, National Center for Biotechnology, Astana, Kazakhstan; e-mail: asel_1388@bk.ru, ORCID: https://orcid.org/0000-0002-5428-1915

Maller Anna Vadimovna — Master's student, Department of General Biology and Genomics, L.N. Gumilyov Eurasian National University, Astana, Kazakhstan; e-mail: anamaller8@gmail.com

Dyussembekova Damira Adilevna — PhD student, Researcher, National Center for Biotechnology, Astana, Kazakhstan; e-mail: dussembekova.damira@gmail.com, ORCID: https://orcid.org/0000-0002-1621-0577

Islamova Symbat Sultanovna — PhD student, Junior researcher, National Center for Biotechnology, Astana, Kazakhstan; e-mail: islamovasimbat@gmail.com, ORCID: https://orcid.org/0009-0000-5349-9149

Nurtaza Aidana Serikbolkyzy — PhD, Leading researcher, National Center for Biotechnology, Astana, Kazakhstan; e-mail: nurtazaaidana6@gmail.com, ORCID: https://orcid.org/0000-0001-6934-3747

Kakimzhanova Almagul Apsalamovna — Doctor of Biological Sciences, Professor, Head of the Laboratory of Biotechnology and Plant Breeding, National Center for Biotechnology, Astana, Kazakhstan; e-mail: kakimzhanova@biocenter.kz, ORCID: https://orcid.org/0000-0002-7797-6867

How to Cite: Andronov, E.E., Darbaeva, T.E., Bakiyev, S.S., Kakishev, M.G., Ermekkaliev, T.S. (2026). Study of the genus Rosehip (*Rosa*) using molecular biological methods. *Fundamental and Experimental Biology*, 31, 3 (123), 192-200. https://doi.org/10.31489/2026FEB3/192-200

Research Article

https://doi.org/10.31489/2026FEB3/192-200

UDC 911:338.48 (574.1) Received: 12.12.2025 | Accepted: 18.02.2026 | Published online: 30.09.2026

E.E. Andronov[1], T.E. Darbaeva[2], S.S. Bakiyev[2*], M.G. Kakishev[2], T.S. Ermekkaliev[2]

[1]*All-Russian Research Institute of Agricultural Microbiology, Saint-Petersburg, Russia;*
[2]*Makhambet Utemisov West Kazakhstan University, Uralsk, Kazakhstan*
[*]*Corresponding author: bakiyevserik@gmail.com*

Study of the genus Rosehip (*Rosa*) using molecular biological methods

This study presents a molecular genetic analysis of a rosehip sample using DNA barcoding and phylogenetic approaches. The aim of the study was to identify the species based on a comparative analysis of nucleotide sequences of nuclear and chloroplast marker genes, including ITS, matK, rbcL, and trn. Genomic DNA was extracted from rosehip leaves using a modified CTAB method optimized for plant material rich in polyphenolic compounds. Target DNA fragments were amplified by polymerase chain reaction (PCR) using specific primer pairs. PCR products were visualized by agarose gel electrophoresis, purified, and sequenced using the Sanger method on an automated genetic analyzer. The resulting nucleotide sequences were edited, assembled into consensus sequences, and analyzed using SeqScape and MEGA software. Species identification was performed by comparing the sequences with those available in the GenBank database using the BLAST algorithm and by constructing phylogenetic trees. The results demonstrated 100% sequence identity for all studied genetic markers with reference sequences of *Rosa majalis*. Phylogenetic analysis confirmed that the investigated sample clustered with other representatives of this species within the genus *Rosa*. These findings indicate the high diagnostic value of the selected DNA markers for reliable molecular identification of the studied rosehip species. The integrated approach combining PCR amplification, sequencing, and phylogenetic analysis proved effective for taxonomic verification. The results may be applied in plant systematics, pharmacognosy, biodiversity studies, and quality control of medicinal plant raw materials.

*Keywords***:** rosehip, *Rosa majalis*, DNA barcoding, PCR, sequencing, phylogenetic analysis.

Introduction

The genus *Rosa* L. (family Rosaceae) includes more than 100 species widely distributed across the temperate regions of the Northern Hemisphere. Representatives of this genus, particularly rosehips, are of significant economic and pharmacological importance due to their high content of biologically active compounds, including ascorbic acid, flavonoids, and organic acids. In this regard, accurate species identification of rosehips is of great importance for botany, pharmacognosy, and quality control of medicinal plant raw materials [1–5].

Traditional morphological methods for species identification within the genus Rosa are often complicated by high phenotypic variability, hybridization, and polyploidy. In recent decades, molecular genetic methods—particularly DNA barcoding—have become reliable tools for taxonomic identification of plants. The use of standard marker genes such as ITS, matK, rbcL, and trn enables accurate comparison of studied samples with reference sequences available in international databases.

The aim of this study was to perform molecular genetic identification of a rosehip sample using PCR amplification, sequencing, and phylogenetic analysis of nucleotide sequences of key marker genes. The obtained results make it possible to refine the systematic position of the studied sample, confirm its affiliation with the species *Rosa majalis*, and demonstrate the effectiveness of an integrated molecular approach in plant systematics.

Experimental

DNA Extraction from Plant Material

At the beginning of the experiment, clean rosehip leaves were dried on kraft paper at 50 °C for 60 minutes. DNA extraction was performed using a sorbitol washing buffer with 1 % DTT containing 100 mM Tris-HCl (pH 8), 0.35 M sorbitol, 5 mM EDTA (pH 8), and 1 % PVP-40. A total volume of 150 mL

of the buffer was prepared from 15 mL of 100 mM Tris-HCl, 3 mL of 5 mM EDTA, 3 g of PVP-40, 19 g of sorbitol, and 5 mL of DTT.

For cell lysis, a CTAB buffer (100 mM Tris-HCl, 3 M NaCl, 3 % CTAB, 20 mM EDTA, 1 % PVP-40, 1 % β-mercaptoethanol), preheated to 65 °C, was used [6, 7].

The extraction protocol included the following steps: grinding of rosehip leaves; washing with a DTT-containing buffer; centrifugation and removal of the supernatant; repeated washing with a buffer containing β-mercaptoethanol; addition of CTAB buffer; incubation at 65 °C; extraction with a chloroform–isoamyl alcohol mixture; DNA precipitation with isopropanol and sodium acetate; washing of the DNA pellet with ethanol; and dissolution of the DNA in TE buffer.

The obtained extracts were used for subsequent purification procedures and PCR analyses. DNA concentration was assessed by a fluorometric method and ranged from 50 to 100 ng/μL. Primers used for PCR amplification are presented in Table 1.

Table 1

Primer pairs used

GEN	Primer_name	Primer_seq	Size (bp)	Primer annealing temperature
MatK	MatK_390-F	CGATCTATTCATTCAATATTTC	801	53°C
	MatK_1326-R	TCTAGCACACGAAAGTCGAAGT		
TRN	trnHF_05-F	CGCGCATGGTGGATTCACAATCC	220	58°C
	psbA3f-R	GTTATGCATGAACGTAATGCTC		
ITS	ITS-Bel3-F	GACGCTTCTCCAGACTACAAT	757	60°C
	ITS-p5-R	CCTTATCACTTAGAGGAAGGAG		
RbcL	rbcLa-F	ATGTCACCACAAACAGAGACTAAAGC	551	62°C
	rbcLr590	AGTCCACCGCGTAGACATTCAT		

The PCR reaction mixture consisted of the following components: forward primer — 1 μL, reverse primer — 1 μL(20 pmol/μL), 2× BioMaster UDG HS-qPCR reaction mix — 12.5 μL, nuclease-free water — 7.5 μL, and DNA template — 3 μL(250–500 ng). The obtained DNA samples were stored in a freezer at −20 °C [8, 9].

The PCR program was as follows: initial denaturation at 95 °C for 2 min; 30 cycles of denaturation at 95 °C for 30 s, primer annealing at 53 °C for 40 s, extension at 72 °C for 40 s; and a final extension at 72 °C for 5 min [10].

Electrophoresis of Amplification Products

Analysis of the amplified DNA fragments was performed by horizontal electrophoresis in a 1.5 % agarose gel containing an intercalating agent, ethidium bromide, used for DNA visualization. Electrophoresis was carried out in a horizontal PowerPac chamber using a Bio-Rad Electrophoretic Bath power supply. A 1× TAE buffer was used as the running (electrode) buffer [11].

PCR Product Purification and Nucleotide Sequencing

Prior to sequencing, PCR products were purified from residual primers and deoxynucleotide triphosphates using magnetic bead-based purification with silica-coated paramagnetic particles [12]. To prepare the binding buffer, 2.00 g of PEG and 1.46 g of NaCl were dissolved in 7 mL of deionized water, mixed thoroughly, and the volume was adjusted to 10 mL. The solution was stored at room temperature.

As the elution solution, 1× TE buffer (10 mM Tris-HCl, pH 8) or deionized water was used. For purification, 15 μL of PCR product (1 ng/μL) was mixed with 15 μL of a 0.1 % suspension of magnetic particles (1–3 μm) in the binding buffer (20 % PEG, 2.5 M NaCl). The particles were pre-washed with 3 % HCl. The mixture was incubated for 10 minutes at room temperature with shaking (1800 rpm, 2 min).

Next, the supernatant was removed on a magnetic stand, the particles were washed twice with 70 % ethanol (100 μL each), and DNA was eluted with the selected buffer at 60 °C for 10 minutes. After removing the particles, the purified PCR product was collected for further analysis [13].

Sequencing Reaction

The sequencing reaction was performed using the BigDye Terminator v3.1 Cycle Sequencing Kit (Applied Biosystems) according to the manufacturer's instructions. Fragment separation was carried out on an automated genetic analyzer (3730xl DNA Analyzer (Applied Biosystems)) [12]. The read length was

900–1000 bp. Leaf samples were collected from a single plant (one bush), and no analysis of variability between different individuals or populations was performed.

Detection of PCR Products and Nucleotide Sequence Analysis

Separation of the sequenced fragments was performed on an automated genetic analyzer, 3730xl DNA Analyzer (Applied Biosystems). The obtained nucleotide sequences, amplified using forward and reverse primers, were analyzed using SeqScape 2.6.0 (Applied Biosystems) and MEGA 11 software [14–16].

Results and Discussion

Molecular Genetic Analysis of Rosehip

The analysis of amplified target DNA fragments was performed by separating the DNA fragments in a 1.5 % agarose gel in the presence of the intercalating agent ethidium bromide, which was used for subsequent DNA visualization (Fig. 1, 2).

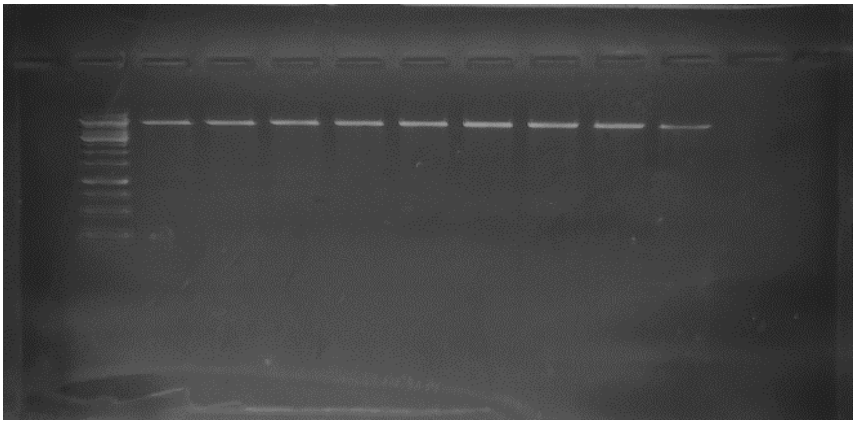

Figure 1. DNA Gel Electrophoresis

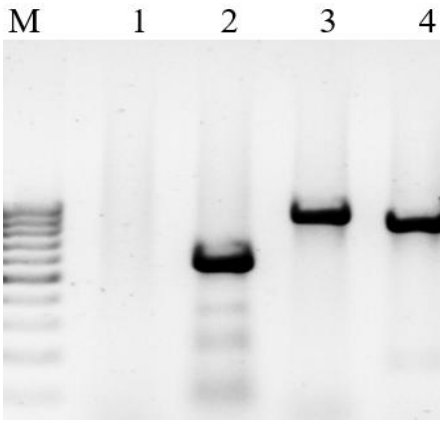

Figure 2. Gel Electrophoresis of PCR-Amplified Gene Fragments:
M — molecular weight marker (Fermentas, 100–1000 bp, 100 bp increments);
1 — negative control; 2 — rbcL (551 bp); 3 — matK (801 bp); 4 — ITS (757 bp)

The electrophoresis results confirmed that a specific fragment was amplified in all samples. No PCR products were observed in the negative control sample, indicating the absence of contamination in the reaction. Figure 2 shows the electrophoresis of the rosehip PCR products.

Figure 2 shows the amplification results, confirming the successful generation of specific fragments for the three target genes, corresponding to the expected molecular sizes.

The obtained nucleotide sequences were analyzed and assembled into a single consensus sequence using SeqMan software (DNASTAR). During processing, terminal regions—including primer sequences and low-quality fragments—were removed. Identification of the obtained sequences was carried out using the BLAST algorithm on the GenBank platform (https://blast.ncbi.nlm.nih.gov/Blast).

1) Nucleotide sequence of the ITS gene:

5’ TGCGGAGGATCATTGTCGAAACCTGCCTAGCAGAACGACCCGAG
AACATGTTTCAACGCTTGGGGGCGGAGGGTCTTGCGGCTCTGCGCCCCCTTATCCTAGGAG
GCAAGTGTCTTGCGCGTTGCATTTCGGTGCTTGCGCTTGACCGACCCTCCCGGGCGTACTGAAC
ACCGGCGTGAATTGCGCCAAGGAACTTGAATGAAAGAGCGTTTCCCCCGCCGTCCCGGAGACG
GTGCTCGTGCGGGTGGTTTCGTCGTCTTCAATATGTCTAAACGACTCTCGGCAACGGATATCTC
GGCTCTCGCATCGATGAAGAACGTAGCGAAATGCGATACTTGGTGTGAATTGCAGAATCCCGT
GAACCATCGAGTCTTTGAACGCAAGTTGCGCCCGAAGCCATTAGGCCGAGGGCACGTCTGCCT
GGGCGTCACACGTCGTTGCCCCCCCCCAACCCCCTCGGGAGTTGGATGGGACGGATGATGGCCTC
CCGTGTGCTCAGTCACGCGGTTGGCATAAATACCAAGTCCTCGGCGACCAACGCCACGACAATC
GGTGGTTGTCAAACCTCGGTTTCCTGTCGTGCGCGCGTGTTGATCGAGTGCTTTCTTAAACAATG
CGTGTCGATCCGTCGATGCTTTCAACGCGACCCCAGGTCAGGCGGGGTTACCCGCTGAATTTAA
GCATATCAATAAGCGGAGGAAAAGAAACTTACAAGGATTCCCTTAGTAACGGCGAGCGAACCG
GGAATAGCCCAGCTG — 3‘.

2) Nucleotide sequence of the matK gene:

5’ AATTATGCATCAGATTGTACTAATTACCCTACCCCATTCATCTGG
AAATCTTGTGTTCAAACCCTTCGCTACTGCGTGAAAGATCCCTCTTCTTTGCATTTATTACG
GCTCTTTCTTCACGAGTATTATAATTGGAATACTCTTATTACTCCAAAAAAATCCATTTTTGCAA
AAAGTAATCAAAGATTATTCTTGCTCCTATATAATTCTTATGTATGTGAATACGAATCCATTTTA
CTTTTTCTCCGTAACCAATCTAATCATTTACGATTAACCTCTTCTGGGATTCTTTTTGAGCGAAT
ACGTTTTTATGAAAAAATAAAATATCCTGTTGAAGAAGTCTTTGCTAACGATTTTCCGGCCACC
TTATGGTTCTTCAAGGATCCTTTTATACAGTATGTTAGATATCAAGGAAAATCGATTCTGGCATC
AAAAGATACTCCTCTTCTGATGAATAAAGTGGAAATATTATCTTGTCCATTTTTGGCAATGTCAT
TTTTATGTATGGTCTCAACCAGGAAGATCCATATAACCAATTATCCAAGCATTCCTTGATTTTTG
GGTTATCTTTCAAGCATCGACCGAATATTTCAGTGGTCGGATCAATTGCTAGAAAATTCGTTTTT
ATGGATAATGCTAGAAGAAGCTTGAACATTATTTCCAATTATTCCAATGATAGGATCGTTGGCT
AAAGTGAAATTTTGTAACACATCAGGGCATCCTATTAGTAAGTCCAGCTGGGCGGATTTGTCGG
ATTCTGAAATTATCGACCGAAATTGTGGCGTTATAAGGGCCGAGGGA — 3’.

3) Nucleotide sequence of the rbcL gene:

5’ — GCTGGTGTTAAAGATTATAAATTGACTTATTATACTCCGGATTA
TGAAACCAAAGATACTAGATATCTTGGCAGCATTTCGAGTAACTCCTCAACCTGGAGTTCCG
CCTGAGGAAGCAGGGGCAGCGGTAGCTGCGGAATCTTCTACTGGTACATGGACAACTGTATGGA
CTGATGGGCTTACCAGTCTTGATCGTTACAAAGGGCGATGCTACCACATTGAACCTGTTGCTGGA
GAAGAAAGTCAATTTATTGCTTATGTAGCTTACCCTTTAGACCTTTTTGAAGAGGGTTCGGTTACT
AACATGTTTACTTCCATTGTAGGTAATGTGTTTGGGTTCAAGGCCTTGCGCGCTCTACGTCTGGAG
GATTTACGAATCCCTACTGCTTATGTTAAAACTTTCCAAGGCCCGCCTCACGGGATCCAAGTTGA
AAGAGATAAATTGAACAAGTATGGCCGCCCCCTATTGGGATGTACTATTAAACCTAAATTGGGG
TTATCCGCTAAGAATTACGGTAGAGCAGTTTATGAATGTCTACGCGGTGGACTAA — 3’.

4) Nucleotide sequence of the trn gene:

5’ TCCGCCCTTGTACTATTTAAATAAAAATTTAAATAAAAATAGAA
ATTACAAATATTTCCACCATTTATCATTACTTGTAAAAGAGAATACAACATAAATGGAAAC
CCTTTTATTTTAATCTTTTAGTAAAAAAAAAGAGTACTAAAATACTAATTTAATTGAAAATACT
AATTTAATTATAGCACTAATTTTAATTAATAATTATAGTAATTAAATTTAA — 3’.

Phylogenetic trees constructed based on the analyzed nucleotide sequences are shown in Figure 3. Figures 4–6 present a comparative analysis of the obtained sequences with nucleotide data available in GenBank for representatives of the species *Rosa majalis*.

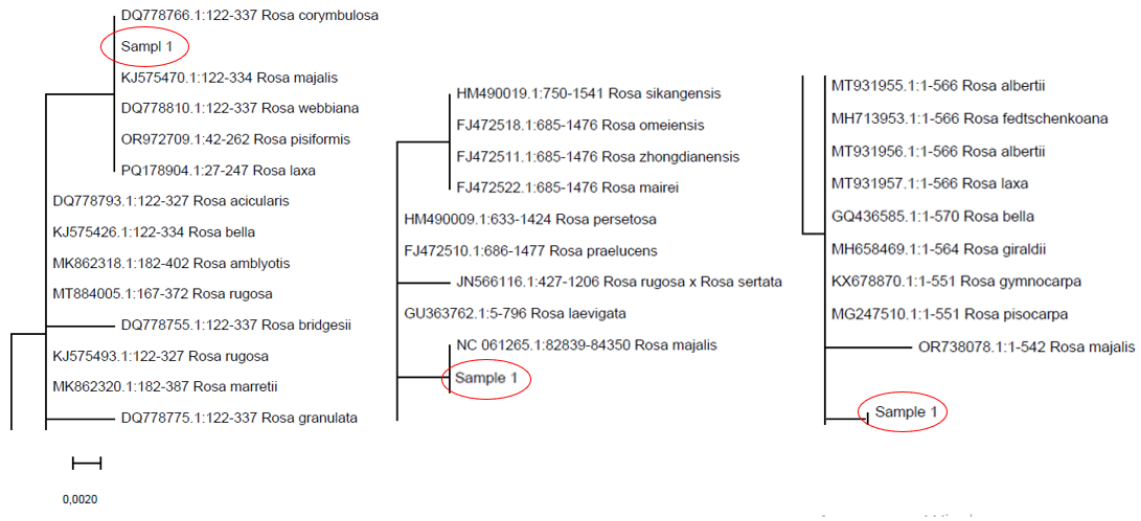

Figure 3. Phylogenetic trees constructed based on the nucleotide sequences of the genes (from left to right): trn, matK, rbcL

Analysis of the phylogenetic trees showed that the studied rosehip species clusters together with other species of the genus Rosa. The closest genetic relative, as demonstrated in Figure 3, is Rosa majalis, based on the analysis of all three investigated nucleotide gene sequences.

Figure 4. Comparative analysis of the nucleotide sequence of the ITS (internal transcribed spacer) gene region (434–504 bp)

As a result of the comparative analysis of the ITS gene nucleotide sequence of the studied rosehip sample, 100 % identity was found with the ITS gene sequences of previously identified *Rosa majalis* samples registered in the GenBank database under accession numbers MZ230091.1 and MZ230112.1.

Figure 5. Comparative analysis of the nucleotide sequence of the matK (maturase K) gene region (282–351 bp)

The comparative analysis of the matK gene nucleotide sequence of the studied rosehip sample revealed 100 % identity with the matK gene sequences of previously identified *Rosa majalis* samples registered in the GenBank database under accession numbers PQ421683.1 and NC_061265.1.

Figure 6. Comparative analysis of the nucleotide sequence of the rbcL (ribulose-1,5-bisphosphate carboxylase large) gene region (30–82 bp)

The comparative analysis of the rbcL gene nucleotide sequence of the studied rosehip sample revealed 100 % identity with the rbcL gene sequence of a previously identified *Rosa majalis* sample registered in the GenBank database under accession number OR738078.1.

Similar results were obtained in the comparative phylogenetic analysis of the other investigated genes, which also showed complete (100 %) identity with representatives of *Rosa majalis*.

Conclusion

Thus, based on molecular genetic data (analysis of nucleotide sequences of protein-coding genes) as well as phenotypic analysis, the studied sample was assigned to the order *Rosales*, family *Rosaceae*, genus *Rosa*, and species *Rosa majalis*. The results obtained in this study may be applied to the conservation of natural heritage sites, as well as to the monitoring and preservation of biodiversity.

Funding

The research work was conducted within the budget program 217 “Development of science”, sub-program 101 “Program-Targeted Funding of Entities Engaged in Scientific and / or Scientific-Technical Activities” according to the priority: Ecology, Environmental Protection, and Sustainable Natural Resource Management; of the BR28712767 research program “Study of ecological, socio-demographic, economic-geographical, and paleobiogeographical aspects of the Urals and assessment of its natural resource potential”. The results of this study correspond to the UN Sustainable Development Goal 15 “Conservation of terrestrial ecosystems”.

Conflict of Interest

The authors declare no conflict of interest.

Authors contribution

The manuscript was written through contributions of all authors. All authors have given approval to the final version of the manuscript. CRediT: **Andronov E.E.** — data curation, investigation, methodology; **Darbaeva T.E**. — data curation, supervision; **Kakishev M.G.** — investigation, formal analysis, methodology; **Bakiyev S.S.** — conceptualization, investigation, methodology, supervision; **Ermekkaliev T.S**. — writing draft, editing, formal analysis.

References

1 Иващенко А.А. Растительный мир Казахстана. Научно-популярное издание / А.А. Иващенко. — Алматы: Алматы кітап баспасы, 2009. — 176 с.

2 Павлов Н.В. Флора Казахстана / Н.В. Павлов. — Алма-Ата: Изд. Наука, 1961. — 639 с.

3 Муранец А.П. Изучение биоразнообразия дикоросов рода *Rosa* L. в Казахстане и их молекулярно-генетическая идентификация / А.П. Муранец, А.К. Есимсеитова, Д.А. Дюсембекова, А.С. Нуртаза, К.Р. Калыбаев, К.З. Кожанов, А.А. Какимжанова // Вестник Евразийского национального университета имени Л.Н. Гумилева. Серия Биологические науки. — 2022. — Т. 139, № 2. — С. 44–60. DOI: 10.32523/2616-7034-2022-139-2-44-60.

4 Аметов А.А. Характеристика растительных сообществ с участием *Lonicera iliensis* Pojark. в условиях среднего течения реки Или / А.А. Аметов, Н.М. Мухитдинов, К.Т. Абидкулова, Л.Н. Карашолакова, А. Ыдырыс // Вестник КазНУ. Серия биологическая. — 2016. — Т.4, № 69. — С. 12–21.

5 Семенютина А.В. Обоснование ассортимента шиповников для обогащения лесомелиоративных комплексов в засушливых условиях / А.В. Семенютина, А.С. Соломенцева // Известия Нижневолжского агроуниверситетского комплекса: наука и высшее профессиональное образование. — 2013. — № 3 (31). — С. 74–79.

6 Healey A. Protocol: a simple method for extracting next-generation sequencing quality genomic DNA from recalcitrant plant species / A. Healey, A. Furtado, T. Cooper et al. // Plant Methods. — 2014. — Vol. 10, No. 21. DOI: https://doi.org/10.1186/1746-4811-10-21.

7 Kim C.S. A simple and rapid method for isolation of high quality genomic DNA from fruit trees and conifers using PVP / C.S. Kim, C.H. Lee, J.S. Shin, Y.S. Chung, N.I. Hyung // Nucleic Acids Res. — 1997. — Vol. 25. — P. 1085-1086. 10.1093/nar/25.5.1085.

8 Johnsen K. Phenotypic and genotypic characterization of phenanthrene-degrading fluorescent *Pseudomonas* biotypes / K. Johnsen, S. Andersen, C.S. Jacobsen // Appl. Environ. Microbiol. — 1996. — Vol. 62, No. 10. — P. 3818–3825.

9 Scarpellini M. Development of PCR assay to identify Pseudomonas fluorescens and its biotype / M. Scarpellini, L. Franzetti, A. Galli // FEMS Microbiol. Lett. — 2004. — Vol. 236 (2). — P. 257–260. DOI: 10.1016/j.femsle.2004.05.043.

10 Ramesh R. Polymerase chain reaction / R. Ramesh, A. Munshi, S.K. Panda // Natl Med J India. — 1992. — Vol. 5, No. 3. — P. 115–119.

11 Lee P.Y. Agarose gel electrophoresis for the separation of DNA fragments / P.Y. Lee, J. Costumbrado, C.Y. Hsu, Y.H. Kim // J. Vis. Exp. — 2012. — No. 62. — Article e3923. DOI: 10.3791/3923.

12 Eren K. DNA sequencing methods: from past to present / K. Eren, N. Taktakoğlu, I. Pirim // Eurasian J. Med. — 2022. — Vol. 54. — P. 47–56. DOI: 10.5152/eurasianjmed.2022.22280.

13 Chen Y. Magnetic particles for integrated nucleic acid purification, amplification and detection without pipetting / Y. Chen, Y. Liu, Y. Shi, J. Ping, J. Wu, H. Chen // Trends Analyt Chem. — 2020. — No. 127. — P. 115912. DOI: 10.1016/j.trac.2020.115912.

14 Liu G-Q. The molecular phylogeny of land plants: progress and future prospects / G-Q. Liu, L. Lian, W. Wang // Diversity. — 2022. — Vol. 14, No. 10. — P. 782. DOI: https://doi.org/10.3390/d14100782.

15 Edwards S.V. Natural selection and phylogenetic analysis / S.V. Edwards // Proc. Natl. Acad. Sci. U.S.A. — 2009. — Vol. 106. — No. 22. — P. 8799–8800. DOI: https://doi.org/10.1073/pnas.0904103106.

16 Bakiyev S.S. Isolation, identification, and characterization of pathogenic Aeromonas hydrophila from critically endangered *Acipenser baerii* / S.S. Bakiyev, I. Smekenov, I. Zharkova, S. Kobegenova, N. Sergaliyev, G. Absatirov, A. Bissenbaev // Aquaculture Reports, 26, 101293. — 2022. — P. 1–11.

Е.Е. Андронов, Т.Е. Дарбаева, С.С. Бакиев, М.Г. Какишев, Т.С. Ермеккалиев

Молекулалық-биологиялық әдістерді қолдану арқылы *Rosa* (итмұрын) туысының түрін зерттеу

Зерттеу жұмысында итмұрын өсімдігінің үлгісіне молекулалық-генетикалық талдау жүргізіліп, ДНҚ-баркодтау және филогенетикалық әдістер қолданылды. Зерттеудің мақсаты — ITS, matK, rbcL және trn ядролық және хлоропластық маркерлік гендерінің нуклеотидтік тізбектерін салыстырмалы талдау арқылы өсімдіктің түрлік сәйкестігін анықтау. Геномдық ДНҚ итмұрын жапырақтарынан полифенолдарға бай өсімдік материалдарына бейімделген модификацияланған ЦТАБ-әдісімен бөлініп алынды. Мақсатты ДНҚ фрагменттері полимеразды тізбекті реакция әдісімен арнайы праймерлерді қолдана отырып амплификацияланды. ПТР өнімдері агарозды гель электрофорезі арқылы талданып, кейін тазартылып, автоматтандырылған генетикалық анализаторда Sanger секвенирлеу әдісімен секвенирленді. Алынған нуклеотидтік тізбектер өңделіп, консенсус-тізбектерге біріктірілді және SeqScape пен MEGA бағдарламалары арқылы талданды. Түрлік идентификация GenBank деректер базасымен BLAST алгоритмі көмегімен салыстыру және филогенетикалық ағаштар құру арқылы жүзеге асырылды. Зерттеу нәтижелері барлық зерттелген генетикалық маркерлердің *Rosa majalis* түрінің тізбектерімен 100 % сәйкестігін көрсетті. Филогенетикалық талдау зерттелген үлгінің *Rosa* туысына жататын *Rosa majalis* түрімен бір кластерде топтасатынын растады. Алынған нәтижелер итмұрын түрлерін молекулалық деңгейде дәл анықтауда қолданылған маркерлердің жоғары тиімділігін көрсетеді.

Кілт сөздер: итмұрын, *Rosa majalis*, ДНҚ-баркодтау, ПТР, секвенирлеу, филогенетикалық талдау.

Е.Е. Андронов, Т.Е. Дарбаева, С.С. Бакиев, М.Г. Какишев, Т.С. Ермеккалиев

Исследование вида рода *Rosa* (шиповник) с применением молекулярно-биологических методов

В работе представлен молекулярно-генетический анализ образца шиповника с использованием методов ДНК-баркодинга и филогенетического анализа. Целью исследования являлась видовая идентификация растения на основе сравнительного анализа нуклеотидных последовательностей ядерных и хлоропластных маркерных генов ITS, matK, rbcL и trn. Геномную ДНК выделяли из листьев шиповника с применением модифицированного ЦТАБ-метода, оптимизированного для растений с высоким содержанием полифенолов. Амплификация целевых фрагментов проводилась методом полимеразной цепной реакции с использованием специфических праймеров. Полученные ПЦР-продукты анализировали с помощью агарозного гель-электрофореза, после чего очищали и подвергали секвенированию методом Sanger на автоматическом генетическом анализаторе. Нуклеотидные последовательности были отредактированы, собраны в консенсус-последовательности и проанализированы с применением программных пакетов SeqScape и MEGA. Видовую принадлежность устанавливали на основе сравнительного анализа с базой данных GenBank с использованием алгоритма BLAST, а также посредством построения филогенетических деревьев. Результаты показали 100 % идентичность всех исследованных генетических маркеров с последовательностями вида *Rosa majalis*. Филогенетический анализ подтвердил кластеризацию исследуемого образца с представителями данного вида рода *Rosa*. Полученные данные свидетельствуют о высокой информативности использованных маркерных генов для молекулярной идентификации шиповника и подтверждают эффективность комплексного подхода, сочетающего ПЦР, секвенирование и филогенетический анализ. Результаты исследования могут быть использованы в систематике растений, фармакогнозии, а также при контроле подлинности лекарственного растительного сырья.

Ключевые слова: шиповник, *Rosa majalis*, ДНК-баркодинг, ПЦР, секвенирование, филогенетический анализ.

References

1 Ivashchenko, A.A. (2009). *Rastitelnyi mir Kazakhstana* [The flora of Kazakhstan]. Almaty: Almaty kitap baspasy [in Russian].

2 Pavlov, N.V. (1961). *Flora Kazakhstana* [Flora of Kazakhstan]. Nauka [in Russian].

3 Muranets, A.P., Yesimseitova, A.K., Dyusembekova, D.A., Nurtaza, A.S., Kalybaev, K.R., Kozhanov, K.Z., & Kakimzhanova, A. A. (2022). Izuchenie bioraznoobraziia dikorosov roda *Rosa* L. v Kazakhstane i ikh molekuliarno-geneticheskaia identifikatsiia [Study of the biodiversity of wild plants of the genus *Rosa* L. in Kazakhstan and their molecular genetic identification]. *Vestnik Evraziiskogo natsionalnogo universiteta imeni L.N. Gumileva. Seriia Biologicheskie nauki — Bulletin of L.N. Gumilyov Eurasian National University. Bioscience Series*, *139*(2), 44–60. https://doi.org/10.32523/2616-7034-2022-139-2-44-60 [in Russian].

4 Ametov, A.A., Muhitdinov, N.M., Abidkulova, K.T., Karasholakova, L.N., & Ydyrys, A. (2016). Kharakteristika rastitelnykh soobshchestv s uchastiem *Lonicera iliensis* Pojark. v usloviiakh srednego techeniia reki Ili [Characteristics of plant communities with the participation of *Lonicera iliensis* Pojark. in the conditions of the middle course of the Ili River]. *Vestnik Kazakhskogo Natsionalnogo Universiteta. Seriia biologicheskaia — Bulletin of the Kazakh National University. Biology Series*, *4*(69), 12–21 [in Russian].

5 Semenyutina, A.V., & Solomentseva, A.S. (2013). Obosnovanie assortimenta shipovnikov dlia obogashcheniia lesomeliorativnykh kompleksov v zasushlivykh usloviiakh [Substantiation of the assortment of dog-rose for enrichment of forest reclamation complexes in arid conditions]. *Izvestiia Nizhnevolzhskogo agrouniversitetskogo kompleksa: nauka i vysshee professionalnoe obrazovanie — Proceedings of Lower Volga Agro-University Complex: Science and Higher Vocational Education*, 31(3), 74–79 [in Russian].

6 Healey, A., Furtado, A., Cooper, T., & Henry, R. J. (2014). Protocol: A simple method for extracting next-generation sequencing quality genomic DNA from recalcitrant plant species. *Plant Methods*, *10*(21). https://doi.org/10.1186/1746-4811-10-21

7 Kim, C.S., Lee, C.H., Shin, J.S., Chung, Y.S., & Hyung, N.I. (1997). A simple and rapid method for isolation of high quality genomic DNA from fruit trees and conifers using PVP. *Nucleic Acids Research*, *25*(5), 1085-1086. https://doi.org/10.1093/nar/25.5.1085

8 Johnsen, K., Andersen, S., & Jacobsen, C.S. (1996). Phenotypic and genotypic characterization of phenanthrene-degrading fluorescent *Pseudomonas* biotypes. *Applied and Environmental Microbiology*, *62*(10), 3818–3825. https://doi.org/10.1128/aem.62.10.3818-3825.1996

9 Scarpellini, M., Franzetti, L., & Galli, A. (2004). Development of PCR assay to identify Pseudomonas fluorescens and its biotype. *FEMS Microbiology Letters*, *236*(2), 257–260. https://doi.org/10.1016/j.femsle.2004.05.043

10 Ramesh, R., Munshi, A., & Panda, S.K. (1992). Polymerase chain reaction. *The National Medical Journal of India*, *5*(3), 115–119.

11 Lee, P.Y., Costumbrado, J., Hsu, C.Y., & Kim, Y.H. (2012). Agarose gel electrophoresis for the separation of DNA fragments. *Journal of Visualized Experiments*, (62), Article e3923. https://doi.org/10.3791/3923

12 Eren, K., Taktakoğlu, N., & Pirim, I. (2022). DNA sequencing methods: From past to present. *The Eurasian Journal of Medicine*, *54*, 47–56. https://doi.org/10.5152/eurasianjmed.2022.22280

13 Chen, Y., Liu, Y., Shi, Y., Ping, J., Wu, J., & Chen, H. (2020). Magnetic particles for integrated nucleic acid purification, amplification and detection without pipetting. *Trends in Analytical Chemistry*, 127, Article 115912. https://doi.org/10.1016/j.trac.2020.115912

14 Liu, G.Q., Lian, L., & Wang, W. (2022). The molecular phylogeny of land plants: Progress and future prospects. *Diversity*, *14*(10), 782. https://doi.org/10.3390/d14100782

15 Edwards, S.V. (2009). Natural selection and phylogenetic analysis. *Proceedings of the National Academy of Sciences*, *106*(22), 8799–8800. https://doi.org/10.1073/pnas.0904103106

16 Bakiyev, S.S., Smekenov, I., Zharkova, I., Kobegenova, S., Sergaliyev, N., Absatirov, G., & Bissenbaev, A. (2022). Isolation, identification, and characterization of pathogenic Aeromonas hydrophila from critically endangered Acipenser baerii. *Aquaculture Reports*, *26*, Article 101293. https://doi.org/10.1016/j.aqrep.2022.101293

Information about the authors

Andronov Evgeny Evgenievich — Doctor of Biological Sciences, All-Russian Research Institute of Agricultural Microbiology, Saint-Petersburg, Russia; e-mail: andronovevgeney64@gmail.com, ORCID: https://orcid.org/0000-0002-5204-262X

Darbaeva Talshen Esenomanovna — Doctor of Biological Sciences, Professor at the Faculty of Natural Geography, Makhambet Utemisov West Kazakhstan University, Uralsk, Kazakhstan; e-mail: dtalshen@mail.ru; ORCID https://orcid.org/0000-0003-2950-0423

Bakiyev Serik Samigullovich — PhD, Faculty of Natural Geography, Makhambet Utemisov West Kazakhstan University, Uralsk, Kazakhstan; e-mail: bakiyevserik@gmail.com; ORCID: https://orcid.org/0000-0001-5095-6869

Kakishev Murat Galikhanovich — PhD, Makhambet Utemisov West Kazakhstan University, Uralsk, Kazakhstan; e-mail: kakishev_murat@mail.ru, ORCID: http://orcid.org/0000-0002-4601-4921

Ermekkaliev Taras Serikkalievich — Master of Natural Sciences, Faculty of Natural Geography, Makhambet Utemisov West Kazakhstan University, Uralsk, Kazakhstan; e-mail: ermekkaliev_07@mail.ru; ORCID: https://orcid.org/0000-0003-0831-1017

How to Cite: Malysheva, A.A, Kazanbassov, T.S., Lopatchenko, T.S., Osikova, K.G., Iskakov, B.K. & Zhigailov, A.V. (2026). Detection of small discrete 5'-terminal fragments of 18S rRNA in mouse cells. *Fundamental and Experimental Biology*, 31, 3 (123), 201-210. https://doi.org/10.31489/2026FEB3/201-210

Research Article

https://doi.org/10.31489/2026FEB3/201-210

UDC 577.217.34+577.123 Received: 12.12.2025 | Accepted: 18.02.2026 | Published online: 30.09.2026

A.A. Malysheva[1, 2], T.S. Kazanbassov[1, 3], T.S. Lopatchenko[1, 4], K.G. Osikova[1, 4], B.K. Iskakov[1], A.V. Zhigailov[1*]

[1]*M. Aitkhozhin Institute of Molecular Biology and Biochemistry, Almaty, Kazakhstan;*
[2]*Al-Farabi Kazakh National University, Almaty, Kazakhstan;*
[3]*Shenzhen University Medical School, Shenzhen University, Shenzhen, China;*
[4]*K.I. Satbayev Kazakh National Research Technical University, Almaty, Kazakhstan*
[*]*Corresponding author: andrzhig@gmail.com*

Detection of small discrete 5'-terminal fragments of 18S rRNA in mouse cells

Protein biosynthesis is a critically important cellular process. With age, structural damage to ribosomes may accumulate, potentially leading to the synthesis of misfolded polypeptides and reduced regenerative capacity and cell viability. Therefore, there is a need to develop universal molecular markers of ribosome integrity. A DNA construct was designed to generate DIG-labeled RNA probes for detecting 5′-terminal fragments of mammalian 18S rRNA. RNA isolated from the liver, lungs, kidneys, and skeletal muscles of young and aging mice was analyzed by Northern blotting using these probes. Small, discrete 5′-terminal fragments of 18S rRNA, similar to the stress-induced 5′18SrRF75 and 5′18SrRF135 molecules identified in plants, were detected in mouse tissues. The levels of these fragments in lung and skeletal muscle tissues were significantly higher than those in the liver and kidneys. Notable differences were observed in the kidneys, lungs, and skeletal muscles of young (3-month-old) versus aging (over 2-year-old) animals. These results suggest that the molecular mechanisms underlying the discrete fragmentation of 18S rRNA may be conserved across species. Such mechanisms may play a role in regulating protein biosynthesis under stress. The small fragments 5′18SrRF75 and 5′18SrRF135 could potentially serve as universal markers of translational apparatus integrity.

Keywords: 18S rRNA, discrete fragmentation, stress markers, mRNA translation, aging, ribosome, small RNAs, oxidative stress.

Introduction

Chronic inflammatory diseases that lead to cell destruction significantly harm human health, society, and economies around the world. In clinical medicine, diagnostic methods commonly involve measuring inflammatory mediators—such as cytokines, chemokines, IgE, histamine, and serotonin—as well as specific groups of leukocytes in patients' blood [1]. However, these stress markers primarily assess the overall immunological and inflammatory status of the body; they cannot evaluate the intracellular processes that cause cell dysfunction and death. Furthermore, these markers are typically detectable only in the later stages of disease progression. Additionally, all of the markers mentioned are species-specific, necessitating the development of unique panels for each individual mammalian species.

In modern laboratory diagnostics, there is a steady trend toward integrating new classes of molecular markers—specifically microRNAs, specific mRNAs, and the pool of small non-coding RNAs—to verify stress-induced and pathological states. The use of these analytes provides a comprehensive assessment of the molecular and genetic mechanisms underlying destructive processes at the cellular and tissue levels. Small, discrete fragments of ribosomal RNA (rRNA) are considered promising candidates for new stress markers in humans and mammals. The high concentration of ribosomes in cells results in a significant copy number of rRNA, which constitutes 80–90 % of the total cellular RNA pool [2]. Consequently, diagnostic test systems targeting rRNA demonstrate analytical sensitivity several orders of magnitude higher than primer kits designed for mRNA and microRNA [3]. Furthermore, the structural organization of rRNA genes, characterized by the presence of highly conserved domains alongside variable regions, enables the development of universal detection systems applicable to a wide range of mammalian biological samples [4].

The mechanism of mRNA translation inhibition in both prokaryotes and eukaryotes is well understood and involves the cleavage of the large ribosomal subunit RNA at a region known as the sarcin-ricin loop.

This process results in the detachment of a small 3′-terminal RNA fragment [5]. This is the exact mode of action for several plant ribosome-inactivating proteins, including abrin, modeccin, and ricin, as well as toxins from bacteria, like Shiga toxin, and from fungi, such as α-sarcin [6]. It is hypothesized that a similar mechanism may occur in eukaryotic cells involving the RNA of the small (40S) ribosomal subunits. The 40S subunits play a crucial role in the initiation of translation, which is the rate-limiting step in the entire protein biosynthesis process. As organisms age, destructive changes in ribosome structure may accumulate, leading to a cumulative effect. The loss of integrity in the cell's translational machinery can significantly impact various cell types. When cells are unable to produce structural, protective, and regulatory proteins in a timely manner due to impaired ribosomal integrity, their regenerative potential declines, causing them to struggle under stress or adverse growth conditions. Moreover, ribosomes with internal defects may result in the synthesis of misfolded or "defective" polypeptides. The accumulation of abnormally folded prion-like proteins in brain cells is a primary cause of many neurodegenerative disorders, including Alzheimer's disease [7].

We hypothesize that small 5′- and 3′-terminal fragments of this molecule can serve as a new class of universal stress markers. Detecting these RNA markers could enable earlier and more timely identification of pathological processes that lead to severe chronic diseases. Previous studies have identified universal stress-induced small 5′-terminal discrete fragments of 18S rRNA in plant cells [8–10]. In the present study, we analyzed the profiles of discrete 5′-terminal 18S rRNA fragments in various tissues from mice in two age groups: young and aging animals. To determine whether similar molecules are detectable in mammalian cells, we investigated the profiles of small 5′-terminal 18S rRNA fragments across four tissue types—liver, lung, kidney, and skeletal muscle—in both young and aging mice.

The results of this study generally confirm the universality of the discrete 18S rRNA fragmentation process in eukaryotic organisms, underscoring the need to explore the underlying molecular mechanisms further. Additionally, the potential use of small discrete fragments of ribosomal RNA in diagnosing chronic diseases and destructive processes in humans and animals is of significant interest.

Experimental

Experiments with animals

The Local Bioethics Commission of the RSE on LPP "M. Aitkhozhin Institute of Molecular Biology and Biochemistry", Ministry of Science and Higher Education of the Republic of Kazakhstan, provided a positive decision for experiments involving laboratory animals (Protocol No. 1, dated May 17, 2024). All procedures using laboratory animals were conducted by qualified specialists with extensive experience, ensuring adherence to the principles of humane treatment and rational use of these animals. The study included two groups of black linear C57BL/6 mice (three males per group): one group consisted of young mature animals aged three months, while the other group included aging animals over two years old.

Computer analysis

Nucleotide sequences of 18S rRNA were analyzed using computer software, specifically the MEGA-X, VectorNTI, and RNA-structure v.5.7 programs, with data obtained from the NCBI GenBank database [11]. To assess the degree of discrete fragmentation of the 18S rRNA semi-quantitatively, the blots were evaluated using densitometry in the ImageJ 1.42q program.

Plasmid construction

Molecular cloning procedures, including phosphorylation/dephosphorylation, restriction, and ligation of DNA, as well as transformation of bacterial cells, were performed according to standard protocols [12]. Plasmid DNA was isolated using the High Pure Plasmid Isolation Kit (Roche), following the manufacturer's instructions. *De novo* synthesized oligonucleotides Rat18S_1-35neg_Acc65-F (5'-gtaccgacaagcatatgctactggcaggatcaaccaggta) and Rat18S_1-35neg-Hind-R (5'-agcttacctggttgatcctgccagtagcatatgcttgtcg) were annealed, phosphorylated, and ligated into the pBluescript KSII vector using *Acc*65I and *Hind*III restriction sites. The inserts were verified through Sanger DNA sequencing, which was carried out using the BigDye™ Terminator v3.1 Cycle Sequencing Kit (Applied Biosystems) with the T7 primer (5'-taatacgactcactataggg) according to the manufacturer's protocol. The reaction mixtures were purified using 70 % ethanol and analyzed on a SeqStudio genetic analyzer (Applied Biosystems).

Northern blotting

Total RNA was extracted from 0.1 g of mouse tissues using Trizol (Sigma), following the manufacturer's protocol. RNA electrophoresis was performed on an 8 % polyacrylamide gel containing 8 M urea. Bands were visualized using the Quantum gel documentation system (Vilber). For the synthesis of DIG-labeled RNA probes, in vitro transcription was conducted after linearizing the plasmids at the *Hind*III restriction site.

The DIG RNA Labelling Kit (SP6/T7) (Roche) was utilized according to the manufacturer's instructions. In the Northern blotting procedure, RNA was transferred to a nylon membrane equilibrated in 0.1x Tris-borate buffer using a semi-dry blotting device (Sci-Plas) at a current of 250 mA for 30 minutes. After the transfer, the membrane was dried and subjected to UV light treatment for 2 minutes at 10 mJ/cm² using a crosslinker (UVP). Hybridization with the DIG-labeled probes and the subsequent detection of bands were performed using the DIG Luminescent Detection Kit for Nucleic Acids (Roche), following the manufacturer's protocol. The hybridization temperature was set to 55 °C. For detecting the bound DIG-labeled probes, Anti-Digoxigenin-AP Fab fragment antibodies (Roche) were employed. The detection phase utilized the alkaline phosphatase substrate CSPD (Roche).

Statistical methods

All measurements were conducted in at least three replicates, and the arithmetic mean ($\bar{X}$) along with the standard error of the mean (m) were calculated. The significance of differences between samples was evaluated using the Student's t-test (t_{st}), with differences considered significant at $p < 0.05$.

Results and Discussion

Creation of a DNA construct for the generation of DIG-labeled RNA probes

To select probe sequences for detecting small fragments of 18S rRNA from mammals, as well as other eukaryotic organisms, nucleotide sequences from reference organisms were sourced from the NCBI GenBank database [11]. These sequences were aligned using the MEGA-X bioinformatics program. The results are illustrated in Figure 1.

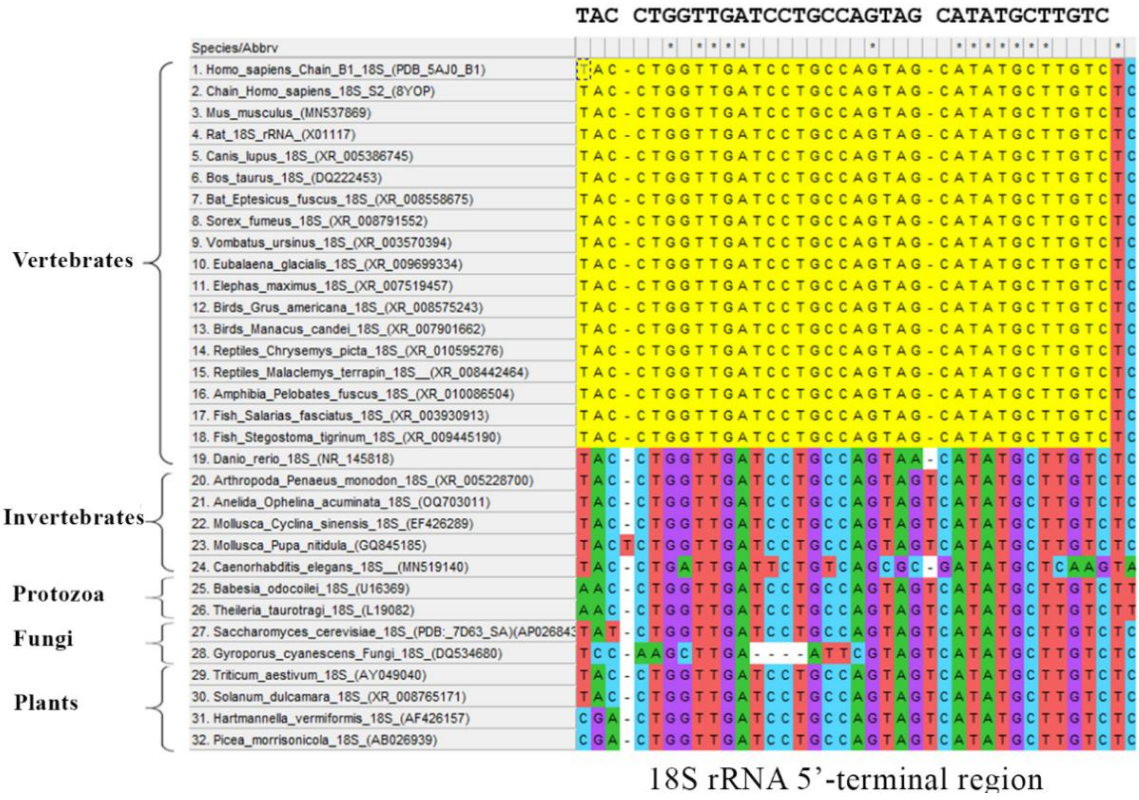

Figure 1. Results of alignment of nucleotide sequences of 5'- 3'-terminal fragments of 18S rRNA of eukaryotic organisms in the MEGA-X program

The 35-nucleotide region at the 5'-end of mammalian 18S rRNA was selected for the detection of 5'-terminal small ribosomal RNAs. This region of the 18S rRNA is highly conserved and remains unchanged across nearly all vertebrates (Fig. 1). Although there may be minor discrepancies in the sequence (one to two letters), probes that are complementary to this 18S rRNA locus are generally effective for detecting small 5'-terminal 18S rRNA fragments from other eukaryotic organisms, with a few exceptions. Notably, the 5'-terminal fragments of the roundworm *Caenorhabditis elegans* and the basidiomycete *Gyroporus cyanescens* do not follow this pattern.

To create DNA constructs for synthesizing DIG-labeled probes using the *in vitro* transcription method, we designed, synthesized, and purified the primers Rat18S_1-35neg_Acc65-F and Rat18S_1-35neg-Hind-R. When these primers were annealed, they formed a 35-nucleotide DNA fragment that corresponds to the 5'-terminal region of eukaryotic 18S rRNA. This fragment is flanked by the restriction sites *Hind*III and *Acc65*I (Fig. 2a).

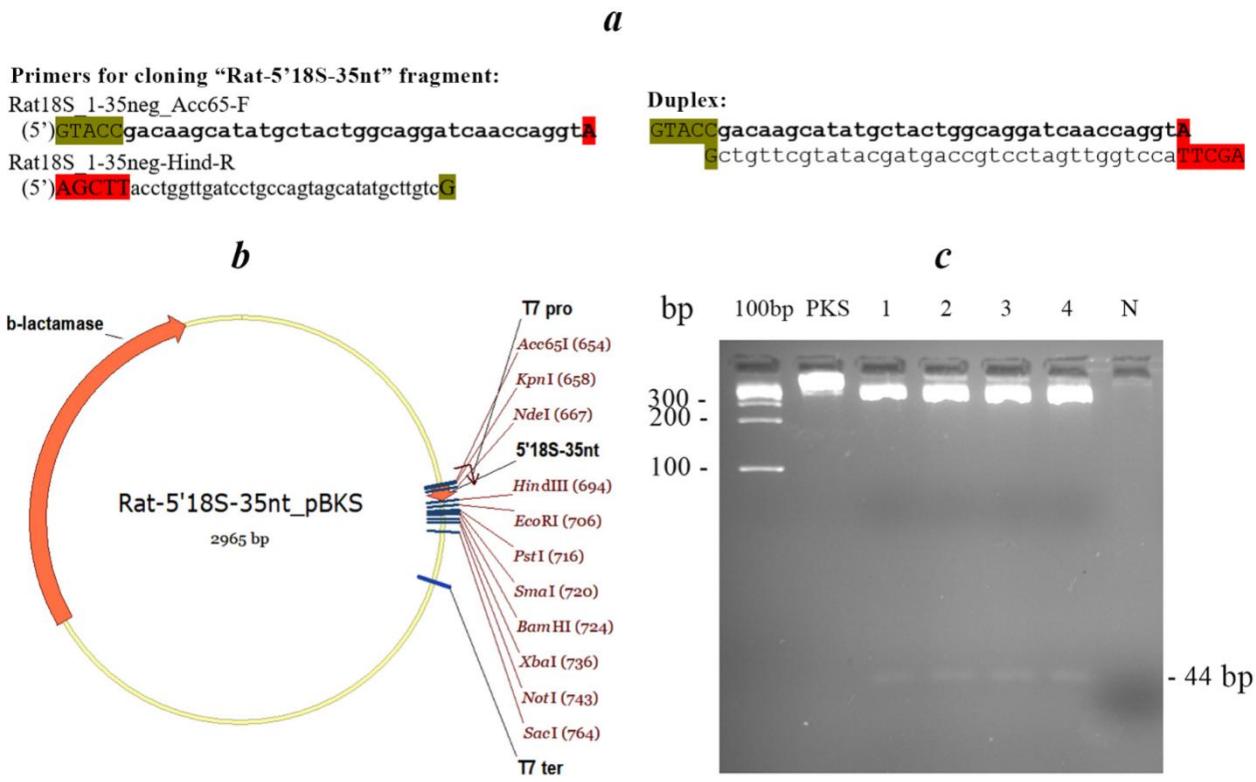

(a) — Formation of oligoDNA duplex for cloning. (b) — Rat-5'18S-35nt_pBKS plasmid map.
(c) — Results of restriction analysis (*Acc65*I/*Hind*III) of DNA clones after ligation.
A 1.5 % agarose gel electrophoregram is shown. 100 bp — GeneRuler 100 bp DNA Ladder (Thermo Fisher Sci.),
PKS — pBluescript KSII vector, 1-4 — DNA clones, N — negative control.

Figure 2. Stages of creating the DNA construct Rat-5'18S-35nt_pBKS for producing an RNA probe to the 5'-end of mammalian 18S rRNA

After phosphorylation, the duplexes were cloned into the pBluescript KS(II) vector at identical restriction sites. The resulting plasmid, designated Rat-5'18S-35nt-pBKS, is illustrated in Figure 2b. We confirmed the presence of inserts of the appropriate size in the DNA clones through restriction analysis using the endonucleases *Hind*III and *Acc65*I, with the results shown in Figure 2c. To verify the accuracy of the cloned nucleotide sequences in these constructs, we performed DNA sequencing using the T7 primer. This resulted in the successful creation of the DNA construct Rat-5'18S-35nt_pBKS, which allows for the synthesis of DIG-labeled probes that target the 5'-terminal region of eukaryotic 18S rRNA from the T7 promoter.

A study of the role of mouse age in the accumulation of 5'-terminal fragments of 18S rRNA

In a study examining the role of mouse age in the accumulation of 5'-terminal fragments of 18S rRNA, we aimed to determine whether specific 5'-terminal fragments of 18S rRNA, similar to those found in plant cells, are present in mammalian cells and whether their abundance varies with age. Total RNA from the liver, lung, spleen, and skeletal muscle of both young and aging mice was analyzed using Northern blotting. The results are displayed in Figure 3.

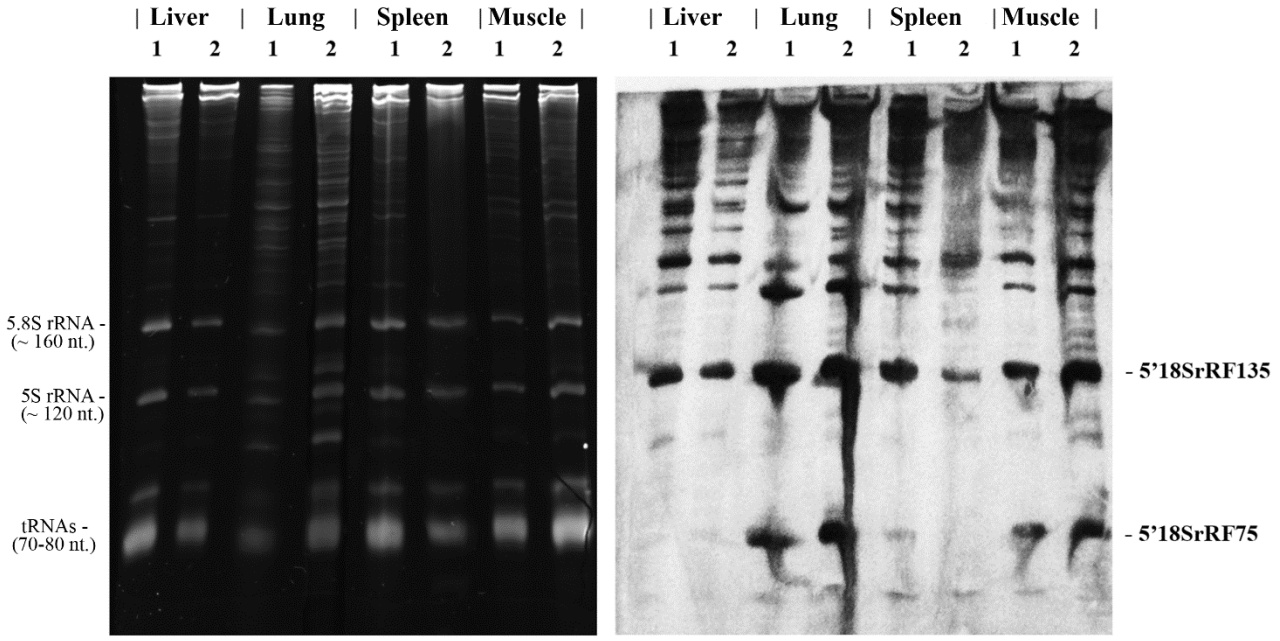

On the left is an 8 % PAA gel, and on the right is a blot of the same gel.
1 — young animals (3 month); 2 — aging animals (over 2 years old).

Figure 3. Northern blot results for detection of 5'-terminal small discrete fragments of 18S rRNA in different tissues of male mice

To confirm the changes in fragmentation levels associated with aging and the differences between tissues, a semiquantitative densitometric analysis of the blots was performed. Although the same amount of total RNA was loaded onto the gel based on calculated values, the actual RNA load may have varied slightly. Additionally, due to potential lane distortions, relying solely on densitometry measurements could result in biased outcomes. To mitigate this issue, the results were normalized to the density of an internal control present in the original electrophoregram. The control used was 5S rRNA, which is consistently expressed across various cell types. By incorporating this internal control into the calculations, we minimized potential errors related to uneven RNA loading or band distortions. Each group of animals (young and aging) consisted of three individuals, allowing for statistical analysis of the results. The findings from the densitometry analysis are summarized in Figure 4.

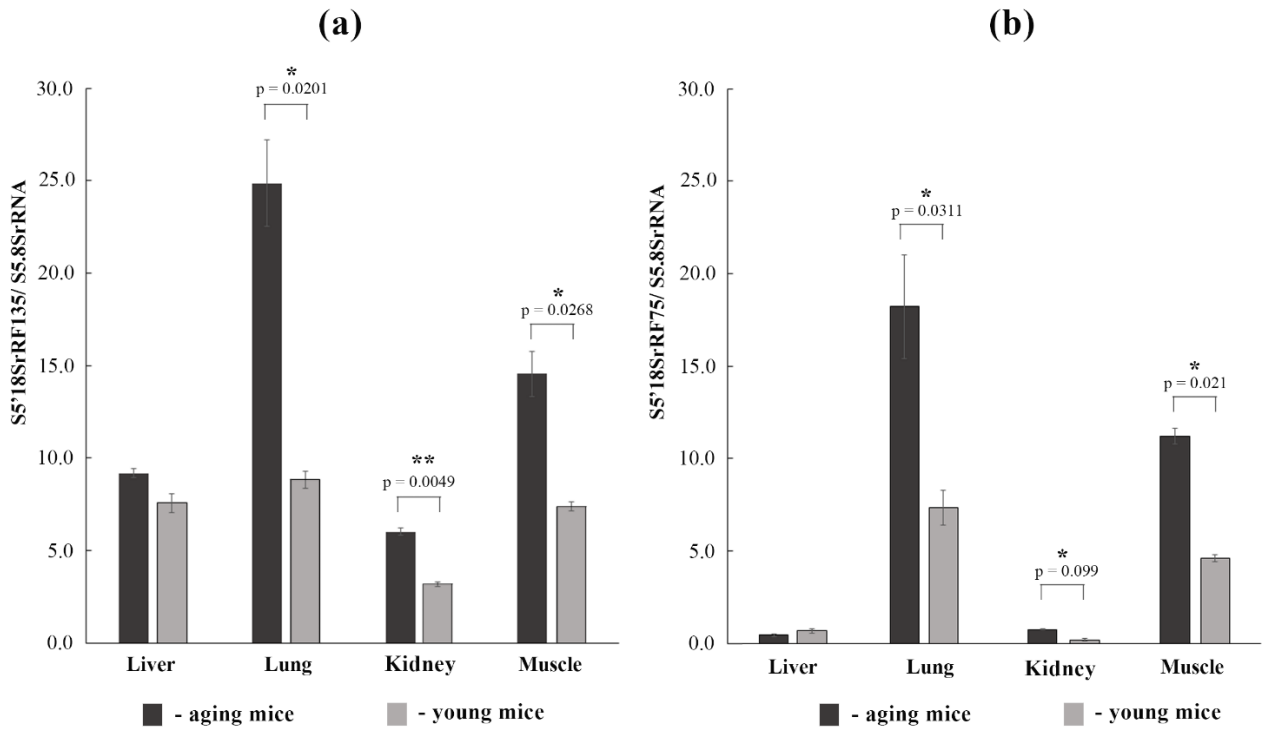

(a) – 5'18SrRF135; (b) — 5'18SrRF75

Figure 4. Results of densitometry analysis assessing the effect of aging on the level of discrete fragmentation from the 5’-terminus in mice

Small ribosomal RNAs similar to the two stress-induced 5′-terminal fragments of plant 18S rRNA (specifically 5’18SrRF75 and 5’18SrRF135) have been identified in mouse cells. The 5’18SrRF135 fragment was detected in all tested tissue types, even in young individuals. In lung cells and skeletal muscle, the levels of this fragment were slightly higher compared to those in liver and kidney cells, although these differences were statistically significant only in aging animals. The 5’18SrRF75 fragment was found in significant amounts only in lung and skeletal muscle cells. These findings may be explained by the fact that mammalian lung and skeletal muscle tissues are subject to elevated oxidative stress. In the lungs, this is due to a high partial pressure of oxygen and constant exposure to external pollutants, which leads to a higher baseline level of reactive oxygen species (ROS) compared to most visceral tissues [13]. Similarly, the increased baseline ROS levels in muscles are attributed to intense metabolism and mitochondrial activity, especially during physical exercise [14].

The data presented in Figure 4 shows that in several tissue types, including the lung, spleen, and skeletal muscle, the levels of both target small fragments of 18S rRNA (5'18SrRF75 and 5'18SrRF135) increase with age. However, this correlation is not observed in the liver, likely due to the low overall levels of these 18S rRNA fragments. Another possible explanation is that liver cells, known as hepatocytes, have an extremely high capacity for proliferation and regeneration. In contrast, lung and kidney tissues are considered stable (expanding) tissues, where cell division occurs infrequently under normal conditions but can be stimulated in response to injury. Generally, the cells in these tissues exhibit moderate to low levels of proliferative activity. Muscle fibers (myofibers), on the other hand, do not divide at all, as they lack centrioles and cannot undergo mitosis.

The detection of small discrete fragments similar to the 5'18SrRF75 and 5'18SrRF135 fragments in mammalian cells, which were previously identified in plants under various stress conditions, suggests that the fragmentation process is universal among eukaryotic organisms. Elevated levels of these fragments have been recorded in cell types that are vulnerable to oxidative stress. Additionally, studies indicate that the levels of both 18S rRNA fragments generally increase in aging animals. The decline in the integrity of the translational machinery with age may have serious consequences, leading to a higher risk of damaging processes

in the body's cells and tissues. Therefore, the 5'18SrRF75 and 5'18SrRF135 molecules can be regarded as universal markers of translational apparatus degradation in mammalian cells.

Conclusion

In conclusion, we have identified small discrete fragments of 5′-terminal 18S rRNA in mouse cells that are similar to the stress-induced small plant rRNAs 5'18SrRF75 and 5'18SrRF135. Quantitatively, these fragments are more abundant in lung and skeletal muscle tissues compared to liver and kidney cells. We hypothesize that this difference is linked to the relatively high ROS in the former two tissue types. Additionally, we found that levels of 5'18SrRF75 and 5'18SrRF135 are elevated in aging animals compared to younger individuals. This age-related decline in the integrity of the cellular translational apparatus may be associated with an increased risk of damaging processes in mammalian cells, potentially leading to chronic diseases. We propose that the small discrete 18S rRNA fragments, 5'18SrRF75 and 5'18SrRF135, should be considered universal markers of translational apparatus damage.

Acknowledgments

The work was carried out in the framework of the scientific program BR27195585 "Creation of new domestic test systems and search for potential biomarkers for the diagnosis of socially significant diseases", funded by the Committee of Science of the Ministry of Science and Higher Education of the Republic of Kazakhstan. The authors express their gratitude to Perfilyeva Y.V., Abdolla N., Kali A. for providing biological samples from mice.

Conflict of Interest

The authors declare no conflict of interest.

Author Contributions

The manuscript was written through contributions of all authors. All authors have given approval to the final version of the manuscript. CRediT: **Malysheva A.A**. — investigation, writing — original draft; **Kazanbassov T.S.** — methodology, investigation; **Lopatchenko T.S**. — investigation; **Osikova K.G**. — investigation; **Iskakov B.K**. — conceptualization, writing — review & editing; **Zhigailov A.V**. — formal analysis, investigation, data curation, writing — review & editing.

References

1 Chen L. Inflammatory responses and inflammation-associated diseases in organs / L. Chen, H. Deng, H. Cui, J. Fang, Z. Zuo, J. Deng, Y. Li, X. Wang, L. Zhao // Oncotarge. — 2017. — Vol. 9 (6). — P. 7204–7218. https://doi.org/10.18632/oncotarget.23208.

2 Deng Z.L. Rapid and accurate identification of ribosomal RNA sequences via deep learning / Z.L. Deng, P.C. Münch, R. Mreches, A.C. McHardy // Nucleic acids research. — 2022. — Vol. 50 (10). — P. 60. https://doi.org/10.1093/nar/gkac112.

3 Law P.P. Ribosomal DNA copy number is associated with body mass in humans and other mammals / P.P. Law, L.A. Mikheeva, F. Rodriguez-Algarra, F. Asenius, M. Gregori, R.A.E. Seaborne, S. Yildizoglu, J.R.C. Miller, H. Tummala, R. Mesnage, M.N. Antoniou, W. Li, Q. Tan, S.I. Hillman, V.K. Rakyan, D.J. Williams, M.L. Holland // Nature communications. — 2024. — Vol. 15 (1). — P. 5006. https://doi.org/10.1038/s41467-024-49397-5.

4 Cawthorn D.M. Evaluation of the 16S and 12S rRNA genes as universal markers for the identification of commercial fish species in South Africa / D.M. Cawthorn, H.A. Steinman, R.C. Witthuhn // Gene. — 2012. — Vol. 491 (1). — P. 40–48. https://doi.org/10.1016/j.gene.2011.09.009.

5 Endo Y. The mechanism of action of ricin and related toxic lectins on eukaryotic ribosomes. The site and the characteristics of the modification in 28S ribosomal RNA caused by the toxins / Y. Endo, K. Mitsui, M. Motizuki, K. Tsurugi // The Journal of biological chemistry. — 1987. — Vol. 262 (12). — P. 5908–5912.

6 Stirpe F. Ribosome-inactivating proteins / F. Stirpe // Toxicon: official journal of the International Society on Toxinology. — 2004. — Vol. 44 (4). — P. 371–383. https://doi.org/10.1016/j.toxicon.2004.05.004.

7 Maccioni R.B. The molecular bases of Alzheimer's disease and other neurodegenerative disorders / R.B. Maccioni, J.P. Muñoz, L. Barbeito // Archives of medical research. — 2001. — Vol. 32 (5). — P. 367–381. https://doi.org/10.1016/s0188-4409(01)00316-2.

8 Zhigailov A.V. Glyphosate treatment mediates the accumulation of small discrete 5'- and 3'-terminal fragments of 18S rRNA in plant cells / A.V. Zhigailov, A.S. Nizkorodova, K.O. Sharipov N.S., Polimbetova, B.K. Iskakov // Вавиловский журнал генетики и селекции. — 2023. — Vol. 27 (2). — P. 93–98. https://doi.org/10.18699/VJGB-23-13.

9 Zhanybekova S.S. Detection of a new small RNA, induced by heat shock, in wheat seed ribosomes / S.S. Zhanybekova, N.S. Polimbetova, N.O. Nakisbekov, B.K. Iskakov // Biokhimiia. — 1996. — Vol. 61 (5). — P. 862–870. — Moscow.

10 Жигайлов А.В. Обнаружение в клетках растений новой цитоплазматической РНК, соответствующей 5’-концевому фрагменту 18S РНК / А.В. Жигайлов, В.Ю. Кислицин, Н.С. Полимбетова, Б.К. Искаков // Вестник КазНУ, Серия биологическая и медицинская. — 2015. — № 2. — С. 109–113.

11 Sayers E.W. GenBank 2025 update / E.W. Sayers, M. Cavanaugh, L. Frisse, K.D. Pruitt, V.A. Schneider, B.A. Underwood, L. Yankie, I. Karsch-Mizrachi // Nucleic acids research. — 2025. — Vol. 53(D1). — P. D56–D61. https://doi.org/10.1093/nar/gkae1114.

12 Sambrook J. The condensed protocols from molecular cloning: a laboratory Manual / J. Sambrook, D.W. Russel. — New-York: ColdSpringHarbor Laboratory Press, 2006. — 800 p.

13 Poulsen H.E. RNA modifications by oxidation: a novel disease mechanism? / H.E. Poulsen, E. Specht, K. Broedbaek, T. Henriksen, C. Ellervik, T. Mandrup-Poulsen, M. Tonnesen, P.E. Nielsen, H.U. Andersen, A. Weimann // Free radical biology and medicine. — 2012. — Vol. 52 (8). — P. 1353–1361. https://doi.org/10.1016/j.freeradbiomed.2012.01.009.

14 Powers S.K. Exercise-induced oxidative stress: cellular mechanisms and impact on muscle force production / S.K. Powers, M.J. Jackson // Physiological reviews. — 2008. — Vol. 88 (4). — P. 1243–1276. https://doi.org/10.1152/physrev.00031.2007.

А.А. Малышева, Т.С. Казанбасов, Т.С. Лопатченко, К.Г. Осикова,
Б.К. Искаков, А.В. Жигайлов

Тышқан жасушаларындағы 18S рРНҚ-ның кіші дискретті 5’-ұшты фрагменттерін анықтау

Нәруыз биосинтезі — өте маңызды биосинтетикалық процесс. Жануарлардың жасы ұлғайған сайын рибосомалар құрылымында деструктивті өзгерістер жинақталып, дұрыс жиналмаған (мисфолдингке ұшыраған) полипептидтердің синтезделуіне, сондай-ақ жасушалардың өміршеңдігі мен регенеративті потенциалының төмендеуіне әкелуі мүмкін. Осыған байланысты рибосомалар тұтастығының әмбебап молекулалық маркерлерін жасау қажеттілігі туындап отыр. Сүтқоректілердің 18S рРНҚ-ның 5'-ұштық фрагменттерін анықтау мақсатында DIG-таңбаланған РНК-зондтарын алуға арналған ДНҚ-конструкциясы жасалды. Алынған зондтарды қолдана отырып, нозерн-блоттинг әдісімен жас және қартайған тышқандардың бауыр, өкпе, бүйрек және қаңқа бұлшықеттерінен бөлінген РНҚ-ға талдау жасалды. Тышқан жасушаларында өсімдіктердегі стресс әсерінен түзілетін 5'18SrRF75 және 5'18SrRF135 молекулаларына ұқсас 18S рРНҚ-ның кішігірім дискретті 5'-ұштық фрагменттері табылды. Олардың мөлшері өкпе және бұлшықет жасушаларында бауыр мен бүйрекке қарағанда айтарлықтай жоғары болды. Жас (3 айлық) және қартайған (екі жастан асқан) жануарлардың бүйрегі, өкпесі және қаңқа бұлшықеттері арасында айтарлықтай айырмашылықтар анықталды. Нәтижелер рибосома құрамындағы 18S рРНҚ-ның дискретті фрагментациясына қатысатын молекулалық механизмдердің әмбебаптығын дәлелдейді. Бұл механизмдер стресс жағдайында нәруыз биосинтезін реттеуге қатысуы мүмкін. Кішігірім 5'18SrRF75 және 5'18SrRF135 фрагменттері трансляциялық аппарат деструкциясының әмбебап маркерлері бола алады.

Кілт сөздер: 18S рРНҚ, дискретті фрагментация, стресс маркерлері, мРНҚ трансляциясы, қартаю, рибосома, кіші РНҚ-лар, тотығу стресі.

А.А. Малышева, Т.С. Казанбасов, Т.С. Лопатченко, К.Г. Осикова,
Б.К. Искаков, А.В. Жигайлов

Обнаружение малых дискретных 5’-концевых фрагментов 18S рРНК в клетках мышей

Биосинтез белка является критически важным биосинтетическим процессом. С возрастом в структуре рибосом могут накапливаться деструктивные изменения, что приводит к синтезу неправильно свернутых (мисфолдированных) полипептидов, а также к снижению регенеративного потенциала и жизнеспособности клеток. В связи с этим существует необходимость в разработке универсальных молекулярных маркеров целостности рибосом. Для детекции 5'-концевых фрагментов 18S рРНК млекопитающих была сконструирована ДНК-конструкция для наработки DIG-меченых РНК-зондов. Методом нозерн-блоттинга с использованием полученных зондов была проанализирована РНК, выделенная из клеток печени, легких, почек и скелетных мышц молодых и стареющих мышей. В клетках мышей были обнаружены малые дискретные 5'-концевые фрагменты 18S рРНК, подобные индуцируемым стрессом молекулам 5'18SrRF75 и 5'18SrRF135 у растений. Их содержание в клетках легких и мышц было значительно выше, чем в клетках печени и почек. Достоверные различия между молодыми (3 месяца) и стареющими (старше двух лет) животными были продемонстрированы для почек, легких и скелетных мышц. Результаты подтверждают универсальность молекулярных механизмов, участвующих в дискретной фрагментации 18S рРНК в составе рибосом. Эти механизмы, вероятно, задействованы в

регуляции биосинтеза белка при стрессе. Малые фрагменты 5'18SrRF75 и 5'18SrRF135 могут служить универсальными маркерами деструкции трансляционного аппарата.

Ключевые слова: 18S рРНК, дискретная фрагментация, маркеры стресса, трансляция мРНК, старение, рибосома, малые РНК, окислительный стресс.

References

1 Chen, L., Deng, H., Cui, H., Fang, J., Zuo, Z., Deng, J., Li, Y., Wang, X., & Zhao, L. (2017). Inflammatory responses and inflammation-associated diseases in organs. *Oncotarget*, *9*(6), 7204–7218. https://doi.org/10.18632/oncotarget.23208

2 Deng, Z.L., Münch, P.C., Mreches, R., & McHardy, A.C. (2022). Rapid and accurate identification of ribosomal RNA sequences via deep learning. *Nucleic Acids Research*, *50*(10), 60. https://doi.org/10.1093/nar/gkac112

3 Law, P.P., Mikheeva, L.A., Rodriguez-Algarra, F., Asenius, F., Gregori, M., Seaborne, R.A.E., Yildizoglu, S., Miller, J.R.C., Tummala, H., Mesnage, R., Antoniou, M.N., Li, W., Tan, Q., Hillman, S.L., Rakyan, V.K., Williams, D.J., & Holland, M.L. (2024). Ribosomal DNA copy number is associated with body mass in humans and other mammals. *Nature Communications*, *15*(1), 5006. https://doi.org/10.1038/s41467-024-49397-5

4 Cawthorn, D.M., Steinman, H.A., & Witthuhn, R.C. (2012). Evaluation of the 16S and 12S rRNA genes as universal markers for the identification of commercial fish species in South Africa. *Gene*, *491*(1), 40–48. https://doi.org/10.1016/j.gene.2011.09.009

5 Endo, Y., Mitsui, K., Motizuki, M., & Tsurugi, K. (1987). The mechanism of action of ricin and related toxic lectins on eukaryotic ribosomes. The site and the characteristics of the modification in 28S ribosomal RNA caused by the toxins. *The Journal of Biological Chemistry*, *262*(12), 5908–5912.

6 Stirpe, F. (2004). Ribosome-inactivating proteins. *Toxicon*, *44*(4), 371–383. https://doi.org/10.1016/j.toxicon.2004.05.004

7 Maccioni, R.B., Muñoz, J.P., & Barbeito, L. (2001). The molecular bases of Alzheimer's disease and other neurodegenerative disorders. *Archives of Medical Research*, *32*(5), 367–381. https://doi.org/10.1016/s0188-4409(01)00316-2

8 Zhigailov, A.V., Nizkorodova, A.S., Sharipov, K.O., Polimbetova, N.S., & Iskakov, B.K. (2023). Glyphosate treatment mediates the accumulation of small discrete 5'- and 3'-terminal fragments of 18S rRNA in plant cells. *Vavilovskii Zhurnal Genetiki i Selektsii — Vavilov Journal of Genetics and Breeding*, *27*(2), 93–98. https://doi.org/10.18699/VJGB-23-13

9 Zhanybekova, S.S., Polimbetova, N.S., Nakisbekov, N.O., & Iskakov, B.K. (1996). Detection of a new small RNA, induced by heat shock, in wheat seed ribosomes. *Biokhimiia — Biochemistry*, *61*(5), 862–870. Moscow [in Russian].

10 Zhigailov, A.V., Kislitsin, V.Y., Polimbetova, N.S., & Iskakov, B.K. (2015). Obnaruzhenie v kletkakh rastenii novoi tsitoplazmaticheskoi RNK, sootvetstvuiushchei 5'-kontsevomu fragmentu 18S RNK [Detection of a new cytoplasmic RNA corresponding to the 5'-terminal fragment of 18S RNA in plant cells]. *Vestnik Kazakhskogo Natsionalnogo Universiteta. Seriia Biologicheskaia i Meditsinskaia — Bulletin of the Kazakh National University. Series Biological and Medical*, 2, 109–113 [in Russian].

11 Sayers, E.W., Cavanaugh, M., Frisse, L., Pruitt, K.D., Schneider, V.A., Underwood, B.A., Yankie, L., & Karsch-Mizrachi, I. (2025). GenBank 2025 update. *Nucleic Acids Research*, *53*(D1), D56–D61. https://doi.org/10.1093/nar/gkae1114

12 Sambrook, J., & Russell, D.W. (2006). *The condensed protocols from molecular cloning: A laboratory manual*. New-York: ColdSpringHarbor Laboratory Press

13 Poulsen, H.E., Specht, E., Broedbaek, K., Henriksen, T., Ellervik, C., Mandrup-Poulsen, T., Tonnesen, M., Nielsen, P.E., Andersen, H.U., & Weimann, A. (2012). RNA modifications by oxidation: A novel disease mechanism? *Free Radical Biology and Medicine*, *52*(8), 1353–1361. https://doi.org/10.1016/j.freeradbiomed.2012.01.009

14 Powers, S.K., & Jackson, M.J. (2008). Exercise-induced oxidative stress: Cellular mechanisms and impact on muscle force production. *Physiological Reviews*, *88*(4), 1243–1276. https://doi.org/10.1152/physrev.00031.2007

Information about the authors

Malysheva Angelina Alexandrovna — PhD-Student, Al-Farabi Kazakh National University, Almaty, Kazakhstan; Junior researcher, Laboratory assistant, Laboratory of Protein and Nucleic Acid Research, M. Aitkhozhin Institute of Molecular Biology and Biochemistry, Almaty, Kazakhstan; e-mail: malysheva_angelina@list.ru; ORCID: 0000-0002-9840-9570

Kazanbassov Temirkhan Serikovich — PhD-Student, Shenzhen University Medical School, Shenzhen University, Shenzhen, China; Laboratory assistant, Laboratory of Protein and Nucleic Acid Research, M. Aitkhozhin Institute of Molecular Biology and Biochemistry, Almaty, Kazakhstan; e-mail: Temirhankazanbasov@gmail.com; ORCID: 0009-0001-4991-102X

Lopatchenko Taisiya Sergeevna — Student, Al-Farabi Kazakh National University, Almaty, Kazakhstan; Laboratory assistant, Laboratory of Protein and Nucleic Acid Research, M. Aitkhozhin Institute

of Molecular Biology and Biochemistry, Almaty, Kazakhstan; e-mail: t.lopatchenko@su.edu.kz; ORCID: 0009-0007-8835-4143

Osikova Kamilla Genadyevna — Student, Al-Farabi Kazakh National University, Almaty, Kazakhstan; Laboratory assistant, Laboratory of Protein and Nucleic Acid Research, M. Aitkhozhin Institute of Molecular Biology and Biochemistry, Almaty, Kazakhstan; e-mail: kamilla.osikova5@gmail.com; ORCID: 0009-0009-4559-4942

Iskakov Bulat Kudaibergenovich — Doctor of Biological Sciences, Professor, Chief Researcher, Laboratory of Protein and Nucleic Acid Research, M. Aitkhozhin Institute of Molecular Biology and Biochemistry, Almaty, Kazakhstan; e-mail: bulat.iskakov2@gmail.com; ORCID: 0000-0002-5204-4377

Zhigailov Andrey Victorovich — Candidate of Biological Sciences, Associate Professor, Head of the Laboratory of Protein and Nucleic Acid Research, M. Aitkhozhin Institute of Molecular Biology and Biochemistry, Almaty, Kazakhstan; e-mail: andrzhig@gmail.com; ORCID: 0000-0002-9646-033X

How to Cite: Sabiyeva, A., Atazhanova, G., Ashirbekova, B., Vlassova, L. & Sabyrova, S. (2026). Study of the antioxidant, antiradical, and antimicrobial activities of the soft extract of *Dracocephalum ruyschiana* L. *Fundamental and Experimental Biology*, 31, 3 (123), 211-219. https://doi.org/10.31489/2026FEB3/211-219

Research Article

https://doi.org/10.31489/2026FEB3/211-219

UDC 616-003.725 Received: 22.02.2026 | Accepted: 12.06.2026 | Published online: 30 September 2026

A. Sabiyeva, G. Atazhanova, B. Ashirbekova, L. Vlassova, S. Sabyrova

Karaganda Medical University, Karaganda, Kazakhstan
**Corresponding author: aseka9520@mail.ru*

Study of the antioxidant, antiradical, and antimicrobial activities of the soft extract of *Dracocephalum ruyschiana* L.

The article presents the results of a study on the antioxidant, antiradical, and antimicrobial activities of a thick extract of *Dracocephalum ruyschiana* L. obtained by ultrasonic extraction from the aerial parts of plants growing in Central Kazakhstan. The aim of the study was to comprehensively evaluate the biological activities of the ultrasonic extract in vitro and assess its potential for further pharmaceutical applications. The results demonstrated that the thick extract exhibits pronounced antiradical activity, indicating its ability to effectively neutralize free radicals and reduce oxidative processes. The antioxidant properties of the extract may be associated with its high content of extractive substances, including biologically active phenolic compounds. Particular attention was paid to the use of ultrasonic cavitation, which facilitates more efficient extraction of active compounds compared with conventional extraction methods. The relevance of the study is related to the important role of free-radical processes in the development of various diseases, including atherosclerosis, ischemic heart disease, cancer, and inflammatory disorders. Substances with antioxidant and antiradical properties are widely investigated for their potential use in the prevention and complex treatment of these conditions. The findings indicate the pharmacological potential of *Dracocephalum ruyschiana* as a promising source of natural biologically active compounds. To the best of our knowledge, this is the first study to provide a comprehensive assessment of the antioxidant, antiradical, and antimicrobial activities of a thick extract of *Dracocephalum ruyschiana* obtained from plant material using ultrasonic cavitation.

*Keywords***:** antioxidant activity, antiradical activity, aerial part, 2,2-diphenyl-1-picrylhydrazyl (DPPH), butylated hydroxyanisole (BHA), optical density, *Dracocephalum ruyschiana*, ultrasonic cavitation, antimicrobial activity.

Introduction

A systematic assessment of the biological potential of dragonhead species (genus *Dracocephalum* L.) has demonstrated promising prospects for their utilization in various domains, particularly in biomedicine. At present, considerable attention from research groups worldwide is directed toward the study of pharmacological applications of extracts derived from *Dracocephalum* plants, as well as the isolation and characterization of their secondary metabolites [1–3]. Accumulating experimental evidence confirms that representatives of this genus exhibit a broad spectrum of biological activities, including anticancer, anti-inflammatory, antioxidant, and antibacterial effects, which have been comprehensively summarized in recent review articles [4–7].

The genus *Dracocephalum* belonging to the family Lamiaceae Lindl. In the flora of Eastern Kazakhstan, the genus *Dracocephalum* occupies a leading position among the genera of the family Lamiaceae, comprising 9 species, which accounts for 12 % of the total number of species within this family. Species of *Dracocephalum* are distributed throughout Central Kazakhstan under various ecological conditions, occurring at altitudes of up to 2500 meters above sea level. They form part of diverse phytocenoses. The genus *Dracocephalum* is widely represented in the flora of Eastern Kazakhstan and is used in traditional medicine (Labiatae), commonly referred to as the mint family, is regarded as a potential source of pharmacologically relevant natural products. According to *The Plant List* (August 2020), the genus comprises 74 accepted species, 20 of which are reported in Kazakhstan [8].

Medicinal plants represent an important reservoir of bioactive secondary metabolites, and increasing research efforts are directed toward approaches that may improve their biosynthetic productivity. Within the Lamiaceae, species of *Dracocephalum*, including *D. ruyschiana*, are characterized by particularly high levels of polyphenolic constituents [9].

A considerable amount of information on the properties of *D. ruyschiana* is available in the literature [10, 11]. According to Iranian, Chinese, and Indian practitioners of traditional medicine, consumption of a cup of *D. ruyschiana* tea exerts a preventive effect against a number of health conditions. *D. ruyschiana* has also been used as a plant-based remedy with antidepressant properties [12–15].

Numerous studies report on the properties of the aerial parts of *D. ruyschiana*, including its phytochemical composition and various types of biological activity, which is associated with the widespread use of this plant in medicine.

Thus, *D. ruyschiana* is an important medicinal plant that, due to its high value, rich chemical composition, and diverse pharmacological effects, attracts considerable attention from researchers worldwide. In addition, *D. ruyschiana* represents a valuable source of phenolic compounds, flavonoids, and rosmarinic acid, and may serve as a widely available and renewable source of raw material for phytopharmacology. Given the broad spectrum of its therapeutic properties, this article presents a comprehensive overview of the composition, pharmacological activity, and methods for obtaining extracts from *D. ruyschiana* [16].

The focus of this study was *D.ruyschiana*, a species broadly distributed across the territory of Kazakhstan and considered a valuable source of raw medicinal material. Histochemical investigation of the aerial organs of *D. ruyschiana* aimed at determining the localization of biologically active compounds represents an important step for the authentication of plant material and for advancing further pharmaceutical and medical research [17].

Dracocephalum ruyschiana is an essential oil–producing plant traditionally employed in folk medicine. Its pharmacological potential is associated with the presence of diverse bioactive constituents in the aerial parts, including cardenolides, alkaloids, tannins, coumarins, and flavonoids. These metabolites underlie its therapeutic applications in the management of respiratory disorders, fever reduction, asthenic conditions, and reproductive health. Moreover, nectar of *D. ruyschiana* has been reported to exhibit antimicrobial properties against both Gram-positive and Gram-negative bacteria [18–20].

Dracocephalum ruyschiana has long been employed in traditional medicine for the treatment of respiratory disorders, as an antipyretic remedy, in cases of asthenia, and as an agent enhancing reproductive function [18]. In addition, the nectar of this species demonstrates antimicrobial efficacy against both Gram-positive and Gram-negative microorganisms [21].

Literature data confirms that Kazakhstani species of Dracocephalum have significant pharmacological potential [22–24], which justifies further preclinical and clinical research to develop safe and effective phytopharmaceutical products based on them.

The aim of the study is to study the antioxidant and radical scavenging activities of the dense extract of *Dracocephalum ruyschiana* (L.) obtained through ultrasonic cavitation, in vitro.

Experimental

The research objects are the above-ground parts of *Dracocephalum ruyschiana* L., collected during the flowering phase from the Karkaraly Mountains (Karaganda Region, N $49^0$43'23", E $75^0$48'38"), in May 2023 (Fig. 1).

Figure 1. *Dracocephalum ruyschiana* in the flowering phase

For the first time, ultrasonic extraction was used to obtain the total extractives from the herb *Dracocephalum ruyschiana*. 20.0 g of air-dried herb were placed in an extraction vessel and covered with 400 ml of extractant—either water or a mixture of ethanol and water (1:20, v/v).

Ultrasonic extraction of the raw material was performed without pre-soaking using the ultrasonic cleaner Sonic-3 at a frequency of 40 kHz and room temperature (20–22 °C) for 30 minutes. Subsequently, the liquid extract was decanted, and extraction was repeated under the same conditions. The extract was prepared using 70 % ethanol and designated as EZR-70 %. The resulting combined liquid extracts of *Dracocephalum ruyschiana* were filtered through a paper filter. The liquid filtrate was poured into a rotary evaporator and the extractant was evaporated at a temperature of 50 °C, resulting in a thick extract of Dracocephalum ruyschiana. Residual solvent was removed from the thick extract in a water bath at 60 °C. The thick extract is an amorphous powder of a greenish-brown color, with a specific odor, and is very hygroscopic. The yield of the extract is 6 % [25].

Determination of Ferric Reducing Antioxidant Power (FRAP assay)

The mechanism of this method can be represented as follows:

$$[Fe(CN)_6]^{3-} + ArOH \rightarrow [Fe(CN)_6]^{4-} + ArO^{\cdot} + H^+$$

$$[Fe(CN)_6]^{4-} + Fe^{3+} + K^+ \rightarrow KFe[Fe(CN)_6] \quad (\lambda = 700\,\text{nm})$$

To 1 mL of the tested extracts at concentrations ranging from 0 to 1 mg/mL, 2.5 mL of phosphate buffer (0.2 M, pH 6.6) and 2.5 mL of 1 % potassium hexacyanoferrate(III) solution were added. The reaction mixture was incubated for 25 minutes at 50 °C. The reaction was stopped by adding 2.5 mL of 10 % trichloroacetic acid. The mixture was then centrifuged for 3 minutes (1,500 rpm). A 2.5 mL aliquot of the upper layer was mixed with 2.5 mL of distilled water and 0.5 mL of 0.1 % $FeCl_3$ solution. The absorbance was measured at 700 nm.

The obtained data are presented in Table 1 and Figure 2, showing the concentration-dependent absorbance values for the studied plant extracts and the standard compound, ascorbic acid (AA).

The antiradical activity of the presented samples was studied using the 2,2-diphenyl-1-picrylhydrazyl radical (DPPH*) [Brand-Williams W., Cuvelier M.E., Berset C. (1995) Lebensm Wiss Technol 28:25–30].

To evaluate the antiradical activity of the tested samples in the DPPH assay, a 100 μM ethanolic DPPH solution was used.

For the selection of samples with pronounced antiradical activity, 2 mL of a 100 μM ethanolic DPPH solution was mixed with 20 μL of the test sample dissolved in ethanol at a concentration of 10 mg/mL. Thus, the final concentration of the test sample in the reaction mixture was 100 μg/mL.

Ten minutes after adding the test sample solution to the DPPH radical solution, the decrease in optical density was measured at 515 nm.

For the tested samples, interaction with the DPPH radical was studied at final concentrations of the extracts ranging from 5 to 100 μg/mL. After that, the concentration of the test extract required to reduce the optical density of the 100 μM DPPH solution by 50 % was determined (IC_{50}, DPPH).

The percentage of DPPH radical inhibition was calculated using the following formula:

$$I = \frac{Ao - Ax}{Ao} \times 100$$

where A_0 is the control optical density of the solution containing all reagents except the test sample; A_x is the optical density of the sample [16].

The antimicrobial activity was studied using the disc diffusion method

Antimicrobial activity was evaluated against standard reference strains: *Staphylococcus aureus ATCC 6538, Bacillus subtilis ATCC 6633, Pseudomonas aeruginosa ATCC 27853, Escherichia coli ATCC 25922, and Candida albicans ATCC 10231*. These strains represent the most common causative agents of purulent-inflammatory diseases and were obtained from the microbial culture collection of the Department of Microbiology of the Non-Commercial Joint-Stock Company "Karaganda Medical University".

The antimicrobial activity was evaluated using the disc diffusion method against Gram-positive bacteria (*Staphylococcus aureus ATCC 6538, Bacillus subtilis ATCC 6633*), Gram-negative bacteria (*Escherichia coli ATCC 25922, Pseudomonas aeruginosa ATCC 27853*), and the yeast *Candida albicans ATCC 10231*. Benzylpenicillin and eucalyptus oil were used as reference drugs for bacteria, while nystatin was used for

Candida albicans. Comparative drugs are benzylpenicillin sodium salt, gentamicin for bacteria and nystatin for the yeast fungus Candida albicans.

For the assay, a microbial suspension containing a standard number of viable cells was prepared and uniformly inoculated onto the surface of nutrient agar in Petri dishes. Sterile filter paper discs were impregnated with 0.01 mL of the test samples and placed on the inoculated agar surface (four discs per plate) at a distance of 2.5 cm from each other. The plates were incubated for 24 h at 36 °C.

Statistical processing was carried out using parametric statistics methods with calculation of the arithmetic mean and standard error.

After incubation, zones of complete or partial inhibition of microbial growth were observed around the discs. Antimicrobial activity was assessed by measuring the diameters of the inhibition zones. Each sample was tested in triplicate [26].

Results and Discussion

For the first time, we carried out ultrasonic extraction of *Dracocephalum ruyschiana*. Given that the authors [27] used solvents with higher polarity for ultrasonic extraction to more effectively extract polyphenolic acids, we chose 70 % ethyl alcohol for ultrasonic cavitation. The result of the evaluation of the anti-radical activity of the obtained extract is presented in Table 1 and Figure 2, which shows the concentration dependence of the optical density for the studied plant extract and the standard, ascorbic acid (AC).

Table 1

Optical density values of *Dracocephalum ruyschiana* extract samples

Concentration range, mg/mL	Optical density values for the samples under study, mg/ml	
	EZR 70	**AA**
0.25	1.19±0.11	1.92±0.01
0.5	1.52±0.18	2.28±0.01
0.75	1.60±0.01	2.25±0.01
1	2.01±0.12	2.31±0.01
EZR 70- *Dracocephalum ruyschiana* extract, AA-ascorbic acid		

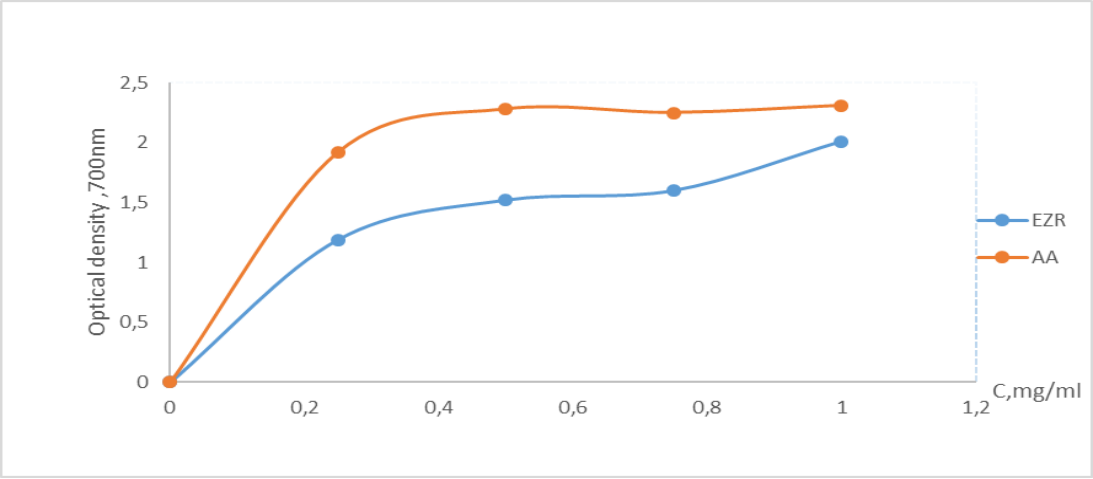

Figure 2. Dependence of the optical density on the concentration of *Dracocephalum ruyschiana* extract

The presented data shows that the ultrasonic extract (EZR) has a relatively high antioxidant activity, as evidenced by a significant increase in the optical density of the solution as its concentration increases.

Table 2 presents the results of screening the given extracts for antiradical activity.

Table 2

Optical density values of a 100 µM DPPH radical solution after 10 min of incubation with *Dracocephalum ruyschiana* extract at a final concentration of 100 µg/mL

№	Test extract	Absorbance, OD
1	extract *Dracocephalum ruyschiana* L.	0,062
2	Control (DPPH solution without the test sample)	0,995

Table 2 shows that the plant extract *Dracocephalum ruyschiana* L. is promising for further research, as it reduces the optical density of the DPPH radical solution by more than 50 %. In the second series of experiments, the ability of the *Dracocephalum ruyschiana* L. extract at various concentrations (from 5 to 100 mg/mL) to interact with the DPPH radical was studied.

Using the constructed calibration curves, the IC_{50} (DPPH) value for the tested extract of *Dracocephalum ruyschiana* was determined (Fig. 3). The IC_{50} (DPPH) values for the extract of *Dracocephalum nutans* are presented in Table 3.

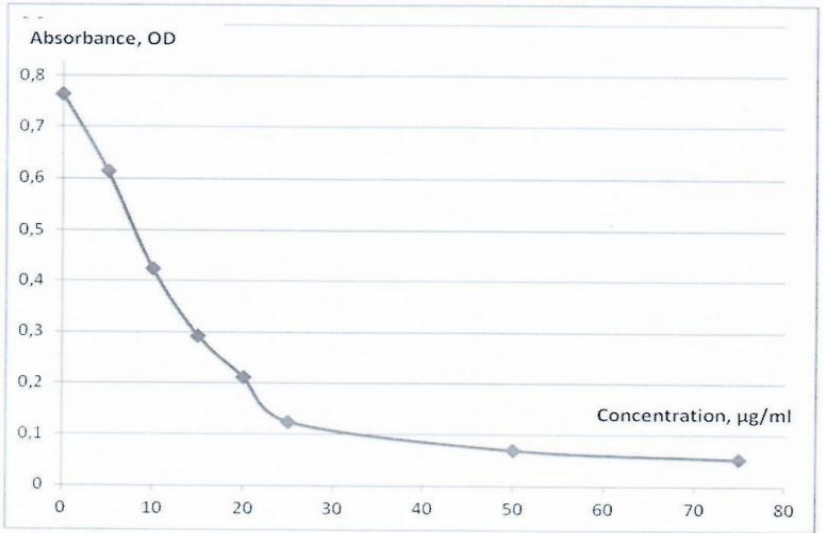

Figure 3. Dose–response curve of DPPH radical scavenging activity of the extract of *Dracocephalum ruyschiana*

Table 3

IC_{50} (DPPH) values for the tested extract of *Dracocephalum ruyschiana*

№	Test extract	IC_{50} (DPPH), mg/mL
1	extract *Dracocephalum ruyschiana*	9,8

The most pronounced antiradical activity under the conditions of this test system was exhibited by the extract of *Dracocephalum ruyschiana* L., for which the concentration capable of reducing the optical density of a 100 µM DPPH radical solution by 50 % was determined. For the *Dracocephalum ruyschiana* L. extract, the IC_{50} (DPPH) value was found to be 9.8 mg/mL.

In the next series of experiments, the antimicrobial activity of the *Dracocephalum ruyschiana* extract was investigated (Tab. 4**)**. Currently, a large number of microorganisms, particularly nosocomial strains, pose a serious threat to human life and health due to the widespread emergence of multidrug resistance and the resulting difficulties in selecting effective chemotherapy. One of the key factors contributing to resistance development is the extensive use of antimicrobial agents, which in some cases leads to adverse effects such as dysbiosis, anaphylactic shock, and the formation of cross-resistance. Therefore, there is an ongoing search for new antimicrobial agents that, on the one hand, exhibit antimicrobial activity via mechanisms distinct from those of conventional antibiotics and, on the other hand, lack significant side effects [28].

Table 4

Antimicrobial activity of the *Dracocephalum ruyschiana* soft extract (inhibition zone diameter, mm)

mm / Sample code	Staphylococcus aureus ATCC 6538	Bacillus subtilis ATCC 6633	Escherichia coli ATCC 25922	Pseudomonas aeruginosa ATCC 27853	Candida albicans ATCC 10231
EZR (70 %)	22± 0.5	25±1	10±0.5	9±1	22± 0.6
Benzylpenicillin sodium salt	16 ± 0.1	14 ± 0.1	15 ± 0.1	12±1	-
Ethyl alcohol (70 %)	10 ± 0.1	10± 0.1	10 ± 0.1	10 ± 0.1	10 ± 0.1
Nystatin	-	-	-	-	21 ± 0.2

Note. n = 3, P ≤ 0.05

Conclusion

A comprehensive study of the antiradical, antioxidant, and antimicrobial activities of the ultrasonic extract of *Dracocephalum ruyschiana* was conducted for the first time. It was established that the thick extract obtained using ultrasonic cavitation exhibits pronounced antiradical and antioxidant activity. The results of antimicrobial assays demonstrated that the *Dracocephalum ruyschiana* extract shows high activity against Gram-positive bacteria (*Staphylococcus aureus* and *Bacillus subtilis*), moderate activity against Gram-negative bacteria (*Escherichia coli* and *Pseudomonas aeruginosa*), and pronounced activity against the yeast *Candida albicans*. These findings indicate the significant pharmacological potential of the extract and highlight its prospects for use in the development of pharmaceutical products.

Acknowledgments

This research was funded by the Science Committee of the Ministry of Science and Higher Education of the Republic of Kazakhstan, grant number AP25794123: “Development of a new wound-healing agent based on *Dracocephalum ruyschiana* L. extract”.

Conflict of interest

The authors declare no conflict of interest.

Author contribution

The manuscript was written through contributions of all authors. All authors have given approval to the final version of the manuscript. CRediT: **Sabiyeva A.** — conceptualization, data analysis, investigation; **Atazhanova G.A.** — plant material collecting, writing draft, data curation; **Ashirbekova B**. — obtaining ultrasonic extracts; **Vlassova L**. — investigation of biological activity and methodology; **Sabyrova S.** — statistical processing of results and collection of raw materials.

References

1 Ranjitha Dhevi, V., & Sundar, M. S. (2019). A comparative study on phytochemical screening, antioxidant and antimicrobial capacities of leaf extracts from medicinal plants. *Research Journal of Pharmacy and Technology, 12*(1), 361–366. https://doi.org/10.5958/0974-360X.2019.00066.0

2 Sabiyeva, A., Ishmuratova, M. Y., Atazhanova, G. A., Smagulov, M. K., & Zhuravel, I. A. (2022). Histochemical analysis of aerial part of *Dracocephalum ruyschiana* L. and *Dracocephalum nutans* L. growing in the territory of Central Kazakhstan. *Research Journal of Pharmacy and Technology, 15*(9), 3831–3835. https://doi.org/10.52711/0974-360X.2022.00642

3 Selenge, E., Murata, T., Kobayashi, K., Batkhuu, J., & Yoshizaki, F. (2013). Flavone tetraglycosides and benzyl alcohol glycosides from the Mongolian medicinal plant *Dracocephalum ruyschiana. Journal of Natural Products, 76*(2), 186–193. https://doi.org/10.1021/np300609u

4 Kleven, O., Endrestøl, A., Evju, M., et al. (2018). SNP discovery in the northern dragonhead *Dracocephalum ruyschiana. Conservation Genetics Resources, 11*(4), 431–435. https://doi.org/10.1007/s12686-018-1045-9

5 Okhlopkova, Z. M., Razgonova, M. P., Pikula, K. S., et al. (2022). *Dracocephalum palmatum S. and Dracocephalum ruyschiana* L. originating from Yakutia: A high-resolution mass spectrometric approach for the comprehensive characterization of phenolic compounds. *Applied Sciences, 12*(3). https://doi.org/10.3390/app12031766

6 Aspé, E., & Fernández, K. (2011). The effect of different extraction techniques on extraction yield, total phenolic and anti-radical capacity of extracts from *Pinus radiata bark. Industrial Crops and Products, 34*(1), 838–844. https://doi.org/10.1016/j.indcrop.2011.02.002

7 Ha, T. V. A., et al. (2015). Antioxidant activity and bioaccessibility of size-different nanoemulsions for lycopene-enriched tomato extract. *Food Chemistry, 178*, 115–121. https://doi.org/10.1016/j.foodchem.2015.01.048

8 Warnasooriya, V., et al. (2024). Nutritional properties, antioxidant activity and heavy metal accumulation in selected marine macro-algae species of Sri Lanka. *Nutraceuticals, 4*(1), 50–64. https://doi.org/10.3390/nutraceuticals4010004

9 Tchani, G. W., et al. (2021). Phytochemical study and comparative antioxidant activity of extracts from aerial parts of *Chenopodium ambrosioides* Linn. *Advances in Biological Chemistry, 11*(5), 220–233. https://doi.org/10.4236/abc.2021.115015

10 Sabiyeva, A., et al. (2026). Phytochemical composition and biological activities of *Dracocephalum* species native to Kazakhstan: A comprehensive review. *Plants, 15*(11), 1722. https://doi.org/10.3390/plants15111722

11 Stappen, I., Wanner, J., Tabanca, N., et al. (2015). Chemical composition and biological activity of essential oils of *Dracocephalum heterophyllum* and *Hyssopus officinalis. Natural Product Communications, 10,* 133–139. https://doi.org/10.1177/1934578X1501000133

12 Abdullaeva, N. S., Khozhimatov, O. K., & Kubakova, K. K. (2020). Synopsis of species of the genus *Dracocephalum* L. (Lamiaceae) growing in Uzbekistan. *The Scientific Heritage, 55*, 24–31.

13 Uchiyama, N., et al. (2006). Trypanocidal constituents of *Dracocephalum komarovi. Tetrahedron, 62*, 4355–4359. https://doi.org/10.1016/j.tet.2006.02.021

14 Chen, Y., Li, J., Wang, H., Zhang, W., Liu, X., & Zhao, F. (2022). Phylogeny and biogeography of the northern temperate genus *Dracocephalum* s.l. (Lamiaceae). *Cladistics, 38*, 429–451. https://doi.org/10.1111/cla.12496

15 Sagdullayevna, A. N., & Nozima, U. (2021). Analysis of herbarium samples of *Dracocephalum* L. distributed in Uzbekistan. *International Journal on Orange Technologies, 3*, 27–29.

16 Laroui, H., et al. (2024). Antioxidant and anti-inflammatory potentials of *Ammodaucus leucotrichus* seeds' extracts: In vitro and in vivo studies. *Journal of Ethnopharmacology, 326*, 117964. https://doi.org/10.1016/j.jep.2024.117964

17 Liu, M. H., et al. (2016). Chemical profiles, antioxidant and anti-obesity effects of extract of *Bambusa textilis leaves. Journal of Functional Foods, 22*, 533–546. https://doi.org/10.1016/j.jff.2016.02.010

18 Abdullaeva, N. S. (2016). Distribution of *Dracocephalum* L. genus species in Uzbekistan's flora. *Uchenyi XXI Veka, 5*, 6–9.

19 Khasanov, D. U., Ismailov, B. A., Rakhmonov, J. T., Karimov, N. R., & Yuldashev, S. K. (2024). Chemical constituents of *Dracocephalum paulsenii. Chemistry of Natural Compounds, 60*, 165–166. https://doi.org/10.1007/s10600-024-04277-8

20 Uchiyama, N., Takahashi, K., Matsumoto, K., Yamamoto, H., & Kato, S. (2003). New icetexane and 20-norabietane diterpenes with trypanocidal activity from *Dracocephalum komarovi. Journal of Natural Products, 66*, 128–131.

21 Zhang, M., et al. (2011). Phytochemicals, antioxidant and antimicrobial activity of Hibiscus sabdariffa, Centella asiatica, *Moringa oleifera and Murraya koenigii leaves. Journal of Medicinal Plants Research, 5*(30), 6672–6680. https://doi.org/10.5897/JMPR11.621

22 Zeng, Q., Jin, H., Fu, J., Qin, J., Hu, H., Yan, L., Chen, M., & Zhang, W. (2010). Chemical constituents of plants from the genus *Dracocephalum. Chemistry & Biodiversity, 7*, 1911–1929. https://doi.org/10.1002/cbdv.200900268

23 Zhou, S., Wei, C., Zhang, C., Han, C., Kuchkarova, N., & Shao, H. (2019). Chemical composition, phytotoxic, antimicrobial and insecticidal activity of the essential oils of *Dracocephalum integrifolium. Toxins, 11*, 598. https://doi.org/10.3390/toxins11100598

24 Ehsani, A., Alizadeh, O., Hashemi, M., Afshari, A., & Aminzare, M. (2017). Phytochemical, antioxidant and antibacterial properties of *Melissa officinalis* and *Dracocephalum moldavica* essential oils. *Veterinary Research Forum, 8*, 223–229.

25 Suja, K. P., Jayalekshmy, A., & Arumughan, C. (2005). Antioxidant activity of sesame cake extract. *Food Chemistry, 91*(2), 213–219. https://doi.org/10.1016/j.foodchem.2003.09.001

26 Sabiyeva, A., Ishmuratova, M. Y., Atazhanova, G. A., et al. (2023). Anatomical study of *Dracocephalum ruyschiana* L. and *Dracocephalum nutans* L. *Research Journal of Pharmacy and Technology, 16*(3), 1193–1198. https://doi.org/10.52711/0974-360X.2023.00198

27 Oliveira, G. D. A. R., Oliveira, A. E., Conceição, E. C., & Leles, M. I. G. (2016). Multiresponse optimization of an extraction procedure of carnosol, rosmarinic and carnosic acids from rosemary. *Food Chemistry, 211*, 465–473. https://doi.org/10.1016/j.foodchem.2016.05.042

28 Sabiyeva, A., Atazhanova, G., Zholdasbayev, M., et al. (2025). Development of composition and technology of antimicrobial gel with *Dracocephalum nutans* L. essential oil growing in the territory of Central Kazakhstan. *Research Journal of Pharmacy and Technology, 18*(5), 2343–2348. https://doi.org/10.52711/0974-360X.2025.00335

А. Сабиева, Г. Атажанова, Б. Аширбекова, Л. Власова, С. Сабырова

Dracocephalum ruyschiana L. қою сығындысының антиоксидантты, радикалға қарсы және микробқа қарсы белсенділігін *in vitro* зерттеу

Мақалада Орталық Қазақстан жағдайында өсетін өсімдіктің жерүсті бөлігінен ультрадыбыстық экстракция әдісі арқылы алынған Dracocephalum ruyschiana L. қою экстрактының антиоксиданттық, антирадикалдық және антимикробтық белсенділігін зерттеу нәтижелері ұсынылған. Зерттеудің мақсаты — ультрадыбыстық экстракттардың *in vitro* жағдайында биологиялық белсенділігін кешенді түрде зерттеу және олардың болашақ фармацевтикалық қолдану мүмкіндіктерін бағалау. Зерттеу нәтижесінде *Dracocephalum ruyschiana* қою экстракты айқын антирадикалдық белсенділікке ие екендігі анықталды, бұл оның бос радикалдарды тиімді бейтараптандыру және тотығу процестерінің қарқындылығын төмендету қабілетін көрсетеді. Экстрактың антиоксиданттық қасиеттері фенолдық табиғаттағы биологиялық белсенді қосылыстарды қамтитын экстрактивті заттардың жоғары мөлшерімен түсіндіріледі. Зерттеуде ультрадыбыстық кавитацияны қолдануға ерекше назар аударылған, себебі ол дәстүрлі экстракция әдістерімен салыстырғанда белсенді компоненттердің тиімдірек бөлініп алынуын қамтамасыз етеді. Зерттеудің өзектілігі бос радикалдық процестердің көптеген аурулардың, соның ішінде атеросклероз, жүректің ишемиялық ауруы, онкологиялық және қабыну ауруларының патогенезіндегі маңызды рөлімен байланысты. Антиоксиданттық және антирадикалдық белсенділігі бар заттар осы патологиялардың алдын алу мен кешенді терапиясында кеңінен қолданылады. Алынған нәтижелер *Dracocephalum ruyschiana* өсімдігінің фармакологиялық әлеуетінің жоғары екенін көрсетіп, оны табиғи биологиялық белсенді қосылыстардың перспективалы көзі ретінде әрі қарай зерттеудің маңыздылығын дәлелдейді.

Кілт сөздер: антиоксиданттық белсенділік, радикалға қарсы белсенділік, жерүсті бөлігі, 2,2-дифенил-1-пикрилгидразил, бутилгидроксианизол, оптикалық тығыздық, *Dracocephalum ruyschiana*, ультрадыбыстық кавитация.

А. Сабиева, Г. Атажанова, Б. Аширбекова, Л. Власова, С. Сабырова

Исследование антиоксидантной, антирадикальной и антимикробной активности густого экстракта Dracocephalum Ruyschiana L. in vitro

В статье представлены результаты исследования антиоксидантной, антирадикальной и антимикробной активности густого экстракта Dracocephalum ruyschiana L., полученного методом ультразвуковой экстракции из надземной части растения, произрастающего в условиях Центрального Казахстана. Целью исследования являлось комплексное изучение биологической активности ультразвуковых экстрактов in vitro и оценка их перспективности для дальнейшего фармацевтического применения. Установлено, что густой экстракт *Dracocephalum ruyschiana* обладает выраженной антирадикальной активностью, что свидетельствует о его способности эффективно нейтрализовать свободные радикалы и снижать интенсивность окислительных процессов. Антиоксидантные свойства экстракта обусловлены высоким содержанием экстрактивных веществ, включая биологически активные соединения фенольной природы. Особое внимание уделено применению ультразвуковой кавитации, которая обеспечивает более эффективное извлечение активных компонентов по сравнению с традиционными методами экстракции. Актуальность исследования обусловлена важной ролью свободнорадикальных процессов в патогенезе многих заболеваний, включая атеросклероз, ишемическую болезнь сердца, онкологические и воспалительные заболевания. Вещества с антиоксидантной и антирадикальной активностью широко применяются в профилактике и комплексной терапии данных патологий. Полученные результаты подтверждают значительный фармакологический потенциал *Dracocephalum ruyschiana* и обосновывают перспективность его дальнейшего изучения как источника природных биологически активных соединений.

Ключевые слова: антиоксидантная активность, антирадикальная активность, надземная часть, 2,2-дифенил-1-пикрилгидразил, бутилгидроксианизол, оптическая плотность, *Dracocephalum ruyschiana*, ультразвуковая кавитация.

Information about the authors

Sabiyeva Assel — PhD in Pharmacy, Associate professor of the School of Pharmacy, Karaganda Medical University, Karaganda, Kazakhstan; e-mail: sabievaa@qmu.kz; ORCID: https://orcid.org/0000-0002-6268-8977

Atazhanova Gayane — Doctor of Chemical Sciences, Professor, Professor-Researcher, Karaganda Medical University, Karaganda, Kazakhstan; e-mail: g-atazhanova@mail.ru; ORCID: https://orcid.org/0000-0003-1615-9967

Ashirbekova Bibigul — Assistant professor at the School of Pharmacy, Karaganda Medical University, Karaganda, Kazakhstan; e-mail: bibigul.ashirbekova.69@mail.ru; https://orcid.org/0000-0001-9380-6297

Vlassova Lenina — Assistant professor, Professor at the School of Pharmacy, PhD in Chemistry, Karaganda Medical University, Karaganda, Kazakhstan; e-mail: vlasova@qmu.kz; https://orcid.org/0000-0003-1530-3859

Sabyrova Sabira — Master of Educational Sciences, Trainee teacher at the School of Pharmacy, Karaganda Medical University, Karaganda, Kazakhstan; e-mail: SabyrovaS@qmu.kz; https://orcid.org/0009-0006-6990-3664

How to Cite: Danilova, A.N., Kotukhov, Y.A., Sumbembaev, A.A., Anufriyeva, O.A. & Ahmetzhanov, A.M. (2026). Status of populations and resource reserves of *Bupleurum multinerve* DC. in various conditions of the Kazakh Altai. *Fundamental and Experimental Biology*, 31, 3 (123), 220-234. https://doi.org/10.31489/2026FEB3/220-234

Review Article

https://doi.org/10.31489/2026FEB3/220-234

UDC 58.009 Received: 1.04.2026 | Accepted: 12.06.2026 | Published online: 30.09.2026

A.N. Danilova, Y.A. Kotukhov, A.A. Sumbembaev*, O.A. Anufriyeva, A.M. Ahmetzhanov

Altai Botanical Garden, Ridder, Kazakhstan
**Corresponding author: aydars@list.ru*

Status of populations and resource reserves of *Bupleurum multinerve* DC. in various conditions of the Kazakh Altai

The results of population and resource studies of *Bupleurum multinerve* in the Kazakh Altai are presented for the Southern and Southwestern Altai, including the Sarymsakty Ridge, Southern Altai Tarbagatai, Narym, and Ivanovsky areas. The aim of the study was to conduct population and resource investigations of *Bupleurum multinerve* under natural growing conditions in the Kazakh Altai. The floristic composition, morphometric parameters, age structure, and resource reserves of the populations were studied. The upper altitudinal limit of the species was established at 1300–2015 m above sea level, where it occurs in mountain-steppe, foothill-shrub, mountain-forest, and subalpine plant communities. Under mountain-steppe conditions in the Southern Altai, the species is a dominant component of the vegetation, with a density of up to 70.0%. The vegetation cover of the studied communities reaches 100%, with herbaceous species forming its basis. The studied populations of *B. multinerve* in the Southern and Southwestern Altai are normal and incomplete, with an age spectrum showing a tendency toward left-sided asymmetry. The species is characterized by relatively stable generative shoot height (coefficient of variation, 13.35–18.65%), high variability in the number of generative individuals per unit area (25.0–36.9%), and the capacity for seed-based regeneration, as indicated by variation in the number of generative shoots (15.1–37.2%). The highest population densities were recorded in mountain-steppe habitats on the Sarymsakty Ridge (75 individuals/m²) and in the Narym area (50.0 individuals/m²). The commercial reserves of aboveground *B. multinerve* biomass in air-dry condition were estimated at 72.02 tons on the Sarymsakty Ridge and 61.46 tons in the Narym area, with potential harvest volumes of 43.21 and 36.87 tons, respectively.

Keywords: Bupleurum multinerve, Southern Altai, Southwest Altai, association, population, species diversity, abundance, age structure, resources.

Introduction

The problem of studying, using, and conserving biological resources under the modern conditions of a changing world is not only a regional but also a geopolitical issue. At present, the relevance of comprehensive research is increasing, based on the integration of various methods and approaches aimed at developing a strategy for the sustainable use of plant resources. Such strategies should take into account not only the demand for already harvested medicinal plant species, but also for new plant species, the harvesting volumes of which are increasing or may increase in the coming years [1].

Among the promising wild medicinal plants in the flora of the Kazakh Altai from the Apiaceae family is *Bupleurum multinerve* (many-nerved hare's ear), a Pleistocene rock and steppe relict of East Siberian origin [2]. The distribution range of this species is quite wide; A.V. Kuminova [3] assigns it to the Asian (North Asian) group of ranges, while G.A. Peshkova [4] classifies it as a Eurasian type. The species occurs in the mountains of Central Asia, Kazakhstan, Mongolia, and China [5].

B. multinerve is a perennial polycarpic taproot caudex herbaceous plant reproducing by seed. It combines features of mesophytes and xerophytes and, due to its dual ecological nature, has broad ecological adaptability to various growth conditions. It is known that species with such dual ecological characteristics are distinguished by a wide range of variability and high productivity; therefore, *B. multinerve* is abundant in many plant associations [6].

In the Kazakh Altai, the coenocomplex of *B. multinerve* is included in groups of meadow-steppe vegetation associations, less frequently in shrub and forest phytocoenoses. The species often extends above the upper forest boundary, where it occurs on rocky slopes among subalpine steppe-like meadows and on fine-stony screes more or less stabilized by vegetation [7].

Interest in studying *B. multinerve* is associated with the possibility of using its raw material in the parapharmaceutical industry due to the accumulation of biologically active substances (BAS) in the vegetative mass, as well as with assessing the prospects for harvesting medicinal raw materials in natural communities, taking into account sustainability and the population's capacity for self-renewal.

B. multinerve is a source of flavonols. The presence of a multi-enzyme system responsible for the breakdown of native flavonols into simple phenolic compounds and the subsequent degradation of aromatic rings were demonstrated by V.G. Minaeva and M.N. Zaprometov [8]. It has been established that the flavonoid-degrading complex includes glycosidases, peroxidases, O-methyltransferases, hydroxylases, and other enzymes [9].

Due to the content of various biologically active compounds—flavonoids, carbohydrates, aliphatic alcohols, vitamins, triterpene saponins, essential oils, and tannins—it is used in official, traditional, and experimental medicine as a capillary-strengthening, anti-inflammatory, anthelmintic, wound-healing, and choleretic agent [10, 11].

Based on the total flavonoids of *B. multinerve*, the preparation "Buplerin" has been developed, containing a flavonol complex composed of quercetin, isorhamnetin, rutin, isoquercetin, and isoquercetin-3-rutinoside. The preparation is recommended for use in hemorrhagic diathesis, bleeding gums and nosebleeds, and edema of vascular origin in hypertension accompanied by increased vascular permeability. The essential oil of *B. multinerve* exhibits antimicrobial and antioxidant activity [12, 13].

Considering the significant role of *B. multinerve* as a medicinal plant, population and resource studies of the species in the flora of the Kazakh Altai have been conducted.

The aim of this work was to carry out population and resource studies of *B. multinerve* under natural growth conditions in the territory of the Southern and Southwestern Altai of the Kazakh Altai.

To achieve this goal, the floristic composition of the communities was studied, the abundance of species forming the phytocoenoses was determined, morphometric and demographic parameters were assessed to identify population responses to growth conditions, and the resource potential of the species in the surveyed communities was established.

Experimental

The research was focused on *B. multinerve* in the phytobiota of the Kazakh Altai (Fig. 1).

Figure 1. *Bupleurum multinerve* in the flora of the Kazakh Altai

The geographical context of the study included four populations in the Southern Altai and two in the Southwestern Altai (Fig. 2).

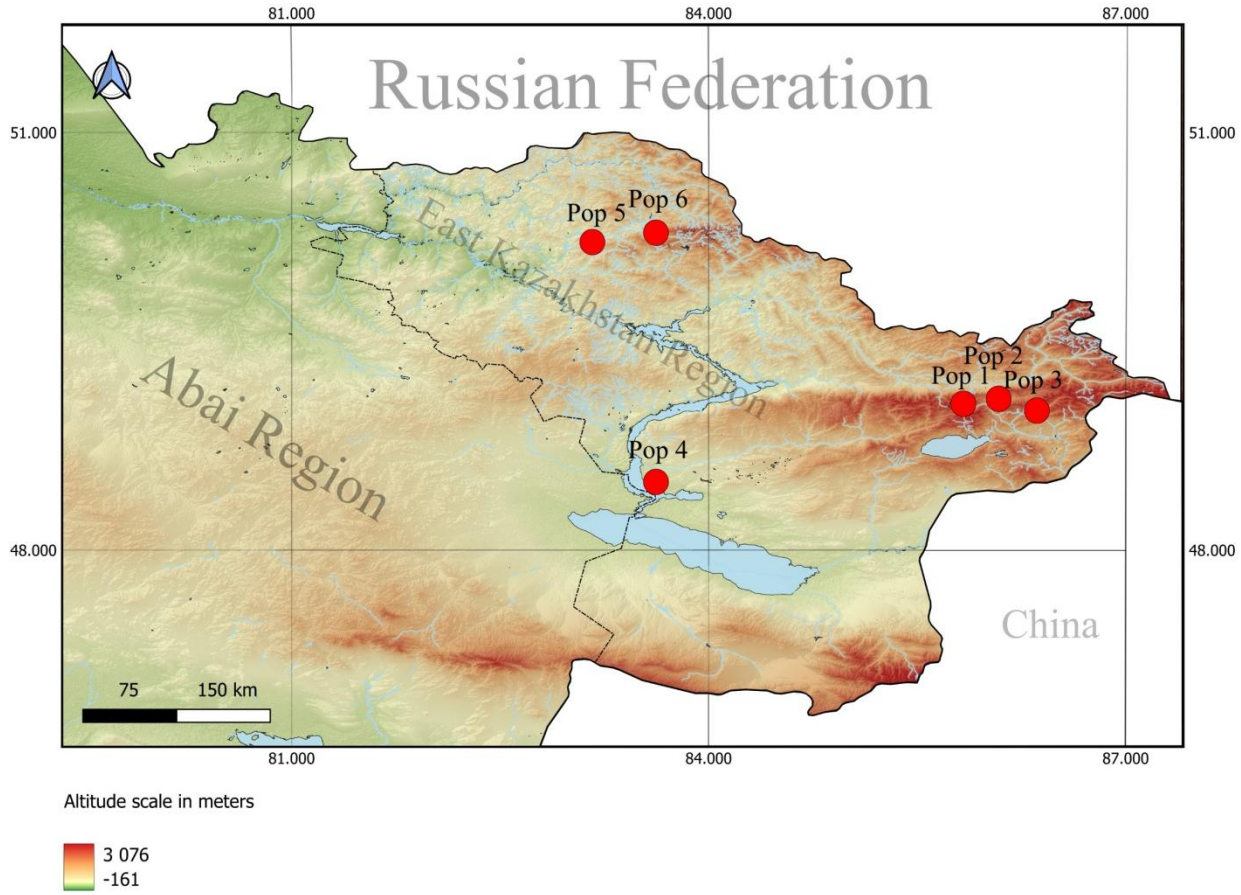

Figure 2. Schematic map of the locations of *Bupleurum multinerve* in the phytobiota of the Kazakh Altai

The mountain system of the Southern Altai, located at the junction of the borders with Russia, Mongolia, and China, has an altitudinal range from 600–700 m above sea level in the western and southwestern foothills to 1500–3400 m in the south and 2000–2500 m in the northeast. The climate is sharply continental, with features determined by altitudinal zonation and the influence of moist northwestern Atlantic air masses, resulting in annual precipitation ranging from 400 mm in the foothills to 800–1000 mm in the mountain forest belt. The Southern Altai is the coldest region within the Kazakh Altai [14].

The Southwestern Altai is characterized by a system of high ridges (1500–2800 m above sea level) and lower mountain and foothill areas (500–700 m above sea level). The climate is sharply continental, with long cold winters, hot summers, significant diurnal and seasonal variations, and pronounced annual fluctuations in air temperature. Annual precipitation ranges from 400–550 mm in the west to 1500 mm in the eastern and northeastern parts of the region [15, 16].

As a result of field studies conducted in the Southern and Southwestern Altai, the floristic composition of plant communities involving *B. multinerve* was examined, including an assessment of species abundance in the Southern Altai. Morphometric and demographic parameters were analyzed, and the resource potential of the species under different growth conditions was determined for six populations, selected based on differences in floristic composition and spatial distribution of the occupied territories.

The coordinates of all populations identified during field research were recorded using a Garmin eTrex 22x GPS navigator. These data were subsequently formatted into an electronic metadata database and uploaded to the Global Biodiversity Information Facility platform (https://gbif.buketov.edu.kz/resourcer=herbarium_abg).

Due to the extensive and topographically complex nature of the study areas, fieldwork was carried out using a route-reconnaissance method [17]. Topographic maps and forest inventory materials were used in planning field routes. A geobotanical method was applied to describe plant communities involving *B. multinerve* [18]. The nomenclature of genera and species of vascular plants in the communities was verified using the Plants of the World Online database [19]. The condition of coenopopulations was assessed using organismal and population-level traits [20]. The resource potential of *B. multinerve* was determined according to the "Methodology for Assessing Reserves of Medicinal Plants" [21]. To estimate raw material re-

serves in specific stands, sample plots of 1 m² were established, with their number varying from 5 to 10 depending on the area of the stand and the uniformity of species distribution within the community [22].

For morphometric measurements, a sample of 15–20 flowering plants of *B. multinerve* was selected in each population, recording the height of generative shoots, the number of generative shoots, and the number of individuals per 1 m². The age states of individuals were determined according to the classification of O.V. Smirnova et al. [23], developed based on the generally accepted scheme of T.A. Rabotnov [24]. Statistical processing was carried out using Microsoft Excel 2010.

Results and Discussion

Our research revealed that the habitats of *B. multinerve* in the Southern Altai are primarily associated with northwestern (Sarymsakty Ridge), southeastern (South Altai Tarbagatai Ridge), and northeastern (Narym Ridge) exposures, with a vertical distribution range from 1300 to 2015 m above sea level. In the Southwestern Altai, both populations were recorded on the southeastern slope of the Ivanovsky Ridge (Prokhodnoy Belok) with a vertical distribution range of 1450–1990 m above sea level.

In the Southern Altai, the species was found in subalpine, mountain-forest, and mountain-steppe associations; in the Southwestern Altai, it occurs in subalpine low-herb and foothill-shrub associations. Surveys showed that *B. multinerve* is widely distributed in mountain-steppe associations, contributing to the formation of meadow-steppe type vegetation, and to a lesser extent, shrub and forest phytocoenoses (Tab. 1).

Table 1

Characteristics of the habitats of the studied *Bupleurum multinerve* populations in the phytobiota of the Kazakh Altai

Population	Location	Coordinates of the main points			The area occupied by the view, ha	Name of the association
		width	longitude	height above sea level.		
	Southern Altai					
Pop 1	Sarimsakty Range, northwestern slope, near the Burkhat Pass	49.1333	86.0103	2015	12,0	Subalpine iris-borage
Pop 2	Sarimsakty Range, northwestern slope, near the Burkhat Pass	49.1586	86.0239	1300	200,0	Mountain-steppe mixed-grass-volodushkovaya
Pop 3	South Altai Tarbagatai Range, southeastern slope, foothill terrace	49.0953	86.2006	1890	15	Mountainous forest grassy-cereal-grassland
Pop 4	Narym Range, northeastern slope	48.5864	83.5764	1380	172	Mountain-steppe mixed-grass-volodushkovaya
	Southwest Altai					
Pop 5	Ivanovsky Range, southeastern slope, (Passing Squirrel)	50.2661	83.5456	1990	25	Subalpine low-grass violet-blue
Pop 6	Ivanovsky Range, southeastern slope, (Passing Squirrel)	50.3211	83.8807	1450	12	Foothill-shrub-grass-and-forb-grass

In the Southern Altai, under subalpine conditions in the iris–Bupleurum association (Pop. 1), the area occupied by the species is 12 ha on eroded rocky slopes of the Sarymsakty Ridge, with a total projective cover of 100 %, of which *B. multinerve* contributes 25.8 % to the community. In the mountain-steppe habitats on the Sarymsakty Ridge (Pop. 2) and Narym Ridge (Pop. 4), *B. multinerve* acts as a landscape-forming species, forming independent stands over areas of 200 ha and 172 ha, respectively, with a total projective cover of 100 %, where the occurrence of *B. multinerve* reaches up to 70.0 %. In the mountain-forest association, *B. multinerve* (Pop. 3) on the South Altai Tarbagatai Ridge occupies a small area of 15 ha at the upper limit of cedar park forests; total projective cover is 100 %, and the species' participation in the phytobiota is 19.8 %.

In the Southwestern Altai, on the Ivanovsky Ridge (Pop. 5) under subalpine conditions, a *Bupleurum* association is established within a sparse larch–cedar forest over an area of 25 ha, where the shrub layer is absent. The herbaceous layer is well-developed, with a projective cover of 100 %, and *B. multinerve* contrib-

utes 13.9 % to the phytocoenosis. The foothill-shrub *Bupleurum–mixed-herb–grass* association (Pop. 6) occurs among a sparse shrub layer with canopy closure of 0.2–0.3, occupying an area of 12 ha. Total projective cover is 100 %, with *B. multinerve* accounting for 15.8 %.

When studying species diversity in communities with *B. multinerve* in the Southern Altai, it was found that the floristic complex consists of 78 species of flowering plants. The floristic composition is mainly represented by mountain-steppe mesoxerophytic herbaceous species. Differences in species richness among the described communities are minor. By species abundance, the mountain-forest mixed-herb–grass–*Bupleurum* association on the South Altai Tarbagatai Ridge at 1890 m a.s.l. (Pop. 3) stands out with 46 species. The lowest contribution to species number comes from the iris–*Bupleurum* population (Pop. 1) under subalpine conditions on the Sarymsakty Ridge at 2015 m a.s.l., with 35 species (Tab. 2).

Table 2

Summary of the floristic composition of plant communities involving *Bupleurum multinerve*, indicating species abundance in the Southern Altai

№	Names of plant species	Name of association			
		Subalpine iris–*Bupleurum* association, 2015 m a.s.l.	**Mountain-steppe mixed-herb–*Bupleurum* association, 1300 m a.s.l.**	**Mountain-forest mixed-herb–grass–*Bupleurum* association, 1890 m a.s.l.**	**Mountain-steppe mixed-herb–*Bupleurum* association, 1380 m a.s.l.**
	Abundance on the Drude scale				
	1	**2**	**3**	**4**	**5**
1	*Spiraea media* Schmidt	sp	-	sp	sp
2	*Cotoneaster uniflorus* Bunge	-	-	un	-
3	*Cotoneaster melanocarpus* G. Lodd.			sol	sp
4	*Sibiraea laevigata* (L.) Maxim	un	-	sol	-
5	*Pentaphylloides fruticosa* (L.)O.Schwarz	un	-	un	-
6	*Rosa acicularis* Lindl.	un	-	un	-
7	*Rosa spinossisima* L.	-	un	-	un
8	*Lonicera caerulea* subsp. *altaica* (Pall.) Gladkova	-	un	-	-
9	*L. microphylla* Willd. ex Roem. & Schult.	sp	-	-	-
10	*Berberis sibirica* Pall.	-	sol	sol	-
11	*Caragana pumila* Pojark	-	-	-	un
12	*Bupleurum multinerve* DC.	cop_1	soc	cop_1	soc
13	*Helictotrichon desertorum* (Less.)Pilg.	-	-	sp	sp
14	*Helictotrichon pubescens* (Huds.) Schult.	-	sp	cop_2	sp
15	*Helictotrichon schellianum* (Hack.)Kitag	sp	-	cop_2	-
16	*Elymus uralensis* (Nevski) Tzvelev	cop_1	-	cop_3	-
17	*E. mutabilis* (Drobov) Tzvelev	un	un	-	-
18	*Artemisia sericea* (Besser) Weber ex Stechm.	sp	sp	sp	sp
19	*A. kotuchovii* Kupr.	-	un	-	-
20	*A. viridis* Willd. ex DC.	-	-	sp	sp
21	*Phleum phleoides* (L.) H. Karst	-	-	sol	-
22	*Poa attenuata* Trin.	-	-	sol	-

Continuation of Table 2

№	Names of plant species	Name of association			
		Subalpine iris–*Bupleurum* association, 2015 m a.s.l.	**Mountain-steppe mixed-herb–*Bupleurum* association, 1300 m a.s.l.**	**Mountain-forest mixed-herb–grass–*Bupleurum* association, 1890 m a.s.l.**	**Mountain-steppe mixed-herb–*Bupleurum* association, 1380 m a.s.l.**
	Abundance on the Drude scale				
	1	**2**	**3**	**4**	**5**
23	*Festuca valesiaca* Schleich. ex Gaudin	-	-	sp	-
24	*Pedicularis cystopteridifolia* Rydb.	-	-	un	-
25	*Pedicularis eriantha* (Boiss. & Buhse) T.N. Popova	-	sp	-	-
26	*Pedicularis proboscidea* Steven	-	-	sp	-
27	*Gentiana decumbens* L..f.	s	-	sp	-
28	*Gentiana macrophylla* Pall.	sp	-	un	-
29	*Oxytropis ambigua* (Pall.) DC.	un	sp	-	un
30	*Oxytropis sulphurea* Bunge	-	-	sp	-
31	*Koenigia alpina* (All.) T.M. & Schult. Reveal	sp	un	soc	un
32	*Campanula glomerata* L.	un	s	sp	un
33	*Gypsophila altissima* L.	un	sp	un	sp
34	*Allium altaicum* Pall.	un	-	-	-
35	*Allium lineare* L.	un	un	un	un
36	*Allium nutans* L.	-	un	-	s
37	*Allium flavidum* Ledeb.	sp	sol	-	-
38	*Allium rubens* Spreng.	-	sol	un	-
39	*Thalictrum flavum* L.	-	s	un	sp
40	*Aconitum anthoroideum* DC.	sp	un	sp	-
41	*Achillea millefolium* L.	-	sp	sp	un
42	*Saussurea parviflora* (Poir.) DC.	sp	un	un	-
43	*Galium cicaezans* Michx.	sp	-	-	-
44	*Galium verum* L.	un	sp	sol	sol
45	*Geranium collinum* Stephan ex Willd.	-	sp	-	sp
46	*G. pseudosibiricum* J. Mayer	sp	sol	-	-
47	*Phlomoides alpina* (Pall.) Adylov, Kamelin & Makhm.	sol	-	sp	-
48	*Phlomoides tuberosa* (L.) Moench	-	-	-	sp
49	*Galatella hauptii* (Ledeb.) Lindl. ex DC.	un	sp	-	-
50	*Galatella sedifolia* subsp. *sedifolia* (L.) Greuter	-	sol	sp	sp-cop_3
51	*Iris ruthenica* Ker Gavl.	cop_2	cop_2	cop_1	cop_2-cop_3
52	*Carex macroura* Meinsh.	cop_2	cop_2,	cop_2	sp
53	*Gentianella amarella* (L.) Börner	sp	sp	sp	sol
54	*Gentianopsis barbata* (Froel.) Ma	sol	sol	sp	sp-cop_1
55	*Dracocephalum ruyschiana* L.	sp	-	sp	-
56	*Dracocephalum discolor* Bunge	-	-	sol	sp
57	*Aster alpinus* L.	sol	sp	sp	-

Continuation of Table 2

№	Names of plant species	Name of association			
		Subalpine iris–*Bupleurum* association, 2015 m a.s.l.	**Mountain-steppe mixed-herb–*Bupleurum* association, 1300 m a.s.l.**	**Mountain-forest mixed-herb–grass–*Bupleurum* association, 1890 m a.s.l.**	**Mountain-steppe mixed-herb–*Bupleurum* association, 1380 m a.s.l.**
	Abundance on the Drude scale				
	1	**2**	**3**	**4**	**5**
58	*Primula macrocalyx* Bunge	un	sol	sol	un
59	*Euphrasia altaica* Serg.	sol	un	-	-
60	*Krascheninnikovia ceratoides* (L.) Gueldenst.	sol	-	-	sp
61	*Pseudoroegneria gmelinii* (Trin. ex Schrad.) Sennikov	-	sol	-	un
62	*Senecio nemorensis* L.	-	sol	-	-
63	*Poa attenuata* Trin	-	sol	un	sol
64	*P. angustifolia* L.	-	-	-	sp
65	*Viola disjuncta* W. Becker	-	sp	-	-
66	*Klasea cardunculus* (Pall.) Holub	-	un	-	-
67	*Scutellaria altaica* Ledeb. ex Sweet	-	sol	-	-
68	*Orostachys spinosa* (L.) Sweet	-	sol	un	-
69	*Thymus serpyllum* L.	-	cop_2	-	sp
70	*Phedimus stoloniferus* (S.G. Gmel.) 't Hart	-	sp	-	-
71	*Dianthus chinensis* L.	-	un	un	un
72	*Sanguisorba officinalis* L.	-	-	sol	-
73	*Scabiosa ochroleuca* L.	-	-	-	sol
74	*Stipa krylovii* Roshev.	-	-	-	sp
75	*Medicago falcata* L.	-	-	-	sol
76	*Fragaria viridis* Weston	-	-	-	sp-cop_2,
77	*Crepis lyrata* (L.) Froel.	-	-	-	un
78	*Seseli buchtormense* (Fisch.) W.D.J. Koch	-	-	-	un
	TOTAL	35	43	46	39

Analysis using the Drude scale showed that shrubs do not play a significant role in the composition of the vegetation cover. In all studied populations, *B. multinerve* acts as the edificator, with an abundance of *soc* under mountain-steppe conditions in the Sarymsakty and Narym Ranges (Fig. 3-4), and with an abundance of cop1 under.

Figure 3. Thickets of *Bupleurum multinerve* in the Narym Range

Figure 4. Thickets of *Bupleurum multinerve* in the Sarymsakty Range

The dominants in the herbaceous layer of the communities are Carex periformis var. macroura — cop2, Elymus uralensis — cop1, Fragaria viridis — sp-cop2, Galatella sedifolia subsp. sedifolia — sp-cop3, Gentianopsis barbata — sp-cop1, Helictotrichon pubescens — cop2, H. schellianum — cop2, Iris ruthenica — cop2, Koenigia alpina — soc, Thymus serpyllum — cop2; other species are considered accompanying.

Considering the potential significance of Bupleurum multinerve as a source of plant raw material for the production of parapharmaceutical products, a resource assessment of the above-ground biomass was conducted in the studied populations in the Southern and Southwestern Altai (Tab. 3).

Table 3

Resource assessment of the potential above-ground biomass productivity of *Bupleurum multinerve* in the studied populations of the Kazakh Altai

Population	Location of the population	The area occupied by the view, ha	Yield, kg/ha (air-dry weight)	Operating stock of air-dry raw materials, t	Operating stock of air-dry raw materials, t Volume of possible preparation of air-dry raw materials, t
Southern Altai					
Pop1	Sarimsakty Range, north-western slope, near Burkhat Pass, 2015 m a.s.l.	12,0	178,85	2,15	1,29
Pop 2	Sarimsakty Range, north-western slope, near Burkhat Pass, 1300 m a.s.l.	200,0	360,10	72,02	43,21
Pop3	South Altai Tarbagatai Range, southeastern slope, foothill terrace, 1890 m a.s.l.	15,0	211,90	3,18	1,91
Pop 4	Narym Range, northeast-ern slope, 1380 m a.s.l.	172,0	357,32	61,46	36,87
Southwest Altai					
Pop 5	Ivanovsky Range, south-eastern slope, (Passing Squirrel), 1990 m a.s.l.	25,0	199,8	4,99	2,99
Pop 6	Ivanovsky Range, south-eastern slope, (Passing Squirrel), 1450m a.s.l.	22,0	221,3	4,87	2,92

In the territory of the Southern Altai, the industrial exploitable reserves of air-dried above-ground biomass of *Bupleurum multinerve* were determined under mountain-steppe conditions in the Sarymsakty (Pop 2) and Narym (Pop 4) Ranges, amounting to 72.02 t and 61.46 t, respectively, with a possible harvest volume of 43.21 t and 36.87 t. This is due to the extensive areas occupied by the species combined with a high density of individuals per unit area. The obtained data allow these populations to be recommended for industrial harvesting of above-ground biomass.

Simultaneously with the assessment of resource potential, certain morphometric parameters of generative individuals were evaluated, with statistically significant differences at $P \leq 0.05$ (Fig. 5). The study revealed that the phenotypes of *Bupleurum multinerve* differ in height depending on their habitat.

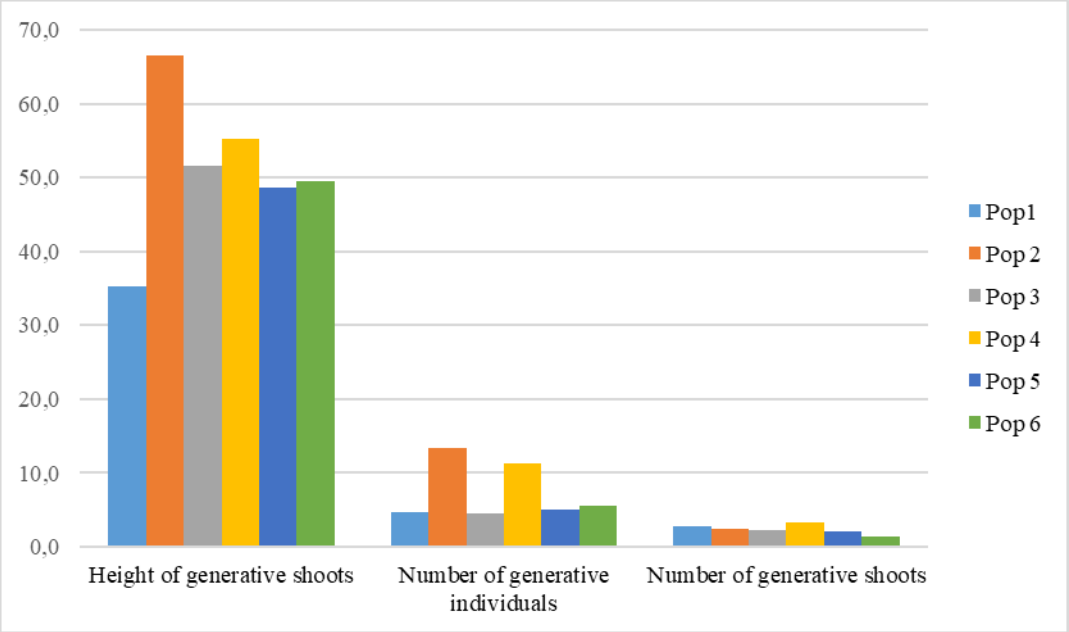

Figure 5. Selected morphometric parameters of above-ground organs of *Bupleurum multinerve* in the studied populations of the Southern and Southwestern Altai

Based on morphometric measurements, the tallest generative individuals were recorded under mountain-steppe conditions in the Southern Altai, in populations Pop2 (Sarymsakty Range) and Pop4 (Narym Range), measuring 66.5 ± 1.93 cm and 55.3 ± 6.23 cm, respectively. The minimum height was observed in the population under subalpine conditions in Pop1 (Sarymsakty Range) at 35.2 ± 1.13 cm. The maximum number of generative individuals per 1 m² was recorded under mountain-steppe conditions in Pop2 (Sarymsakty Range) and Pop4 (Narym Range), with values of 13.37 ± 2.06 and 11.23 ± 3.23 individuals/m², respectively. In natural conditions of the Southern and Southwestern Altai, generative individuals were characterized by a low number of generative shoots, ranging from 1.48 ± 0.26 to 3.39 ± 0.86 shoots per individual.

Based on morphometric data, the populations under mountain-steppe conditions in the Sarymsakty and Narym Ranges can be considered promising for seed collection for introduction and inclusion in a seed gene bank.

According to statistical guidelines, when the coefficient of variation is less than 12 %, the trait variability is considered low; from 13 % to 20 % — medium; from 21 % to 40 % — high; and above 40 % — very high [25]. In our study, the height of generative plants in all populations varied at a medium level of variability, ranging from 13.35 % to 18.65 %, indicating the stability of this trait in individuals of the species in the surveyed ranges of the Kazakh Altai. Traits with high variability in *B. multinerve* included the number of individuals per unit area, varying from 25.0 % to 36.9 %, while the variability of generative shoot number ranged from medium to high, from 15.1 % to 37.2 %, demonstrating high plasticity and the species' ability to self-renew under natural conditions in the Southern and Southwestern Altai.

Bupleurum multinerve is a rhizome-taproot perennial with a monocyclic, oligocarpic, or polycarpic biomorph type [26]. According to E.L. Nukhimovskij [27], individuals of different biomorphs of *B. multinerve* may occur within the same cenotic population, undergoing a complete ontogenetic cycle, the du-

ration of which is directly dependent on growth conditions. Considering the ontogenetic development characteristics of *B. multinerve* [28], a single individual was used as the counting unit in the study of the age structure of populations. Counts were conducted across four age groups: juvenile (j), immature (im), virginal (v), and generative (g) individuals, as senescent and dying plants were not observed (Fig. 6).

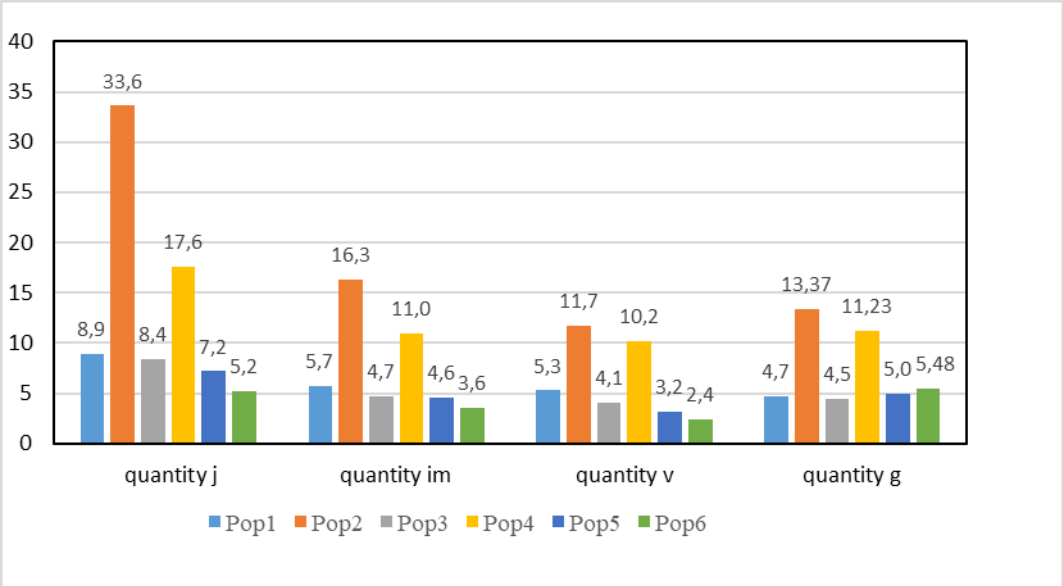

Figure 6. Quantitative composition of age groups in the studied populations of *Bupleurum multinerve* in the Southern and Southwestern Altai

The studied populations of *Bupleurum multinerve* in the Southern and Southwestern Altai, despite inhabiting different geographic locations, are normal and complete, exhibiting an age spectrum with a tendency toward left-skewed asymmetry. In all populations, the young fraction dominates over the adult fraction according to the index (j + im)/(v + g), which confirms that the species maintains its population density primarily through seed reproduction within the associations. At the current stage, minor differences in the ratio of virginal (v) to generative (g) individuals across all populations indicate that the environmental conditions for *B. multinerve* in the studied populations are optimal.

When assessing the economic traits of *B. multinerve*, the density of individuals per unit area is considered a key economic indicator. The results of the study show that, except for populations Pop2 and Pop4, the density of individuals per 1 m² varies slightly despite heterogeneous natural conditions (Fig. 7). Under Southern Altai conditions, this indicator was 24.6 individuals/m² in Ror1 and 21.7 individuals/m² in Pop3; in the Southwestern Altai, it was 20.0 individuals/m² in Pop5 and 18.7 individuals/m² in Pop6. The highest density of individuals was observed in Pop2 (75.0 individuals/m²) and Pop4 (50.0 individuals/m²) under mountain-steppe conditions in the Sarymsakty and Narym Ranges. Based on these data, it can be inferred that the surveyed populations are currently in a stable state and that the habitat conditions correspond to the species' ecological optimum.

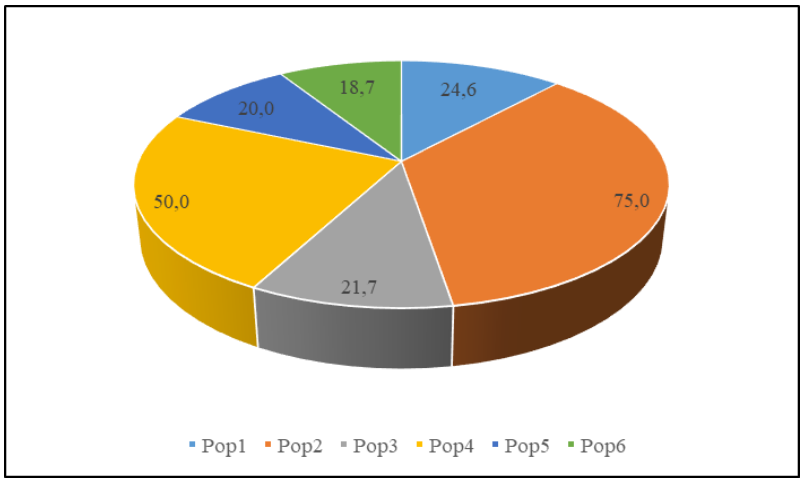

Figure 7. Density of *Bupleurum multinerve* individuals in populations of the Southern and Southwestern Altai, individuals/m²

Thus, the integration of ecological-phytocoenotic and morphometric indicators, along with the assessment of age structure and productivity of *Bupleurum multinerve*, demonstrates the potential for the species' use at the present stage as an unconventional wild medicinal plant in the Kazakh Altai. Future studies, including assessments of genetic diversity, reproductive biology, and modeling of climate resilience, will significantly enhance the prospects for sustainable utilization of the species in the region.

Conclusion

Population and resource studies in the phytobiota of the Kazakh Altai have shown that the Southern and Southwestern Altai regions hold significant potential for the economic use of natural populations of the unconventional wild medicinal plant *B. multinerve*. Habitat analysis demonstrated specific preferences with respect to plant communities; populations were recorded in mountain-steppe, foothill-shrub, mountain-forest, and subalpine associations, with the species in the mountain-steppe conditions of the Southern Altai acting as a landscape-forming element with dominance levels *soc* and *sor1*.

The vertical distribution of the species ranges from 1,300 to 2,015 m a.s.l. The rich species diversity of floristic composition in these associations, combined with a significant level of variation in morphometric parameters—such as the height of generative shoots, the number of generative shoots per individual, and the number of generative individuals per unit area—confirms the stability of populations and the ecological plasticity of *B. multinerve* in the phytobiota of the Kazakh Altai.

The dominance of juvenile and immature individuals over virginal and generative individuals in the age structure indicates the effectiveness of seed reproduction and the species' capacity for self-maintenance through seeds. The left-skewed age spectrum reflects population youth and serves as a current indicator of high vitality and the ability to maintain occupied territories.

Resource assessment demonstrated the industrial significance of the species in the Southern Altai under mountain-steppe conditions, where *B. multinerve* formed the most extensive and highly productive industrial stands (ranging from 357.32 kg/ha to 360.10 kg/ha of air-dry weight). The most resource-rich populations should be prioritized when planning the harvest volumes of plant raw materials as a valuable medicinal plant of the Kazakh Altai flora, while also ensuring the conservation of populations in their natural habitats.

Funding

This article was written with the financial support of the Committee of Science of the Ministry of Higher Education and Science of the Republic of Kazakhstan as part of the BR28712367 project "Comprehensive Study of Unconventional Wild Medicinal Plants, Mobilization of Their Genetic Resources in the Botanical Gardens of Western, Eastern, and Central Kazakhstan, and Creation of a Bioinformation Database for the Development of the Parapharaceutical Industry", 2025–2027.

Conflict of interest

The authors declare no conflict of interest.

Author Contributions

The manuscript was written through contributions of all authors. All authors have given approval to the final version of the manuscript. CRediT. **Danilova A.N.** — development of relevance, analysis of results, **Kotukhov Y.A.** — field work, development of methodology; **Sumbembayev A.A.** — geobotanical research, analysis, **Anufriyeva O.A**. — field work, conclusion, **Akhmetzhanov A.M.** — study of the age structure of populations, literature sources.

References

1 Кубентаев С.А. Ресурсная оценка лекарственных растений Западного Алтая в пределах Восточно-Казахстанской области / С.А. Кубентаев, Н.Г. Гемеджиева, А.К. Агаджаева, С.К. Мухтубаева, К.С. Исбастина, Д.Т. Алибеков, Ж.Т. Идрисова // Матер. Междун. науч.-практ. конф. «Современное состояние и перспективы развития ботанических садов и дендариев Казахстана», посвященной 5-летию Астанинского ботанического сада. — Астана, 2023. — С. 67–70. ISBN 978-601-7511-63-0.

2 Каримова О.А. Результаты интродукции двух ресурсных видов из рода *Bupleurum* L. в Республике Башкортостан / О.А. Каримова // Научные ведомости. Сер. Естественные науки. — 2011. — № 3(98). — Вып. 14/1. — С. 14–20.

3 Куминова А.В. Растительный покров Алтая / А.В. Куминова. — Новосибирск, 1960. — 449 с.

4 Пешкова Г.А. Флорогенетический анализ степной флоры гор Южной Сибири [Электронный ресурс] / Г.А. Пешкова. — Новосибирск, 2001. — 192 с. ISBN 5-02-031931-7. — Режим доступа: http://nskhuman.ru/shipunov/biblbook.php?nbook=10170

5 Грубов В.И. Определитель сосудистых растений Монголии / В.И. Грубов. — Л., 1982. — 189 с.

6 Байтулин И.О. Казахстанский Алтай как ресурсная база лекарственных растений / И.О. Байтулин, А.Б. Мырзагалиева // Известия Национальной академии наук. Серия биологическая и медицинская. — 2015. — 6(312). — С. 5–11. ISSN 2224 — 5308

7 Кубентаев С.А. Современное состояние и запасы володушки многожильчатой на хребтах Сарымсакты и Южноалтайский Тарбагатай / С.А. Кубентаев, А.Н. Данилова // Сб. Международ. научн. конф. «Изучение, сохранение и рациональное использование растительного мира Евразии». — 2017. — С. 271–276.

8 Минаева В.Г. О превращении флавонолов в бесклеточных экстрактах репродуктивных органов володушки (Bupleurum L.) / В.Г. Минаева, М.Н. Запрометов // Доклады Академии наук СССР. — 1973. — Т. 211, № 5. — С. 1213–1216.

9 Altantsetseg S. Comparative study of essential oil constituents of Bupleurum species from Mongolia / S. Altantsetseg, S. Shatar, N. Javzmaa N. Altantsetseg // Mongolian Journal of Chemistry. — 2012. — Vol. 13. — P. 28–30. DOI: https://doi.org/10.5564/mjc.v13i0.156

10 Дикорастущие полезные растения России. — СПб., 2001. — 664 с.

11 Грудзинская Л.М. Аннотированный список лекарственных растений Казахстана / Л.М. Грудзинская, Н.Г. Гемеджиева, Н.В. Нелина, Ж.Ж. Каржаубекова. — Алматы, 2014. — Т. 20 (1). — 200 с.

12 Саратиков А.С. Новые фармакологические свойства препарата буплерина из надземной части *Bupleurum multinerve* DC. / А.С. Саратикова, И.Г. Минаева, В. Г., Лившиц Н.С. Жанаева Т. А., И.Е. Лобанова // Растительные ресурсы. — 1990. —Т. 26, № 1. — С. 88–90.

13 Мирович В.М. Флавоноиды и фенилпропаноиды надземных органов володушки многожилковой (*Bupleurum multinerve* DC.) флоры Прибайкалья / В.М. Мирович, Д.Н. Олейников, С.А. Петухова, А.А. Посохина // Химия растительного сырья. — 2020. — № 4. — С. 121–128. DOI: 10.14258/jcprm.2020047530

14 Kotukhov Y.A. Ecological and biological features of Cypripedium at Katon-Karagay State National Natural Park / Yu. A. Kotukhov, A.N. Danilova, O.A. Anufriyeva, A.N. Suleimenov, A.A. Sumbembayev, S.A. Kubentaev // Plant Archives. — 2018. — Vol. 18, No. (2). — P. 1499–1502.

15 Sumbembayev A.A. Assessment of state of Dactylorhiza fuchsia (Orchidaceae) populations from the Altai mountains of Kazakhstan / A.A. Sumbembayev, Z.H.T. Tergenbaeva, G.M. Kudabayeva, R.S. Tashmetova, Y.A. Genievskaya, D.L. Szlachetko // Biodiversitas. — 2022. — Vol. 23, No. 9. — P. 4385–4399. DOI: 10.13057/biodiv/d230903.

16 Kubentayev S.A. Current State of Natural Populations of Paeonia anomala (Paeoniaceae) in East Kazakhstan / S.A. Kubentayev, O.N. Khapilina, M.Y. Ishmuratova, A.K. Sarkytbayeva, A. S.Turzhanova, A.A. Imanbayeva, M.Z. Zhumagul // Diversity. — 2023. — Vol. 15, No. 11. — P. 1127. DOI: 10.3390/d15111127

17 Щербаков А.В. Полевое изучение флоры и гербаризация растений / А.В. Щербаков А.В. Майоров. — М.: Изд-во МГУ, 2006. — 84 с.

18 Румянцева Д.Е. Основы геоботаники: учеб.-мет. пос. [Электронный ресурс] / Д.Е. Румянцев, В.А. Липаткин, А.Б. Загреева. — 2023. — 66 с. — Режим доступа: https://mf.bmstu.ru/assets/info/science/dendro/books/17.pdf.

19 Plants of the World Online (POWO 2025). — [Electronic resource]. — Access mode: https://powo.science. kew.org/cite-us

20 Заугольнова Л.Б. Структура популяций семенных растений и проблемы их мониторинга: автореф. дис. … д-ра биол. наук [Электронный ресурс] / Л.Б. Заугольнова. — 1994. — 72 с. — Режим доступа: https://viewer.rusneb.ru/ru/000199_000009_000286782? page=1&rotate=0&theme=white

21 Методика определения запасов лекарственных растений. — М., 1986. — 50 с.

22 Гемеджиева Н.Г. Алкалоидоносные растения Казахстана и перспективы их использования (на примере Джунгаро-Северотяньшаньской провинции) / Н.Г. Гемеджиева. — Алматы, 2012. — Т. 18 (8). — 312 с.

23 Смирнова О.В. Критерии выделения возрастных состояний и особенностей хода онтогенеза у растений различных биоморф / О.В. Смирнова, Л.Б. Заугольнова, Н.А. Торопова, Л.Д. Фаликова // Ценопопуляции растений (основные понятия и структура). — 1976. — С. 14–44.

24 Работнов Т.А. Геоботаника. Жизненный цикл многолетних травянистых растений в луговых ценозах / Т.А. Работнов // Труды Ботанического института АН СССР. Серия III. — 1950. — Вып. 6. — С. 7–204.

25 Зайцев Н.Г. Методика биометрических расчетов. Математическая статистика в экспериментальной ботанике [Электронный ресурс] / Н.Г. Зайцев. — М.: Наука, 1973. — 256 с. — Режим доступа: https://knigogid.ru/books/1923293

26 Михайлова С.И. Морфология и анатомия *Bupleurum multinerve (Apiaceae)* на Алтае [Электронный ресурс] / С.И. Михайлова // Ботанический журнал. — 1989. — Т. 74. — С. 1455–1461. — Режим доступа: http://nskhuman.ru/shipunov/bibljourn.php? nbook=52

27 Нухимовский Е.Л. Основы биоморфологии семенных растений / Е.Л. Нухимовский. — М.: Недра, 1997. — Т. 1. Теория организации биоморф. — 629 с.

28 Астешенков А.Ю. Состояние ценопопуляций *Bupleurum multinerve* DC. в различных условиях Хакасии и Алтая / А.Ю. Астешенков, В.А. Черемушкина // Растительный мир Азиатской России. — 2009. — № 1(3). — С. 94–99.

А.Н. Данилова, Ю.А. Котухов, А.А. Сумбембаев, О.А. Ануфриева, Ә.М. Ахметжанов

Қазақстан Алтайының әртүрлі жағдайларындағы *Bupleurum multinerve* DC. ресурстық қоры және популяциялар күйі

Қазақстан Алтайында *Bupleurum multinerve* бойынша зерттеулердің нәтижелері ұсынылған. Зерттеудің мақсаты — Қазақстан Алтайындағы табиғи өсу жағдайларында *Bupleurum multinerve* түрінің популяциялық және ресурстық көрсеткіштерін зерттеу. Популяциялардың флористикалық құрамы, морфометриялық параметрлері, жас құрылымы және ресурстық қоры анықталды. Түрдің тік таралу шегі теңіз деңгейінен 1300–2015 м аралығында екені анықталып, ол тау-далалық, тау бөктеріндегі бұталы, тау орманды және субальпілік қауымдастықтар құрамында кездесетіні белгіленді. Оңтүстік Алтайдың тау-далалық жағдайында бұл түр ландшафт түзуші, оның үлесі 70,0 %-ға дейін жетеді. Қауымдастықтардың өсімдік жамылғысы 100 % қалыптасқан, негізін шөптесін өсімдіктер құрайды. Оңтүстік және Оңтүстік-Батыс Алтайдағы зерттелген *B. multinerve* қалыпты, толық құрамды емес, жастық спектрі сол жақты асимметрияға бейім. Түр генеративті өркеннің биіктігі бойынша 13,35 %-дан 18,65 %-ға дейін тұрақтылықпен сипатталады, ал бірлік ауданға шаққандағы генеративті дарақтар саны бойынша 25,0–36,9 % аралығында жоғары өзгергіштік көрсетеді. Сонымен қатар генеративті өркендердің 15,1–37,2 % деңгейінде ауытқуы есебінен тұқым арқылы өздігінен жаңару қабілетіне ие. Дарақтардың ең жоғары тығыздығы Сарымсақты (75 дана/м²) және Нарым (50,0 дана/м²) жоталарының тау-далалық жағдайларында тіркелген. *B. multinerve* түрінің жерүсті массасының өнеркәсіптік қоры ауа-құрғақ күйде Сарымсақты және Нарым жоталарында сәйкесінше 72,02 т және 61,46 т болып анықталды, ал мүмкін болатын дайындау көлемі — 43,21 т және 36,87 т.

Кілт сөздер: Bupleurum multinerve, Оңтүстік Алтай, Оңтүстік-Батыс Алтай, ассоциация, популяция, түрлік әртүрлілік, молшылық, жас құрылымы, ресурстар.

А.Н. Данилова, Ю.А. Котухов, А.А. Сумбембаев, О.А. Ануфриева, А.М. Ахметжанов

Состояние популяций и ресурсные запасы *Bupleurum multinerve* DC. в различных условиях Казахстанского Алтая

Представлены результаты исследований *Bupleurum multinerve* в Казахстанском Алтае. Цель исследования — популяционные и ресурсные исследования *Bupleurum multinerve* в естественных условиях произрастания в Казахстанском Алтае. Изучены флористический состав, морфометрические параметры, возрастной состав, ресурсные запасы популяций. Установлен порог вертикального распространения вида — 1300–2015 м н. у. м. в составе горно-степных, предгорно-кустарниковых, горно-лесных и субальпийских ассоциаций. В горно-степных условиях Южного Алтая вид является ландшафтообразующим с плотностью до 70,0 %. Растительный покров ассоциаций сформирован на 100 %, основу составляют травянистые виды растений. Популяции *B. multinerve* на Южном и Юго-Западном Алтае нормальные, неполночленные, возрастной спектр с тенденцией к левосторонней асимметрии. Вид характеризуется стабильностью по высоте генеративного побега от 13,35 % до 18,65 %, высокой вариабельностью по количеству генеративных особей на единице площади от 25,0 до 36,9 %, способностью к самовозобновлению семенным путем за счет варьирования генеративных побегов на уровне от 15,1 до 37,2 %. *Наибольшая плотность особей отмечена в горно-степных условиях произрастания на хр. Сарымсакты (75 шт./м^2) и Нарымском (50,0 шт./м^2).* Промышленные запасы надземной массы *B.*

multinerve в воздушно-сухом состоянии установлены *в горно-степных условиях на хр. Сарымсакты и Нарымском соответственно* — 72,02 и *61,46 т, а объем возможной заготовки* — 43,21 и 36,87 т.

Ключевые слова: Bupleurum multinerve, Южный Алтай, Юго-Западный Алтай, ассоциация, популяция, видовое разнообразие, численность, возрастная структура, ресурсы.

References

1 *Kubentaev, S.A.,* Gemedzhieva, N.G., Agadzhaeva, A.K., Mukhtubayeva, S.K., Isbastina, K.S., Alibekov, D.T., & Idrisova, Zh.T. (2023). *Resursnaia otsenka lekarstvennykh rastenii Zapadnogo Altaia v predelakh Vostochno-Kazaxstanskoi oblasti [*Resource assessment of medicinal plants of Western Altai within East Kazakhstan region*]. Materialy Mezhdunarodnoi nauchno-prakticheskoi konferentsii «Sovremennoe sostoianie i perspektivy razvitiia botanicheskikh sadov i dendrariev Kazakhstana», posviashchennoi 5-letiiu Astaninskogo botanicheskogo sada — Materials of the International Scientific and Practical Conference "Current state and prospects of development of botanical gardens and arboretums of Kazakhstan", dedicated to the 5th anniversary of the Astana Botanical Garden* (pp. 67–70). Astana [in Russian].

2 *Karimova, O.A. (2011). Rezultaty introduktsii dvukh resursnykh vidov iz roda Bupleurum L. v Respublike Bashkortostan [*Results of the introduction of two resource species of the genus *Bupleurum* L. in the Republic of Bashkortostan*]. Nauchnye vedomosti. Seria Estestvennye nauki — Scientific bulletin. Natural Sciences Series, 3(98), 14–20* [in Russian].

3 *Kuminova, A.V. (1960). Rastitelnyi pokrov Altaia [*Vegetation cover of the Altai*]*. Novosibirsk [in Russian].

4 *Peshkova, G.A. (2001). Florogeneticheskii analiz stepnoi flory gor Yuzhnoi Sibiri [*Florogenetic analysis of the steppe flora of the southern Siberian mountains*]. nskhuman.ru. Retrieved from* http://nskhuman.ru/shipunov/biblbook.php? nbook=10170 [in Russian].

5 *Grubov, V.I. (1982). Opredelitel sosudistykh rastenii Mongolii [*Guide to vascular plants of Mongolia*]*. Leningrad [in Russian].

6 *Bajtulin, I.O.,* & Myrzagalieva, A.B. *(2015). Kazakhstanskii Altai kak resursnaia baza lekarstvennykh rastenii [*Kazakh Altai as a resource base for medicinal plants*]. Izvestiia Natsionalnoi Akademii Nauk. Seriia biologicheskaia i meditsinskaia — Proceedings of the National Academy of Sciences. Series is biological and medical, 6(312), 5–11* [in Russian].

7 Kubentaev, S.A., & Danilova, A.N. *(2017). Sovremennoe sostoianie i zapasy volodushki mnogozhilchatoi na khrebtakh Sarymsakty i Yuzhnoaltaiskii Tarbagatai [*Current state and resources of *Bupleurum multinerve* on the Sarymsakty and South-Altai Tarbagatai ranges*]. Sbornik Mezhdunarodnoi nauchnnoi konferentsii «Izuchenie, sokhranenie i ratsionalnoe ispolzovanie rastitelnogo mira Evrazii» — Collection of the International Scientific Conference "Study, conservation and rational use of the flora of Eurasia" (pp. 271–276)* [in Russian].

8 *Minaeva, V.G., & Zaprometov, M.N. (1973). O prevrashchenii flavonolov v beskletochnykh ekstraktakh reproduktivnykh organov volodushki (Bupleurum L.) [*On the transformation of flavonols in cell-free extracts of reproductive organs of *Bupleurum* L.*]. Doklady Akademii Nauk SSSR — Reports of the Academy of Sciences of the USSR, 211(5), 1213–1216* [in Russian].

9 *Altantsetseg, S., Shatar, S., & Javzmaa, N. (2012). Comparative study of essential oil constituents of Bupleurum species from Mongolia. Mongolian Journal of Chemistry, 13, 28–30. DOI: https://doi.org/10.5564/mjc.v13i0.156*

10 *(2001). Dikorastushchie poleznye rasteniia Rossii [*Wild Useful Plants of Russia*]. Saint Petersburg* [in Russian].

11 Grudzinskaya, L.M., Gemedzhieva, N.G., Nelina, N.V., & Karzhaubekova, Zh. Zh. (2014). *Annotirovannyi spisok lekarstvennykh rastenii Kazakhstana [*Annotated list of medicinal plants of Kazakhstan*]. Vol. 20(1).* Almaty [in Russian].

12 Saratikov, A.S., Minaeva, I.G., Livshits, V.G., Zhanaeva, T.A., & Lobanova, I.E. *(1990). Novye farmakologicheskie svoistva preparata buplerina iz nadzemnoi chasti Bupleurum multinerve DC. [*New pharmacological properties of the drug buplerin from the aerial part of *Bupleurum multinerve* DC.*]. Rastitelnye resursy — Plant resources, 26(1), 88–90* [in Russian].

13 Mirovich, V.M., Oleinikov, D.N., Petukhova, S.A., & Posokhina, A.A. (2020). *Flavonoidy i fenilpropanoidy nadzemnykh organov volodushki mnogozhilkovoi (Bupleurum multinerve DC.) flory Pribaikalia [*Flavonoids and phenylpropanoids of aerial organs of *Bupleurum multinerve* DC. in the flora of the Baikal region.*]. Khimiia rastitelnogo syria — Chemistry of plant raw materials, 4, 121–128* [in Russian]. DOI:10.14258/jcprm.2020047530.

14 Kotukhov, Y.A., Danilova, A.N., Anufriyeva, O.A., Suleimenov, A.N., Sumbembayev, A.A., & Kubentaev, S.A. (2018). *Ecological and biological features of Cypripedium at Katon-Karagay State National Natural Park. Plant Archives*, *18*(2), 1499–1502.

15 Sumbembayev, A.A., Tergenbaeva, Z.H.T., Kudabayeva, G.M., Tashmetova, R.S., Genievskaya, Y.A., & Szlachetko, D.L. (2022). Assessment of state of *Dactylorhiza fuchsia* (Orchidaceae) populations from the Altai mountains of Kazakhstan. *Biodiversitas*, *23*(9), 4385–4399. https://doi.org/10.13057/biodiv/d230903

16 Kubentayev, S.A., Khapilina, O.N., Ishmuratova, M.Y., Sarkytbayeva, A.K., Turzhanova, A.S., Imanbayeva, A.A., & Zhumagul, M.Z. (2023). Current state of natural populations of *Paeonia anomala* (Paeoniaceae) in East Kazakhstan. *Diversity*, *15*(11), 1127. https://doi.org/10.3390/d15111127

17 *Shherbakov, A.V.,* & Mayorov, A.V. (2006). *Polevoe izuchenie flory i gerbarizatsiia rastenii [*Field study of flora and herbarium techniques*]*. Moscow: Izdatelstvo Moskovskogo Gosudarstvennogo Universiteta [in Russian].

18 *Rumyantseva, D.E.,* Lipatkin, V.A., & Zagreeva, A.B. *(2023). Osnovy geobotaniki [*Fundamentals of geobotany*]. mf.bmstu.ru. Retrieved from* https://mf.bmstu.ru/assets/info/science/dendro/books/17.pdf. [in Russian].

19 *Plants of the World Online (POWO 2025). powo.science. kew.org. Retrieved from https://* powo.science. kew.org/cite-us.

20 *Zaugolnova, L.B. (1994). Struktura populiatsii semennykh rastenii i problemy ikh monitoringa [*Structure of seed plant populations and problems of their monitoring*]. Extended abstract of candidate's thesis. Saint Petersburg* [in Russian]. *Retrieved from* https://viewer.rusneb.ru/ru/000199_000009_000286782? page=1&rotate=0&theme=white

21 *(1986). Metodika opredeleniia zapasov lekarstvennykh rastenii [*Methodology for determining stocks of medicinal plants*]. Moscow* [in Russian].

22 *Gemedzhieva, N.G. (2012). Alkaloidonosnye rasteniia Kazakhstana i perspektivy ikh ispolzovaniia (na primere Dzhungaro-Severotian-Shanskoi provintsii) [*Alkaloid-bearing plants of Kazakhstan and prospects for their use (example of the Dzungaro-North Tian Shan Province)*]. Vol. 18 (8), 312. Almaty* [in Russian].

23 *Smirnova, O.V.,* Zaugolnova L.B., Toropova, N.A., & Falikova, L.D. *(1976). Kriterii vydeleniia vozrastnykh sostoianii i osobennostei khoda ontogeneza u rastenii razlichnykh biomorp [*Criteria for distinguishing age states and ontogenetic features in plants of various biomorphs. In Plant cenopopulations: main concepts and structure*]. Tsenopopuliatsii rastenii (osnovnye poniatiia i struktura) — Coenopopulations of plants (basic concepts and structure)* [in Russian].

24 *Rabotnov, T.A. (1950). Geobotanika. Zhiznennyi tsikl mnogoletnikh travianistykh rastenii v lugovykh tsenozakh [*Geobotany: Life cycle of perennial herbaceous plants in meadow cenoses.*]. Trudy Botanicheskogo instituta Akademii Nauk SSSR — Proceedings of the Botanical Institute of the USSR Academy of Sciences. Series III, Issue 6, 7–204* [in Russian].

25 *Zajcev, N.G. (1973). Metodika biometricheskikh raschetov. Matematicheskaia statistika v eksperimentalnoi botanike [*Methodology of biometric calculations: Mathematical statistics in experimental botany*]. Moscow: Nauka* [in Russian]. *Retrieved from* https://knigogid.ru/books/1923293

26 *Mixajlova, S.I. (1989). Morfologiia i anatomiia Bupleurum multinerve (Apiaceae) na Altae [*Morphology and anatomy of *Bupleurum multinerve* (*Apiaceae*) in the Altai*]. Botanicheskii zhurnal — Journal Botanical, 74, 1455–1461* [in Russian]. *Retrieved from* http://nskhuman.ru/shipunov/bibljourn.php? nbook=52

27 *Nukhimovskij, E.L. (1997). Osnovy biomorfologii semennykh rastenii [*Fundamentals of biomorphology of seed plants]. *Teoriia organizatsii biomorp — Theory of biomorph organization, 1, 629* [in Russian].

28 *Asteshenkov, A.Yu. Sostoianie cenopopuliatsii Bupleurum multinerve DC. v razlichnykh usloviiakh Khakasii i Altaia [*State of *Bupleurum multinerve* DC. cenopopulations under different conditions in Khakassia and Altai*]. Rastitelnyi mir Aziatskoi Rossii — Flora of Asian Russia, 1(3), 94–99* [in Russian].

Information about the authors

Danilova Alevtina Nikolaevna — Candidate of Biological Sciences, Leading Researcher, Altai Botanical Garden, Ridder, Kazakhstan; e-mail: a-n-danilova@yandex.ru; ORCID: 0000-0002-1096-9339

Kotukhov Yuriy Andreevich — Candidate of Biological Sciences, Leading Researcher, Altai Botanical Garden, Ridder, Kazakhstan; e-mail altai_bs@mail.ru; ORCID: 000-0002-7700-5390

Sumbembayev Aidar Aitkazyevich — PhD, General Director of Altai Botanical Garden, Ridder, Kazakhstan; e–mail: aydars@list.ru, ORCID: https://orcid.org/0000-0003-0682-9162

Anufriyeva Olga Alexandrovna — Senior Researcher, Altai Botanical Garden, Ridder, Kazakhstan; e-mail: anufrievaolgaalex59@yandex.kz, ORCID: https://orcid.org/0000-0001-9675-7654

Akhmetzhanov Alisher Meirkhanuly — Junior Researcher, Altai Botanical Garden, Ridder, Kazakhstan; e-mail: alisherahmetzanov2000@gmail.com; ORCID: https://orcid.org/0009-0007-1572-0886